Author:
Wallis, Stephanie

Title:
Investigating the pathogenesis of tau protein in stem cell models of neurodegenerative disease

Investigating the pathogenesis of tau protein in stem cell models of neurodegenerative disease

Stephanie Wallis

A dissertation submitted to the University of Bristol in accordance with the requirements for award of the degree of Doctor of Philosophy (PhD) in the Faculty of Clinical Sciences November 2017.

Word count: 69930

Declaration

I, Stephanie Wallis, declare that the work in this dissertation was carried out in accordance with the requirements of the University's Regulations and Code of Practice for Research Degree Programmes and that it has not been submitted for any other academic award. Except where indicated by specific reference in the text, the work is my own work. Work done in collaboration with, or with the assistance of, others, is indicated as such.

Signed: ..... Date: .....

Abstract

Tauopathies are neurodegenerative diseases characterised by the pathological phosphorylation and accumulation of tau protein within the brain. Despite considerable efforts, the molecular pathways underlying tau pathogenesis have not yet been fully elucidated. This has been partially attributed to the limitations of traditionally used *in vitro* and *in vivo* models to recapitulate the complex molecular pathways involved in the pathogenesis of tau.

The use of human induced pluripotent stem cell (hiPSC) technology has enabled the derivation of disease-relevant cell types from patients with tauopathy. During this project, models of sporadic Alzheimer's disease (sAD) and frontotemporal dementia with Parkinsonism linked to chromosome 17 (FTDP-17) were developed through the derivation of vulnerable neuronal subtypes from hiPSC. Tau-related molecular pathology was assessed in these models and compared to that within human brain tissue to determine the ability of these models to recapitulate the molecular aspects of the disease niche and to inform on the underlying pathways contributing to tau pathogenesis.

hiPSC derived from a patient carrying Val337Met *MAPT* were differentiated to produce cortical glutamatergic neurons (CGNs) to model FTDP-17. This model successfully recapitulated the abnormal tau phosphorylation characteristic of tauopathy and decreased levels of synapsin, indicative of synaptic loss. Additionally, analysis of alterations in the gene expression, protein levels and activity of tau kinases involved in tauopathy recapitulated those seen in the brain, demonstrating the value of this model as a platform for further investigation of the pathogenesis of frontotemporal dementia.

Basal forebrain cholinergic neurons (bfCNs) and CGNs, which are vulnerable in sAD, were derived from control human pluripotent stem cell lines and treated with Amyloid-β (Aβ) oligomers for 48 hours to probe the molecular mechanisms underlying Aβ-induced tau pathology. While no evidence of abnormal tau phosphorylation or increased levels of tau were found, the model was found to recapitulate the development of neuronal varicosities and the loss of synapsin. The knowledge gained from this model serves to inform future models employing Aβ oligomer treatment.

Acknowledgements

I gratefully acknowledge the James Tudor Foundation for providing the funding that made this project possible.

I would also like to express my gratitude for the support and tutorage of my supervisors, Dr. Shelley Allen and Prof. Maeve Caldwell. Many thanks to Prof. Maeve Caldwell, who initially took me on as her PhD student for this project and has stayed in touch with me throughout the process of completing it, providing guidance and support. My sincere thanks to Dr. Shelley Allen for her excellent advice, patience and support during this project.

I am gratefully indebted to Dr. Lucy Crompton and Dr. Paul Nistor who spent many hours helping me to develop cell culture techniques, checking problematic cell cultures with me and for providing advice on the neuronal differentiation protocols. Many thanks to Dr. Lucy Crompton for carrying out the reprogramming of hiPSC lines V337M-C and V337M-E. Many thanks also to Dr. Daniel Whitcomb for his help with the preparation of Amyloid-β. Many thanks to Prof. Peter Davies (Albert Einstein College of Medicine, New York, USA) for supplying tau antibodies DA9, PHF-1, CP13, RZ3 and MC1.

I would like to thank my fellow PhD students in the Regenerative Medicine Labs at the University of Bristol. A special thanks to Jal and Renata, who kept me sane during late working hours and brightened challenging days in the lab with their sense of humour. Many thanks also to Petros for his calm attitude, humour and advice on cell culture work. I would also like to thank Aida and Hadil for their lovely cakes.

I wish to thank my parents, who have instilled in me a sense of resilience; they have demonstrated through their own challenges that there is always a way to solve difficult problems. I have always admired their determination and work ethic. Thank you both so much for your support during this project.

This PhD project has taught me to have resilience and patience. I feel privileged to have been able to contribute to this fascinating and important area of research.

Table of Contents

List of Tables

List of Figures

List of Abbreviations

$[Ca^{2+}]i$	Intracellular calcium concentration
µl	Microlitres
µM	Micromolar
µm	Micrometres
3D	Three dimensional
aa	Amino acid
AA	Ascorbic acid
ACh	Acetylcholine
ACID	APP intracellular cytoplasmic domain
AD	Alzheimer's disease
ADP	Adenosine diphosphate
AGD	Argyrophilic grain disease
$AlCl_3$	Aluminium chloride
ALS	amyotrophic lateral sclerosis
AP-1	Activator protein 1
ApoE	Apolipoprotein E
APP	Amyloid precursor protein
ATP	Adenosine triphosphate
Aβ	Amyloid-β peptide
$Aβ_{40}$	Amyloid-β 1-40
$Aβ_{42}$	Amyloid-β 1-42
$Aβ_{42}O$	Amyloid-β 1-42 oligomers
AβO	Amyloid-β oligomers
BfCNs	Basal forebrain cholinergic neurons
BIN1	Bridging integrator 1
BMPs	Bone morphogenic proteins
Bp	Base pair
BSA	Bovine serum albumin
bvFTD	Behavioural variant frontotemporal dementia
C83	C-terminus fragment of 83aa
C99	C-terminus fragment of 99aa
Ca^{2+}	Calcium ion
$CaCl_2$	Calcium chloride
cAMP	Cyclic adenosine monophosphate
CBD	Corticobasal degeneration

Cdc42/Rac	Cell division control protein 42 homolog/Ras-related C3 botulinum toxin substrate 1
Cdk5	Cyclic dependent kinase 5
CDK5	Cyclic dependent kinase 5 gene
CDM	Chemically defined media
cDNA	Complementary DNA
CGN	Cortical glutamatergic neurons
ChAT	Choline acetyltransferase
c-myc	Myelocytomatosis viral oncogene homologue
CR1	Complement receptor 1
CSF	Cerebrospinal fluid
CT	Threshold cycle number
CTE	chronic traumatic encephalopathy
Cu^{2+}	Copper (II) ion
DAPT	N-[N-(3,5-diflurorphenacetyl) – l-alanyl]-S-phenylglycine t-butyl ester
DIV	days *in vitro*
DMEM	Dulbecco's Modified Eagle medium
DMSO	Dimethyl sulfoxide
DNA	Deoxyribonucleic acid
DTT	1,4-Dithiothreitol
EB	Embryoid body
EDTA	Ethylenediamine tetraacetic acid
EGF	Epidermal growth factor
EOAD	Early-ons*et* Alzheimer's disease
ERK	Extracellular signal-regulated protein kinase
ESC	Embryonic stem cell
fAD	Familial AD
FAM	Fluorochrome 6-carboxyfluorescein (FAM)
FBS	Foetal bovine serum
FGF2	Fibroblast growth factor 2 (also known as basic fibroblast growth factor – bFGF)
FTD	Frontotemporal dementia
FTDP	Frontotemporal dementia with Parkinsonism
FTDP-17	Frontotemporal dementia with Parkinsonism linked to chromosome 17
FTD-tau	Frontotemporal dementia associated with tau pathology
FTLD	Frontotemporal lobar degeneration
FUS	Fused in sarcoma
GAPDH	Glyceraldehyde-3-phosphate dehydrogenase
gDNA	Genomic DNA

GDNF	Glial derived neurotrophic factor
GFP	Green fluorescent growth factor
GSK3	Glycogen synthase kinase 3
GSK3α	Glycogen synthase kinase 3 alpha
GSK3β	Glycogen synthase kinase 3 beta
GSK3β	Glycogen synthase kinase 3 beta gene
HCl	Hydrochloric acid
HD	Huntington's disease
hESC	Human embryonic stem cell
hFib	Human fibroblast
hiPSC	Human induced pluripotent stem cell
HiPSC-bfCNs	Basal forebrain cholinergic neurons derived from human induced pluripotent stem cells
HiPSC-CGN	Cortical glutamatergic neurons derived from human induced pluripotent stem cells
HIV	Human immunodeficiency virus
hPSC	Human pluripotent stem cell
hPSC-bfCNs	Basal forebrain cholinergic neurons derived from human pluripotent stem cells
HPSC-CGN	Cortical glutamatergic neurons derived from human pluripotent stem cells
ICM	Inner cell mass
iMEFs	Inactivated mouse embryonic fibroblasts
IPC	Intermediate progenitor cells
iPSC	Induced pluripotent stem cell
IRES	Internal ribosome response element
IVS	Intervening sequence
JNK	c-Jun N-terminal kinase
Kb	Kilobase pair
Klf4	Kruppel-like factor 4
KO	Knock-out
KO DMEM	Knock-out DMEM
LTD	Long-term depression
LTP	Long-term potentiation
M	Molar
mA	Milliamps
MAPs	Microtubule associated proteins
MAPT	Microtubule binding protein tau gene
MARK	Microtubule-affinity regulating kinase
MBD	Microtubule binding domain

MBP	Microtubule binding protein
MC1	Mild cognitive impairment
MEF	Mouse embryonic fibroblast
MEFs	Mouse embryonic fibroblasts
$MgCl_2$	Magnesium chloride
ml	Millilitres
mM	Millimolar
mRNA	Messenger RNA
MT	Microtubule
NaCl	Sodium chloride
NAD	Nicotinamide adenosine dinucleotide
$NaHCO_3$	sodium bicarbonate
nbM	Nucleus Basalis of Meynert
NEAA	Non-essential amino acids
NEM	Neural expansion media
NFT	Neurofibrillary tangle
NIM	Neural induction media
nM	nanomolar
NMM	Neural maintenance media
NPC	Neural progenitor cell
NTC	Non-template control
OCT4	Octamer binding transcription factor 4
p	Phosphorylated
PAK	P21 activated kinase
PAK1	P21 activated kinase 1
PAK1	P21-activated kinase 1 gene
PAK3	P21 activated kinase 3 gene
PAK3	P21-activated kinase 3
Pax6	Paired box protein gene 6
PBS	Phosphate buffered saline
PBs	Pick bodies
PBS-Tx	PBS + 0.1 % Triton-X-100
PCR	Polymerase chain reaction
PD	Parkinson's disease
PFA	Paraformaldehyde
PICALM	Phosphatidylinositol binding clatherin assembly protein
PiD	Pick's disease
PKB	Protein kinase B

PMD	Post-mortem delay
PNFA	Progressive non-fluent aphasia
POR	Poly-L-ornithine
PSD95	Post-synaptic protein 95
PSP	Progressive supranuclear palsy
ptau	Phosphorylated tau
PVDF	Polyvinylidene difluoride
qPCR	Quantitative polymerase chain reaction
RNA	Ribonucleic acid
ROCK	Rho-associated protein kinase inhibitor, also known as Y-27632
ROS	Reactive oxygen species
RT	Reverse transcription
S.D.	Standard deviation
S.E.M.	Standard error of the mean
sAD	Sporadic Alzheimer's disease
Sarkosyl	N-Dodecanoyl-N-methylglycine sodium salt
SD	Semantic dementia
SDS	Sodium dodecyl sulfate
sFTD	Sporadic frontotemporal dementia
Shh	Sonic hedgehog
SORL1	Sortilin-related receptor 1
SOX1	Sex determining region Y-box 1
SOX2	Sex determining region Y box 2
SSEA4	Stage-specific embryonic antigen 4
TAMRA	Tetramethylrhodamine
Tau	Tau protein
Tbr1	T-domain transcription factor 1
Tbr2	T-domain transcription factor 2
TBS-T	20 mM Tris–Cl pH 7.6, 137M NaCl, 0.1 % Tween 20
TDM	Terminal differentiation media
TDP-43	Transactive response DNA binding protein of 43 kilodalton molecular weight
Tg	Transgenic
TGFβ	Transforming growth factor beta
Thr	Threonine
TOD	Tangle only dementia
Tra-1-60	Trafalgar antigen 1-60
TRIS	Tris(hydroxymethyl) aminomethane
TRIS HCl	Tris(hydroxymethyl) aminomethane HCl

Tyr	Tyrosine
UNG	Uracil-N glycosylase
UP	Ultrapure
UPS	Ubiquitin protease system
V	Volts
VCP	Valosin-containing protein
VGlut1	Vesicular glucose transporter 1
vGlut2	Vesicular glucose transporter 2
VPA	Valproic acid
VTN	Vitronectin
VTN-T	Truncated vitronectin
WMT-GGI	White matter tauopathy with globular glial inclusions
Wnt	Wingless
WT	Wild type
Y-27632	Rho-associated protein kinase inhibitor, also known as ROCK

Chapter 1

General Introduction

1.1 Tau protein

Tau is a microtubule binding protein present abundantly within the axons and the somatodendritic compartments of neurons, as well as in relatively low levels within glial cells (Lee *et al.,* 2001; Trojanowski *et al.,* 1989; Tashiro *et al.,* 1997). This natively unfolded, hydrophilic protein has four main regions: an N-terminal projection region, a proline-rich domain, a microtubule-binding domain and a C-terminal region (Mandelkow *et al.,* 1996) (Figure 1.1). The primary role of tau within neurons is to provide stability to the microtubules (Chapter 1.1.2.1).

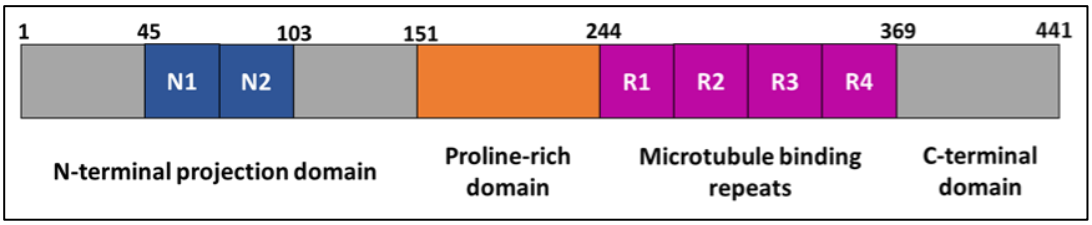

Figure 1.1 Schematic representation of the structure of tau protein

Schematic representation of the structure of the longest isoform of tau protein (441 amino acids (aa)) depicting the N-terminal domains N1 and N2 (blue), the proline rich domain (orange) and the microtubule binding domains R1, R2, R3 and R4 (purple). Tau binds to the microtubules via the microtubule binding domains and the N-terminal domains project outwards.

1.1.1 Expression of tau in the brain

In humans, tau is encoded by microtubule-associated protein tau gene (*MAPT*), which is situated on chromosome 17q21 and contains 16 exons. Six isoforms of tau are generated through alternative splicing of exons 2, 3 and 10; exons 2 and 3 each encode a 29-residue N-terminal repeat sequence (N), while exon 10 encodes a microtubule repeat domain (R). The resultant isoforms are denoted according to the number of these sequences that they contain, as 3R0N, 3R1N, 3R2N, 4R0N, 4R1N and 4R2N (Lee *et al.,* 2001; Andreadis *et al.,* 1992; Goedert *et al.,* 1989) (Figure 1.2). Although adults express all six isoforms, during the first year of neurodevelopment only 3R0N tau, also known as foetal tau, is expressed (Goedert *et*

al., 1989). Within the adult brain the ratio of 3R to 4R containing isoforms is approximately 1:1. Isoforms containing 0N, 1N and 2N comprise approximately 37 %, 54 % and 9 % of tau, respectively (Andreadis *et al.,* 1995; Goedert and Jakes, 1990). Abnormal alternative splicing of exon 10 results in an imbalance in the ratio of 3R:4R tau and is associated with particular tauopathies (Dickson *et al.,* 2011). The regulation of tau expression levels is brain region specific; the highest expression of tau in the brain occurs in the frontal and temporal lobes (Trabzuni *et al.,* 2012; Majounie *et al.,* 2013; McMillan *et al.,* 2008).

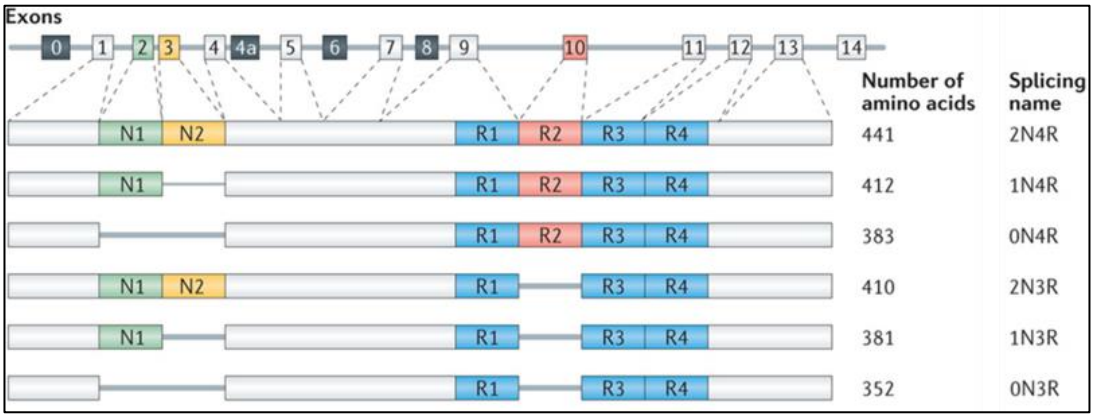

Figure 1.2 The isoforms of tau

Alternative splicing of MAPT produces six isoforms of tau; three of these include exon 10 and therefore have four microtubule binding domains (4R), three exclude this exon so have three microtubule binding domains (3R). Within these two groups the isoforms differ based on their inclusion or exclusion of exons 2 and 3. Exon 3 can only be included with exon 2, therefore allowing for three options; isoforms can have no N-terminal domains (0N), one N-terminal domain (1N) or two N-terminal domains (2N).
Image from Wang and Mandelkow, 2015, with permission.

1.1.1.2 Haplotypes

The locus containing the *MAPT* gene has two major haplotypes, H1 and H2. H2 differs in comparison to H1 by a 238-base pair (bp) deletion upstream of exon 10, as well as the inversion of a 900 kilo base pair (kb) sequence (Pittman *et al.,* 2006; Myers *et al.*, 2007; Caillet-Boudin *et al.*, 2015). Genome wide association studies have associated non-inverted H1 haplotypes with increased plasma tau levels (Allen *et al.,* 2016). This haplotype has also been associated with 4R tauopathies (Beevers *et al.,* 2017; Caffreys, 2006), frontotemporal dementia (FTD) and Alzheimer's disease (AD) (Pastor *et al.,* 2015; Pastor *et al.,* 2002; Chen *et al.,* 2017; Winder-Rhodes *et al.,* 2015). The H2 haplotype has been suggested to be

protective in neurodegenerative disease (Allen *et al.,* 2016), however this haplotype has also been implicated as a risk factor in the development of Pick's disease (PiD) (Russ *et al.*, 2001) and early onset AD (EOAD) (Kaivorinne *et al.*, 2008).

1.1.2 The physiological functions of tau

The most established function of tau is in microtubule stabilisation and as a conduit for the regulation of microtubule dynamics (Drubin and Kirschner 1986; Caceres and Kosik 1990; Avila *et al.,* 2004) (Chapter 1.1.2.1). As such tau also plays important roles in axonogenesis (Sayas *et al.,* 2015; Dawson *et al.,* 2001), synaptogenesis and synaptic plasticity in long-term depression (LTD) (Regan *et al.,* 2015; Kimura *et al.,* 2014). Increasing evidence has demonstrated tau's role in other cellular functions, unrelated to microtubule dynamics, such as in neurodevelopment, DNA repair, the transfer of information between neurons and in cell signalling (Hanger *et al.,* 2014; Wang and Mandelkow, 2015). The phosphorylation-dependent role of tau in microtubule regulation, however, remains the primary focus when considering the pathological roles of tau in tauopathy.

1.1.2.1 The role of tau as a microtubule binding protein

Microtubules are cylindrical polymers, comprised of alpha and beta tubulin heteromers, which form part of the cytoskeleton in all cells (Kirschner and Mitchison, 1986). In neurons, these linear structures, found grouped into bundles, have important roles in maintaining cell morphology, mitosis, scaffolding signalling molecules to form signalling hubs, synaptic plasticity and neurite growth (Kadavath *et al.,* 2015). Together with motor proteins, such as dynein and kinesin, which associate with the microtubule through microtubule associated proteins (MAPs), they are crucial for the transport of organelles, vesicles, nutrients and other cellular cargo in both in anterograde and retrograde directions throughout neurons. As highly polarised cells with great energy demands, efficient cellular transport is particularly important for the maintenance of healthy biomolecular functioning within neurons. Dysfunction in microtubule transport is associated with neurodegenerative disease (Su *et al*., 2010).

To carry out their functions effectively, microtubules must exist in a state of dynamic instability, which means they are constantly being assembled and disassembled. This state is maintained and regulated by a plethora of proteins, including tau (De Forges *et al.,* 2012; Roll-Mecak and McNally, 2010; Akhmanova and Steinmetz, 2015).

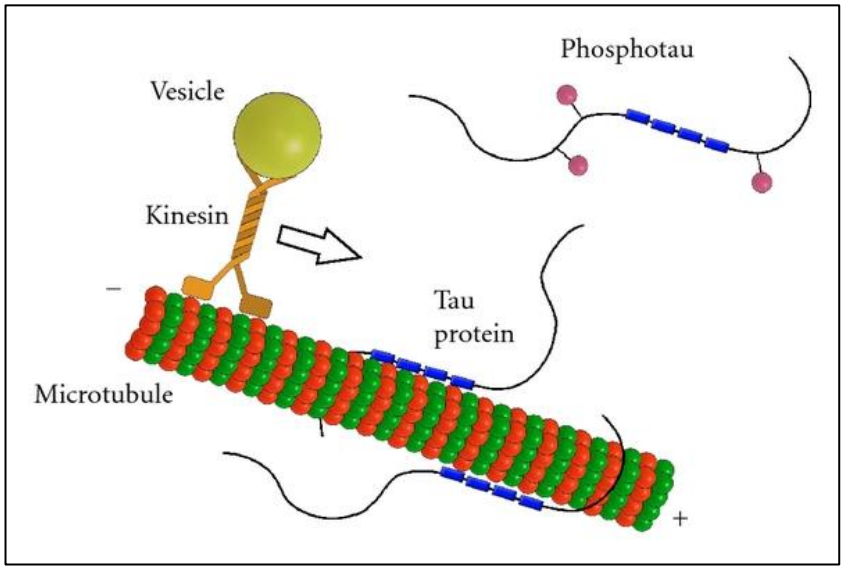

Figure 1.3 Tau binds to microtubules to regulate the transport of cellular cargo

Tau binds to the microtubules via its microtubule binding domains (blue rectangles). The binding of tau to the microtubules is regulated by phosphorylation through the activity of phosphatases and kinases; phosphate groups are indicated by the pink circles. Phosphorylation of tau regulates axonal transport, which is carried out by motor proteins, such as kinesin.

Tau binds to microtubules via its microtubule binding domains, with its N-terminals and C-terminals projecting outwards, at the interface between tubulin heterodimers (Santarella *et al.,* 2004; Kar *et al.,* 2003; Buée *et al.,* 2000) (Figure 1.3). The binding of specific isoforms of tau (Chapter 1.1.2) dictates the degree of microtubule stability of each bound tau molecule (Stanford *et al.,* 2003; Kosik *et al.,* 1989; Lu and Kosik, 2001). 4R isoforms have a greater affinity for the microtubules compared to 3R isoforms, owing to their possession of an extra microtubule-binding repeat domain, which explains their superior efficiency at promoting microtubule stability in comparison to 3R isoforms (Utton *et al.,* 2001; Goedert and Jakes, 1990). The N-terminals of tau can also bind to microtubules to form part of a membrane-

associated complex and to regulate the spacing between microtubules (Maas *et al.,* 2000; Frappier *et al.,* 1994; Al-Bassam *et al.,* 2002; Buée *et al.,* 2000; Kadavath *et al.,* 2015).

The exact mechanism through which tau regulates microtubule transport via the microtubules is unclear, however, increased binding of tau to the microtubules is thought to inhibit transport (Ebneth *et al.,* 1998; Trinczek *et al.,* 1999; Stamer *et al.,* 2002; Dixit *et al.,* 2008; Stoothoff *et al.,* 2009; Vossel *et al.,* 2010; Shahpasand *et al.,* 2012). The amount of tau bound to the microtubules influences cellular transport and the concentration of tau exists in a gradient throughout mature neurons such that a greater amount of tau is present within the synapses to encourage release of cellular cargo (Medina *et al.,* 2016).

1.1.2.1.1 Regulation of microtubule binding by phosphorylation of tau

Tau is subject to many modes of post-translational modification including phosphorylation, glycosylation, ubiquitination, sumoylation, glycation, polyamination, nitration, cleavage and truncation (Martin *et al.,* 2011). Primarily, however, it is the degree of phosphorylation of tau which dictates its binding affinity to the microtubules. There are 85 possible phosphorylation sites within the longest isoform of tau (4R2N), of which 80 are serine or threonine residues and five tyrosine (Hanger *et al.,* 2009). Tau phosphorylation is tightly regulated by the activity of tau kinases and phosphatases (Chapter 1.3), to allow for control of microtubule function.

In general, increased phosphorylation of tau results in decreased microtubule binding (Lindwall and Cole, 1984; Jenkins and Johnson, 1999; Sontag *et al.,* 1996; Drewes *et al.,* 1995; Sengupta *et al.,* 1998). It is recognised that phosphorylation of particular phosphorylation sites has a greater influence on the affinity of tau to the microtubules; for example, phosphorylation at Ser262, Ser214 and Thr231 is known to greatly reduce the affinity of tau for microtubules compared to phosphorylation at other residues (Sengupta *et al.,* 1998). Foetal tau is highly phosphorylated, containing approximately seven moles of phosphate compared to the two moles within the adult brain (Kanemaru *et al.,* 1992). It is thought that this is important for neurogenesis; for example, it has been demonstrated that tau must be phosphorylated at serine 205 and threonine 205 (Ser202/Thr205) to allow for neurite extension (Rösner *et al.,* 1995; Riederer *et al.,* 2001).

1.1.3 Pathological phosphorylation of tau leads to neurodegeneration

Many post-translational modifications of tau (Chapter 1.1.2) have been implicated in tauopathy (Martin *et al.,* 2011; Héraud *et al.,* 2014; Zilka *et al.,* 2006; Paholikova *et al.,* 2015; Cook *et al.,* 2014; Irwin *et al.,* 2013; Yan *et al.,* 1994; Gong and Iqbal 2008), however, hyperphosphorylation of tau at abnormal sites is the hallmark of tauopathies. It is believed that initial phosphorylation events lead to the formation of pathological conformations of tau, which are predisposed to become further phosphorylated and to subsequently aggregate (Zheng-Fischhöfer *et al.,* 1998; Kimura *et al.,* 1996). The molecular pathways underlying the aberrant phosphorylation and aggregation of tau, leading to neurodegeneration, is an area of intense research. Pathological tau is thought to contribute to neurodegeneration through several pathways (Figure 1.4).

Hyperphosphorylation of tau is known to lead to the detachment of tau from the microtubules (Goedert, 1993), which leads to the destabilisation and disassembly of the microtubules. Consequently, the loss of cellular structural integrity as well as cellular transport of critically important cargo, such as mitochondria, to distal areas of the neuron follows. This contributes to synapse loss and neuronal death (Spires-Jones and Hyman, 2014) (Figure 1.4). The detachment of tau from the microtubules also leads to an increase in free intracellular tau, which is susceptible to further phosphorylation and aggregation.

The formation of tau with a pathogenic conformation occurs due to hyperphosphorylation (Gendron and Petrucelli, 2009; LaPointe *et al.,* 2009) and has been proposed to seed the formation of aggregates of tau (Jicha *et al.,* 1999; Jicha *et al.,* 1997). Hyperphosphorylated tau has also been proposed to be more resistant to degradation, thereby contributing to the accumulation and subsequent aggregation of the protein (Paglini and Cáceres, 2001). For example, tau aberrantly phosphorylated at Ser422, Ser262 and Ser356 is resistant to proteasomal degeneration (Dickey *et al.,* 2006). Hyperphosphorylated, aggregated tau may further impede cellular transport, affect cell signalling and enforce toxicity through overloading protein clearance pathways.

The interaction of tau with other proteins is also altered through increased phosphorylation, contributing to dysregulation of critically important biomolecular pathways. This is exemplified by the fact that only hyperphosphorylated tau can interact with the kinesin-associated protein JUN N-terminal kinase-Murray *et al*, 2014. Additionally, abnormal phosphorylation of tau at specific sites 'primes' tau for further sequential phosphorylation

by other tau kinases, which would not usually occur in physiological conditions, establishing a pathogenic feed-forward system (Zheng-Fischhöfer *et al.,* 1998; Cho and Johnson, 2003; Cho and Johnson, 2004).

We have not yet completely mapped out which sites are aberrantly phosphorylated in all cases of tauopathy, however, mounting evidence supports the role of hyperphosphorylation of specific phospho-sites in AD and other tauopathies (Martin *et al.,* 2013; Luna-Muñoz *et al.,* 2007). Hanger and collegues have used mass spectrometry to map novel tau phosphorylation sites (Hanger *et al.*, 2007).

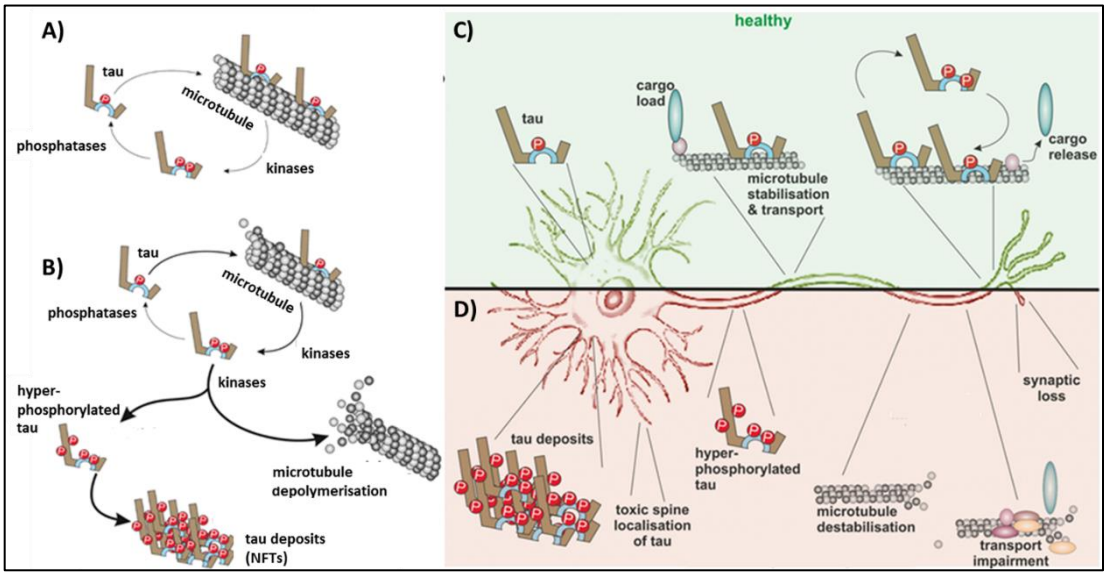

Figure 1.4 Physiological and pathological phosphorylation of tau

In normal physiological function (A and C), kinases and phosphatases work in concert to control the phosphorylation of tau, which determines its ability to bind to the microtubules. Upon phosphorylation by kinases, tau detaches from the microtubules and is then dephosphorylated by phosphatases (A). This regulation of tau phosphorylation facilitates stabilisation of the microtubules as well as transport of cargo along the microtubules; at the synapses cargo is released by phosphorylation of tau by kinases (C).

Under pathological conditions (B and D), there is an imbalance between the action of kinases and phosphatases, leading to hyperphosphorylation of tau. Hyperphosphorylation of tau causes tau to detach from the microtubules, leading to microtubule depolymerisation and the aggregation of hyperphosphorylated tau into tau deposits (NFTs) (B), which build-up within the neuron (D). Destabilisation of neurons contributes to the impairment of cellular transport and to the loss of synapses (D).

Interestingly, hyperphosphorylation of tau at sites associated with tauopathy have been found in mammals that undergo hibernation. Hibernation is a physiological state

characterised by significant decreases in body temperature and oxidative metabolism during prolonged inactivity to minimise energy expenditure during inhospitable environmental conditions. Hibernation is accompanied by dramatic decreases in neuronal function (Arendt *et al.*, 2003). Previous studies have demonstrated that hyperphosphorylated tau has been found within the entorhinal cortex and hippocampus of European ground squirrals (Arendt *et al.*, 2003) and within the brains of Arctic ground squirrels (Su *et al.*, 2008). The increase in tau phosphorylation was found to correspond to changes in the activity of tau kinases and phosphatases during hibernation; activity of tau kinases GSK3β and PKA increased and activity of tau phosphatase PP2A decreased during hibernation of the Arctic squirrel (Su *et al.*, 2008). This hyperphosphorylation is fully reversible when hibernation ends or during the periodic re-warmings of the animals body during hibernation and has been suggested to be a neuroprotective mechanism enabling the brain to adapt to dramatically decreased metabolism and temperature thus demonstrating a physiological role for hyperphosphorylation of tau in the adult mammal brain (Arendt *et al.*, 2003; Su *et al.*, 2008; Arendt and Bullmann, 2013).

Hyperphosphorylation of tau has also been found within in the adult, healthy human brain; Matsuo and colleagues demonstrated that healthy, human brain biopsies have tau phosphorylated at many of the same sites associated with PHF tau found in patients with AD (Matsuo *et al.*, 1994) and later rapid processing of biopsied healthy human and monkey brain tissues also revealed tau is hyperphosphorylated at sites associated with pathological tau (Garver et al., 1996). Phosphorylation of tau at certain sites is known to be lost rapidly after death and time taken to process post-mortem brain samples has been demonstrated to be an important consideration in investigations into tau phosphorylation .

1.2 Tauopathies

Tauopathies are a group of heterogenous, progressive neurodegenerative diseases characterised by the pathological hyperphosphorylation and accumulation of tau within the brain. The most common tauopathy is Alzheimer's disease (AD), initially described by Alois Alzheimer (Alzheimer, 1907). The second most prevalent is frontotemporal dementia (FTD) (Yoshiyama *et al.,* 2001). Hyperphosphorylated, aggregated tau pathology is also the primary culprit underlying many other dementing disorders including progressive supranuclear palsy

(PSP), corticobasal degeneration (CBD), argyrophilic grain disease (AGD), Huntington's disease (HD), amyotrophic lateral sclerosis (ALS) and chronic traumatic encephalopathy (CTE) (Murray *et al.*, 2014).

1.2.1 Frontotemporal Dementia

The highly heterogeneous group of diseases circumscribed by the term frontotemporal dementia (FTD) (or frontotemporal lobar degeneration (FTLD)) are characterised by a predominant, progressive loss of neurons within the frontal and temporal lobes. Over time and with growing knowledge, our classification of these diseases has been refined. Histologically, there are four subtypes within the group; FTD-tau, FTD-TDP, FTD-FUS and FTD-UPS, which are so called due to their association with the aggregation of tau, transactive response DNA-binding protein (TDP), fused in sarcoma (FUS) proteins or ubiquitin protease system (UPS) proteins, respectively (Figure 1.5).

Between 50-80 % of FTD cases are thought to be sporadic, while the rest of the cases are accounted for by mutations within a number of genes. FTD-TDP can be caused by mutations in *GRN*, *TARDBP* or VCP, which encode progranulin protein, transactive response DNA-binding protein of 43 kilodalton (kDa) molecular weight *(TDP-43)* and valosin-containing protein, respectively. Each of the mutations responsible for FTD-TDP cause formation of glial and neuronal inclusions of TDP-43, a DNA and RNA binding protein involved in RNA processing. Mutations in *CHMP2B*, which encodes charged multivesicular body protein 2B are associated with FTD-UPS. Mutations in C9orf72, which is important for lysosomal storage function (Clayton *et al.*, 2015) and in the regulation of endosomal trafficking (Farg *et al.*,

2014), lead to FTD-FUS (Hardy, 2014; Goedert and Spillantini, 2000). Mutations in *MAPT* cause FTD-tau.

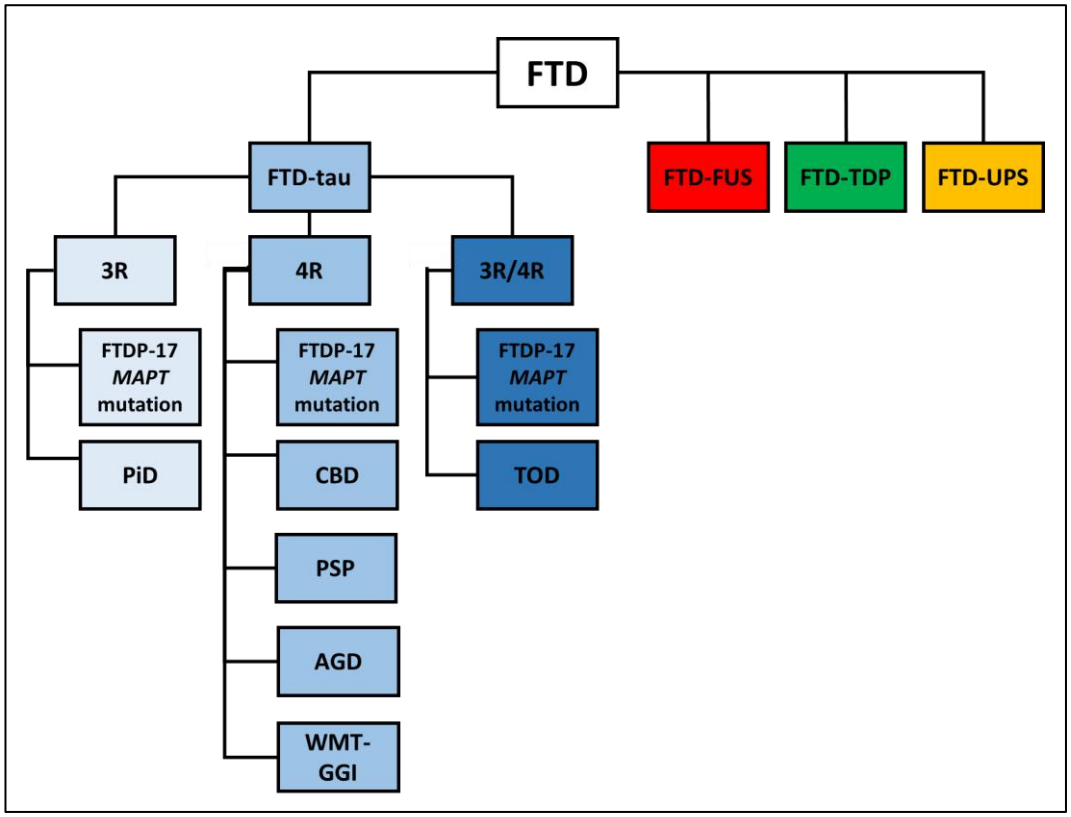

Figure 1.5 Histological classification of frontotemporal dementias

FTD can be classified due to its association with different protein pathologies. FTD-tau is associated with tau pathology, FTD-fus is associated with ubiquitinated Fused-in-Sarcoma (FUS) pathology, FTD-TDP is associated with the presence of ubiquitinated TAR DNA-binding protein of 43 kDa (TDP-43) pathology and FTD-UPS includes pathology positive for components of the ubiquitin-proteasome system (UPS) but negative for FUS or TDP-43. Tauopathies are also classified according to the predominant isoforms, 3R or 4R, of tau that accumulate. Depending on the specific mutation responsible for FTDP-17, either of these isoforms, or a mixture, can be dominant. PiD is associated with 3R tau accumulation. Tauopathies known to contain more 4R tau include white matter tauopathy with globular glial inclusions (WMT-GGI), argyrophilic grain disease (AGD), progressive supranuclear palsy (PSP) and corticobasal degeneration (CBD).

FTD-tau includes sporadic and familial forms of FTD with tau pathology. The group includes Pick's disease (PiD), frontotemporal dementia with Parkinsonism linked to chromosome 17 (FTDP-17), progressive supranuclear palsy (PSP), corticobasal degeneration (CBD), white matter tauopathy with globular glial inclusions (WMT-GGI), argyrophilic grain disease (AGD) and tangle only dementia (TOD) (Halliday *et al.,* 2012) (Figure 1.5). While histologically

classified as distinct diseases, these diseases are all highly heterogenous and there are extensive histological and clinical overlaps between them (Luna-Muoz *et al.,* 2014).

In general, the presentation of FTD is associated with cognitive decline heeded by disinhibition, behavioural changes and emotional changes, however, the disease is highly variable in its clinical presentation. Clinical presentations of FTD are classified into three main groups. Behavioural variant FTD (bvFTD) accounts for approximately 60 % of all FTD cases and includes PiD and FTDP-17, while semantic dementia (SD) accounts for approximately 20 % of cases and progressive non-fluent aphasia (PNFA) accounts for the remaining 20 % of cases.

bvFTD is recognised by behavioural disinhibition, apathy, loss of empathy, hyperorality, dietary changes, executive function deficits and compulsive, perseverative or ritualistic behaviours (Piguet *et al.,* 2011). Memory is relatively spared in bvFTD, however, when memory dysfunction does present it is similar in phenotype to that in AD patients. SD, also called temporal variant FTD, is characterised by a loss of language semantics caused by degeneration of an area of the left temporal lobe critical for assigning meaning to words. Right-sided SD occurs where neurodegeneration begins in the right temporal lobe and is characterised by problems remembering the faces of familiar people and loss of empathy. Patients with SD usually live longer than those with bvFTD, however, will always develop symptoms associated with bvFTD eventually. Patients with PNFA have difficulty producing fluent speech despite their understanding of the meaning of the words remaining intact (Goedert *et al.,* 2012). Classification is further complicated by the co-presentation of motor dysfunction similar to that of Parkinson's disease (PD), termed 'frontotemporal dementia with Parkinsonism' (FTDP), which most commonly is recognised in cases of bvFTD (Goedert *et al.,* 2012).

1.2.1.1 Neurodegeneration in frontotemporal dementia associated with tau pathology

The presentation of FTD is influenced by the areas of the brain affected, the underlying pathology and the large-scale neural networks involved (Finger, 2016). Each clinical group is associated with different patterns of neurodegeneration; bilateral degeneration of the medial frontal lobes and anterior temporal lobes underlies bvFTD, whereas SD is associated with more pronounced, usually asymmetric temporal lobe atrophy and PNFA is accompanied by atrophy of the left lateral sulcus.

Cortical glutamatergic neurons (CGNs) and glutamatergic transmission are particularly vulnerable in FTD (Procter *et al.,* 1999; Ferrer, 1999; Sposito *et al.,* 2015), demonstrated by reduced numbers of dendritic branches, numbers of dendritic spines and levels of synaptic proteins, including synapsin I (Ferrer, 1999). Surprisingly few studies have been carried out aimed at understanding why glutamatergic neurons are selectively lost in the disease. In AD, tau is linked to molecular pathways resulting in glutamate toxicity (Campos-Pea and Antonio, 2014) and similar pathways may underlie loss of these neurons in FTD.

1.2.1.2 Pick's Disease

Pick's disease (PiD) is a sporadic, progressive and highly heterogenous frontotemporal dementia (FTD) that accounts for approximately 2 % of all cases of dementia. Clinically, PiD manifests at around age 40-60 years as bvFTD (Hodges 2001; Luna-Munoz *et al*., 2014). Patients live an average of 10.4 years after diagnosis (Josephs *et al.,* 2005). Histologically, PiD is recognised by frontal and anterior temporal lobe cortical atrophy due to the loss of synapses dendrites and neurons, white matter degeneration, achromatic neurons (Pick cells) and intraneuronal tau inclusions called Pick bodies (PBs) (Lewis *et al.,* 2001; Kertesz, 2003), which have been found in the cerebral cortex, the hippocampus and in selected brainstem nuclei (Zhukareva *et al*., 2002). Recent studies suggest that neurodegeneration first occurs in the frontotemporal limbic regions and neocortical regions before progressing to subcortical regions, then the primary motor cortex and pre-cerebellar nuclei and finally the visual cortex (Lewis *et al.,* 2001). Tau aggregations are mainly composed of 3R tau (Delacourte *et al.,* 1998; Delacourte *et al.,* 1996; Dickson *et al.,* 2011; Buée and Delacourte 1999) loosely arranged into straight filaments (Takauchi *et al.,* 1984).

1.2.2 Frontotemporal dementia with Parkinsonism linked to chromosome 17

We have known for a long time that tau is the major component of the intracellular filamentous deposits found in the brains of those suffering from many neurodegenerative diseases. In 1998, mutations within *MAPT* were demonstrated to be the cause of familial FTD (Hutton *et al.,* 1998; Poorkaj *et al.,* 1998), emphatically demonstrating that dysfunction of tau protein can cause neurodegenerative disease.

FTD caused by mutations in *MAPT* account for approximately 30 % of cases of heritable FTD and are associated with autosomal dominant inheritance of disease (Hardy, 2014). These

diseases are named frontotemporal dementia with Parkinsonism linked to chromosome 17 tau (FTDP-17) (Foster *et al*., 1997) as patients tend to clinically present with Parkinson's disease-like motor symptoms along with bvFTD (Siuda *et al.,* 2014). Patients usually initially present with psychiatric symptoms, alongside language dysfunction in some cases, and are often misdiagnosed with PiD, primary progressive aphasia, AD, PSP or CBD (Ghetti *et al.,* 2015). Memory impairment, as a predominant presenting feature, has been reported in only a few cases of FTDP-17 (Doran *et al.,* 2007), however, the phenotype of the memory disturbance phenotype is similar to that in AD (Doran *et al.,* 2007).

The clinical presentation, age of onset and duration of these diseases varies between patients with different *MAPT* mutations, in line with the heterogeneity reflected in the neuropathology and patterns of brain atrophy in these patients. For example, while the average age of onset is 49 years and the life expectancy after diagnosis is 8.5 years, patients have presented with FTDP-17 in their early 20s as well as in the late 70s and lived for only 1.5 years or as long as 26 years (Wszolek *et al.,* 2003; Reed *et al.,* 2000). There is also a high level of heterogeneity between families carrying the same mutation and even within families (Larner, 2009; Larner and Doran, 2008; Wszolek *et al*., 2003; Bugiani *et al*., 1999), demonstrating that environmental factors or genetic modifiers play a role in the pathogenesis of tauopathies. Phenotypic differences between patients with the same FTDP-17 mutation may be explained by the tau haplotype (Chapter 1.1.1.2) (Baba *et al*., 2005) carried by these patients or their ApoE genotype (Mann *et al.,* 2001). Through understanding how each of these mutations, which exert specific changes to tau protein or the splicing of tau isoforms, result in different disease pathology and presentation, we can gain insight into the importance of particular pathogenic alterations to tau in disease.

1.2.2.1 *MAPT* mutations

Linkage analysIs of 150 families affected by FTDP-17 have led to the identification of 53 intronic and exonic *MAPT* mutations (van der Zee and Van Broeckhoven, 2014). Approximately half of these are exonic mutations of exons 1, 9, 11, 12 and 13, which affect the ability of tau to interact with microtubules or increase its propensity to assemble into abnormal filaments (Hasegawa *et al.,* 1998; Deture *et al.,* 2000; Dayanandan *et al.,* 1999; Hong *et al.,* 1998; Matsumura *et al.,* 1999; Ghetti *et al.,* 2015). The other mutations occur within exon 10 or in the adjacent introns (Figure 1.6). Some of these intronic mutations of these mutations prevent or disrupt the formation of the stem loop structure of tau's pre-

RNA, which forms because the non-mutant sequence is palindromic, thereby preventing the splicing machinery from splicing out exon 10 (Wolfe, 2008). Another mechanism through which mutations affect the splicing of exon 10 is by altering linear cis-splicing elements (Wolfe, 2008). This results in the overproduction of 4R tau, thus perturbing the normal ratio of 3R:4R tau isoforms (Ghetti *et al.,* 2015). Disturbances in the normal function and expression of tau lead to neurodegeneration due to altered microtubule dynamics.

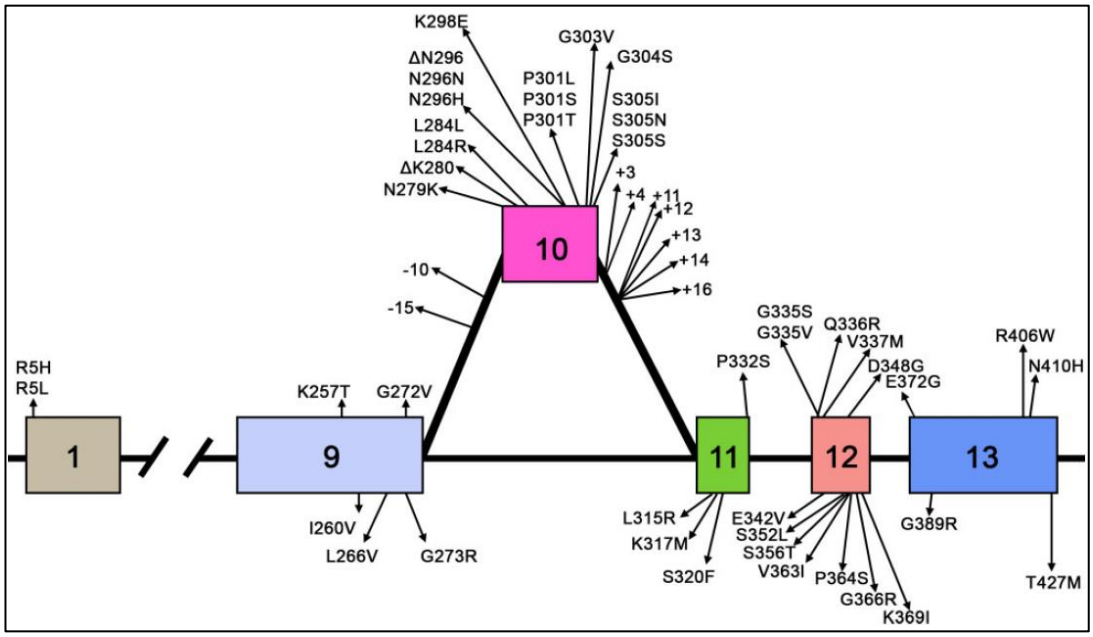

Figure 1.6 MAPT mutations in FTDP-17

Schematic representation of the positions of MAPT mutations in FTDP-17. Approximately half of these are either intronic or exonic mutations near, or in exon 10; These mutations affect the alternative splicing of exon 10. Other exonic mutations exist in exon 1, 9, 11, 12 and 13 and these affect either the binding of tau to the microtubules or the propensity of tau to aggregate.

Image from Ghetti et al., 2015, permission granted, Copyright © 1999 - 2017 John Wiley & Sons, Inc.

Different mutations lead to different tau pathology, patterns of atrophy and clinical presentations. For example, Whitwell and colleagues demonstrated that although all cases of FTDP-17 exhibit degeneration of the anterior temporal lobes, mutations that alter the splicing of tau pre-mRNA lead to grey matter loss focused within the medial temporal lobes, including the hippocampus, amygdala, parahippocampal gyrus and fusiform gyrus. On the other hand, mutations that lead to altered structure of tau are more commonly associated

with relative sparing of the medial temporal lobes and degeneration of the lateral temporal lobes (Whitwell *et al.*, 2009).

In the studies presented here, hiPSC from patients carrying a missense mutation resulting in a change of valine to methionine at 337 (V337M) within *MAPT* were differentiated into neurons. A more detailed description of the clinical presentation and tau pathology associated with this mutation is given in Chapter 4 (Chapter 4.1.1). Tau pathology within the frontal and temporal lobes of patients with a missense mutation resulting in a change of arginine to tryptophan at 406 (R406W), and within those with a point mutation resulting in a change of cysteine to tyrosine within intron 10 (IVS 10+16 C>T) *MAPT*, have been investigated in Chapter 6.

1.2.2.1.1 The clinical and pathological features of IVS 10+16 C>T *MAPT*

The point mutation from cysteine to tyrosine within intron 10 of *MAPT* (IVS 10+16 C>T *MAPT*) destabilises the stem-loop structure of intron 10 of *MAPT* (Figure 1.6), leading to a two- to six-fold increase in the ratio of 4R:3R tau mRNA by altering the splicing of exon 10 (Connell *et al.*, 2005). The clinical presentation of individuals with this mutation is heterogenous within and between families (Larner and Doran, 2008); patients have been diagnosed with FTD (Janssen *et al.*, 2002; Pickering-Brown *et al.*, 2002), AD (Doran *et al.*, 2007; Larner et al., 2008, 2009) and PSP (Morris *et al.*, 2003). A range of symptoms have been described including those more commonly associated with FTDP-17; motor dysfunction including Parkinsonism, anomia, language impairment and disinhibition have been reported (Pickering-Brown *et al.,* 2002; Janssen *et al.,* 2002; Larner *et al.,* 2009; Stanford *et al.,* 2004; Morris *et al.,* 2003). Age of onset varies from the late 30's to the early 60's of patients (Janssen *et al.*, 2002; Pickering-Brown *et al.*, 2002; Morris *et al.*, 2003; Stanford *et al.*, 2004; Larner and Doran, 2006; Larner, 2009).

While the frontal and temporal lobes are affected in patients with this mutation, neuropathology, including the loss of neurons, neuropil vacuolation, grey matter gliosis, tau phosphorylation and tau aggregation, also varies in location and reports have concluded particularly severe loss of temporal lobe tissue (Larner *et al.,* 2009), global loss of cortical regions of the brain (Larner *et al.,* 2009) and the severe neurodegeneration of the globus pallidus and subthalamic nucleus (Morris *et al.,* 2003) within the brains of patients with this

mutation. Hyperphosphorylated tau aggregates within the brains of these patients have been reported to be diffuse or globular in structure (Morris *et al.,* 2003).

1.2.2.1.2 The clinical and pathological features of R406W *MAPT*

The point mutation arginine to tryptophan at 406 (R406W *MAPT*), occurs in exon 13 of *MAPT*. The residue it alters is highly conserved, which highlights its probable importance in the function of tau. The mutation results in a change in the structure of tau, which results in alterations in the ability of tau to bind to the microtubules (Hong *et al*., 1998).

Clinically, patients with this mutation present with AD-like symptoms, including memory impairment, as well as FTDP-17 symptoms including Parkinsonism, disinhibition and impulsivity (Ostojic *et al*., 2004; Carney *et al.,* 2014; Van Swieten *et al.,* 1999; Rademakers *et al*., 2003; Ebrahimi 2015; Passant *et al.,* 2004; Hirschbichler *et al.,* 2015; Behnam *et al.,* 2015; Ng *et al*., 2015). As with those with other FTDP-17 mutations, presentation is heterogenous between individuals with the disease. Language disturbances have been reported in some cases (Rademakers *et al.,* 2003; van Swieten *et al.,* 1999), however, this is not the case for all cases of R406W *MAPT* FTDP-17 (Ikeuchi *et al.,* 2008; Hirschbichler *et al.,* 2015; van Swieten *et al.,* 1999). This mutation can result in one of two disease trajectories; in most cases reported the disease progresses slowly (Passant *et al.,* 2004; Ostojic *et al.,* 2004; Ikeuchi *et al.,* 2008; Lindquist *et al.,* 2008; Rademakers *et al.,* 2003; Carney *et al.,* 2014), however, in one patient progression of cognitive decline was observed to be rapid (Carney *et al.,* 2014). Onset varies considerably from the 3rd to the 6th decade of the patients' lives (Rademakers *et al.*, 2003; Ostojic *et al.*, 2004; Passant *et al.*, 2004; Ikeuchi *et al.*, 2008; Carney *et al.*, 2014; Behnam *et al.*, 2015; Hirschbichler *et al.*, 2015) .

The pathology associated with this mutation is described as bilateral frontotemporal degeneration (Basiri *et al.,* 2015). As well as the loss of neurons, gliosis and widespread aggregation of tau within the cortex are pathological features of this mutation. Amyloid pathology has also been reported in some cases (Ishida *et al.*, 2015).

1.2.3 Alzheimer's disease

Alzheimer's disease (AD) is responsible for the majority of cases of dementia worldwide (Alzheimer's Association, 2016). The symptoms of AD are caused by neurodegeneration of large scale neuroanatomic networks resulting in severe cortical atrophy (Weintraub *et al.,*

2012; Seeley *et al.,* 2009; Dennis and Thompson, 2014). Neuropathologically, AD is hallmarked by the accumulation of intracellular tau protein and extracellular amyloid-beta (Aβ) within areas of the brain related to this circuitry. There are two forms of AD with equivalent pathology and symptoms, which are clinically distinguished by their age of onset; the majority of cases are sporadic (sAD) and generally present after age 65, while 2-10 % of cases are familial (fAD), which present before age 65 (Alzheimer's Association, 2016; Zhu *et al.,* 2015).

The predominant symptom of AD is memory failure, which is subtle upon initial presentation, becoming more severe with progression and is eventually incapacitating. Patients also exhibit a range of other cognitive deficits, language disturbances and neuropsychological changes including depression, poor judgement, confusion, sleep disturbance, mutism, agitation, withdrawal, hallucinations and seizures (Landes *et al.,* 2001; Peter-Derex *et al.,* 2015; Weintraub *et al.,* 2012; Caraci *et al.,* 2010; Selkoe 2011; Chi *et al.,* 2014). In the later stages of disease, patients may also experience motor symptoms (Wirths and Bayer, 2008).

1.2.3.1 Neurodegeneration in Alzheimer's disease

Neurodegeneration begins in the basal forebrain and entorhinal cortex, considered an invariant focus of pathology in all AD cases, which gives rise to bidirectional projections connecting the hippocampus and the cortex (Schmitz *et al.*, 2016). Degeneration of the hippocampus follows and then neurons are lost in other neocortical areas including the temporal cortex (Buckner *et al.,* 2008; Jack *et al.,* 1998). The hippocampus plays a prominent role in memory acquisition and consolidation, while the temporal lobe governs language function and is also involved in memory functions (Buckner *et al*., 2008; Jack *et al*., 1998), which explains the prominent memory dysfunction associated with AD. In the later stages of AD, wide-spread neurodegeneration occurs, evidenced by shrinkage of the cerebral cortex and enlarged ventricles, precipitating additional symptoms (Braak *et al.,* 2011; Braak and Braak, 1991; Braak and Braak, 1996; Braak and Braak, 1995) (Figure 1.7).

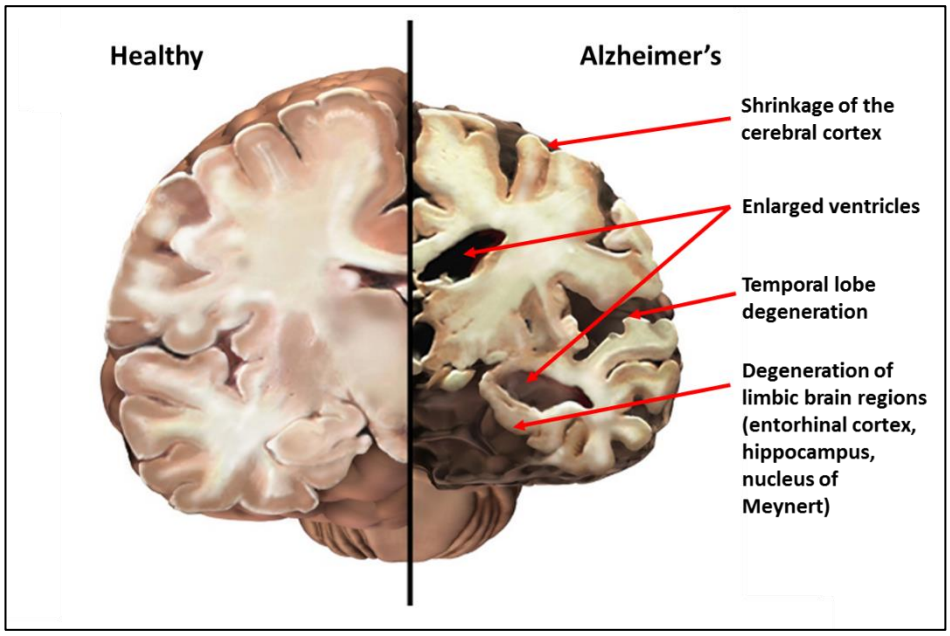

Figure 1.7 Neurodegeneration in Alzheimer's disease

The image above depicts a coronal section through a healthy brain (left hand side) and a late-stage AD brain (right hand side). Upon comparison of the two, gross atrophy of the brain can be recognised by shrinkage of the cerebral cortex and ventricle enlargement. The limbic regions and temporal lobes are labelled and demonstrate severe loss of brain tissue.

Adapted with permission from www.alz.org ©2017 Alzheimer's Association. All rights reserved. Illustrations by Stacy Jannis.

1.2.3.1.1 Vulnerable neuronal populations in AD

The cholinergic and glutamatergic neurotransmission systems are preferentially targeted in AD (Sims *et al*., 1983; Bartus *et al*., 1982; Francis *et al*., 1993; Greenamyre, 1986). It is thought that neurodegeneration in the AD brain occurs in a dichotomous pattern, beginning with the basal cholinergic forebrain neurons (bfCNs), which originate from within the basal nucleus of Meynert (nbM) and provide cholinergic innervation to the hippocampus and cortex (Coyle *et al.,* 1983; Auld *et al.,* 2002; Wicklund *et al.,* 2010; Prado *et al.,* 2016; Duan *et al.,* 2014.; Palmer and Gershon 1990; Whitehouse *et al.,* 1982; Kuhn *et al.,* 2015; Arendt *et al.,* 1983; Bartus *et al.,* 1982; Schmitz *et al.,* 2016; Candy *et al.,* 1983; Liu *et al.,* 2015). These neurons play important roles in encoding novel information, the regulation of cortical plasticity and attention, which are all important processes in memory function (Auld *et al.,* 2002; Olton, 1990; Zaborszky *et al.,* 2012; Janocko *et al.,* 2012; Schmitz *et al.,* 2010; Schmitz *et al.,* 2016; Schmitz *et al.,* 2014; Quigley *et al.,* 2010; McGaughy 2005; Pinto *et al.,* 2013; Goard and Dan, 2009). Aβ plaques occur early in these neurons and degeneration of the

nbM is correlated with dementia (Kerbler *et al.*, 2015). BfCNs are very long and project elaborate, richly arborised processes (Woolf, 1991). Consequentially, they have high metabolic demands deeming them particularly vulnerable in AD (Wu *et al.,* 2014).

Glutamatergic neurons, particularly those within the cortex, are also particularly vulnerable in AD, leading to severe disruption of glutamatergic neurotransmission within the hippocampus and neocortical areas (Francis *et al.,* 1993; Francis, 2003; Lee *et al.,* 2002; Greenamyre *et al.,* 1988; Campos-Pea and Antonio, 2014; Palmer and Gershon, 1990; Frisardi *et al.,* 2011; Revett *et al.,* 2013). Since glutamatergic neurotransmission within the medial temporal lobes is important in learning and memory functions, the loss of these neurons may underlie dementia in AD (Squire and Zola-Morgan, 1991).

1.2.3.2 Tau and Amyloid-beta pathology in Alzheimer's disease

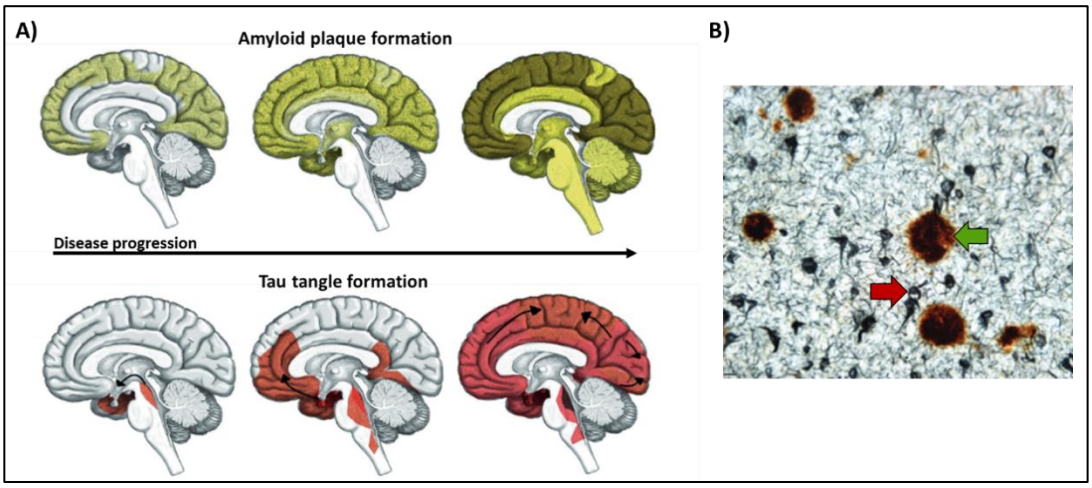

Figure 1.8 Neurofibrillary tangles and Amyloid plaques in the Alzheimer's disease brain

A) Schematic representation of the spread of Amyloid plaque (green) and tau tangle (red) pathology with disease progression. Darker colours resemble areas of higher concentrations of aggregations. Plaques develop profusely within the cortex and later in disease can be found within the allocortex, diencephalon and eventually throughout the majority of the brain. NFTs first appear within the basal forebrain and entorhinal cortex, then within the temporal lobes and other cortical areas. Image adapted, with permission, from Candela et al., 2013.

B) Amyloid plaques immunostained with anti-beta-amyloid antibody (green arrow) and tau tangles immunostained with anti-PHF-1 antibody (red arrow) within a hippocampal slice from an AD brain. Image adapted, with permission, from Rohn, 2013.

1.2.3.2.1 Propagation of tau pathology

A study by Braak and colleagues compared tau pathology within the brain using immunostaining with antibodies against hyperphosphorylated tau and silver staining at Braak stages. The group found that at Braak stage I, mild tau pathology is confined to the transentorhinal region. At stage II, the density of NFT lesions increases and the pathology extends to the entorhinal cortex with pathological hyperphosphorylated tau found within the deep entorhinal plexus. By stage III, tau pathology worsens and lesions extend to the hippocampus and the adjoining neocortical association areas. Stage IV is characterised by increased lesion density within the entorhinal region and fusiform gyrus, as well as pathology within the medial temporal gyrus and insular cortex. Lesions widely extend into the occipital lobe and the pristriate region in stage V and in stage VI lesions are visible within the parastriate and striate areas of the occipital neocortex (Braak *et al.*, 2006).

The stereotypical, spaciotemporal pattern of tau pathology progression associated with certain tauopathies, such as AD and AGD, supports the hypothesis that tau spreads trans-synaptically in a manner resemblent of the progression of prion protein pathology (Seeley *et al.*, 2009; Raj *et al*., 2012; Zhou *et al.*, 2012; Clavaguera *et al.*, 2015). Prions are infectious agents, which propagate via protein-protein interactions, templating further aggregation of normally folded proteins (Prusiner, 1982). Specific aggregations of tau, or stains, distinct in different tauopathies, are thought to conformationally template native tau into pathological fibrils. Prions also stably maintain unique conformations that connect the structure of the prion to the pattern of pathology (Sanders *et al.*, 2014), akin to the distinct patterns of neuropathology and rates of progression associated with different conformations of aggregated tau in specific tauopathies.

Clavaguera and colleagues were the first to illustrate the transmission of tau pathology in prion manner. The group injected brain extracts derived from P301S tau-expressing mice into the hippocampi of Tg mice overexpressing WT human tau and noted that this triggered the assembly of WT human tau into filaments. This pathology spread from the site of injection to anatomically connected brain regions (Clavaguera *et al.*, 2009). Similar observations regarding the progression of tau pathology have also been achieved through injection of P301S tau-mice (Iba *et al.*, 2013) or WT mice (Sanders *et al.*, 2014) with synthetic pre-formed fibrils and within Tg mice expressing human P301S *MAPT* restricted to the entorhinal cortex (de Calignon *et al.*, 2012; Liu *et al.*, 2012). Further studies involving the injection of aggregated tau isolated from patients with AD, PiD, AGD, PSP, TD and CBD

(Lasagna-Reeves *et al.*, 2012; Clavaguera *et al.*, 2013; Um *et al.*, 2013; Kaufman *et al.*, 2017; Narasimhan *et al.*, 2017) into WT mice support this work, demonstating that tau aggregation was initiated through the introduction of pathogenic tau at the site of injection and within anatomically connected regions. Interestingly, in the case of mice injected with tau isolated from AGD, PSP and CBD site specific lesions associated with disease were noted (Clavaguera *et al.*, 2013), differences in the potency of particular tau stains to induce aggregation of endogenous tau was noted (Narasimhan *et al.*, 2017) and different neuronal networks were differentially vulnerable to specific stains (Narasimhan *et al.*, 2017), supporting the hypothesis of prion-like tau transmission. Stains from CBD and PSP were found to be capable of causing tau aggregation within glial cells, further demonstrating the differences in the propensity of particular strains of tau to affect certain cell types (Narasimhan *et al.*, 2017). Sanders and colleagues illustrated the faithfully templating of two synthetic pathogenic tau stains by inoculating WT mice with one of each strain. Each stain faithfully produced different patterns of tau pathology progression within mice and later tau was purified from these mice revealing that the strains were unchanged, further supporting the similarities of tau pathology propagation with prion diseases (Sanders *et al.*, 2014). These observations may explain the distinct neuroanatomical patterns of tau aggregation and histopathology of different tauopathies.

Soluble tau has been shown to be released into interstitial space within *in vivo* models, or media within *in vitro* models, and this release is increased with neuronal activity (Pooler *et al.*, 2013; Yamada *et al.*, 2014; Wu *et al.*, 2016). *In vitro* and *in vivo* experimental models have demonstrated that both synthetic, misfolded tau fibrils (Frost *et al.*, 2009; Guo and Lee, 2011) as well as those from AD patients (Santa-Maria *et al.*, 2012) can be taken up by cells, seeding fibrillisation of endogenous tau. Wu and colleages have demonstrated that tau misfolds into low molecular weight oligomers before further aggregation into fibrils and that these oligomers can be internalised after release by neighbouring cells (Wu *et al.*, 2013).

Experimental evidence supports several mechanisms by which tau may be released and reabsorbed by neighbouring neurons. Oligomeric, misfolded 'naked' tau may be released into the interstital space (Chai et al., 2012; Kfoury *et al.*, 2012; Pooler *et al.*, 2013), to be taken up directly through the plasma membrane of the neighbouring cell, by macropinocytosis (Frost *et al.,*, 2009; Santa-Maria *et al.*, 2012; Holmes *et al.*, 2013; Wu *et al.*, 2013), a form of actin-mediated endocytosis whereby the cell membrane internalises a large intracellular vesicle containing extracellular fluid and biomolecules (Lim and Gleeson, 2011).

Alternatively, tau may be released within exosomes, which fuse with the membranes of neighbouring cells (Saman *et al.*, 2012). Tunnelling nanotubes, which are membranous, tunnel-like structures that connect two cells allowing for cytoplasmic continuity, have been demonstrated to be involved in the spreading of prion proteins (Gousset *et al.*, 2009) and have recently been implicated in tau transmission (Abounit *et al.*, 2016; Tardivel *et al.*, 2016). Additional research is needed to provide clarity on the mechanisms of transmission of misfolded 'seed' tau strains between neurons and glia of patients with tauopathy.

1.2.3.2.2 Generation of Amyloid pathology

Aβ is produced through proteolytic processing of its precursor protein, APP. APP is a transmembrane protein and processing occurs through two pathways, the non-amyloidogenic and the amyloidogenic pathway. The amyloidogenic pathway is responsible for the production of Aβ. In this pathway, APP is initially cleaved by β-secretase, generating a C-terminus fragment of 99 aa (C99), which remains in the membrane, as well as a soluble APP fragment (sAPPβ), which is released extracellularly. Subsequent cleavage of C99 by γ-secretase leads to the release of Aβ into the extracellular space and the APP intracellular cytoplasmic domain (AICD) is deposited intracellularly. γ-secretase is a large protein complex consisting of at least four main proteins; presenilin 1 or presenilin 2, PEN2, APH1 and Nicastrin (Vetrivel *et al*., 2006). Different forms of Aβ are produced, most commonly $Aβ_{38}$, $Aβ_{40}$ and $Aβ_{42}$. While the majority of Aβ produced in normal physiology is $Aβ_{40}$ (Seubert *et al*., 1992), $Aβ_{42}$ is the most abundant form found to be aggregated which is thought to be due

to its increased propensity to aggregate thereby resisting degradation (Roher *et al.,* 1993; Snyder *et al.,* 1994).

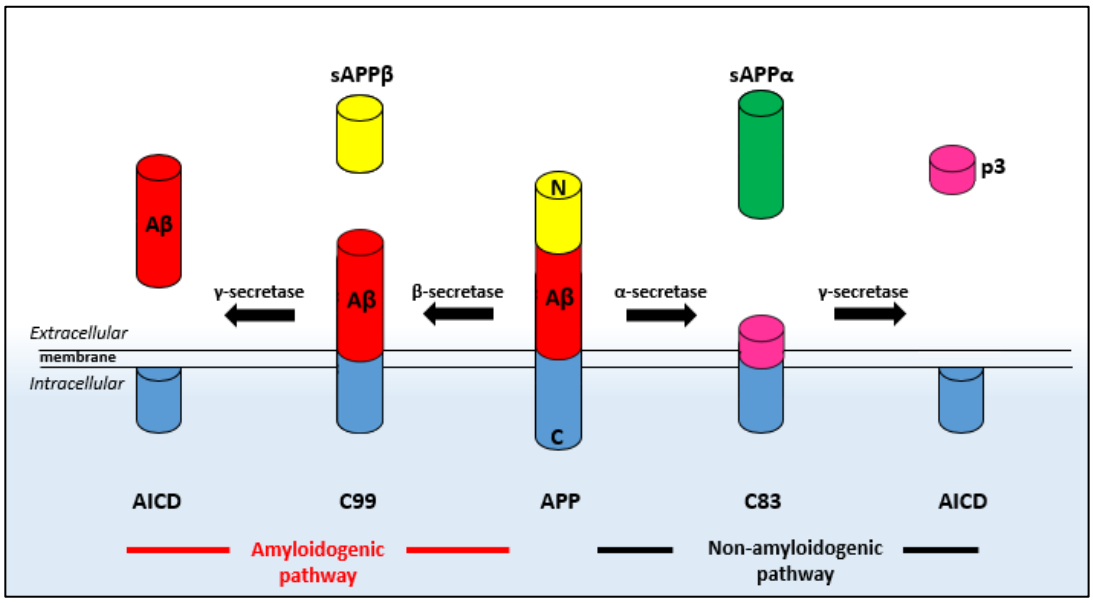

Figure 1.9 Schematic representation of amyloid beta precursor protein cleavage via the amyloidogenic and non-amyloidogenic pathways

Aβ is produced through cleavage of APP via the amyloidogenic pathway, depicted on the left. APP is first cleaved by β-secretase releasing sAPPβ into the extracellular space and leaving a 99 aa C-terminus fragment within the membrane (C99). After further cleavage of C99 by γ-secretase, Aβ is released into the extracellular space and AICD is left within cell. APP is cleaved via the non-amyloidogenic pathway initially by α-secretase to release sAPPα leaving C83 behind embedded in the membrane. Subsequent cleavage of the C-terminus fragment leads by γ-secretase leads to the release of p3 leaving AICD within the cell.

The non-amyloidogenic pathway does not result in the production of Aβ as APP is first cleaved by α-secretase within the Aβ peptide region. This initial cleavage leads to release of sAPPα into the extracellular space, leaving a C-terminus fragment of 83aa (C83) embedded in the membrane. sAPPα is thought to be neuroprotective (Mattson *et al.,* 1993; Furukawa *et al.,* 1996; Ma *et al.,* 2009), while sAPPβ lacks these neuroprotective properties (Furukawa *et al.,* 1996). C83 is then cleaved by γ-secretase to produce the APP intracellular domain (AICD) and a small 3 kDa peptide called p3, both of which are rapidly degraded (Zhang *et al*., 2012). The non-amyloidogenic pathway and the amyloidogenic pathway are depicted in Figure 1.9.

The formation of Aβ into plaques is thought to occur through well-defined sequential aggregation events. Monomers form oligomers, which are most likely the principle toxic

species of Aβ in AD (Klein, 2013; Verma *et al.,* 2015), and then protofibrils of various sizes. Protofilaments then further aggregate to form amyloid fibrils and eventually these fibrils compose plaques (Martins *et al.*, 2008).

1.2.3.2.3 Amyloid toxicity

In healthy people, the normal physiological levels of Aβ are approximately 1.5 nM, however, in AD patients much higher levels of have been reported (Kuo *et al.*, 1996; Höglund *et al.*, 2008). Toxic Aβ aggregates in the form of soluble Aβ oligomers, intraneuronal Aβ and amyloid plaques impair synapses and ultimately cause neurodegeneration and dementia. $A\beta_{42}$ in comparison to $A\beta_{40}$, elicits considerably greater toxicity in cell culture studies (Krishtal *et al.*, 2015), possibly due to its greater propensity for aggregation (Harada and Kuroda, 2011; Vandersteen *et al.*, 2012; Tiiman *et al.*, 2015) and effect on the structure of Aβ aggregations (Pauwels *et al.,* 2012). For example, $A\beta_{42}$, but not $A\beta_{40}$, has been reported to decrease the functionality of forebrain cholinergic neurons differentiated from mouse embryonic stem cells (Wicklund *et al.*, 2010), form ion channels in cell membranes in an immortalised neural cell line (Bode *et al.,* 2017) and attenuate synaptic AMPA receptor function in primary CA1 hippocampal neurons (Parameshwaran *et al.*, 2007). Oligomers are thought to be able to interact with the cell membrane non-specifically through electrostatic force and specifically by associating with ligand and receptors on pre- and post-synaptic terminals (Hertel *et al.,* 1997; Jarosz-Griffiths *et al.,* 2016; Malinow *et al.,* 2011; Spires-Jones and Hyman, 2014). $A\beta_{42}$ oligomers have also been demonstrated to cause membrane disruptions through the creation of pores in the membrane (Sepulveda *et al.*, 2010).

1.2.3.2.4 Phosphorylation of tau in AD

Over 40 of tau's phosphorylation sites are phosphorylated in AD and not in controls (Hanger *et al.*, 2007; Martin *et al.*, 2013). We know that for tau to become highly phosphorylated, to the degree that it is in the AD brain, certain phosphorylation sites must initially be phosphorylated to 'prime' for further deleterious phosphorylation (Hashiguchi *et al.*, 2002). In a comprehensive study aimed at revealing the sequential phosphorylation of specific sites of tau protein during disease progression, the brains of cases with mild cognitive impairment (MCI) and AD of different Braak stages were immunostained using 429 antibodies against phosphorylated tau (ptau) species. The authors found that the tau phosphorylation site Thr231 was initially phosphorylated, followed by Ser202 and Ser205. Phosphorylation at

Ser396 and Ser404 ensued, with Thr214 and Ser212 phosphorylated subsequently (Luna-Muñoz *et al.*, 2007).

Many of the sites phosphorylated in AD, including Thr181, Ser202, Ser205, Thr231, Ser396 and Ser422, have been found to be phosphorylated *in vitro* as a consequence of AβO treatment in human and murine neural cell lines (Busciglio *et al.*, 1995; Billingsley and Kincaid, 1997; Iqbal *et al.*, 1998; Wang *et al.*, 2000; Zheng *et al.*, 2002; Johansson *et al.*, 2006; Ma *et al.*, 2009; Jin *et al.*, 2011).

1.2.3.3 Mutations of familial AD

fAD is caused by highly penetrant mutations within three genes encoding proteins involved in the amyloid processing pathways (Zhu *et al.,* 2015) (Figure 1.12), which result in the abnormal production of Aβ. The disease, also called early onset AD (EOAD) owing to the unusually young age of onset in comparison to sAD, is diagnosed in patients who present before age 65 (Rossor *et al.,* 2010; Zhu *et al.,* 2015), have at least one affected, closely-related family member and have a mutation in one of these genes (Bird, 1993). Over 200 mutations (Cruts *et al.,* 2012), which are inherited in an autosomal dominant manner, have been found in the genes encoding APP (Goate *et al.,* 1991), PSEN1 (Sherrington *et al.,* 1995) and PSEN2 (Levy-Lahad *et al.,* 1995). Pathological mutations within *PSEN1* are the most common, affecting between 30-70 % of patients, while *APP* mutations are responsible for 10-15 % of cases and *PSEN2* mutations account for less than 5 % of cases (Bird, 1993; Janssen *et al.,* , 2003; Tedde *et al.,* 2003; Rogaeva *et al.,* 2001; Lleó *et al.,* 2002). Different clinical presentations are associated with specific mutations (Bird, 1993).

The realisation that EOAD is caused by mutations these genes resulting in an increased ratio of cerebral $A\beta_{42}$ as opposed to $A\beta_{40}$ (Scheuner *et al.*, 1996; Price *et al.*, 1998), or by an increase in the self-aggregation of Aβ if the mutations are within the Aβ of *APP* (Selkoe and Hardy, 2016), was the main contributing factor in the development of the amyloid cascade hypothesis of AD (Hardy and Higgins, 1992). The hypothesis is based on the central role of Aβ in initiating the cascade of pathological molecular events resulting in AD (Hardy and Selkoe, 2002). Additional genetic evidence in support of the hypothesis is that patients with Down Syndrome, which is caused by a trisomy of chromosome 21 resulting in an additional copy of *APP*, leads to the abnormal deposition of Aβ and early-onset dementia (Hardy and Higgins, 1992).

Whilst the Amyloid cascade hypothesis is centred around the role of Aβ in pathogenesis, studies using tau null mice have demonstrated the critical role of tau in AD. Roberson and colleagueds demonstrated the importance of tau in disease pathogenesis through the production of Tg mice each expressing human *APP* (K670M/N671L/V717F) (hAPP) and either two (h*APP*/Tau+/+), one (h*APP*/*Tau*$^{+/-}$) or no (h*APP*/*Tau*$^{-/-}$) endogenous tau alleles (Roberson *et al.*, 2007). While mice with two endogenous tau alleles were found to have learning and memory deficits as well as spacial memory deficits, mice with just one endogenous tau allele demonstrated reduced deficits and tau null mice showed no impairment compared to controls, indicating the importance of tau as a mediator for disease pathogenesis. Santacruz and colleagues have also demonstrated the amelioration of memory function deficits, behavioural impairments and neuronal loss by decreasing levels of tau in mice expressing Tg *MAPT* P301L that could be supressed using doxycycline (Santacruz *et al.*, 2005). In other studies, a 3xTg AD mouse, which expresses APP_{Swe}, tau_{P301L}, and $PS1_{M146V}$ transgenes was found to generate Aβ pathology earlier than tau pathology, suggesting a causal relationship between the pathogenesis of the two proteins (Oddo *et al.,* 2003). This mouse model also suggests tau as a mediator of the disease as severe cognitive deficits are not observed until tau pathology is present (Oddo *et al.*, 2004; Billings *et al.*, 2005). Additionally, the cognitive deficits recognised in the 3xTg AD mouse are only mitigated when immunotherapy is used to reduce both Aβ and tau, and not Aβ alone (Oddo *et al.*, 2006). Further evidence of the mediatory role of tau has been found in patients with AD; the presence of neurofibrillary tangles more strongly correlates to cognitive decline in comparison to Aβ pathology (Bennett *et al.*, 2004).

1.2.3.4 Risk factors of Alzheimer's disease

The primary risk factor of AD is ageing; however, genetic and environmental risks have also been implicated. Environmental risk factors include obesity (Beydoun *et al.*, 2008), smoking (Lee *et al.*, 2010), lack of exercise (Morris *et al.*, 2017), lower levels of education and alcohol abuse (Anstey *et al*., 2009). Previous medical conditions such as hypertension (Qiu *et al.*, 2005), diabetes (Lu *et al.,* 2009) and stroke (Savva *et al.*, 2010) also increase the risk of developing AD.

The major genetic risk determinant for sAD is the presence of Apolipoprotein E (ApoE) polymorphic alleles ε2, ε3 or ε4. ApoE is a major cholesterol carrier, which functions in lipid transportation, glucose metabolism, neuroinflammation, neuronal signalling and

mitochondrial function in the brain. ApoE isoforms differentially regulate Aβ aggregation and clearance in the brain; the ε2 allele decreases risk, ε3 is considered neutral, one copy of ε4 increases risk by two fold and two copies of ε4 increases risk by 12 fold (Liu *et al.,* 2013). Genome wide association studies and next-generation sequencing have revealed over 20 gene loci associated with AD risk, including those within clusterin (apolipoprotein J) (Harold *et al.,* 2009; Lambert *et al.,* 2009), phosphatidylinositol binding clatherin assembly protein (PICALM) (Harold *et al.,* 2009; Lambert *et al.,* 2009), complement receptor 1 (CR1) (Lambert *et al.,* 2009), bridging integrator 1 (BIN1) (Seshadri *et al.,* 2010; Tan *et al.,* 2013) and sortilin-related receptor 1 (SORL1) (Rogaeva *et al.,* 2007).

1.3 Tau kinases and phosphatases

The balanced activities of many tau kinases and phosphatases allow for precise control of the phosphorylation status of tau protein within neurons under physiological conditions. In tauopathy, the equilibrium of kinase and phosphatase activity is thought to become imbalanced, leading to the accumulation of aberrant changes in tau protein over time due to abnormal phosphorylation. Understanding how the levels and activity of tau kinases and phosphatases change in tauopathy may allow us to deduce key initiating pathological events in tauopathy (Boutajangout *et al.*, 2011; Martin *et al.,* 2013).

Many tau kinases that have been implicated in tauopathy including glycogen synthase-3 (GSK3), cyclin-dependent kinase 5 (Cdk5) p21-activated kinase 3 (PAK3), p38, extracellular-signal related kinase (ERK), c-Jun N-terminal kinase (JNK), Akt and microtubule-affinity regulating kinase (MARK) (Lee *et al.,* 2011; Tell and Hilgeroth, 2013). Protein phosphatase 2A (PP2A) is the major tau phosphatase in the brain and is reduced within the AD brain (Gong *et al.,* 1993), however there are other known phosphatases including PP1, PP2B, PP2C and PP5 (Hanger *et al.,* 2009).

Glycogen synthase kinase 3β (GSK3β) and cyclin dependent kinase 5 (Cdk5) are considered to be particularly important kinases in tau pathogenesis and are considered potential therapeutic targets for the treatment of tauopathies (Mazanetz and Fischer 2007; Boutajangout *et al.,* 2011; Pandey and DeGrado, 2016; Tell and Hilgeroth 2013; Eldar-Finkelman and Martinez, 2011; Tolosa *et al.,* 2014; Lovestone *et al.,* 2014; Llorens-Martín *et al.,* 2014). GSK3β has been reported to phosphorylate more aberrantly phosphorylated sites

in disease than any other tau kinase (Martin *et al.,* 2013). There are few studies into the role of p21-activated kinase 3 (PAK3) in tau phosphorylation and tauopathy, however, recent work suggests that the tau kinase may be upregulated in FTDP-17 and involved in AD (Zhao *et al.*, 2006; Ma *et al.*, 2008; Nguyen *et al.*, 2008; Arsenault *et al.*, 2013; Ehrlich *et al.,* 2015; Hallmann, *et al.*, 2015).

1.3.1 GSK3β

Glycogen synthase kinase 3 (GSK3) is a highly conserved, proline directed serine/threonine kinase, which is highly enriched in the brain, especially within the neocortex, hippocampus and cerebellum (Yao *et al.*, 2002). Glycogen synthase kinase 3β (GSK3β) is one of two related paralogs that encode GSK3, the other of which is glycogen synthase kinase 3α (GSK3α), which produce two highly homologous proteins of 52 and 47 kDa, respectively (Doble and Woodgett, 2003). Both proteins are expressed ubiquitously, although GSK3β is expressed at higher levels within the brain, and are distinguished by differences in their C-terminal and N-terminal domains (Woodgett 1990; Leroy *et al.,* 2002).

GSK3β is involved in the regulation of a myriad of cellular processes within the brain and is recognised as a master regulator in many signalling pathways including insulin signalling and glycogen synthesis, neurotransmitter signalling, neurotrophic factor signalling and Wnt signalling (Llorens-Martín *et al.,* 2014; Wu and Pan, 2010; An *et al.,* 2010; Hemmings *et al.,* 1981; Embi *et al.,* 1980). GSK3β also phosphorylates cytoskeletal proteins, including tau, to regulate microtubule architecture and dynamics (Hanger and Noble, 2011; Hashiguchi and Hashiguchi 2013; Goold and Gordon-Weeks 2004; Trivedi *et al.,* 2005; Castaño *et al.,* 2010; Wu *et al.,* 2011). Through its role in regulating microtubule dynamics, it is a crucial kinase in neurodevelopment, synaptic transmission and synaptic plasticity including the regulation of LTP and LTD (Conde and Cáceres, 2009; Geraldo and Gordon-Weeks, 2009; Ciani *et al.,* 2004; Purro *et al.,* 2008; Krylova *et al.,* 2000; Salinas, 2005; Lucas *et al.,* 1998; Hall *et al.,* 2000; Lucas and Salinas, 1997; Eickholt *et al.,* 2002; Shi *et al.,* 2004; Yoshimura *et al.,* 2005; Jiang *et al.,* 2005; Davis *et al.,* 2008; Plattner *et al.,* 2006; Clayton *et al.,* 2010; Huang 1998; Peineau *et al.,* 2007; Stanton, 1996; Hooper *et al.,* 2007; Lisman 2003; Cai *et al.,* 2008; Malenka and Bear, 2004; Giese, 2009; Chen *et al.,* 2006; Zhu *et al.,* 2007; de Barreda *et al.,* 2010).

GSK3β is an unusual kinase as it is constitutively active, however, due to its involvement in a plethora of physiological processes, regulation of GSK3β must be tightly controlled. GSK3β

is primarily regulated by phosphorylation; phosphorylation of Tyr216 can enhance enzyme activity and, conversely, phosphorylation of Ser9 is inhibitory (Wang *et al.,* 1994). Akt, which is also a tau kinase and will be discussed later (Chapter 1.3.4), is a kinase involved in the PI3K/PKB/Akt signal transduction cascade, stimulated by insulin and growth factors, capable of phosphorylating GSK3β at Ser9 (Delcommenne *et al.,* 1998; Cross *et al.,* 1994; Cross *et al.,* 1995). The activity of GSK3β can also be inhibited through N-terminal cleavage by calcium-dependent protease calpain (Goni-Oliver *et al.,* 2007; Jin *et al.,* 2015a).

GSK3β is capable of phosphorylating at least 36 of tau's phosphorylation sites (Martin *et al.,* 2013; Hanger *et al.,* 2007). However, GSK3β preferably phosphorylates tau at Ser199, Ser202, Ser396, Ser400, Ser 412 Ser413 and Thr231 (Billingsley and Kincaid 1997; Imahori and Uchida, 1997) and moderately phosphorylates tau at Ser46, Thr50 and Ser202/Thr205 (Illenberger *et al.,* 1998), while other sites are phosphorylated to a lesser degree. Tau can be phosphorylated by GSK3β in the absence of a previous priming event (Cho and Johnson 2003), however, many of the sites associated with tauopathy, including Ser404 (Plattner *et al.,* 2006; Sengupta *et al.,* 2006) and Thr231 (Li and Paudel, 2006; Li *et al.,* 2006), have been demonstrated to require priming by another kinase before phosphorylation of GSK3β can occur. In order for these two particular sites to become phosphorylated Cdk5 primes tau before phosphorylation by GSK3β (Li and Paudel, 2006; Li *et al.*, 2006; Plattner *et al.*, 2006; Sengupta *et al.*, 2006). Sites found phosphorylated exclusively in AD by GSK3β include Ser422, Ser409, Thr403, Ser368, Ser289, Ser262, Ser238, Ser237, Ser214, Ser210, Ser184, Thr175, Thr153 and Thr69 (Martins *et al.,* 2013). It seems that to affect tau's MT binding ability, tau must be phosphorylated at previously primed sites, indicating the importance of priming by other kinases, before GSK3β activity, to affect microtubules (Cho and Johnson, 2003).

1.3.1.1 GSK3β in tauopathy

Since 1992, we have known that GSK3β is an important kinase associated with the abnormal hyperphosphorylation of tau leading to NFT formation in tauopathies (Hanger *et al.,* 1992; Mandelkow *et al.,* 1992). Increased GSK3β activity has been observed in the brains of AD patients (DaRocha-Souto *et al.,* 2012; Leroy *et al.,* 2007), through the application of AβO to primary neuronal cultures (Alvarez *et al.,* 1999; DaRocha-Souto *et al.,* 2012; Takashima *et al.,* 1996; Takashima *et al.,* 1993) and in murine models of AD (Deng *et al.,* 2014; DaRocha-Souto *et al.,* 2012; Shipton *et al.,* 2011).

Increased activity and overexpression of GSK3β have been shown to result in increased tau phosphorylation at sites consistent with those hyperphosphorylated in AD brains within both *in vitro* (Lovestone *et al.,* 1994; Moreno *et al.,* 1995; Sperbera *et al.,* 1995; Li and Paudel, 2006; Hanger *et al.,* 1992; Mandelkow *et al.,* 1992) and transgenic (Tg) animal models (Lucas 2001; Engel *et al.,* 2008; Spittaels *et al.,* 2000; Brownlees *et al.,* 1997). Inhibition has been shown to decrease tau phosphorylation (Malm *et al.,* 2007; Zhang *et al.,* 2011; Shi *et al.,* 2008; Noble *et al.,* 2005; Crouch *et al.,* 2009; Greco *et al.,* 2009; Kozikowski *et al.,* 2006; Leclerc *et al.,* 2001; Takahashi *et al.,* 1999), as well as total tau protein levels (Martin *et al.,* 2009; Rametti *et al.,* 2008) and *MAPT* mRNA (Rametti *et al.,* 2008). The activity of GSK3β has also been associated with increased aggregation of tau (Lei *et al.,* 2011; Chun and Johnson 2007; Engel *et al.,* 2006; Rankin *et al.,* 2007).

In Tg murine and drosophila models of tauopathy, concurrent overexpression of GSK3β has been demonstrated to accelerate neurodegeneration (Lucas 2001; Engel *et al.,* 2008; Spittaels *et al.,* 2000; Chun and Johnson 2007) and inhibition of GSK3β has been shown to reduce tau-induced neurotoxicity (Nakashima *et al.,* 2005; Pérez *et al.,* 2003; Engel *et al.,* 2006; Alvarez *et al.,* 1999; Qing *et al.,* 2008; Sofola *et al.,* 2010; Hurtado *et al.,* 2012).

GSK3β is thought to be intimately related to the pathogenesis of tauopathy and its dysregulated activity may participate in pathological feed forward loops in tandem with Aβ and tau in AD (Llorens-Martín *et al.*, 2014). One example of a feed-forward loop is the activation of GSK3β through hyperphosphorylated tau, mediated by an increase in oxidative stress, neuroinflammation and apoptotic processes (Saeki *et al.,* 2011; Shim *et al.,* 2007). *In vitro* overexpression of GSK3β has been demonstrated to alter the transport of organelles along microtubules, microtubule structure and microtubule assembly, alongside abnormal phosphorylation of tau (Sang *et al.,* 2001; Lovestone *et al.,* 1996; Cho and Johnson 2003; Utton *et al.,* 1997; Cuchillo-Ibanez *et al.,* 2008; Dill *et al.,* 2008; Tatebayashi *et al.,* 2004; Reddy, 2013). Polymorphisms in GSK3β have been demonstrated to occur at over twice and thrice the frequency in FTD patients and AD patients, respectively, as in aged healthy subjects (Schaffer *et al.,* 2008).

GSK3β also interacts with different components of the amyloid plaque producing system, such as APP and presenilin (Aplin *et al.,* 1996; Terracciano *et al.,* 2010; Kirschenbaum *et al.,* 2001b; Kirschenbaum *et al.,* 2001; Twomey and McCarthy, 2006) influencing the production of greater levels of Aβ (Phiel *et al.,* 2003). The kinase also influences the expression of β-

secretase in triple Tg AD murine models, leading to increased Aβ (Ly *et al.,* 2013). Reciprocally, mounting evidence in Tg murine and *in vitro* models carrying mutations resulting in increased production of Aβ supports the role of Aβ in increasing GSK3β activity (Takashima *et al.,* 1993; Takashima *et al.,* 1996; Hoshi *et al.,* 2003; Takashima *et al.,* 1998; Ma *et al.,* 2006; Terwel *et al.,* 2008), representing a pathogenic feed-forward mechanism. Furthermore, genetic or pharmacological deactivation of GSK3β in these models prevents increased levels and neurotoxicity of Aβ (Takashima *et al.,* 1993; Takashima *et al.,* 1996; Koh *et al.,* 2008; Aplin *et al.,* 1997; Ryder *et al.,* 2003; Serenó *et al.,* 2009; Rockenstein *et al.,* 2007; Decker *et al.,* 2010; Ly *et al.,* 2013).

Investigations using tau null mice show these mice are protected against neurotoxicity mediated by Aβ (Ittner *et al.,* 2010; Roberson *et al.,* 2007) or GSK3β (de Barreda *et al.,* 2010), indicating that tau is required in order for the function of pathogenic feed-forward systems established by the complex interactions between GSK3, Aβ and tau. These studies strongly implicate GSK3β in AD pathogenesis and have led to the development and clinical testing of several GSK3β inhibitors aimed at reducing tau phosphorylation in disease.

1.3.2 CDK5

Cyclin dependant kinase 5 (Cdk5) belongs to the cyclin dependant kinase (CDK) family of proline-directed serine threonine kinase proteins (Kimura *et al.,* 2014). Many of Cdk5's substrates are involved in the regulation of microtubule dynamics (Shah and Lahiri, 2016; Contreras-Vallejos *et al.,* 2014); while tau is the most well-known of these, others include collapsing response mediator protein 2 (Brown *et al.,* 2004), axin (Fang *et al.,* 2011), stathmin (Hayashi *et al.,* 2006), doublecortin (Tanaka *et al.,* 2004), tubulin polymerization-promoting protein (Hlavanda *et al.,* 2007) and microtubule associated protein 1B (Paglini *et al.,* 1998). Therefore, the activity of Cdk5 influences neurotransmission, neurogenesis, trafficking of cellular cargo, synaptic plasticity, LTP and LTD as these rely on rapid changes in microtubule structure (Hawasli *et al.,* 2007; Angelo *et al.,* 2006; Hisanaga and Endo 2010; Nakayama *et al.,* 1999; Kawauchi 2014; Kawauchi *et al.,* 2005).

It is important for Cdk5 activity to be tightly regulated as it functions in so many important pathways. Cdk5 is active when complexed with specific activator proteins, p39 and p35 (Tsai *et al.,* 1994; Tang *et al.,* 1997). The expression of these activator proteins is restricted to the neurons, therefore, the activity of Cdk5 is neuron specific (Li *et al.,* 2016; Guidato *et al.,* 1998;

Miyajima *et al.,* 1995; Paglini and Cáceres, 2001; Humbert *et al.,* 2000) and developmentally regulated such that p39 is expressed in foetal development whereas p35 is expressed in adults (Dhariwala and Rajadhyaksha, 2008). When Cdk5 complexes with its activators p35 or p39, which have membrane-targeting motifs, the complex translocates from the cytoplasm to the membrane allowing for interaction with its substrates (Asada *et al.,* 2008). Both p35 and p39 have short half-lives and are degraded via ubiquitin-mediated proteasome system, allowing for tightly regulated Cdk5 activity (Li *et al.,* 2016).

P35 can be cleaved by calpain to produce p25, which retains the Cdk5 binding domain and therefore also complexes with Cdk5 (Tang *et al.,* 1997; Tsai *et al.,* 1994; Lew *et al.,* 1994; Uchida *et al.,* 1994; Lee *et al.,* 2000; Patrick *et al.,* 1999). P25 makes a stronger association with Cdk5 and Cdk5-p25 has a half-life estimated to be six times greater than Cdk5-p35 (Patrick *et al.,* 1998; Angelo *et al.,* 2006). Cdk5-p25 is also not restricted to the membrane, as Cdk5-p35 is, allowing the complex access to additional substrates within the cytoplasm and nucleus. Due to these properties of Cdk5-p25 it is considered hyperactive (Lee *et al.,* 2000; Noble *et al.,* 2003; Patzke and Tsai 2002). An increase in Cdk5-p25 is associated with neurotoxic events and neurodegenerative disease.

1.3.2.1 Cdk5 in tauopathy

Cdk5 is a particularly interesting kinase as all of the 11 serine/threonine sites of tau protein that it phosphorylates are found to be phosphorylated in AD brains (Chauhan *et al.,* 2005; Hanger *et al.,* 2009; Martin *et al.,* 2013). Major sites phosphorylated by Cdk5 include Ser404, Ser235, Ser202 and Thr205, while minor sites include Ser199, Ser396, Thr153, Thr181, Thr212, Thr217 and Thr231 (Kimura *et al.,* 2014; Lund *et al.,* 2001; Wada *et al.,* 1998; Sakaue *et al.,* 2005; Kimura *et al.,* 2013). Cdk5 is deregulated in AD and has been intimately associated with the pathological processes leading to neurodegeneration (Chang *et al.,* 2010; Kanungo *et al.,* 2009). The mechanism behind this dysregulation is thought to hinge on increased intracellular calcium ($[Ca^{2+}]i$), which occurs in pathological conditions, including in the presence of Aβ1-42 or oxidative stress (Lee *et al.,* 2000; Kusakawa *et al.,* 2000; Patzke and Tsai, 2002), within the brains of patients with tauopathy. Increased $[Ca^{2+}]i$ results in the activation of calpain, which subsequently cleaves p35 to produce p25 and leads to increased levels of hyperactive Cdk5 (Lee *et al.,* 2000). Importantly, Cdk5-p25 has a higher tau kinase activity than Cdk5-p35 (Hashiguchi *et al.,* 2002; Sakaue *et al.,* 2005; Kimura *et al.,* 2014; Patrick *et al.,* 1999; Imahori and Uchida, 1997; Dhavan and Tsai, 2001).

Studies that provide support for the hypothesis that Cdk5 is hyperactivated in tauopathy brain report increased levels of Cdk5-p25, increased p25 and increased p25/p35 ratios within AD brains compared to controls (Tseng *et al.,* 2002; Camins *et al.,* 2006; Lee *et al.,* 1999; Grynspan *et al.,* 1997; Liu *et al.,* 2016; Zhu *et al.,* 2001). Cdk5 protein levels have also been reported to be increased two-fold in AD brains compared to age-matched controls (Lee *et al.,* 1999; Pei *et al.,* 1998; Zhu *et al.,* 2001). Increased Cdk5 levels have also been observed in pre-tangle neurons isolated from AD brains, suggesting that dysregulation of Cdk5 may be an early event in tau pathogenesis (Pei *et al.,* 2001).

A transgenic mouse overexpressing p25 in the forebrain has been used to demonstrate that increased p25 alone is sufficient to elicit neurofibrillary tangles and subsequent neuronal loss in otherwise healthy mice through bolstering Cdk5 activity (Cruz *et al.,* 2003). Furthermore, the pathology observed in these mice occurred in the cortex and hippocampus, which are primary regions of neurodegeneration in AD and FTD (Chapter 1.2) suggesting a link between aberrantly activated Cdk5 and tauopathy. In an additional study, this transgenic mouse was crossed with FTDP-17 model mice carrying the P301L *MAPT* mutation and the authors reported markedly increased tau phosphorylation, tau pathology and neurodegeneration in double transgenic mice compared to mice carrying the tau mutation alone (Noble *et al.,* 2003).

Cdk5-p25 phosphorylates the same sites on tau as Cdk5-p35 (Sakaue *et al.,* 2005), therefore, it is suspected that Cdk5-p25 is capable of causing hyperphosphorylation of tau as it binds to tau with greater affinity (Hashiguchi *et al.,* 2002) and has a longer half-life leading to an imbalance in the rate of phosphorylation verses dephosphorylation of tau. Additionally, as Cdk5-p25 can phosphorylate 'free' tau within the cytoplasm it increases the propensity for tau to become aggregated (Giese, 2014). Indeed, Cdk5 has been found co-localised with tau tangles in AD brains (Augustinack *et al.,* 2002b).

Increased levels of Aβ are also linked to the activity of Cdk5. Cleavage of p35 to produce p25 can be induced by Aβ peptide treatment (Lee *et al.,* 2000; Town *et al.,* 2002; Li *et al.,* 2003). Additionally, Cdk5-p25 is involved in the synthesis of amyloid-β (Cruz *et al.,* 2006) via increasing levels of β-secretase (Wen *et al.*, 2008) and as APP, presenilin-1 (PSEN1) and amyloid-β are among its substrates (Baumann *et al.,* 1993; Morfini *et al.,* 2004; Lau *et al.,* 2002; Iijima *et al.,* 2000). Furthermore, Cdk5 has been suggested to play a role in mediating tau pathology and neurotoxicity caused by the presence of Aβ in AD. Numerous *in vitro*

studies involving the application of Aβ peptides have demonstrated increased phosphorylation of tau at sites phosphorylated by Cdk5, with concurrent increase in Cdk5-p25 (Otth *et al.,* 2002; Zempel *et al.,* 2010; Shukla *et al.,* 2012; Hernandez *et al.,* 2009; Han 2005; Lopes *et al.,* 2007; Zheng *et al.,* 2005; Zheng *et al.,* 2010). Inhibition of Cdk5 activity has been demonstrated to ameliorate Aβ peptide-induced toxicity and tau phosphorylation in AD Tg murine models and within cells treated with Aβ peptides (Hernandez *et al.,* 2009; Alvarez *et al.,* 1999; Chang *et al.,* 2010; Lopes *et al.,* 2010; Lee *et al.,* 2000). P35 overexpression potentiates Aβ-induced apoptosis in neuronal cultures (Utreras *et al.,* 2009).

Furthermore, overexpression of p25 in cortical neurons not only results in aberrant phosphorylation of tau but also cytoskeletal disruption and apoptotic cell death, indicating that aberrant Cdk5 activation is neurotoxic. Cdk5-p25 has been demonstrated to increase oxidative stress and cause mitochondrial dysfunction (Sun *et al.,* 2008). Increased levels of Cdk5 also promotes neuronal apoptosis (Li *et al.,* 2002; Hamdane *et al.,* 2005; Cheung *et al.,* 2008).

CDK5 gene expression has also been proposed to be altered in tauopathy, which could explain changes to its activity, however this is controversial. Liang and colleagues found *CDK5* expression was decreased in the entorhinal cortex, hippocampus, posterior cingulate cortex and medial temporal gyrus in patients with AD in comparison to controls (Liang *et al.,* 2008). Interestingly, the same study also revealed an increase in *p35* expression and it was speculated that this may represent a neuroprotective mechanism to prevent further tau pathology (Liang *et al.,* 2008). Within PC12 cells overexpressing APP, *CDK5* expression was found to be increased (Czapski *et al.,* 2011).

1.3.3 P21 activated kinases

P21 activated kinases (PAKs) are a family of serine/threonine kinases, activated by cell division control protein 42 homolog/Ras-related C3 botulinum toxin substrate 1 (Cdc42/Rac), which are classified into two groups of isoforms based on their structural and biochemical properties. Group 1 consists of PAKs 1-3, while group 2 includes PAKs 4-6 (Arias-Romero and Chernoff 2008; Minden 2012). All PAKs contain an N-terminal Cdc42/Rac-binding domain and a C-terminal protein kinase domain, which are highly conserved (Kelly and Chernoff 2011). PAK3 shares 95 % homology with PAK1 and is believed to have many similar, redundant functions (Kelly and Chernoff, 2011; Huang *et al.,* 2011). Both of these tau kinases

are expressed throughout the brain, particularly in the hippocampus, and are distributed throughout the soma and within the proximal dendrites of differentiated neurons (Allen *et al.,* 1998; Huang *et al.,* 2011). There are two other main differences between these two isoforms of PAK, which may allude to unknown functional discrepancies of the two isoforms; PAK1 is able to enter the nucleus of neurons, whereas PAK3 cannot (Lightcap *et al.,* 2009), and PAK1 requires binding with Rho GTPases to become active, whereas Pak3 does not. The binding of Rho GTPases to PAK3 is, however, essential for the translocation of PAK3 to the dendrites (Bagrodia and Cerione, 1999).

These PAKs are known to play roles in the regulation of synapse formation, dendritic spine morphology, synaptic transmission, neurite outgrowth, growth cone guidance, apoptosis and cell cycle control (Arias-Romero and Chernoff, 2008; Zhao *et al.,* 2006; Hayashi *et al.,* 2004; Nakayama *et al.,* 2000; Obermeier *et al.,* 1998; Zhang *et al.,* 2005; Boda *et al.,* 2004; Malinow and Malenka 2002; Thévenot *et al.,* 2011; Huang *et al.,* 2011; Ding *et al.,* 2015). The involvement of PAK 1 and 3 in these roles may be due to their ability to regulate actin and microtubule dynamics through phosphorylation of cytoskeletal proteins, including tau (Arias-Romero and Chernoff, 2008; Zhao *et al.,* 2006; Szczepanowska, 2009).

Several lines of evidence demonstrate that the loss of PAK 1 and 3 functions is detrimental to neurogenesis and instrumental in neurodegeneration. *PAK3* mutations that result in loss of function cause X-linked non-syndromic mental retardation (Hayashi *et al.,* 2007; Kreis and Barnier, 2009; Peippo *et al.,* 2007). *PAK1/PAK3* null mice have severely impaired memory and learning functions, major loss of brain volume and hyperactive behaviour as well as reduced dendrite lengths and dendrite tip number (Huang *et al.,* 2011). Both Tg null PAK1 and Tg null PAK3 mice exhibit changes in synaptic morphology and LTP, however these mice are otherwise viable, fertile and healthy probably owing to their function redundancy (Hayashi *et al.,* 2004; Meng *et al.,* 2005; Asrar *et al.,* 2009). *PAK3* null rat hippocampal slices and primary neuron cultures also exhibit abnormal spine morphology, abnormal activity-mediated spine dynamics and reduced LTP. Furthermore, in the prefrontal cortex and hippocampus of patients with depression *PAK1* and *PAK3* expression are decreased, which corresponds with decreased volume of these areas in these patients (Fuchsova *et al.,* 2016).

1.3.3.1 PAK3 in tauopathy

In the hippocampi of early-stage AD patients, increased levels of total and active PAK3 levels have been reported (Nguyen *et al.,* 2008), while significantly decreased levels of PAK3 have been measured in late-stage AD within the hippocampus, temporal lobes and neocortex (Ma *et al.,* 2008; Nguyen *et al.,* 2008; Arsenault *et al.,* 2013; Zhao *et al.,* 2006a). This disparity in PAK3 levels has been replicated in young and aged mutant *APP* Tg mice (Nguyen *et al.,* 2008). The variation in PAK3 levels was demonstrated to be a response to increased Aβ; limiting the production of Aβ in these mice, by preventing the cleavage of APP by caspase, prevented the increased activity of PAK3 in young mice and the decreased activity in aged mice (Nguyen *et al.,* 2008). This finding was replicated in rat hippocampal neurons treated with $A\beta_{42}O$, which were found to exhibit abnormal activation of PAK3 and translocation of PAK3 from the cytosol to the membrane (Ma *et al.,* 2008). Additionally, in fAD murine models PAK3 has been shown to mediate the pathways leading to apoptosis and abnormal DNA synthesis through its interaction with the C-terminus of APP (McPhie *et al.,* 2003). An increase in PAK3 has been proposed to signify a protective mechanism in early AD as the loss of PAK3 is detrimental, evidenced by a more pronounced loss of synaptic proteins and a loss in social recognition abilities in Tg AD mice crossed with *PAK3* null mice, compared to those with two copies of *PAK3* (Arsenault *et al.,* 2013). Alternatively, the initial increase in the activation of PAK 1 and 3 in AD may be a consequence of microtubule instability, as this has been demonstrated to result in PAK1 activation in non-neuronal cell cultures (Zang *et al.,* 2001).

Comparatively fewer studies have investigated the involvement of PAK3 on tau pathogenesis in tauopathy. A high-content siRNA screen revealed PAK3 phosphorylates tau at Ser262 (Azorsa *et al.,* 2010), however, further investigation is required to understand which other sites PAK3 may phosphorylate. Arsenault and colleagues demonstrated that loss of PAK function within a Tg AD murine model corresponds with increased aggregation of tau, however, no change in soluble tau levels or tau phosphorylation at Ser202, Ser205, Ser396 or Ser404 was detected (Arsenault *et al.,* 2013). In a recent study, however, PAK3 depletion in 3xTg-AD mice led to increased pSer202/pSer205 and pSer396/pSer404 tau (Bories *et al.,* 2017).

Dysregulation of PAK3 activity may indirectly result in aberrant tau phosphorylation through its effects on other tau kinases. Extracellular signal regulated kinase 3 (Erk3), a tau kinase implicated in neurodegenerative disease (De La Mota-Peynado *et al.,* 2011), is a substrate of

PAK3. Furthermore, PAK3 forms a complex with the tau phosphatase protein phosphatase 2 (PP2A) (Westphal *et al.,* 1999), found to be deactivated and expressed at lower levels in tauopathy (Torrent and Ferrer, 2012). Since PP2A is thought to be regulated through complexing with other proteins, this may suggest that PAK3 regulates PP2A activity (Westphal *et al.,* 1999).

PAK3 is downregulated is hiPSC dopaminergic neurons carrying mutations N279K and V337M *MAPT*, suggesting that tau pathology resulting from these mutations may influence the expression of *PAK3* (Ehrlich *et al.,* 2015). Tau activates AP-1 transcription factor via MAPK (Leugers and Lee, 2010) and AP-1 transcription factor is responsible for *PAK3* transcription (Parker *et al.,* 2013), therefore it is possible that aberrant species of tau affect the expression of *PAK3*. Furthermore, PAK3 phosphorylates tau kinase GSK3β as well as tau (Killick *et al.,* 2014; Zhou *et al.,* 2014; Inestrosa and Varela-Nallar, 2014).

1.4 Models of tauopathy

Investigating the pathogenesis of tauopathy is particularly challenging for several reasons. Firstly, these diseases are unique to the aged, human brain, which is inaccessible before death. Secondly, tauopathies are clinically, pathologically and biochemically heterogeneous, therefore tissue from large cohorts of patients is required to allow us to form firm inferences about disease. Thirdly, the neuropathological phenotypes of various tauopathies are distinguished based on the involvement of different anatomical areas, cell types and presence of distinct isoforms of tau in the pathological deposits, calling for a multidisciplinary approach including biomolecular techniques to understand these diseases.

Recent progression in imaging techniques, specifically in positron emission tomography, computed tomography, magnetic resonance imaging and multiphoton imaging has furthered our ability to study the brains of individuals with AD and FTD. While these techniques provide valuable data in living patients, particularly concerning the anatomical location of neurodegeneration, they are limited in their ability to provide biomolecular information. Yet, whilst post-mortem histology and biomolecular study of brain tissue allows us to see end-stage properties of disease, we are unable to study the mechanisms of initial pathogenesis. This is particularly important as AD and FTD are progressive diseases, whereby pathology is accumulated over a long prodromal period. Furthermore, it is not feasible to obtain brain

tissue from a large cohort of patients with very low post-mortem delay (PMD) and proteins, post-translational modifications and mRNA are particularly vulnerable to degradation (Matsuo *et al.,* 1994). Prolonged agonal conditions including hypoxia, coma and ischaemia, further complicate assessment of tauopathy-related pathology in these samples as these conditions can alter molecular pathways associated with neurodegenerative disease. To address research questions concerning the biomolecular basis of tauopathy, animal models and cell-based models, such as those using neuroblastoma cell lines and primary murine neuron cultures, have traditionally been used, however, the use of these models have limitations.

1.4.1 Animal models

The aetiology of idiopathic tauopathy is unknown. Therefore, animal models have been created using transgenic (Tg) and knockout (KO) technology to modulate the expression of pathogenetically important proteins, with the intention of replicating the neuropathology and clinical phenotypes recognised in humans. The most popular vertebrate animals used in neurodegenerative research are rodents. Invertebrate animals, including the nematode *Caenorhabditis elegans (C. elegans)* and the fruit fly *Drosophila melanogaster (Drosophila)*, are particularly useful for genetic screening. While each of these have provided important insights into tauopathy (Götz and Ittner, 2008), no model is capable of recapitulating all aspects of human tauopathy and each of them have limitations.

1.4.1.1 Murine models

Murine models of AD are a mainstay of research into tauopathy and have facilitated many important discoveries, including those regarding the biology of formation of amyloid plaques and neurofibrillary tangles. Tg technology, coupled with behavioural analysis techniques cultivated over decades, has enabled *in vivo* investigation in animals that have a similar number of genes and considerable chromosomal synteny with humans (Chinwalla *et al.,* 2002). The structure and function of the circuitry of the hippocampus and entorhinal cortex is also largely phylogenetically conserved between humans and mice. There are limitations, however; the use of rodents is costly, time-intensive and restricted by ethical considerations due to animal rights laws. Failed translation of promising therapeutic solutions for tauopathies into humans is also a major problem with the use of mice in pre-clinical research (Franco and Cedazo-Minguez, 2014; Laurijssens *et al.,* 2013; Windisch, 2014).

Murine models of AD successfully recapitulate age-dependent accumulation of amyloid plaques, which are structurally similar to those found in humans, as well as memory impairment and cognitive deficits that occur before the presence of pathology (Meyer-Luehmann *et al.,* 2008; Morrissette *et al.,* 2009). Physiological differences are thought to underlie the lack of faithful recapitulation of important features of human tauopathy, such as widespread neuronal loss (Sullivan and Young-Pearse, 2015). Rodents and humans differ neurally: human cortical and hippocampal neurons have more elaborate dendritic branching and a greater density of dendritic spines compared to mice (Ballesteros-Yáñez *et al.,* 2006; Benavides-Piccione *et al.,* 2006; Elston *et al.,* 2011); humans' astrocytes are larger with more complex processes (Oberheim *et al.,* 2006; Oberheim *et al.,* 2009); only humans have Von Economo (also known as Spindle) neurons, which are important in pathogenesis of FTD (Seeley *et al.,* 2006). Another important consideration is that the splicing of exon 10 *MAPT* varies in mice and humans with 4R tau predominantly expressed in adult mice (McMillan *et al.,* 2008). There are also disparities between humans and rodents in drug metabolism, drug pharmacokinetics and immune system modulation (Geerts, 2009; Seok *et al.,* 2013).

Another concern is the fact that murine Tg models may in fact be representative of the consequences of overexpression of human genes, at levels significantly above those that are physiologically relevant, rather than tauopathy. Indeed, many proteins will become toxic if overexpressed at sufficient levels and human genes within a rodent may cause abnormal interactions. While murine models have been invaluable in deciphering the biology of amyloid and tau aggregation, the subtle molecular changes that result in pathogenesis in human AD and FTD, particularly in sporadic cases, may not be involved in generation of the observed pathology in these animals. Furthermore, many popular murine models overexpress multiple mutated genes and this does not occur in people with familial disease. Additionally, the majority of cases of tauopathy are sporadic whereas these animal models are representative of familial disease. As we do not yet understand whether the molecular mechanisms that instigate sporadic disease are equal to those that cause familial disease these models are thought to be limited in their applicability for the study of tau pathogenesis.

1.4.1.3 *Drosophila* models

The genome and neurobiology of *Drosophila* is well characterised, owing to over 100 years of research using these animals. There are no ethical restrictions according to animal protection laws for the use of *drosophila,* which when coupled with the fact that they are

time and cost effective to maintain makes them a good option for modelling neurodegenerative disease. Drosophila can be genetically modified inexpensively and very quickly, which, along with their short-life span deems them particularly applicable to genetic screens (Prüßing *et al.,* 2013). Tg *drosophila* expressing *MAPT* mutations do exhibit hyperphosphorylation of tau and neurodegeneration, however, they do not demonstrate large aggregations of tau (Wittmann, 2001).

Although drosophila are more complex organisms compared to *C. elegans*, they are far less complex than humans both physiologically and genetically. The anatomy of the drosophila brain, although well characterised, is very different to that of humans. There is also poor conservation of many proteins important in neurodegenerative disease and a lower level of genetic redundancy. They also have a simpler, less adaptive immune system in comparison to humans and drug metabolism is likely to be very different. It is also very difficult to measure complex behaviour and cognitive decline in these animals (Prüßing *et al.,* 2013).

1.4.1.3 *C. elegans* models

C. elegans are time-effective, cheap and unrestricted by ethical considerations due to animal rights laws. There are also advantages in using *C. elegans* for screening, including the ease of genetic modification, the ability to generate Tg strains rapidly and the short lifespan of the worms. Kraemer and colleagues developed a tauopathy model using *C. elegans* expressing wild type or FTDP-17 mutant tau, which recapitulated the aggregation of hyperphosphorylated tau and age-dependent neuronal degeneration, that was later used alongside screening to demonstrate the possible involvement of many unexpected genes in tauopathy (Kraemer *et al.,* 2003; Kraemer *et al.,* 2006). These models are limited, however, by their applicability to human tauopathy due to major differences in physiology compared to humans (Teschendorf and Link, 2009). In total, there are just 302 neurons in the nervous system of these animals and no active immune system. Furthermore, it is very difficult to carry out electrophysiological studies using *C. elegans* neurons as these are small and difficult to patch clamp (Ramot *et al.,* 2008).

1.4.2 Cell-based models of tauopathy

The main advantages of using *in vitro* models are that these can be used alongside biomolecular techniques to study the biomolecular mechanisms involved in tauopathy. Traditional cell-based disease modelling approaches rely on animal primary neurons or

cancerous cell lines. To model tauopathy, these cells are most commonly treated with tau or Aβ peptides and can be genetically modified to knockout or overexpress genes encoding proteins involved in tauopathy. Whilst these models have provided invaluable contributions to neurodegenerative research, they also have limitations.

1.4.2.1 Primary neuronal cultures

Primary cortical and hippocampal neuron cultures, which are lost in tauopathy, represent a valuable research tool for the study of biomolecular mechanisms underlying tauopathy and for electrophysiological studies. These neurons are usually isolated from either wild type (WT) or Tg murine animals, and therefore are limited in their ability to model human tauopathy by their physiological differences. These cells are more likely to recapitulate neurons in the body, however, compared to cancer-derived cell lines (Gordon *et al.,* 2013) (Chapter 1.4.2.2). Perhaps the most technically challenging aspect faced by researchers working with these cultures is the inability of isolated neurons to proliferate; cultures must be skilfully established and maintained to ensure a healthy culture is obtained (Gordon *et al.,* 2013). Additionally, isolation of these cells from animal tissues is difficult as neurons must be separated from other neural cell types and the purity of each culture must be determined. The use of primary neuronal cultures is also subject to ethical considerations under animal rights laws.

1.4.2.2 Cancer-derived cell lines

Models of tauopathy based on cancer-derived cell lines circumvent many of the limitations posed by primary cell culture models. These cells are immortal, banked, easy to culture and are not subject to ethical considerations. These properties, alongside the ability of these lines to be rapidly expanded *in vitro*, facilitates the establishment of unlimited cultures of homogenous cells, limiting variablily in experimental design. It is also easier to genetically modify these cells as they are easy to transfect (Gordon *et al.,* 2013).

Numerous human cancer-derived cell lines exist; NT2 and SH-SY5Y are commonly used and are derived from cell lines established from a neuronally committed teratocarcinoma and a neuroblastoma, respectively. Although these cells are derived from humans, they are considered to be less representative of human neurons compared to cultured primary neurons as these cells lack important neuronal phenotypes such as ion channels, receptors, functional synapses and long neuritic processes usually found in neurons. This has been

somewhat overcome by directed differentiation of these cells to produce 'neuron-like' cells, most commonly using retinoic acid.

Differentiated SH-SY5Y cells express mature neuronal markers, including tau, and have neuritic processes, synaptophysin-positive functional synapses, increased membrane excitability, neurotransmitters (NT) and NT receptors (Adem *et al.,* 1987; Påhlman *et al.,* 1981; Påhlman *et al.,* 1984; Lopes *et al.,* 2010; Tosetti *et al.,* 1998; Encinas *et al.,* 2000; Kovalevich and Langford, 2013). These cultures are nevertheless limited in their ability to recapitulate tau pathogenesis due to the interaction of biomolecular pathways with expressed cancer genes (Zheng *et al.,* 2010). An important consideration in the development of models of tauopathy using these lines is that neuroblastoma cell lines do not express all six isoforms of tau, therefore may not be appropriate for studying molecular aspects of tau pathogenesis (Sullivan and Young-Pearse, 2015).

1.4.3 Modelling tauopathy using induced pluripotent stem cells

1.4.3.1 Stem cells

Stem cells are undifferentiated cells of a multicellular organism capable of replicating indefinitely to give rise to cells of the same type or differentiating to become other types of cells. The zygote, which is the cell created after fertilisation of an egg, is a totipotent stem cell; this cell can give rise to all cells of the body as well as forming the extra-embryonic tissue, including the placental and umbilical tissues (Mitalipov and Wolf, 2009). The blastocyst is generated early in embryogenesis and consists of the embryoblast and the trophoblast, which are the inner and outer layers of this structure, respectively.

The inner cell mass forms within the blastocyst and consists of human embryonic stem cells (hESC) which can form all the cells of the body, except extra-embryonic tissues, and are thus described as pluripotent (Gilbert, 2000). These cells differentiate to form multipotent stem cells restricted to differentiation into one of the three primary germ layers; mesoderm, endoderm and ectoderm. Neural tissue arises from the ectoderm, as does tissue that makes up the skin, teeth, hair and many exocrine glands (Gilbert, 2000). These multipotent cells further differentiate to produce progenitor cells with further restricted potential for differentiation. This includes the neuroblasts, which differentiate to form neurons, and glioblasts, which differentiate to produce glial cells such as oligodendrocytes and astrocytes.

The differentiation of totipotent, pluripotent and multipotent cells is schematically represented in Figure 1.10.

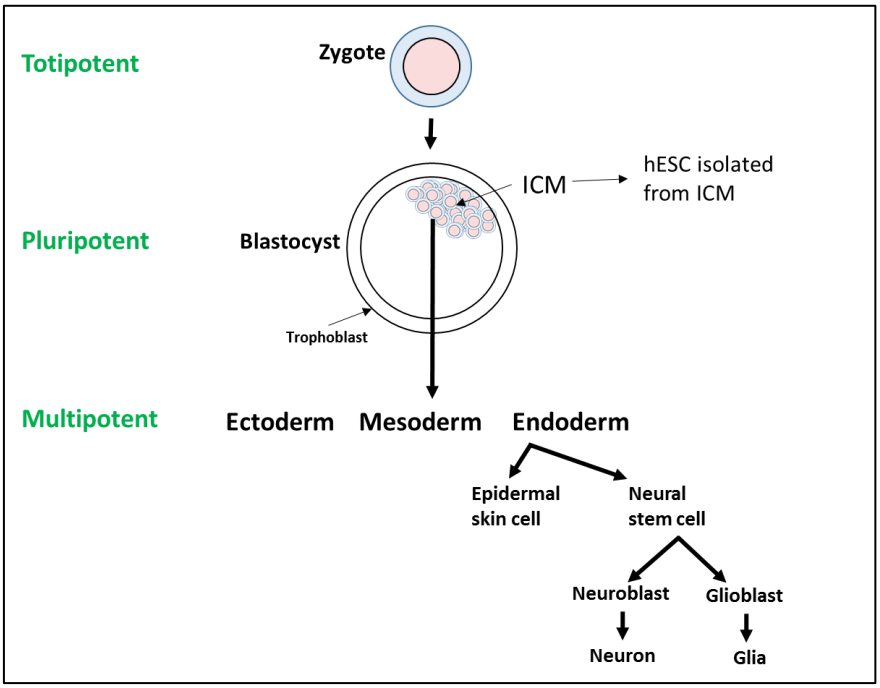

Figure 1.10 Schematic representation of totipotent, pluripotent and multipotent stem cell differentiation during development

Zygotes are totipotent and differentiate to produce embryonic stem cells (hESC), which comprise the inner cell mass (ICM) and are pluripotent. hESC of the inner cell mass differentiate to form germ layer specific multipotent stem cells, which give rise to tissue specific progenitors. Neurons are formed from neural stem cells, which give rise to neuroblasts.

1.4.3.1.1 Embryonic stem cells

The ability of pluripotent stem cells to replicate indefinitely, coupled with the development of protocols allowing directed differentiation to produce cells of the nervous system, provided researchers with a non-exhaustive supply of human neurons with which to study neurodegenerative disease *in vitro*. For use experimentally, hESC are derived from within the inner cell mass of the blastocyst of donated embryos (Vazin and Freed, 2010).

In 2000, the first neurons were derived from hESC (hESC-neurons) (Reubinoff *et al.,* 2000). Subsequently protocols for directing differentiation to produce neurons, which involve manipulation of the *in vitro* environment as well as treatment with growth factors and small

molecules, have been refined allowing for the derivation of specific cells including motor neurons, dopaminergic neurons, GABAergic neurons, oligodendrocytes, astrocytes, glutamatergic neurons and cholinergic neurons (Crompton *et al.,* 2013; Nilbratt *et al.,* 2010; Bissonette *et al.,* 2011; Perrier *et al.,* 2002; Gerrard *et al.,* 2005; Yan *et al.,* 2005; Erceg *et al.,* 2008; Zhang *et al.,* 2006; Wichterle *et al.,* 2002).

One important limitation of disease modelling using hESC is that these cells are derived from embryos, rather than adult humans, therefore we do not know whether this person would have developed sporadic tauopathy since we still do not understand every genetic and epigenetic factor that contributes to increased risk. Additionally, donated embryos are rare and precious resources, limiting the creation of a large bank of cell lines thought to be necessary to account for the heterogeneity in tauopathy. Furthermore, research using hESC is fraught with political and ethical concerns as collection of the inner cell mass obligates the destruction of the embryo.

1.4.3.1.2 Induced pluripotent stem cells

In 2006, Nobel Laurette Yamanaka demonstrated that terminally differentiated, somatic cells can be reprogrammed to produce pluripotent stem cells (Takahashi and Yamanaka, 2006). These cells, called induced pluripotent stem cells (iPSC) are identical to embryonic stem cells in their pluripotent potential and epigenetic profile (Mallon *et al.,* 2014). The first human induced pluripotent stem cells (hiPSC) were generated in 2007 (Yamanaka *et al.,* 2007) using human immunodeficiency virus (HIV) derived lentiviral vectors to transfer genes encoding transcription factors that drive pluripotency into fibroblasts. These factors, commonly referred to as 'Yamanaka's factors', include Octamer binding transcription factor 4 (OCT4), Kruppel-like factor 4 (Klf4), Sex determining region Y box 2 (SOX2) and myelocytomatosis viral oncogene homologue (c-myc). Further developments in reprogramming led to the use of various other combinations of factors to achieve reprogramming, allowing for the elimination of c-myc, which is a known oncogene (Yu *et al.,* 2007).

The hiPSC lines, V337M-C and V337M-E, generated for this project (Chapters 3 and 4) were created through reprogramming of fibroblasts using lentiviral vectors. Whilst the use of lentiviral vectors delivers good reprogramming efficiency, the main disadvantage of using this method is that the reprogramming vectors are integrated into the infected somatic cell's genome leaving a 'footprint'. The presence of this 'footprint' may affect experimental results

through transient expression of transgenes (Rao and Malik, 2012). Furthermore, the use of retroviral and lentiviral vectors can introduce the risk of deleterious DNA recombination associated with viral integration into the nucleus (Vannucci *et al.*, 2013).

The use of non-integrating viral delivery systems such as sendai viral vectors (Fusaki *et al.*, 2009), mRNA reprogramming (Warren *et al.*, 2010), PiggyBac transposition (Wang *et al.*, 2008; Woltjen *et al.*, 2009; Yusa *et al.*, 2009), small molecule reprogramming (Jung *et al.,* 2014) and episomal factor delivery methods such as lipofection (Okita *et al.*, 2008) and nucleofection (Yu *et al.*, 2011; Okita *et al.,* 2010) have vanquished the risk of deleterious DNA recombination, improving the reliability of iPSC models (Schlaeger *et al.*, 2015).

The field is rapidly progressing and has overcome many of the initial limitations recognised. Reprogramming efficiency has been vastly improved using small-molecule compounds such as valproic acid (Huangfu et. al., 2008), genetic alterations such as knockdown of the p53 gene (Hong et. al., 2009) and optimisation of the *in vitro* environment, for example through culturing in normoxic conditions (Prado-Lopez *et al.,* 2010). Techniques enabling reprogramming of many other non-invasively obtained cells, including blood cells (Okabe *et al.,* 2009; Loh *et al.,* 2009) has been developed.

1.4.3.1.3 Differentiation of pluripotent stem cells to produce neurons

The generation of specific subtypes of human pluripotent stem cell (hPSC)-derived neurons intended to model tauopathy often begins with generation of forebrain neurons. Since the 'default' fate for neural differentiation of hiPSC is to become cortical neurons, further differentiation into specific neuronal subtypes is achieved through dual SMAD inhibition within a monolayer culture (Chambers *et al.,* 2009; Shi *et al.,* 2012), embryoid body (EB) culture (Crompton *et al.,* 2013; Eiraku *et al.,* 2008) or in tandem with the development of three-dimensional organoid culture system (Lancaster *et al.,* 2012). Small molecules, growth factors and the forced expression of transcription factors (Bissonnette *et al.,* 2011; Duan *et al.,* 2014) can be used to modulate developmental patterning pathways to produce specific cell types; for example, glutamatergic neurons (Boisvert *et al.,* 2013; Shi *et al.,* 2012; Vazin *et al.,* 2014) and bfCNs (Crompton *et al.,* 2013; Bissonnette *et al.,* 2011). hiPSC-derived glutamatergic neurons have been demonstrated to be more vulnerable to Aβ-induced pathogenesis compared to hiPSC-GABAergic neurons (Vazin *et al.,* 2014), supporting the

utility of hiPSC-neurons for research into the selective vulnerability of neuronal subtypes in tauopathy.

1.4.3.1.4 The role of dual Smad inhibition in neural induction

Smads are proteins that mediate intracellular signalling triggered by transforming growth factor β (TGFβ) ligands, which include TGFβs and bone morphogenic proteins (BMPs) (Ueberham and Arendt, 2013). The TGFβ superfamily signalling pathways have diverse and complex roles in the regulation of cell growth, differentiation and development of neural cells (Yun *et al.,* 2008). TGFβ signals are transmitted through transmembrane serine/threonine (Ser/Thr) kinase receptors, which when activated phosphorylate TβRI-associated Smads. These activated Smads form a complex with the co-mediator Smad (Smad 4), which translocates to the nucleus where it activates or suppresses target gene expression (Massagué *et al.,* 2000).

There are Smads associated with two main pathways; Smad1/5/9 are part of the BMP pathway and Smad2/3 are part the TGFβ/activin pathway. Inhibition of the BMP pathways, associated with mesoderm lineage development, have previously been shown to be involved in neural induction (Sasai *et al.,* 1994; Hemmati-Brivanlou *et al.,* 1994; Smith *et al.,* 1992) and inhibition of either the BMP or TGFβ pathways aids neural induction of hESCs (Smith *et al.,* 2008; Elkabetz *et al.,* 2008; Lee *et al.,* 2007). Inhibition of either of these pathways alone is not sufficient to induce neural induction, however, dual pathway inhibition has been shown to enable neural induction through directed differentiation towards the neuroectoderm in human embryonic stem cell cultures (Chambers *et al.,* 2009).

1.4.3.1.5 Modelling tauopathy using induced pluripotent stem cells

This advent, when paired with protocols facilitating the derivation of hESC-neurons, invited the generation of neurons differentiated from hiPSC that had been reprogrammed from disease patient's somatic cells (hiPSC-neurons), creating a new opportunity for modelling disease *in vitro*. Patient-derived hiPSC-neurons were first cultured by Dimos and colleagues to model ALS (Dimos et. al., 2008) and later Ebert and colleagues demonstrated that iPSC-motor neurons from spinal muscular atrophy (SMA) patients recapitulated deficits of the disease (Ebert et. al., 2009). The first iPSC model of AD was reported in 2011 (Yagi *et al.,* 2011) and significant progression has been made since then.

There are still limitations in the use of hiPSC as models of tauopathy. Recent studies have revealed heterogeneity between cell lines generated from patients with fAD (Kondo *et al.,* 2013), sAD (Kondo *et al.,* 2013; Israel *et al.,* 2012) and FTDP-17 carrying the same *MAPT* mutation (Hallmann *et al.,* 2017; Wren *et al.,* 2015), which reflects the heterogeneity noted in patients. This finding calls for studies using hiPSC-neurons derived from larger cohorts of patients and although biorepositories, such as The Human Pluripotent Stem Cell (hPSC) Repository project (California, USA) have been established, it may take some time before large numbers of cell lines are available. Further to this, the generation of neurons from large numbers of cell lines is labour intensive and expensive. Genetic background variability between lines may also hinder reliable results (Kim *et al.,* 2010), although the development of isogenic lines circumvents this problem (Fong *et al.,* 2013). As the field advances, developments in reprogramming and differentiation efficiency are hoped to overcome counter these factors (Ebrahimi, 2015).

1.4.3.1.6 Modelling frontotemporal dementia using induced pluripotent stem cells

hiPSC-neuron models have been derived through reprogramming somatic cells from patients with various *MAPT* mutations, including V337M (Ehrlich *et al.,* 2015), N279K (Wren *et al.,* 2015; Ehrlich *et al.,* 2015; Iovino *et al.,* 2015), P301L (Iovino *et al.,* 2015), A152T (Silva *et al.,* 2016; Fong *et al.,* 2013), R406W (Imamura *et al.,* 2016), IVS 10+16 (Esteras *et al.,* 2017) and IVS 10+14 *MAPT* (Imamura *et al.,* 2016). These hiPSC lines have been used to derive mixed populations of neurons (Ehrlich *et al.,* 2015; Fong *et al.,* 2013), as well as specific neuronal subtypes including cortical neurons (Esteras *et al.,* 2017; Imamura *et al.,* 2016; Wren *et al.,* 2015; Silva *et al.,* 2016; Iovino *et al.,* 2015; Usenovic *et al.,* 2015), dopaminergic neurons (Ehrlich *et al.,* 2015) and astrocytes (Hallmann *et al.,* 2017). hiPSC-neuron models have also been derived through overexpression of P301L *MAPT* within control hiPSC lines (Verheyen *et al.,* 2015). One model of sFTD-tau has been developed through seeding of control hiPSC-neurons with oligomeric tau species to initiate tau pathology, rather than through deriving hiPSC from patients carrying mutations (Usenovic *et al.,* 2015). A summary of the key findings of these studies is given in Table 1.1.

Table 1.1 hiPSC models of FTDP-17

Mutation	Neuronal Subtype	Findings	Reference
A152T *MAPT*	Mixed	Gene-dose-dependent effect of the A152T *MAPT* mutation on neurodegeneration and increased tau phosphorylation at Ser202/Thr205. Dopaminergic neurons are more susceptible to neurodegeneration that other neuronal subtypes.	(Fong *et al.,* 2013)
N279K and P301L *MAPT*	Cortical glutamatergic	N279K and P301L increase levels of tau during maturation and cause mitochondrial transport dysfunction. N279K express tau prematurely leading to an increased 4R:3R tau ratio, have increased pThr212/pSer214 tau and tau aggregates. P301L neurons have contorted processes with varicosities containing tau and α-synuclein.	(Iovino *et al.,* 2015)
P301L	Cortical glutamatergic	No tau pathology could be detected in mutant neurons, except on priming with pre-formed aggregates, which then revealed substantially increased pSer202/Thr205 tau, total tau levels and tau aggregation compared to controls.	(Verheyen *et al.,* 2015)
N279K	Cortical glutamatergic	N279K increased tau protein, 4R:3R tau ratio and cellular stress. Increased levels of vesicle components.	(Wren *et al.,* 2015)
No mutation	Cortical	Treatment of control neurons with oligomeric tau species increased pThr231 and pSer396/404 tau, numbers of MC1 positive neurons and tau aggregation.	(Usenovic *et al.,* 2015)
N279K V337M	Mixed 50% dopaminergic 45% GABAergic 2-4% Cholinergic	N279K and V337M *MAPT* hiPSC-neurons exhibit increased tau fragmentation, increased pSer202/Thr205 tau, activation of the unfolded protein response and disease associated changes to the gene expression profile. N279K neurons were found to have increased tau aggregation, an increased 4R:3R tau ratio, decreased neurite extension and increased oxidative stress response to inhibition of mitochondrial respiration.	(Ehrlich *et al.,* 2015)
IVS 10+16 *MAPT*	Cortical glutamatergic	An increased ratio of 4R:3R tau ratio in IVS 10+16 *MAPT* compared to controls was found. Additionally, full splicing of tau was recognised after prolonged culture of neurons for 1 year.	(Sposito *et al.,* 2015)
A152T *MAPT*	Mixed	Increased levels of tau and ptau at Ser202/Thr205, Ser396/404 and Thr231/235 were found in A152T *MAPT* hiPSC-neurons. No aggregates were detected and *MAPT* expression was found to be unchanged. A152T *MAPT* hiPSC-neurons were more vulnerability to cellular stress.	(Silva *et al.,* 2016)
R406W IVS 10+14 C>T	Cortical neurons	R406W and IVS 10+14 *MAPT* hiPSC-neurons have accumulations of misfolded tau accumulations and increased extracellular release of misfolded tau. Cultures of hiPSC-neurons carrying these mutations also show increased neurodegeneration. Upon electrical stimulation,	(Imamura *et al.,* 2016)

		evoked calcium ion (Ca^{2+}) transients are dysregulated. IVS 10+14 *MAPT* neurons also exhibited increased 4R tau.	
N279K	Astrocytes	Astrocytes from one mutant line were larger and contained tau, as well as being more vulnerable to oxidative stress and having increased levels of GFAP indicative of astrocytic activation. 4R1N tau expressed early in mutant neurons and astrocytes compared to controls.	(Hallmann *et al.,* 2017)
IVS 10+16 *MAPT*	Cortical glutamatergic	Increased vulnerability of control neurons cultured with FTD-astrocytes to cellular stress. Altered mitochondrial function. Overproduction in ROS in mitochondria, which leads to oxidative stress. Increased cell death in neurons dependent on increased ROS in mitochondria.	(Esteras *et al.,* 2017)

Table 1.1 hiPSC models of FTDP-17

hiPSC models of FTDP-17 derived from patients, apart from for Verheyen et al., 2015 in which control neurons were genetically altered to express 2R4N P301L and for Usenovic et al., 2015, in which control neurons were pre-seeded with pre-aggregated tau to induce tau pathology. 'Mixed' refers to a mixed population of neuronal subtypes. In Esteras et al., 2017 control hiPSC neurons were cultured with hiPSC-astrocytes carrying the IVS 10+16 MAPT mutation.

These studies have demonstrated that hiPSC-neuron FTDP-17 models are capable of recapitulating the neuronal pathology found in disease patient brains. Neuronal pathology, including decreased neurite extension in hiPSC-neurons carrying N279K *MAPT* (Iovino *et al.,* 2015) and contorted processes with varicosities containing tau and α-Synuclein in P301L hiPSC-neurons (Iovino *et al.,* 2015), has been reported.

Some of these studies have investigated the molecular mechanisms underlying the observed neurodegeneration, tauopathy and response to cellular stress. The results demonstrate that these models are useful for probing tau pathogenesis. For example, N279K and P301L *MAPT* hiPSC-neurons exhibit mitochondrial transport dysfunction (Iovino *et al.,* 2015), which may result from these mutations and underlie neurodegeneration. Increased levels of vesicle components have been noted in A152T *MAPT* neurons (Wren *et al.,* 2015). N279K and V337M *MAPT* hiPSC-neurons exhibit increased activation of the unfolded protein response (Ehrlich *et al.,* 2015), responsible for protein clearance, which may show a compensatory increased clearance mechanisms to cope with excess tau within these cells. Healthy hiPSC-neurons co-cultured with hiPSC-astrocytes from a patient carrying 10+16 *MAPT* showed reduced mitochondrial function, demonstrating that astrocytes carrying the mutation can cause neuronal dysfunction in nearby neurons within the brain (Esteras *et al.,* 2017). This

study demonstrated that these *in vitro* hiPSC models can be used to probe relationships between different cell types in isolation during the development of disease. The models have also demonstrated changes in the levels of tau protein, tau phosphorylation and tau aggregation as a result of different mutations within *MAPT.*

These studies have also provided insights into the effects of *MAPT* mutations during neuronal maturation. Tau mutations have been found to have no effect on reprogramming efficiency (Fong *et al.,* 2013; Imamura *et al.,* 2016) or the propensity of hiPSC to differentiate into neuronal subtypes (Hallman *et al.,* 2015; Ehrlich *et al.,* 2015; Imamura *et al.,* 2016; Fong *et al.,* 2013). However, N279K hiPSC-neurons express 4R1N much earlier than control neurons (Iovino *et al.,* 2015).

These studies have also been used to provide proof-of-principle that these models can be used in drug discovery. For example, hiPSC-dopaminergic neurons from patients with V337M *MAPT* and N279K *MAPT* were found to have a pronounced oxidative stress response compared to controls, which could be rescued through GSK3β inhibition (Ehrlich *et al.,* 2015). Imamura and colleagues also demonstrated that treatment of hiPSC-neurons derived from patients carrying the 10+14 *MAPT* mutation with glutamate receptor blockers or genetic correction of using CRISPR/Cas9 gene editing ameliorated evidence of pathology in these cells (Imamura *et al.,* 2016). Similarly, Hallmann and colleagues have demonstrated the genetic correction of N279K *MAPT* neurons with CRIPSR/Cas9 (Hallmann *et al.,* 2017).

1.4.3.1.7 Modelling Alzheimer's disease using induced pluripotent stem cells

To date, the majority of AD models established using hiPSC-derived neurons have been developed through reprogramming somatic cells from fAD patients carrying mutations in genes involved in the production of Aβ i.e. *PSEN1, PSEN2* and *APP* (Chapter 1.2.3.3). Models of sAD have also been developed that rely on both the differentiation of hiPSC-neurons from sAD patients (Kondo *et al.,* 2013; Israel *et al.,* 2012; Duan *et al.,* 2014; Young *et al.,* 2015; Hossini *et al.,* 2015) and the treatment of control hiPSC-neurons with Aβ peptides (Xu *et al.,* 2013; Zhang *et al.,* 2014; Vazin *et al.,* 2014; Nieweg *et al.,* 2015). hiPSCs reprogrammed from Down's syndrome (DS) patients have been developed to study AD (Shi *et al.,* 2012; Chang *et al.,* 2015), as DS is caused by a triplication of chromosome 21, which contains the genes for *APP* and some tau kinases, such as dual specificity tyrosine-phosphorylation-regulated *kinase* 1A (DYRK1A) (Kimura *et al.,* 2007; Jin, Yin, Gu, *et al.,* 2015), and patients

with DS also develop dementia, akin to AD. Models of AD using hiPSC-neurons have also been developed through culture of hiPSC-neurons in three dimensional (3D) scaffolds (Zhang *et al.,* 2014; Choi *et al.,* 2015) and the development of hiPSC-derived cerebral organoids (Raja *et al.,* 2016). These studies are summarised in Table 1.2.

The most common experimental output reported in these studies is a change in the levels of either amyloid (Shi *et al.,* 2012; Israel *et al.,* 2012; Yagi *et al.,* 2011; Kondo *et al.,* 2013), or in the ratio of Aβ 1-42 to Aβ 1-40 ($A\beta_{42}/A\beta_{40}$) (Sproul *et al.,* 2014; Duan *et al.,* 2014; Muratore *et al.,* 2014; Koch *et al.,* 2012; Moore *et al.,* 2015), both of which are associated with AD. Studies have revealed a developmental increase in the production of Aβ (Muratore *et al.,* 2014; Koch *et al.,* 2012) and provided proof-of-principle that both sAD and fAD hiPSC models are capable of recapitulating this aspect of AD pathology. So far, only three models have exhibited Aβ aggregates (Chang *et al.,* 2015; Choi *et al.,* 2014; Raja *et al.,* 2016).

Increased levels of tau phosphorylation (Yagi *et al.,* 2011; Hossini *et al.,* 2015; Choi *et al.,* 2014; Shi *et al.,* 2012; Chang *et al.,* 2015; Muratore *et al.,* 2014; Moore *et al.,* 2015; Raja *et al.,* 2016; Israel *et al.,* 2012), altered tau kinase activity (Israel *et al.,* 2012; Muratore *et al.,* 2014), altered tau kinase gene expression (Hossini *et al.,* 2015) and abnormal translocation of PAK3 (Zhang *et al.,* 2014) have been described in hiPSC-neurons modelling AD. Other studies have reported altered glutamate metabolism (Hossini *et al.,* 2015), increased sensitivity to Ca^{2+} mediated cell death, increased cell stress after glutamate-induced excitation (Duan *et al.,* 2014), production of reactive oxygen species (ROS) (Hossini *et al.,* 2015; Kondo *et al.,* 2013) and the increased expression of genes involved in oxidative stress and in the proteasome (Kondo *et al.,* 2012; Hossini *et al.,* 2015). These studies indicate that hiPSC-neurons can be used to investigate the molecular pathways involved in AD.

Some of these studies have provided proof-of-principle that hiPSC-neurons can be used to screen drugs capable of influencing tau phosphorylation. Israel and colleagues demonstrated that treatment of fAD and sAD hiPSC-neurons with β-secretase inhibitors, but not γ-secretase inhibitors, significantly reduced levels of pThr231 tau and active GSK3β (Israel *et al.,* 2012). Furthermore, both β- and γ-secretase inhibitors decreased the number of *APP(*K670N/M671L,V717L) or ΔE9 *PSEN1* hiPSC-neurons, that were positively stained for ptau (Choi *et al.,* 2014). In a recent study, hiPSC-derived neurons from six controls donors and seven sAD patients were used to investigate effects the expression of a protective or AD risk variant of *SORL1*, a gene encoding an endocytic trafficking factor, on Aβ burden. The

group demonstrated that only those with the protective variant responded to brain derived neurotrophic factor (BDNF) treatment (Young *et al.,* 2015), demonstrating the usefulness of these models to investigate the impact of gene variants on specific pathways.

Table 1.2 hiPSC-neuron models of AD

sAD/fAD	Genetics	Neuron subtype	Findings	Reference
fAD	N141I *PSEN1* and *PSEN2*	Cholinergic	Increased production of $A\beta_{42}$ ameliorated by γ-secretase inhibitors.	(Yagi *et al.,* 2011)
DS	Down's Syndrome Trisomy 21	Cortical	Increased Aβ, increased secreted tau, pSer396/pSer404 tau and pSer202/205 tau.	(Shi *et al.,* 2012)
fAD	L166P and D385N *PSEN1*	Mixed*	Decreased $A\beta_{40}$.	(Koch *et al.,* 2012)
fAD and sAD	APP duplication	Mixed*	Increased $A\beta_{40}$, increased ptau (Thr231), increased levels of active GSK3β, early large endosomes.	(Israel *et al.,* 2012)
fAD and sAD	sAD, E693 and V717L *APP* hiPSC	Mixed*	Accumulation of intracellular AβO (E693 APP), increased ROS production, increased oxidative stress-related gene expression.	(Kondo *et al.,* 2013)
sAD	N/A	Forebrain	Aβ-induced cell cycle re-entry, neuronal apoptosis and increased Cdk2.	(Xu *et al.,* 2013)
sAD	N/A	GABAergic and glutamatergic	Increased apoptosis of control hESC- and hiPSC-neurons with increasing concentrations of Aβ.	(Vazin *et al.,* 2014)
fAD and sAD	*APOε3/ε4* genotype	BfCNs	Increased $A\beta_{42}/A\beta_{40}$ ratio increased cell stress after glutamate-induced excitation.	(Duan *et al.,* 2014)
fAD	V717L *APP*	Cholinergic	Increased $A\beta_{42}/A\beta_{40}$ ratio, two-fold increase in tau, increased pSer262 tau and increased active GSK3β.	(Muratore *et al.,* 2014)
fAD	*PSEN1* A246E; *PSEN1* M146L	Mixed*	Increased $A\beta_{42}/A\beta_{40}$ ratio.	(Sproul *et al.,* 2014)
sAD	N/A	Mixed* (3D)	Abnormal translocation of PAK3 and decreased pre-synaptic protein (drebrin) within neurons in response to $A\beta_{42}O$.	(Zhang *et al.,* 2014)
fAD	K670N/M671L and V717L *APP* or ΔE9 *PSEN1*	Mixed* (3D)	Aβ and tau aggregations within neurons, beaded neurites, pSer396/404 and pSer202/Thr205 tau reduced upon treatment with γ- and β-secretase inhibitors.	(Choi *et al.,* 2014)
sAD	N/A	GABAergic and glutamatergic	Control hiPSC-neurons were treated with Aβ for 8 days, increased pSer202 and pThr231, impaired synaptic transmission and increased stress response.	(Nieweg *et al.,* 2015)

sAD	*SORL1* protective and risk alleles	Mixed*	SORL1 variant dependant decrease of Aβ after treatment with brain derived neurotrophic factor (BDNF).	(Young *et al.,* 2015)
sAD	N/A	Mixed*	Downregulation of GSK3 and CDK5, altered gene expression of genes involved in the ubiquitin proteasome system, treatment with *γ*-secretase inhibitors reduced tau and pThr231.	(Hossini *et al.,* 2015)
DS	Down's Syndrome Trisomy 21	Mixed*	Aβ, aggregates, increased secreted tau, redistribution of pSer396/pSer404 and pSer202/Thr205 tau.	(Chang *et al.,* 2015)
fAD	V717I *APP* APP duplication ΔI4 *PSEN1* Y115C *PSEN1* Down's Syndrome Trisomy 21	Cortical glutamatergic neurons	Increased ratio of $A\beta_{42}$ to $A\beta_{40}$. Increased total tau, pSer396 tau, pSer404 tau and pSer202/Thr205 tau in hiPSC carrying *APP* mutants but no increase in those carrying *PSEN1* mutations.	(Moore *et al.,* 2015)
fAD	APP duplication M136I PSEN1 A264E PSEN1	Mixed* (3D)	Increased phosphorylation of tau at Ser396 or Thr181 at 90 days. Increased levels and aggregation of Aβ. Endosome abnormalities.	(Raja *et al.,* 2016)

Table 1.2 hiPSC-neuron models of AD

Models are derived from patients with fAD and sAD patients apart from in the six highlighted publications. Models of sAD developed through treatment of control hiPSC-neurons with $A\beta_{42}O$ are highlighted in green. A fAD model developed through treatment of Tg modified control neurons with $A\beta_{42}O$ is highlighted in blue. Tg fAD hiPSC-neurons are highlighted in red.
**Mixed includes cell cultures derived from hiPSC consisting of many types of neuronal subtypes, including dopaminergic, GABAergic, glutamatergic and cholinergic neurons.*

Chapter 2

General Methods

2.1 Cell culture

All cell lines were cultured within a humidified incubator at 37 ^{o}C and 5 % CO_2. All cell work was carried out in a class II cell culture hood.

2.1.1 Mouse embryonic fibroblast culture

2.1.1.1 Mouse embryonic fibroblast (MEF) media

Mouse embryonic fibroblasts (MEFs) and inactivated MEFs (iMEFs) were grown in media comprised of the following:

Table 2.1 Mouse embryonic fibroblast (MEF) media

Volume	Reagent	Product ID
87 %	Dulbecco's Minimum Essential Medium (DMEM)	Sigma, D6546
10 %	Foetal Bovine Serum (FBS) (Heat Inactivated)	Invitrogen, 10500
1 %	GlutaMAX™ (100x)	Invitrogen, 35050
1 %	Non-Essential Amino Acids (NEAA) (100x)	Invitrogen, 11140
1 %	Penicillin-Streptomycin solution stabilised (Pen-Strep)	Sigma, P4458

2.1.1.2 Derivation of mouse embryonic fibroblasts (MEF)

Animals were maintained and treated under the Home Office's animals (Scientific Procedures) act 1986 and in agreement with the University of Bristol Animal Welfare and Ethical Review Body guidelines. Pups were removed from a pregnant mouse at gestational day 12-13 (E12-13). After removal of the yolk sack using a sterile scalpel and forceps, the

head was removed to kill each foetus. This is necessary in accordance with Home Office Schedule 1 requirement for all foetuses over gestational day 10. After removal of the internal organs of each foetus the remaining tissue was pooled into a 50 ml falcon tube with 20 ml TrypLE™ Express (1X) [Life Technologies, 12604-021]. The tissue incubated for 10 minutes in the TrypLE™ Express after homogenisation of the tissue through repeated trituration with a P1000 pipette tip and a glass aspirating needle. 20 ml of FBS was added to the foetal material after completion of the incubation period to quench the TrypLE. The cell suspension was centrifuged (300 g; 5 minutes) before the cells were resuspended in MEF media (Chapter 2.1.1.1). The cells were split between 175 cm^3 flasks; the same number of flasks as foetuses were used. The cells were allowed to proliferate, cultured in MEF media, until approximately 80 % confluent before being passaged three times at a ratio of 1:5 to expand the population of cells. To passage the cells, the flasks were washed with PBS three times and incubated with 5 ml of TrypLE for 10 minutes at 37 ^oC within the incubator.

2.1.1.3 Mouse embryonic fibroblast (MEF) inactivation

MEFs were inactivated through incubation with mitomycin C for 2 hours within the incubator. A 100 µg/ ml stock solution of mitomycin C was first prepared by dissolving 10 mg of mitomycin C from *Streptomyces Caespitosus* [Tocris, 3258] in 100 ml of MEF media (Table 2.1). 2 ml of the stock solution of mitomycin C was then added to each flask, which contained 18 ml of MEF media, to give a final concentration of 10 µg/ ml. After completion of the incubation period, each flask was washed three times with phosphate buffered saline (PBS), pH 7.2 [Invitrogen, 20012] before being incubated for a further 10 minutes in 4 ml of TrypLE™ Express. The TrypLE™ Express was the quenched with MEF media and the cells were washed and collected into 50 ml falcon tubes. The MEFs were centrifuged (300 g; 5 minutes), resuspended in freezing media (10 % DMSO; 90 % FBS) and counted (Chapter 2.1.3.1). The cells were cryopreserved (Chapter 2.3.1.2) and stored within -80 ^oC freezer in aliquots of 4-8 x 10^6 cells per cryovial. From this point the cells are referred to as iMEFs.

2.1.1.4 Plating down inactivated mouse embryonic fibroblasts (iMEFs) as feeders for human induced pluripotent stem cells

Tissue culture plates [Corning, 430167] were coated by incubating with 0.1 % gelatin (prepared from powder [Sigma, G1890] in ddH_20) for 10 minutes within the incubator. An aliquot of iMEFs was thawed, resuspended in 10 ml of MEF media within a 15 ml falcon tube

and centrifuged (300 g; 3 minutes). The iMEFs were resuspended in MEF media. Once the gelatin coating was aspirated from the tissue culture plates, iMEFs were plated at a density of 21,000 cells/cm^2. The cells were allowed to adhere to the plates overnight. The media was changed to human pluripotent stem cell (hPSC) media (Table 2.2) at least 2 hours before passaging pluripotent cells onto the layer of iMEFs to allow the iMEFs to condition the media.

2.1.2 Human pluripotent stem cell culture

2.1.2.1 Culturing human pluripotent stem cells on an iMEF feeder layer

Table 2.2 Human pluripotent stem cell media

Volume	Reagent	Product ID
76.7 %	Knock-Out DMEM	Invitrogen, 10829
20 %	Knock-Out Serum Replacement	Invitrogen, 10828
1 %	GlutaMAX™ (100x)	Invitrogen, 35050
1 %	Non-essential amino acids NEAA (100x)	Invitrogen, 11140
1 %	Penicillin-Streptomycin solution stabilised (Pen-Strep)	Sigma, P4458
0.2 %	2-Mercaptoethanol (50 mM)	Invitrogen, 991827
10-20 ng/ ml	Human Fibroblast Growth Factor – basic (FGF2)	PeproTech, 100-18B
0.1 %	Fungizone	Invitrogen, 15290-018

2.1.2.1.1 Mechanical passaging of human induced pluripotent stem cells

Differentiated areas of colonies were aspirated before passaging using a P200 pipette tip and an aspirator. A sterile insulin needle [VWR, 613-0740] was used to score colonies into squares of approximately equal sizes (Figure 2.1). This was done within the hood under a dissection microscope (Leica). A new needle was used for each cell line. The colony pieces were then detached and collected from the tissue culture plate using a P1000 pipette. 30-40 colony pieces were collected and plated onto a tissue culture plate with a layer of iMEFs. The colony pieces were allowed to attach to the tissue culture plates for 24 hours and the media was changed 48 hours later. Colonies were allowed to grow for 5-10 days before being passaged.

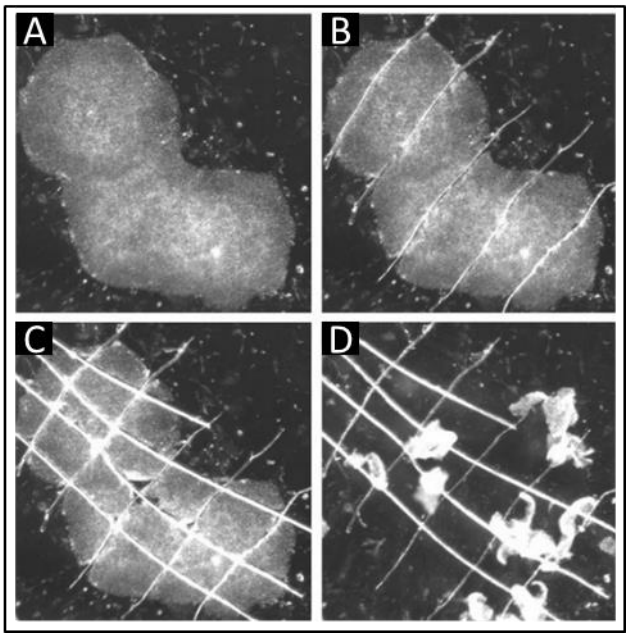

Figure 2.1 Mechanical stem cell colony passaging

Mechanical passaging of hESC colonies views under a stereomicroscope. Once the colony has reached an appropriate size for passaging (A), a 20 G needle is used to score the colony, viewed under a stereomicroscope within the cell culture hood (B). Next, the colony is scored again perpendicularly to the direction of initial scoring (C) to create colony pieces of ideal size for re-plating. These colony pieces are collected within a P1000 pipette tip and transferred to a new plate, pre-seeded with iMEFs (D).

2.1.2.2 Culturing human pluripotent stem cells (hPSC) within the Essential 8™ feeder free system

Human pluripotent stem cells were grown in Essential 8™ (E8) media within 6-well tissue culture plates [Fisher, 10119831], coated with either Vitronectin, Matrigel™ or Geltrex™. Essential 8™ Medium was developed in the laboratory of James Thomson (Chen *et al.,* 2011) before being validated and refined by Cellular Dynamics International. The E8 system has been extensively tested for its ability to support maintenance of pluripotency in various hiPSC lines. The complete media requires combination of Essential 8™ Medium with a 1:50 v/v of Essential 8™ Supplement, to consist of DMEM/F12, 64 mg/L l-ascorbic acid-2-phosphate magnesium, 14 µg/L sodium selenium, 100 µg/L FGF2, 19.4 mg/L insulin, 543 mg l^{-1} sodium

bicarbonate ($NaHCO_3$) and 10.7 mg/L transferrin, 2 µg/L TGFβ1 or 100 µg/L Nodal (Chen et. al., 2011).

2.1.2.2.1 Tissue culture plate surface coatings

The advantages of using the following cell culture substrates for culturing hiPSC are reduced variability compared to using an iMEF feeder layer, which results in more stable cultures from passage to passage.

2.1.2.2.1.1 Geltrex™

Geltrex™ is a gelatinous substrate composed of a complex mixture of basement membrane proteins derived from the spontaneous tumours of Engelbreth-Holm-Swarm mice, which provide a physical support for cultured cells to grow on top of. An aliquot of Geltrex™ [Life Technologies] was thawed overnight at 4 °C. The aliquot was kept on ice during handling. The contents of the aliquot were diluted in cold DMEM/F12 [Invitrogen, 31331028] to a concentration of 150 µg/ ml. 1 ml of the solution was applied to each well of a 6-well plate. The plates were incubated for 1 hour with Geltrex™ within the cell culture incubator before being incubated for 1 hour at room temperature. The Geltrex™ was then aspirated and 2 ml of Essential 8 media was added to each well.

2.1.2.2.1.2 Matrigel™

Matrigel™ also consists of basement membrane proteins derived from spontaneous Engelbreth-Holm-Swarm mouse tumours, is a gelatinous substrate and provides a physical support for the growth of cells in vitro. An aliquot of 300 µl Matrigel™ [BD Bioscience] was thawed overnight at 4 °C. The aliquot was kept on ice during handling. 500 µl of cold KO DMEM media, which consists of Knockout DMEM [Invitrogen, 10829] supplemented with Knockout Serum Replacer [Invitrogen, 10828] was added to the aliquot to dilute it. The contents of the aliquot were then added to 29.3 ml of cold KO DMEM within a 50 ml falcon. After mixing, 1 ml of the solution was applied to each well of a 6-well plate and incubated for at least 2 hours within the cell culture incubator. The Matrigel™ was then aspirated and the wells were washed once with KO DMEM. 2 ml of Essential 8 media was added to each well.

2.1.2.2.1.3 Vitronectin

Vitronectin is an abundant, secreted glycoprotein found in serum, the extracellular matrix and bone, which promotes cell adhesion and spreading when used as a surface coating. Vitronectin is relatively inexpensive compared to other available synthetic surfaces and requires minimal preparation. The truncated recombinant human vitronectin (rhVTN-N) [Life Technologies, A14701SA], corresponding to the amino acid fragment 62–478 of human vitronectin expressed in *E. coli*, is purified from inclusion bodies and refolded for use as a substrate for the feeder-free culture of human pluripotent stem cells (hPSCs) in Essential 8™ medium. This form of vitronectin was used at a concentration of 5 µg/ ml. An aliquot of stock vitronectin, at concentration 0.5 mg/ ml, was diluted 1:100 in PBS. 1 ml of vitronectin was added to each well of a 6-well plate and incubated at room temperature for 1 hour. The solution was aspirated before Essential 8 media was added to the well.

2.1.2.2.1.4 Poly-L-ornithine and laminin

200 µl poly-L-ornithine (POR) hydrochloride [Sigma P2533] was added at stock concentration to each well and incubated for 2 hours within the incubator. The poly-L-ornithine was then removed and 250 µl of 10 µg/ ml laminin (diluted from stock [Sigma, L2020] in PBS) was added to each well. The wells were incubated with laminin within the incubator for 2 hours or overnight. Upon completion of the incubation period, the laminin was removed and media was added to the wells. At this point to plates are referred to as POR/L coated.

2.1.2.2.2 Passaging human pluripotent stem cells using ethylenediamine tetraacetic acid

UltraPure™ 0.5M EDTA, pH 8.0 [Life Technologies, 15575-020] was diluted to a stock of 0.5 mM in PBS and warmed in a water bath to 37 ^{o}C. Wells with cells to be passaged within them were treated with ROCK inhibitor (Y27632) (10 ng/ ml) [Tocris, 1254], which was added to the media, 30 minutes prior to being passaged. The Essential 8 media was aspirated and each well was washed once with the EDTA stock solution. 1 ml of ethylenediamine tetraacetic acid (EDTA) was applied to each well before incubating at room temperature for 6 minutes. The EDTA was aspirated and 1-2 ml of Essential 8 media was sprayed onto the tissue culture surface to dislodge the colonies. The colonies were gently triturated until they had broken up into smaller colony pieces. 20-30 colony pieces were added to a freshly coated well of a 6-well plate. The colonies were allowed to adhere to the tissue culture surface

overnight. The media was changed after 48 hours. Colonies growing within the E8 culture system were passaged every 4-8 days.

2.1.2.2.3 Passaging human pluripotent stem cells from iMEFs to E8 cell culture system

Tissue culture plates with colonies to be passaged within them were treated with ROCK inhibitor (10 ng/ ml). Colonies were scored and 20-30 pieces were collected (Chapter 2.1.2.1.2) before being transferred to a freshly coated well of a 6-well plate. The colony pieces were allowed to adhere to the tissue culture surface overnight. The media was changed after 48 hours.

2.1.3 General Cell Techniques

2.1.3.1 Counting cells

To calculate the number of cells within a given volume of cell suspension, cells were first centrifuged and re-suspended in 1 ml of media, pipetting with a P1000 to ensure the cells were evenly suspended. To gain a dilution factor of 10, 10 µl of the cell suspension was collected into a 0.5 ml Eppendorf tube before 80 µl of media and 10 µl of 0.4 % Trypan Blue [Invitrogen, 15250] was added. The mixture was pipetted using a P1000 pipette to ensure it was evenly mixed.

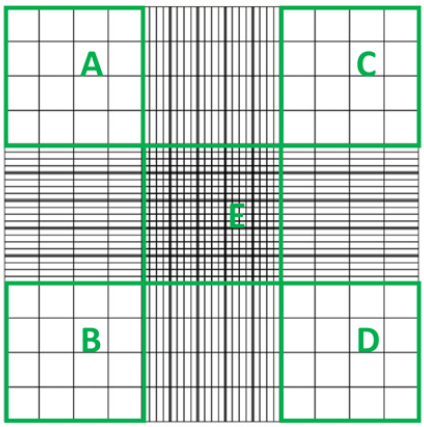

Equation used to calculate the number of cells within the original 1 ml cell suspension:

$$\text{Cell number} = \frac{\text{(Total number of live cells) x Dilution factor (10) x Scale factor } (10^4)}{\text{Number of squares}}$$

Figure 2.2 Schematic demonstrating the grid within the counting chamber of the haemocytometer used

Cells brightly stained with Trypan blue within highlighted areas (green) with lettered numbers were counted to give a total of five counts. Within the highlighted areas, only cells which crossed over the outer borders on the left-hand side and the top and were included in the count. Each highlighted area represents the number of cells within 1 µl of the cell suspension; therefore, the scale factor is 10^4. The number of live cells was calculated using the equation shown in the figure.

A coverslip was placed onto a clean haemocytometer and 10 µl of the cell suspension within the Eppendorf tube was carefully pipetted at the edge of the coverslip. Capillary action ensured the suspension was taken under the coverslip to fill the counting chamber. Only live cells were counted. Trypan blue is not absorbed by live cells so these cells appear colourless, with a bright, refractive border; the dye transverses the membranes of non-viable cells so that these cells appear blue.

2.1.3.2 Cryopreservation of cells

2.1.3.2.1 Cryopreservation of MEFs and iMEFs

After aspirating the media from the cells, the cells were washed with PBS and an appropriate volume of TripLE Express™ was added to the cells. The cells were incubated for 10 minutes in the incubator. After completion of the incubation the TripLE Express™ was quenched with an equal volume of MEF media and the cells were collected into a falcon tube. For cryopreservation of cells in a volume greater than 10 ml, cells were collected into a 50 ml falcon and centrifuged (300 g; 5 minutes); for cryopreservation of cells in a volume less than 10 ml cells were collected into a 15 ml falcon and centrifuged [300 rpm; 3 minutes]. The cells were resuspended in freezing media, consisting of 10 % Dimethyl sulfoxide (DMSO), which acts as a cryoprotectant, and 90 % foetal bovine serum (FBS) [Life Technologies, 10500064]) and 700 µl of the cell suspension was added into each labelled 1 ml cryovial [Greiner, 123278]. The cryovials were placed in a Mr Frosty™ , at room temperature, and immediately stored at -80 °C. Mr Frosty™ is a freezing container consisting of a plastic chamber of compartments in which to place individual vials of cells, surrounded by 100 % isopropyl alcohol, which allows for a uniform cooling rate of approximately 1 °C per minute, determined to be ideal for optimal cell survival.

2.1.3.2.2 Cryopreservation of human pluripotent cells grown on an iMEF feeder layer

The media was aspirated from the cells and 1 ml of warm 1 mg/ ml collagenase IV [Life Tech, 17104-019] (made up from stock concentration of 10 mg/ ml diluted in KO DMEM)] was added to each tissue culture plate. The cells were incubated with collagenase IV for 20 minutes in the incubator before KO DMEM and a P1000 pipette were used to spray the colonies from the tissue culture surface. The colonies were collected into 15 ml falcon tubes and topped up to 10 ml with KO DMEM before being centrifuged (1100 g; 3 minutes). The media was removed from the cell pellet and the colonies were gently resuspended in freezing media. For each tissue culture plate, colonies were resuspended in 700 µl of freezing media and this volume was added to a labelled, 1 ml cryovial. The cells were placed into a Mr Frosty™ and immediately frozen at -80 °C.

2.1.3.2.3 Cryopreservation of human pluripotent cells cultured within the E8 system

A 2x freezing media consisting of 20 % DMSO and 80 % E8 media was prepared. An appropriate number of cryotubes were labelled. The media was removed from E8 cells and the cells were washed once with warmed EDTA, before being incubated with EDTA for 6 minutes. After the incubation period the EDTA was removed and the cells were sprayed from the tissue culture well surface with an appropriate volume of E8 media, for example 1 ml for each well of a 6-well plate and 0.5 ml for each well of a 12-well plate. An equal volume of freezing media was then added to each well drop wise. 500 µl to 700 µl was pipetted into each cryovial and the cryovials were placed into a Mr Frosty™, which was placed into -80 °C freezer. When hPSC cultured within the E8 system were thawed they were plated in E8 media supplemented with 10 µg/ ml ROCK inhibitor to limit cell death.

2.1.3.2.4 Cryopreservation of neurospheres

Neurospheres to be cryopreserved were collected from within the tissue culture flask into a 15 ml falcon with 10 ml of media. The neurospheres were centrifuged (300 g; 3 minutes) and the media removed from the falcon. Freezing media (10 % DMSO in foetal bovine serum (FBS)) was added to the spheres. An average of 40 neurospheres were frozen in a 1 ml cryovial with 700 µl of freezing media. The cryovials were placed in a Mr Frosty™ and immediately stored at -80 °C.

2.1.3.2.5 Cryopreservation of neural progenitors and neurons at day 20-25 of the cortical glutamatergic neuron differentiation protocol

The cells were washed once with PBS before 200 µl of Accutase™ [Sigma, A6964] was applied to each well with cells to be cryopreserved. The cells were incubated with Accutase™ for 5 minutes within the incubator. After completion of the incubation period the cells were gently pipetted, using a P1000 pipette, to dissociate the cells to give a single-cell suspension. 800 µl of neural maintenance media was added to each well to quench the Accutase™, and this mixture was transferred to a 15 ml falcon tube. The cells were centrifuged (200 g; 5 minutes) and resuspended at 2 x 10^6 cells/ ml in neural stem cell freezing media [neural maintenance media supplemented with 10 % DMSO; 20 ng/ ml FGF2].

2.2 Biomolecular Techniques

2.2.1 Western Immunoblotting

2.2.1.1 Protein extraction from neurospheres

The media was gently aspirated from the wells containing neurospheres before the neurospheres were washed once with ice cold PBS. 100 µl Ice cold RIPA buffer (50 mM Tris HCl [pH7.4], 150 mM NaCl,1 % Triton-X-100 (v/v), 0.5 % Sodium deoxycholate (w/v), 0.1 % sodium dodecyl sulphate (SDS) (w/v)) plus 1 tablet of Protease Inhibitor [Roche, cOmplete Mini, 04693124001] per 10 ml of RIPA buffer and 1 tablet of Phosphatase Inhibitor PhosStop, [Roche] per 10 ml was used to dissolve neurospheres within 3 wells. Neurospheres were manually detached from the surface of the wells whilst in RIPA buffer using a P1000 pipette tip. The RIPA buffer and neurospheres from three wells were collected into a sterile, labelled 1.5 ml Eppendorf and triturated using a P200 pipette tip before being left on ice for 10 minutes. The sample was then further homogenised by triturating using a 1 ml syringe and 18G needle. The sample was then centrifuged (4 ^{o}C; 12,000 g, 15 minutes) and the supernatant was collected into a clean, cold Eppendorf. The sample was immediately stored at -80 ^{o}C overnight.

2.2.1.2 Protein quantification

A bicinchoninic acid (BCA) assay [Pierce, 23225] was used to quantify the concentration of protein within each sample. The manufacturer's protocol was followed. A set of standards of known protein concentrations comprised of bovine serum albumin (BSA) dissolved in RIPA buffer (50 mM tris HCl, 150 mM NaCl, 1 % Triton X-100 (v/v), 1 % sodium deoxycholate (w/v), 0.1 % sodium dodecyl sulfate (w/v), pH 7.4) were prepared and pipetted in triplicate into wells of a 96-well plate, alongside triplicates of each protein sample, and incubated with the reaction solution for 30 minutes at 37 ^{o}C on a shaking platform. The protein in the samples degrades the Cu^{2+} within the reaction solution to Cu^{1+}, which forms a complex with BCA leading to a colorimetric reaction. This reaction causes the contents of the wells to change colour from green to purple. The relationship between BSA/Cu^{1+} complex and the concentration of protein is linear, allowing the protein within each well to be then quantified by measuring the absorbance, read at 562 nm (1 minute) using a photospectrometer. The values from the BCA assay standards were used to create a standard curve and calculate the

equation for this curve, using MS Excel™. The equation can then be used to calculate the concentration of protein within each sample.

2.2.1.3 Buffers and solutions used during western immunoblotting

Table 2.3 Components of SDS Sample Buffer (5 X)

Reagent	Product	Concentration
TRIS-HCl [Tris(hydroxymethyl) aminomethane HCl]	Melford, T1513	50 mM – pH 6.8
Dithiothreitol (DTT)	Sigma, D9779	100 mM
SDS	Sigma, L3771	2 % (w/v)
Bromophenol Blue	Sigma, B0126	0.1 % (w/v)
Glycerol	Sigma, G5516	10 % (w/v)

Table 2.4 Components of Loading Gel (12 %)

Reagent	Product	Concentration	Volume (v/v)
H_2O*	Sigma, W3500	N/A	32.96 %
Acrylamide	Sigma, A3574	30 %	40.00 %
TRIS [(hydroxymethy)aminomethane]	Melford, B2005	1.5 M – pH 8.8	25.00 %
SDS	Sigma, L3771	10 % (w/v)	1.00 %
Ammonium Persulfate (APS)	Sigma, A3678	10 % (w/v)	1.00 %
TEMED	Fluka BioChemika, RA12027	N/A	0.04 %

Table 2.5 Components of Stacking Gel (4 %)

Reagent	Product	Concentration	Volume (v/v)
H_2O*	Sigma, W3500	N/A	68.65 %
Acrylamide	Sigma, A3574	30 %	16.75 %
TRIS [(hydroxymethy)aminomethane]	Melford, B2005	1 M – Ph 6.8	12.50 %
SDS	Sigma, L3771	10 % (w/v)	1.00 %
Ammonium Persulfate (APS)	Sigma, A3678	10 % (w/v)	1.00 %
TEMED	Fluka BioChemika, RA12027	N/A	0.10 %

Table 2.6 Components of Running Buffer (10x)

Reagent	Product	Amount
TRIS	Melford, B2005	30.2 g
Glycine	Melford, GO709	188.0 g
SDS	Sigma, L3771	0.5 % (w/v)
H_2O*	N/A	Made up to 2 L using H_2O

Table 2.7 Components of Transfer Buffer (10x)

Reagent	Product	Amount
TRIS	Melford, B2005	58 g
Glycine	Melford, GO709	29.2 g
SDS	Sigma, L3771	3.7 % (w/v)
H_2O*	N/A	Made up to 2 L using H_2O

Table 2.8 Components of TRIS Buffer Saline (TBS) (10x)

Reagent	Product	Amount
TRIS	Melford, B2005	30 g
$NaCl^2$	Sigma, S7653	80 g
KCl	Sigma, P9541	2 g
H_2O*	N/A	Made up to 2 L using H_2O

*H_20 was purified using The Milli-Q Integral System, Millipore.

2.2.1.4 Sample Preparation

The lysate samples were thawed on ice. The volume of each lysate required to add 20 µg of protein for each sample was calculated, using the concentration of the protein samples calculated using the BCA assay (Chapter 2.2.1.2). The volume of H_20 required to prepare the samples to a total volume of 20 µl was also calculated. The water was pipetted into labelled PCR tubes before adding the 4 µl sample buffer (Table 2.3) containing dithiothreitol (DTT), which is required to denature the protein. Finally, the correct volume of protein was added to the corresponding labelled PCR tube. The samples were heated to 100 ^oC for 5 minutes

within a heat block to facilitate denaturisation of the protein. Following this treatment, the samples were kept on ice before loading.

2.2.1.5 Preparation of the loading and stacking gels

12 % acrylamide loading gel was used for all western blotting experiments (Table 2.4). The apparatus for running the protein and the gels were prepared before the protein samples were prepared, to limit the time from thawing the samples to preparation for western blotting ensuring minimal sample degradation. 7 ml of the loading gel was pipetted, immediately after preparation in a 50 ml falcon tube, between two clean 1.5 mm^2 plates, secured within the Mini Protean II Apparatus (Biorad). 500 µl of butanol was then pipetted on top of the loading gel, to ensure the gel set with an even upper surface to allow all samples to run equally through the gel. The gel was allowed to set for 30 minutes before the butanol was removed, and the gel washed with water to remove traces of butanol. The stacking gel was then prepared (Table 2.5) and 2 ml pipetted onto the loading gel. To create the wells within the stacking gel for protein loading, a comb with 10 'teeth' was inserted into the top of the gap between the two plates and the gel was allowed to set for 15 minutes. The plates containing the set gel were transferred from the Mini Protein II Apparatus into the running cassette and the tank (Mini Trans-Blot® Cell, Biorad) was filled with 1L 1 X running buffer (Table 2.6), making sure that the running buffer covered the top of the gel. The comb was removed from the gel and the gel was loaded with the protein samples. A note of the order of the protein samples was taken and the wells created by the comb were checked to ensure they had not been distorted in the process. 5 µl of protein ladder (Precision Plus Protein™ Kaleidoscope™ Standards, [Bio-Rad 161-0375]) was loaded in a well alongside the protein samples. The samples were run at 100 V until they had passed the stacking gel, at which point the voltage was increased to 150 V. The gel was run until the blue sample buffer could be seen at the bottom of the gel, which takes approximately 70 minutes. The plates were removed from the apparatus and separated carefully before the stacking gel was removed and discarded, leaving the loading gel.

2.2.1.6 Wet transfer of proteins to a polyvinylidene difluoride membrane

Two pieces of sponge and two pieces of blotting paper were soaked in 1 X transfer buffer with 10 % methanol (Table 2.7). Polyvinylidene difluoride (PVDF) membrane was cut into an appropriate size and soaked for one minute in methanol, before being transferred to a

container with 1 X transfer buffer, with 10 % methanol, to soak for an additional 5 minutes. Soaking the membrane in methanol ensures it is 'active', while soaking in 1 X transfer buffer ensures the membrane is at isotonic equilibrium. The gel and membrane were layered between filter paper and sponge within the transfer cassette as depicted (Figure 2.3) rolling each layer upon addition to minimise the chance of air bubbles becoming trapped. The cassette was secured close and placed into the western transfer apparatus. To limit degradation of the protein, an ice block was added into the tank next to the cassette as the process of transferring produces heat. The tank was then filled with 1 X transfer buffer with 10 % methanol and the lid fitted. The apparatus was placed into a plastic bucket containing ice to minimise heating. The transfer was performed by passing 200 mA of current through the apparatus for 90 minutes. Upon completion of the transfer, the membrane was removed from the apparatus and the gel discarded. The membrane was 'reactivated' by soaking in methanol for five minutes.

Figure 2.3 Schematic of western transfer

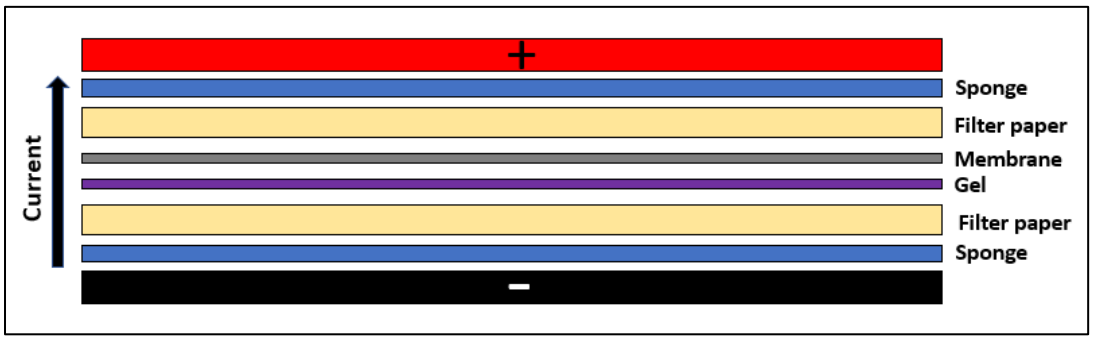

Figure 2.3 Schematic of western transfer

The current was passed from the negative anode to the positive anode through the gel and then the membrane to transfer the protein. The sponges and filter paper were arranged such as to ensure the membrane and gel remained soaked by the transfer buffer.

2.2.1.7 Probing the PVDF membrane with antibodies

The membrane was rolled into a 50 ml falcon tube, ensuring no overlapping, and then blocked in 10 ml of 10 % skimmed milk [Marvel] in 1 X TBS (Table 2.8) + 20 % Tween (TBS-T) for an hour at room temperature on a roller. After washing the membrane 3 times (10 minutes/wash) in 10 ml of TBS-T within a clean falcon tube, the membrane was added to a new, clean falcon tube with 5 ml of the prepared primary antibody solution. The primary

antibodies were prepared in 5 % milk in 1 x TBS-T to the required concentration. The membrane was incubated with the antibody overnight at 4^{o}C on a roller. The following day, the membrane was removed from the primary antibody and placed into a clean falcon tube and washed 3 times as before. An appropriate secondary horseradish peroxidase (HRP)-conjugated antibody was diluted 1:5000 in 5 % milk in 1 x TBS-T in a clean falcon tube and the membrane was incubated with the secondary antibody for 1 hour at room temperature on a roller. The membrane was washed 3 times as before.

2.2.1.8 Enhanced chemiluminescence (ECL) detection of antibodies

The membrane was placed within a plastic folder. 0.75 ml of Luminol Enhancer and 0.75 ml Stable Peroxide Buffer were mixed in a 15 ml falcon tube [Supersignal west pico chemiluminescent substrate (ECL) kit; Thermo Scientific, 34080] and this solution was added to the membrane within the folder. The solution was spread over the membrane, ensuring even coverage, for one minute. The solution was then removed and the folder sealed airtight. The folder containing the membrane was then affixed within a Hypercassette^{TM} [GE Healthcare Amersham]. In a dark room, autoradiograph film (Amersham Hyperfilm ECL, [GE Healthcare, 28-9068-40]) was added to the hypercassette to expose the film to the membrane. The film was developed using a Kodak X-OMAT 1000 auto processor.

2.2.1.9 Stripping the western

Western blots were re-probed after initial probing with a 'housekeeping' antibody to allow normalisation of signals. Before re-probing, the membrane was stripped using western blot stripping buffer [Fisher, 21059]. The membrane was incubated with the stripping buffer for 5-10 minutes at room temperature within a 50 ml falcon tube on a roller, before being washed three times (10 minutes/wash) and re-activated by soaking in methanol for five minutes. The membrane was blocked for one hour in 10 % milk in 1 X TBS-T before re-probing. Each blot was probed with an antibody against GAPDH before being probed with a tau antibody, either DA9, PHF-1 or CP13. Each western blot was then probed with an antibody against a tau kinase, either GSK3β, GSK3β pTyr216, Akt pSer273 or PAK3. Other blots were probed with GAPDH and then either antibodies against synapsin or p25-p35. This information is also given within Chapter 5.2.4.1.

2.2.1.10 Densitometric analysis of protein bands

Densitometric analysis was performed using the software Image J, downloaded from http://rsbwb.nih.gov/ij/. The blot was scanned using an Epsom scanner 1250 and saved as a Tiff file. Each band was individually selected to generate a histogram. The areas under the peaks of each histogram were calculated and imported into an Excel file for processing for analysis.

2.2.2 Immunocytochemistry

2.2.2.1 List of solutions

Table 2.9 Components of blocking/permeabilisation solution

Reagent	Amount	Product
Triton-X-100	0.1 %-0.4 %	Sigma, T8787
Horse serum	10 %	Life technologies, 26050088
Bovine serum albumin (BSA)	2 %	Sigma, A9418
Phosphate buffered Saline (PBS) + $CaCl_2$ + $MgCl_2$	Up to 10 ml	Sigma, D8662

Table 2.10 Components of antibody incubation solution

Reagent	Amount	Product
Primary/secondary antibody	Various	Various
Triton-X-100	0.1 %	Sigma, T8787
Horse serum	1 %	Life technologies, 26050088
Bovine serum albumin (BSA)	0.2 %	Sigma, A9418
Phosphate buffered Saline (PBS) + $CaCl_2$ + $MgCl_2$	Up to 10 ml	Sigma, D8662

2.2.2.2 Preparation of cells for immunocytochemistry

Cells were washed with PBS and an appropriate volume of 4 % paraformaldehyde (PFA) at room temperature was added to the cells (i.e. 150 µl per well of a 4-well or 24-well plate). The cells were incubated at room temperature; 15 minutes for cells in a monolayer, or 20 minutes for neurospheres. Cells were then incubated with blocking/permeabilisation solution for 2 hours at room temperature, or overnight at 4 ^{o}C, on a rocker. Cells were then gently washed 3 times (10 minutes/wash) in PBS + 0.1 % Triton-X-100 (PBS-Tx).

2.2.2.3 Probing cells with antibodies

Cells were incubated with the primary antibody, prepared in antibody incubation solution, overnight at 4 °C on a rocker. The following day the cells were gently washed 3 times (10 minutes/wash) in PBS-Tx before being incubated with the appropriate fluorescent secondary, at a concentration of 1:400, for 2 hours on a rocker, protected from light. After washing the cells 3 times (10 minutes/wash) Hoechst solution at a concentration of 1:1000 in PBS was added to the cells for 5 minutes, protected from light. After the incubation period the cells were washed 3 times (10 minutes/wash).

2.2.2.4 Mounting coverslips

Cells cultured on coverslips and immunostained were mounted. The coverslips were removed from the cell culture well using forceps and placed inverted onto a ~30 µl drop of Vectorshield® Mounting Medium on a slide. Care was taken to avoid placing any pressure on the coverslips. The coverslips were allowed to rest on the slides for approximately two minutes to allow the mounting medium to spread through capillary action. Any excess medium was removed using blotting paper. A layer of clear nail varnish was painted around the edge of the coverslip to seal the coverslip to the slide and contain the mounting medium. After allowing 1 hour to dry, a second coat of nail varnish was applied. A fluorescence microscope (Leitz DMRB, Leica) was used to image the cells, captured by a camera (DC 500, Leica) and processed using Leica imaging software.

2.2.3 Analysis of Gene Expression

The expression of specific genes present within hPSCs, embryoid bodies (EBs), hPSC-derived neurons and brain tissue was quantified by quantitative polymerise chain reaction (qPCR) using Taqman® probes. Briefly, total RNA was isolated from the cells, purified and converted to cDNA. The cDNA is representative of the RNA present within the sample and therefore can be used to quantify RNA expression. This technique involves the amplification of target DNA, representative of the gene in question, using sequence specific Taqman® DNA probes, which consist of oligonucleotides labelled with a fluorescent reporter. Fluorescence is only detected after hybridisation of the probe with the complimentary target DNA sequence. The fluorescent sequence was detected using a StepOnePlus™ System [Applied Biosciences] and the complimentary software used to quantify the number of cDNA copies present within each sample.

2.2.3.1 Extraction and purification of total RNA

RNA extraction and purification was performed by using TRIzol reagent [Ambion, 15596-026] with the PureLink® RNA Mini Kit [Ambion, 12183018]. TRIzol® [Ambion] is a monophasic solution of phenol and guanidine isothiocyanate, designed to isolate separate RNA, DNA and proteins from cell and tissue samples into fractions.

hiPSC colonies were grown in feeder-free conditions in 9 cm diameter cell culture plates until 50 % confluent. Cortical glutamatergic neurons were grown in 6 cm diameter 6-well plates until confluent and basal forebrain neurons were grown in 24-well plates. The media from the cells was removed and an appropriate volume of TRIzol®, dependent on the surface area of the culture surface, was added to the cells. hPSC and neurons were homogenised directly in the plate by pipetting 20 times with a P1000 pipette tip. EBs and brain tissue were collected into RNAse-free tubes and an appropriate amount of TRIzol® was added to each tube. Embryoid bodies and brain tissue were homogenised within the tubes using a tissue homogeniser and then by pipetting 20 times with a P1000 pipette tip.

After homogenisation the plates or tubes were incubated on ice for 5 minutes. The incubation period ensured the complete homogenisation and extraction of nucleic materials from the cells. After incubation on ice, homogenised hPSC and neurons were transferred to RNAse-free tubes. The samples were frozen immediately at -80 ^{o}C or processed using the PureLink® RNA Mini Kit to isolate RNA.

The PureLink® RNA Mini Kit relies on spin column technology. PureLink® DNase [Ambion, 12185010] is optimised for use with the PureLink® RNA Mini Kit and was used to remove genomic DNA from the RNA samples; this product is an endonuclease that breaks apart double- and single-stranded DNA and is free of ribonucleases and proteases. Briefly, the bench area, pipettes and tube stands were cleaned using RNase AWAY™ surface decontaminant [Thermo Scientific, 7002] to ensure an RNA-free environment. The manufacturer's instructions for the PureLink® RNA Mini Kit were followed to complete extraction and purification of RNA and to remove any residual DNA. RNA-free filter pipette tips were used throughout the protocol.

2.2.3.2 Quantification of RNA

A spectrometer [NanoPhotometer™, Implen, Pearl Edition] was used to quantify the concentration of the RNA within the sample by first vortexing the sample for 2 seconds and

then adding 1 µl of the sample to the sensor. The value of the concentration was recorded, along with the absorbance ratio values; absorbance ratio of 260nm/280nm should equate to 2.0 +/- 0.05, which indicates a pure RNA sample, whereas the ratio 260nm/230nm should be between 2.0 and 2.2, indicating pure nucleic acid. If this ratio value deviates from this it indicates there may be protein contaminants within the sample, therefore, samples outside of these ranges were discounted.

2.2.3.3 Reverse Transcription of RNA to cDNA

The High-Capacity cDNA Reverse Transcription (RT) Kit [Applied Biosystems, 4368814] was used to convert up to 2 µg of RNA per sample to cDNA. A 2 X reaction mix was prepared on ice according to the manufacturer's instructions (Table 2.11). An equal amount of RNA, for example 1 µg, for each sample was added to the reaction to allow for accurate quantification of gene copy number during qPCR. To create a negative template control for each sample, the protocol was performed without Multiscribe™ Reverse Transcriptase. When used alongside qPCR, the negative template control ensured there was no DNA contamination within the samples before reverse transcription.

Table 2.11 Reaction mix for reverse transcription of RNA to cDNA.

Component	Volume/Reaction (µL)	
	Kit with Multiscribe™ Reverse Transcriptase to create a positive template	Kit without Multiscribe™ Reverse Transcriptase to create a negative template
5 x RT Buffer	2.0	2.0
25x dNTP* Mix (100 nM)	0.8	0.8
10x RT Random Primers	2.0	2.0
Multiscribe™ Reverse Transcriptase	1.0	-
RNAse Inhibitor	1.0	1.0
Nuclease-free H_2O	3.2	4.2
Total per Reaction	10.0	10.0

*dNTPs comprise dATP, dCTP, dTTP and dGTP

The manufacturer's instructions for High-Capacity cDNA Reverse Transcription Kit were followed. Briefly, the volumes of each component (10x RT Buffer, 25x dNTP Mix (100 nM)), 10 X RT Random Primers, Multiscribe™ Reverse Transcriptase, RNAse Inhibitor and Nuclease-free H_20) (Table 2.11) needed to make up the volume of reaction mixture, was calculated to create a positive and negative template for each sample, plus 10 % to account for any pipetting error. The positive template and negative template mixtures were made in RNAse free Eppendorf tubes, vortexed to mix, briefly centrifuged and kept on ice. 10 µl of RNA mixture for each sample, containing the correct amount of RNA and made up to 10 µl with nuclease-free H_20, was pipetted into clean, RNAse free tubes. 10 µl of the positive or negative reaction mixtures were pipetted into the RNAse-free PCR tubes containing the RNA mixture. The samples were inverted three times to mix before centrifuging briefly. The tubes were placed into the thermal cycler [Biorad, MJ Mini] programmed with the following heat cycle: 25 ^oC for 10 minutes, 37 ^oC for 120 minutes and 85 ^oC for 5 minutes. Once the cycle was complete, the synthesised cDNA was stored at 4 ^oC before being used for qPCR.

2.2.3.4 Quantitative Polymerise Chain Reaction

The required volume, plus 10 % to account for pipetting error, of 2X TaqMan® Universal PCR Master Mix (Applied Biosystems, 4364340) was determined to perform qPCR reactions for all samples, endogenous control assays and non-template controls (NTC) for each gene assay. Glyceraldehyde-3-phosphate dehydrogenase (*GAPDH*) was used as an endogenous reference gene throughout. The 2X TaqMan® Universal PCR Master Mix contains AmpliTaq Gold® DNA Polymerase, UP (Ultra-pure), Uracil-N glycosylase (UNG), dNTPs with dUTP, dNTPs with dUTP, ROX™ Passive Reference and optimized buffer components. The Taqman® Gene Expression Assay (20 X) was added to the master mix (Table 2.12) within an RNAse-free Eppendorf. Taqman® Gene Expression Assays for real-time PCR were purchased from Applied Biosystems (Table 2.13; at the 5' end, the probes were conjugated to the fluorochrome 6-carboxyfluorescein (FAM); and at the 3' end to the quencher tetramethylrhodamine (TAMRA).

Table 2.12 Components required per qPCR Taqman® Gene Expression Assay reaction.

Component	Volume (µl)
2X TaqMan® Universal PCR Master Mix	10
Taqman® Gene Expression Assay (20 X)	1
cDNA template	Varies
RNase free H_20	To 20

Table 2.13 Taqman® probes

Gene	TaqMan® Gene Expression Assay Catalog no. ID
Glyceraldehyde-3-Phosphate Dehydrogenase (GAPDH)	Hs02758991
Cyclin-Dependent Kinase 5 (CDK5)	Hs00358991
Glycogen synthase kinase 3 beta (GSK3β)	Hs01047719
P21 Protein (Cdc42/Rac)-Activated Kinase 3 (PAK3)	Hs00176828
Repeat Microtubule Associated Protein Tau (*MAPT*)	Hs02758991

Within strip PCR tubes the appropriate volume (Table 2.12) required for a triplicate of each assay was measured out. The appropriate volume of cDNA, consistent between all samples and assays, for a triplicate of each assay was then added to each tube. The tubes were vortexed and centrifuged for 5 seconds to ensure adequate mixing of the components. 20 µl of each assay and cDNA mixture was then added to the side of a well of a 96-well plate (MicroAmp, Applied Biosystems). This was repeated to ensure a triplicate of each assay.

Non-template controls (NTC) were also mixed and pipetted in the same way with the same volumes, however, in the place of the cDNA template RNAse free H_20 was added. The plate was covered with an optical adhesive cover (Applied Biosystems; Cat No. 4313663) to prevent evaporation and contamination during the reaction and then centrifuged at 300 g for one minute at room temperature in a centrifuge to eliminate any bubbles that may have formed during pipetting and ensure the mixture was at the bottom of each well. The instructions in the instrument user guide for the StepOnePlus™ Real-Time PCR System were used to set the thermal cycling parameters of the PCR system as described in Table 2.14.

Table 2.14 Thermal cycling parameters used for qPCR

Parameter	UNG incubation	Polymerase activation	PCR (40 cycles)	
	Hold	Hold	Denature	Anneal/extend
Temperature	50 °C	95 °C	95 °C	60 °C
Time (mm:ss)	02.00	10.00	00.15	01.00

2.2.3.5 Analysis of qPCR results

The threshold cycle number for product detection (Δ CT value) for the housekeeping gene (*GAPDH*) and the genes being tested (*MAPT*, *CDK5*, *GSK3β* or *PAK3)* were calculated within the StepOnePlus™ Real-Time PCR System complimentary software, for both the control samples and experimental samples. These values were copied into Microsoft Excel and the average relative gene expression of each gene in comparison to the controls was then calculated. In Chapter 4, control samples were from Shef 6-CGN and experimental samples were from V337M-C-CGN. In Chapter 5, control samples were Nas 2-bfCN or Shef 6-CGN not treated with $A\beta_{42}O$ and experimental samples were those treated with $A\beta_{42}O$. The average of the CT values for each sample in triplicate were averaged. ΔCT values for the experimental (ΔCTE) and control (ΔCTC) conditions were generated subtracting the average CT value of the housekeeping gene from the average CT value of the gene being tested for the experimental sample. The difference between ΔCTE and ΔCTC (ΔCTE-ΔCTC) was calculated to work out the Double Delta CT Value (ΔΔCT). The value of 2^-ΔΔCT was then calculated to arrive at the value for average relative gene expression. This value, for each sample, was normalised to the average 2^-ΔΔCT value of the control samples.

2.2.4 Statistical analysis of western immunoblotting and gene expression results

Analysis was carried out to determine the statistical significance of results from western immunoblotting densitometry and qPCR. Graphpad Prism 7 was used to analyse the data and statistical tests were recommended by Prism.

An unpaired Student's t-test was used to analyse the statistical significance of western immunoblotting results in which two groups were compared, as recommended by Graphpad Prism 7. Upon analysis of the effects multiple concentrations of $A\beta_{42}O$ on tau-related pathogenesis within Shef 6-bfCN (Chapter 5.3), the Friedman test was used followed by the Dunn post-hoc test to allow for comparison of results across separate blots.

Statistical analysis of gene expression data was carried out using non-parametric tests as sample sizes are too small to reliably confirm normal distribution of data. Where two groups were compared, statistical analysis was carried out using the Mann-Whitney test. Where more than two groups were compared the Kruskal-Wallis test followed by a post-hoc Dunn's test. *=$p \leq 0.05$. **=$p \leq 0.01$. ***=$p \leq 0.001$. ****=$p \leq 0.0001$.

2.2.5 Definition of technical and biological replicates

For each biological sample collected for western immunoblotting or gene analysis via qPCR of cortical glutamatergic neurons (CGNs), protein lysates were collected from one well of a 6-well plate (Chapter 4 and Chapter 5). Lysates from three wells of a 24-well plate were pooled for each biological sample collected for western immunoblotting or gene analysis for basal forebrain cholinergic neurons (bfCNs) (Chapter 5). Each western blot was repeated three times to account for technical variation. Three technical replicates of the resultant cDNA created were carried out on each qPCR plate.

Chapter 3

Generation of V337M *MAPT* induced pluripotent stem cell lines

3.1 Introduction

Val337Met (V337M) *MAPT* is a rare mutation, otherwise known as the Seattle family A mutation, described as a missense, single nucleotide polymorphism within exon 12 of *MAPT* resulting in a change in the amino acid (aa) at 337 from valine to methionine, resulting in frontotemporal dementia with Parkinsonism linked to chromosome 17 (FTDP-17) (Poorkaj *et al.*, 1998). Four human pluripotent stem cell (hPSC) lines were used during this PhD project: Shef 6, a human embryonic stem cell (hESC) line; Nas 2 a human induced pluripotent stem cell (hiPSC) line; and two hiPSC lines derived from a patient carrying V337M *MAPT.* Characterisation of the pluripotency of the Nas 2 hiPSC and Shef 6 hESC lines has been carried out previously within the Kunath lab (Devine *et al.,* 2011) and by the UK Stem Cell Bank, respectively. The study was approved by National Research Ethics Service (NRES Committee – South West) reference 09/H0102/47. The work in this chapter describes the generation, establishment and characterisation of hiPSC lines V337M-C and V337M-E.

Reprogramming of V337M *MAPT* lines was carried out previously within the Caldwell lab by Dr. Lucy Crompton while clonal selection and characterisation was carried out by the author of this thesis, under the supervision of Dr. Lucy Crompton. A skin biopsy was obtained from a 44 year old female with the heterozygous mutation V337M *MAPT*. Cells from the skin biopsy were cultured *in vitro* to expand a population of fibroblasts, which were obtained from Corriell Biorepository (http://ccr.coriell.org/, catalogue no: ND40082) (New Jersey, USA), where they had been genetically characterised. These fibroblasts were reprogrammed using lentiviral transduction of pluripotency transcription factors (TFs), *OCT4*, *KLF4*, *SOX2, LIN28* and *NANOG*, along with the gene for green fluorescent protein (GFP), to produce human induced pluripotent stem cells (hiPSC) carrying the mutation. Clones were selected for expansion and two of these were taken forward for characterisation of pluripotency and karyotyping: V337M-C and V337M-E. After expansion of the clones, the established cell lines

were cultured and continually banked up until passage 10. hESC and hiPSC lines between passages 10 and 16 were differentiated to produce cortical glutamatergic neurons (CGNs).

At the start of this PhD, there were concerns within the scientific community that hiPSC lines may not be identical to hESC with regards to their genetic and epigenetic regulation of pluripotency, genome integrity and gene expression (Bilic and Belmonte, 2012; Puri and Nagy, 2012). Additionally, concerns over the inability of hiPSC-models to recapitulate certain aspects of particular diseases, previously recapitulated in hESC-models, were also raised (Halevy and Urbach, 2014). Potential differences between these two cell types would hinder the comparison of the results in such studies to those found within studies using hESC-models. To allow for control of these possible differences, the gold standard of the time was to use a control hESC line alongside a control hiPSC line within studies involving modelling using hiPSC lines derived from patients. This is no longer deemed necessary as differences between these two cell types have been confirmed to be minimal (Bates and Silva, 2017).

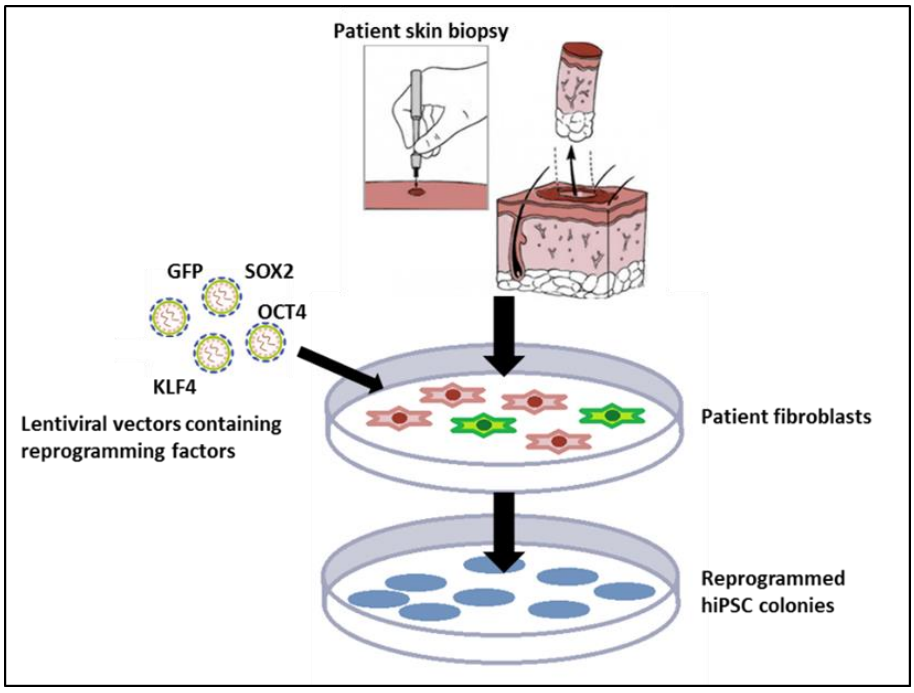

Figure 3.1 Reprogramming of hFibs to produce hiPSC

A skin biopsy was collected from the patient, which was cultured in vitro to expand a population of fibroblasts. Lentiviral vectors were used to transduce reprogramming factors (OCT4, SOX2, KLF4), along with GFP, into patient fibroblasts. The silencing of GFP was used to monitor the completion of reprogramming.

3.2 Methods

3.2.1 Human fibroblast culture

Human fibroblast culture was carried out by Dr. Lucy Crompton within the Caldwell lab to gain fibroblasts from a skin biopsy.

3.2.2 Reprogramming

Reprogramming of these fibroblasts was originally carried out within the Caldwell lab by Dr. Lucy Crompton using lentiviral vectors (pRRL-Sin-cppt-PGK-EGFP, pSin4-EF2-Oct4-Sox2, pSin4-EF2-Nanog-Lin28, pWXPL-Klf4) originally from the James Thomson lab (Yu *et al.,* 2007). A discussion on the disadvantages of retroviral reprogramming and 'start-of-the-art' approaches is given in Chapter 1.4.3.1.2.

Table 3.1 Transduction Media

Volume or concentration	Reagent	Product
76.8 % (v/v)	Knock-out DMEM	[Invitrogen, 10829]
20 % (v/v)	Knock-out serum replacement	[Invitrogen, 10828]
1 % (v/v)	GlutaMAX™ (100x)	[Invitrogen, 35050]
1 % (v/v)	Non-essential amino acids NEAA (100x)	[Invitrogen, 11140]
1 % (v/v)	Penicillin-streptomycin (Pen/Strep). solution stabilised	[Sigma, P4458]
0.2 % (v/v)	2-Mercaptoethanol (50 mM)	[Invitrogen, 991827]
100 ng/ ml	Human fibroblast growth factor – basic (FGF2)	[Peprotech, 100-18B]
8 µg/ ml	Polybrene® (Hexadimethrine bromide)	[Sigma, 107689]
2 mM	Valproic acid	[Calbiochem, 676380]

3.2.3 Clonal Selection of hFibs

Clonal selection of hFibs was carried out by the author supervised by Dr. Lucy Crompton. After transduction, the cells were plated onto inactivated mouse embryonic fibroblasts (iMEFs), within a 9 cm diameter cell culture plate, in 3 ml transduction media containing 100 ng/ml of fibroblast growth factor 2 (FGF2) and 20 mM valproic acid (VPA). Over the following

14 days, the cells were half-fed daily; 1.5 ml of the media was removed and replaced with fresh transduction media. After 7 days, VPA was removed from the media and the cells were viewed under a fluorescent microscope [Leica, BS7270] to detect 'clumping' of GFP positive hFibs. After a further 14 days, the hFibs had clumped and swirled, forming early colonies with defined borders. The location of these colonies were marked on the bottom of the plate using a permanent marker. GFP positive colonies were manually passaged, viewed under a dissection microscope within the tissue culture hood, one colony at a time. Each colony was transferred into one well of a 6-well plate, pre-seeded with iMEFs, and cut into smaller pieces using an insulin needle. From this point, the cells were treated as independent clones and labelled by letter A-F. The passaged colony pieces were allowed to form colonies and monitored for morphology and the expression of GFP. At this point, cells are morphologically different compared to hFibs and more similar to a stem cell colony, however, they still express GFP indicating incomplete reprogramming.

The amount of FGF2 was reduced to 50 ng/ml for one week, before being reduced to 20 ng/ml. The colonies of each clone were passaged again into 6 wells of a 6-well plate after a period of two weeks had passed since the last passage. GFP expression is silenced at this point, identified by a lack of fluorescence, indicating complete reprogramming of the cells. The pluripotency was determined by analysis of morphology of the cells and colonies, alkaline phosphatase staining and fluorescent immunocytochemistry using pluripotency markers. Four of these clones were chosen for cryopreservation and two were finally selected for use in modelling FTDP-17 (Chapter 4).

Table 3.2 Table of cell lines used

Name	Type	Control or carrying mutation	Source
Shef 6	hESC	Control	UK Stem Cell Bank
Nas 2	hiPSC	Control	Prof. Kunath's lab
V337M-C	hiPSC	Carrying mutation V337M *MAPT*	Prof. Caldwell's lab
V337M-E	hiPSC	Carrying mutation V337M *MAPT*	Prof. Caldwell's lab

3.2.4 Alkaline Phosphatase Staining

hiPSC were cultured for approximately five days until medium-sized colonies had formed. The media was aspirated from the plate and cells were fixed in 4 % paraformaldehyde for 1.5

minutes. The fixative was then aspirated, the plate was washed gently with TBS-T (20 mM Tris-HCl, 0.15 M NaCl and 0.05 % Tween-20) and 1.5 ml of alkaline phosphatase stain from the alkaline phosphatase staining kit [Sigma, AP0100] was pipetted onto each plate. The plates were incubated with alkaline phosphatase stain, protected from the light, for 15-30 minutes at room temperature. The stain was then aspirated off of the cells and the cells were rinsed with TBS-T. Epsom scanning software was used obtain images of the plates. Pink colonies indicate pluripotent cells, whereas non-coloured cells represent differentiated cells.

3.2.5 Fluorescent immunocytochemistry

Immunocytochemistry was carried out as detailed in Chapter 2.2.2.

Table 3.3 Antibodies for characterisation of hiPSC

Antibody	Code and manufacturer	Concentration	Species	Details
SSEA4	ab16287, Abcam	1:300	Mouse	IgG3, monoclonal
Tra-1-60	ab16288, Abcam	1:300	Mouse	IgM, monoclonal

3.2.6 Karyotyping

hiPSC were cultured almost to confluence within a 25cm^3 flask in the E8 system and sent live to The Doctors Laboratory Ltd. for karyotypic analysis to ensure sound chromosomal integrity after reprogramming.

3.2.7 Genotyping

A 25 cm^3 flask of V337M *MAPT* hFibs was grown until confluent. The media was aspirated and the cells were washed twice with PBS to remove traces of media. The 25 cm^3 flask was stored overnight in a -80 ^{o}C freezer to aid the lysis of cells. The next day lysis buffer [10 mM Tris-HCl pH 7.5-8, 10 mM EDTA, 10 mM NaCl, 0.5 % SDS, 18 µg/ml Proteinase K (Roche, 03115887001)] was added to the cells. The flask was then incubated overnight in a humified incubator set to 55 ^{o}C. 2 x the volume of -20 ^{o}C ethanol/salt solution (75 mM NaCl in 100%, ethanol) was added to the flask and the flask was placed on an orbital rocker for 30 minutes to elute the DNA from the cells. Genomic DNA (gDNA) could be seen, precipitated within the liquid in the flask. The liquid and gDNA was removed from the flask and placed into a 15 ml falcon tube and centrifuged at 4000 g for 10 minutes. The supernatant was removed from

the falcon tube leaving a gDNA pellet, which was then washed twice with 100 % ethanol. The gDNA was then carefully removed with a pipette tip and placed into an Eppendorf tube. All excess liquid was removed and the pellet was allowed to air dry within the tube for 15 minutes at room temperature. 250 µl of TE buffer (Tris 10 mM, EDTA 1 mM, pH 8) was then added to the gDNA at room temperature and the DNA was allowed to resuspend after pipetting for 1 hour. Samples were then haplotyped in Dr Roger Barker's lab, Brain Repair Centre, Cambridge, UK.

3.2.8 Maintenance of hiPSC

hiPSC were maintained on either iMEFs or within the Essential 8^{TM} system as described in Chapter 2.1.2.1 and 2.1.2.2, respectively.

3.3 Results

3.3.1 Characterisation of pluripotency

Characterisation of hiPSC is essential to verify that pluripotent stem cells have been created. This was achieved through observation of the morphology of the cells and the colonies that they form. True hiPSCs should resemble pluripotent hESCs, and both the V337M-E and V337M-C hiPSC lines displayed hESC-like morphology; colonies had defined edges and consisted of small, round cells with a large proportion of each cell taken up by its nucleus (Vallier *et al.,* 2004). Similar to hESCs, cells within the V337M-E and V337M-C hiPSC lines were compact within the colonies (Vallier *et al.,* 2004). Shef 6 was used to compare the morphology of the cells within the colonies of Tau-V337M hiPSC. All cells within the colonies expressed both Tra-1-60 and Stage-Specific Embryonic Antigen-4 (SSEA4) (Figure 3.2), which are gold-standard markers of pluripotency. Colonies of each line also contained cells with a high level of alkaline phosphatase activity, which is also indicative of pluripotency.

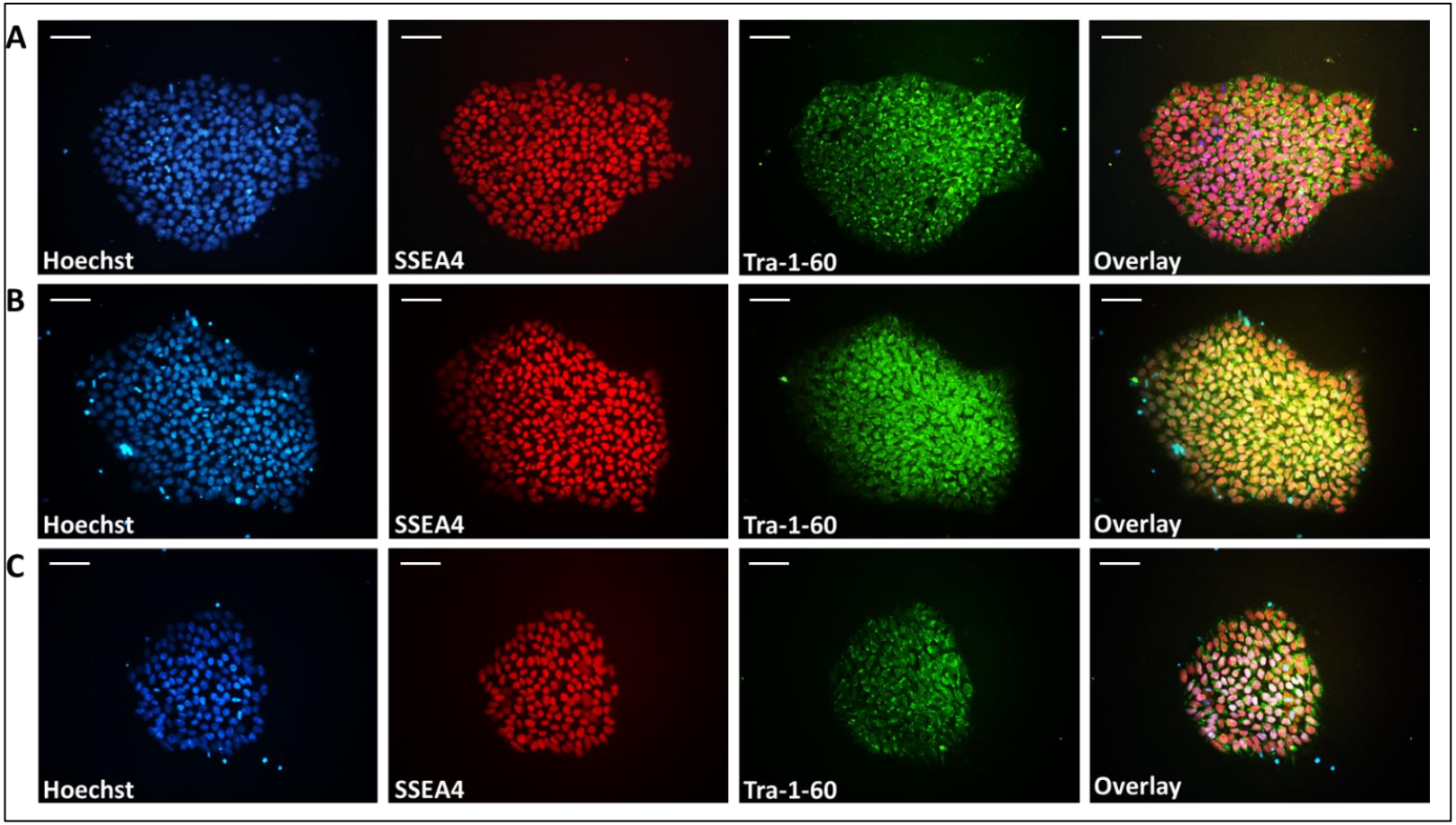

Figure 3.2 Morphology and immunocytochemical staining of V337M hiPSC and Shef 6 hESC colonies

Cells within colonies of V337M-C-hiPSC (A), V337M-E-hiPSC (B) and Shef 6-hESC (C) immunostained using Hoechst nuclear stain (blue), Anti-SSEA 4 (red) and Anti-Tra-1-60 (green). In the far right-hand side panels the overlay of this immunostaining is demonstrated. Each cell line expresses the two markers of pluripotency within each cell of its colony and colonies have well defined edges. The nucleus occupies a large proportion of each cell. Scale bars indicate 50 µM.

Figure 3.3 Colonies of V337M-C and V337M-E hiPSC express high levels of alkaline phosphatase

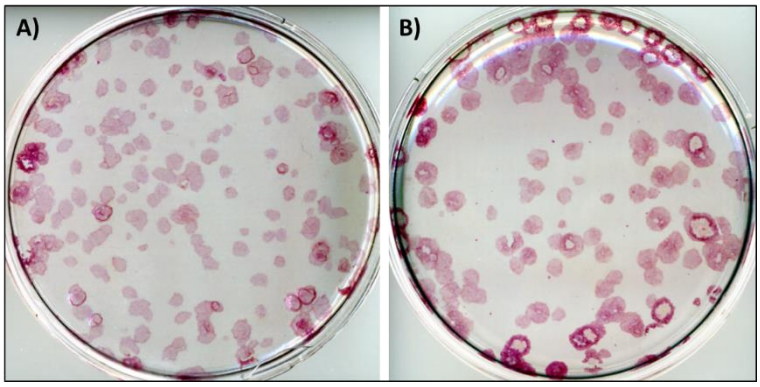

Figure 3.3 Colonies of V337M-C and V337M-E hiPSC express high levels of alkaline phosphatase

Alkaline phosphatase staining demonstrating colonies of V337M-C hiPSC (A) and V337M-E hiPSC (B) expressing high levels of alkaline phosphatase, as illustrated by pink colonies. Non-uniform colonies are those that have been manually pruned to remove any cells that may be differentiating to ensure the stability of the culture.

3.3.2 V337M *MAPT* lines have normal karyotypes

The process of reprogramming carries a small risk of introducing chromosomal abnormalities and through the culture of hiPSC culture these can be introduced. Therefore, the karyotypes of these cells were examined. No abnormalities were seen within the chromosomes of V337M-C-hiPSC or V337M-E-hiPSC with karyotyping (Figure 3.4), indicated by matching pairs of 23 chromosomes, each with appropriate chromosomal size and shape.

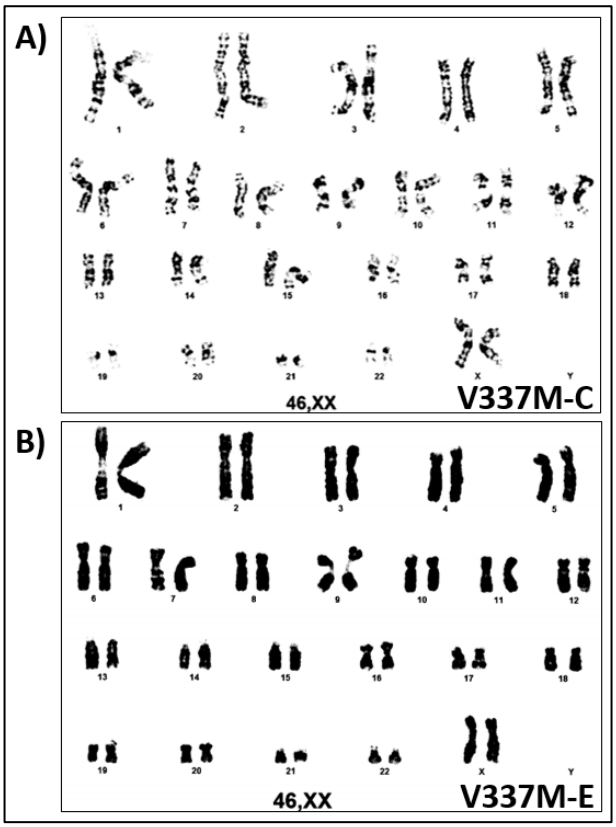

Figure 3.4 Karyotyping of V337M-C and V337M-E hiPSC

No chromosomal abnormalities were revealed by karyotyping in either V337M-C (A) or V337M-E (B) hiPSC, as indicated by the presence of matching pairs of 23 chromosomes, each with appropriate chromosomal size and shape.

3.3.3 V337M *MAPT* hiPSC are homozygous H1

MAPT can exist as one of two haplotypes, H1 or H2. Both of these are associated with the development of tauopathy and are described in Chapter 1 (Chapter 1.1.1.2). The patient fibroblasts used to generate these hiPSC were genotyped to understand whether they carry the H1 or H2 haplotypes of *MAPT.* The fibroblasts were found to be homozygous H1, therefore, hiPSC carrying V337M *MAPT* are also homozygous H1. Shef 6 hESC lines are also homozygous H1 (Sposito *et al.,* 2015).

3.3.4 Summary

HiPSC lines V337M-C and V337M-E exhibit morphology consistent with pluripotency, express hallmark pluripotency markers and have high levels of alkaline phosphatase, indicative of pluripotency. Genotyping of these lines revealed that these hiPSC have the H1 haplotype, the significance of which in tauopathy is described in Chapter 1 (Chapter 1.1.1.2). These results indicate that reprogramming was successful and that hiPSC have been derived, therefore, these lines are suitable for the development of hiPSC-neuron models.

Chapter 4

The development of a model of frontotemporal dementia with Parkinsonism linked to chromosome 17 using induced pluripotent stem cell technology

4.1 Introduction

The molecular pathways underlying tau pathogenesis is an area of intense research as improved comprehension of these of these may facilitate the development of effective therapeutics. Inferences gained through investigating the pathways affected by specific *MAPT* mutations may provide valuable knowledge on the pathogenesis of tau, applicable to sporadic tauopathies as well as to those that are heritable. Neurodegenerative diseases caused by mutations in *MAPT* are termed frontotemporal dementia with Parkinsonism linked to chromosome 17 (FTDP-17). The clinical presentation, pathology and known mutations of FTDP-17 are described in Chapter 1 (Chapter 1.2.2).

To develop a model with the potential to allow research into the initial pathogenic events that occur due to *MAPT* mutations, induced pluripotent stem cell (iPSC) technology was used to develop a model of FTDP-17. The work in this chapter describes the differentiation of hiPSC, derived from a patient carrying V337M *MAPT*, to produce cortical glutamatergic neurons (CGN), which are particularly vulnerable in FTD (Chapter 1.2.2). Current knowledge of the specific pathology and symptoms associated with this mutation are discussed below (Chapter 4.1.1). Two cell lines, V337M-C and V337M-E, were derived from a patient carrying the mutation Val337Met (V337M) *MAPT* (Chapter 3) and differentiated alongside a human embryonic stem cell (hESC) control line (Shef 6) and a hiPSC control line (Nas 2), to produce these neurons.

At the start of this project, the gold standard in experiments using iPSC was to include a hESC line, which is why an hESC line was included in these experiments. The western blotting results included in this chapter use one control line, Shef 6 hESC or Nas 2 hiPSC, and one line

carrying V337M *MAPT,* V337M-C or V337M-E, on each blot allowing for comparison between controls and cells carrying the mutation on the same blot. Unfortunately, a control was not included to allow for comparison of results from western immunoblots containing Shef-6-CGN and V337M-E-CGN samples with western immunoblots containing Nas-2-CGN and V337M-C-CGN samples. Samples from lines Shef 6 and V337M-C were used for gene expression analysis as it was not possible to gain enough CGNs from V337M-E and Nas 2 to carry this out.

To characterise changes in tau protein due to the mutation, the levels of tau protein, expression of *MAPT* and phosphorylation of tau at sites associated with tauopathy were investigated. The levels, activity and gene expression of key tau kinases, thought to be involved in deregulated hyperphosphorylation of tau in patients with FTDP-17 and other tauopathies (Chapter 1.3), were also investigated to interrogate the molecular pathways underlying early pathogenesis.

4.1.1 Val337Met *MAPT*

V337M *MAPT* is a rare, missense mutation also referred to as the 'Seattle family A' mutation after the family in which it was first discovered (Poorkaj *et al.,* 1998). V337M *MAPT* is caused by a change in the amino acid (aa) valine to methionine at position 337 within exon 12. Although we do not completely understand how this mutation results in tauopathy, valine at 337 of *MAPT* is present in other tau protein homologues and is highly conserved (Poorkaj *et al.,* 1998) alluding to its importance in tau's function.

Recent research has described patients with this mutation as presenting as young as in their 30's but more typically in their 50's with a disease duration of approximately 10 years (Spina *et al.,* 2017; Bird *et al.,* 1997; Poorkaj *et al.,* 1998; Domoto-Reilly *et al.,* 2017; Sumi *et al.,* 1992). Patients present initially with irritability, compulsive behaviour and mental inflexibility (Spina *et al.,* 2017). As the disease progresses, hallmark symptoms of behavioural variant frontotemporal dementia (bvFTD) are observed including loss of inhibition, antisocial behaviour, paranoia and loss of empathy (Ghetti *et al.,* 2015; Spina *et al.,* 2017; Bird *et al.,* 1997; Poorkaj *et al.,* 1998; Sumi *et al.,* 1992). In the later stages, language problems become apparent alongside dementia, which includes disturbance in memory, episodic function and loss of semantic knowledge (Spina *et al.,* 2017).

The mutation results in symmetrical frontotemporal atrophy (Connell *et al.,* 2001; Spina *et al.,* 2017) (Figure 4.1). Tau aggregates, including neurofibrillary tangles (NFTs), are present in the highest density within the medial frontal lobes and to a lesser extent within the lateral temporal lobes (Spina *et al.,* 2017; Sumi *et al.,* 1992; Spillantini *et al.,* 1996). Neurodegeneration also has been reported in parahippocampus, amygdala and neocortical areas (Sumi *et al.,* 1992; Spina *et al.,* 2017).

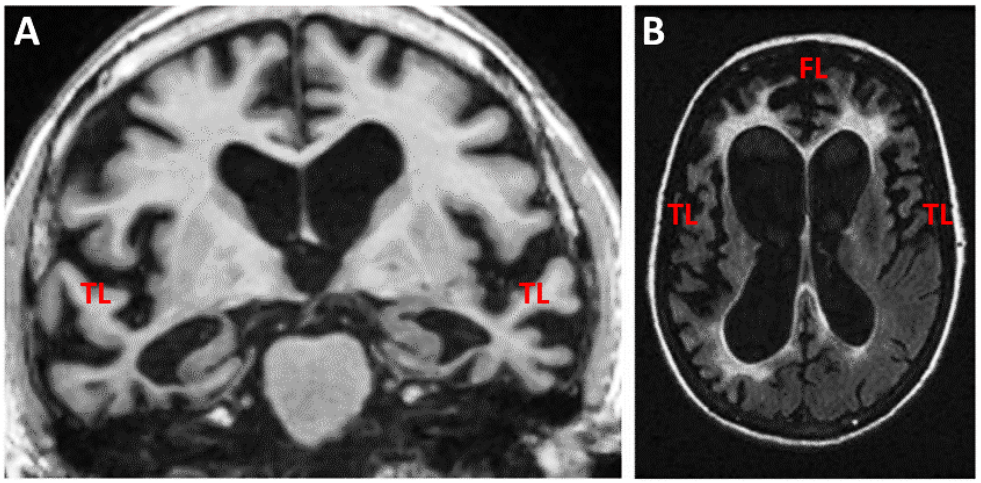

Figure 4.1 MRI images of the brains of two patients with V337M MAPT

(A) MRI scan showing coronal section of a 65 year old male patient with FTDP-17 caused by V337M MAPT mutation. His symptoms evolved over 20 years. The MRI shows moderate to marked, bilateral frontal and temporal cortical atrophy as well as severe anterior temporal lobe atrophy. Image adapted with permission from Ghetti et al., 2015 © 1999 – 2017 John Wiley and Sons, Inc.

(B) MRI scan showing transverse section of a 58 year old male patient with V337M MAPT. Image adapted with permission from Spina et al., 2017 © 2017 American Academy of Neurology.

Degeneration within the hippocampus is spared even when tau aggregates are present within the region (Spina *et al.,* 2017). This suggests that the molecular events resulting in degeneration due to this mutation occur before the aggregation of tau. Indeed, in V337M *MAPT* Tg drosophila, no filamentous tau aggregates could be identified in neurons despite neurodegeneration, suggesting that tau-induced neurodegeneration is not dependent on the aggregation of filamentous tau (Wittmann, 2001). Considerable variability in the clinical presentation and neuropathology of the disease has been reported, akin to FTDP-17 caused by other *MAPT* mutations (Larner and Doran, 2008). For example, Spina and colleagues demonstrated the presence of amyloid pathology, which is not normally observed, within the

brain of a member of a V337M *MAPT* family (Spina *et al.,* 2017). Additionally, Domoto-Reilly and colleagues reported one member of a family with V337M *MAPT* presenting with an unusually long duration of disease and delayed penetrance (Domoto-Reilly *et al.,* 2017). This patient was found to carry the ApoE genotype E2/E3, thought to be protective in neurodegenerative disease (Liu *et al.,* 2013), implicating the influence of other genetic factors in the heterogeneity of this disease (Domoto-Reilly *et al.,* 2017).

The NFTs in the brains of individuals with this mutation are composed of straight and paired helical filaments (PHF) of tau composed of all six isoforms of tau (Poorkaj *et al.,* 1998; Sumi *et al.,* 1992; Spillantini *et al.,* 1996; Ghetti *et al.,* 2015). Aggregations of tau are found mainly in neurons of V337M *MAPT* patient brains (Brandt *et al.,* 2005) and are similar in structure to those recognised in AD (Kidd *et al.,* 1963; Goedert *et al.,* 1989). The mutation has no effect on the splicing of exon 10 of *MAPT* (Ehrlich *et al.,* 2015; Brandt *et al.,* 2005), therefore, tau hyperphosphorylation within the brains of patients with this mutation is not initiated through an alteration in the ratio of 4R:3R isoforms of tau.

The mutation encourages aggregation of tau, which may explain the formation of NFTs in the brains of patients with V337M *MAPT.* Tau with this mutation forms filaments upon heparin treatment, *in vitro,* after incorporation of 4-6 moles of phosphate per mole of tau protein, whereas wild type (WT) tau will not form filaments until approximately 10 moles of phosphate per mole of tau have been incorporated (Arawaka *et al.,* 1999). Tau inclusions in the brains of these patients stain for tau within an abnormal conformation associated with early tauopathy (Sumi *et al.,* 1992), however, it is not clear how the mutation causes tau to become hyperphosphorylated. Importantly, V337M *MAPT* does not create additional phosphorylation sites in tau protein, therefore, the resultant hyperphosphorylation of tau due to this mutation must involve downstream molecular pathways triggered by this mutation (Brandt *et al.,* 2005). These pathways are unclear; however, studies have been undertaken to understand whether this mutation can affect the susceptibility of tau to be phosphorylated by tau kinases, including GSK3β and Cdk5 (Connell *et al.,* 2001; Han *et al.,* 2009) or the activity of tau kinases (Lambourne *et al.,* 2005).

One mechanism through which tau mutations are thought to cause neurodegeneration is by impairing the ability of tau protein to stabilise microtubules. Several studies have been carried out to examine the effect of V337M *MAPT* on the ability of tau to bind and stabilise microtubules. In cell free, *in vitro* systems, V337M *MAPT* reduces the affinity and binding

capacity of tau to microtubules (Hasegawa *et al.,* 1998; Dayanandan *et al.,* 1999; Rizzu *et al.,* 1999; Hong *et al.,* 1998) and the ability of tau to facilitate microtubule polymerisation (Hong *et al.,* 1998; Hasegawa *et al.,* 1998). V337M tau has also been shown to disrupt microtubule organisation within non-neuronal mammalian (Arawaka *et al.,* 1999) and insect (Frappier *et al.,* 1999) cells. In a baculovirus system, expression of V337M *MAPT* tau led to fewer microtubules per process and altered microtubule spacing (Frappier *et al.,* 1999).

4.1.2 Aims

The aim of the work in this chapter was to develop and probe a hiPSC-model of V337M *MAPT* FTDP-17 and to investigate the ability of the model to be used to gain insight into the influence of V337M *MAPT* on total tau levels, tau phosphorylation at sites associated with tauopathy and the expression of *MAPT*. The protein levels, activity and gene expression levels of tau kinases associated with tauopathy were also investigated.

4.2 Methods

4.2.1 Use of Tg4510 mice for antibody screening

Tg4510 mice were used to optimise tau antibodies used within this thesis project. Tg4510 mice overexpress human mutant P301L *MAPT* 4R0N tau (Ramsden *et al.,* 2005; Santacruz *et al.,* 2005). Expression is mostly restricted to neurons of the forebrain, driven by the Ca^{2+}-calmodulin kinase II promoter, and can be suppressed by treatment with doxycycline (Denk and Wade-Martins, 2009; Santacruz *et al*., 2005). Tg4510 mice develop severe NFT pathology in the form of pre-tangles from 2.5 months of age and argyrophilic tangle-like inclusions from 4 months of age onwards, which dramatically worsens with age (Santacruz *et al.,* 2005).

These mice are ideal for optimisation of a panel of tau antibodies for western immunoblotting for number of reasons: firstly, these mice develop prominent tau pathology and this tau pathology is well characterised (Ramsden *et al.,* 2005; Santacruz *et al.,* 2005; Song *et al.,* 2015); secondly, many of these antibodies have previously been used to investigate tau phosphorylation of tissue from these mice allowing for comparison of the results obtained in this study (Song *et al*., 2015; Ramsden *et al*., 2005; Santacruz *et al*., 2005); thirdly, this transgenic mouse model expresses human tau thereby ensuring that the antibodies are capable of detecting human tau.

A panel of tau antibodies was optimised for probing western blots to ensure their suitability for use in the experiments. Antibodies DA9, PHF-1, CP13 and RZ3 have been used previously to establish the pathology within post-mortem brain tissue of Alzheimer's patients (Luna-Munoz *et al.,* 2007). Basal forebrain, hippocampus and cortex tissue from a well-established FTDP-17 murine model, Tg4510, at 5 and 10 months of age was western immunoblotted alongside tissue from aged matched wild type (WT) mice.

All animal tissues were supplied from Eli Lily, where animals were maintained and treated under the Home Office's animals (Scientific Procedures) act 1986 and in agreement with the University of Bristol Animal Welfare and Ethical Review Body guidelines. Female animals were euthanised at 5 months and 10 months of age according to the schedule 1 method of cervical dislocation and brain tissue was immediately removed and frozen for histological or molecular analysis.

4.2.2 Differentiation of human pluripotent cells to produce cortical glutamatergic neurons

This protocol describing the derivation of cortical glutamatergic neurons (CGNs) from human pluripotent stem cells (hPSC) has been adapted from work carried out within the Livesey Lab (University of Cambridge) (Shi *et al.,* 2012) to allow for the derivation of these cells from hiPSC cultured within the E8 culture system (Chapter 2.1.2.2).

During neural development, glutamatergic projection neurons, which go on to form the cerebral cortices affected in FTD, are formed in a stereotyped temporal order, whereby deep layer neurons are produced first and upper layer neurons last (Mountcastle, 1998). The use of dual Smad (Sma and Mad Related family) pathway inhibition in this protocol directs the differentiation of hiPSC firstly into cortical stem and progenitor cells, which then undergo the same temporal process of differentiation and neurogenesis recognised during development to generate projection neurons of all layers of the cerebral cortex, in appropriate proportions (Shi *et al.,* 2012).

LDN-193189 and SB431542 are the two small molecule Smad inhibitors used in this protocol. LDN-193189 is a cell permeable inhibitor of BMP type I receptors ALK2 and ALK3 (Yu *et al*, 2008). SB421542 is a potent and selective inhibitor of the TGFβ type I receptor activin receptor-like kinase ALK5, and its relatives ALK4 and ALK7 (Inman *et al.,* 2002). Additional information on the roles of dual Smad inhibition is detailed in Chapter 1.4.3.1.4.

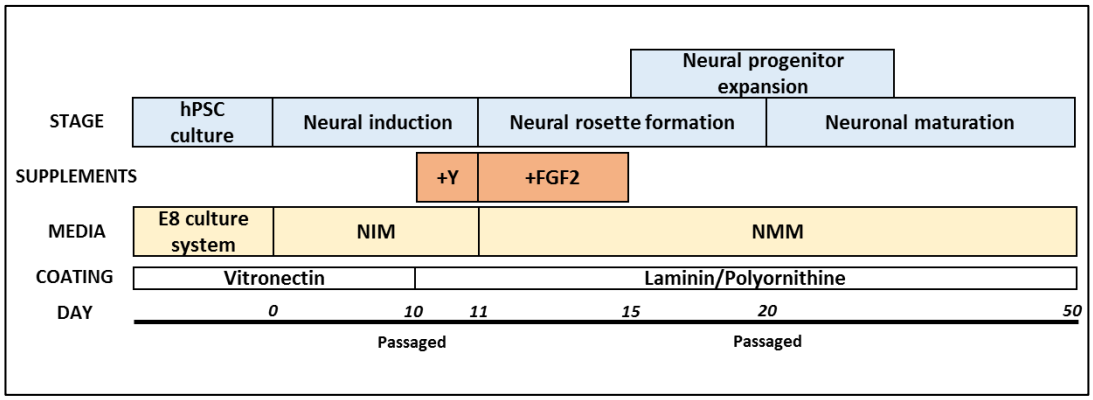

Figure 4.2 Schematic detailing the protocol used for the derivation of cortical glutamatergic neurons from human pluripotent stem cells

Y= Y-27632 (ROCK inhibitor). The protocol can be divided into five stages; hPSC culture, neural induction, neural rosette formation, neural progenitor expansion and neuronal maturation. hPSC are first cultured, on truncated Vitronectin (VTN-T)-coated 6-well plates within the Essential 8 (E8) culture system, to gain a culture of healthy pluripotent stem cell colonies at 50-70 % confluency and these cells are cultured in neural induction media (NIM) to direct them to differentiate into cells a neural lineage. The start of neural induction is considered to be 'day 1'. Once a monolayer of neuroepithelial cells has formed, the cells are passaged onto plates pre-coated with polyornithine-laminin (POL) before being cultured within neural maturation media (NMM) supplemented with fibroblast growth factor 2 (FGF2) for 4 days. After this period, the cells are cultured in NMM for the duration of the protocol and are passaged once more at day 20.

4.2.2.2 Media used during the derivation of cortical glutamatergic neurons

Table 4.1 Components of Neural Maintenance Media (NMM)

Product	Amount	Supplier and product code
Advanced DMEM/F12	47.5 %	Life Technologies, 12634028
Neurobasal	47.5 %	Life Technologies, 21103049
B27 supplement	2 %	Life Technologies, 17504044
N2 supplement	1 %	Life Technologies, 17502048
Penicillin-Streptomycin solution stabilised (Pen-Strep)	1 %	Sigma, P4458
GlutaMAX™ (100x)	1 %	Invitrogen, 35050
2-Mercaptoethanol (50mM)	0.2 %	Invitrogen, 991827
Insulin solution (from bovine pancreas) (stock solution 10 mg/ml)	0.025 %	Sigma, I0516

Table 4.2 Components of Neural Induction Media (NIM)

Product	Amount	Supplier and product code
Neural Maintenance Media	To 100%	As above
LDN-193189	1 ng/ml	[Sigma–Aldrich, SML0559]
SB431542 (Selective inhibitor of activin receptor-like kinase, TGF-beta type I receptor)	10 µM	[Tocris, 1614]

4.2.2.3 Neural Induction

Human pluripotent stem cells (hPSP) were cultured in xeno-free and feeder-free culture conditions, within the wells of 6-well plates [Fisher, 10098870]. The cells were cultured in the E8 culture system [LifeTechnologies, A1517001], in which cells are cultured within E8 media on truncated Vitronectin [VTN-N; LifeTechnologies, A14700] (Chapter *2.1.2.2.1.3*) coated plastic surfaces (Chapter 2.1.2.2.1.3). Cells were cultured in 2 ml of media, which was removed and replaced with fresh media each day. Once a monolayer of 50-70 % confluence had been achieved, which takes approximately 4 days after initial passaging of hiPSC colonies, the media was changed to neural induction media (NIM), containing the Smad inhibitors LDN-193189 and SB431542. This day of the protocol is referred to as day 1. Cells were cultured within this media for 10 days allowing for the formation of a uniform monolayer of cells consisting of cells with small, round nuclei, indicating neuroepithelial cells, as opposed to large, round nuclei, indicative of hiPSC and hESC (Shi *et al.,* 2012).

At this point, cells were dissociated by adding 250 µl of 37 °C Dispase stock, consisting of 10 mg/ml Dispase [Life Technologies, 17105] in PBS, directly to the cell culture media and incubating for 7 minutes at 37 °C. After incubation, the monolayer was broken into aggregates of 300-500 cells by pipetting with a P1000 pipette three times. The media containing the aggregates was collected into a 15 ml falcon tube and the aggregates were allowed to settle into the bottom of the tube before the media was aspirated. The aggregates were resuspended in 1 ml of NIM, supplemented with 10 ng/ml Rho-associated protein kinase (ROCK) inhibitor (Y-27632) [Tocris, 1524] to inhibit cell apoptosis. The clumps of cells were passaged into wells of a 6-well plate pre-coated with poly-L-ornithine and laminin (POR/L) (Chapter 2.1.2.2.1.4) containing 1.7 ml of NIM, supplemented with 10 ng/ml Y-27632, by adding 330 µl of the resuspended cell aggregate mixture to each well to achieve a passaging ratio of 1:3.

4.2.2.4 Neural Rosette Formation

The cells were allowed to adhere onto the cell surface overnight, after passaging on day 10, and the next day the media was replaced with neural maintenance media (NMM) supplemented with human fibroblast growth factor 2 (FGF2) [PeproTech, 100-18B]. The media was replaced every day and FGF2 was kept in the media until day 15. FGF2 has an important role in the differentiation, development and function of the central nervous system (CNS) (Woodbury and Ikezu, 2014) and its expression co-occurs with neurogenesis in the developing brain (Powell *et al.,* 1991). In this protocol, it is added to media after neural induction to stimulate neurogenesis (Shi *et al.,* 2012). Neural rosette structures formed between days 11-19, observed using an inverted microscope.

4.2.2.5 Terminal differentiation and maturation of neurons

The rosettes were allowed proliferate and differentiate to produce neural progenitors and neurons for the duration of the protocol, for which they were maintained in NMM and fed every day. Between day 20-30 substantial neurogenesis is observed. Between days 20-23, the cultures were passaged and re-plated to continue differentiation, to plate cells for immunocytochemistry and to allow for cryopreservation (Chapter 4.3.1.6). After day 30, 2 µg/ml laminin, from Engelbreth-Holm-Swarm murine sarcoma basement membrane [L2020, Sigma], was added to the media on one day each week, to prevent detachment of neurons from the culture surface (Nistor *et al*., 2015).

4.2.2.6 Passaging cells at day 20-23

Between day 20-23 the neural progenitor and neuron cultures were passaged using Accutase™ [Sigma, A6964], which is a gentle enzyme mixture with proteolytic and collagenolytic enzyme activity. After the media was aspirated from the cells, the cells were washed gently with PBS once, and 1 ml of Accutase™ was added to each well. The cultures were incubated in Accutase™ for 1-2 minutes at 37 ^{o}C. After the incubation period, 4 ml of 37 ^{o}C NMM, supplemented with Y-27632 to prevent apoptosis, was added to each well to quench the Accutase™ and the media was gently pipetted to detach the cells from the culture surface. The cell suspension was added to a 15 ml falcon tube and centrifuged (200 g; 5 minutes). For re-plating, the cells were resuspended in NMM supplemented with 10 ng/ml Y23532 to inhibit apoptosis, gently pipetting with a P1000 pipette to ensure a fully dissociated cell suspension, counted and plated at a concentration of 50000 cells/cm^2 onto

either POR/L pre-coated 6-well plates or POR/L pre-coated glass coverslips within 4-well plates for subsequent immunocytochemistry. For cryopreservation, the cell pellet collected was re-suspended in neural stem cell cryopreservation media (1260 µl E8 media supplemented with 10 ng/ml Y23532 and 140 µl Dimethyl sulfoxide (DMSO)) at a concentration of $2x10^6$ cells/ml and the cell suspension was divided equally between two sterile cryovials [Greiner Bio One, 123278] and frozen at -80 ^oC within a Mr. Frosty™ freezing container (Chapter 2.1.3.2.1).

4.2.3 Immunocytochemistry

Cells were washed once with PBS and 200 µl of room temperature, 4 % paraformaldehyde (PFA) was added to the cells. The cells were incubated with PFA for 15 minutes before the PFA was removed and the cells were washed gently three times with PBS to ensure residual PFA was removed. Non-specific binding of proteins was blocked by incubation of the cells for 1 hour, or overnight, in blocking/permeabilisation solution (Chapter 2.2.2.1). Upon completion of the incubation period the blocking/permeabilisation solution was removed and the primary antibody was added. The cells were incubated with the primary antibody (Table 4.4) overnight before being washed gently three times with PBS. Primary and secondary antibodies were prepared and diluted in 1 % HS, in 0.1 % TX-PBS. The secondary fluorophore antibody was then added and incubated for two hours, protected from the light, at room temperature on a rocking plate. After the two hour incubation period, the cells were washed with PBS for five minutes on a rocking table, three times. After the final aspiration of the washing liquid, the glass coverslips were carefully lifted from the wells and placed facing down-wards onto a droplet of Vectorshield™ on a glass slide. The circumference of the coverslips were sealed with clear nail varnish and allowed to dry overnight, protected from the light.

4.2.4 Western Immunoblotting

A panel of tau antibodies, including PHF-1, DA9, CP13 and RZ3 was first assessed in Tg 4510 mice (Chapter 4.3.1). After assessment and optimisation of the western blotting protocols, required to achieve clear results using these antibodies, a complement of antibodies was used to probe hPSC-neuron lysates via western immunoblotting (Table 4.4). Western blotting protocols described in Chapter 2.2.1 were followed. The bands analysed by densitometry were normalised to those created through probing with anti-GAPDH for each

result. The western immunoblots shown within figures in this chapter are representatives of the three western immunoblots carried out for each result. For phosphorylated tau antibodies, density of bands after normalisation to GAPDH were also compared to those for total tau after normalisation to GAPDH. Where multiple bands were produced through probing with anti-tau antibodies, all bands were included in the densitometric analysis. Analysis of PAK3 levels included only bands at 65 kDa. For analysis of synapsin levels only bands at 75 kDa were included. For p25 and p35 level analysis, only bands at 25 kDa and 35 kDa, respectively, were included in analysis. For analysis of the levels of GSK3β and pTyr216 GSK3β, only bands at 48 kDa and 52 kDa were included in analysis.

Table 4.3 Primary antibodies in immunocytochemistry and western immunoblotting

Primary antibody	Protein detected	Host	Source and catalogue number	References	Dilutions	
					Western	ICC
Akt pSer273	pSer273 Akt	Rabbit	9271, Cell Signalling	(Ksiezak-Reding *et al.,* 2003)	1:500	N/A
βIII Tubulin	βIII Tubulin	Mouse	ab6046, Abcam	(Huidong *et al.,* 2015)	N/A	1:1000
CP13	pSer202 tau	Mouse	Prof. Davies*	(Petry *et al.,* 2014; Vingtdeux, *et al.,* 2011)	1:1000	N/A
DA9	Pan-tau	Mouse	Prof. Davies*	(Petry *et al.,* 2014)	1:5000	N/A
GAPDH	GAPDH	Mouse	AM4300, Invitrogen	(de Oliveira *et al*., 2017)	1:5000	N/A
GSK3β	GSK3β	Rabbit	D5C5Z, Cell Signalling	(Burk *et al.,* 2017)	1:500	N/A
GSK3β pTyr216	pTyr216 GSK3β	Rabbit	ab75745, Abcam	(Porquet *et al.,* 2015; Rui *et al.,* 2013)	1:500	N/A
p25-p35	p25-p35	Rabbit	C64B10, Cell Signalling	(Porquet *et al.,* 2014)	1:300	N/A
PAK3	PAK3	Rabbit	2609S, Cell Signalling	(Murata and Constantine-Paton, 2013)	1:300	N/A
PHF-1	pSer396/pSer404 tau	Mouse	Prof. Davies*	(Otvos *et al.,* 1994)	1:5000	N/A
PSD-95	PSD-95	Mouse	ab2723, Abcam	(Frandemiche *et al.,* 2013)	1:1000	1:300
RZ3	pThr231	Mouse	Prof. Davies*	(Vingtdeux *et al.,* 2011)	1:250	N/A
Synapsin	Synapsin I	Rabbit	ab64581, Abcam	(Stefanova *et al.,* 2016)	1:750	1:300
RD3	3R tau	Mouse	05-803, Merck Millipore	(de Silva et al., 2003)	1:1000	N/A
RD4	3R tau	Mouse	05-804, Merck Millipore	(de Silva et al., 2003)	1:100	N/A

*Prof. Peter Davies (Albert Einstein College of Medicine, New York, USA) kindly supplied CP13, DA9, PHF-1 and MC1 antibodies.

4.2.4.1 Preparation of mouse brain tissue lysates

Mouse hippocampal or cortical brain areas, from control or Tg4510 mice were homogenised, in 10 µl per mg of tissue in ice cold RIPA buffer (Chapter 2.2.1.1) plus one tablet of Protease Inhibitor [Roche, cOmplete Mini, 04693] per 10 ml of RIPA buffer and one tablet of Phosphatase Inhibitor PhosStop, [Roche] per 10 ml. To homogenise, the tissue was firstly compressed using a sterile plastic disposable 1.5 ml microtube pestle 20 times. The tissue was then passed through a series of sterile, disposable needles of descending size, from 14 gauge to 20 gauge, attached to a sterile syringe. The resultant crude homogenate was centrifuged at 11,000 g for 15 minutes at 4 ^{o}C to clarify it by removing any remaining non-homogenated brain tissue. The homogenates were kept on ice throughout this process and used immediately in western blotting or stored immediately at -80 ^{o}C.

4.2.5 qPCR

Shef 6-CGNs and V337M-C-CGNs were cultured after terminal differentiation to maturity before being collected and processed to extract and purify RNA. See Chapter 2.2.3 for details of the protocols used for extraction and purification of RNA from hPSC-CGN cultures, conversion into cDNA, qPCR and analysis of the results. A list of the Taqman® probes used during this chapter are detailed in Table 2.13 and include probes against *GSK3β*, *CDK5*, *MAPT*, *PAK3* and also *GAPDH,* which was used as a quantitative control for analysis.

To calculate the average relative gene expression, the cycle threshold (CT) values (Chapter 2) for each gene were normalised to those gained through qPCR using the probe against *GAPDH* and each result was normalised against the average of Shef 6-CGNs, which was used as the healthy control for these experiments. Statistical analysis of qPCR data in this chapter was performed using a Mann-Whitney test.

4.3 Results

4.3.1 Optimisation of a panel of tau antibodies for western immunoblotting

Figure 4.3 Western immunoblots of Tg4510 mice basal forebrain, cortex and hippocampus with tau antibodies

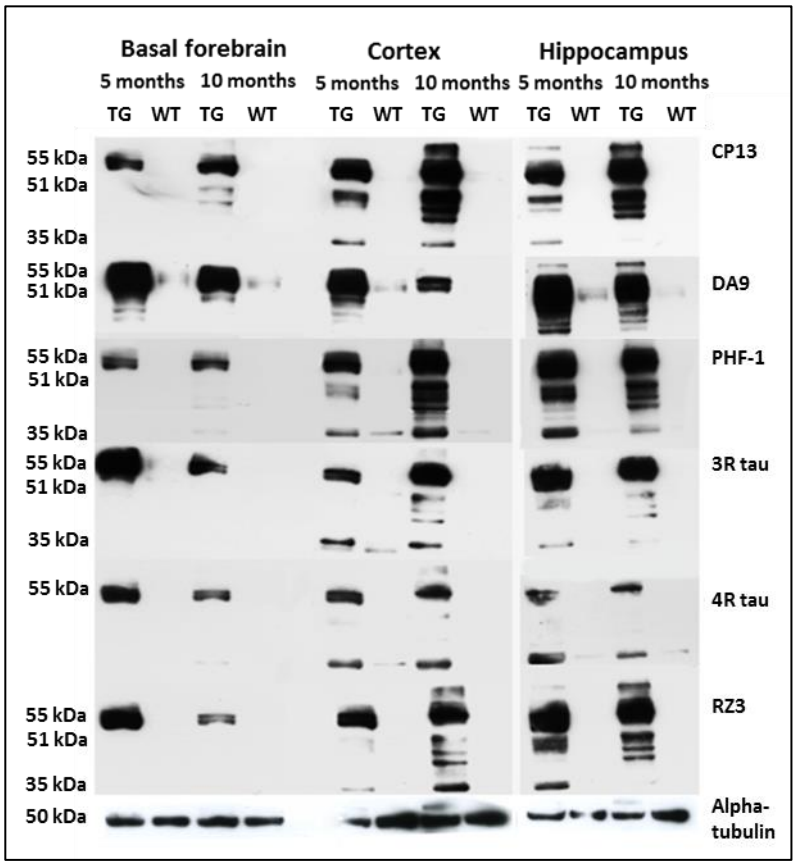

Figure 4.3 Western immunoblots of Tg4510 mice basal forebrain, cortex and hippocampus with tau antibodies

Western immunoblots of Tg4510 mice and WT mice basal forebrain, cortex and hippocampus at ages 5 months and 10 months probed using antibodies CP13, DA9, PHF-1, 3R tau, 4R tau and RZ3 alongside alpha-Tubulin, which is used as a loading control antibody to allow for the consideration of the total amount of protein loaded.

Western immunoblots using antibodies CP13, PHF1, RZ3, DA9, 4R tau, 3R tau and α-Tubulin as a control antibody, demonstrate clearly that tau pathology is more prominent in the hippocampus, cortex and basal forebrain of Tg mice compared to WT mice (Figure 4.3). Tau pathology in Tg4510 mice begins within the cortex (Santacruz et. al., 2005); therefore, it is

unsurprising that the immunoblots indicate the greatest staining, using total and phosphorylated tau antibodies, within the cortex of these mice.

DA9 detects both dephosphorylated and phosphorylated tau, therefore is an antibody used to detect total tau. In 10 month old Tg4510 mice, immunoblotting for DA9 is decreased in comparison to 5 month old mice, which likely corresponds to the gross neurodegeneration observed at 10 months in a previous study (Spires *et al*., 2006).

CP13 detects pSer202 tau, which is associated with early phosphorylated tau pathology (Luna-Muñoz *et al.,* 2007) and the immunoblots indicate greater amounts of this form of tau especially in the cortex and hippocampus of Tg mice, which corresponds to the increased staining seen in CA1 neurons within the hippocampus of Tg4510 mice at 10 months old (Ramsden *et al.,* 2005). In these western blots, CP13 staining is increased in Tg mice compared to WT in both 5 month and 10 month old mice and is more pronounced in Tg mice of 10 months of age compared to those of 5 months of age. A similar pattern is found for antibodies PHF-1 and RZ3, demonstrating that these western blots are consistent with previous reports of increased phosphorylated tau pathology, exacerbated with age, within Tg4510 mice compared to controls.

RZ3 detects pThr231 tau and immunoreactivity is seen in a variety of tau transgenic AD model mice and in the brains of patients with AD (Acker *et al*., 2013). Although RZ3 has not previously been cited as being used on Tg4510 mouse brain tissue, the increased presence of pThr231 tau as detected here by this antibody is commensurate with the known increase in NFT pathology, in particular in the cortex and hippocampus, of these mice.

PHF-1 is a well-characterised antibody, which detects pSer396/404 tau and is a marker for late-stage NFTs. Previous studies parallel results from these immunoblots (Ramsden *et al.,* 2005; Santacruz *et al.,* 2005), which show that PHF-1 staining was increased within 10 month old mice in comparison to 5 month old mice and most intense staining was found within the cortex. The antibody MC1 was also included in the panel of antibodies used within this project. MC1 can be used to detect abnormal conformations of tau associated with early tangle formation (Gotz *et al*., 2001). MC1 loses specificity when used for western immunoblotting, therefore, it was not used to probe western blots of hPSC-neurons (Petry *et al.,* 2014).

Immunostaining with 3R tau and 4R tau antibodies, which detect tau with three C-terminal repeats and four C-terminal repeats respectively, indicates that these mice have increased amounts of both of these isoform groups of tau in comparison to wild type mice, however, this is to be expected due to the increase in total tau detected by DA9. At the beginning of this study, these isoform specific antibodies were intended to be used to understand whether tau pathology resulting from V337M *MAPT* could alter the ratio of 3R:4R tau as changes in the ratio are associated with tauopathy. However, the recent discovery that 4R tau is not expressed within hPSC-neurons until they have been cultured for at least 100 days (Sposito *et al.,* 2015), with the exception of those hPSC-neurons carrying mutations that are capable of altering the splicing of *MAPT* leading to early expression of 4R tau (Iovino *et al.,* 2015; Hallman *et al.,* 2015; Wren *et al.,* 2015), deemed this analysis unnecessary.

The parallels between previous reports of tau pathology within Tg4510 mice and the western immunostaining detected in these immunoblots indicated that this panel of antibodies is suitable for the detection of changes in tau and may enable a deeper understanding of the changes of tau phosphorylation in neurons derived from hiPSC with mutations within *MAPT.*

4.3.2 Characterisation of CGNs derived from pluripotent stem cells

During the generation of CGNs from hiPSC, cell cultures pass various milestones during differentiation, mimicking cortical neurogenesis during development (Shi *et al*., 2012). These milestones can be assessed and characterised by immunocytochemistry. During the development of the cortex, cortical glutamatergic neurons (CGNs) are produced from radial glia, which are capable of differentiating into intermediate cell types that terminally differentiate to form neurons and glia (Heins *et al.,* 2002; Noctor *et al.,* 2001; Miyata *et al.,* 2001; Malatesta *et al.,* 2000; Englund *et al.,* 2005). Radial glia express paired box protein 6 (Pax 6), a homeodomain transcription factor that exerts high-level control over cortical development (Manuel *et al*., 2015). Radial glia differentiate to produce intermediate progenitor cells (IPCs), which express T-domain transcription factor 2 (Tbr2) and are committed to a glutamatergic neuron fate (Englund *et al.,* 2005; Hevner *et al.,* 2006). Pax 6 and Tbr 2 expression overlaps within cells during development of CGNs (Englund *et al.,* 2005; Hevner *et al.,* 2006). The presence of Pax 6 (Figure 4.4) and Tbr 2 (Figure 4.5) were detected in cultures at day 15 of the protocol via fluorescent immunocytochemistry.

Figure 4.4 Neural progenitors express Pax6 at day 15

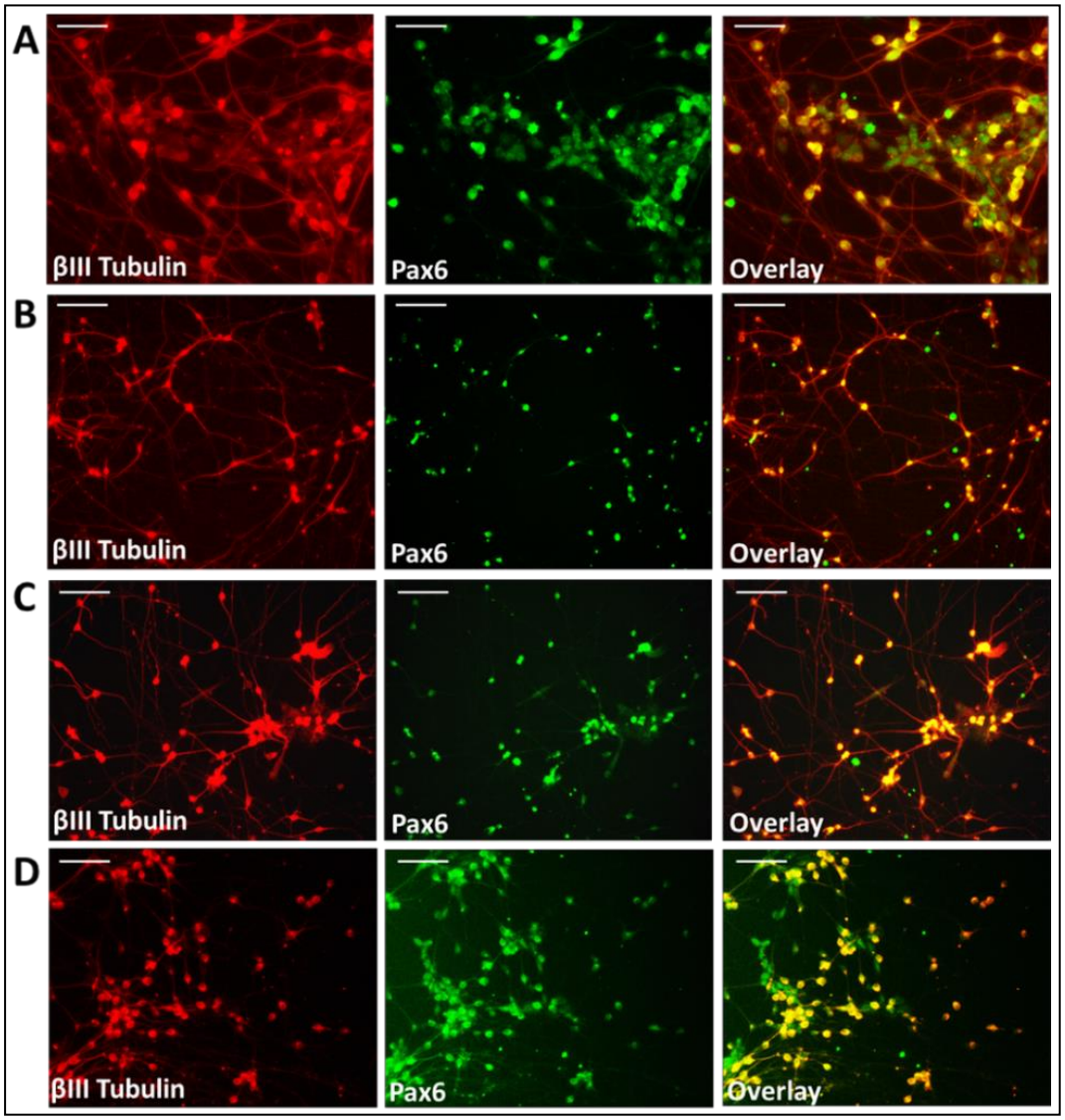

Figure 4.4 Neural progenitors express Pax6 at day 15

Neural progenitors differentiated from Shef 6 (A), Nas 2 (B), V337M-E (C) and V337M-C (D), express Pax 6 at day 15 of the protocol. Scale bars indicate 50 µM.

Figure 4.5 Neural progenitors express Tbr2 at day 15

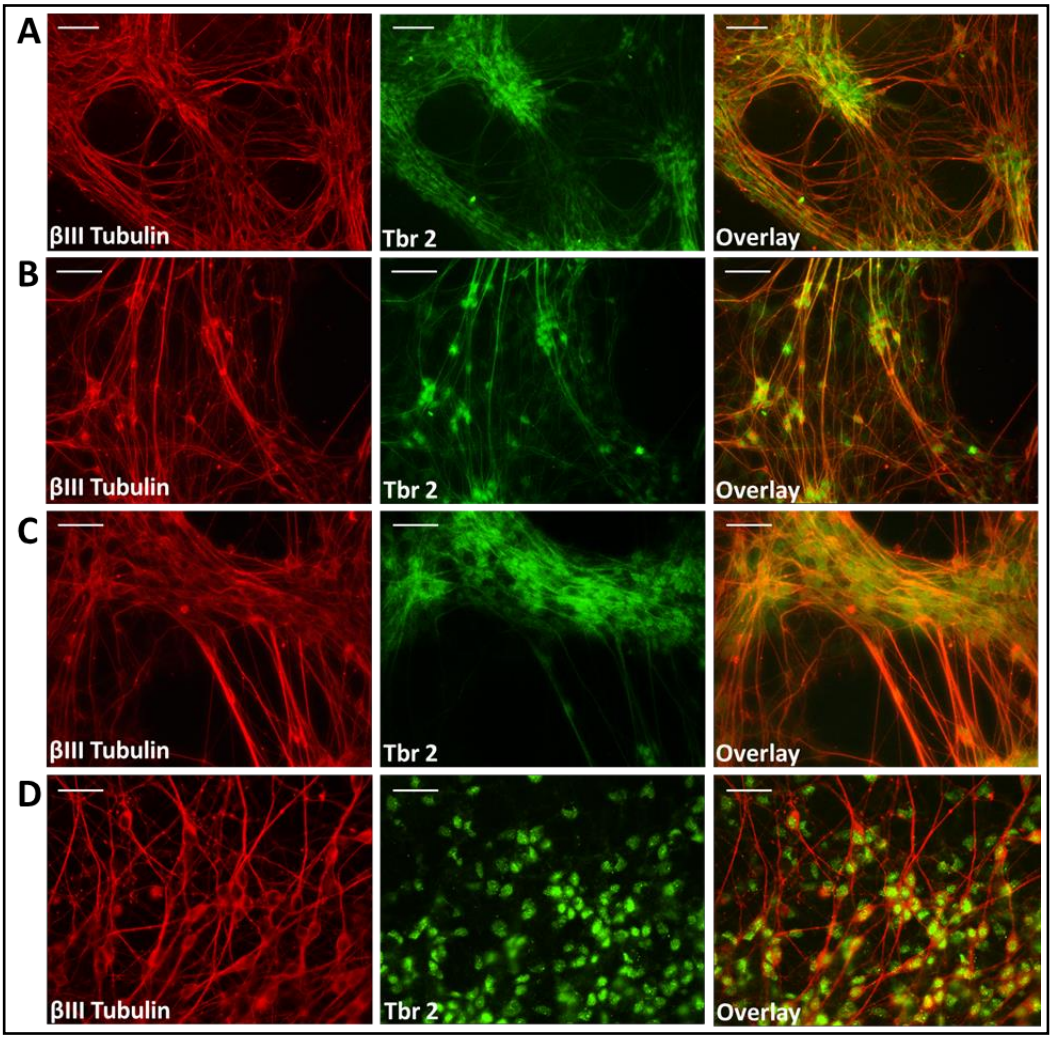

Figure 4.5 Neural progenitors express Tbr2 at day 15

Neural progenitors differentiated from Shef 6 (A), Nas 2 (B), V337M-E (C) and V337M-C (D), express Tbr2 at day 15 of the protocol. Scale bars indicate 50 µM

The mixture of neural progenitors and young neurons at day 15 of the protocol express both Pax 6 and Tbr 2. The presence of these two proteins in day 15 cultures indicates the presence of both radial glia and IPCs, indicating that the cells are following the correct route for differentiation.

Figure 4.6 Neural progenitors express Tbr1 at day 25

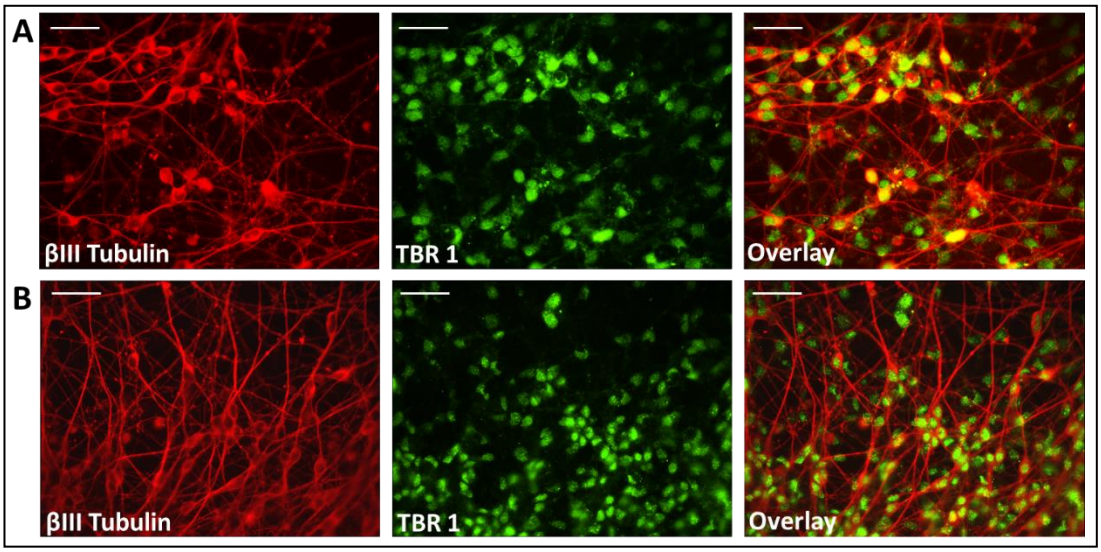

Figure 4.6 Neural progenitors express Tbr1 at day 25

Neural progenitors differentiated from Nas 2 (A) and V337M-C (B), express Tbr1 at day 22 of the protocol. Scale bars indicate 50 µM.

Later in cortical neurogenesis, T-domain transcription factor 1 (Tbr1) is expressed. Tbr1 is expressed by virtually all post-mitotic glutamatergic cortical neurons (Hevner *et al.,* 2001; Hevner *et al.,* 2006; Englund *et al.,* 2005) and is not present in GABAergic neurons (Hevner *et al.,* 2001). At day 25 of the differentiation protocol, the cultures of neurons positively co-immunostained with an antibodies against βIII Tubulin and Tbr1, indicating that these neurons are glutamatergic (Figure 4.6).

Figure 4.7 hPSC-CGN express vGlut1 at day 50

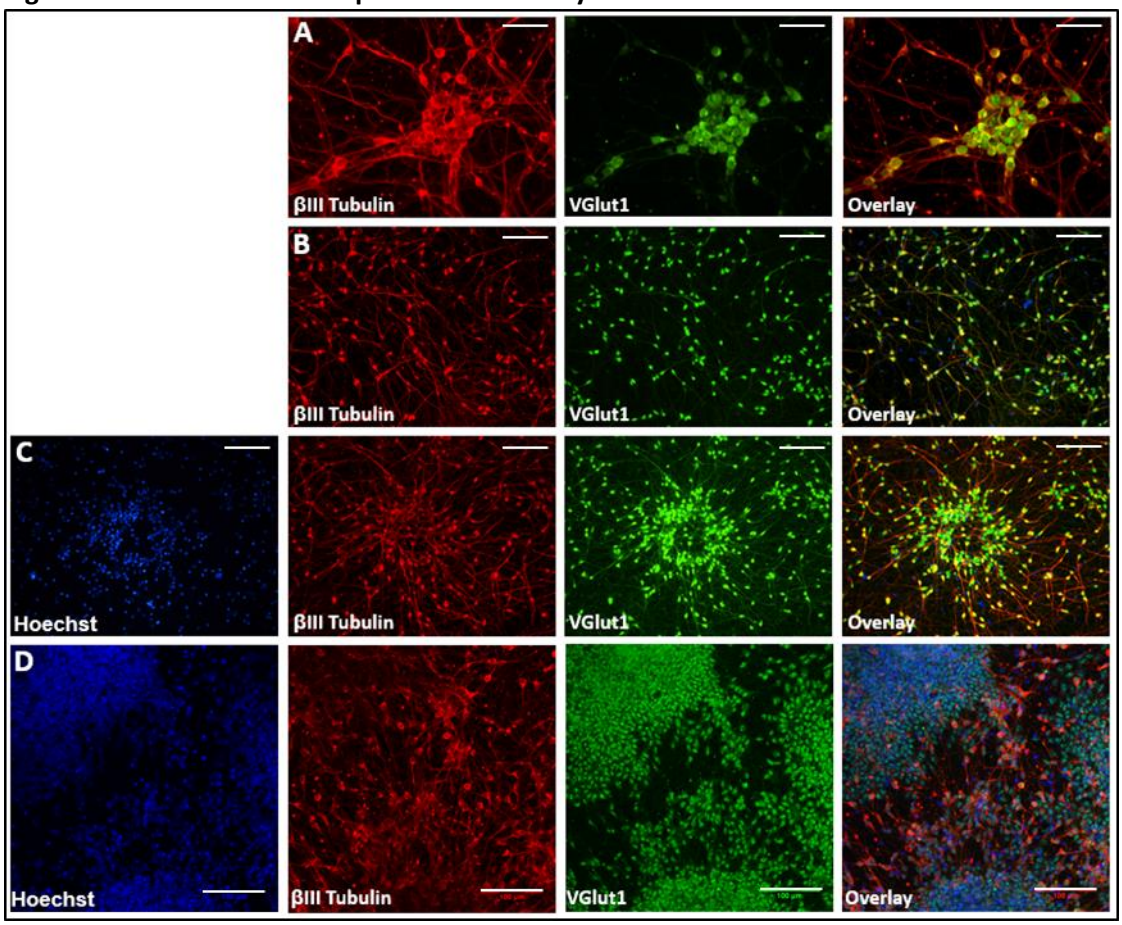

Figure 4.7 hPSC-CGN express VGlut1 at day 50

Nas 2-CGN (A), Shef 6-CGN (B), V337M-C-CGN (C) and V337M-E-CGN (D) immunostained with βIII Tubulin (red) and VGlut1 (green). V337M-C-CGN and V337M-E-CGN were also immunostained with Hoechst solution (blue) to indicate cell nuclei. The overlays are depicted in the panels furthest to the right. Scale bar for Nas 2-CGN (A) indicates 50 µm, scale bars for Shef 6-CGN (B), V337M-C-CGN (C) and V337M-E-CGN (D) indicate 100 µm.

Vesicular glutamatergic transporter 1 (vGlut1) is a vesicular glutamatergic transporter, present within neurons that use the neurotransmitter glutamate and within the cortex, hippocampus or cerebellar cortex (Bellocchio *et al*., 2000). Mature cortical glutamatergic neurons should express vGlut1, therefore, an antibody against this protein was used in combination with fluorescent immunocytochemistry to visualise the presence of vGlut1. Nas 2-CGN, Shef 6-CGN, V337M-C-CGN and V337M-E-CGN cultures all have neurons, highlighted by βIII Tubulin, that co-stain positively with VGlut1 (Figure 4.4). Positive immunostaining of these neurons, therefore, indicates post-mitotic cortical glutamatergic neurons (CGNs).

Figure 4.8 Day 50 hPSC-CGN express synapsin I

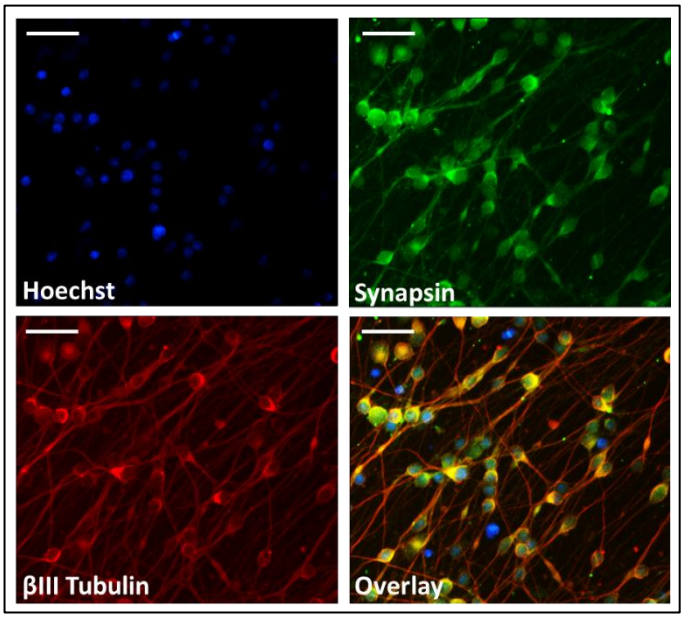

Figure 4.8 Day 50 hPSC-CGN express synapsin I

Shef 6-CGN express synapsin I at day 50 as indicated by positive fluorescent immunostaining using antibodies against synapsin I and βIII Tubulin. Scale bars indicates 50µm.

Dysfunction and loss of synapses precedes neurodegeneration in tauopathy, therefore, it was important to confirm the presence of synapses within hPSC-CGNs. Immunocytochemistry using antibodies against synapsin, a pre-synaptic protein important for vesicle trafficking within the synapse present within early and mature synapses (Evergren *et al.,* 2007) (Figure 4.8) and βIII Tubulin, demonstrated the presence of this synaptic protein in hPSC-CGNs at day 50 of the differentiation protocol. These hPSC-CGNs also express post-synaptic density protein 95 (PSD-95) (Figure 4.9), a protein present within the post-synaptic density of mature synapses (Naisbitt *et al*., 2000).

Figure 4.9 hPSC-CGN express post-synaptic density protein 95 at day 50

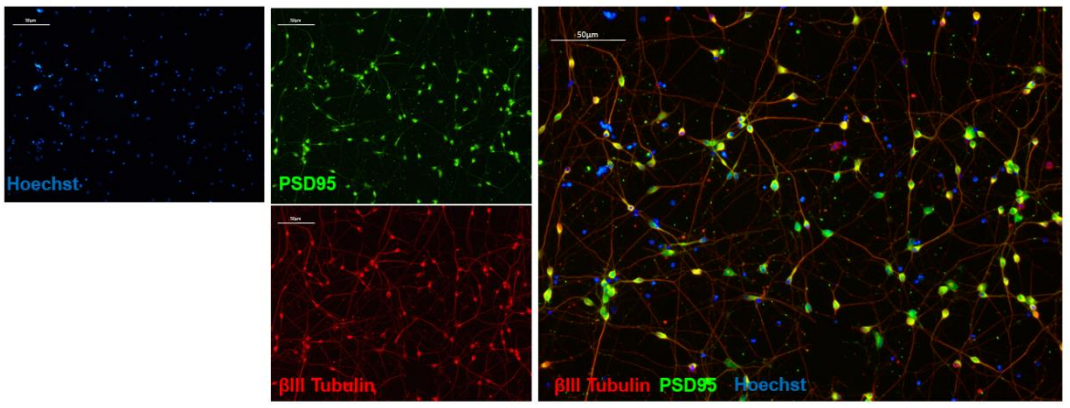

Figure 4.9 hPSC-CGN express post-synaptic density protein 95 at day 50

Shef 6-CGN express Synapsin at day 50 as indicated by positive fluorescent immunostaining using antibodies against PSD 95 and βIII Tubulin. Scale bars indicate 50µm.

4.3.3 Tau and phosphorylated tau levels in CGNs

After terminal differentiation, hPSC-CGNs were cultured to maturity, i.e. 50 days, from lines Nas 2, Shef 6, V337M-C and V337M-E before the cells were washed, lysed and frozen. The resultant samples were western immunoblotted and probed with total tau antibody, DA9, as well as antibodies PHF-1, CP13 and RZ3 to detect tau phosphorylated at Ser396/Ser404, Ser202 and Thr231, respectively. The calculated density and size of each band was normalised to bands produced by probing with the housekeeping control antibody GAPDH. The bands produced by probing with the phosphorylated tau antibodies were also normalised against those revealed by probing with DA9, after normalisation against GAPDH, allowing for consideration of total tau variation within sample. Prepared lysates from V337M-C-CGN were western immunoblotted alongside Nas 2-CGN, while V337M-E-CGN were western immunoblotted alongside Shef 6-CGN.

Figure 4.10 Level of total tau in hiPSC-CGNs

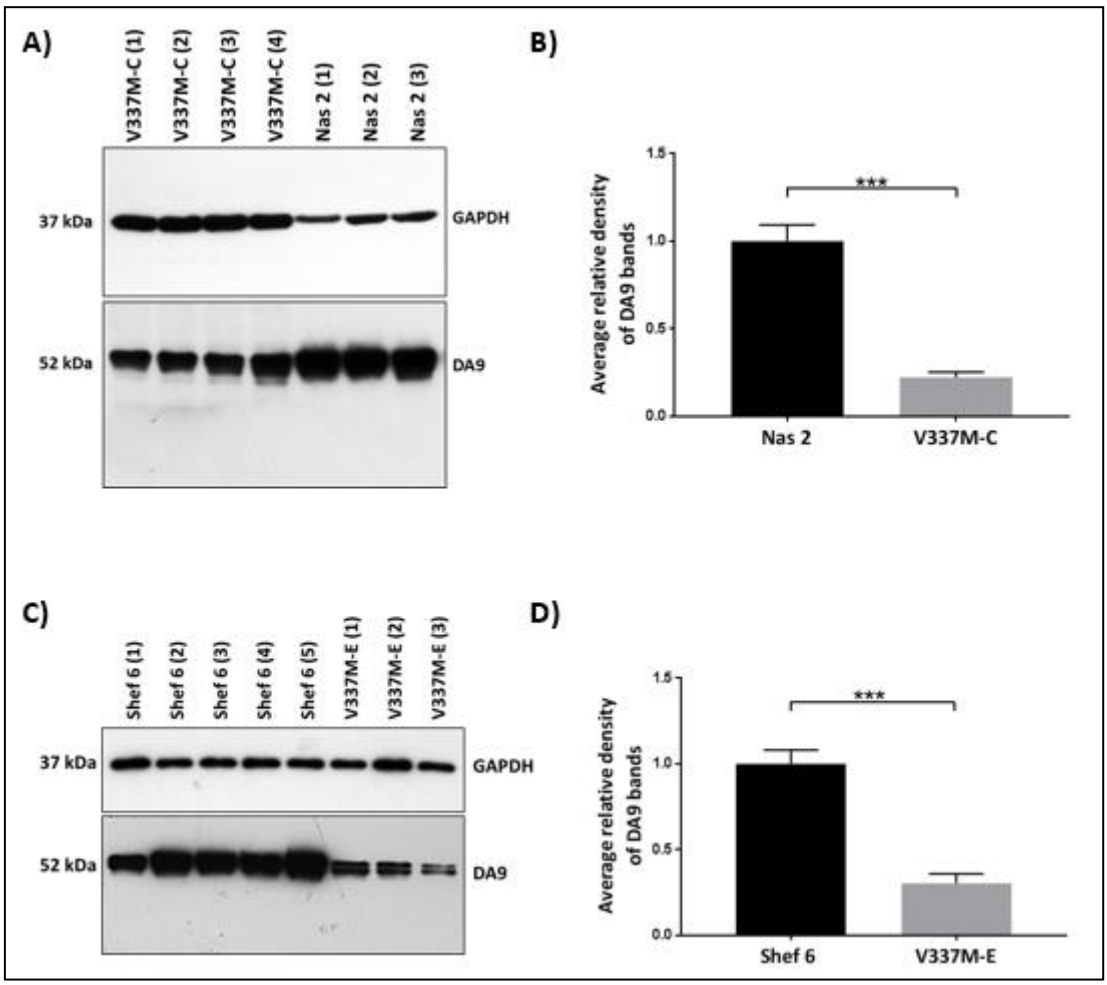

Figure 4.10 Levels of total tau in CGNs

*Representative western blots showing CGN derived from V337M-C and Nas 2 (V337M-C-CGN n=4; Nas 2-CGN n=3) (A) and from derived from V337M-E and Shef 6 (V337M-E-CGN n=4; Shef 6-CGN n=3) (B) probed with GAPDH and DA9 antibodies. Bar charts represent the density of DA9 bands compared to GAPDH bands for CGN derived from (B) V337M-C and Nas 2 (***p=0.0005) and from (C) V337M-E and Shef 6 (*** p=0.0007).*

Levels of total tau are decreased in neurons carrying the V337M mutation, derived from V337M-C (p= 0.0005) and V337M-E (p= 0.0007), compared to control neurons derived from Nas 2 and Shef 6, respectively (Figure 4.10).

To detect the amount of tau phosphorylated at Ser396 and Ser404 within cells carrying V337M *MAPT* compared to control cells, lysates from V337M-C-CGN, V337M-E-CGN, Shef 6-CGN and Nas 2-CGN were immunoblotted and western blots were probed with PHF-1 (Figures 4.11 and 4.12).

Figure 4.11 Level of tau phosphorylation Ser396 and Ser404 in V337M-C-CGNs and Nas 2-CGNs

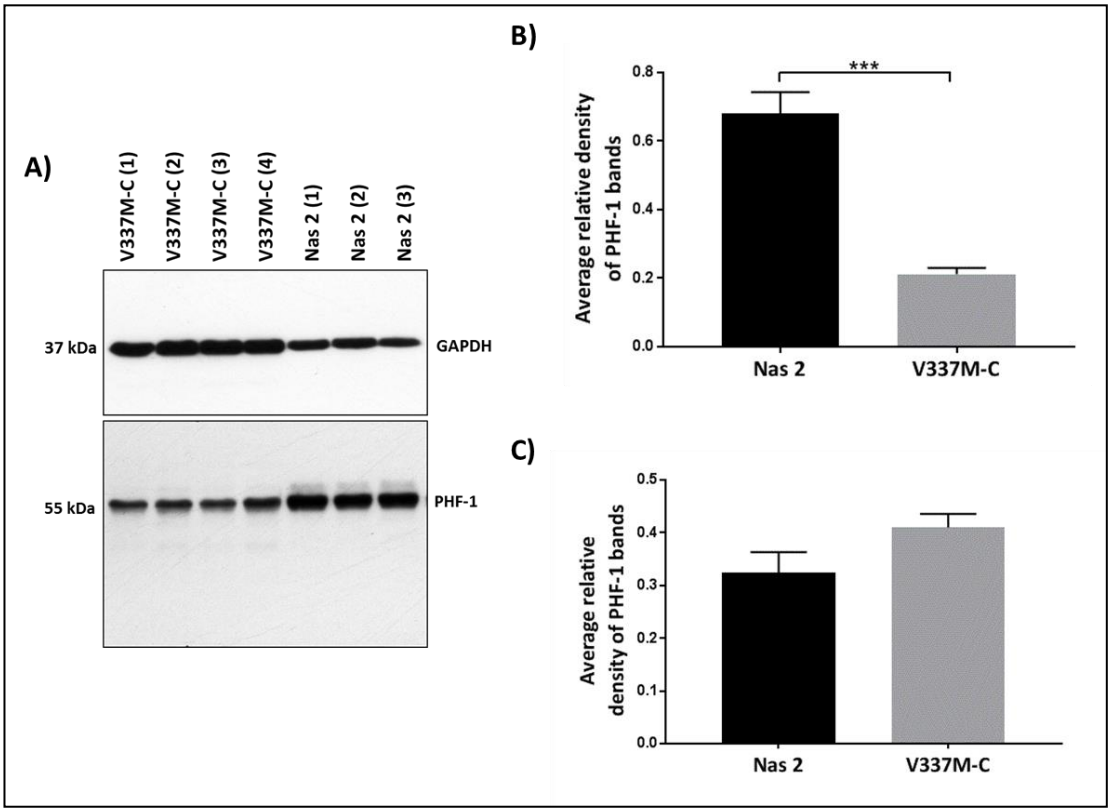

Figure 4.11 Levels of tau phosphorylated at pSer396 and pSer404 in V337M-C- and Nas 2-CGNs

*Representative western blot (A) showing CGN derived from V337M-C and Nas 2 probed with GAPDH and PHF-1 antibodies (V337M-C-CGN n=4; Nas 2-CGN n=3) and corresponding bar charts representing the density of PHF-1 bands normalised to GAPDH bands (***p=0.0005) (B) and then normalised to DA9 bands (C).*

Data was analysed using an unpaired Student's t-test. Error bars indicate +1 S.E.M.

Levels of pSer396/404 tau are decreased in V337M-C-CGN before normalisation to total tau levels (p= 0.0005), however, there was no significant difference in levels of tau phosphorylation at these sites between Nas 2-CGN and V337M-C-CGN after normalisation to total tau (p= 0.2677).

Figure 4.12 Levels of tau phosphorylated at Ser396 and Ser404 in V337M-E-CGNs and Shef 6-CGNs

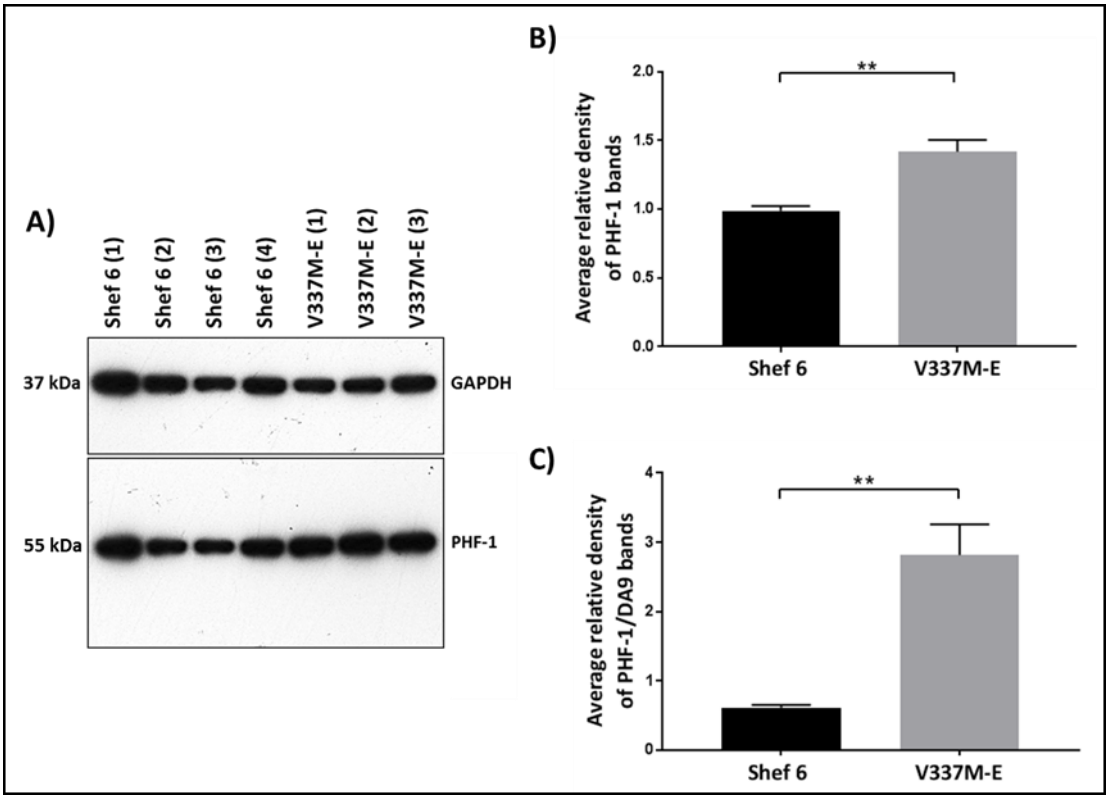

Figure 4.12 Levels of tau phosphorylated at Ser396 and Ser404 in V337M-E-CGNs and Shef 6-CGNs

*Representative western blot (A) showing CGN derived from V337M-E and Shef 6 probed with GAPDH and PHF-1 (V337M-E-CGN n=3; Shef 6-CGN n=5). Bar charts representing the density of (B) PHF-1 bands normalised to GAPDH bands (** p= 0.0013) and then (C) normalised to DA9 bands (** p= 0.0014).*

Data was analysed using an unpaired Student's t-test. Error bars indicate +1 S.E.M.

Levels of pSer396/404 tau are decreased in V337M-E-CGN before normalisation to total tau levels (p= 0.0013), and after normalisation to total tau (p= 0.0014).

Figure 4.13 Level of tau phosphorylation Ser202 in V337M-C-CGNs and Nas 2-CGNs

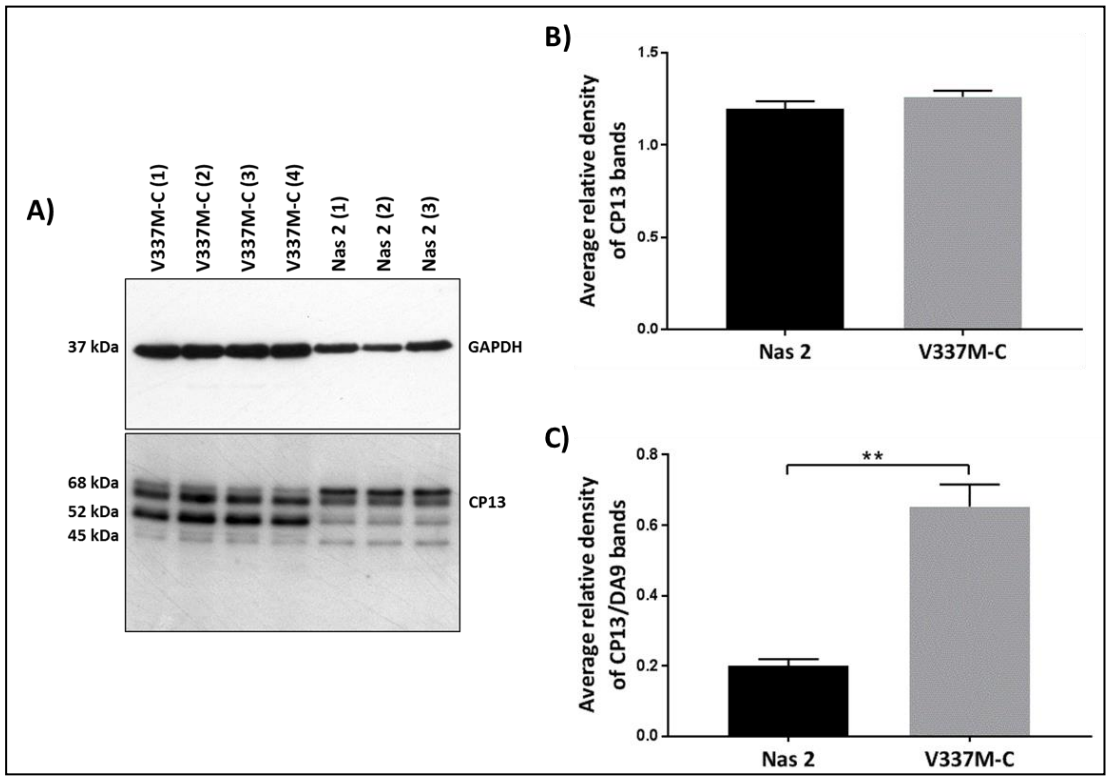

Figure 4.13 Levels of tau phosphorylated at pSer202 and pSer205 in V337M-C- and Nas 2-CGNs

*Representative western blot showing CGN derived from V337M-C and Nas 2 probed with GAPDH and CP13 (V337M-E-CGN n=4; Nas 2-CGN n=3). Bar charts representing the density of (B) CP13 bands normalised to GAPDH bands and (C) then normalised to DA9 bands (** p= 0.0019).*

Data was analysed using an unpaired Student's t-test. Error bars indicate +1 S.E.M.

Before normalisation to total tau, no difference was found in phosphorylation of tau at Ser202 between V337M-C-CGN and Nas 2-CGN, however, upon normalisation to total tau within the neurons, tau was found to be phosphorylated within V337M-C-CGN compared to Nas 2-CGN (p= 0.0019) (Figure 4.13).

Thr231 phosphorylation of tau is associated with pre-tangle pathology (Augustinack *et al.,* 2002a) and has been shown to inhibit tau's ability to bind microtubules by approximately 25 % (Sengupta *et al*., 1998). To investigate the phosphorylation of tau at this site western blots of V337M-C-CGN and Nas 2-CGN were probed with RZ3 (Figure 4.14).

Figure 4.14 Level of tau phosphorylation Thr231 in V337M-C-CGNs and Nas 2-CGNs

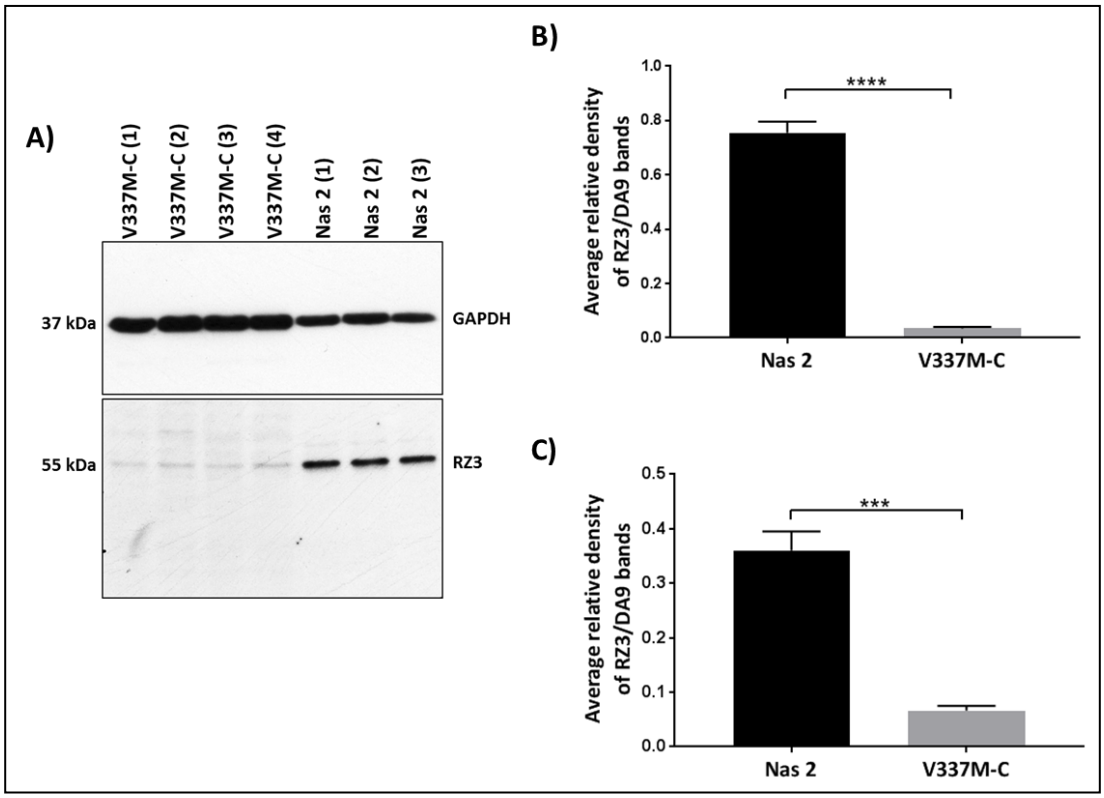

Figure 4.14 Levels of tau phosphorylated at pThr231 in V337M-C- and Nas 2-CGNs

*Representative western blot (A)showing CGN derived from V337M-C and Nas 2 probed with GAPDH and RZ3 (V337M-C-CGN n=4; Nas 2-CGN n=3) and corresponding bar chart representing the density of RZ3 bands normalised to GAPDH bands (**** p<0.0001) (B) and then to DA9 (*** p=0.0002) (C).*

Data was analysed using an unpaired Student's t-test. Error bars indicate +1 S.E.M.

pThr231 tau is significantly reduced in V337M-C-CGN compared to Nas 2-CGN both before (p≤ 0.0001) and after (p= 0.0002) normalisation to total tau. Unfortunately, the signal generated through probing western blots of V337M-E-CGN and Shef 6-CGN was too weak to enable analysis of tau phosphorylation at this site.

4.3.4 Gene expression of *MAPT* in Shef 6-CGNs and V337M-C CGNs

Shef 6-CGNs and V337M-C-CGNs were cultured after terminal differentiation to maturity (Chapter 4.2.1), before the cells were collected and processed to extract and purify RNA. RNA was converted to cDNA and qPCR was carried out using Taqman® probes to discern expression levels of *MAPT* (Chapter 2.7). The average relative gene expression *MAPT* was calculated for V337M-C-CGN and compared to that in Shef 6-CGN.

Figure 4.15 Levels of *MAPT* gene expression in V337M-C-CGNs and Shef 6-CGNs

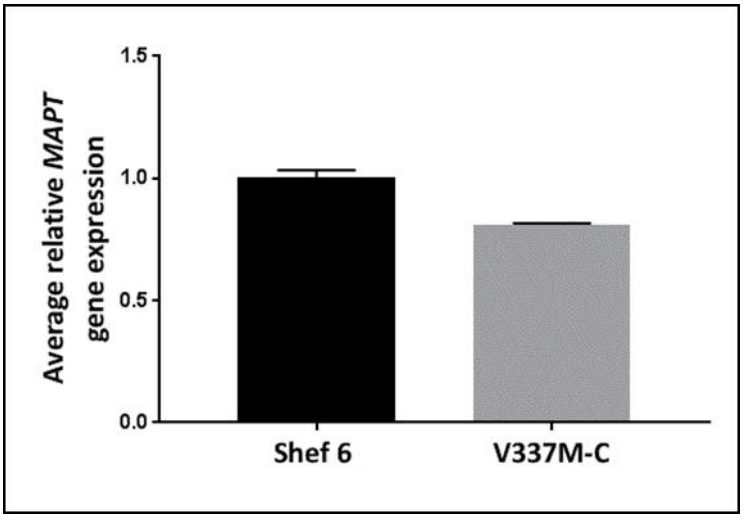

Figure 4.15 Levels of MAPT gene expression in V337M-C-CGN and Shef 6-CGN

Bar chart representing the average MAPT gene expression within V337M-C-CGN and Shef 6-CGN (V337M-C-CGN n=4; Shef 6-CGN n=3).

Data was analysed using a Mann-Whitney test. Error bars indicate +1 S.E.M.

While the average relative expression of *MAPT* is not statistically different in V337M-C-CGN compared to Shef 6-CGN (p= 0.0571) (Figure 4.15), this result approaches statistical significance.

4.3.5 Tau kinase levels and activity in hiPSC-CGNs

To investigate the levels and activity of GSK3β within hiPSC-CGN carrying the V337M *MAPT* mutation compared to control neurons, western blots were probed with antibodies against total GSK3β and GSK3β phosphorylated at pTyr216. Phosphorylation of GSK3β at this site is necessary for GSK3β activity (Chapter 1.3.1) and by comparing levels of pTyr216 GSK3β to total GSK3β it is possible to investigate the activity of this kinase.

Levels of GSK3β (p= 0.2225), pTyr216 GSK3β (p= 0.6334) and the ratio of pTyr216 GSK3β normalised to total GSK3β (p= 0.2106), were not significantly different in V337M-C-CGN compared to Nas 2-CGN (Figure 4.16). However, in V337M-E-CGNs levels of GSK3β were found to be significantly increased compared to Shef 6-CGN (p= 0.0122) while levels of pTyr216 GSK3β were decreased (p= 0.0159) (Figure 4.17). This was reflected in a decreased ratio of pTyr216 GSK3β to total GSK3β (p= 0.0016) (Figure 4.17, E), indicating that while GSK3β levels overall rise in cells carrying V337M *MAPT* compared to Shef 6-CGN, the activity of GSK3β is decreased. Banding patterns varied between western blots for pTyr216 GSK3β and total GSK3β for both V337M-C and Nas-2 derived CGNs (Figure 4.16) and V337M-E and Shef 6 derived CGNs (Figure 4.17).

Figure 4.16 Levels of active GSK3β in V337M-C-CGN and Nas 2-CGNs

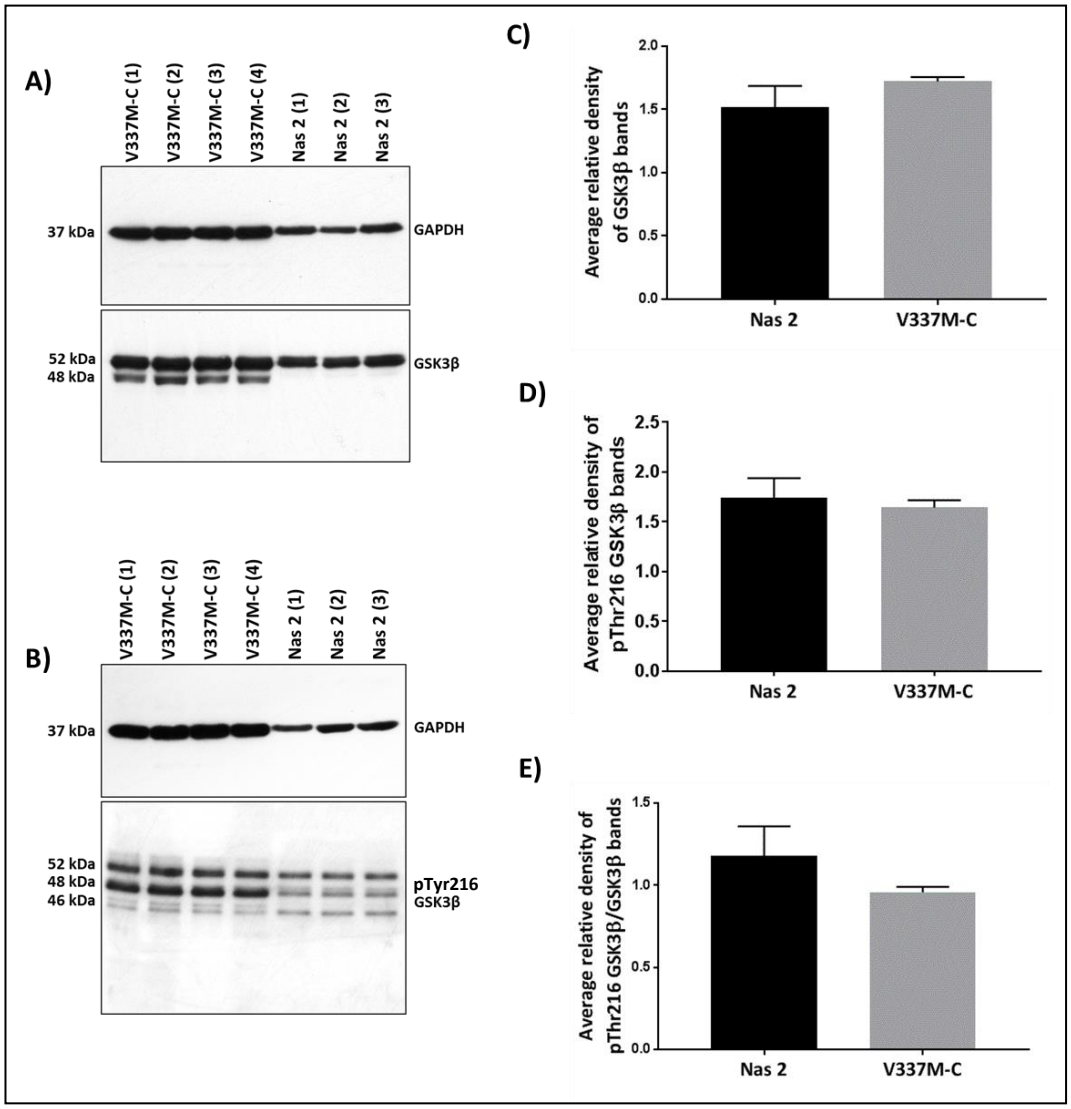

Figure 4.16 Level of GSK3β and pTyr216 GSK3β in V337M-C-CGN and Nas 2-CGN

Representative western blots showing CGNs derived from V337M-C and Nas 2 probed with antibodies against (A) GAPDH and GSK3β and (B) GAPDH and pTyr216 GSK3β (V337M-C-CGN n=4; Shef 6-CGN n=3). Bar charts representing the density of (C) GSK3β bands normalised to GAPDH bands, (D) pTyr216 GSK3β bands normalised to GAPDH bands and (E) pTyr216 GSK3β bands normalised to total GSK3β bands, then to GAPDH bands.

Data was analysed using an unpaired Student's t-test. Error bars indicate +1 S.E.M.

Figure 4.17 Levels of active GSK3β in V337M-E-CGN and Shef 6-CGNs

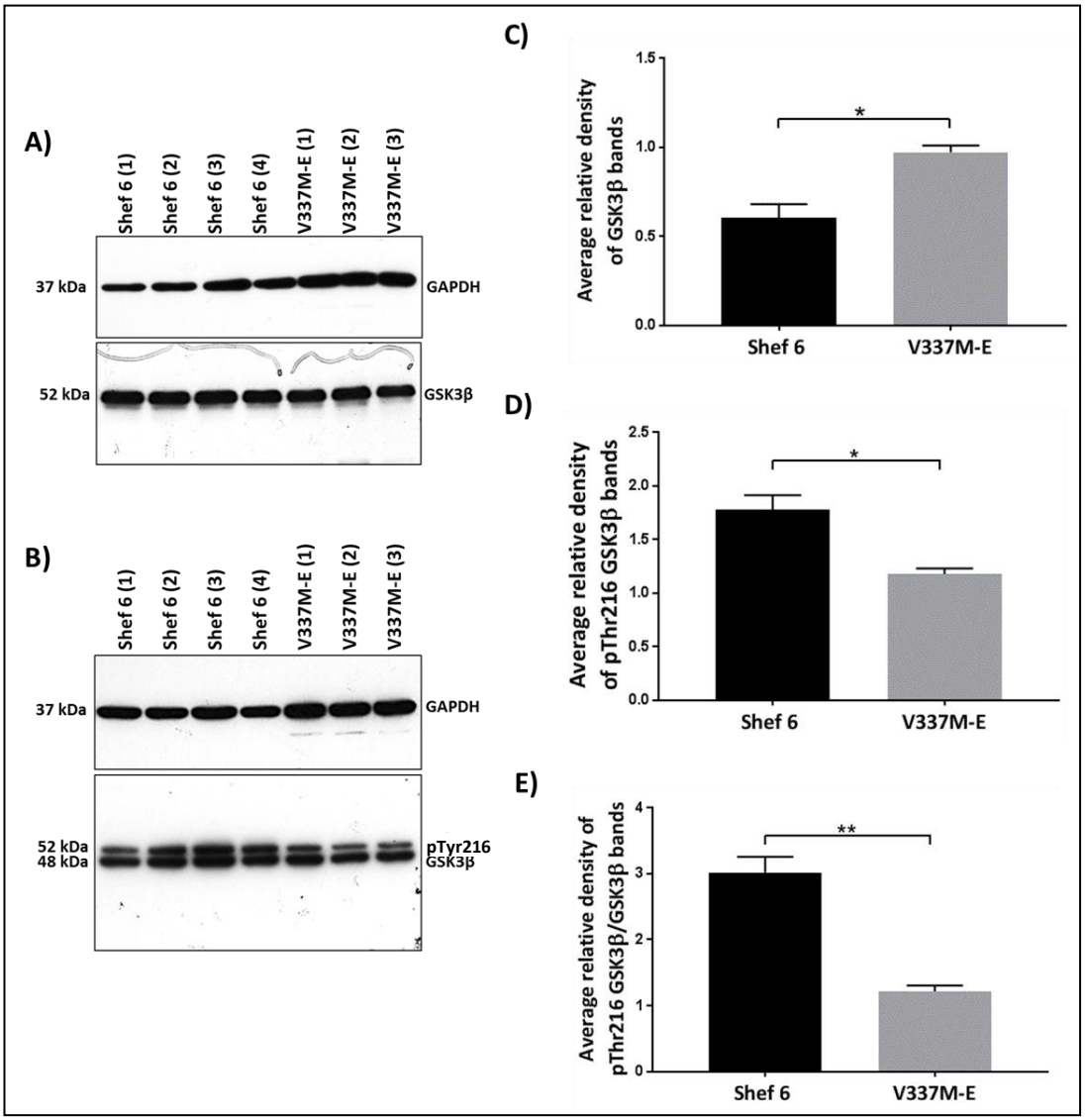

Figure 4.17 Level of GSK3β and pTyr216 GSK3β in V337M-E-CGN and Shef 6-CGN

Representative western blots showing CGNs derived from V337M-E and Shef 6 probed with antibodies against (A) GAPDH and GSK3β and (B) GAPDH and pTyr216 GSK3β (V337M-E-CGN n=3; Shef 6-CGN n=4). Corresponding bar charts represent the density of (C) GSK3β bands normalised to GAPDH bands (p= 0.0122), (D) pTyr216 GSK3β bands normalised to GAPDH bands (* p= 0.0159) and (E) pTyr216 GSK3β bands normalised to total GSK3β bands, then to GAPDH bands (** p= 0.0016).*

Data was analysed using an unpaired Student's t-test. Error bars indicate +1 S.E.M.

To investigate the activity of Cdk5, the relative ratio of p35 to p25 in brain samples was examined by probing western blots with an antibody against p25 and p35. An increase in the activity of Cdk5 is indicated by increased levels of p25 and decreased levels of p35 as described in more detail in Chapter 1 (Chapter 1.3.2).

Figure 4.18 Levels of p35 in hPSC-CGN

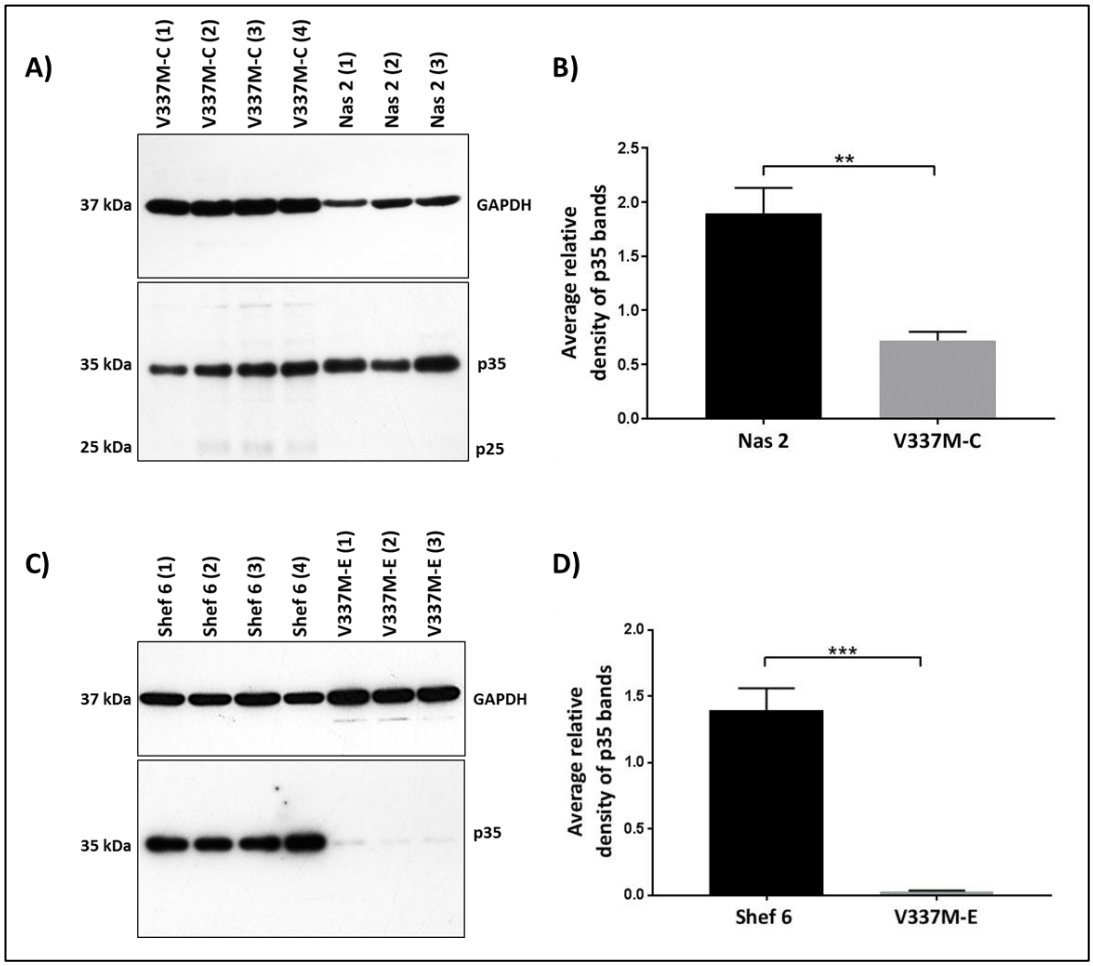

Figure 4.18 Levels of p35 in hPSC-CGNs

*Representative western blots showing CGNs derived from (A) V337M-C and Nas 2 (V337M-C-CGN n=4; Nas 2-CGN n=3) and (C) V337M-E and Shef 6 (V337M-E-CGN n=3; Shef 6-CGN n=5) probed with antibodies against GAPDH and p25/p35. Bar charts representing the density of p35 bands normalised to GAPDH bands for (B) V337M-C and Nas 2 (** p= 0.0037) and (D) V337M-E and Shef 6 (*** p= 0.0004).*

Data was analysed using an unpaired Student's t-test. Error bars indicate +1 S.E.M.

Levels of p25 were too low to be quantified in these western immunoblots. Levels of p35 were significantly decreased in V337M-C-CGN compared to Nas 2-CGN ($p= 0.0037$) and in V337M-E-CGN compared to Shef 6-CGN ($p= 0.0004$) (Figure 4.18).

Western blots were probed with anti-PAK3 to investigate the effects of V337M *MAPT* on levels of this tau kinase. PAK3 levels were significantly decreased in V337M-C-CGN compared to Nas 2-CGN ($p< 0.0001$). Although PAK3 levels appear to be decreased in V337M-E-CGN compared to Shef 6-CGN, this result is not statistically significantly ($p= 0.0601$) (Figure 4.19).

Figure 4.19 Levels of PAK3 in V337M-C-CGNs and Nas 2-CGNs

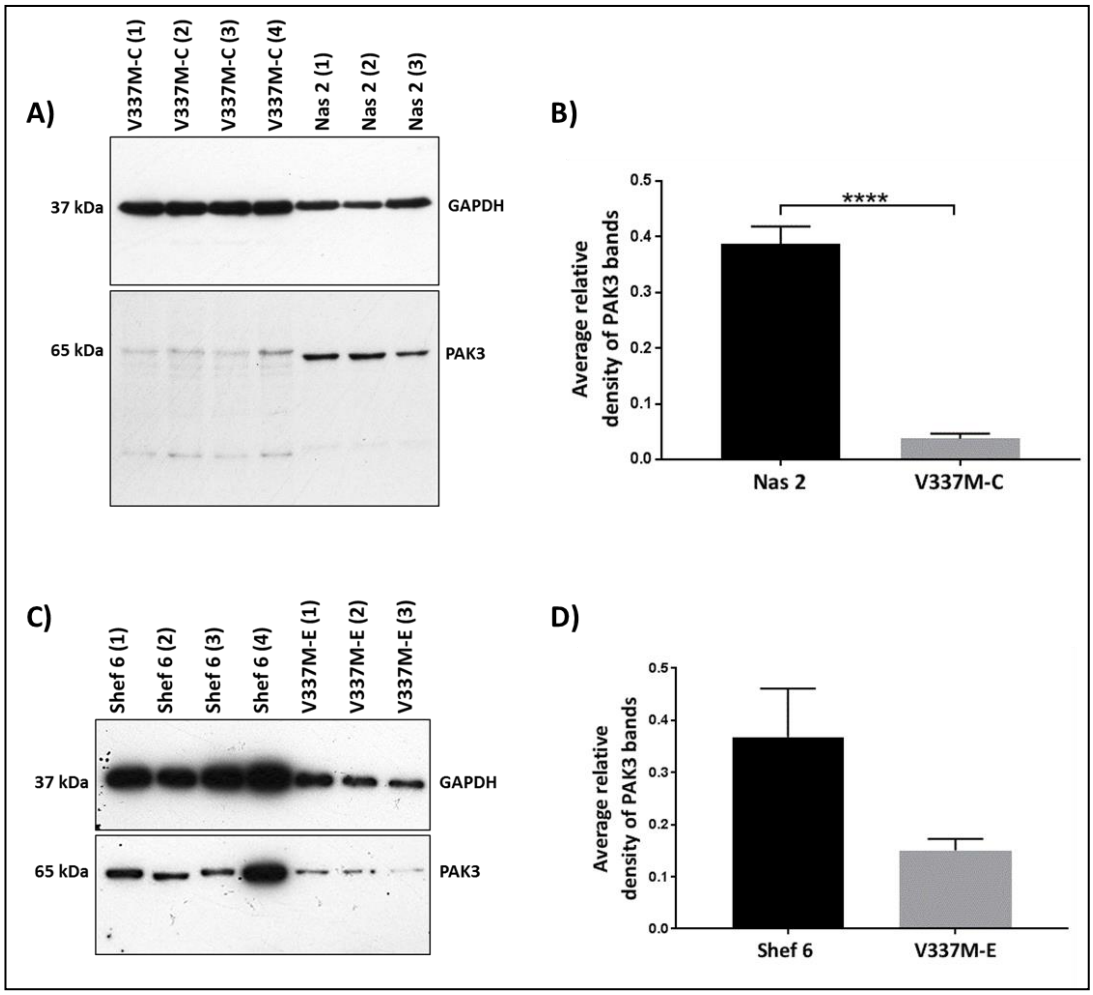

Figure 4.19 Levels of PAK3 in hiPSC-CGNs

*Representative western blot showing CGNs derived from (A) V337M-C and Nas 2 (V337M-C-CGN n=4; Nas 2-CGN n=3) and (C) V337M-E and Shef 6 (V337M-E-CGN n=3; Shef 6-CGN n=5) probed with antibodies against GAPDH and PAK3. Corresponding bar charts representing the density of PAK3 bands normalised to GAPDH bands for (B) V337M-C and Nas 2 (**** p< 0.0001) and (D) V337M-E and Shef 6.*

Data was analysed using an unpaired Student's t-test. Error bars indicate +1 S.E.M.

Akt, also known as protein kinase B (PKB), is a serine/threonine protein kinase capable of phosphorylating tau directly at Thr212 and Ser214 (Kyoung *et al.,* 2004; Ksiezak-Reding *et al.,* 2003) and regulating the activity of other tau kinases via phosphorylation; for example, Akt phosphorylates GSK3β at Ser9, therefore inhibiting it (Chalecka-Franaszek and Chuang, 1999; Doble and Woodgett, 2003; De Sarno *et al*., 2002). Phosphorylation of Akt at Ser473 is necessary for its activation (Kyoung *et al.,* 2004; Ksiezak-Reding *et al.,* 2003). The influence of V337M *MAPT* on the activity of Akt were investigated by probing western blots with an antibody against this phosphorylated form of Akt. The levels of pSer473 Akt within V337M-C-CGN ($p= 0.0749$) and V337M-E-CGN ($p= 0.9459$) are not significantly different compared to Nas 2-CGN and Shef 6-CGN, respectively (Figure 4.20).

Figure 4.20 Level of pSer473 Akt in hPSC-CGNs

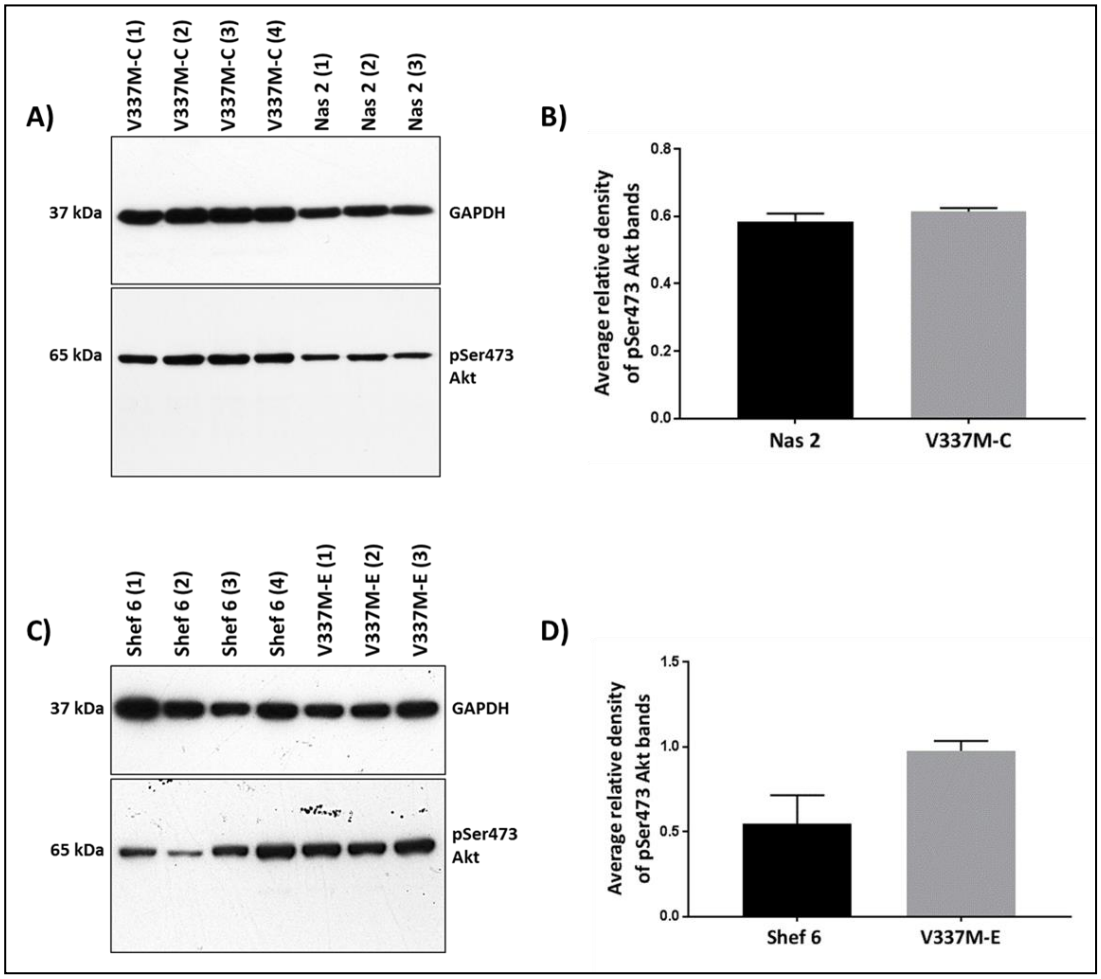

Figure 4.20 Level of pSer473 Akt in hPSC-CGNs

Representative western blots showing CGNs derived from (A) V337M-C and Nas 2 (V337M-C-CGN n=4; Nas 2-CGN n=3) as well as (C) V337M-E and Shef 6 (V337M-E-CGN n=3; Shef 6-CGN n=4) probed with GAPDH and pSer473 Akt antibodies. Corresponding bar charts represent the density of pSer473 Akt bands normalised to GAPDH bands for (B) V337M-C and Nas 2 and (D) V337M-E and Shef 6.

Data was analysed using an unpaired Student's t-test. Error bars indicate +1 S.E.M.

4.3.6 Gene expression of tau kinases in CGN

To determine the effect of V337M *MAPT* on the expression levels of tau kinases, *GSK3β, CDK5* and *PAK3,* qPCR was carried out using probes to detect cDNA of these kinases.

Figure 4.21 Levels of tau kinase gene expression in V337M-C-CGNs and Shef 6-CGNs

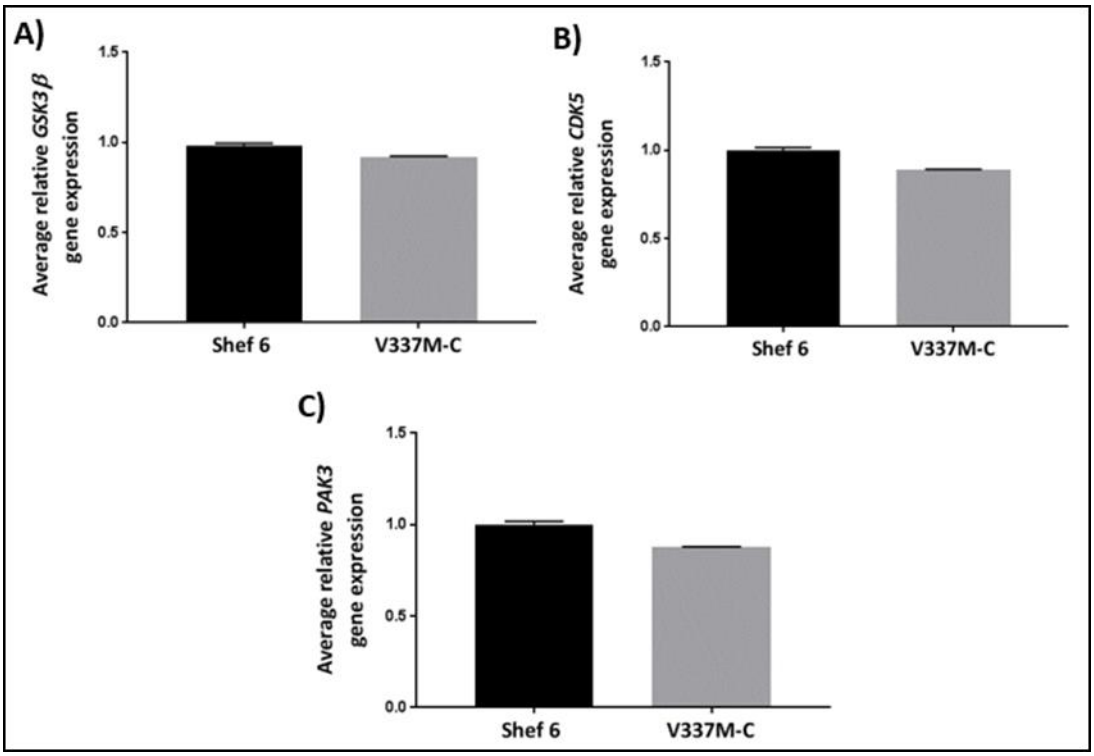

Figure 4.21 Levels of tau kinase gene expression in V337M-C-CGNs and Shef 6-CGNs

Bar charts representing the average gene expression of (A) GSK3β, (B) CDK5 and (C) PAK3 within V337M-C-CGN and Shef 6-CGN (V337M-C-CGN n=4; Nas 2-CGN n=3).

Data was analysed using a Mann-Whitney test. Error bars indicate +1 S.E.M.

GSK3β (p= 0.0571), *CDK5* (p= 0.0571) and *PAK3* (p= 0.1000) gene expression levels are not significantly different in V337M-C-CGN compared to Shef 6-CGN (Figure 4.21), however, results for *GSK3β* and *CDK5* approach statistical significance.

4.3.7 Loss of synapsin I in CGN

Figure 4.22 Level of synapsin in hPSC-CGNs

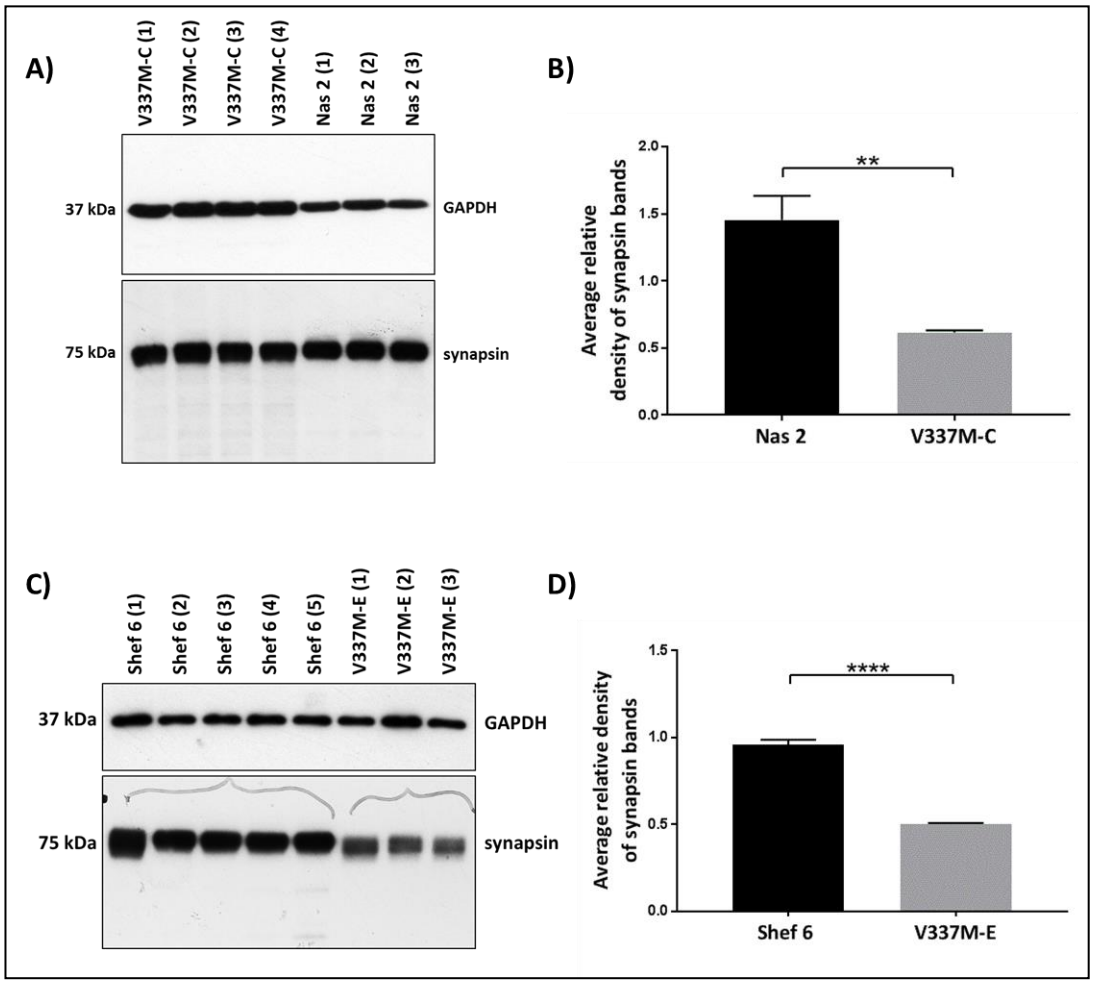

Figure 4.22 Levels of synapsin I in hPSC-CGNs

*Representative western blots showing (A) V337M-C-CGN and Nas2-CGN (V337M-C-CGN n=4; Nas 2-CGN n=3) and (C) Shef 6-CGNs and V337M-E-CGNs probed with antibodies against GAPDH and synapsin (control n=5; Aβ 0.5μM n=3). Corresponding bar charts show the average relative density of synapsin I bands normalised to GAPDH bands for (B) V337M-C-CGN and Nas2-CGN (** p=0.0018) and (D) Shef 6-CGNs and V337M-E-CGNs (**** p<0.0001).*

Data was analysed using an unpaired Student's t-test. Error bars indicate +1 S.E.M.

Levels of synapsin are significantly decreased in V337M-C-CGN compared to Nas 2-CGN (p= 0.0018). Similarly, levels of synapsin are significantly decreased in V337M-E-CGN compared to Shef 6-CGN (p= <0.0001) (Figure 4.22).

4.4 Discussion

4.4.1 Limitations in the use of a V377M *MAPT* iPSC derived from a single patient

The work in this chapter compares tau protein levels, *MAPT* gene expression levels, tau phosphorylation levels, tau kinase protein levels, tau kinase protein activity and tau kinase gene expression levels between CGNs derived from two iPSC lines derived from a single patient and control cell lines. It is important to recognise the limitations of using a single patient to understand the pathological changes involving tau protein due to FTDP-17. FTDP-17 is known to be caused by over 53 mutations, each producing different pathological phosphorylation of tau, which may involve different pathways to hyperphosphorylation or different levels of kinase activity. As discussed in more depth in Chapter 1, patients with the same mutations are also known to present in different ways. The heterogeneity of these diseases is not reflected through the work in this chapter as iPSC-CGN derived from one patient was examined. Further studies, addressing the pathological changes to tau and tau kinases assessed in this chapter, within a cohort of patients carrying V337M *MAPT* would shed additional light on the heterogeneity of pathological tau and tau kinases between patients carrying this mutation. Additional studies addressing these within patients carrying other mutations would also illuminate the heterogeneity of these within FTDP-17 patients in general. This work is likely necessary before the results gained through this study could inform clinical drug discovery efforts (Cabana *et al.*, 1999; Greenfield *et al.*, 2007). In the future, statistical techniques, such as Bayesian and adaptive statistical methods, may be employed to pool results gained through single patient studies to understand tau pathology in a wider population of FTDP-17 patients (Duan et al., 2013).

4.4.2 Levels of tau and *MAPT* expression in V337M-CGN

The work in this chapter has demonstrated that hiPSC-CGNs carrying V337M *MAPT* have markedly decreased levels of tau protein and *MAPT* expression compared to controls, suggesting that a decrease in *MAPT* expression contributes to decreased levels of tau.

The finding of decreased levels of tau within these cells aligns with previously reported decreased levels of full-length tau within a mixed population of neurons, comprised mainly of GABAergic neurons and dopaminergic neurons, derived from V337M *MAPT* hiPSC (Ehrlich *et al.,* 2015). In this study, the authors demonstrate increased fragmentation of tau and

conclude that this is at the expense of full-length tau, however, increased fragmentation was not observed within these V337M *MAPT* hiPSC-CGNs. The decrease in tau found within V337M *MAPT* hiPSC-CGNs contrasts increased levels of total tau reported within in N297K (Wren *et al.,* 2015), A152T (Silva *et al.,* 2015) and P301L (Verheyen et. al., 2015) *MAPT* hiPSC-neurons, indicating that this aspect of tau pathology may be exclusive to this mutation.

Although levels of tau protein have not yet been investigated within the brains of patients with this mutation, a recent study reported similar levels of tau within the CSF of V337M *MAPT* patients compared to controls (Spina *et al.,* 2017). Similar levels of CSF-tau in comparison to controls has also been reported in patients carrying P301L and G272V *MAPT* (Rosso *et al.,* 2003) and within those diagnosed with FTD (Sjögren *et al*., 2001). Analysis of total tau levels within the brain tissue of a patient carrying IVS 10+3 G>A *MAPT* (Spillantini *et al.,* 1997) and in patients with FTD-tau (Adamec *et al*., 2001; van Eersel *et al*., 2009) has also revealed similar levels compared to controls. The decrease in total tau levels within V337M *MAPT* hiPSC-CGNs does not reflect levels reported in the cerebrospinal fluid (CSF) or brain tissue of those with FTDP-17 and other sporadic forms of FTD-tau.

The decrease in *MAPT* expression found in V337M *MAPT* hiPSC-CGNs in this study was unexpected as Ehrlich and colleagues found that V337M *MAPT* hiPSC-dopaminergic neurons express *MAPT* at similar levels to controls (Ehrlich *et al.,* 2015). Furthermore, no difference in expression levels were found in Drosophila overexpressing human V337M *MAPT* compared to those expressing WT human *MAPT* (Haddadi *et al*., 2016). In A152T *MAPT* hiPSC-neurons *MAPT* expression has also been reported to be similar to that within controls (Silva *et al.,* 2016).

Ehrlich and colleagues reported considerable variation in *MAPT* expression levels between FTDP-17 hiPSC-neurons created from different clones (Ehrlich *et al.,* 2015). Non-disease related variation of *MAPT* expression between hiPSC clones could explain the difference in *MAPT* expression reported by Ehrlich and colleagues compared to those measured here, as only one clone was analysed here due to a lack of those derived from V337M-E. The disparity between levels of *MAPT* expression in this study and within Ehrlich *et al.,* 2015 may also be explained by neuronal subtype variability in *MAPT* expression changes due to V337M *MAPT. MAPT* expression levels and the expression of different isoforms of tau varies between different areas of the brain, with the temporal and frontal lobes expressing the highest levels of tau (Majounie *et al.,* 2013; Trabzuni *et al.,* 2012). Liang and colleagues have demonstrated

that in AD brains *MAPT* expression is differentially altered in a regionally specific manner; specifically regions particularly targeted in AD express lower levels of *MAPT* compared to healthy brains (Liang *et al*., 2008). CGNs are abundantly present within the frontal and temporal cortices, therefore, gene expression of *MAPT* may be decreased in these as they represent the areas principally degenerated in FTDP-17, whereas Ehrlich and colleagues measured *MAPT* expression within cells that contained a large proportion of dopaminergic neurons, which are not associated in such high numbers within these brain areas. Further investigation into changes in the gene expression of *MAPT* within brain tissue isolated from the frontal and temporal cortices compared to other areas of the brain may help us to understand whether the effects of *MAPT* mutations alter gene expression in a region-specific manner.

The reduced levels of tau protein and *MAPT* expression within V337M *MAPT* hiPSC-CGNs found in this study may reflect the state of these cells early in disease; before tauopathy has become apparent. A reduction in the levels of tau protein has been demonstrated previously to diminish the severity of disease (Cheng *et al*., 2014; Santacruz *et al*., 2005). Therefore, the reduction of tau measured in these cells could indicate a protective mechanism.

4.4.3 Levels of phosphorylated tau in V337M-CGN

Levels of pSer396/404 tau were found to be increased within CGN derived from one hiPSC cell line with the mutation (V337M-E), both before and after normalisation to total tau. Within CGN derived from V337M-C, however, levels of pSer396/404 were found to be not significantly different in comparison to controls after normalisation to total tau.

Although phosphorylation of tau at this site has not yet been investigated within hiPSC-neurons carrying V337M *MAPT* or within the brain tissue of patients with this mutation, increased phosphorylation of tau at this site has been reported within the hippocampal neurons of 11 month old V337M *MAPT* mice (Tanemura *et al*., 2002). It has also been demonstrated, *in* vitro, that V337M *MAPT* tau is more rapidly phosphorylated at Ser396 and Ser404 and phosphorylated to a greater degree than WT tau at Ser404 upon treatment with kinases isolated from the rat brain (Alonso *et al*., 2004). In another study, pSer396/404 tau was found to be increased in H4 neuroblastoma overexpressing V337M tau compared to those overexpressing WT tau (DeTure *et al.,* 2002). Although tau is phosphorylated at pSer396/404 during neurodevelopment (Bramblett *et al.,* 1993), which

potentially could be a limitation in the recognition of increased phosphorylation due to *MAPT* mutations in these cells, this site has been found to be more intensely phosphorylated in hiPSC-neurons carrying A152T *MAPT* (Silva *et al.,* 2016) and in hiPSC-neurons seeded with pre-aggregated tau oligomers (Usenovic *et al.,* 2015) compared to controls, illustrating that hiPSC-neurons are capable of overcoming this limitation. It was, therefore, expected that V337M *MAPT* hiPSC-CGNs would also have increased phosphorylation of tau at these sites.

Evidence of interclonal variability upon disease specific phenotypic analysis has been previously documented within studies involving the derivation of neurons and other cell types from hiPSC (Martelli *et al.,* 2012; Ehrlich *et al.,* 2015; Yokobayashi *et al*., 2017; Sheridan *et al.,* 2011), which is suggested to be at least partially due to variability occurring during reprogramming and differentiation (Liang and Zhang, 2013; Vitale *et al*., 2012). Clonal variability may explain the difference in the phosphorylation of tau at pSer396/404 between clones V337M-C and V337M-E.

Levels of tau phosphorylated at pSer202 are increased within V337M-C-CGN after normalisation to total tau in comparison to the control line, Nas 2-CGN. In agreement with the results in this present study, widespread pSer202/205 tau positive immunostaining has been reported within the midbrains of V337M *MAPT* patients (Ehrlich *et al.,* 2015,) as well as within the hippocampal neurons of Tg V337M *MAPT* mice at 6-12 months of age compared to controls (Lambourne *et al.,* 2005; Tanemura *et al.,* 2002). These are also supported by previous *in vitro* studies, which have provided evidence to suggest that the mutation may increase the propensity for tau to become phosphorylated at these sites. In a cell-free system, V337M *MAPT* tau is phosphorylated *in vitro* to a greater degree, upon phosphorylation with kinases isolated from the rat brain, at Ser202 compared to WT tau (Alonso *et al*., 2004) demonstrating that V337M *MAPT* may result in tau with a greater propensity to be phosphorylated at these sites. Additionally, co-overexpression of V337M *MAPT* and GSK3 in CHO cells has been shown to result in increased pSer202 tau compared to CHO cells co-expressing WT tau and GSK3 (Dayanandan *et al.,* 1999). hiPSC-neuron models have so far demonstrated increased pSer202 tau within hiPSC-neurons carrying N279K, P301L and A152T *MAPT* (Ehrlich *et al.,* 2015; Fong *et al.,* 2013; Verheyen *et al.,* 2015, Silva *et al.,* 2016) despite pSer202 tau being present at high levels during neurodevelopment (Goedert *et al.,* 1993).

The banding patterns revealed by probing western blots with CP13 are different for Nas 2-CGN compared to V337M-C-CGN samples. In V337M-C-CGN samples, the bands at 68 kDa are lower in density compared to the same bands within Nas 2-CGN samples. Additionally, bands at 52 kDa are much more dense in V337M-C-CGN compared to those in Nas 2. Kimera and collegues have previously used phospho-tagging alongside western immunoblotting to demonstrate that certain mutations affect the banding pattern produced by phosphorylation of tau by Cdk5 when probing with different total tau and phospho-tau antibodies. Upon further investigation, the group did not find R406W *MAPT* affected major phosphorylation sites known to be phosphorylated by Cdk5 (Ser202, Thr205, Ser235 and Ser404), therefore it was concluded that minor phosphorylation sites may be affected by the mutation resulting in the altered pattern of phosphorylation. Whilst Kimura and colleagues found that R406W *MAPT* altered these banding patterns, V337M *MAPT* was not found to alter the phosphorylation of tau by Cdk5 (Kimura *et al.*, 2016). The altered pattern of phosphorylation in V337M-C-CGN compared to Nas 2-CGN may suggest that V337M *MAPT* alters the order in which tau is phosphorylated, possibly resulting in fewer tau species phosphorylated at Ser202 being hyperphosphorylated to a degree resulting in the band at 68 kDa. As other tau kinases apart from Cdk5, for example GSK3β, PKC and Erk 1/2 (Martin et al., 2013), are known to phosphorylate tau at pSer202 it possible that V337M *MAPT* alters the propensity for tau to become phosphorylated by kinases other than Cdk5; further investigation is needed to examine this hypothesis.

Phosphorylation of tau at Thr231 was found to be markedly decreased in V337M-C-CGN compared to Nas 2-CGN, suggesting that the mutation alters tau phosphorylation at this site. In support of this result, overexpression of V337M *MAPT* within H4 neuroblastoma cells was shown to decrease phosphorylation of tau at Thr231 tau (DeTure *et al*., 2002). Additionally, V337M *MAPT* overexpression within HEK-297 cells has been demonstrated to increase dephosphorylation of tau at this site by protein phosphatase 2A (PP2A) compared to overexpression of WT tau (Han *et al.,* 2009). This result was unexpected, however, as increased phosphorylation at this site is associated with tauopathy (Acker *et al*., 2013). Furthermore, increased pThr231 tau has been detected in Tg V337M *MAPT* mice at six months of age (Lambourne *et al.,* 2005). In line with these studies, within a cell-free *in vitro* system V337M *MAPT* tau is phosphorylated more rapidly by rat brain kinases and to a greater degree at Thr231 compared to WT tau (Alonso *et al.,* 2004). In control hiPSC-neurons seeded with pre-aggregated tau (Usenovic *et al.,* 2015) and in hiPSC-neurons

derived from a patient with A152T *MAPT* increased pThr231 tau has been reported (Silva *et al.,* 2016), demonstrating that the decrease in pThr231 tau found in V337M *MAPT* hiPSC-CGNs is likely to be an effect of this specific mutation. The decrease in phosphorylation of tau within V337M *MAPT* hiPSC-CGN in this study may represent the effect of the mutation in early disease, possibly due to its influence on the ability of tau to be dephosphorylated at this site.

4.4.4 Protein levels, activity and expression levels of tau kinases in V337M-CGN

Levels of GSK3β and active (pTyr216) GSK3β, as well as expression levels of *GSK3β* in V337M-C-CGN, are not significantly different compared to Nas 2-CGN. In V337M-E-CGN, however, total GSK3β levels are increased and the amount of active GSK3β is decreased compared to Shef 6-CGN, both before and after comparison to total GSK3β. These results suggest that the activity of GSK3β is not increased within V337M *MAPT* hiPSC-CGNs. Increased activity of GSK3β is associated with neurodegenerative disease and GSK3β is capable of phosphorylating the majority of sites phosphorylated in AD, therefore it is considered an important therapeutic target (Chapter 1.3.1).

It is uncertain whether GSK3β levels and activity are altered in V337M *MAPT* FTDP-17. No change in pTyr216 GSK3β could be found in Tg V337M *MAPT* mice compared to controls (Lambourne *et al.,* 2005) and phosphorylation of V337M *MAPT* tau by GSK3β within a cell-free system, *in vitro*, was similar compared to WT tau (Connell *et al.,* 2001), suggesting that this mutation does not alter the propensity of tau to become phosphorylated by this kinase. These results, therefore, corroborate existing evidence and suggest that GSK3β is not involved in the initial phosphorylation events early in tauopathy resulting from V337M *MAPT*. Therefore, the changes in phosphorylation levels of tau at pSer202, pSer396/404 and pThr231, which are sites phosphorylated by GSK3β (Reynolds *et al.,* 2000; Goedert *et al.,* 1995), in V337M-CGN are unlikely to be due to increased GSK3β activity.

The banding patterns produced by probing western blots for pTyr216 GSK3β and total GSK3β for both V337M-C and Nas-2 derived CGNs and V337M-E and Shef 6 derived CGNs were found to vary. Total GSK3β bands for V337M-C-CGN were found at 48 kDa as well as 52 kDa, whereas there was just one total GSK3β band for Nas 2-CGN at 52 kDa. This may be due to the greater levels of protein present within the samples loaded on the blots for V337M-C-

CGN, allowing for visualisation of the minor band at 48 kDa. Mukai and colleagues suggested that the upper band may indicate GSK3β2, the alternative spliced variant of GSK3β with a 13 amino acid-insertion, whereas the lower band may indicate GSK3β1 (Mukai *et al.*, 2002). An additional band at approximately 46 kDa was also produced by probing western blots of V337M-C-CGN and Nas 2-CGN for pThr216 GSK3β, which was not present within western blots of V337M-E-CGN and Shef-6-CGN probed with the same antibody. The additional minor bands may indicate non-specific binding and therefore were not included in the analysis of these results.

The protein levels of p35 were found to be decreased in V337M *MAPT* hiPSC-CGN in comparison to control hiPSC-CGN. The regulation of Cdk5 activity is discussed in detail in Chapter 1 (Chapter 1.3.2); to briefly reiterate, Cdk5 must bind to p35 or p25 to become active. It is considered to be 'hyperactive' when bound to p25 and increased levels of p25 or decreased levels of p35 are associated with neurodegenerative disease (Chapter 1). While the levels of p25 cannot be commented on due to the insufficient staining of western blots, the decrease in p35 levels detected within V337M-CGN compared to controls suggests that p35 has been cleaved to p25, indicative of increased Cdk5 activity.

Previous reports of the effects of V337M *MAPT* on the activity of Cdk5 are controversial. A decrease in p35 was not found via western blotting in cells carrying this mutation, therefore, increased activity of Cdk5 may underlie the increased levels of tau phosphorylation recognised at pSer396/404, pSer202 and pThr231 in V337M-CGN, as these are sites known to be phosphorylated by this kinase (Martin *et al*., 2013; Imahori and Uchida, 1997). FTDP-17 mutations have been shown previously to result in increased levels of caspase 3 (Stanford *et al*., 2003). Indeed, cultures of V337M *MAPT* hiPSC-dopaminergic neurons have greater numbers of cleaved-caspase 3 positive neurons compared to control neurons after treatment with Rotenone, indicating increased vulnerability of neurons with the mutation (Ehrlich *et al.,* 2015). Since p35 is cleaved to p25 by caspase, increased levels of caspase could lead to increased Cdk5 activity (Chapter 1.3.2).

PAK3 protein levels of were found to be significantly decreased in V337M-C-CGN compared to Nas 2-CGN. While levels of PAK3 are not significantly decreased in V337M-E-CGN compared to Shef 6-CGN controls, there is a trend towards decreased PAK3 protein in V337M-E-CGN compared to Shef 6 controls ($p= 0.061$). A decrease in PAK3 protein levels has been demonstrated to result in neurodegeneration, specifically involving dysregulation of

microtubule dynamics and the loss of synapses (Chapter 1.3.3). PAK3 protein levels and gene expression was expected to be decreased in these cells as expression of *PAK3* was found to be downregulated in V337M *MAPT* hiPSC-dopaminergic neurons compared to controls in a previous study (Ehrlich *et al.,* 2015). However, gene expression analysis of *PAK3* in these cells demonstrated that *PAK3* is not expressed at significantly different levels in V337M *MAPT* hiPSC-CGNs compared to controls, which may represent a difference between *PAK3* expression in these two different cell types. *PAK3* has not been found to be expressed at lower levels within the midbrains of FTDP-17 patients previously (Ehrlich *et al.,* 2015), however, which may be due to the association of decreased *PAK3* expression with early pathogenesis. In AD, PAK3 levels have been demonstrated to be low in early stage disease only (Nguyen *et al.,* 2008) (Chapter 1.3.3).

The activity of Akt is not affected by V337M *MAPT* in these hiPSC-CGNs, as there is no significant difference in the levels of pSer473 Akt between hiPSC-CGNs carrying V337M *MAPT* compared to controls. These results suggest that Akt phosphorylation of tau is not involved in early pathogenesis of FTDP-17 caused by this mutation. Although there have been no previous studies on the activity of Akt in V337M *MAPT* patients or models, in P301S *MAPT* Tg mice, no change in the levels of Akt or its activity were found (Barini *et al*., 2016), therefore, this result agrees with previously published work.

4.4.5 Levels of synapsin I in V337M-CGN

Levels of synapsin I were found to be markedly decreased in V337M-CGN compared to controls, implicating a loss of post-synaptic densities and impaired synaptic localisation of NMDARs (Warmus *et al.,* 2014). In C. elegans, V337M *MAPT* causes pre-synaptic dysfunction of cholinergic neurons (Kraemer *et al*., 2003). Synapses have been demonstrated to be affected early in FTDP-17, before evidence of neurodegeneration and in some cases tauopathy, in FTDP-17 mouse models (Yoshiyama 2008; Umeda *et al.,* 2013; Crescenzi *et al.,* 2014; Hoffmann *et al.,* 2013; Eckermann *et al.,* 2007; Harris *et al.,* 2012; Rocher *et al.,* 2010). One possible explanation for the loss of synapses could be explained by a disruption of the regulation of microtubule dynamics, which has been documented to be associated with V337M *MAPT* (Hong *et al.,* 1998; Hasegawa *et al.,* 1998; Dayanandan *et al.,* 1999; Rizzu *et al.,* 1999; Frappier *et al.,* 1999; Arawaka *et al.,* 1999; Deture *et al*., 2000). These results suggest that hiPSC-CGNs may be highly suited for the investigation of synaptopathy in neurodegenerative disease.

4.4.6 Summary

This study has provided proof-of-concept that patient derived hiPSC-CGNs can be used to investigate changes in tau protein levels, tau phosphorylation, kinase activity and gene expression caused by V337M *MAPT*. hiPSC-CGNs carrying the mutation have been demonstrated to have lower levels of tau protein in comparison to controls. Furthermore, hiPSC-CGNs derived from this patient had increased levels of pSer202 tau and decreased levels of pSer231 tau, indicating that this mutation is capable of altering the tau phosphorylation at these sites, which are associated with tauopathy. The hiPSC-CGNs have also provided an insight into altered kinase activity due to the mutation; Cdk5 activity is decreased, as evidenced by decreased levels of p35, while levels of PAK3 are also decreased. Surprisingly, GSK3β activity, a tau kinase considered to be a 'master regulator' of tau phosphorylation, was not increased in these cells, which suggests that the increase in pSer202 was not due to GSK3β but another kinase, possibly Cdk5, which also phosphorylates tau at this site.

Chapter 5

The development of a model of Alzheimer's disease using pluripotent stem cell technology

5.1 Introduction

An extensive body of experimental evidence from biomarker analysis in Alzheimer's disease (AD) patients, *in vitro* models and *in vivo* models supports the hypothesis that pathological tau phosphorylation and aggregation is initiated by aberrant accumulation of amyloid-β (Aβ) in AD (Stancu *et al.,* 2014). A therapeutic solution may transpire through precise manipulation of the molecular pathways coupling these proteins to prevent prodromal pathological events, which occur decades before cognitive symptoms arise. Currently, the molecular pathways that facilitate Aβ-induced tau phosphorylation early in the disease remain unclear. Traditional *in vitro* and *in vivo* models cannot accurately represent the subtle molecular changes important in early stage AD (Chapter 1.4). A clinically relevant, human model allowing for improved resolution of these pathways would, therefore, be an invaluable tool for this line of investigation.

Chapter 4 described altered tau phosphorylation and kinase activity in V337M *MAPT* hiPSC-neurons compared to controls, demonstrating that hiPSC technology can be used to gain inferences into frontotemporal dementia with Parkinsonism linked to chromosome 17 (FTDP-17). To examine whether neurons derived from human pluripotent stem cells (hPSC-neurons) can also be used to investigate the early changes in tau phosphorylation in sporadic AD (sAD), hPSC-neurons were treated with Aβ 1-42 oligomers ($A\beta_{42}O$), described as the most pathogenic form of Aβ (Chapter 1.2.3.2.2). Two control hPSC lines were differentiated to produce mature basal forebrain cholinergic neurons (bfCNs) and cortical glutamatergic neurons (CGNs), which are two particularly vulnerable neuronal subtypes in AD (Chapter 1.2.3.1.1). The effects of $A\beta_{42}O$ on the levels of total tau, *MAPT* expression, tau phosphorylation at specific sites associated with AD and tau kinase activity were investigated.

5.1.1 The relationship between Aβ and tau in Alzheimer's disease

AD is defined not only by the presence of abnormally phosphorylated tau (ptau) but also Aβ pathology. The pathology and pathogenesis of AD is discussed in detail in Chapter 1, along with the pathological processing of amyloid protein and the pathological phosphorylation of tau in AD (Chapter 1.3.3). Deleterious interactions between tau and Aβ seem to be necessary for initiation and progression of AD. Indeed, a recent study using regression models to analyse cognitive decline and clinical progression in patients with mild cognitive impairment (MCI), with aggregations of both proteins, demonstrated that Aβ and tau interact synergistically, rather than additively, to drive AD (Pascoal *et al.,* 2017).

Evidence from murine AD models, with concurrent Aβ and tau pathology, supports the hypothesis that abarent Aβ processing exacerbates tau pathology. For example, intracerebral injection of $A\beta_{42}O$ into transgenic (Tg) mice with mutations in *MAPT* results in greater hyperphosphorylation of tau, as well as higher levels of tau in abnormal conformations, not only at the injection site but also in distant regions of the brain (Bolmont *et al.,* 2007; Frautschy *et. al.*, 1991; Götz *et al.,* 2001; Sigurdsson *et al.,* 1997; Chabrier *et al.,* 2004; Lewis *et al.,* 2001; Pooler *et al.,* 2015). Likewise, the resultant offspring born by crossing mice with an *APP* duplication with mice expressing human P301L *MAPT* exhibit increased neurofibrillary tangle (NFT) pathology within the limbic and olfactory areas of the brain compared to P301L *MAPT* parent mice. This was despite expressing similar levels of tau as P301L *MAPT* parent mice and similar Aβ pathology to *APP* parent mice (Lewis *et al.,* 2001). Chabrier and colleagues generated a double Tg mouse through crossing a mouse overexpressing human *MAPT* with mice overexpressing human V717L or KM670/671NL *APP,* and reported acceleration of cognitive impairment, tau pathology and dendritic spine loss, in comparison to either parent (Chabrier *et al.,* 2014), linking Aβ-dependent acceleration of tau pathology with other synaptic and symptomatic AD hallmarks. Pooler and colleagues also reported a dramatic increase in the speed and distribution of tau propagation from the entorhinal cortex to synaptically-connected brain regions of the offspring produced by crossing mice overexpressing P301L *MAPT* within layer II of the entorhinal cortex with Tg 3xfAD (*K670M/N671L APP,* Δ*E9 PSEN1*) mice, compared to either parent (Pooler *et al.,* 2015).

The presence of tau has been demonstrated to be necessary for Aβ-induced changes to cytoskeletal structure, neurodegeneration and subsequent cognitive decline recognised in AD. Application of AβO (Aβ oligomers) to tau null *MAPT* mouse primary hippocampal

neurons does not result in the cytoskeletal changes and neurodegeneration, which occur when it is applied to WT mouse primary hippocampal neurons (Jin *et al.,* 2011; Rapoport *et al.,* 2002). Furthermore, cross-breeding mutant Tg h*APP(K670M/N671L,V717F)* or 5xFAD (*APP*(*K670N/M671L,I716V,V717I/PSEN1M146L,L286V)* mice with null *MAPT* mice ameliorates cognitive dysfunction and early mortality (Roberson *et al.,* 2007; Leroy *et al.,* 2012). In patients with a high cerebrospinal fluid (CSF) Aβ load, the presence of pThr181 tau was reported to be necessary for cognitive decline (Desikan *et al.,* 2012), demonstrating the requirement of abnormal ptau for the pathogenesis of AD. Collectively, this body of research suggests that Aβ exerts its toxic potential through interactions with tau protein.

Although we do not yet have a thorough understanding of the mechanisms through which Aβ causes pathological phosphorylation of tau protein, evidence collected over the last two decades supports numerous pathways, which may work in concert with each other to drive disease progression. Aβ and tau can form soluble complexes *in vitro* (Guo *et al.,* 2006) and it has been hypothesised that the interaction of Aβ with tau seeds an initial structural change in tau, which templates further misfolding and hyperphosphorylation of tau thereby propagating tau pathology (Guo *et al.,* 2006; Bolmont *et al.,* 2007). Furthermore, AβO interacts with the membranes of neurons initiating molecular cascades associated with dyshomeostasis of intracellular calcium concentration ($[Ca^{2+}]i$), disturbed Wnt signalling and neuroinflammation. These molecular cascades are intimately associated with the dysregulation and activation of tau kinases and phosphatases, resulting in the hyperphosphorylation of tau.

5.1.2 Rational for sAD hiPSC-model design

The glutamatergic and cholinergic systems are especially affected in AD, of which CGNs and bfCNs are particularly vulnerable, respectively (Chapter 1.2.3). This model of sAD benefits from hiPSC-technology to produce these specific neuronal subtypes from control hPSC lines. The hiPSC line, Nas 2 (Chapter 3), was differentiated alongside the hESC line, Shef 6 (Chapter 3), and synthetic $A\beta_{42}O$ was applied to mature hiPSC-neurons over a period of 48 hours. Two control lines were used in this study to evaluate the reproducibility of model should different hPSC cell lines be used. hPSC-bfCNs were derived through plating neural stem cells, derived from hPSCs, for 35 days and hPSC-CGN were derived by culturing cells for 50 days from the first day of differentiation. The reason for these time points was so that the hPSC-bfCNs and hPSC-CGNs would be of similar 'age' or maturation point as by approximately day 15 of the

protocol for the production of hPSC-CGN hPSC have differentiated to become neural progenitors (Chi *et al*., 2012).

sAD is a highly heterogenous disease; various environmental and lifestyle factors are thought to influence the pathogenesis, alongside the cumulative effects of many unknown genetic risk factors (Chapter 1.2.3.4). Genetic factors are conserved through the process of reprogramming and differentiation of hiPSC (Rouhani *et al.,* 2014), however, environmental influences and the effects they exert on a patient's epigenetics, are not (Hewitt and Garlick, 2013). Therefore, many of the cumulative factors that impact on the development of sAD may be lost in reprogramming, which may explain the lack of clear phenotype in some hiPSC-neuron lines derived from sAD patients (Kondo *et al.,* 2013; Israel *et al.,* 2011; Duan *et al.,* 2014). Molecular pathology within hiPSC-neurons generated from different sAD patients has been demonstrated to be highly variable (Duan *et al.,* 2014; Kondo *et al.,* 2013; Israel *et al.,* 2012) and to model this heterogeneous disease comprehensively hiPSC-neurons will likely need to be differentiated from a large cohort of donor sAD patients. To circumvent these challenges, synthetic $A\beta_{42}O$ was applied to hiPSC-neurons created from control cell lines, rather than from sAD patient somatic cells, to allow for examination of the effects of $A\beta_{42}O$ on tau pathogenesis in isolation of influential environmental and genetic factors.

Oligomeric $A\beta_{42}$ is the most toxic form of Aβ in neurodegenerative disease (Chapter 1.2.3.2.2), therefore, treatment of cells with this form of Aβ was used to model AD. Previous studies are at odds on the effects of $A\beta_{42}O$ at various concentrations upon treatment of different cell types, however, the majority of the literature overall suggests that greater concentrations of Aβ (*e.g.,* between 5 μM and 10 μM) are acutely toxic to cells, whereas concentrations lower than this are more likely to be closer to physiological levels and therefore be more representative of AD pathology (Wicklund *et al.,* 2010). Concentrations ranging from 0.1 μM to 1 μM $A\beta_{42}$ are most commonly used for AD modelling to study changes in tau phosphorylation using cell culture systems (Wicklund *et al.,* 2010; Zempel *et al.,* 2010; Gilson *et al.,* 2015). The aggregation of $A\beta_{42}$ depends on concentration and it has been reported that application of concentrations of Aβ 1-42 to cell media in the micromolar range result in aggregation of monomers to produce oligomers, whereas application of nanomolar to low micromolar concentrations result in aggregation into a mixture of monomers and oligomers (Hellstrand *et al.,* 2010). This study aims to investigate the effect of $A\beta_{42}O$ on tau pathology, rather than toxicity; therefore, a range of concentrations from 0.1

μM to 1 μM were used in this study. Cells were incubated with $A\beta_{42}O$ over a period of 48 hours as many publications have been produced demonstrating application of $A\beta_{42}O$ over this time period (Wei *et al.*, 2002; de Felice *et al.*, 2008; Ferreira *et al.*, 1997; Zheng *et al.*, 2002; Choi *et al.*, 2014) and it was hoped this would allow for comparison of the results from this study with those from other publications.

Unfortunately, it was not possible to generate enough Nas 2-CGNs during this project to allow for treatment of these cells with $A\beta_{42}O$ to be evaluated. It also was not possible to generate enough Nas 2-bfCN or Shef 6-CGN to evaluate the effects of 0.1 μM $A\beta_{42}O$.

5.1.3 Aims

The aim of the work in this chapter was to develop a model of sAD and to investigate changes in tau related-molecular pathology within it to gain insight into the pathogenesis of AD.

5.2 Methods

Cortical glutamatergic neurons (CGNs) were derived from control hPSC cell lines, Nas 2 and Shef 6 using the protocol described in Chapter 4 (Chapter 4.2.1).

5.2.1 Differentiation of human pluripotent cells to produce basal forebrain cholinergic neurons using a non-adherent, embryoid body based system

This protocol was developed within the Caldwell lab (Crompton *et al.,* 2013). The method is dependent on a non-adherent, embryoid body based system. This reductionist approach to hPSC differentiation allows the cells to establish their own developmental cues, parallel to those recognised during embryonic patterning within the neural tube, to produce basal forebrain cholinergic neurons (bfCNs) (Crompton *et al.,* 2013).

The non-adherent system promotes endogenous sonic hedgehog (SHH) signalling within cultures of embryoid bodies, which directs the expression of key transcription factors, homeobox protein Nkx 2.1 and Lim homeobox 8 (LHX8), required to drive the fate of the cells towards basal forebrain neural progenitors. Subsequent adherent culture of the neurospheres allows the cells to terminally differentiate to produce bfCNs. This protocol has been demonstrated to produce bfCNs capable of releasing acetylcholine and that have a functional electrophysiological profile (Crompton *et al.,* 2013).

5.2.1.1 Media used during the derivation of basal forebrain cholinergic neurons

Table 5.1 Chemically Defined Media (CDM)

Product	Amount	Supplier and product code
IMDM + GlutaMAX™	49 %	Life Technologies, 31980-022
F12 + GlutaMAX™	49 %	Life Technologies, 31765-027
Penicillin-Streptomycin solution stabilised (Pen-Strep)	1 %	Sigma, P4458
Albumax®	200 mg/ ml	Life Technologies, 11021-029
Monothioglycerol	100 ng/ ml	Sigma M6145
Insulin	10 mg/ ml	Sigma, I6634
SB431542	20 µM	Tocris, 1614
ROCK inhibitor	10 µM	Tocris, 1254

Table 5.2 Neural Expansion Media (NEM)

Product	Amount	Supplier and product code
KO DMEM	68 %	Life Technologies, 10829018
F12 + GlutaMAX™	28 %	Life Technologies, 31765-027
B-27® Supplement	2 %	Gibco, A14867-01
GlutaMAX™	1 %	Invitrogen, 35050
Penicillin-Streptomycin solution stabilised (Pen-Strep)	1 %	Sigma, P4458
Fibroblast Growth Factor 2 (FGF2)	20 ng / ml	Peprotech, 100-18B
Heparin	5 µg / ml	Sigma, H-1349
Epidermal Growth Factor (EGF)	20ng/ ml	Sigma, E-9644

Table 5.3 Terminal Differentiation Media (TDM)

Product	Amount	Supplier and product code
KO DMEM	68 %	Life Technologies, 10829018
F12 + GlutaMAX™	28 %	Life Technologies, 31765-027
B-27® Supplement	2 %	Gibco, A14867-0
GlutaMAX™	1 %	Invitrogen, 35050
Penicillin-Streptomycin solution stabilised (Pen-Strep)	1 %	Sigma, P4458

5.2.1.2 Formation of embryoid bodies from human pluripotent stem cells

Six 9 cm diameter tissue culture plates, each containing approximately 30 colonies of hPSC, grown on a layer of iMEFs, were required for each neuralisation. Any differentiated areas of the colonies were removed using an aspirator before incubating the cells with warm 1X collagenase (1 ml per plate) within the cell culture incubator at 37 ^{o}C for 20 minutes to detach the colonies from the tissue culture surface. Upon completion of the incubation period the collagenase was quenched with DMEM (4 ml per plate) to prevent further activity. The colonies were gently sprayed from the tissue culture surface using a P1000 pipette tip and collected in a 50 ml falcon tube. The colony pieces were allowed to settle at the bottom of the falcon tube before the media was aspirated. The colony pieces were resuspended in 5 ml of hPSC media without FGF2 to wash and allowed to settle again. After removing the media, the colonies were resuspended in 1 ml hPSC media without FGF2. The colonies were collected using a P1000 pipette and placed in a droplet onto the lid of a 6 cm diameter chopping plate. The excess media was carefully removed using a P200 pipette tip. A McIlwain tissue chopper (Mickle Laboratory Engineering Ltd.) was used to chop the colonies in a uniform fashion into 150 µM pieces. hPSC media, without FGF2 and supplemented with 10 ng/ ml ROCK inhibitor, was then added to the pieces on the chopping plate and a P200 pipette tip was used to gently lift the colony pieces and transfer them into a 25 cm^3 tissue culture flask, pre-coated with poly 2-hydroxyethyl-methacrylate and containing 6 ml of hPSC media without FGF2 and supplemented with 10 ng/ ml of the ROCK inhibitor, Y27632 (Tocris, 1254). The cells were allowed to form neurospheres for 4 days.

5.2.1.3 Neuralisation of embryoid bodies

To begin the neuralisation, the embryoid bodies (EBs) were collected with the media within the 25 cm^3 flask into a 15 ml falcon tube and centrifuged (300 g; 5 minutes). The media was removed and the EBs were resuspended in 10 ml CDM (Table 5.2), which contains the SMAD inhibitor SB431542. The 25 cm^3 tissue culture flask was washed with PBS, before the resuspended EBs were added back into the flask. The EBs were cultured in CDM for 8 days. At the end of this period the spheres of cells, which were once EBs, are now referred to as neurospheres as they now consist of neural stem cells.

5.2.1.4 Expansion of neural stem cells within neurospheres

After completion of this period the neurospheres were centrifuged (300 g; 5 minutes) and re-suspended in NEM (Table 5.3), supplemented with 10 µM ROCK inhibitor and 20 µM SB431542 for the first 10 days of expansion. Every 7 days, the neurospheres were chopped into 200 µm uniform pieces using the McIlwain tissue chopper to prevent the neurospheres becoming too large and to expand the population of cells. If a neurosphere becomes too large during expansion, the cells at the centre of the spheres will not have adequate access to nutrients in the media and will not respire correctly, leading to molecular and possibly genetic changes within these cells and cell death. The cells were also regularly triturated with a P1000 pipette to ensure a pure population of NSCs (Crompton *et al.,* 2013).

5.2.1.5 Terminal Differentiation of neural stem cells and progenitors

13 mm glass coverslips [VWR, 631-0149], stored in ethanol after sterilisation through treatment with nitric acid, were passed through a Bunsen burner flame to ensure sterility and remove ethanol. Each coverslip was placed into a well of a 12-well plate and coated with poly-L-ornithine and laminin (POR/L) (Chapter 2.1.2.2.1.4) and 250 µl TDM (Table 5.4) was added to each well, supplemented with 10 ng/ml N-[(3,5-Difluorophenyl)acetyl]-L-alanyl-2-phenylglycine-1,1-dimethylethylester (DAPT). DAPT is an inhibitor of the γ-secretase complex, for which Notch is a key target, therefore DAPT indirectly inhibits the Notch pathway leading to enhanced neuronal differentiation (Crawford and Roelink, 2007). Through inhibition of Notch, 3-5 neurospheres were plated onto each well on the coverslip, taking care to ensure space between each sphere. The spheres were allowed to attach, without the plate being disturbed, for 48 hours within the incubator. The media was then fully changed to TDM without DAPT. The media was changed every 2 days; alternating feeds were supplemented with 0.1 % laminin to aid attachment of the spheres to the culture surface. After 3-6 days axons sprouting from the spheres could be seen. Plated neurospheres were cultured for 35 days before processing for protein extraction (Chapter 2.2.1.1) or being subjected to a period of toxin application for 48 hours.

5.2.2 Application of toxins

$A\beta_{42}O$ were prepared and added to media as described below. The cells were incubated for 48 hours with media containing the $A\beta_{42}O$ in concentrations ranging from 0.1 µM to 1 µM.

5.3.2.1 Preparation of $A\beta_{42}O$

Lyophilised $A\beta_{42}$ peptide [Anaspec, AS-24224] was dissolved to a concentration of 1.6 M in 35 % acetonitrile (Ryu *et al.,* 2004) and 10 µl aliquots were stored in clean 0.5 ml Eppendorf tubes at -20 ^{o}C until required. The day before application of $A\beta_{42}$ onto the cells, an aliquot was thawed and diluted to 300 mM by addition of knockout (KO) DMEM. The solution was pipetted using a P200 pipette to ensure the solution was mixed. The solution was stored for 18 hours, overnight, within the cell culture incubator at 37 ^{o}C to allow polymerisation of protein monomers to oligomers. After the 18 hour incubation period, on the day of application of the toxin to the cells, warmed cell culture media was prepared within a 15 ml falcon tube with the correct concentration of Aβ and mixed thoroughly by inversion of the tube five times (van Helmond *et al.,* 2009). The media was then ready to add to the cells.

5.2.3 Immunocytochemistry

Immunostaining was performed as described in Chapter 2 (Chapter 2.2.2). The antibodies used during immunostaining in this chapter are listed in Table 5.5.

5.2.4 Western Immunoblotting

Immunostaining was performed as described in Chapter 2 (Chapter 2.2.1) using tau and ptau antibodies previously optimised in Tg 4510 mice (Chapter 4.3.1). The antibodies used during western immunoblotting in this chapter are listed in Table 5.5.

5.2.4.1 Stripping and re-probing of western immunoblots

Apart from western blots of samples obtained from Shef 6 -CGN treated with 1 µM $A\beta_{42}O$ and associated controls, western blots were stripped between probing with each antibody using western blot stripping buffer [Fisher, 21059]. Each blot was probed with an antibody against GAPDH before being probed with a tau antibody, either DA9, PHF-1 or CP13. Each western blot was then probed with an antibody against a tau kinase, either GSK3β, GSK3β pTyr216 or PAK3. Other blots were probed with GAPDH and then either antibodies again synapsin or p25-p35. DA9, PHF-1 or CP13 bands were analysed on separate blots because

stripping of these antibodies was determined to be difficult and bands for these antibodies are at similar weights.

Western blots of samples obtained from Shef 6 -CGN treated with 1 μM $A\beta_{42}O$ and associated controls were carried out through probing the same blots as these blots were produced and probed early in this PhD project. The process of probing separate western blots for each tau antibody was employed after this set of western blots throughout the PhD project to mitigate the risk of traces of previous tau antibodies being left behind on the blot after stripping. For these western blots, westerns were probed with secondary antibody after stripping to ensure primary antibodies were fully stripped from the blots before probing with an additional antibody. For this reason, the same GAPDH blot is used to compare results for Shef 6 -CGN treated with 1 μM $A\beta_{42}O$. These results are depicted in figures 5.6, 5.8, 5.11, 5.14, 5.16 and 5.17.

5.2.4.2 Analysis of western blots

The density of bands was analysed as described in Chapter 2 (Chapter 2.2.1.10). Each band, for a specific antibody, was normalised to its bands for control antibody, GAPDH. For each blot, the result for each case were compared to averaged controls. For phosphorylated tau antibodies, density of bands was also compared to those for total tau, after individual normalisation to GAPDH. Where anti-tau antibodies revealed multiple bands, all bands were included in the densitometric analysis. Analysis of PAK3 and synapsin were determined by analysis of only the main predicted bands at 65 kDa and 75 kDa, respectively. For p35 and p25 level analysis, only bands at 35 kDa and 25 kDa, respectively, were included. For analysis of the levels of GSK3β and pTyr216 GSK3β, only bands at 48 kDa and 52 kDa were included in analysis.

Statistical analysis for Nas 2-bfCN and Shef 6-CGN results was carried out using an unpaired Student's t-test. Statistical analysis for Shef 6-bfCN results was carried out using the Friedman test, with multiple comparisons undertaken between each concentration, including the controls, using Dunn's post hoc test. The Friedman test is a non-parametric test used to compared three or more matched or paired groups and allows for comparison of bands across different blots. This statistical test was chosen as samples for each concentration for Shef 6-bfCN are spread across three sets of blots. *=$p \leq 0.05$. **=$p \leq 0.01$. ***=$p \leq 0.001$.

Table 5.4 Antibodies used in western immunoblotting and immunocytochemistry

Primary antibody	Protein detected	Host	Manufacturer and catalogue number	References	Dilutions	
					Western	ICC
βIII Tubulin	βIII Tubulin	Mouse	ab6046, Abcam	(Tong *et al.,* 2015)	N/A	1:1000
βIII Tubulin	βIII Tubulin	Rabbit	ab15568, Abcam	N/A	N/A	1:1000
CP13	pSer202 tau	Mouse	Prof. Davies*	(Petry *et al.,* 2014; Vingtdeux, *et al.,* 2011)	1:1000	N/A
DA9	Pan-tau	Mouse	Prof. Davies*	(Petry *et al.,* 2014)	1:5000	N/A
GAPDH	GAPDH	Mouse	AM4300, Invitrogen	(de Oliveira *et al.,* 2017)	1:5000	N/A
GSK3β	GSK3β	Rabbit	D5C5Z, Cell Signalling	(Burk *et al.,* 2017)	1:500	N/A
GSK3β pTyr216	pTyr216 GSK3β	Rabbit	Ab75745, Abcam	(Porquet *et al.,* 2015)	1:500	N/A
p25-p35	p25-p35	Rabbit	C64B10, Cell Signalling	(Porquet *et al.,* 2015)	1:300	N/A
PAK3	PAK3	Rabbit	2609S, Cell Signalling	(Murata and Constantine-Paton, 2013)	1:300	N/A
PHF-1	pSer396/pSer404 tau	Mouse	Prof. Davies*	(Otvos *et al.,* 1994)	1:5000	N/A
PSD-95	PSD-95	Mouse	ab2723, Abcam	(Frandemiche *et al.,* 2013)	1:1000	1:300
Synapsin	Synapsin I	Rabbit	ab64581, Abcam	(Stefanova *et al.,* 2016)	1:750	1:300
ChAT	ChAT	Rabbit	ab181023, Abcam	(Crompton *et al.,* 2013)	N/A	1:250
MC1	Abnormal conformation tau	Mouse	Prof. Davies*	(Jicha *et al.,* 1997; Jicha *et al.,* 1999; Petry *et al.,* 2014)	N/A	1:250
Mushashi	Mushashi	Rabbit	ab154497, Abcam	N/A	N/A	1:300
Nestin	Nestin	Mouse	ab105389, Abcam	(Pijuan-Galitó *et al.,* 2016)	1:300	N/A

*Prof. Peter Davies (Albert Einstein College of Medicine, New York, USA) kindly supplied CP13, DA9, PHF-1 and MC1 antibodies.

5.2.5 Quantitative PCR

Quantitative PCR (qPCR) was carried out as described in Chapter 2 using probes to detect the gene expression of *GAPDH, MAPT, GSK3β, CDK5* and *PAK3.* The details of these probes can also be found in Chapter 2 (Chapter 2.2.3). Statistical analysis of qPCR data was performed using the Mann-Whitney test where one concentration of $A\beta_{42}O$ was used to treat the same cells or a Kruskal-Wallis test followed by a post-hoc Dunn's test where more than one concentration was used. *=$p \leq 0.05$. **=$p \leq 0.01$. ***=$p \leq 0.001$.

5.3 Results

5.3.1 Characterisation of bfCN differentiation

The intermediate cells generated during this differentiation protocol have already been characterised in Crompton *et al.,* 2013. However, to ensure a homogenous population of neural stem cells (NSC) were obtained within the neurospheres before plating down for terminal differentiation, cells from within neurospheres at day 30 of neural expansion were dissociated and plated for two hours before fixing for immunocytochemistry with two NSC markers, nestin and mushashi (Figure 5.1).

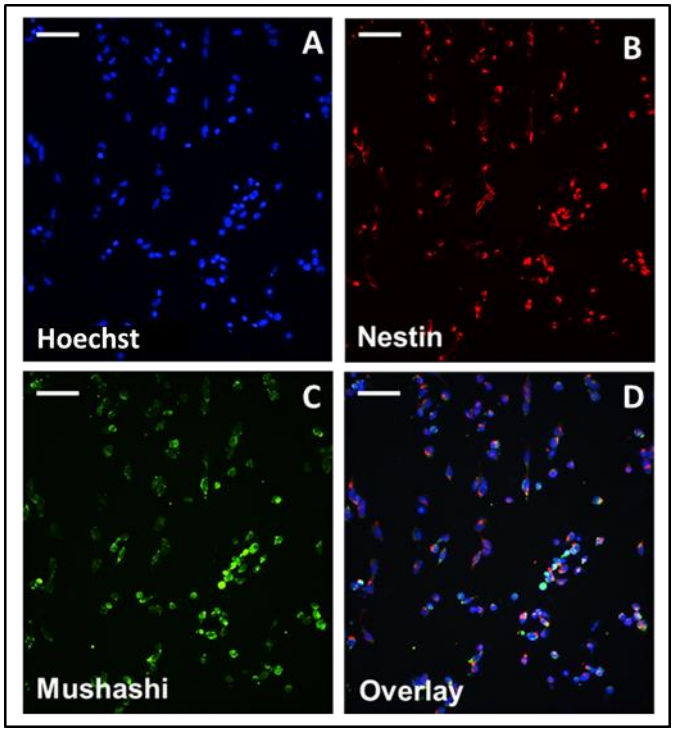

Figure 5.1 Cells within neurospheres express neural stem cell markers at day 30 during of expansion phase of Crompton protocol

Dissociated cells from within neurospheres at day 30 of differentiation of Nas 2 line, plated and cultured for two hours, immunostain positively for nestin (B, red) and mushashi (C, green), two neural stem cell markers as shown in the overlay (D). Hoechst stain was used to highlight the cell nuclei (A, blue). Scale bars indicate 30 µM.

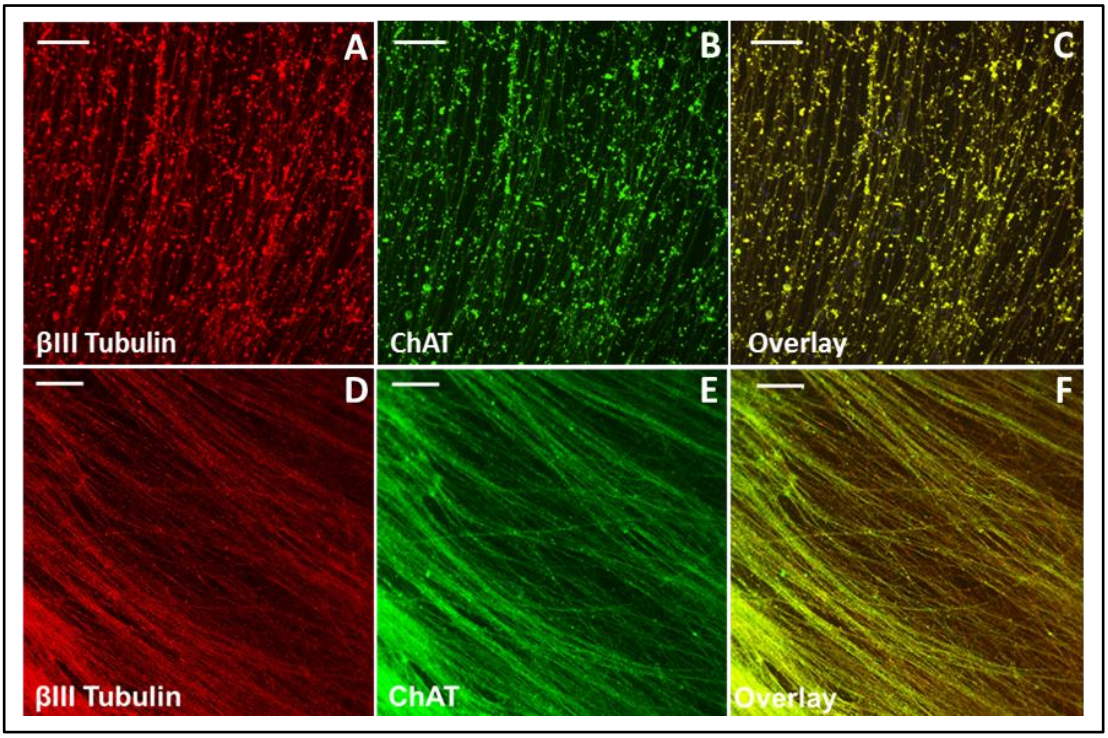

Figure 5.2 Characterisation of day 35 differentiated bfCNs

Images in the upper panels demonstrate Shef-6 bfCNs immunostained with antibodies against βIII tubulin (A, red), ChAT (B, green) and the overlay of these (C). Images in the lower panels show Nas 2-bfCNs immunostained with antibodies against βIII tubulin (D, red), ChAT (E, green) and the overlay of these (F). Scale bars indicate 50µm.

Choline acetyltransferase (ChAT) is the enzyme responsible for biosynthesis of the neurotransmitter acetylcholine (ACh), by catalysing the transfer of an acetyl group from acetyl coenzyme A to choline. ChAT is expressed by cholinergic neurons in the central nervous system (CNS) (Oda, 1999) and can be used as a marker for cholinergic neurons. Terminally differentiated cells, cultured for 35 days after neurosphere plate down, were fixed and immunostained with an anti-ChAT antibody and anti-βIII tubulin. BfCNs differentiated from both Shef 6 and Nas 2 lines positively stain with anti-ChAT (Figure 5.2).

Terminally differentiated bfCNs were fixed and immunostained to detect synapsin I and post-synaptic density protein 95 (PSD-95). Synapsin is a protein integral to the pre-synaptic membrane and important for vesicle trafficking within the synapse (Evergren *et al.,* 2007), therefore can be used to indicate pre-synaptic membranes. PSD-95 is a key constituent protein of the post-synaptic density, which is associated with the post-synaptic membrane,

and is therefore used as a post-synaptic marker (Naisbitt *et al.,* 2000). Distribution of these proteins from the soma throughout the axon is an indicator of synapse formation.

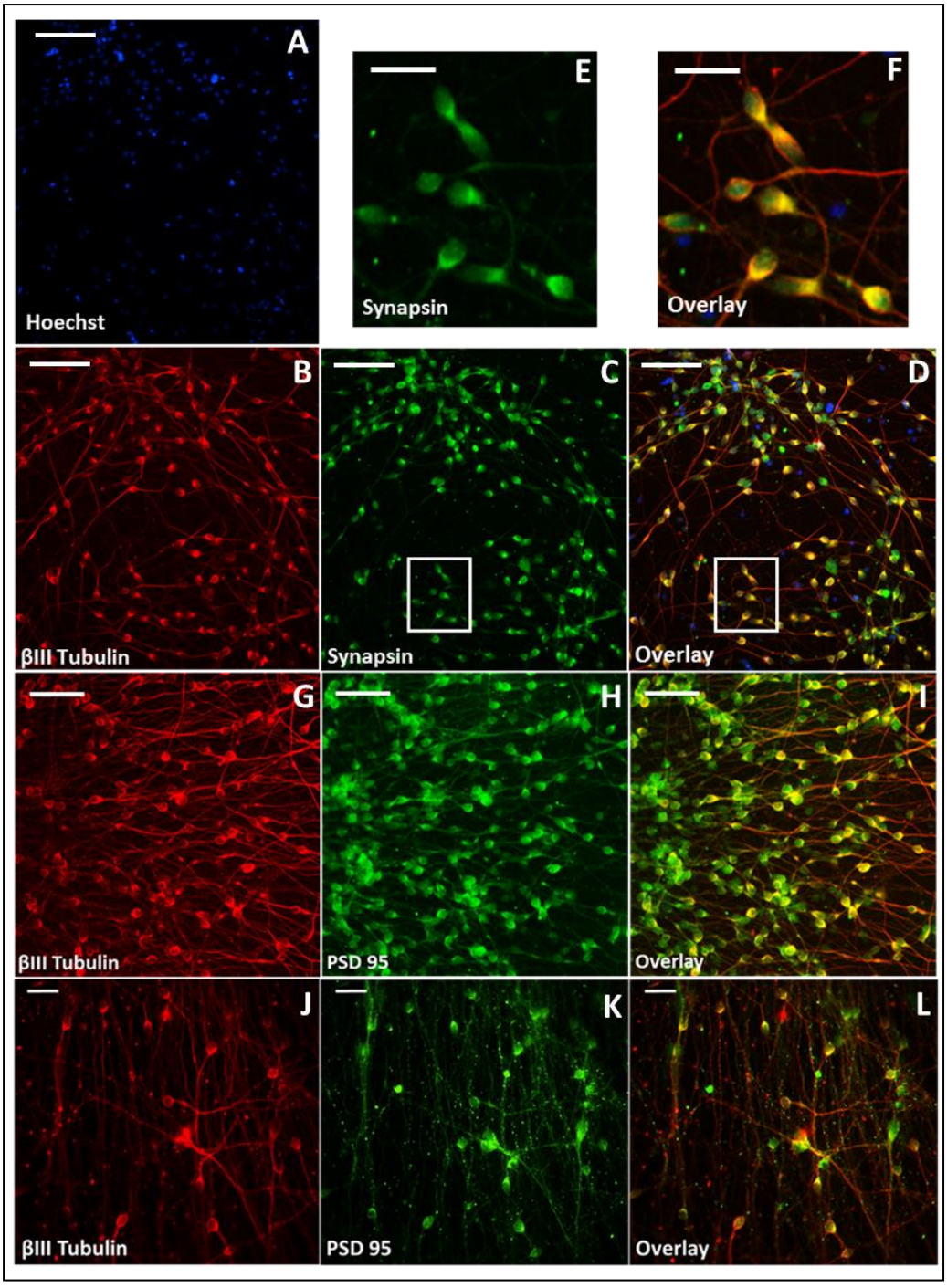

Figure 5.3 Immunostaining demonstrating positive staining for anti-synapsin I and anti-PSD 95 in Shef 6-bfCN and Nas 2-bfCN

A, B, C and D show immunostaining of Shef 6-bfCN with Hoechst nuclear stain (A, blue), anti-βIII Tubulin (B, red), anti-synapsin I (C, green) and the overlay of these (D). E and F show enlargements of the areas outlined by white boxes in C and D, respectively. G, H and I show Shef 6-bfCN immunostained with anti-βIII Tubulin (G, red), anti-PSD 95 (H, green) and the overlay of these (I). J, K and L show Nas 2-bfCN immunostained with anti-βIII Tubulin (J, red), anti-PSD 95 (K, green) and the overlay of these (L). Scale bars for A, B, C and D indicate 100 µm; scale bars for E and F indicate 25 µm; Scale bars for G, H, I, J, K and L indicate 50 µm.

Nas 2-bfCN and Shef 6-bfCN both positively stained for synapsin I and PSD-95 (Figure 5.3). Confocal microscopy, along with epifluorescence microscopy, was used to demonstrate the proximity of puncta stained with anti-synapsin I and anti-PDS-95 (Figure 5.4) indicating mature synaptic structure (Nieweg *et al.,* 2015). Nas 2-CGN and Shef 6-CGN also demonstrate positive staining for anti-synapsin I and anti-PDS-95, as described in Chapter 4 (Figures 4.8 and 4.9).

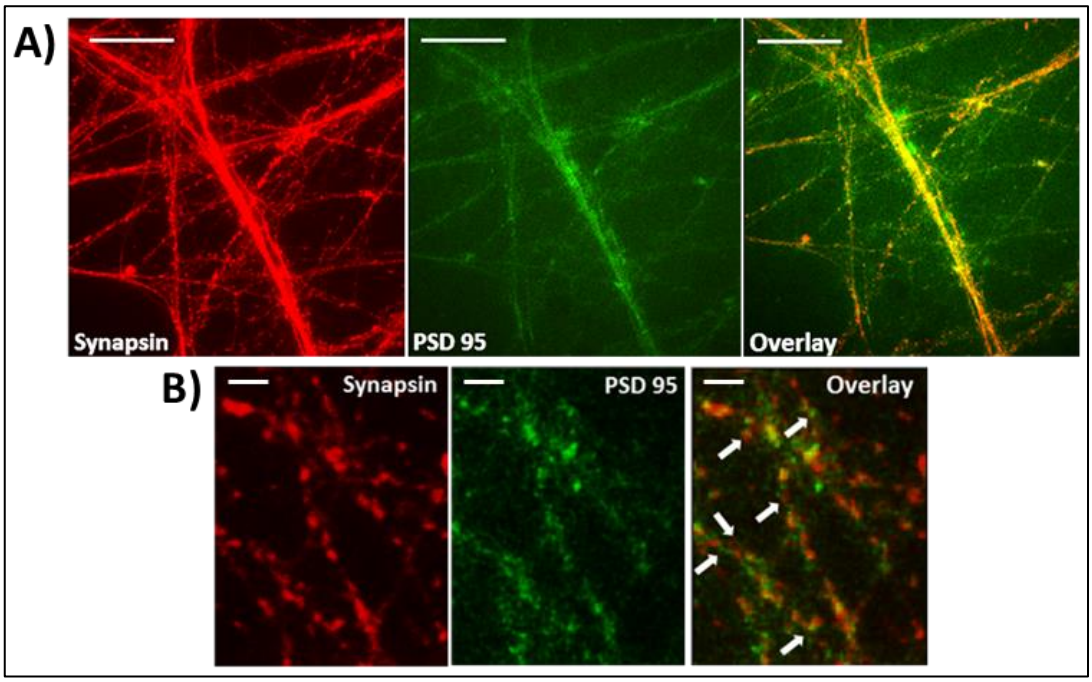

Figure 5.4 Synapsin and PSD-95 puncta are within close proximity to each other in mature bfCNs

Nas 2-bfCNs at day 35 positively immunostain for PSD-95 (green) and synapsin (red) with puncta along axons within close proximity to each other as can be seen in enlarged images. Images in A were taken using epifluorescence microscopy, while images in B were taken using confocal microscopy. Scale bars indicate 25 µM for those in A and 5 µM for those in B.

5.3.2 Tau and ptau levels in Shef 6-bfCNs, Nas 2-bfCNs Shef 6-CGNs treated with $A\beta_{42}O$

To investigate the levels of total tau and ptau within mature Shef 6-bfCNs, Nas 2-bfCNs and Shef 6-CGNs, cells were cultured after terminal differentiation to maturity, which equates to 35 days after final plate down for bfCNs and 50 days in culture for CGNs (Chapter 5.2.1), and treated with $A\beta_{42}O$ for 48 hours before being washed, lysed and immunoblotted. Levels of total tau and tau phosphorylated at Ser396/404 and Ser202 were detected by probing western blots with tau and ptau specific antibodies. The calculated density and size of each band was normalised firstly to bands produced by probing with the housekeeping control antibody GAPDH and subsequently to the average of the controls; therefore, these results are graphically represented as a ratio of the controls. To allow for consideration of total tau variation within each sample, the bands produced by probing with ptau antibodies were also normalised against those revealed by probing with DA9, which specifies total tau, after normalisation to GAPDH levels and before normalisation to the average of the controls. PHF-1 detects tau phosphorylated at Ser396/404 and CP13 detects tau phosphorylated at Ser202.

Figure 5.5 Levels of total tau in bfCNs treated with Aβ$_{42}$O

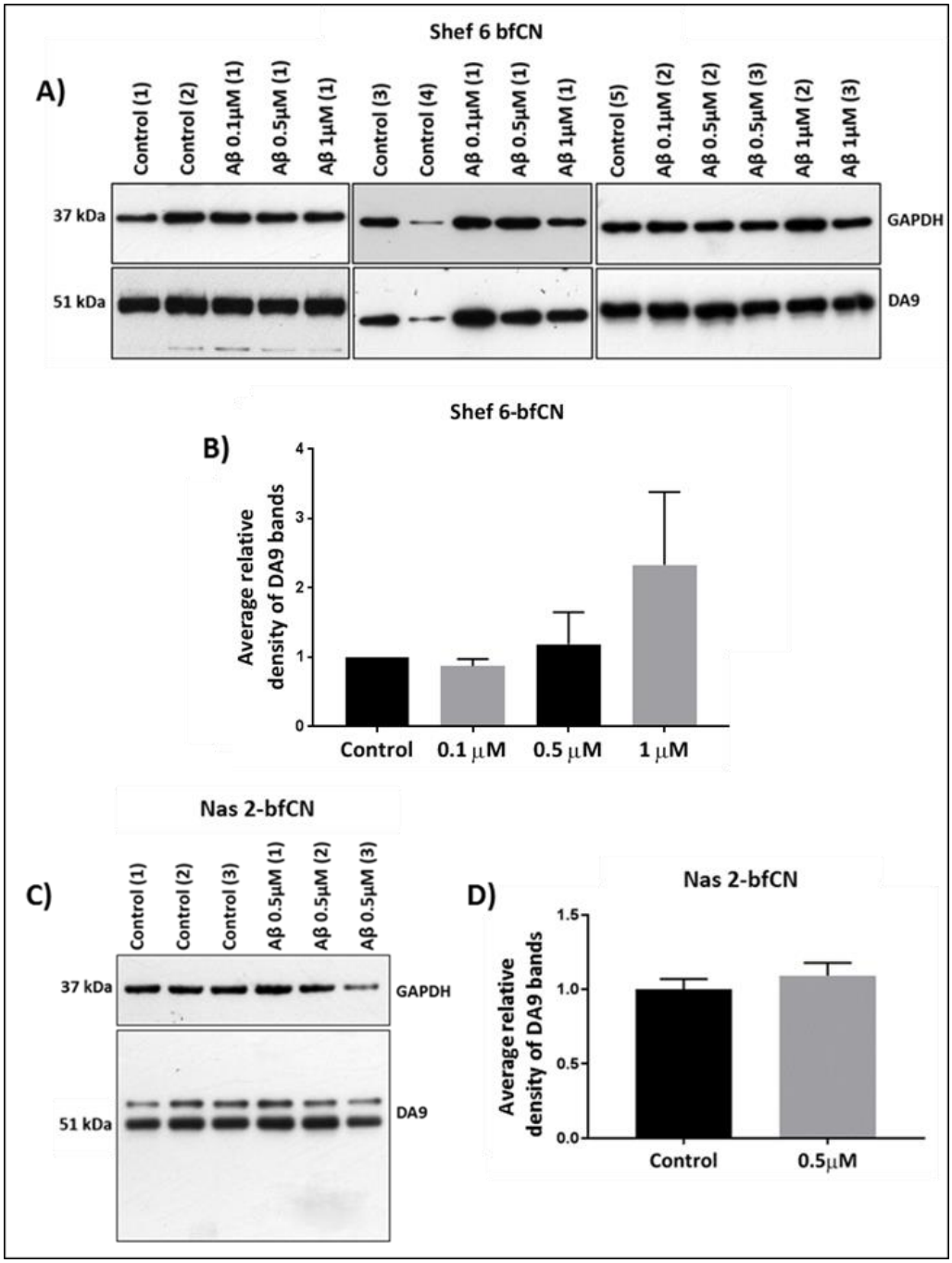

Figure 5.5 Level of total tau in bfCNs treated with Aβ$_{42}$O

Representative western blots showing Shef 6-bfCNs treated with 0.1 μM, 0.5 μM, 1 μM Aβ$_{42}$O (control n=5; Aβ 0.1 μM n=3; Aβ 0.5 μM n=4; Aβ 1 μM n=4) (A) and Nas 2-bfCNs treated with 0.5μM Aβ$_{42}$O (control n=3; Aβ 0.5 μM n=3) (C), probed with GAPDH and DA9 antibodies. Graphs representing the average relative density of DA9 bands normalised to GAPDH bands for Shef 6-bfCN (B) and for Nas 2-bfCN (D) treated with Aβ$_{42}$O.

Data represented in B) was analysed using a Friedman test with post-hoc Dunn's test. Data represented in D) was analysed using an unpaired Student's t-test. Error bars indicate +1 S.E.M.

Western immunoblots of hiPSC-neurons treated with $A\beta_{42}O$ were probed with DA9, an antibody against total tau, to understand whether the oligomers affect the total amount of tau within the cells. Treatment of Shef 6-bfCNs with incrementally increasing concentrations of $A\beta_{42}O$ (0.1 µM, 0.5 µM and 1 µM) did not have a statistically significant effect on total tau ($p= 0.0747$) (Figure 5.5, A and B). Nas 2-bfCNs were treated with 0.5 µM $A\beta_{42}O$, which did not have an effect on total tau levels ($p= 0.4509$) (Figure 5.5, C and D). Likewise, no statistically significant change in the levels of total tau was caused by treatment of Shef 6-CGN with 0.5 µM or 1 µM $A\beta_{42}O$ ($p= 0.4638$ and $p= 0.5098$, respectively) (Figure 5.6).

Figure 5.6 Level of total tau in Shef 6-CGNs treated with Aβ$_{42}$O

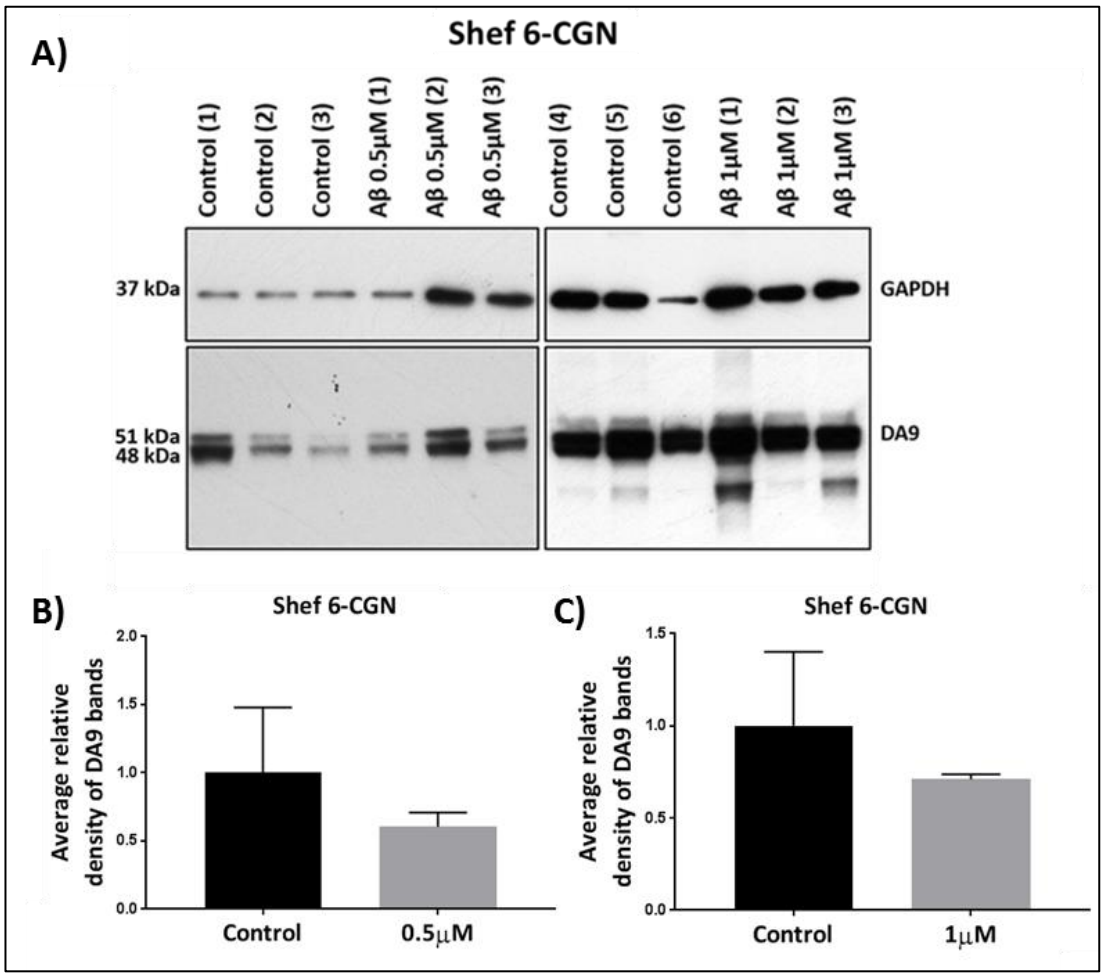

Figure 5.6 Level of total tau in Shef 6-CGNs treated with Aβ$_{42}$O

Representative western blot (A) showing Shef 6-CGNs treated with 0.5 μM (control n=3; Aβ 0.5 μM n=3) and 1 μM (control n=3; Aβ 1 μM n=3) Aβ$_{42}$O, alongside controls, probed with GAPDH and DA9. Representation of the average relative density of DA9 bands normalised to GAPDH bands for those treated with 0.5 μM (B) and 1 μM (C) Aβ$_{42}$O compared to controls.

Data was analysed using an unpaired Student's t-test. Error bars indicate +1 S.E.M.

Figure 5.7 Levels of tau phosphorylated at pSer396 and pSer404 in Nas 2-bfCNs treated with $A\beta_{42}O$

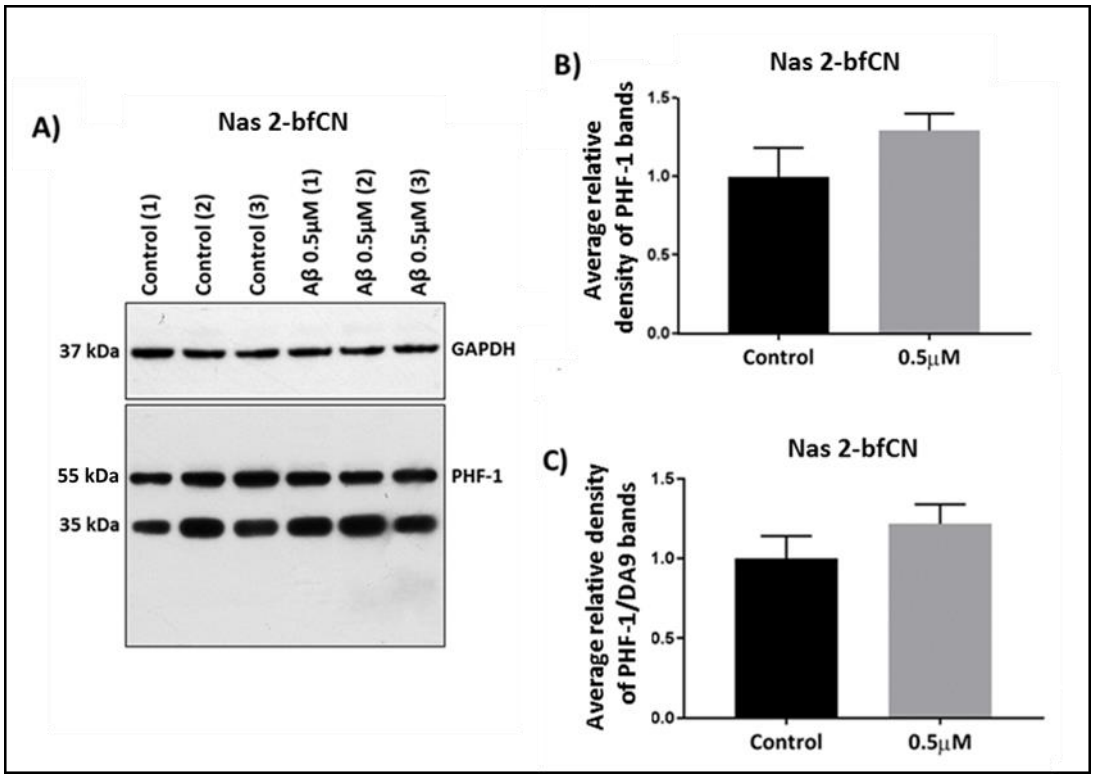

Figure 5.7 Level of tau phosphorylated at pSer396 and pSer404 in Nas 2-bfCNs treated with $A\beta_{42}O$

Representative western blot (A) showing Nas 2-bfCNs treated with 0.5μM $A\beta_{42}O$ alongside controls probed with GAPDH and PHF-1 (control n=3; Aβ 0.5μM n=3) and graphical representation of the average relative densities of PHF-1 bands normalised to GAPDH bands (B) and then normalised to DA9 bands (C).

Data was analysed using an unpaired Student's t-test. Error bars indicate +1 S.E.M.

Figure 5.8 Levels of tau phosphorylated at Ser396 and Ser404 in Shef 6-CGNs treated with $A\beta_{42}O$

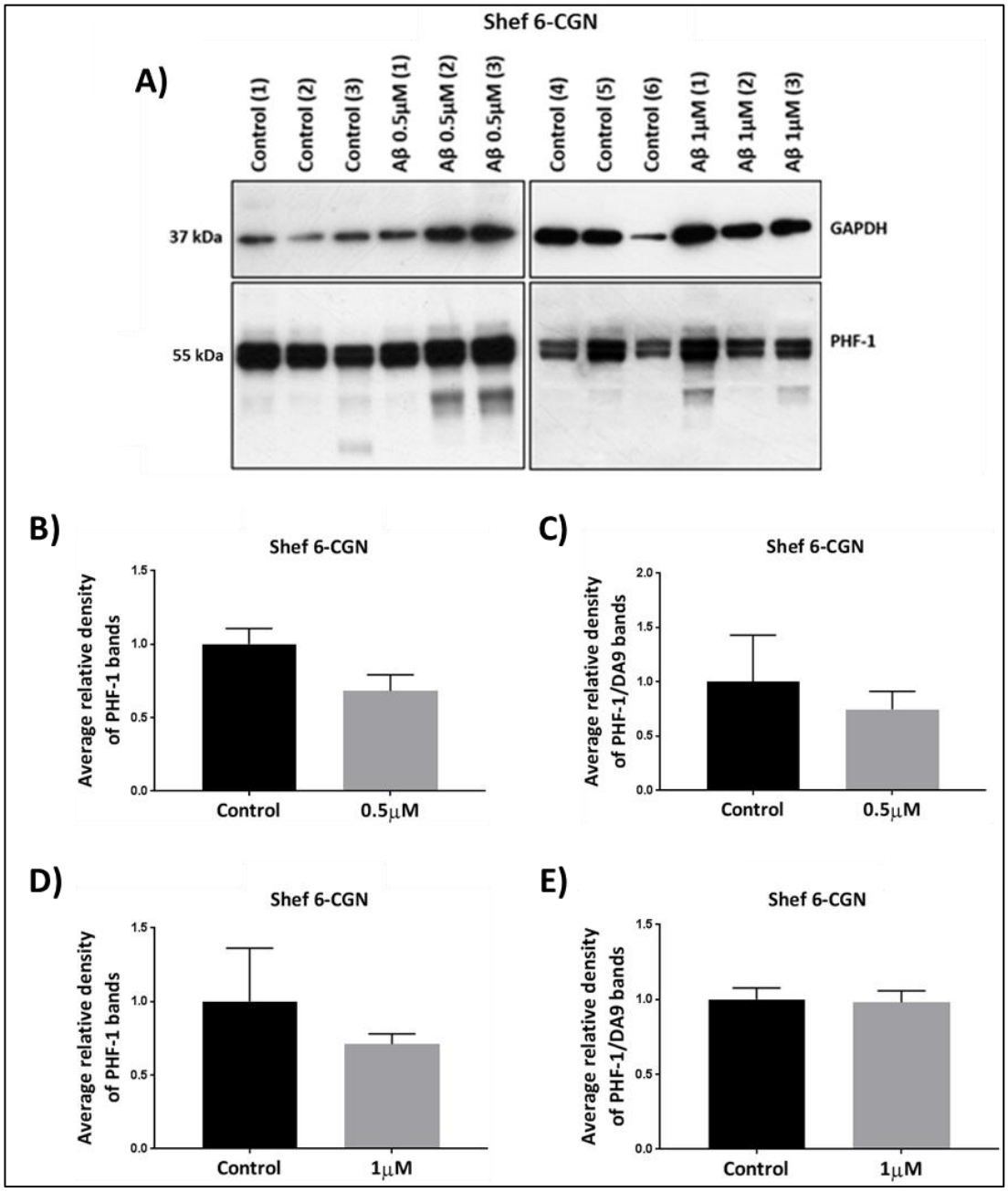

Figure 5.8 Level of tau phosphorylated at Ser396 and Ser404 in Shef-6 CGNs treated with $A\beta_{42}O$

Representative western blots (A) of Shef 6-CGNs treated with 0.5μM (control n=3; Aβ 0.5 μM n=3) and 1 μM (control n=3; Aβ 1 μM n=3) $A\beta_{42}O$ alongside controls, probed with GAPDH and PHF-1. Graphs representing the average relative density of PHF-1 bands normalised to GAPDH bands (B and D) and then to DA9 bands (C and E) for Shef 6-CGNs treated with 0.5μM $A\beta_{42}O$ (B and C) and 1 μM $A\beta_{42}O$ (D and E), compared to controls.

Data was analysed using an unpaired Student's t-test. Error bars indicate +1 S.E.M.

No significant difference in pSer396/404 tau was found in Nas 2-bfCNs treated with 0.5 µM $A\beta_{42}O$ compared to controls either before normalisation to total tau (p= 0.2417), or afterwards (p= 0.3096) (Figure 5.7). No statistically significant diffference was found in Shef 6-CGN treated with 0.5 µM or 1 µM $A\beta_{42}O$ before normalisation to total tau (p= 0.1018 and p=4765, respectively) or after normalisation to total tau (p= 0.6089 and p= 0.3808, repectively) (Figure 5.8).

Figure 5.9 Levels of tau phosphorylated at Ser202 in Shef 6-bfCNs treated with $A\beta_{42}O$

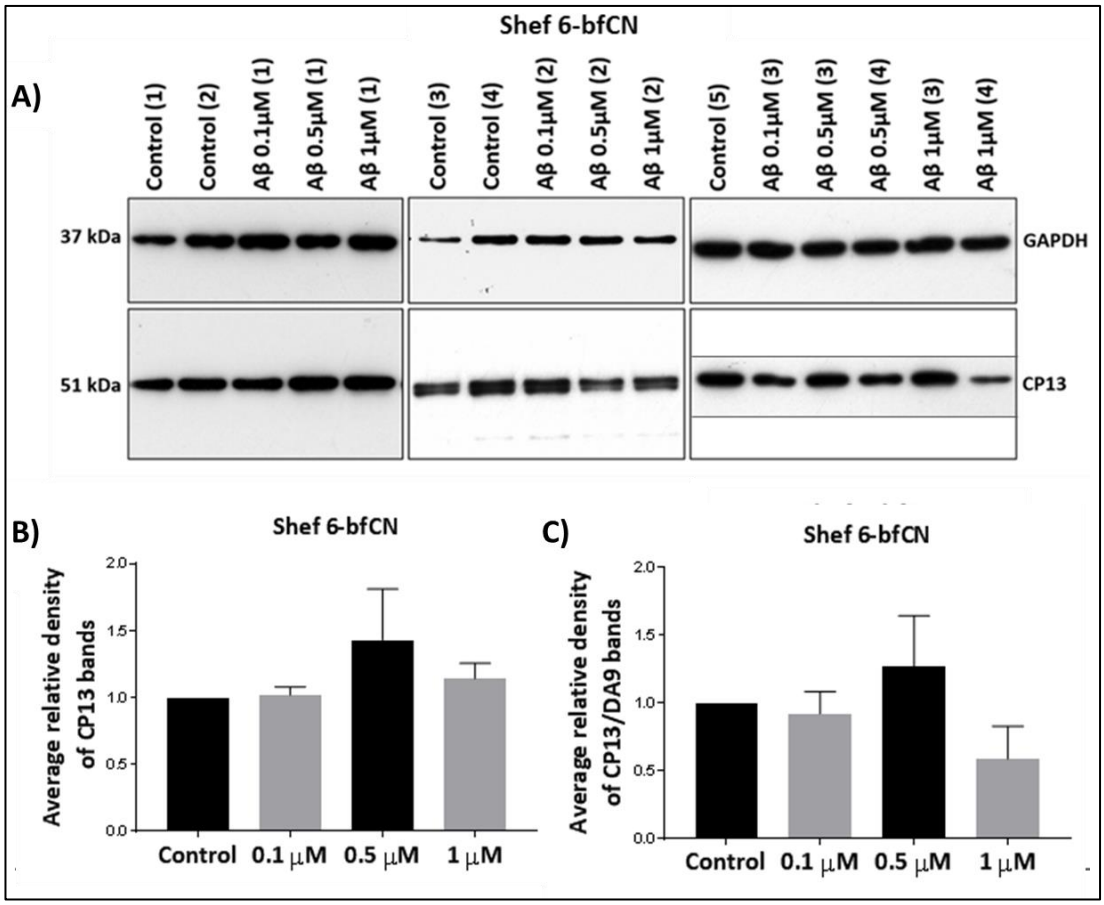

Figure 5.9 Level of tau phosphorylated at Ser202 in Shef 6-bfCNs treated with $A\beta_{42}O$
Representative western blots showing Shef 6-bfCNs treated with 0.1 µM, 0.5 µM, 1 µM $A\beta_{42}O$ (control n=5; Aβ 0.1 µM n=3; Aβ 0.5 µM n=4; Aβ 1 µM n=4) probed with GAPDH and CP13 antibodies (A). Graphs representing the average relative density of CP13 bands normalised to GAPDH bands (B) and then to DA9 bands (C) for Shef 6-bfCN treated with $A\beta_{42}O$.

Data was analysed using a Friedman test with post-hoc Dunn's test. Error bars indicate +1 S.E.M.

Figure 5.10 Levels of tau phosphorylated at Ser202 in Nas 2-bfCNs treated with $A\beta_{42}O$

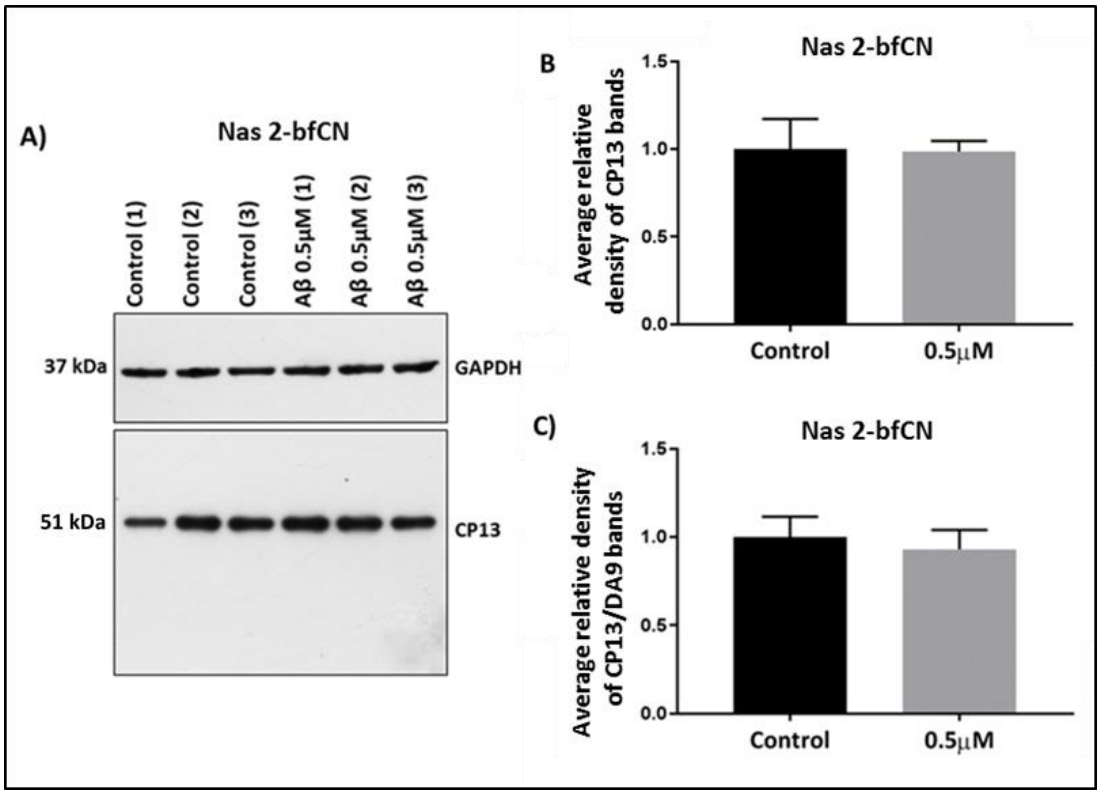

Figure 5.10 Level of tau phosphorylated at Ser202 in Nas 2-bfCNs treated with $A\beta_{42}O$

Representative western blot (A) showing Nas 2-bfCNs treated with 0.5 μM $A\beta_{42}O$ and probed with GAPDH and CP13 (control n=3; Aβ 0.5 μM n=3). Graphs representing the density of CP13 bands normalised to GAPDH bands (B), then normalised to DA9 bands (C), for Nas 2-bfCN treated with $A\beta_{42}O$.

Data was analysed using an unpaired Student's t-test. Error bars indicate +1 S.E.M.

Figure 5.11 Levels of tau phosphorylated at Ser202 in CGNs treated with Aβ$_{42}$O

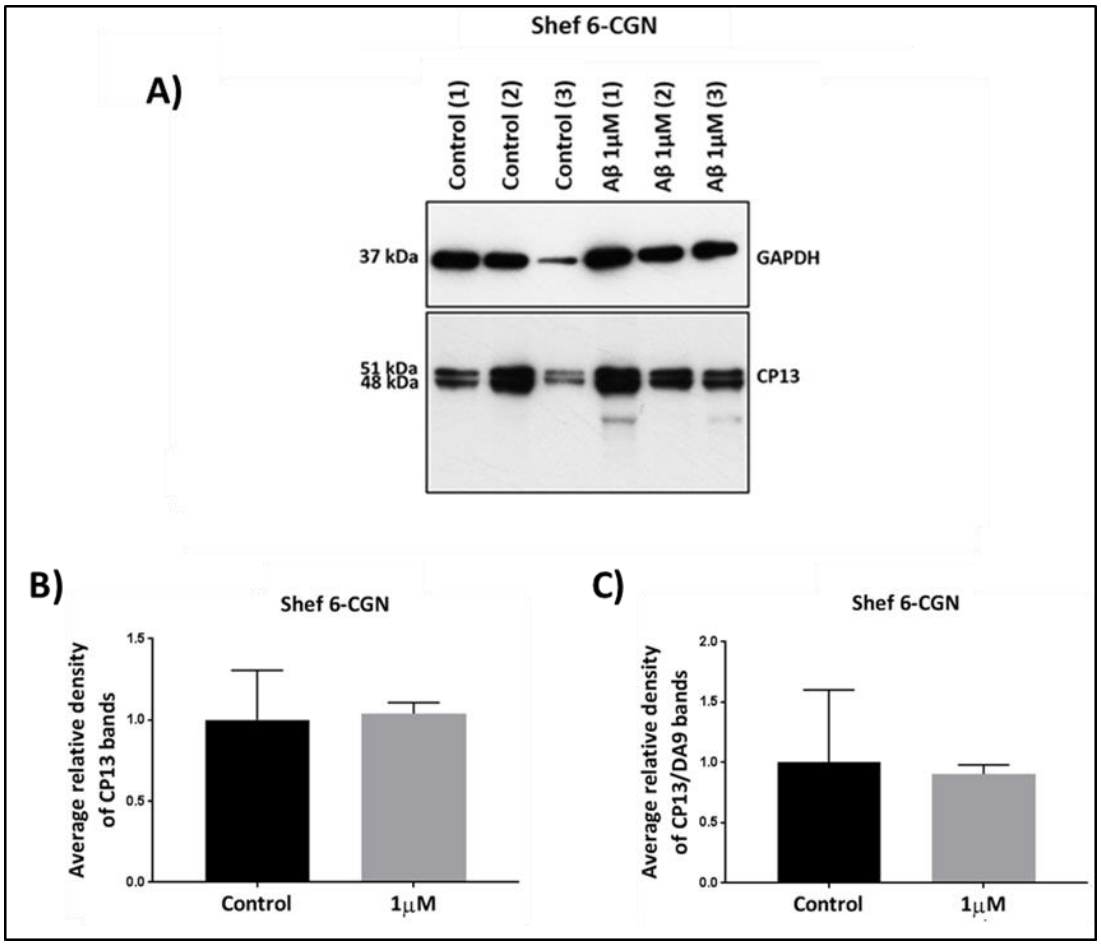

Figure 5.11 Level of tau phosphorylated at Ser202 in Shef 6-CGNs treated with Aβ$_{42}$O
Representative western blots (A) of Shef 6-CGNs treated with 1 μM (control n=3; Aβ 1 μM n=3) Aβ$_{42}$O alongside controls, probed with GAPDH and CP13. Graphs representing the average relative density of CP13 bands normalised to GAPDH bands (B) and then to DA9 bands (C).

Data was analysed using an unpaired Student's t-test. Error bars indicate +1 S.E.M.

No statistically significant difference in pSer202 tau levels was found in Shef 6-bfCN treated with 0.1 μM, 0.5 μM or 1 μM Aβ$_{42}$O compared to controls, either before normalisation to total tau (p= 0.7813), or afterwards (p= 0.2449) (Figure 5.9). Similarly, within Nas 2-bfCN treated with 0.5 μM Aβ$_{42}$O no statistically significant change in levels of tau phosphorylated at these sites was detected compared to controls before normalisation to total tau (p= 0.9405) or following normalisation (p= 0.6862) (Figure 5.10). Application of 1 μM Aβ$_{42}$O to Shef 6-CGN also did not statistically significantly alter levels of pSer202 tau before normalisation to total tau (p= 0.9071) or after normalisation to total tau (p= 0.8817), compared to controls (Figure 5.11).

5.3.3 Gene expression of *MAPT* in Shef 6-CGN and Nas 2-bfCNs treated with $A\beta_{42}O$

MAPT expression levels within Shef 6-CGN treated with 1 µM $A\beta_{42}O$ and Nas 2-bfCN treated with 0.5 µM $A\beta_{42}O$ were investigated. The average relative gene expression was calculated for cells treated with each concentration of $A\beta_{42}O$ compared to controls. Neither Nas 2-bfCNs treated with 0.5 µM $A\beta_{42}O$ (p= 0.2286) or Shef 6-CGNs treated with 1 µM $A\beta_{42}O$ (p= 0.4000) were found to express significantly higher levels of *MAPT* compared to controls (Figure 5.12).

Figure 5.12 Relative expression of *MAPT* in Nas 2-bfCN and Shef 6-CGN treated with $A\beta_{42}O$

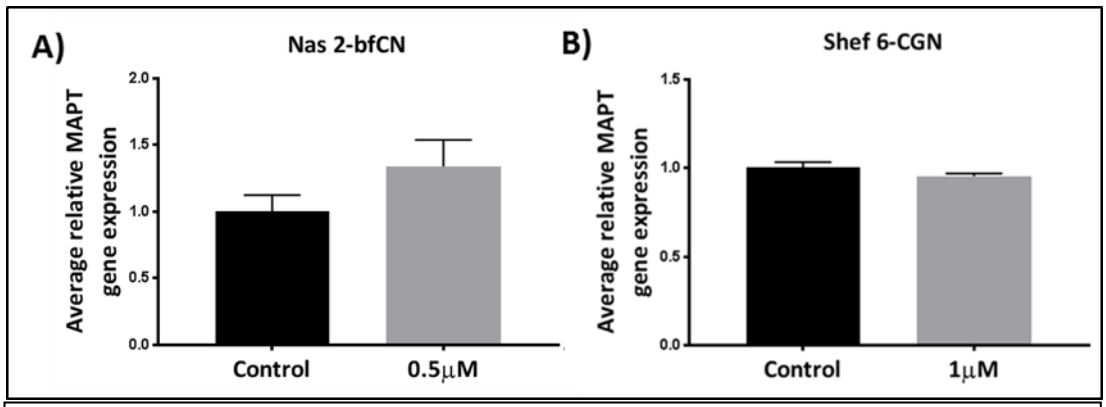

Figure 5.12 ***Relative expression of MAPT in Nas 2-bfCN and Shef 6-CGN treated with*** **$A\beta_{42}O$**

Graphs representing the average relative gene expression of MAPT within Nas 2-bfCN treated with 0.5 µM $A\beta_{42}O$ (control n=3; Aβ 0.5 µM n=4) (A) and within Shef 6-CGN treated with 1 µM $A\beta_{42}O$ (control n=3; Aβ 1 µM n=3) compared to controls.

Data was analysed using a Mann-Whitney test. Error bars indicate +1 S.E.M.

5.3.4 Tau kinase levels and activity in Shef 6-CGNs and Nas 2-bfCNs treated with $A\beta_{42}O$

To discern whether the activity of tau kinases GSK3β, Cdk5 and PAK3 are affected by treatment of hPSC-neurons with $A\beta_{42}O$, protein levels of GSK3β, GSK3β pTyr216, p25, p35 and PAK3 in Nas 2-bfCNs treated with 0.5 µM $A\beta_{42}O$ and Shef 6-CGN treated with 0.5 µM $A\beta_{42}O$ or 1 µM $A\beta_{42}O$ were investigated via western immunoblotting.

Phosphorylation of GSK3β at pTyr216 is necessary for the kinase to become fully active (Chapter 1.3.1), therefore levels of GSK3β phosphorylated at this site were compared to total GSK3β to distinguish the effects of 0.5µM $A\beta_{42}O$ treatment on GSK3β activity in Nas 2-bfCNs. Levels of total GSK3β are unchanged in Nas 2-bfCN treated with 0.5 µM $A\beta_{42}O$ compared to controls ($p= 0.7450$), however, levels of pTyr216 GSK3β are increased ($p= 0.0127$) and remain increased when normalised against total GSK3β ($p= 0.0273$) (Figure 5.13).

Figure 5.13 Levels of total and active GSK3β in Nas 2-bfCNs treated with $A\beta_{42}O$

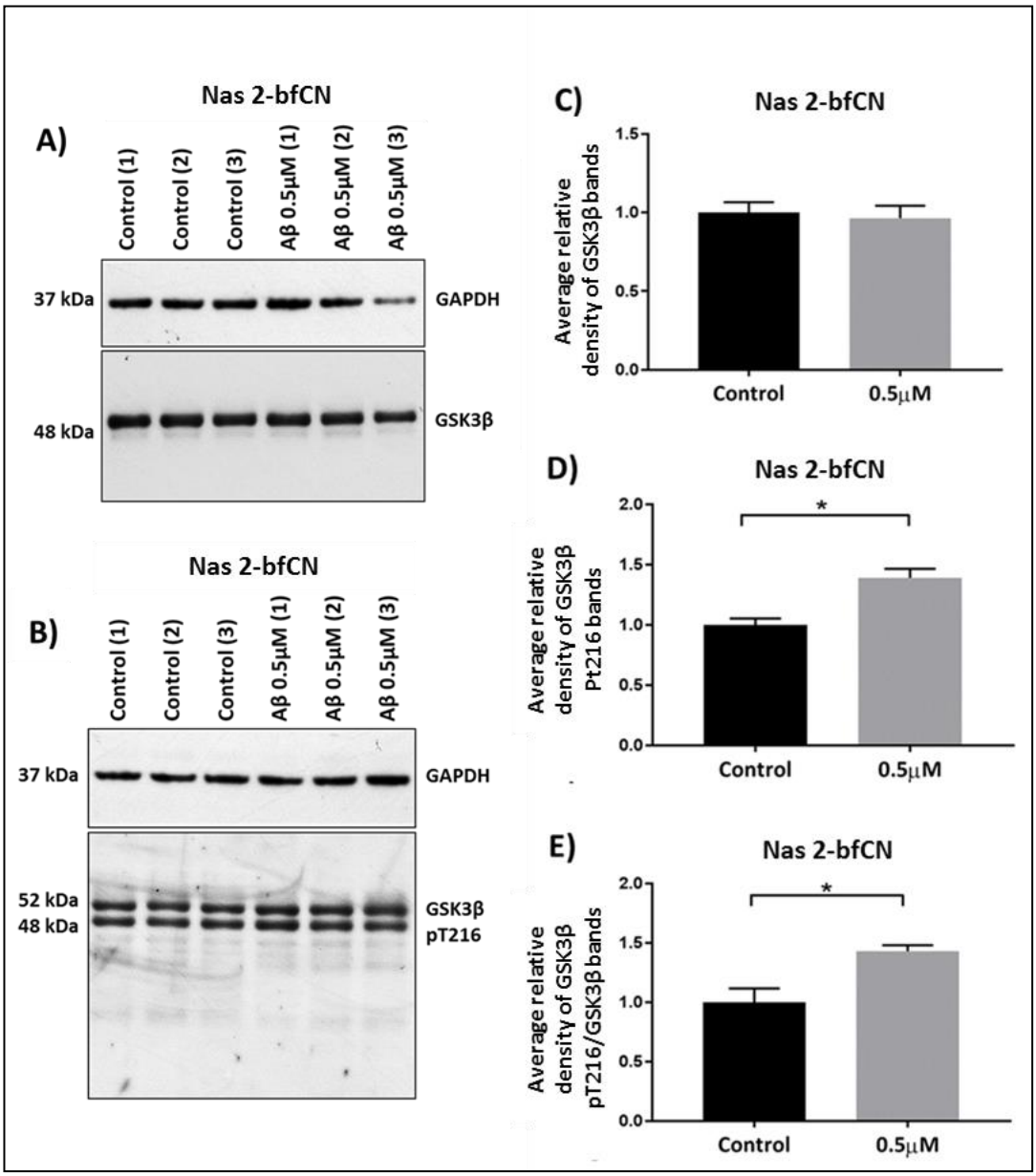

Figure 5.13 Levels of total and active GSK3β in Nas 2-bfCNs treated with $A\beta_{42}O$

*Representative western blots of Nas 2-bfCNs treated with 0.5μM $A\beta_{42}O$ alongside controls, probed with GAPDH and anti-GSK3β (A) and GAPDH and anti-GSK3β (B) (control n=3; Aβ 0.5 μM n=3). Graphs representing the average relative density of anti-GSK3β bands normalised to GAPDH bands (C), of anti-GSK3β pTyr216 bands normalised to GAPDH * p= 0.0127 (D), and of anti-GSK3β pTyr216 bands normalised to anti-GSK3β bands * p= 0.0273 (E).*

Data was analysed using an unpaired Student's t-test. Error bars indicate +1 S.E.M.

Figure 5.14 Levels of active GSK3β in Shef 6-CGNs treated with Aβ$_{42}$O

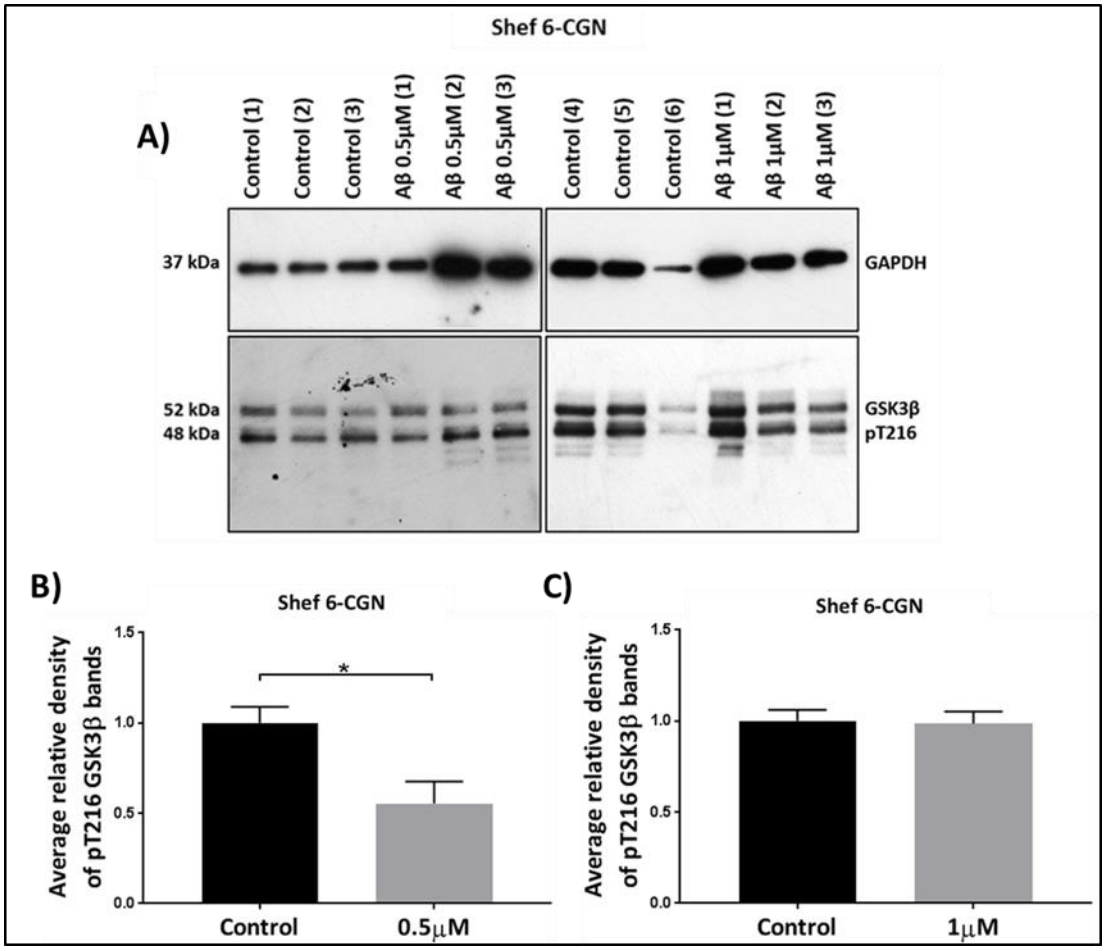

Figure 5.14 Levels of active GSK3β in Shef 6-CGNs treated with Aβ$_{42}$O

Representative western blot (A) of Shef 6-CGNs treated with 0.5 μM (control n=3; Aβ 0.5 μM n=3) and 1 μM (control n=3; Aβ 1 μM n=3) Aβ$_{42}$O alongside controls, probed with GAPDH and anti-GSK3β pTyr216. Graphs representing the average relative density of anti-GSK3β pTyr216 bands normalised to GAPDH bands, averaged to the controls, for Shef 6-CGNs treated with 0.5 μM (B) and 1 μM (C) Aβ$_{42}$O.

Data was analysed using an unpaired student's T test. Error bars indicate +1 S.E.M.

Conversely, statistical analysis revealed levels of GSK3β pTyr216 were reduced in Shef 6-CGNs treated with 0.5 μM compared to controls and treatment with 1 μM Aβ$_{42}$O (p= 0.0413) (Figure 5.14). There was no statistical difference in the levels of GSK3β pTyr216 between controls and Shef 6-CGNs treated with 1 μM Aβ$_{42}$O.

Increased p25, decreased p35 and increased p25:p35 ratio are indicative of increased Cdk5 activity, as discussed in Chapter 1.3.2. Therefore, western immunoblots of Nas 2-bfCNs treated with 0.5 μM Aβ$_{42}$O and Shef 6-CGNs treated with 0.5 μM and 1 μM Aβ$_{42}$O alongside

controls were probed with anti-p25/p35 to investigate Cdk5 activity. The ratio of each to GAPDH was measured, however, p25 levels were too low to be detected for Shef 6-CGN treated with 0.5 µM $A\beta_{42}O$. Where p25 could be calculated in controls and Shef 6-CGN treated with 1 µM $A\beta_{42}O$ on the same blot, and within Nas 2-bfCNs, anti-p25 bands were normalised against GAPDH and then normalised to p35 bands to calculate the p25:p35 ratio.

Levels of p35 ($p>0.9999$), p25 ($p= 0.4111$) and the ratio of p25:p35 ($p= 0.3327$) were not significantly changed through the application of 0.5 µM $A\beta_{42}O$ to Nas 2-bfCNs (Figure 5.15). Levels of p25 ($p= 0.2464$) and the ratio p25:p35 ($p= 0.1183$) were found to be not significantly different in Shef 6-CGN treated with 1 µM $A\beta_{42}O$ compared to controls (Figure 5.16, C and D), however, levels of p35 were significantly decreased in cells treated with 1 µM or 0.5 µM $A\beta_{42}O$ ($p= 0.0019$) (Figure 5.16).

Figure 5.15 Levels of p25 and p35 in Nas 2-bfCNs treated with $A\beta_{42}O$

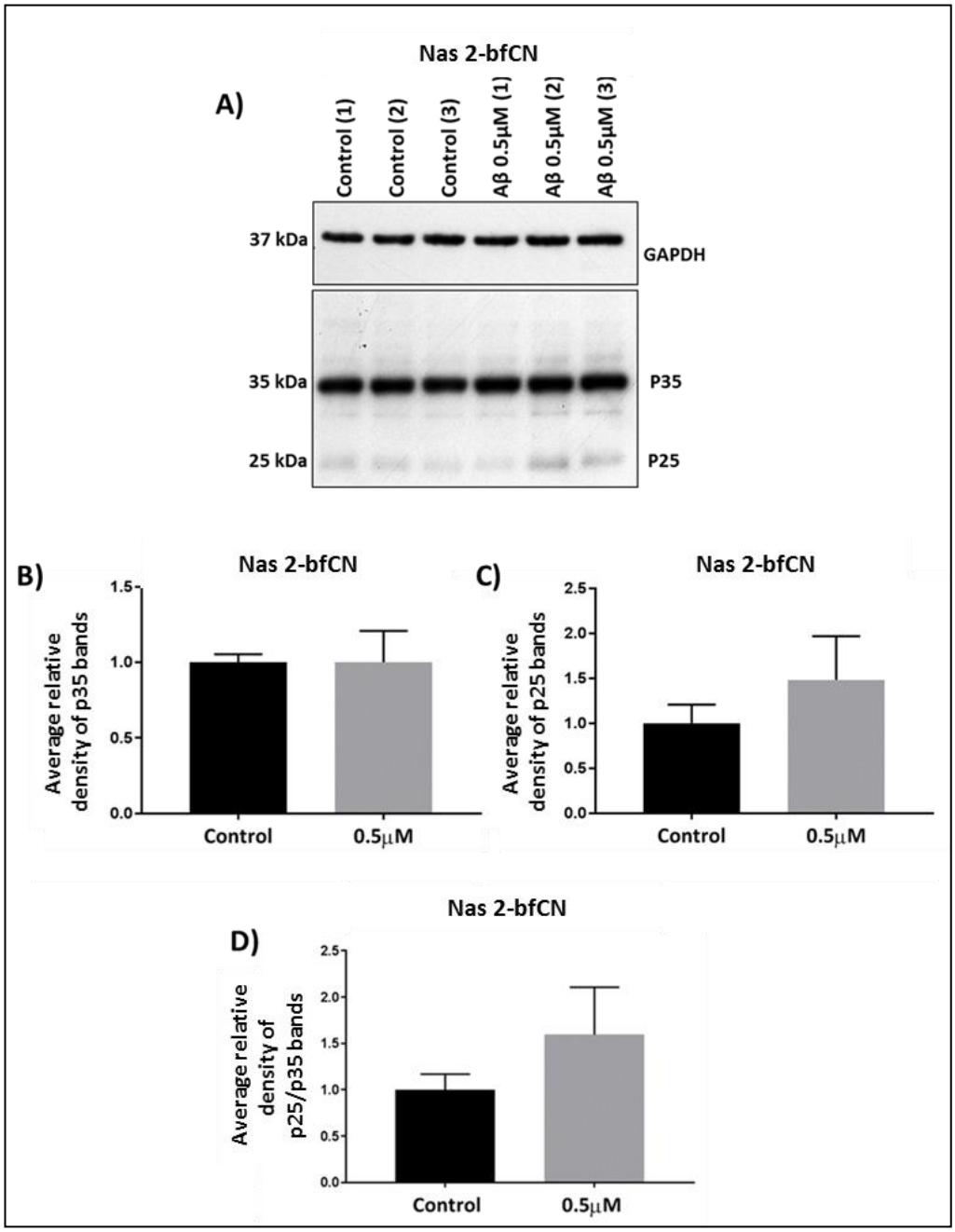

Figure 5.15 Levels of p25 and p35 in Nas 2-bfCNs treated with $A\beta_{42}O$

Representative western immunoblot (A) of Nas 2-bfCNs treated with 0.5 μM $A\beta_{42}O$ alongside controls, probed with GAPDH and anti-p25/p35 (control n=3; Aβ 0.5 μM n=3). Graphical representations of average relative density of p35 bands normalised to GAPDH bands (B), of p25 bands normalised to GAPDH bands (C) and of p25 bands normalised to p35 bands (D) for Nas 2-CGNs.

Data was analysed using an unpaired Student's t-test. Error bars indicate +1 S.E.M.

Figure 5.16 Levels of p25 and p35 in Shef 6-CGNs treated with Aβ$_{42}$O

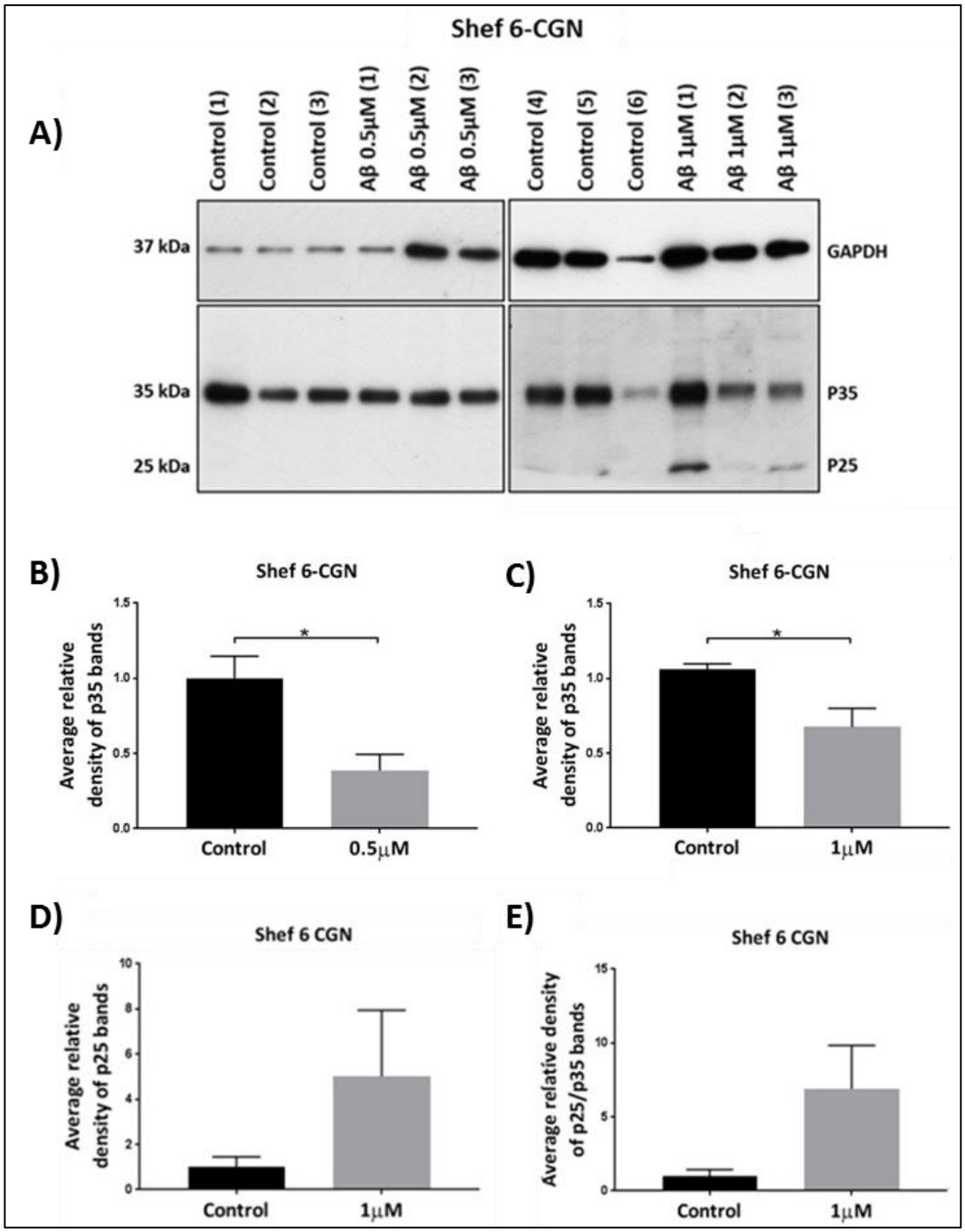

Figure 5.16 Levels of p25 and p35 in Shef 6-CGNs treated with Aβ$_{42}$O

*Representative western blot of Shef 6-CGNs treated with 0.5μM (control n=3; Aβ 0. 5 μM n=3) and 1μM (control n=3; Aβ 1 μM n=3) Aβ$_{42}$O alongside controls, probed with GAPDH and anti-p25/p35 (A). Graphs representing the average relative density of anti-p35 bands normalised to GAPDH bands for Shef 6-CGN treated with 0.5 μM Aβ$_{42}$O * p= 0.0419 (B) and 1 μM Aβ$_{42}$O * p=0.0274 (C). Graphs representing the average relative density of anti-p25 bands normalised to GAPDH bands (D) and then to p35 bands (E) for Shef 6-CGN treated with 1 μM Aβ$_{42}$O.*

Data was analysed using an unpaired Student's t-test. Error bars indicate +1 S.E.M.

Figure 5.17 Levels of PAK3 in Shef 6-CGNs and Nas 2-bfCNs treated with Aβ$_{42}$O

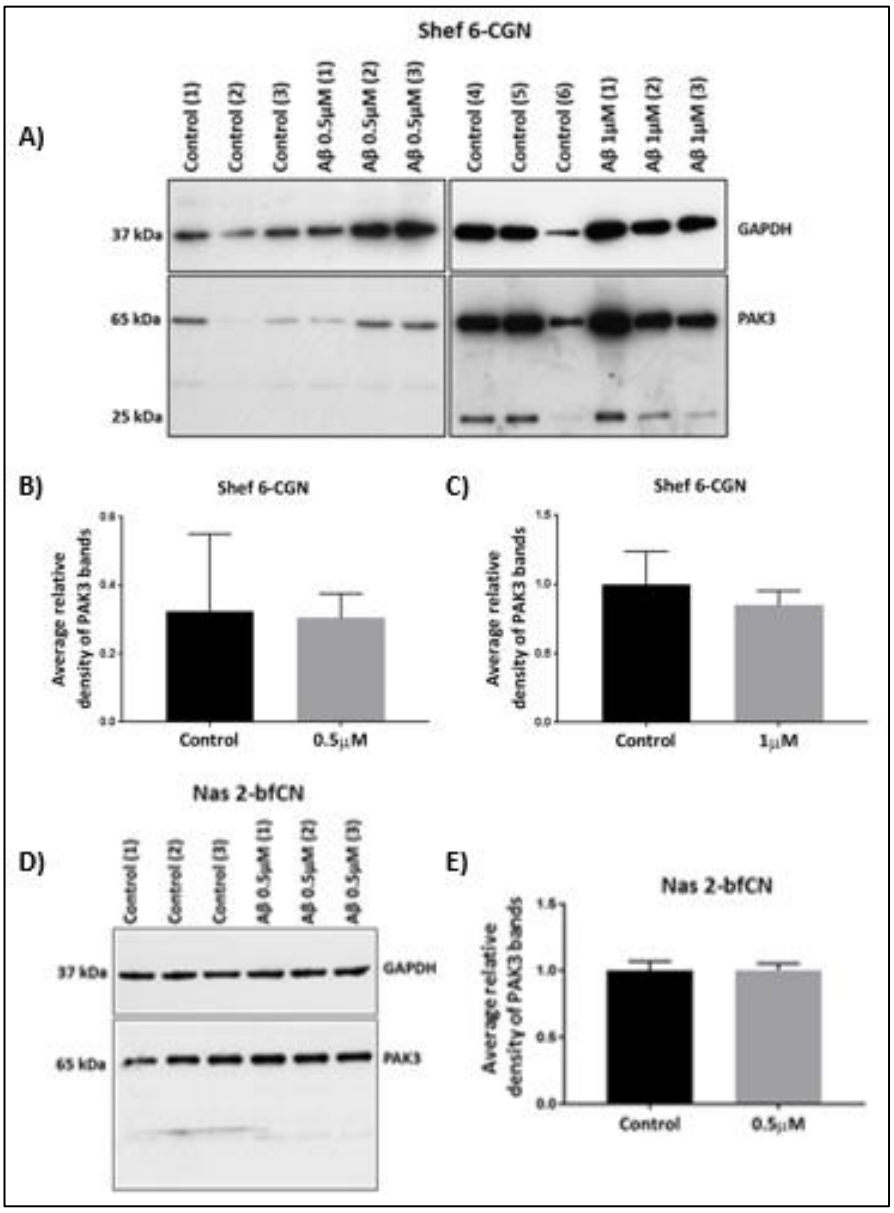

Figure 5.17 Levels of PAK3 in Shef 6-CGNs and Nas 2-bfCNs treated with Aβ$_{42}$O

Representative western blots of Shef 6-CGNs treated with 0.5 μM (control n=3; Aϐ 0.5 μM n=3) and 1 μM Aϐ$_{42}$O (control n=3; Aϐ 1 μM n=3) alongside controls (A) and Nas 2-bfCN treated with 0.5 μM Aϐ$_{42}$O (control n=3; Aϐ 0.5 μM n=3) (D) probed with GAPDH and anti-PAK3. Graphs representing the average relative density of anti-PAK3 bands normalised to GAPDH bands for Shef 6-CGNs treated with 0.5 μM (B) and 1 μM (C). Graph representing the average relative density of anti-PAK3 bands normalised to GAPDH bands for Nas 2-bfCNs treated with 0.5 μM Aϐ$_{42}$O alongside controls (E).

Data represented was analysed using an unpaired student's t-test. Error bars indicate +1 S.E.M.

Western blots of Shef 6-CGNs and Nas 2-bfCNs treated with Aβ$_{42}$O were probed with anti-PAK3 antibody to investigate the effects of Aβ$_{42}$O on the levels of this tau kinase within these

cells. PAK3 levels were not significantly different in Shef 6-CGNs treated with 0.5 µM (p= 0.9379) and 1 µM $A\beta_{42}O$ (p= 0.5859) or Nas 2-bfCNs 0.5 µM $A\beta_{42}O$ (p> 0.9999) treated with $A\beta_{42}O$ compared to controls (Figure 5.17).

5.3.5 Gene expression of tau kinases in Shef 6-CGN and Nas 2-bfCNs treated with $A\beta_{42}O$

To determine whether changes in expression levels of tau kinases are concomitant with altered tau kinase activity or tau phosphorylation in response to $A\beta_{42}O$ treatment within Shef 6-CGN and Nas 2-bfCN, qPCR was carried out using probes to detect *GSK3β, CDK5* and *PAK3* cDNA.

Whilst *GSK3β* expression was found to be greater within Nas 2-bfCN treated with 0.5 µM $A\beta_{42}O$ compared to those treated with 1 µM $A\beta_{42}O$ (p= 0.0128), there was no significant difference in Nas 2-bfCN treated with 0.5 µM $A\beta_{42}O$ (p= 0.2715) or 1 µM $A\beta_{42}O$ (p= 0.0714) compared to both controls (Figure 5.18, A). Similarly, no significant change in expression was detected for Shef 6-CGN treated with 1 µM $A\beta_{42}O$ (p= 0.1000) (Figure 5.18, B).

Expression of *CDK5* was not found to be significantly different in Nas 2-bfCN treated with 0.5 µM $A\beta_{42}O$ (p=0.0571) (Figure 5.18, C) compared to controls, or in Shef 6-CGN treated with 1 µM $A\beta_{42}O$ (p >0.9999) (Figure 5.18, D). The expression of *PAK3* was not significantly altered in Nas 2-bfCN after application of either 0.5 µM $A\beta_{42}O$ (Figure 5.18, E) or 1 µM $A\beta_{42}O$ (p= 0.4990) or in Shef 6-CGN treated with 1 µM $A\beta_{42}O$ (p= 0.4000) (Figure 5.18, F) compared to controls.

Figure 5.18 Relative expression of tau kinases in hiPSC-neurons treated with Aβ$_{42}$O

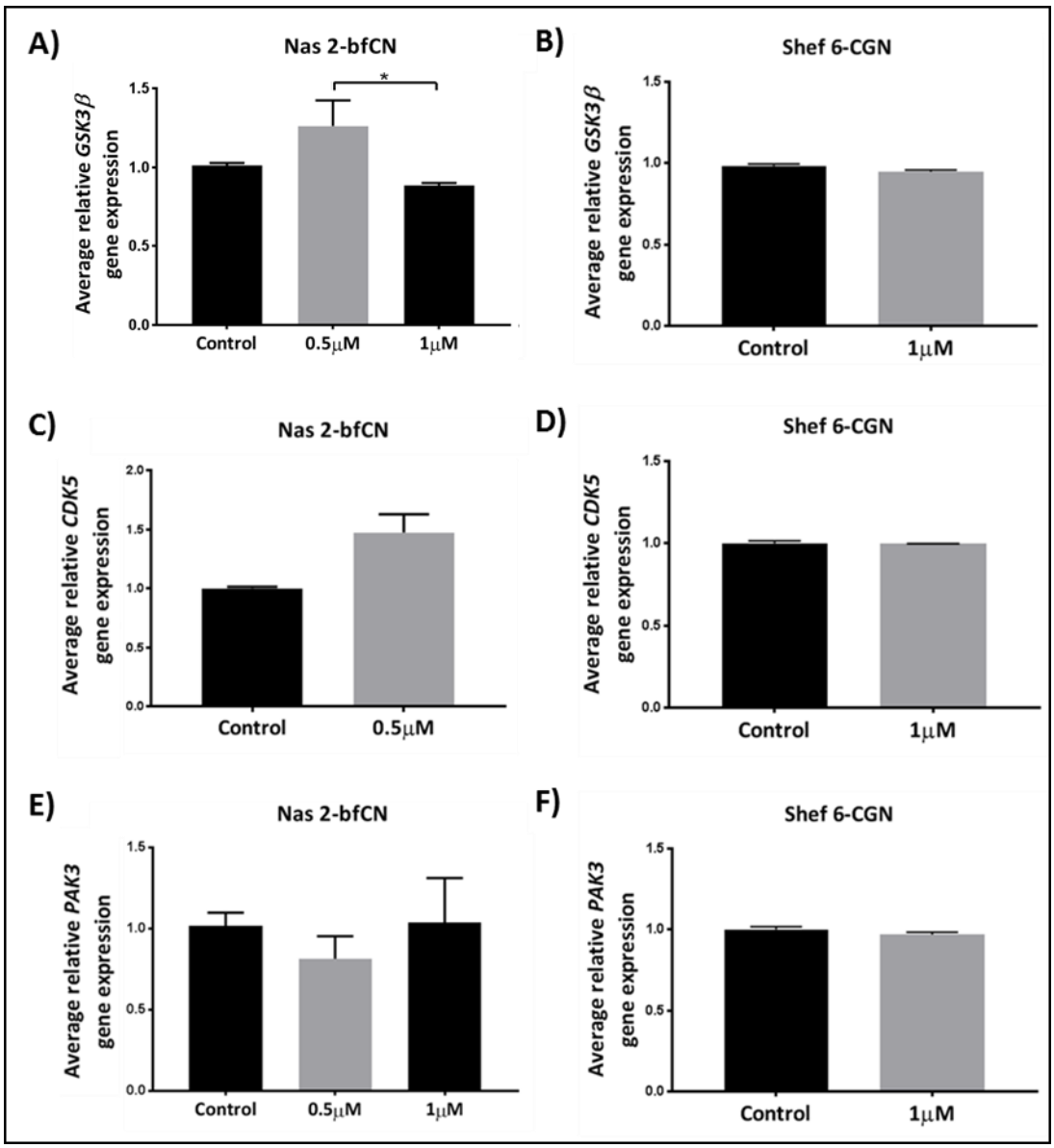

Figure 5.18 Relative gene expression of tau kinases in hiPSC-neurons treated with Aβ$_{42}$O

Graphs representing the average relative gene expression of GSK3β (A) p= 0.0128 (control n=7; Aβ 0.5 μM n=4; Aβ 1 μM n=3); CDK5 (C) (control n=3; Aβ 0.5 μM n=4) and PAK3 (E) (control n=7; Aβ 0.5 μM n=4; Aβ 1 μM n=3) within Nas 2-bfCN treated with 0.5 μM and 1 μM Aβ$_{42}$O alongside controls.*

Graphs representing the average relative gene expression of GSK3β (B), CDK5 (D) and PAK3 (F) within Shef 6-CGN treated with 1 μM Aβ$_{42}$O compared to controls (control n=3; Aβ 1 μM n=4).

Data represented in A) and E) was analysed using a Kruskal-Wallis with post-hoc Dunn's test. Data represented in B), C), D) and F) was analysed using a Mann-Whitney test. Error bars indicate +1 S.E.M.

5.3.6 Level of synapsin I in Shef 6 and Nas 2 derived CGNs and bfCNs treated with $A\beta_{42}O$

To investigate the synaptotoxic effects of treatment with Shef 6-CGNs and Nas 2-bfCNs, western blots of lysates from these cells after treatment were probed with anti-synapsin I. Shef 6-CGN treated with 0.5 µM $A\beta_{42}O$ had lower synapsin I levels compared to controls ($p= 0.0274$) (Figure 5.19, B), however, no change in synapsin I levels was detected in Nas 2-bfCNs after the same treatment ($p= 0.0929$) (Figure 5.19, D).

Figure 5.19 Decrease in protein level of synapsin I in Shef 6-CGNs and Nas 2-bfCNs with Aβ$_{42}$O as indicated by western immunoblotting using anti-synapsin

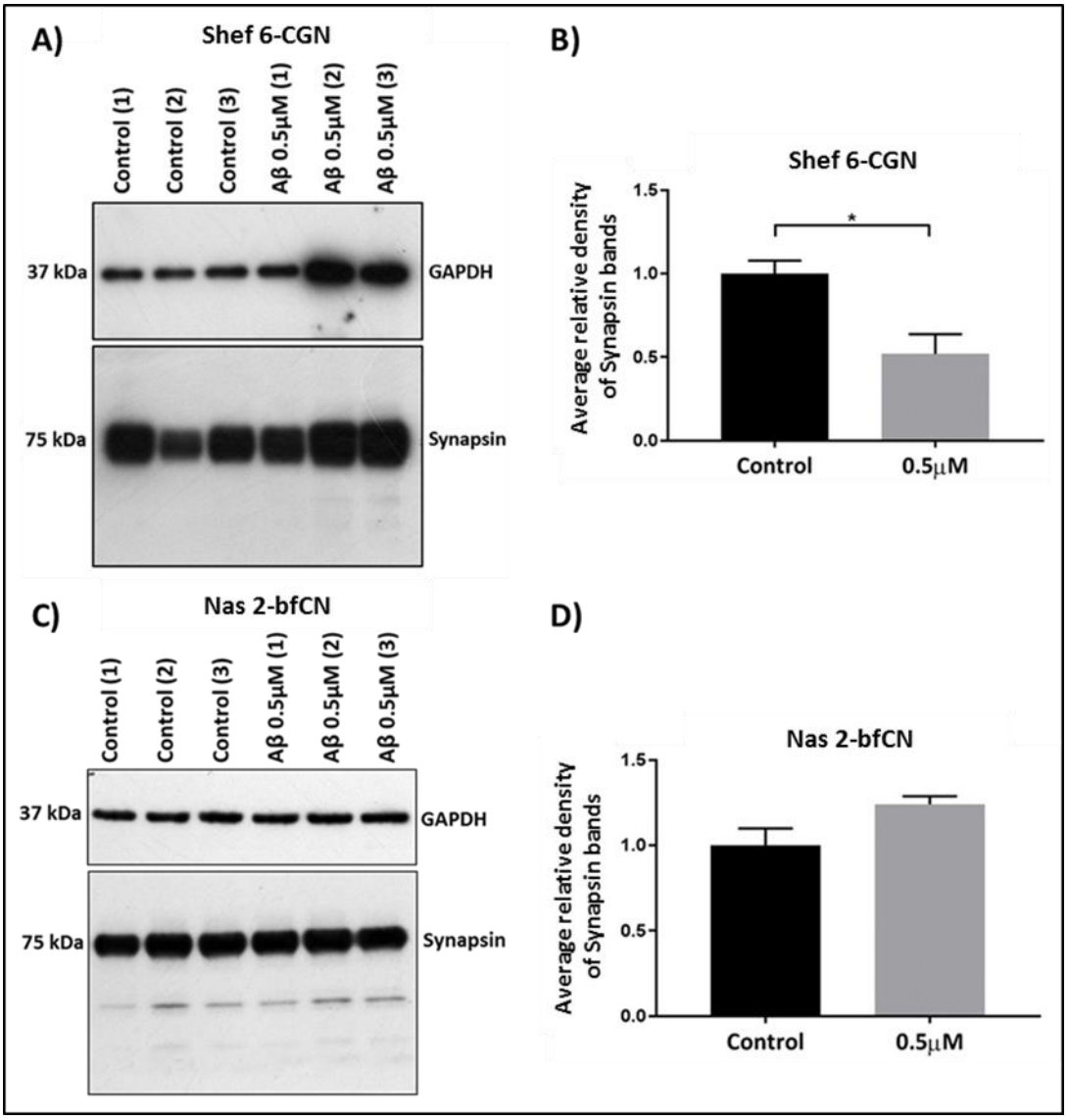

Figure 5.19 Decrease in protein level of synapsin I in Shef 6-CGNs and Nas2-bfCNs with Aβ$_{42}$O as indicated by western immunoblotting using anti-Synapsin

Representative western blots showing Shef 6-CGNs treated with 0.5 μM Aβ$_{42}$O (control n=3; Aβ 0.5 μM n=3) (A) and Nas 2-CGNs treated with 0.5 μM (control n=3; Aβ 0.5 μM n=3) (C), alongside controls, probed with GAPDH and anti-synapsin I. Graphs represent the average relative density of anti-synapsin I bands normalised to GAPDH bands for Shef 6-CGN treated with 0.5 μM Aβ$_{42}$O (B) and Nas 2-bfCN treated with 0.5 μM Aβ$_{42}$O (D).

Data was analysed using an unpaired Student's t-test. Error bars indicate +1 S.E.M.

5.3.7 Varicosities in Nas 2-bfCN treated with 1 µM $A\beta_{42}O$

To investigate the presence of pathogenic tau within neurons, Nas 2-bfCN treated with 1µM $A\beta_{42}O$ were fixed and immunostained with MC1, an antibody which specifically recognises a form of tau with an abnormal conformation associated with early AD (Weaver *et al.,* 2000; Jicha *et al.,* 1997). Nas 2-bfCN treated with 1 µM $A\beta_{42}O$ have greater numbers of neurons positively stained with MC1 and axonal varicosities that positively stain with MC1 (Figure 5.20; B and C, white arrows) compared to controls from the same differentiation set (Figure 5.20, A).

Trafficking of vital organelles, including mitochondria, has also been reported to be disrupted in tauopathies (Chapter 1.1.2). Mitochondria have a vital role within neurons and their dysfunction is intimately associated with neurodegenerative disease (Cabezas-Opazo *et al.,* 2015; Moreira *et al.,* 2010). To investigate the transport of mitochondria with Nas 2-bfCN treated with 1 µM $A\beta_{42}O$, cultures were immunostained with anti-ATPβ, which detects the beta subunit of ATP (adenosine triphosphate) synthase, an enzyme responsible for phosphorylating ADP (adenosine diphosphate) to ATP. This enzyme is richly present within mitochondria and so anti-ATPβ can be used as a mitochondrial marker (Jonckheere *et al.,* 2012). Staining was too dim to use for controls, however, varicosities containing mitochondria were observed in Nas 2-bfCNs treated with $A\beta_{42}O$ (Figure 5.21; B, C, E, F).

Figure 5.20 Nas 2-bfCNs treated with 1 µM $A\beta_{42}O$ contain varicosities containing an abnormal conformation of tau

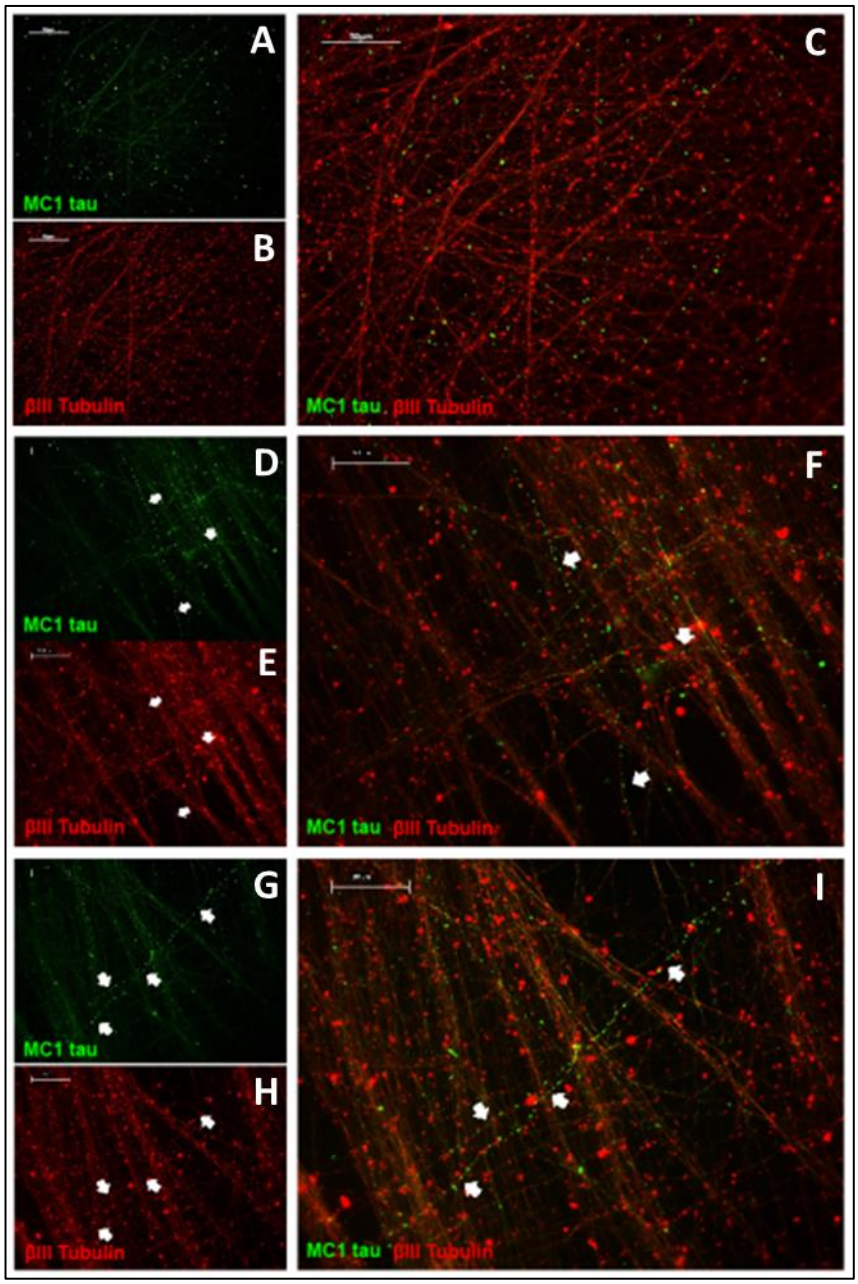

Figure 5.20 Nas 2-bfCNs treated with 1 µM $A\beta_{42}O$ contain varicosities containing an abnormal conformation of tau

Nas2-bfCNs positively immunostained for tau with an abnormal conformation in neuronal varicosities, as indicated by positive staining using MC1 antibody (green) and βIII Tubulin antibody (red). Arrows indicate individual neurons with varicosities containing MC1 tau found in neurons treated with 1 µM $Aβ_{42}O$, but not in controls. Controls are shown stained with antibodies A) MC1, B) βIII Tubulin and both C) MC1 and βIII Tubulin. Nas 2-bfCNs treated with 1 µM $Aβ_{42}O$ are shown stained with D) MC1, E) βIII Tubulin and both F) MC1 and βIII Tubulin. Another example of Nas 2-bfCNs treated with 1 µM $Aβ_{42}O$, taken from a different well, are shown stained with G) MC1, H) βIII Tubulin and both I) MC1 and βIII Tubulin. Scale bars indicate 50 µM.

5.21 Nas 2-bfCNs treated with 1 µM $A\beta_{42}O$ have varicosities containing mitochondria

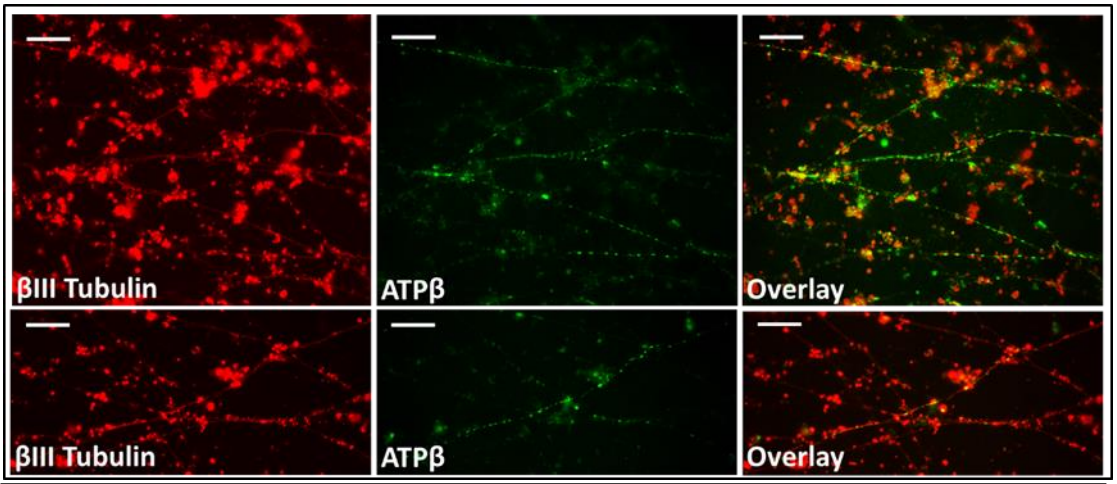

Figure 5.21 Nas 2-bfCNs treated with 1 µM $A\beta_{42}O$ have varicosities containing mitochondria
Nas 2-bfCNs were immunostained with anti-βIII Tubulin (A and D, red) and anti-ATPβ (B and E, green). Overlays (C and F) demonstrate axonal varicosities positively stained with ATPβ along axons. Scale bars indicate 50 µM.

5.4 Discussion

The work in this chapter was untaken to investigate whether the application of pre-aggregated, synthetic $A\beta_{42}O$, within a concentration range of 0.1 µM to 10 µM, to hPSC-bfCNs and hPSC-CGNs can recapitulate molecular aspects of early tauopathy recognised in AD. Specifically, the levels of tau protein and phosphorylated species of tau have been measured, which are reported to be increased in the AD brain and are considered to be indicators of tau pathology. Levels of *MAPT* expression were also investigated to determine whether altered levels contribute to the levels of tau protein. To investigate the culpability of the tau kinases GSK3β, Cdk5 and PAK3, reportedly dysregulated in AD, within the model, the protein levels, activity and gene expression of these proteins were also investigated.

5.4.1 Characterisation of hPSC-bfCN

BfCNs were differentiated from Nas 2-hiPSC and Shef 6-hESC after the generation of neurospheres from these lines. Acutely plated cells from these neurospheres, from each line, positively immunostain for nestin, an intermediate filament protein specific to CNS precursor cells (Zimmerman *et al.,* 1994; Fukuda *et al.,* 2003) and RNA-binding protein Mushashi homolog 1 (Mushashi), which is highly enriched within mammalian CNS and selectively expressed in neural stem cells (NSCs) (Sakakibara *et al.,* 1996; Kaneko *et al.,* 2000). The positive expression of these two markers in acute plate-downs of dissociated neurospheres indicates a homogenous population of NSCs, necessary to ensure a population of terminally differentiated cells of purely neural lineage. At 35 days after plating the neurospheres to initiate terminal differentiation, these neurons express the cholinergic marker, ChAT, as indicated by positive immunostaining of cultures with anti-ChAT and anti-βIII Tubulin.

Furthermore, at day 35 of terminal differentiation, these neurons also express synapsin, known to be present within early synapses, and PSD-95, a marker for mature synapses. Since synapsin is a pre-synaptic marker and PSD-95 is a post-synaptic marker, the proximity of puncta positive for these two proteins indicates the formation of synapses (Micheva *et al.,* 2010; Pratt *et al.,* 2008). The presence of mature synapses within *in vitro* AD models is an important consideration as dysfunction and loss of synapses are fundamental elements in early AD pathogenesis (Ferreira and Klein, 2011). Additionally, it has been postulated that tau pathology propagates throughout neural networks upon neuronal excitation via release of tau at synapses (Kfoury *et al.,* 2012; Wu *et al.,* 2016; Wang *et al.,* 2017; Liu *et al.,* 2012),

therefore the presence of a network of functional neurons is required in order to recapitulate AD pathogenesis as accurately as possible *in vitro*.

Characterisation of Shef 6-CGNs and Nas 2-bfCNs has been described previously in Chapter 4. At 50 days, derived neurons expressed the vesicular glutamate transporter 1 (vGlut1), a marker of glutamatergic neurons (Chapter 4.3.2). Immunostaining of hiPSC-CGNs also revealed the presence of synapsin I and PSD-95 in neurons.

5.4.2 $A\beta_{42}O$-induced tau pathology

Increased tau and ptau are widely reported in studies in post-mortem brain tissue, CSF and blood of AD patients (Sjögren *et al.,* 2001; Iqbal *et al.,* 2010; Zetterberg *et al.,* 2013) (Chapter 1.3). AD pathology develops over decades and it is not known if this pathological feature can be recapitulated in control hiPSC-neurons treated with $A\beta_{42}O$, although studies in primary neurons suggest this may be feasible (Zheng *et al.,* 2002; Billingsley and Kincaid 1997; Iqbal *et al.,* 1998; Busciglio *et al.,* 1995; Johansson *et al.,* 2006; Jin *et al.,* 2011; Ma *et al.,* 2009; Wang *et al.,* 2000; Alvarez *et al.,* 1999).

In an attempt to examine this aspect of pathology in these hiPSC-neurons, levels of tau protein were investigated by western immunoblotting and qPCR, respectively. Tau protein levels were not significantly altered through the treatment of Nas 2-bfCNs with 0.5 µM, Shef 6-CGNs with 0.5 µM or 1 µM $A\beta_{42}O$, or Shef 6-bfCNs with 0.1 µM, 0.5 µM or 1 µM $A\beta_{42}O$. These results indicate that treatment of hPSC-neurons with these concentrations of $A\beta_{42}O$ over 48 hours does not result in altered levels of total tau protein, therefore, this aspect of AD pathology was not recapitulated in this model.

This is predictable as so far, no sAD hiPSC-neuron model has reported increased levels of total tau or the presence of NFTs (for references see Table 1.2) and one sAD model based on the application of Aβ to hiPSC-neurons reported similar levels of total tau after treatment (Nieweg *et al.,* 2015). There have also been reports of increased tau secretion into the media of hiPSC-neurons derived from DS patients (Chang *et al.,* 2015; Shi *et al.,* 2012).

The cause of increased total tau within the AD brain is unclear; some have hypothesised that the increase may be due to the resistance of pathologically phosphorylated and aggregated tau to proteasomal degradation and removal through clearance pathways (Paglini and

Cáceres, 2001; Moore *et al*., 2015). In this hiPSC-models of AD, 48 hour treatment with $A\beta_{42}O$ may not allow sufficient time for the accumulation of tau.

To determine whether increased transcription of *MAPT* early in disease could play a role in the increased levels of tau in AD brains, gene expression was investigated. *MAPT* expression was not altered by treatment of Nas 2-bfCNs or Shef 6-CGNs with 0.5 µM or both 0.5 µM and 1 µM $A\beta_{42}O$, respectively. These results are in line with results from a previous study in which *MAPT* expression levels were reported to be unchanged within hiPSC-neurons derived from fAD patients carrying various mutations (Moore *et al.,* 2015). Studies examining levels of *MAPT* mRNA in AD brains compared to aged healthy brains have produced controversial results. While Liang and colleagues demonstrated decreased *MAPT* gene expression within the entorhinal cortex, hippocampus, middle temporal gyrus and posterior cingulate cortex of AD patients (Liang *et al.,* 2008), no statistically significant change was determined in two other studies where expression in specific brain regions was examined (Farnsworth *et al.,* 2016; Fukasawa *et al.,* 2017). However, it should be noted that upon amalgamation of results obtained from various brain regions, Fukasawa and colleagues did note statistically decreased *MAPT* in AD brains compared to controls (Fukasawa *et al.,* 2017). Liang and colleagues suggested that the decrease in *MAPT* expression in AD brains may represent a neuroprotective mechanism of remaining neurons (Liang *et al.,* 2008). If so, decreased *MAPT* expression occurs later in disease as hiPSC-neurons are thought to represent the early stages of disease pathogenesis.

An elevated level of ptau is one of the defining molecular features of the AD brain; pSer396/404 and pSer202 tau are found in AD brain NFTs. Phosphorylation of tau at Ser396 and Ser404 is associated with the later stages of AD, while phosphorylation at Ser202 is associated with early AD (Luna-Munoz *et al*., 2007). The application of 0.5 µM $A\beta_{42}O$ to Nas 2-bfCN, or of 0.5 µM or 1 µM $A\beta_{42}O$ to Shef 6-CGN did not result in statistically significant changes in tau phosphorylation at sites Ser396/404 compared to controls. Similarly, pSer202 tau levels were not significantly altered in Shef 6-CGN or Nas 2-bfCN after treatment with 0.5 µM $A\beta_{42}O$, or in Shef 6-bfCN after treatment with 0.1 µM, 0.5 µM or 1 µM $A\beta_{42}O$. These results indicate that the application of $A\beta_{42}O$, in concentrations between 0.1 µM and 1 µM, to hiPSC-derived CGNs and bfCNs for 48 hours does not cause elevated tau phosphorylation at these sites.

These results are unsurprising as so far, no sAD hiPSC-neuron model has recapitulated increased pSer396/404 tau, although one study has demonstrated increased pSer202 tau (Nieweg *et al.,* 2015). Increased phosphorylation of tau at these sites has been reported in previous fAD hiPSC-neuron models, suggesting that models based on fAD mutations may reproduce tau hyperphosphorylation at these sites more reliably. Increased pSer396/404 and pSer202/205 tau have been detected in V717L *APP* hiPSC and within hiPSC carrying a duplication of *APP* (Moore *et al.,* 2016). Increased phosphorylation of tau at Ser396, as well as Thr181, has also been reported within hiPSC-derived cerebral organoids carrying *APP* duplication (Raja *et al.,* 2016). Choi and colleagues reported a dramatic increase in pSer396/404 and pSer202/205 tau within select neurons, via immunocytochemistry, within 3xfAD (K670N/M671L,V717L *APP/*ΔE9 *PSEN1*) hiPSC-neurons (Choi *et al.,* 2014).

In a recent publication, an increase in pSer202/pSer205 tau could not be found in rat primary neurons treated with $A\beta_{42}O$ via western immunoblotting, however, increased immunostaining at the dendrites of these cells was reported (Tanokashira *et al.,* 2017). Mislocalised pSer202/202 and pSer396/404 tau has been detected, via immunocytochemistry, in some hiPSC-neuron models derived from DS patients (Chang *et al.,* 2015). These studies, along with immunostaining results reported by Choi and colleagues (Choi *et al.,* 2014), suggest that the use of immunocytochemistry to detect abnormal translocation and increased levels of ptau facilitate identification of early AD pathology in hiPSC-neurons in which protein levels are not significantly altered. While no change in the levels of pSer396/404 tau or pThr231 was detected within cells of hiPSC-neurons derived from patients with DS, increased levels of tau phosphorylated at these sites was detected within the media of these cultures (Shi *et al.,* 2012), which may signify that ptau cannot be detected in some hiPSC-neuron models of AD via western immunoblotting due to secretion of ptau.

Further investigation of levels of pThr231 tau in this model may reveal increased tau phosphorylation, as increased phosphorylation of tau at this site has been reported in sAD hiPSC-neuron models (Hossini *et al.,* 2015; Israel *et al.,* 2013; Nieweg *et al.,* 2015) as well as within hiPSC-neurons derived from fAD patients with *APP* duplication (Israel *et al.,* 2013). The age of the neurons in these studies seems to be critical to successful recapitulation of increased tau phosphorylation at these sites. Muratore and colleagues noted that pSer262 tau levels were not increased at day 35 of culture but were at 100 days (Muratore *et al.,*

2013), while Raja and colleagues detected increased ptau at 90 days but not at 60 days (Raja *et al.,* 2016). Choi and colleagues measured phosphorylation within their model at 70 days after differentiation of hiPSC-neurons (Choi *et al.,* 2014), while Moore and colleagues detected ptau within hiPSC-neurons at day 90 (Moore *et al.,* 2016). The culture period for hiPSC-bfCN and hiPSC-CGN in this study may not be sufficient to allow for detection of increased ptau.

Previous studies involving the application of Aβ to murine primary neurons report increased pSer396/404 and pSer202/205 tau levels after treatment (De Felice *et al.,* 2008; Ramser *et al.,* 2013; Alvarez *et al.,* 1999; Zempel *et al.,* 2010). Recapitulating increased increased phosphorylation at these sites in hiPSC-neurons appears to be more challenging. In the foetal brain, tau is heavily phosphorylated at sites hyperphosphorylated in AD (Matsuo *et al.,* 1994) and recently, we have learned that hiPSC-neurons, once differentiated, mature at a similar rate to those within the developing human brain (Sposito *et al.,* 2015). High levels of phosphorylation in young hiPSC-neurons may mask the effects of $A\beta_{42}O$-induced changes to pathways leading to aberrant tau phosphorylation in the hPSC-CGN and hPSC-bfCN used in this project.

5.4.3 $A\beta_{42}O$-induced alterations in kinase activity, levels and expression

Levels of GSK3β were not significantly altered by treatment with $A\beta_{42}O$ in Nas 2-bfCNs and Shef 6-CGNs, however GSK3β activity, indicated by levels of GSK3β phosphorylated at Tyr216, was altered in both cell types. Treatment of Nas 2-bfCNs with 0.5 μM $A\beta_{42}O$ significantly increased GSK3β activity, while the same treatment of Shef 6-CGNs decreased activity, as indicated by levels of active (pTyr216) GSK3β. These results suggest that GSK3β activity is differentially affected in these two neuronal subtypes.

Varying levels of GSK3β activity have been reported in different areas of the brain. Within the frontal cortex of AD brains, pTyr216 GSK3β has been reported to be increased (Leroy *et al.,* 2007), while activity has been found to be unchanged within the AD hippocampus (Pei *et al.,* 1997). In another study, the activity of GSK3β was found to be decreased in the pre-frontal cortex of AD brains (Swatton *et al.,* 2004), indicating that further research is required to understand the regional differences in GSK3β activity within the AD brain. Increased activity of GSK3β has previously been reported within V717L *APP* hiPSC-derived cholinergic neurons (Muratore *et al.,* 2014) and in rat cholinergic septal neurons after treatment with

AβO (Zheng *et al.,* 2002), in line with the increase in pTyr216 GSK3β in hiPSC-bfCN reported in this chapter. Increased levels of pTyr216 GSK3β have also been found within a mixed population of hiPSC-neurons carrying a duplication of *APP* (Israel *et al.,* 2012).

The gene expression of *GSK3β* within Nas 2-bfCN and Shef 6-CGN was not significantly altered by treatment with 1 µM $A\beta_{42}O$ or 0.5 µM $A\beta_{42}O$. Expression was significantly increased, however, in Nas 2-bfCN treated with 0.5 µM $A\beta_{42}O$ compared to those treated with 1 µM $A\beta_{42}O$. These results suggest that *GSK3β* expression is not altered by treatment of these neurons for 48 hours with concentrations 1 µM $A\beta_{42}O$ or 0.5 µM $A\beta_{42}O$.

GSK3β expression has been reported to be upregulated in AD and MCI patients, within the hippocampus (Blalock *et al.,* 2004), in post-synaptosomal supernatants (Pei *et al.,* 1997) and in peripheral lymphocytes (Hye *et al.,* 2004). Conversely, decreased expression of *GSK3β* has also been described within the hippocampus, medial temporal gyrus and posterior cingulate cortex of AD patients compared to healthy age-matched controls (Liang *et al.,* 2008). In this publication, the authors suggest that healthy neurons that remain in the brains of AD patients may respond to the disease by decreasing *GSK3β* expression as a neuroprotective mechanism. The results in this study align with the decrease in *GSK3β* expression previously reported in hiPSC-cortical neurons derived from a patient with sAD (Hossini *et al.,* 2015). These studies do not support thes lack of gene expression difference in Nas 2-bfCN and Shef 6-CGN treated with $A\beta_{42}O$ in this study.

As described, greater levels of p35 compared to p25 can be associated with physiological activity of Cdk5, while greater levels of p25 indicate hyper-activated Cdk5 (Chapter 1.3.2). Levels of p25 and levels of p35 are unchanged in Nas 2-bfCN treated with 0.5 µM $A\beta_{42}O$, while levels of p35 are decreased in Shef 6-CGN treated with either 1 µM or 0.5 µM $A\beta_{42}O$. In agreement with this, AβO treatment of rat primary cortical neurons has been demonstrated to cause decreased levels of p35 (Hsiao *et al.,* 2008).

CDK5 expression was observed to be unchanged in Nas 2-bfCN treated with 0.5 µM $A\beta_{42}O$ and Shef 6-CGN treated with 1 µM $A\beta_{42}O$ compared to controls. These results differ compared to a previous report in which *CDK5* expression was demonstrated to be decreased in sAD hiPSC-neurons (Hossini *et al.,* 2015). Conversely, in PC12 cells overexpressing *APP* gene, expression of *CDK5* was increased (Czapski *et al.,* 2011). Two studies have reported decreased expression of *CDK5* in specific brain areas including the entorhinal cortex, hippocampus, posterior cingulate cortex and medial temporal gyrus in patients with AD in

comparison to controls (Liang *et al.,* 2008; Fukasawa *et al.,* 2017). Interestingly, Liang and colleagues also reported an increase in *p35* expression alongside decreased *CDK5* expression and hypothesised that these expression changes may represent neuroprotective processes in the remaining healthy cells in an attempt to prevent further tau pathology (Liang *et al.,* 2008).

PAK3 levels and *PAK3* expression are unchanged in Nas 2-bfCN and Shef 6-CGN treated with 0.5 µM and 1 µM $A\beta_{42}O$. While changes in PAK3 levels have not been reported in hiPSC-neurons via western immunoblotting, the application $A\beta_{42}O$ to hiPSC-neurons within a 3D culture system has been shown to stimulate translocation of PAK3 into the somatodendritic compartments (Zhang *et al.,* 2014), which agrees with previous research in rat primary cortical neurons (Ma *et al.,* 2008). Elevated levels of PAK3 and phosphorylated PAK3 have, however, been reported in rat cortical neurons after treatment with $A\beta_{42}O$ (Ma *et al.,* 2008). These results suggest that the pathways affected in AD that result in changes to PAK3 protein and gene expression levels, described in Chapter 1 (Chapter 1.3.3), may not be recapitulated fully in hPSC-bfCNs and CGNs upon treatment with $A\beta_{42}O$.

5.4.4 The effects of $A\beta_{42}O$ on synapsin I protein levels

The loss of synapses is an early event in AD pathogenesis and is thought to occur before the loss of neurons (Scheff *et al.,* 2006; Hong *et al.,* 2016). Levels of synapsin I have been found to be decreased within affected brain regions of AD patients compared to controls, indicating the loss of synapses (Hamos *et al.,* 1989; Perdahl *et al.,* 1984). To investigate the loss of synapses within this model of AD, levels of synapsin I within hPSC-CGNs and hPSC-bfCNs treated with $A\beta_{42}O$ were investigated.

In this study, levels of synapsin I were found to be decreased in Shef 6-CGN treated with 1 µM $A\beta_{42}O$, indicating that treatment of these cells with this concentration of $A\beta_{42}O$ recapitulates this aspect of AD. No change in synapsin I levels was found in Nas 2-bfCN treated with 0.5 µM $A\beta_{42}O$. Although functional synaptic impairment has been demonstrated in hiPSC-glutamatergic neurons treated with 25-50 ng/ml $A\beta_{42}O$ for 8 days, the levels of the pre-synaptic protein vGlut1 were reported to be unchanged in this AD hiPSC-model (Nieweg *et al.,* 2015). Similarly, Israel and colleagues demonstrated no change in synapsin I within hiPSC-neurons derived from patients with a duplication of APP or sAD patients, compared to controls (Israel *et al.,* 2011). The cultures of hiPSC-neurons

differentiated by Israel and colleagues consisted of a mixed population of neurons and were estimated to contain 15 % of glutamatergic neurons, therefore, the lack of decreased synapsin I in these hPSC-neurons may represent the relative resilience of other neuronal subtypes. Differences in the relative resilience of hPSC-CGN compared to hPSC-bfCN to the loss of synapsin could be explained by phenotypic differences or differences in culture conditions. Additionally, these differences may be due to the insufficiency of 0.5 μM $A\beta_{42}O$ to cause synapsin I loss relative to the higher concentration of 1 μM.

Reports on the relative resilience of different neuronal subtypes in AD and models of AD are conflicting. Counts and colleagues examined the protein levels of pre-synaptic proteins, synaptophysin and synaptotagmin, alongside post-synaptic drebrin in the hippocampi of patients with mild-to-moderate AD compared to those with no cognitive impairment. They found that while drebrin levels were diminished by 40 % in AD, synaptophysin and synaptotagmin levels were preserved (Counts *et al.,* 2012). The same group previously demonstrated a loss of approximately 35 % of synaptophysin levels in the temporal cortex of patients with MCI compared to controls (Counts *et al.,* 2006), suggesting that the loss of specific synaptic proteins in AD may be regionally distinct. This may explain that while there is no loss in synapsin I levels within hiPSC-bfCNs, which represent the basal forebrain projecting to the hippocampus, synapsin I levels are reduced in hiPSC-CGN, which represent cortical neurons.

Within an *in vitro* model of AD, the treatment of KM670/671NL *APP* mouse primary cortical neurons with 1 μM AβO had no effect on levels of synapsin I, while post-synaptic proteins were found to be decreased (Almeida *et al.,* 2005). On the contrary, treatment of control mouse primary hippocampal neurons with $A\beta_{40}O$ significantly decreased synapsin (Sepulveda *et al.,* 2010). These reports, coupled with the results in this chapter, highlight the need for further clarification of the synaptic proteins loss in different neuronal subtypes in AD.

5.4.5 $A\beta_{42}O$-induced varicosities containing pathogenic tau and mitochondria

Axonal varicosities, which can be described as swellings or beading, are well documented in AD (Geula *et al.,* 2008; Grutzendler *et al.,* 2007; Notter and Knuesel, 2013; Terwel *et al.,* 2002). These varicosities are thought to be caused by impaired transport of vesicles containing cargo along the microtubules, caused by aberrant phosphorylation of tau through

the interaction of AβO and tau (Mertens *et al.,* 2013; Krstic and Knuesel, 2012; Khan and Bloom, 2016). Individual neurons within cultures of Nas 2-bfCN treated with 1 μM $A\beta_{42}O$ were found to have axonal varicosities, which positively immunostained for a pathological conformation of tau and mitochondria, in this study.

Varicosities have been demonstrated before in hiPSC-neuron models of tauopathy. Varicosities within hiPSC-neurons, carrying mutations in *APP* (K670N/M671L and V717L) as well as in *PSEN1* (ΔE9), have been reported within those neurons exhibiting increased levels of tau phosphorylation, identified by immunostaining with antibodies to detect pSer396/404 and pSer199/202/205 tau (Choi *et al.,* 2014). Additionally, Iovino and colleagues have demonstrated varicosities, which positively immunostain with a 4R tau antibody, within P301L *MAPT* hiPSC-CGNs, which also exhibited impairments in the transport of mitochondria (Iovino *et al.,* 2015). This study suggests a link between pathological tau, varicosities and mitochondrial impairment.

Increased phosphorylation of tau, specifically at Ser396/404 and Ser199/202/205, has also been demonstrated to lead to abnormalities in mitochondrial transport in P301L *MAPT* mice and within the human AD brain (Kopeikina *et al.,* 2011). In PC12 cells, as well as in mouse cortical neurons, carrying *MAPT* mutations associated with increased phosphorylation of tau at Ser199, Ser202 and Ser205, individual neurons within cultures that were positively immunostained with MC1 also exhibited reduced mitochondrial transport, indicating a link between tau phosphorylation, the formation of tau with an abnormal conformation and reduced transport of mitochondria (Shahpasand *et al.,* 2012). Furthermore, acute application of synthetic AβO to rat hippocampal neurons has been previously shown to result in prompt and severe disruption of mitochondrial transport, indicating that this treatment can be used to recapitulate this aspect of pathology (Rui *et al.,* 2006).

These results suggest that Nas 2-bfCN treated with 1 μM $A\beta_{42}O$ may, therefore, be a suitable model for investigating the pathways through which Aβ causes changes to tau protein resulting in a pathogenic conformation of tau. The model may also be suitable for investigating microtubule transport deficits. Since it has been previously demonstrated that varicosities and impaired axonal transport occur before overt AD pathology in the AD brain (Stokin, 2005), the varicosities recognised in this study may be representative of early, prodromal pathology linked to AD.

5.4.6 Summary

This study has shown that bfCN neurons respond to $A\beta_{42}O$ with changes in kinase activity of GSK3β and Cdk5. The development of varicosities in response to $A\beta_{42}O$ in Nas 2-bfCN and reduction of synapsin I levels in Shef 6-CGN also indicate early pathological changes. Furthermore, the differences in the responses of the two types of neurons examined suggests that distinct neuronal subtypes have different responses to $A\beta_{42}O$, which may relate to the progression of neurodegeneration through specific pathways in the brain.

This model failed to recapitulate key changes in tau pathology on a molecular level; increased levels of tau protein and tau phosphorylation were not observed. Although this is not unexpected, based on the literature, this limitation of the model may affect its utility for drug discovery. It is hoped that further development of the model could overcome these limitations.

One important consideration when modelling with hiPSC-neurons is that these cells are relatively immature, despite being cultured for a long time *in vitro*, compared to those of the AD brain. HiPSC-neurons are thought to mature at a similar rate to that recognised in the developing human brain and since the most significant risk factor in AD is age, these neurons may not recapitulate molecular changes recognised in aging. For example, NFTs in the AD brain are made up of all six isoforms and development of tau pathology may depend on interactions between tau isoforms. Due to the relative immaturity of these cells, only one of the six isoforms of tau is expressed; 3R0N. Furthermore, it has been shown that AβO more readily bind to the surface of aged neurons and have a greater effect on membrane stability compared to younger neurons (Ungureanu *et al*., 2016). Therefore, the relative immaturity of these hiPSC-neurons may contribute to a lack of complete AD phenotype.

A review of AD hiPSC models to date has revealed some possible avenues for improvement of this model. Three publications detailing 3D AD hiPSC-neuron models have demonstrated AD phenotypes that could not be observed in equivalent 2D models. Zhang and colleagues treated hiPSC-neurons within a 3D culture system with 0.1 µM $A\beta_{42}O$ for 24 hours and demonstrated abnormal translocation of PAK within neurons in their 3D system, but not in a 2D system (Zhang *et al.,* 2014). The only hiPSC-neuron models reported to develop tau aggregations were created through 3D culture system (Choi *et al.,* 2014; Raja *et al.,* 2016). Recently, the use of layered hydrogels for 3D modelling has been demonstrated to accelerate the maturation of neurons and allow for co-culture of different cell types (Zhang *et al.,* 2016).

Co-culturing neurons with glial cells has also been shown to advance neuronal maturation (Qi *et al*., 2017). At 365 days *in vitro*, hiPSC-CGNs begin to express the adult isoforms of tau (Sposito *et al.,* 2015), therefore culturing cells for longer periods after terminal differentiation may allow more complete modelling of AD.

The work in this chapter contributes to the base level research that must be carried out to understand the behaviour of tau in hiPSC-neurons to move towards creating improved models for research and drug discovery.

Chapter 6

Tau pathology in the brain tissue of patients with frontotemporal dementia and Alzheimer's disease

6.1 Introduction

Frontotemporal dementia (FTD) is a clinically and pathologically diverse group of progressive neurodegenerative diseases (Chapter 1.2.1), the majority of which are sporadic. In this project, hiPSC-neurons have been derived from a patient carrying a mutation that causes FTDP-17 (Chapter 4) to model FTD. Although we do not yet understand the initial causative events that instigate pathogenesis in sporadic cases of FTD, we do know that mutations in *MAPT* result in FTDP-17, therefore it is logical to create hiPSC-models based on these mutations. Mutations of *MAPT* only make up an estimated 10 % of FTD cases (Hardy, 2014), however; for this reason it would be valuable to understand how closely these models represent the sporadic cases of FTD, as well as FTDP-17. PiD is a sporadic FTD (sFTD) covering a variety of symptoms and pathology, although it has many important features in common with FTDP-17 (Chapter 1.2.1). Both PiD and FTDP-17 most commonly clinically present as behavioural variant FTD (bvFTD), are classified as FTD-tau (Figure 1.4) and follow similar patterns of neurodegeneration (Chapter 1.2.1).

Accordingly, the work described in the first part of this chapter was carried out to investigate post-mortem tau-related pathology within the frontal and temporal cortices of patients with FTDP-17 and PiD, using the same molecular tools used to investigate tau pathology in hiPSC-neurons (Chapter 4.2) to limit variability during comparison. Western immunoblotting was carried out to determine soluble tau protein levels and their phosphorylation status, alongside the protein levels and activity of the tau kinases glycogen synthase kinase 3β (GSK3β), cyclic dependent kinase 5 (Cdk5) and p21 activated kinase 3 (PAK3), in six controls, three PiD patients and three FTDP-17 patients. Two of the three patients with FTDP-17 carried the mutation IVS 10+16 *MAPT*, while one carried the mutation R406W *MAPT*. Below

the known pathology and clinical presentations of these mutations are discussed (Chapter 6.1.1).

Tau within hiPSC-neurons carrying *MAPT* mutations has been demonstrated to be soluble, with no aggregates of tau (Silva *et al.,* 2016; Hallmann *et al.,* 2017; Ehrlich, Hallmann, *et al.,* 2015; Wren *et al.,* 2015); therefore, to allow for comparison of tau pathology in human brains with hiPSC-models the levels and phosphorylation status of soluble tau protein was investigated. This project focuses on tau pathogenesis since phosphorylated, soluble tau has been suggested to be the precursor of tau aggregates (Šimić *et al.,* 2016).

This knowledge will further our understanding regarding whether hiPSC-models created using patients with mutations in *MAPT* can be used to model not only FTDP-17 but also sporadic FTD, and to what extent. An evaluation of the ability of V337M *MAPT* hiPSC-neurons to recapitulate the pathology found in these tissues is discussed in Chapter 8 (Chapter 8.1).

In the second part of this chapter, the gene expression levels of *MAPT* and two selected tau kinases were determined within the basal forebrain nucleus basalis of Meynert (nbM) in patients with Alzheimer's disease (AD) compared to controls, using qPCR. This area of the brain is affected early in AD and is particularly vulnerable, as discussed in Chapter 1 (Chapter 1.2.3). An evaluation of the ability of the hiPSC-neuron model of AD described in Chapter 5 (Chapter 5) to recapitulate these changes is discussed in Chapter 8 (Chapter 8.2).

6.2 Methods and reagents

6.2.1 Brain tissue samples

Temporal and frontal brain tissue from three FTDP-17 patients, with either R406W *MAPT* or IVS 10+16 *MAPT* mutations, along with three control patients tissue, was obtained from the Queen's Square Brain Bank for Neurological Disorders (QSBB) (London, UK) (Ethics ref 08/H0718/54+5]. Temporal and frontal brain tissue was obtained from three patients with PiD and three control patients, and compared with tissue from four patients with AD (nbM) from the South West Dementia Brain Bank (SWDBB) [Ethics ITA074]. Table 6.1 lists the known, relevant details regarding these patients. Brain tissue from patients carrying the rare V337M *MAPT* mutation proved very difficult to find and could not be obtained for this project. An alternative mutation, R406W *MAPT*, was obtained instead. Both R406W and V337M are nonsense, exonic mutations, which increase tau aggregation, reduce tau microtubule binding (Hutton *et al.,* 1998; Poorkai *et al.,* 1998), do not affect splicing of exon 10 of *MAPT* and have equal numbers of 3R and 4R tau isoforms within aggregations of tau (Hong *et al.,* 1998). Tissue from only one patient with R406W *MAPT* was available, therefore, frontal and temporal cortex tissue of patients with IVS 10+16 *MAPT* was also obtained. Details of the pathology and clinical presentation of patients with these two mutations are given in Chapter 1 (Chapter 1.2.3.1).

Table 6.1 Brain tissue samples

Group	Name	Code	Source	Tissue	Age	Sex	Diagnosis	PMD	Pathology notes	Cause of death	Genetic
1	PiD 1	197	SWDBB	TL and FL	68	M	PiD	16	AD diagnosis	Respiratory tract infection	ApoE2/3
1	PiD 2	493	SWDBB	TL and FL	77	M	PiD	61	Pick's disease		ApoE3/3
1	PiD 3	514	SWDBB	TL and FL	76	M	PiD	56	Pick's disease		ApoE2/3
1	Control 1	150	SWDBB	TL and FL	69	M	Control	66	No abnormal changes	Primary pulmonary hypertension	ApoE 3/3
1	Control 2	894	SWDBB	TL and FL	74	M	Control	57.5	Mild Argyrophilic grain disease	Disseminated metastatic cancer	
1	Control 3	927	SWDBB	TL and FL	78	M	Control	51.5	Mild Small Ventricular Disease	Prostate cancer	ApoE3/3
2	MAPT R406W	P6/07	QSBB	TL and FL	66	M	FTDP-17				
2	MAPT 10+16 (1)	P2/08	QSBB	TL and FL	66	M	FTDP-17				
2	MAPT 10+16 (2)	P6/11	QSBB	TL and FL	52	M	FTDP-17				
2	Control 4	P78/06	QSBB	TL and FL	68	F	Control				
2	Control 5	P15/10	QSBB	TL and FL	69	M	Control				
2	Control 6	P18/03	QSBB	TL and FL	56	F	Control				
3	AD 1	691	SWDBB	nBM	80	M	AD	99	Braak tangle stage IV; Moderate density of neuritic plaques	Broncho-pneumonia	ApoE 3/4
3	AD 2	765	SWDBB	nBM	80	M	AD	24	Braak tangle stage IV; Moderate density of neuritic plaques;	Broncho-pneumonia	
3	AD 3	794	SWDBB	nBM	80	F	AD	26	Braak tangle stage IV; moderate density of neuritic plaques	Gist tumour	ApoE 3/4
3	Control 7	800	SWDBB	nBM	92	F	Control	34.5	Braak tangle stage IV; sparse neuritic plaques	Old age	ApoE 3/3
3	Control 8	870	SWDBB	nBM	90	F	Control	41	Mild argyrophilic grain disease; moderate cerebral amyloid angiopathy	Biventricular heart failure	
3	Control 9	877	SWDBB	nBM	82	M	Control	67	Very mild arteriosclerotic small vessel disease with an occasional microinfarct	Cerebrovascular event; renal failure	
3	Control 10	887	SWDBB	nBM	74	F	Control	39.5		Infective exacerbation of COPD	ApoE 3/3

Table 6.1 Brain tissue sample details (legend continued on following page)

TC= temporal cortex; FC= frontal cortex; nbM = nucleus basalis of Meynert. Group 1 mean and S.D of age is 73.67+/-4.23 and of PMD is +/- 51.33+/-17.98. Group 2 mean and S.D. of age is 62.83 +/- 7.05. Group 3 mean and S.D of age is 81.14 +/- 4.74 and of PMD is 51.92+/-27.07. Group 1 and 2 combined mean and S.D. of age is 68.25 +/- 7.92.

6.2.2 Western immunoblotting

6.2.2.1 Lysate preparation of brain samples

This method was adapted from Mair *et al*., 2016 and buffer recipes selected for their ability to prevent degradation changes to post translational modifications (PTM) during processing. 300 mg of frozen brain tissue was weighed out and homogenised in 1.5 ml of Buffer 1 (Table 6.2). The tissue was homogenised firstly by compressing 20 times using a sterile plastic disposable 1.5 ml microtube pestle, then by passing the tissue through a series of sterile, disposable needles of descending size, from 14 gauge to 20 gauge, attached to a syringe. After centrifuging 15 minutes; 11,000 g; 4 ^{o}C to clarify the crude homogenate, 1 % Sarkosyl (Sigma, L9150) was added to each sample from a 10 % stock solution and the samples were incubated on a vertically rotating platform for 60 minutes at 4 ^{o}C. The samples were then centrifuged at 100,000 g for 120 minutes at 4 ^{o}C. The supernatant was removed and kept in a clean Eppendorf labelled 'soluble fraction'. Samples were stored at -80 ^{o}C and thawed on ice just before preparation of western immunoblotting samples.

Table 6.2 Reagents for Buffer 1

Reagent	Manufacturer and code	Concentration
Tris HCl pH 7.4	Melford, T1513	25 mM
NaCl	Melford, S0520	150 mM
EDTA	Sigma, E6758	10 mM
EGTA	Sigma, E3889	10 mM
DTT	Thermal Fisher, R0862	1 mM
Nicotinamide	Sigma, 72340	10 mM
Trichostatin A	Selleck Chemicals, S1045	0.002 mM or 2 µM
PhosStop™ phosphatase inhibitor tablet	Roche, 04906845001	1 tablet/10 - 50 ml ddH_2O
cOmplete™ protease inhibitor cocktail tablet	Roche, 11697498001	1 tablet/ 10 - 50 ml ddH_2O

Western immunoblotting samples were prepared as described in Chapter 2 (Chapter 2.2.1). 30 µg of protein was loaded into each well, as measured by bicinchoninic acid (BCA) assay (Chapter 2.2.1.2). The samples were run on 12 % SDS-page gels and the antibodies for pan-tau and phospho-tau were run on separate western blots to avoid any residual staining,

which could affect the results as analysed by densitometry. All tau kinase antibodies were also run on separate blots. Each western blot was performed three times. Densitometric analysis and other western immunoblotting steps were carried out as described in Chapter 2 (Chapter 2.2.1). The details for the antibodies used to probe western immunoblots in this chapter are as detailed in Table 5.5 (Table 5.5; Chapter 5.2.4).

6.2.2.2 Analysis of western immunoblots

Upon completion of densitometric analysis of western bands for tau antibodies, analysed as described in Chapter 2 (Chapter 2.2.1.10), bands were normalised against those measured for GAPDH, a housekeeping protein. All bands revealed by western immunoblotting using anti-tau antibodies were included in densitometric analysis, for each sample. The statistical significance of differences, calculated as a P value, between patient and control groups was calculated using a Student's T-test. Analysis of PAK3 levels included only bands at 65 kDa. For analysis of synapsin levels only bands at 75 kDa were included. For p25 and p35 level analysis, only bands at 25 kDa and 35 kDa, respectively, were included in analysis. For analysis of the levels of GSK3β and pTyr216 GSK3β, only bands at 41 kDa to 52 kDa were included in analysis. Graphs were annotated with asterisks to denote the level of significance; * with $P < 0.05$, ** with $P < 0.01$ and *** with $P < 0.001$.

6.2.3 qPCR analysis of gene expression in brain tissue

6.2.3.1 RNA extraction, purification and conversion to cDNA

1 ml of TRIzol® reagent (Thermo Fisher, 15596026) was added to 100 mg of brain tissue. The tissue was then homogenised as described above (Chapter 6.3.1) before being incubated for 5 minutes at room temperature to allow for complete dissociation of nucleoprotein complexes. 0.2 ml of chloroform was then added to each sample and the samples were vigorously mixed for 15 seconds before being left to incubate for 2-3 minutes at room temperature. The samples were then centrifuged at 12,000 g at 4 ^{o}C for 5 minutes. The sample separated into three layers; a lower red phenol-chloroform layer, a white interphase and a colourless upper aqueous phase containing RNA. A wide 200 µl pipette tip was used to carefully extract the upper layer ensuring none of the interphase was collected with it. The aqueous phase was transferred into a clean, RNAse-free Eppendorf and either immediate frozen within a -80 ^{o}C freezer or processed to purify and concentrate the RNA, as described

in Chapter 2 (Chapter 2.2.3.1). The concentration and purity of the resultant RNA samples were measured using the NanoPhotometer™ Pearl (Implen) as outlined in Chapter 2 (Chapter 2.2.3.2). Reverse transcription of RNA to cDNA was performed as detailed in Chapter 2 (Chapter 2.2.3.3) and qPCR was carried out in triplicate as described previously (Chapter 2.2.3.4). The analysis of qPCR was also carried out as detailed in chapter 2 (Chapter 2.2.3.5). The threshold cycle (CT) values for *MAPT, GSK3β*, *CDK5* or *PAK3* were normalised against the CT values for the housekeeping gene, *GAPDH*. The statistical significance of differences, between patient and control groups, was calculated using the Mann-Whitney test where expression within brain tissue of controls were compared to brain tissue of AD patients (Chapter 6.3.5) and the Kruskal-Wallis test followed by a post-hoc Dunn's test where expression within the brains of controls, FTDP-17 patients and PiD patients were compared (Chapter 6.3.2 and Chapter 6.3.3). *=$p \leq 0.05$. **=$p \leq 0.01$. ***=$p \leq 0.001$.

6.3 Results

6.3.1 Tau pathology within the frontal and temporal cortices of patients with FTD

To investigate the total levels of tau protein within the frontal and temporal cortices of patients with PiD, compared to controls, western immunoblots were probed with the antibody to total tau, DA9.

Figure 6.1 Levels of total tau in frontal and temporal cortex brain tissue from PiD patients

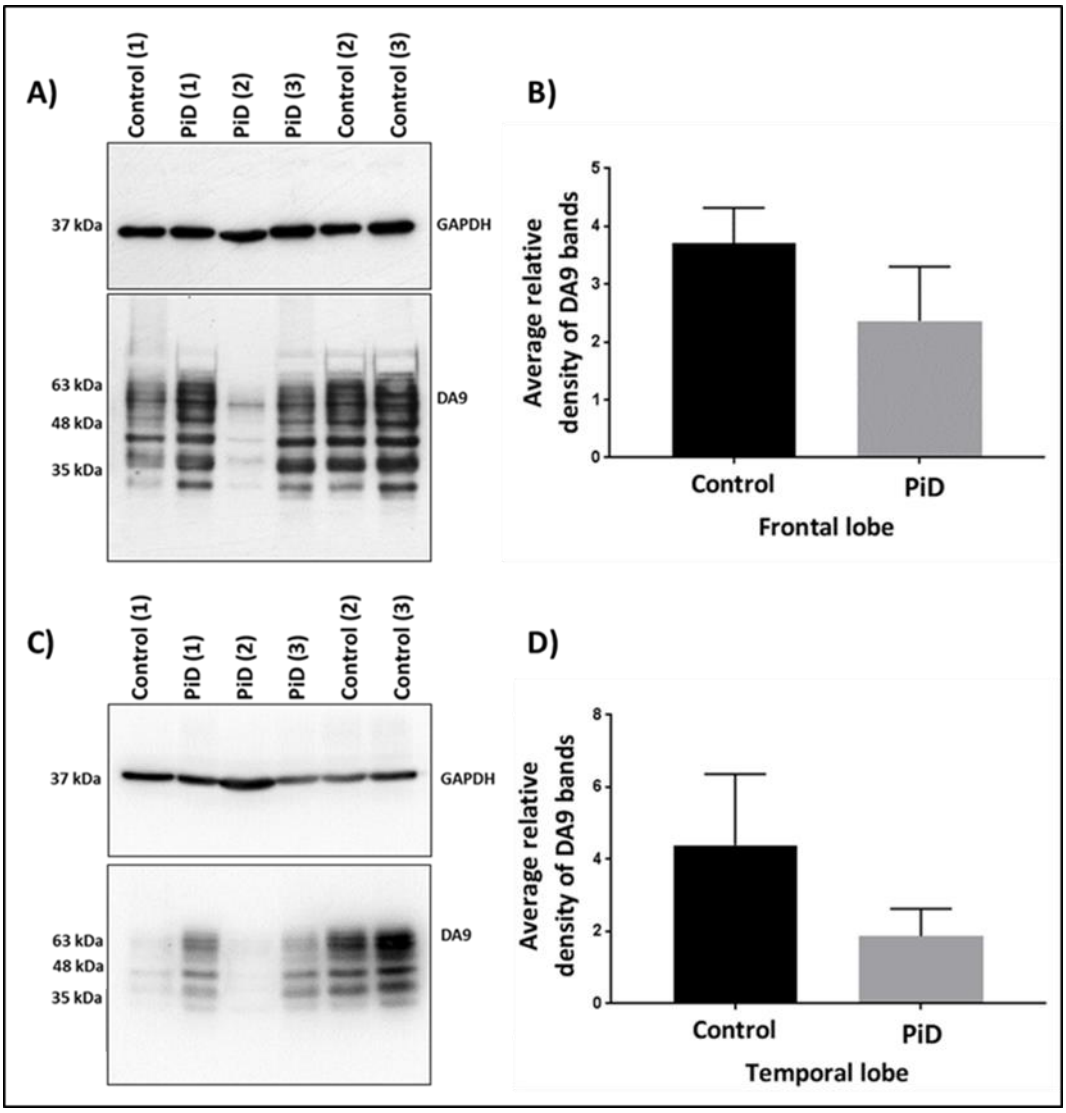

Figure 6.1 Levels of total tau in frontal (A & B) and temporal (C & D) cortex brain tissue from PiD patients

Representative western blots showing frontal cortex tissue (A) and temporal cortex tissue (B) from PiD patients alongside healthy controls probed with GAPDH and DA9 (Control n=3; PiD n=3). Graphs representing the density of DA9 bands normalised to GAPDH bands for frontal cortex tissue (C) and temporal cortex tissue (D).

Data was analysed using an unpaired Student's t-test. Error bars indicate +1 S.E.M.

No statistically significant change in levels of total tau were detected in frontal (p= 0.2952) or temporal (p= 0.2976) cortices of PiD compared to controls. The total levels of tau protein within the frontal cortices of patients with FTDP-17, compared to controls, were also detected by probing western immunoblots with DA9 (Figure 6.1).

Figure 6.2 Levels of total tau in frontal cortex brain tissue from FTDP-17 patients

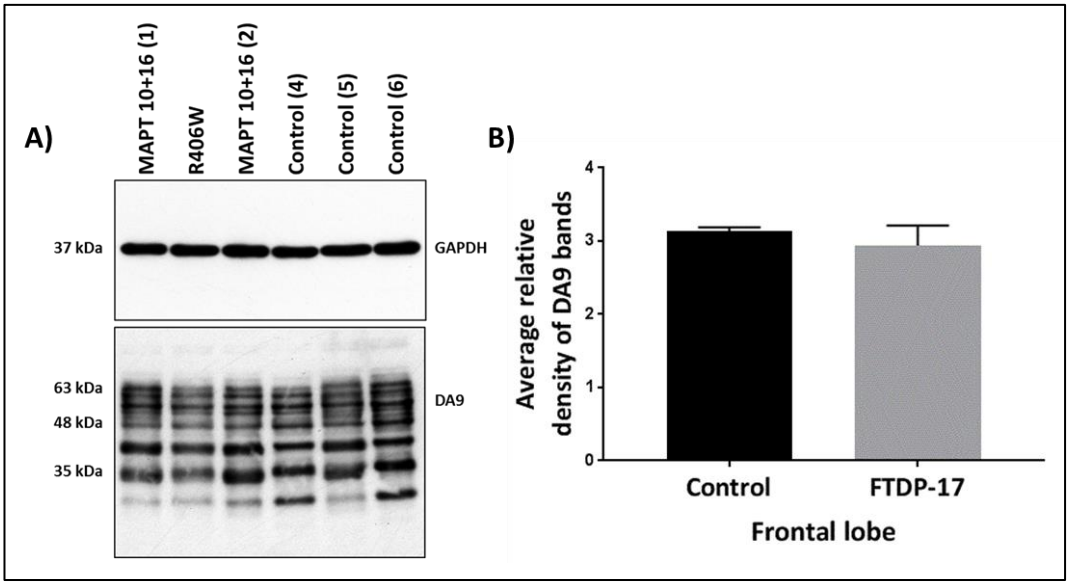

Figure 6.2 Levels of total tau in frontal brain tissue from PiD patients

Representative western blot (A) showing frontal cortex tissue from patients with FTDP-17 alongside healthy controls probed with GAPDH and DA9 (Control n=3; FTDP-17 n=3). Graph representing the density of DA9 bands normalised to GAPDH bands (B).

Data was analysed using an unpaired Student's t-test. Error bars indicate +1 S.E.M.

No change in levels of total tau were detected in the frontal cortices of patients with FTDP-17 compared to controls (p= 0.5155) (Figure 6.2).

Figure 6.3 Levels of pSer404/pSer396 tau in frontal cortex brain tissue from PiD patients

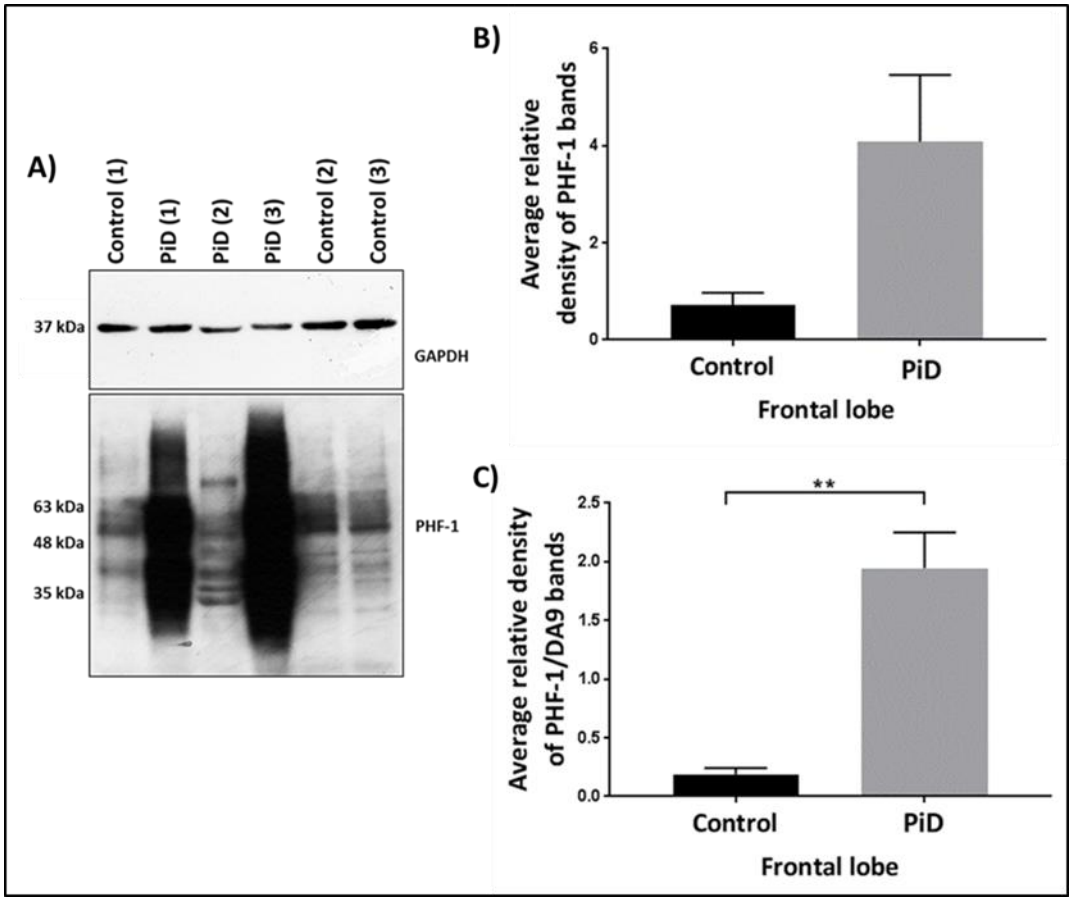

Figure 6.3 Levels of pSer396/404 tau in frontal cortex brain tissue from PiD patients

*Representative western blot (A) showing frontal cortex tissue from patients with PiD alongside healthy controls probed with GAPDH and PHF-1 (Control n=3; PiD n=3). Graphs representing the density of PHF-1 bands normalised to GAPDH bands (B) and of PHF-1 bands normalised to DA9 bands ** p= 0.0049 (C).*

Data was analysed using an unpaired Student's t-test. Error bars indicate +1 S.E.M.

In the frontal cortices of patients with PiD pSer396/404 tau levels were not significantly increased before normalisation to DA9 (p= 0.0717) but were found to be increased after normalisation to total tau (p= 0.0049), compared to controls (Figure 6.3).

Levels of pSer396/404 tau were also investigated in the frontal cortices of patients with FTDP-17 compared to controls by probing western blots with the antibody PHF-1.

Figure 6.4 Levels of pSer396/404 tau in frontal cortex tissue from FTDP-17 patients

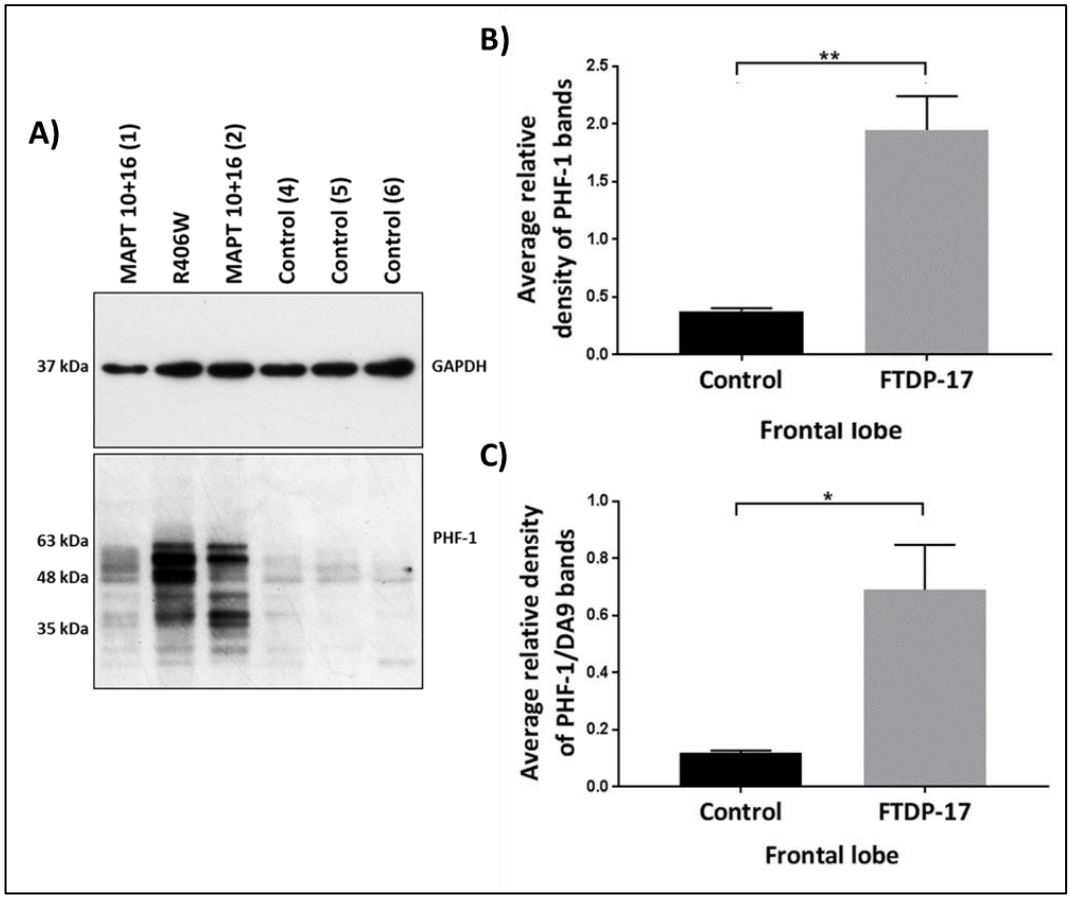

Figure 6.4 Levels of pSer396/404 tau in frontal cortex brain tissue from FTDP-17 patients

*Representative western blot (A) showing frontal cortex tissue from patients with FTDP-17 alongside healthy controls probed with GAPDH and PHF-1 (Control n=3; FTDP-17 n=3) Graphs representing the density of PHF-1 bands normalised to GAPDH bands ** p= 0.0059 (B) and of PHF-1 bands normalised to DA9 bands *p= 0.0221 (C).*

Data was analysed using an unpaired Student's t-test. Error bars indicate +1 S.E.M.

pSer396/404 tau was significantly increased in the frontal cortices of patients with FTDP-17 compared to controls both before (p= 0.0059) and after comparison to DA9 (p= 0.0221) (Figure 6.4).

To investigate the levels of pSer202 tau within the frontal and temporal cortices of patients with PiD, compared to controls, western immunoblots were probed with the antibody CP13.

Figure 6.5 Levels of pSer202 tau in frontal cortex brain tissue from PiD patients

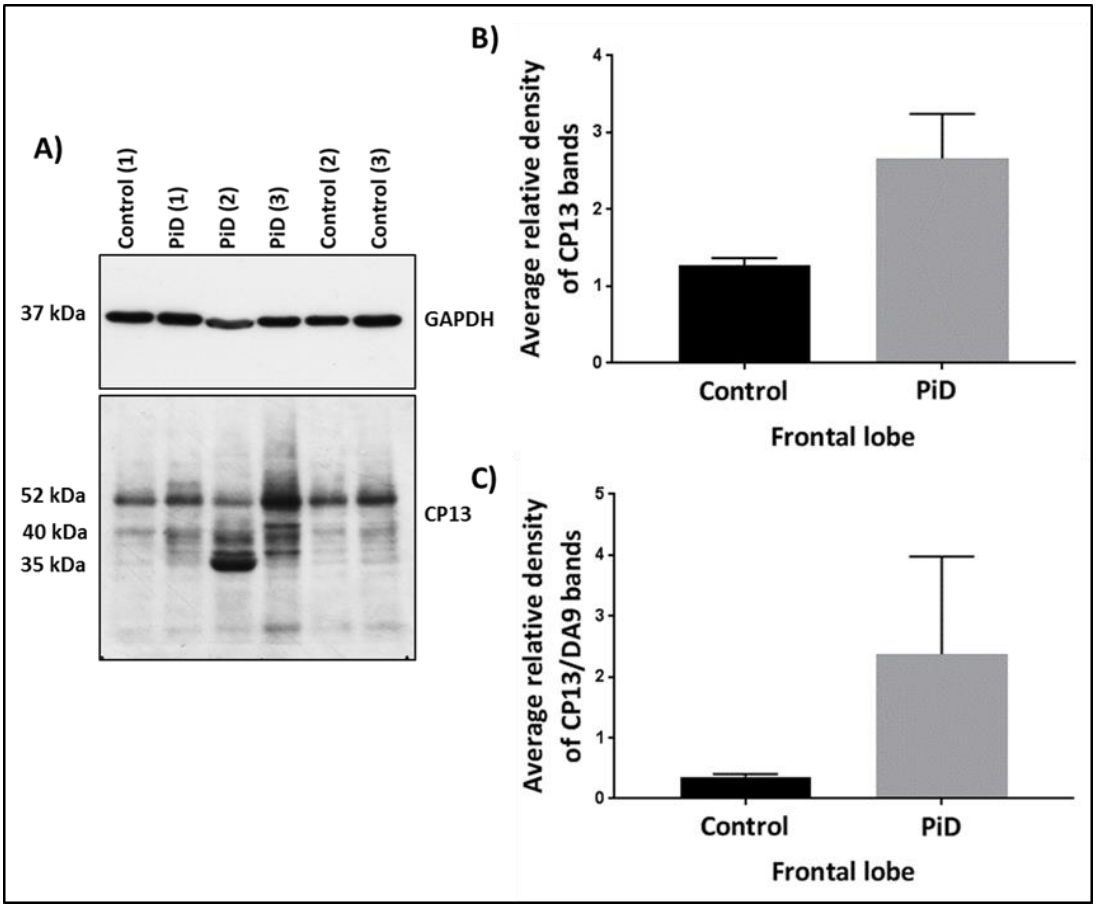

Figure 6.5 Levels of pSer202 tau in frontal cortex brain tissue from PiD patients

Representative western blot (A) showing frontal cortex tissue from patients with PiD alongside healthy controls probed with GAPDH and CP13 (Control n=3; PiD n=3). Graphs representing the density of CP13 bands normalised to GAPDH bands (B) and of CP13 bands normalised to DA9 bands (C).

Data was analysed using an unpaired Student's t-test. Error bars indicate +1 S.E.M.

No significant difference was detected in the total levels of pSer202 tau within the frontal cortices of patients with PiD compared to controls, either before (p= 0.0775) or after normalisation to DA9 (p= 0.2766) (Figure 6.5).

Similarly, no significant difference in levels of tau phosphorylated at these sites was detected in the temporal cortices of PiD patients compared to controls either before (p= 0.4680) or after (p= 0.4306) normalisation to total tau (Figure 6.6).

Figure 6.6 Levels of pSer202 tau in temporal cortex brain tissue from PiD patients

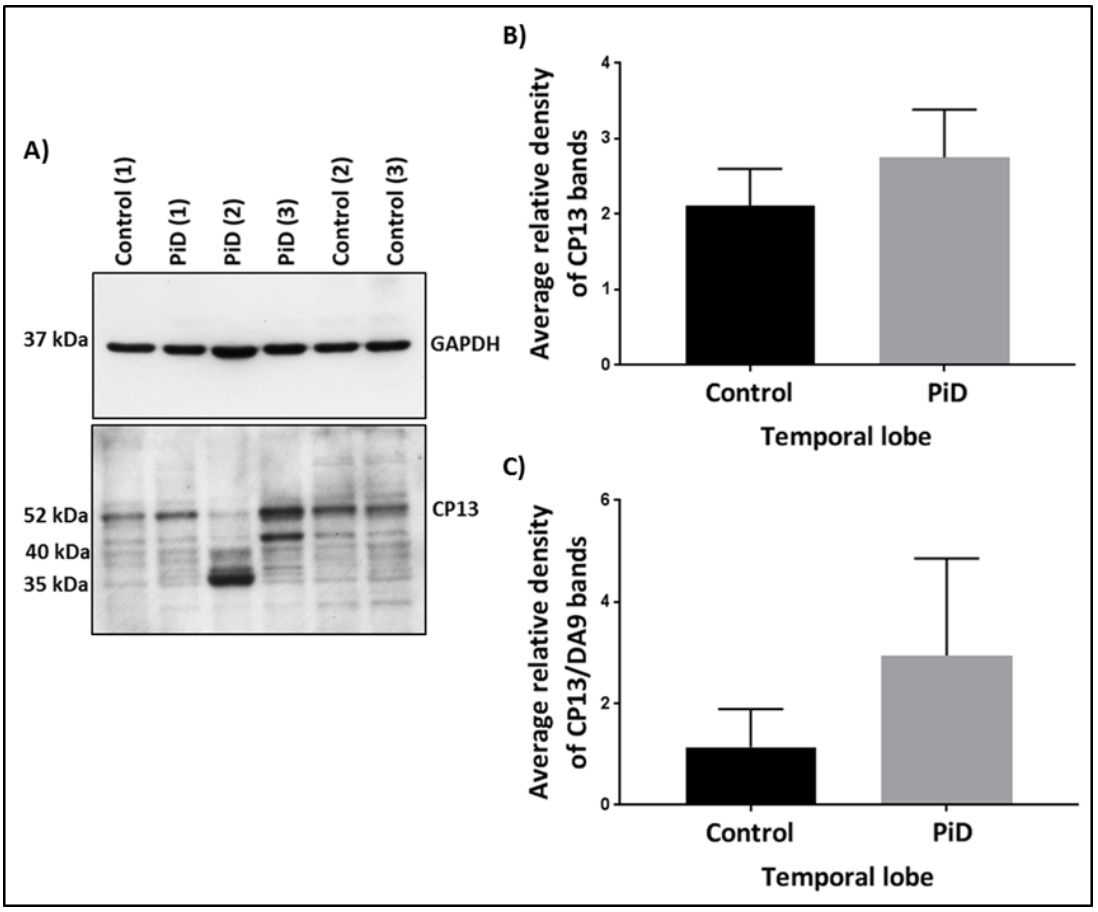

Figure 6.6 Levels of pSer202 tau in temporal cortex brain tissue from PiD patients

Representative western blot (A) showing temporal cortex tissue from patients with PiD alongside healthy controls probed with GAPDH and CP13 (Control n=3; PiD n=3). Graphs representing the density of CP13 bands normalised to GAPDH bands (B) and CP13 bands normalised to DA9 bands (C).

Data was analysed using an unpaired Student's t-test. Error bars indicate +1 S.E.M.

Within the temporal cortices of patients with PiD total levels of pSer202 tau are not significantly different compared to controls either before comparison to total tau (p= 0.9639) or after (p= 0.4896) (Figure 6.6).

The levels of pSer202 tau were also investigated within the frontal cortices of patients with FTDP-17 compared to controls by probing western blots with CP13.

Figure 6.7 Levels of pSer202 tau in frontal cortex brain tissue from FTDP-17 patients

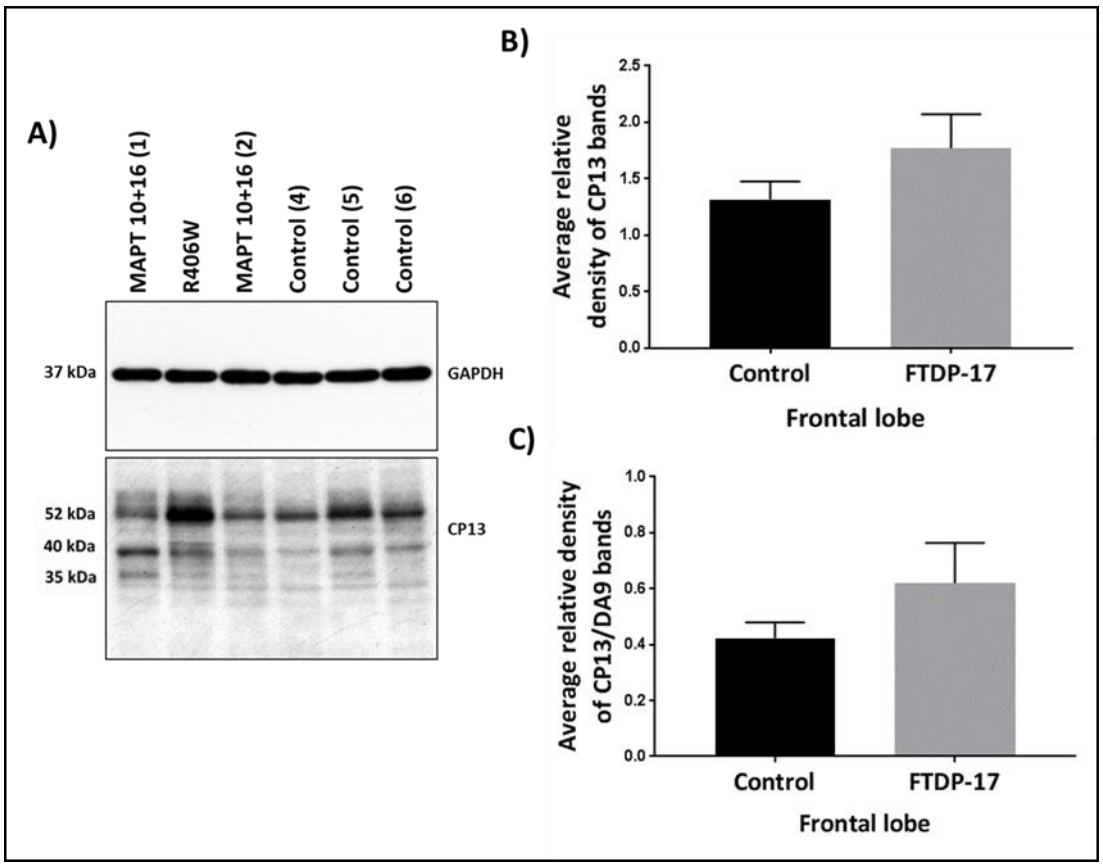

Figure 6.7 Levels of pSer202 tau in frontal cortex brain tissue from FTDP-17 patients

Representative western blot (A) showing frontal cortex tissue from patients with FTDP-17 alongside healthy controls probed with GAPDH and CP13 (Control n=3; FTDP-17 n=3). Graph representing the density of CP13 bands normalised to GAPDH bands (B) and CP13 bands normalised to DA9 bands (C).

Data was analysed using an unpaired Student's t-test. Error bars indicate +1 S.E.M.

No significant difference was detected in the levels of pSer202 in frontal cortex tissue from controls and FTDP-17 patients either before normalisation to total tau (p= 0.2591) or after (p= 0.2721) (Figure 6.7).

6.3.2 Levels of *MAPT* gene expression within the frontal and temporal cortices of patients with FTD

The levels of *MAPT* gene expression within the frontal and temporal cortices of patients with PiD and FTDP-17, compared to controls, were determined using qPCR.

6.8 Levels of *MAPT* gene expression in frontal and temporal cortex tissue from patients with PiD and FTDP-17

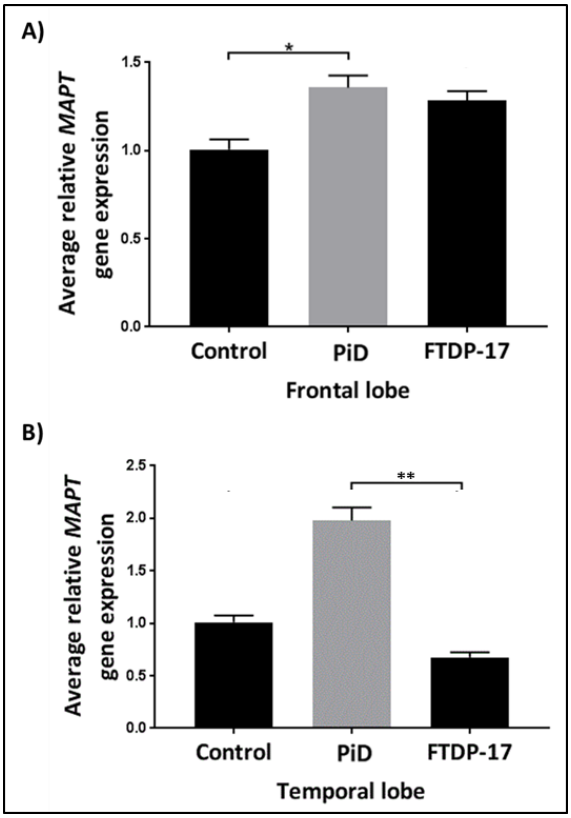

Figure 6.8 Levels of MAPT gene expression in frontal and temporal cortex tissue from patients with PiD disease and FTDP-17

*Graphs representing the average MAPT gene expression within frontal cortex tissue *p= 0.0348 (A) and within temporal cortex tissue **p= 0.0094 (B) from patients with FTDP-17 and PiD disease (Control n=6; PiD n=3; FTDP-17 n=3).*

Data was analysed using a Kruskal-Wallis test followed by a Dunn's post hoc test. Error bars indicate +1 S.E.M.

Gene expression of *MAPT* was found to be significantly greater in the frontal cortices (p= 0.0348) (Figure 6.8, A) but not the temporal cortices (p= 0.2948) (Figure 6.8, B) of patients with PiD. *MAPT* expression was not found to be significantly different in the frontal cortices (p=0.2147) (Figure 6.8, A) or temporal cortices of patients with FTDP-17 (p= 0.2948) (Figure

6.8, B) compared to controls. However, *MAPT* expression was lower within the temporal cortices of patients with FTDP-17 compared to those with PiD (p= 0.0094) (Figure 6.8, B).

6.3.3 Levels and activity of tau kinases within the frontal and temporal cortices of patients with FTD

To explore the potential roles of tau kinases in PiD and FTDP-17, the levels and activity of GSK3β, CDK5 and PAK3 were investigated within the frontal and temporal cortices of PiD patients compared to controls, as well as in the frontal cortices of patients with FTDP-17 compared to controls. The total levels of GSK3β and the levels of GSK3β phosphorylated at Tyr216, necessary for the kinase to be maximally active (Chapter 1.3.1), were investigated through probing immunoblots with antibodies specific against these proteins.

Figure 6.9 Levels of GSK3β and pTyr216 GSK3β in frontal cortex brain tissue from PiD patients

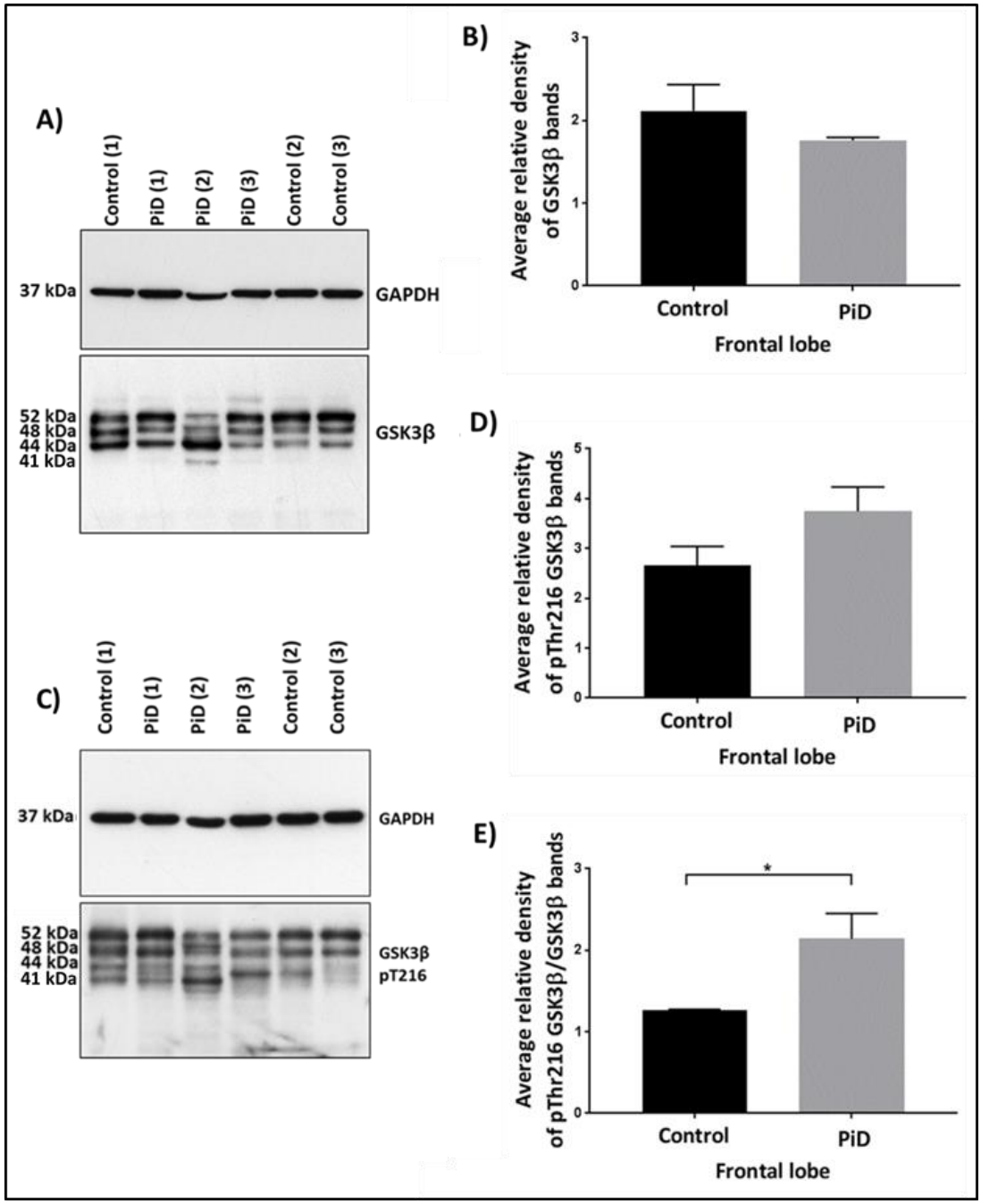

Figure 6.9 Levels of GSK3β and pTyr216 GSK3β in frontal cortex brain tissue from PiD patients

*Representative western blots showing frontal cortex tissue from patients with PiD alongside healthy controls probed with GAPDH and GSK3β (A) and GAPDH and pTyr216 GSK3β (C) (Control n=3; PiD n=3). Graphs representing the density of GSK3β bands normalised to GAPDH bands (B), of pTyr216 GSK3β normalised to GAPDH bands (D) and of pTyr216 GSK3β normalised to GSK3β bands * p= 0.0464 (E).*

Data was analysed using an unpaired Student's t-test. Error bars indicate +1 S.E.M.

No significant difference in the levels of GSK3β (p= 0.3279) or pTyr216 GSK3β (p= 0.1523) were detected in the frontal cortices of patients with PiD compared to controls. However, after normalisation of pTyr216 GSK3β levels to total GSK3β, the frontal cortices of patients with PiD were found to have increased levels of active GSK3β (p= 0.0464) (Figure 5.10). Similarly, within the temporal cortices of PiD patients there was no significant difference in GSK3β (p= 0.6749) or pTyr216 GSK3β (p= 0.9815) levels compared to controls. Furthermore, there is no significant difference in pTyr216 GSK3β levels after normalisation to total GSK3β levels (p= 0.5306) between controls and patients with PiD (Figure 6.10).

Figure 6.10 Levels of GSK3β and pTyr216 GSK3β in temporal cortex brain tissue from PiD patients

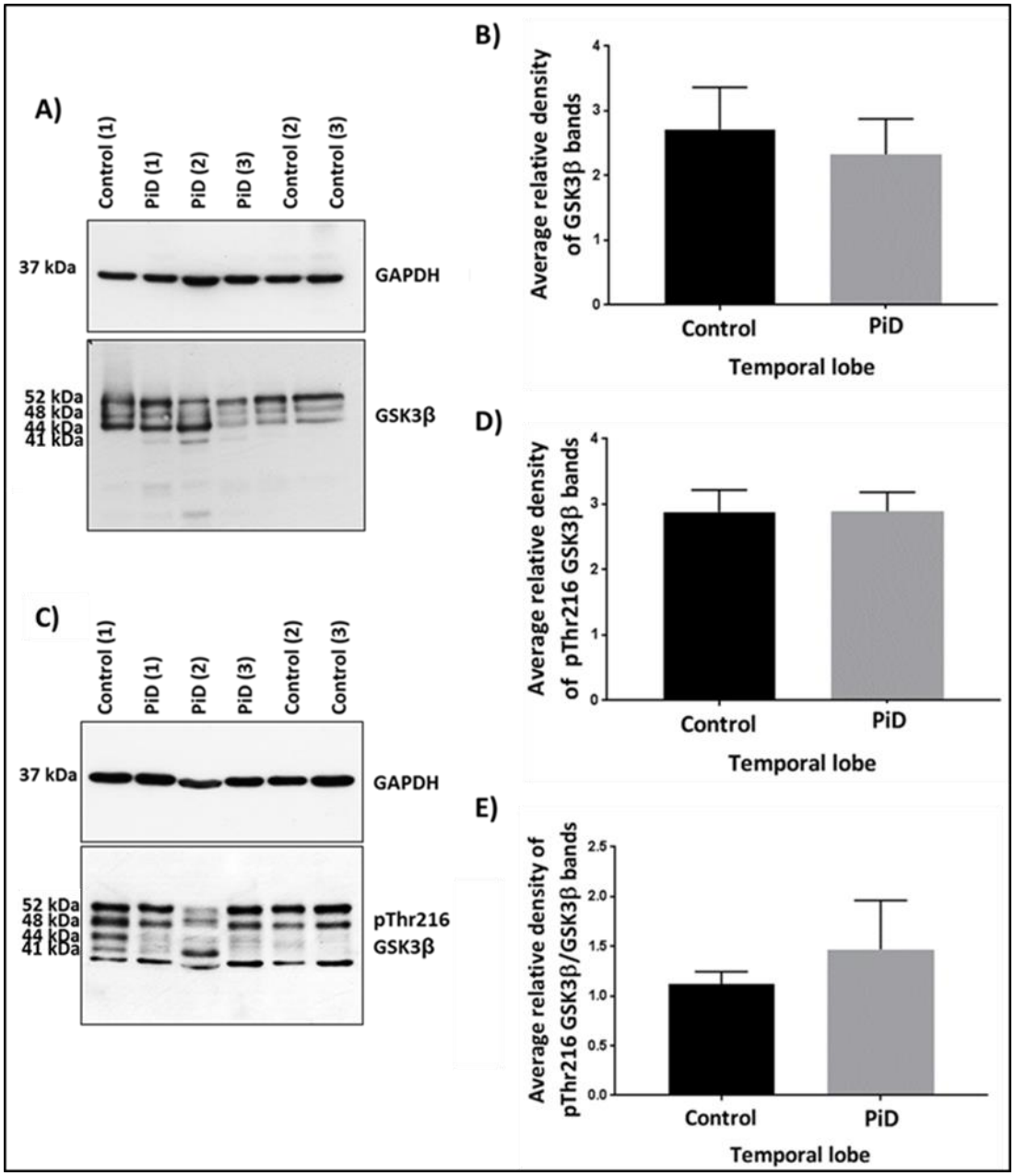

Figure 6.10 Levels of GSK3β and pTyr216 GSK3β in temporal cortex brain tissue from PiD patients

Representative western blots showing temporal cortex tissue from patients with PiD alongside healthy controls probed with GAPDH and GSK3β (A) or pTyr216 GSK3β (C) (Control n=3; PiD n=3). Graphs representing the density of GSK3β bands normalised to GAPDH bands (B), of pTyr216 GSK3β normalised to GAPDH bands (D) and of pTyr216 GSK3β normalised to GSK3β bands (E).

Data was analysed using an unpaired Student's t-test. Error bars indicate +1 S.E.M.

Figure 6.11 Levels of GSK3β in frontal cortex brain tissue from FTDP-17 patients

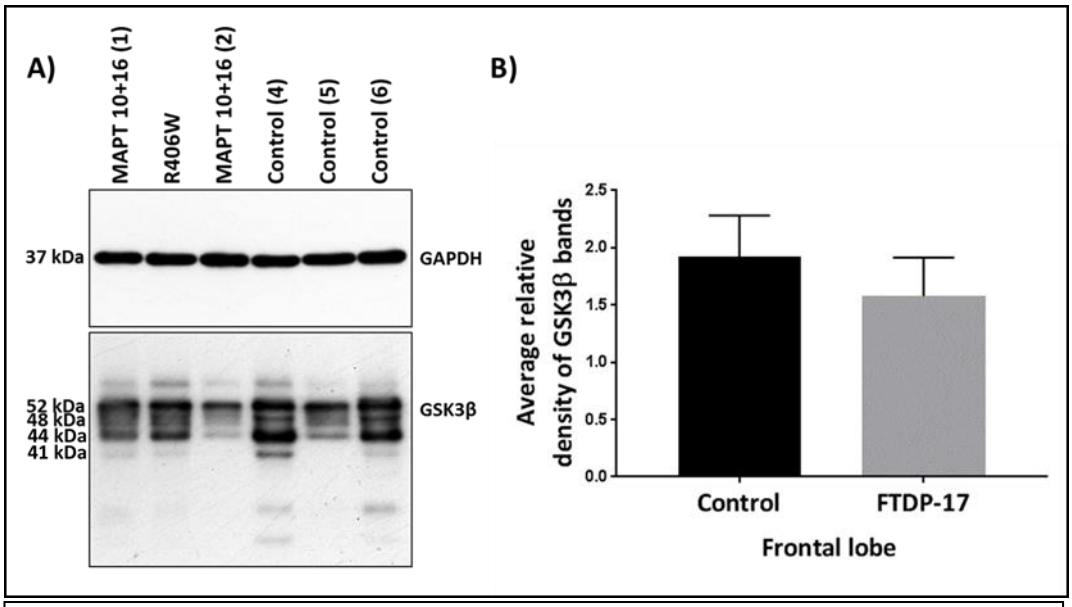

Figure 6.11 Levels of GSK3β in frontal lobe brain tissue from FTDP-17

Representative western blot (A) showing frontal cortex tissue from patients with FTDP-17 alongside healthy controls probed with GAPDH and GSK3β (Control n=3; FTDP-17; n=3). Graph representing the density of GSK3β bands normalised to GAPDH bands (B).

Data was analysed using an unpaired Student's t-test. Error bars indicate +1 S.E.M.

There was no significant difference in the levels of GSK3β in the frontal cortices of patients with FTDP-17 compared to controls (p= 0.5268) (Figure 6.11).

To investigate the activity of Cdk5 in PiD and FTDP-17, western immunoblots were probed with an antibody against p25 and p35, the activator proteins of Cdk5. Increased p25 protein levels and decreased p35 protein levels are associated with aberrant hyperactivity of Cdk5, which contributes to pathological hyperphosphorylation of tau (Chapter 1.3.2).

Figure 6.12 Levels of p25 and p35 in frontal cortex brain tissue from PiD

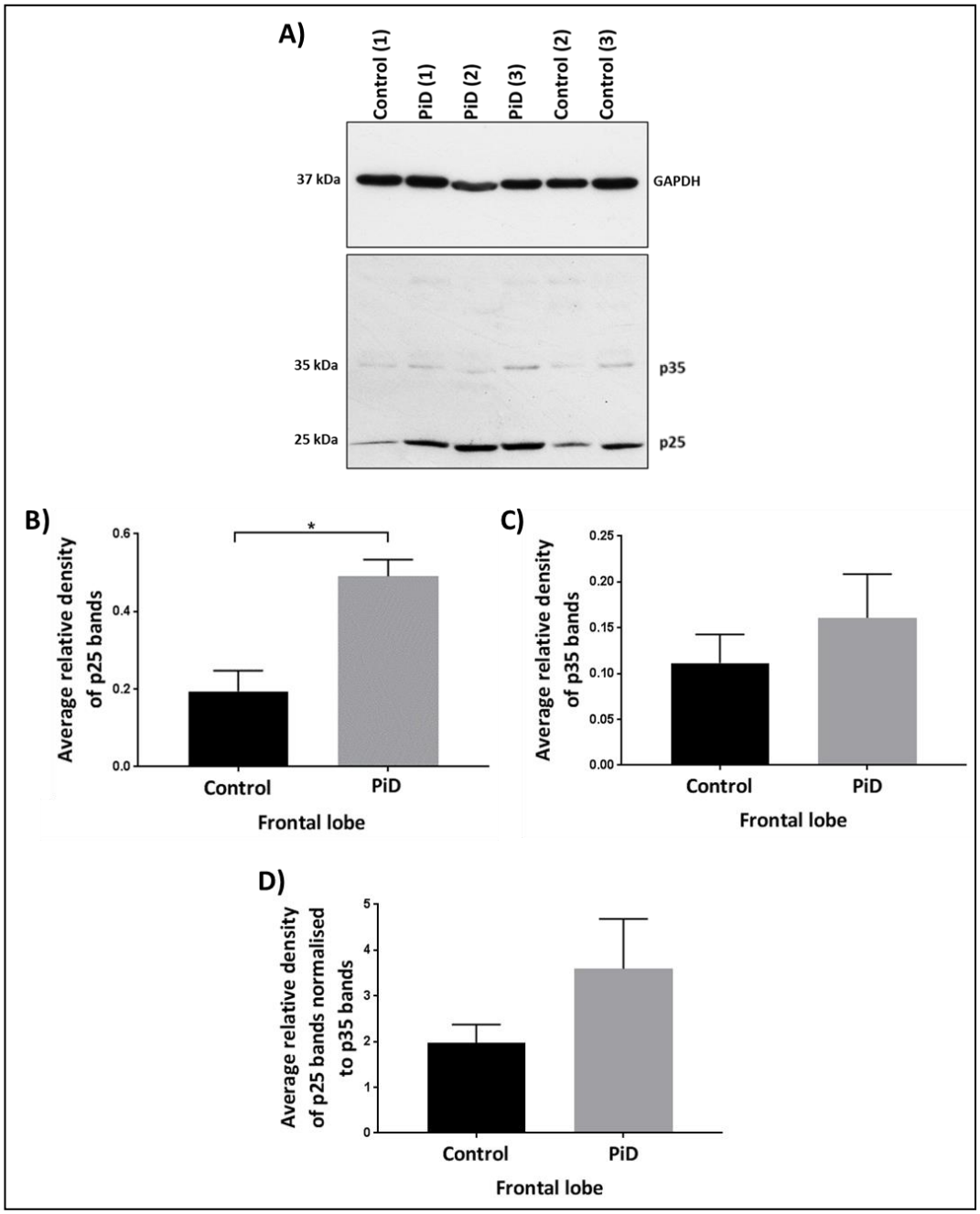

Figure 6.12 Levels of p25 and p35 in frontal cortex brain tissue from PiD

*Representative western blot (A) showing frontal cortex tissue from patients with PiD alongside healthy controls probed with GAPDH and p25/p35 (Control n=3; PiD n=3). Graph representing the density of p25 bands normalised to GAPDH bands * p= 0.0126 (B), p35 bands normalised to GAPDH bands (C) and p25 bands normalised to p35 bands.*

Data was analysed using an unpaired Student's t-test. Error bars indicate +1 S.E.M.

Levels of p25 were increased (p= 0.0126) while levels of p35 were unchanged (p= 0.4367) in the frontal cortices of PiD patients compared to controls as indicated by densitometric analysis of the p25 and p35 bands, respectively, normalised to GAPDH bands (Figure 6.12). There was no change in the ratio of p25/p35 levels within the frontal cortices of patients with PiD compared to controls, calculated by normalising p25 bands to p35 bands (Figure 6.12, D).

Figure 6.13 Levels of p25 in temporal cortex brain tissue from PiD

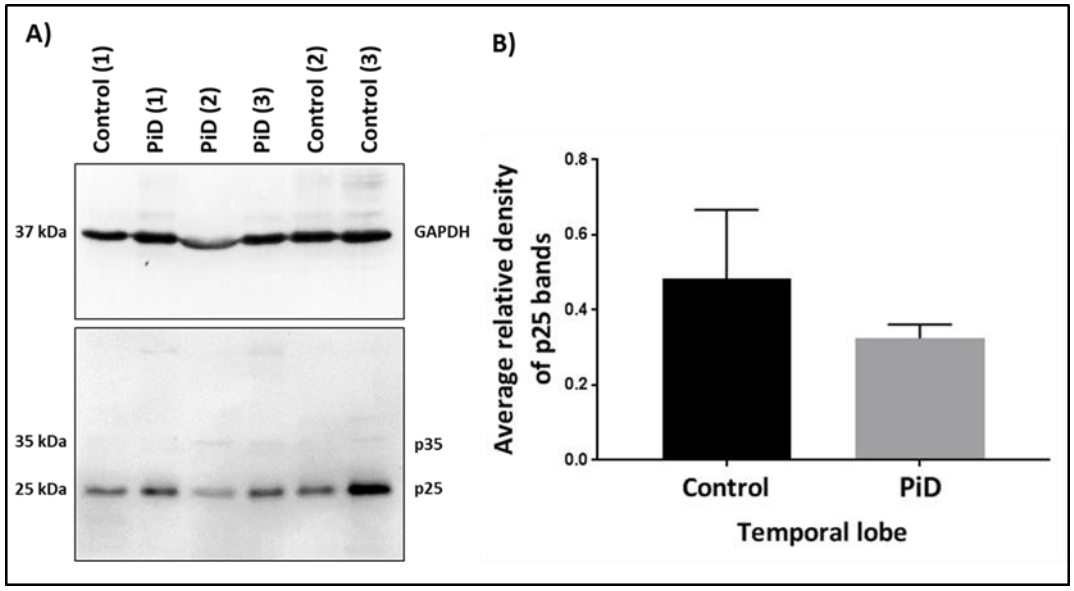

Figure 6.13 Levels of p25 in temporal cortex brain tissue from PiD

Representative western blot (A) showing frontal cortex tissue from patients with PiD alongside healthy controls probed with GAPDH and p25 (Control n=3; PiD n=3). Bar chart representing the density of p25 bands normalised to GAPDH bands (B).

Data was analysed using an unpaired Student's t-test. Error bars indicate +1 S.E.M.

Levels of p25 are not significantly different within the temporal cortices of PiD patients compared to controls (p= 0.4415) as indicated by densitometric analysis of p25 bands normalised to GAPDH bands. Levels of p35 could not be detected in these samples as the immunoreactivity was not sufficient (Figure 6.13).

Figure 6.14 Levels of PAK3 in frontal and temporal cortex brain tissue from PiD patients

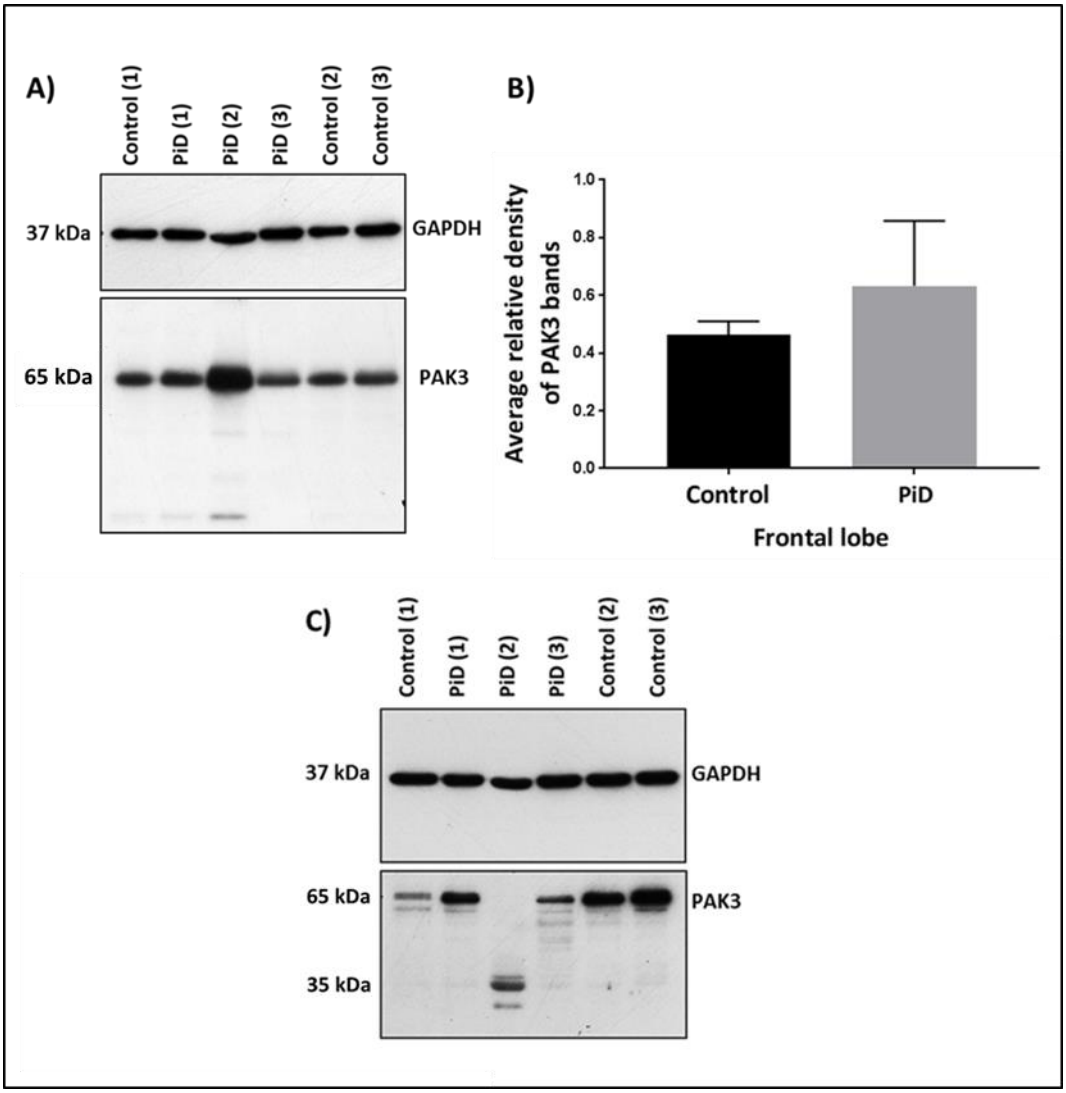

Figure 6.14 Levels of PAK3 in frontal and temporal cortex brain tissue from PiD patients

Representative western blots showing frontal cortex PiD (A) and temporal cortex (C) tissue from patients with and alongside healthy controls probed with GAPDH and PAK3 (control n=3; PiD n=3). Graph representing the density of PAK3 bands normalised to GAPDH bands for frontal cortex brain tissue (B).

Data was analysed using an unpaired Student's t-test. Error bars indicate +1 S.E.M.

PAK3 is not changed in PiD patients compared to control patients within the frontal cortices (p= 0.5016) as indicated by densitometric analysis of PAK3 bands normalised to GAPDH bands (Figure 6.14). PAK3 levels could not be compared within in the temporal cortices of patients with PiD compared to controls as the band for PAK3 expected at 65 kDa was not present and an additional band was present at 35 kDa.

Figure 6.15 Levels of PAK3 in frontal cortex brain tissue from FTDP-17 patients

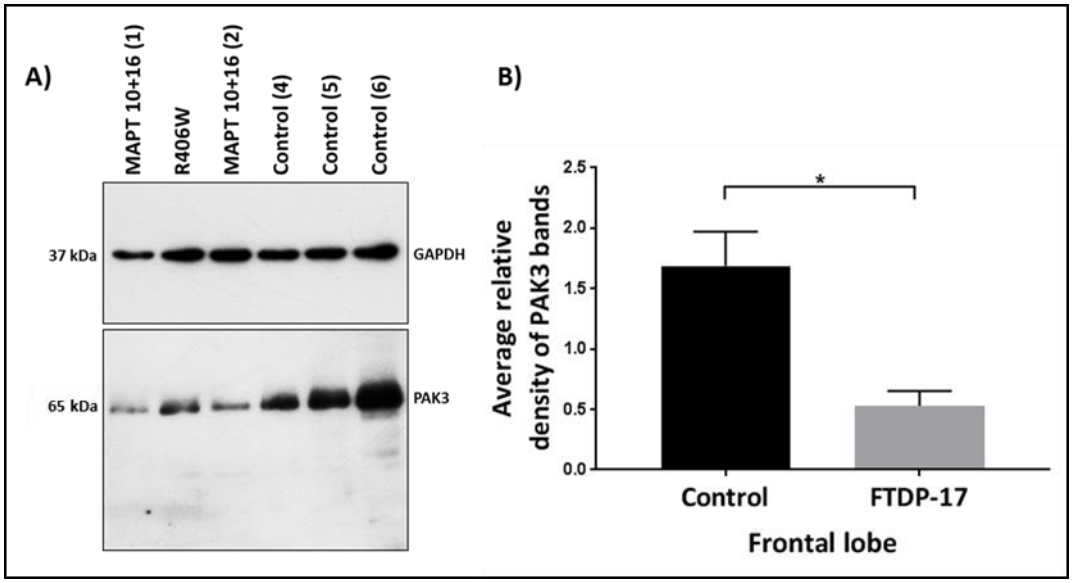

Figure 6.15 Levels of PAK3 in frontal cortex brain tissue from FTDP-17

*Representative western blot (A) showing frontal cortex tissue from patients with FTDP-17 alongside healthy controls probed with GAPDH and PAK3 (Control n=3; FTDP-17; n=3). Graph representing the density of PAK3 bands normalised to GAPDH bands * p= 0.0201.*

Data was analysed using an unpaired Student's t-test. Error bars indicate +1 S.E.M.

Densitometric analysis of PAK3 normalised to GAPDH bands demonstrate that PAK3 is decreased in the frontal cortices of patients with FTDP-17 compared to controls (p= 0.0201) (Figure 6.15).

Figure 6.16 Gene expression levels of *GSK3β, CDK5* and *PAK3* in frontal and temporal cortices of patients with PiD and FTDP-17

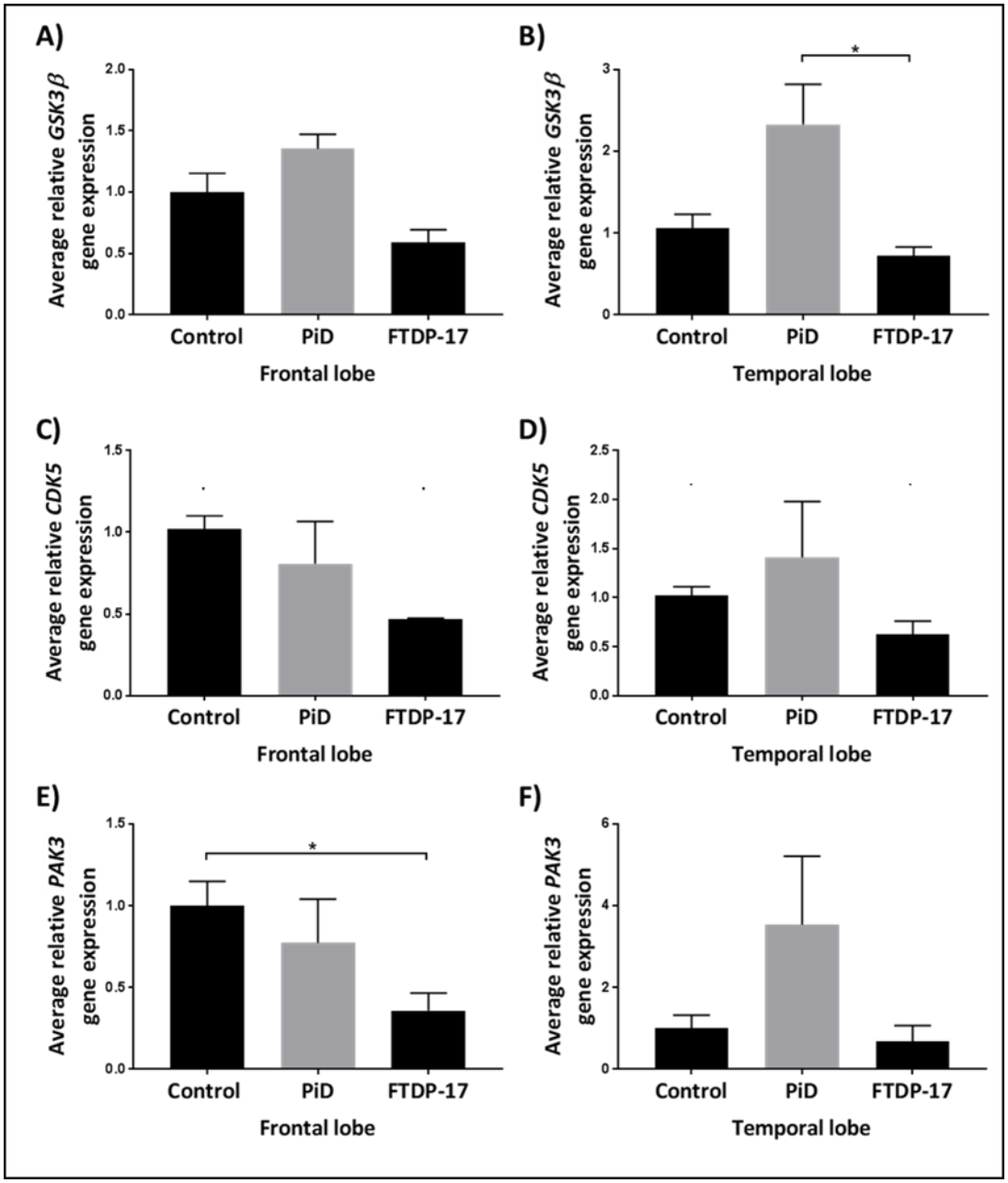

Figure 6.16 Gene expression levels of GSK3β, CDK5 and PAK3 in frontal lobe brain tissue from PiD disease and FTDP-17 patients

*Graphs representing the average GSK3β (A), CDK5 (C) and PAK3 * p= 0.0494 (E) gene expression within frontal cortices of patients with PiD and FTDP-17 (Control n=6; PiD n=3; FTDP-17 n=3). Graphs representing the average GSK3β *p= 0.0415 (B), CDK5 (D) and PAK3 (F) gene expression within temporal cortices of patients with PiD and FTDP-17 (Control n=6; PiD n=3; FTDP-17 n=3).*

Data was analysed using a Kruskal-Wallis test followed by a Dunn's post hoc test. Error bars indicate +1 S.E.M.

Gene expression of *GSK3β* was not found to be significantly different in the temporal cortices (p= 0.2795) or frontal cortices (p= 0.7430) of patients with PiD compared to controls (Figure 6.16, B and A). In the frontal (p= 0.8492) and temporal cortices (p= 0. 0.4339) of patients with FTDP-17, gene expression of *GSK3β* was not significantly different compared controls (Figure 6.16, A and B). *GSK3β* gene expression was found to be significantly lower within the temporal cortices of patients with FTDP-17 compared to PiD (p= 0.0415), however, this was not found to be true within the frontal cortices (p= 0.0580).

CDK5 expression levels were not found to be significantly different within the frontal (p= 0.1093) and temporal cortices (p= 0.4511) of FTDP-17 patients compared to controls (Figure 6.16, C and D). Similarly, levels of *CDK5* expression were not found to be significantly different within the frontal (p >0.9999) and temporal cortices (p >0.9999) of PiD patients. There is also no significant difference in *CDK5* expression within the frontal (p= 0.7726) or temporal cortices (p= 0.5227) between PiD and FTDP-17 patients.

In the frontal cortices of patients with FTDP-17 *PAK3* expression levels were found to be decreased compared to controls (p= 0.0494), although this was not found to be the case in the temporal cortices of these patients (p= 0.4511). In PiD patients, no significant difference was found within the frontal (p >0.9999) or temporal cortices (p >0.9999). There was also no significant difference in *PAK3* expression in the temporal cortices of patients with FTDP-17 compared to those with PiD (p= 0.5227), or within the frontal cortices (p= 0.1391).

6.3.4 Levels of synapsin I in within the frontal and temporal cortices of patients with FTD

Figure 6.17 Levels of synapsin I in temporal cortex brain tissue from patients with PiD

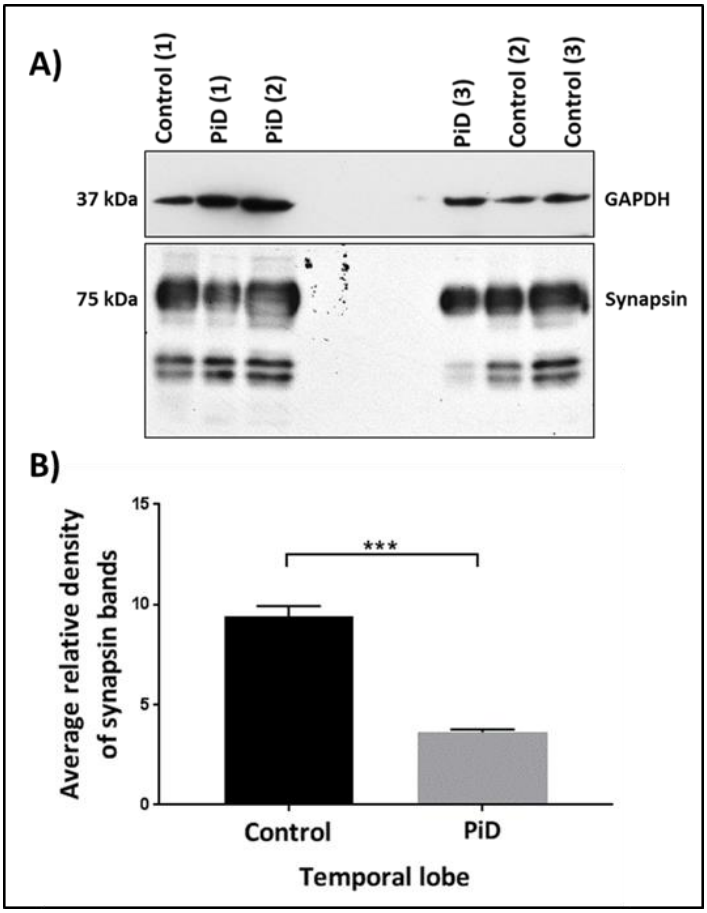

Figure 6.17 Levels of synapsin I in temporal cortex brain tissue from PiD

Representative western blot (A) showing temporal cortex tissue from patients with PiD alongside healthy controls probed with GAPDH and synapsin I (Control n=3; PiD n=3). Bar chart representing the density of synapsin I bands normalised to GAPDH bands *** p= 0.0004 (B).

Data was analysed using an unpaired Student's t-test. Error bars indicate +1 S.E.M.

Levels of synapsin I, indicated by the top two bands at approximately 75 kDa, in the temporal cortices of patients with PiD are significantly decreased compared to controls (p= 0.0004).

Figure 6.18 Levels of synapsin I in frontal cortex brain tissue from patients with FTDP-17

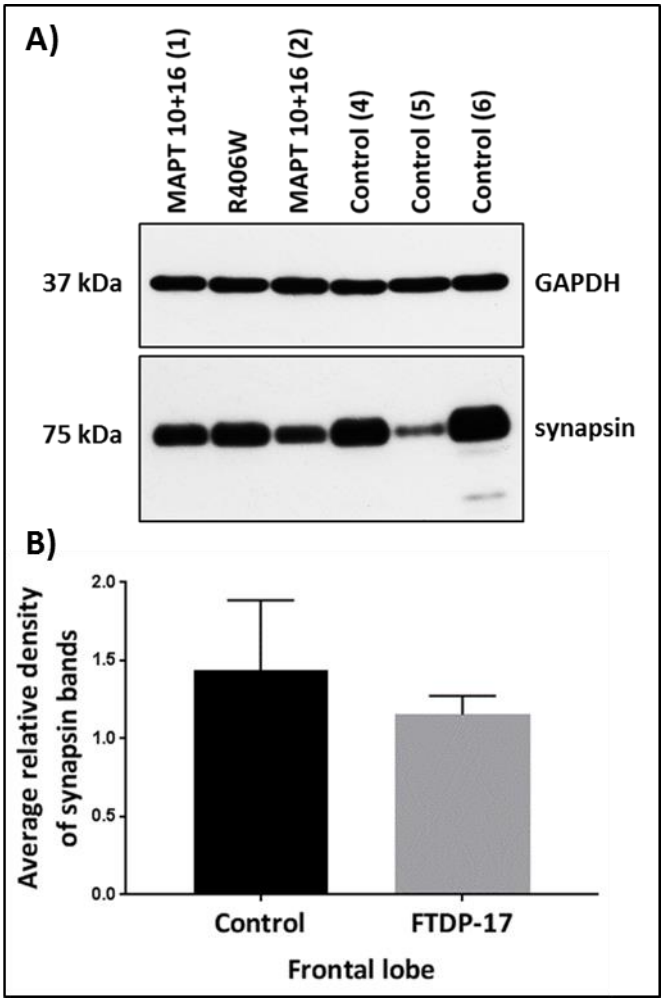

Figure 6.18 Levels of synapsin I in frontal cortex brain tissue from FTDP-17 patients

Representative western blot (A) showing frontal cortex tissue from patients with FTDP-17 alongside healthy controls probed with antibodies against GAPDH and synapsin I (Control n=3; FTDP-17 n=3). Graph representing the density of synapsin I bands normalised to GAPDH bands (B).

Data was analysed using an unpaired Student's t-test. Error bars indicate +1 S.E.M.

Levels of synapsin I in the frontal cortices of patients with FTDP-17 are unchanged compared to controls (p= 0.5790).

6.3.5 Gene expression of *MAPT*, *CDK5* and *PAK3* in basal nucleus of Meynert of patients with AD

Figure 6.19 Levels of *MAPT*, *CDK5* and *PAK3* gene expression in basal nucleus of Meynert from patients with AD

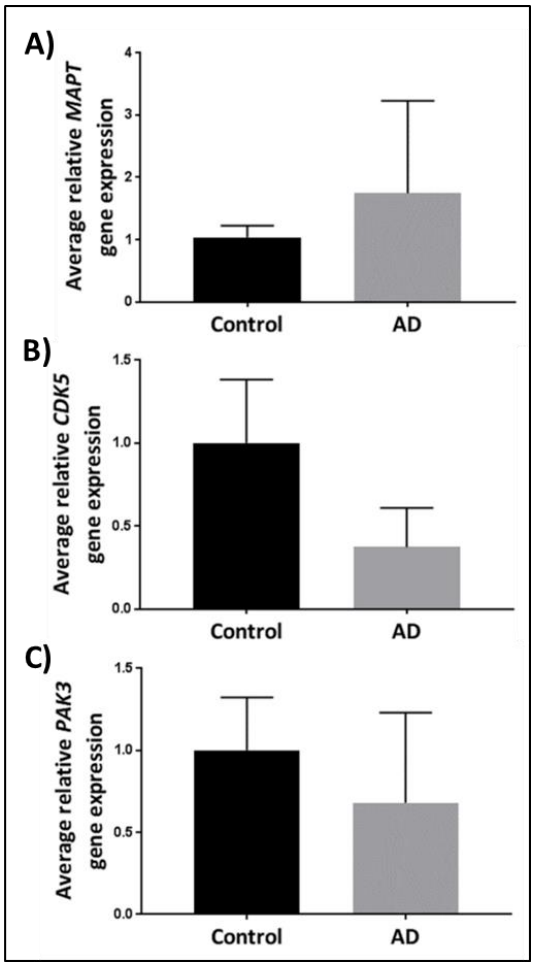

Figure 6.19 Levels of MAPT, CDK5 and PAK3 gene expression, normalised to GAPDH, in basal nucleus of Meynert (nbM) of patients with AD.

Graphs representing the average MAPT (A), CDK5 (B) and PAK3 (C) gene expression within nbM of patients with AD compared to controls (Control n=4; AD n=3).

Data was analysed using a Mann-Whitney test. Error bars indicate +1 S.E.M.

Relative gene expression levels of *MAPT* ($p < 0.9999$), *CDK5* ($p = 0.4000$) and *PAK3* ($p = 0.7000$) are unchanged within basal forebrain of AD patients compared to controls.

6.4 Discussion

6.4.1 Rational behind inclusion of sample PiD2 and sample heterogeneity

Unlike cell-based experiments, there is a great deal of heterogeneity in biological measurements in post-mortem human tissues. To establish statistically significant difference between disease and control brain tissue it is therefore necessary to use a large cohort. Tissue obtained from FTD individuals is rare and there are also multiple sub-types of FTD which may have differing pathological presentation; together this makes it difficult to determine highly significant similarities or differences from other diseases or even control brain tissue. For this study it was only possible, unfortunately, to obtain small numbers of samples. Nevertheless, the results have highlighted certain aspects which may inform the rationale for further studies. Therefore, particularly because it seems that the PiD samples are heterogenous, all samples, including apparent outliers (for instance PiD2), have been included here.

Examples of this heterogeneity are given here. For instance, in Figure 6.1, lower levels of total tau is evident not only within both frontal and temporal cortex of PiD2, compared with PiD1 and PiD3, but also in the temporal cortex for control 1, compared with the other 2 controls. Given this heterogeneity appears to be a part of the natural heterogeneity of human samples, all have been included. Additionally, in Figure 6.3, p396/404 tau levels are much higher in the frontal cortex tissue of PiD1 and PiD3 than controls and PiD2 levels, although PiD2 levels are still increased in comparison to controls. Considerable variation was also seen in p396/404 tau levels between samples *MAPT* 10+16 (1) and *MAPT* 10+16 (2) (Figure 6.4) indicating the variability of tau phosphorylated at this site even between different patients with the same tauopathy. Interestingly, western blots indicating pSer202 tau banding patterns, particularly those at approximately 35kDa and 52kda, that varied considerably for PiD 2 within the frontal (Figure 6.4) and temporal cortex (Figure 6.5), compared to both controls and PiD 1 and PiD 3 samples. In Figure 6.7, pSer202 levels in *MAPT* 10+16 (1) and *MAPT* 10+16 (2) vary especially in the bands at 52 kDa and 40 kDa.

Interestingly, western blots probed with CP13, indicating pSer202 tau, demonstrated banding patterns that varied considerably for PiD 2 within the frontal and temporal cortex compared to both controls and PiD 1 and PiD 3 samples. Specifically, a band at approximately 35kDa has much greater density compared to the other samples, whereas the band at

approximately 52kda is much less dense. Additionally, the 40 kDa band revealed by probing with CP13 in *MAPT* 10+16 (1) is denser than the band at 52 kDa, whereas in *MAPT* 10+16 (2) the band at 52 kDa is denser than the one at 40 kDa (Figure 6.7).

Additionally, in western blots probed with both antibodies against GSK3β and pTyr216 GSK3β, PiD2 samples of both frontal and temporal lobes, show a different banding pattern compared to the other PiD samples. In particular, 48 and 52kda pTyr216 GSK3β bands are much fainter, whereas the 41 kDa band is much darker. Further to these results, heterogeneity in banding patterns has also been described by others, in samples taken from different patients with tauopathy (Espinosa et al., 2008)

Western blots probed with anti-PAK3 of controls and PiD patient temporal cortex tissue revealed that the expected band for PAK3 at 65 KDa was missing for PiD2 and an additional major band at 35 kDa was present. Unfortunately, it was only possible to obtain three samples from PiD patients, therefore statistical analysis could not be carried out on the results gained from probing western blots from the temporal lobes using PAK3 antibody. For this reason, quantification and statistical analysis of this result has been omitted. The reason for this unexpected result remains unclear, however, may be attributed to the heterogeneity of the disease. One possible explanation is that PAK3 may have been cleaved within the temporal cortex of PiD2. Caspase 3 is known to be able to cleave another isoform of PAK, hPAK65, at a single site, between the N-terminal regulatory p21-binding domain and the C-terminal kinase domain, to produce a smaller protein of approximately 35 kDa (Lee et al., 1997). Although PAK1 is known to unaffected by caspase 3 cleavage (Lee et al., 1997), it is possible that PAK3 may be cleaved by caspase 3, which is known to have increased activity and to play multiple roles in neurodegenerative disease (Zhang, 2013).

6.4.2 Protein and gene expression levels of tau within the frontal and temporal cortices of patients with PiD and FTDP-17

Western immunoblots of lysates from the frontal and temporal cortices of controls, patients with PiD and patients with FTDP-17, probed using an antibody against total tau, revealed six bands at approximately 48-68 kDa, indicating the presence of the six adult isoforms of tau protein in these patients, as well as lower molecular weight bands indicating products of tau degradation (Adamec *et al.,* 2001; Goedert *et al.,* 1989). In the frontal and temporal cortices of patients with PiD, and the frontal cortices of patients with FTDP-17, total levels of soluble tau are not significantly different compared to controls. These results are in line with

previously reported levels of soluble tau within the frontal cortex tissue of patients with PiD and FTLD associated with tau pathology compared to those within controls (van Eersel *et al.,* 2009; Adamec *et al.,* 2001).

MAPT expression levels were found to be higher in the frontal cortices of patients with PiD but not FTDP-17, or within the temporal cortices of patients with either disease. Previously, *MAPT* expression in patients with FTLD associated with tau pathology has been previously shown to be similar to controls, therefore the higher levels of expression within the frontal cortices of PiD patients were unexpected. Although the levels of *MAPT* expression have not been evaluated in the brains of patients with the mutations carried by these FTDP-17 patients, previous studies in hiPSC-neurons derived from patients with FTDP-17 (Ehrlich *et al.,* 2015) and Tg drosophila models of FTDP-17 (Haddadi *et al.,* 2016) have reported similar levels of *MAPT* mRNA. Furthermore, *MAPT* expression levels have been demonstrated to largely correlate with tau protein levels within the brain (Trabzuni *et al.,* 2012) whereas here soluble protein levels of tau do not reflect *MAPT* expression. The higher levels of expression within the frontal cortices of patients with PiD may be explained by the fact that here only soluble levels of tau were measured, and additional tau may have been aggregated and so insoluble. Further investigation into the insoluble levels of tau may provide insight into this.

MAPT expression levels and the expression of different isoforms of tau have been demonstrated to be brain region specific (McMillen *et al.,* 2008; Majounie *et al.,* 2013; Trabzuni *et al.,* 2012), suggesting distinctions in the regulation of *MAPT* expression between brain areas. Therefore, in these PiD patients, the higher levels of *MAPT* expression in the frontal cortices, in contradiction to the similar levels of expression compared to controls found in the temporal cortices, could be explained by the different effects of the *MAPT* mutations on the pathways that regulate *MAPT* expression within these areas.

6.4.3 Levels of phosphorylated tau in the frontal and temporal cortices of patients with PiD and FTDP-17

In this study, pSer396/404 tau levels were found to be increased within the frontal cortices of patients with PiD and FTDP-17, compared to controls, after normalisation to total tau. This was expected as increased phosphorylation at this site has previously been reported in PiD cases in which Pick bodies positively stain with anti-pSer396/404 tau antibodies (van Eersel *et al*., 2009; Zhukareva *et al*., 2002; Love *et al*., 1988; Ishizawa *et al*., 2000; Sparks *et al*.,

1994). Furthermore, in cortical tissue of patients with IVS 10+16 *MAPT* and other FTDP-17 mutations, tau is phosphorylated at Ser396/404 (Irwin *et al.,* 2013). While phosphorylation of R406W *MAPT* tau at Ser396/404 has been reported to be decreased into Chinese hamster ovary cells compared to controls, in Tg R406W *MAPT* mice, pSer396/404 tau is increased (Ikeda *et al.,* 2005).

No difference was found in the phosphorylation of tau at pSer202 in PiD and FTDP-17 frontal and temporal cortices in comparison to controls. Interestingly, levels of tau phosphorylated at this site have been shown by others to be increased within the brains of patients with PiD (Zhukareva *et al.,* 2002; Espinoza *et al.,* 2008; Koga *et al.,* 2017; van Eersel *et al.,* 2009; Nölle *et al.,* 2013) and also FTDP-17 patients carrying G272V *MAPT* (Nölle *et al.,* 2013). Sections of the midbrains of patients carrying V337M *MAPT* also immunostain more intensely with an antibody against pSer202/Thr205 tau, indicating increased levels (Ehrlich *et al*., 2015). Furthermore, increased tau phosphorylation at Ser202 has been reported in Tg R406W *MAPT* mice (Ikeda *et al.,* 2005), as well as Tg P301L *MAPT* mice (de Calignon *et al.,* 2012).

Shiarli and colleagues demonstrated, via immunohistochemistry using AT8, an antibody that recognises tau phosphorylated at pSer202 as well as Thr205, that the levels of tau phosphorylated at pSer202 are approximately 90 % lower in frontal cortex tissue of PiD and FTDP-17 patients, including those with R406W and IVS 10+16 *MAPT* mutations, compared to those in AD patients (Shiarli *et al*., 2006). Furthermore, this publication mentions the significant decrease in western blot immunoreactivity using AT8 observed via western immunoblotting in FTDP-17 and PiD patients compared to AD patients (Hasegawa, unpublished data). As FTDP-17 and PiD are heterogenous diseases and variation in the phosphorylation of tau at these sites has been demonstrated between patients (Shiarli *et al.,* 2006), tissue from a larger cohort of patients may be required to gain statistically significant results to confirm changes in the levels of pSer202 tau.

Phosphorylation of tau at Thr231 could not be detected in the temporal and frontal cortices of controls or patients with either PiD of FTDP-17 using RZ3 antibody. Tau phosphorylated at Thr231 is associated with AD as brain lysates from healthy human controls do not react with this antibody via western blotting (Acker *et al.,* 2013). Previously, pThr231 tau has been demonstrated to be significantly decreased in the frontal cortices of patients with PiD and FTDP-17, including those with mutations in R406W and IVS 10+16, compared to patients with

AD (Shiarli *et al.,* 2014). These studies, along with the results in this study, suggest that hyperphosphorylation of this site may be specific to AD and not present in all tauopathies.

6.4.4 Protein levels and expression of tau kinases in the frontal and temporal cortices of patients with PiD and FTDP-17

Within the frontal and temporal cortices of patients with PiD as well as the frontal cortices of patients with FTDP-17, there was no significant difference in the levels of total GSK3β protein. GSK3β levels have not been investigated in PiD or FTDP-17, although no change has been seen in the brains of patients with AD (Leroy *et al.,* 2007). GSK3β enzyme activity was not measured here, however, an indication of this can be seen by the levels of pTyr216 GSK3β present. In that respect, GSK3β activity within the temporal cortices of patients with PiD was comparable to that within controls. Within the frontal cortices of PiD patients, however, pTyr216 GSK3β was found to be increased. Previous studies have reported an increase in GSK3β activity within the brains with those with tauopathy. Leroy and colleagues demonstrated an increase in pTyr216 GSK3β via western immunoblotting, in the frontal cortices of AD patients compared to controls (Leroy *et al.,* 2007). Another group demonstrated decreased inhibition of GSK3β, determined by increased phosphorylation of GSK3β at its inhibitory site Ser9 (Chapter 1.3.1), in the temporal cortices of AD patients (DaRocha-Souto *et al.,* 2012). The differences in activation of GSK3β within the frontal and temporal cortices of PiD patients could be due to differences in the regulation of GSK3β, of which little is known, in various brain areas, which has previously been demonstrated in mice overexpressing GSK3β (Fuster-Matanzo *et al*, 2011).

GSK3β gene expression was not found to be significantly different in the frontal cortices or temporal cortices of patients with both PiD and FTDP-17 compared to controls. These results reflect the similar protein levels of total GSK3β in the frontal and temporal cortices of PiD patients, as well as the frontal cortices of FTDP-17 patients, compared to controls. Additionally, these results are in line with previous studies, which overall suggest that, after development, GSK3β is rarely regulated through increased or decreased expression (Beural *et al.,* 2015).

Contrary to the results within this study, upregulation of GSK3β has previously been demonstrated within the temporal and frontal cortices of patients with ALS, a tauopathy related to PiD (Luna-Morenz *et al.,* 2007), although not within the cerebellum or

hippocampus (Yang *et al.,* 2008). Another study also described altered expression of *GSK3β* within the medial temporal gyrus and the hippocampus of AD patients, although difference in gene expression was found within the superior frontal gyrus or visual cortex (Liang *et al.,* 2008).

While there was no significant difference in the levels of p25 within the temporal cortices of PiD patients, p25 levels were found to be increased in the frontal cortices in comparison to controls. This indicates increased activity of Cdk5 within the frontal cortices but not the temporal cortices of these patients. In the frontal cortices, levels of p35 were found to be unchanged compared to controls. Immunoreactivity indicating p35 was very faint and, unfortunately, levels within the temporal cortices could not be detected. This is in line with previous reports demonstrating the rapid cleavage of p35 within a short post-mortem delay (PMD) in human AD and control brains (Taniguchi *et al.,* 2001; Patrick *et al.,* 2001), which would explain the low levels of p35 protein.

The increase of p25 within the frontal cortices of PiD patients is in disagreement with a previous study reporting no difference in the protein levels of p25 or p35 within this area in PiD and FTD patients in comparison to controls (Tandon *et al.,* 2003). It should be mentioned, however, that reports of these protein levels in AD patients vary; two publications mention the increase of p25 in AD brains (Tseng *et al.,* 2002; Patrick *et al.,* 1999), whilst others were unable to reproduce this (Tandon *et al.,* 2003; Taniguchi *et al.,* 2001). The variation in Cdk5 activity in the frontal and temporal cortices of PiD patients compared to controls may be indicative of different pathological mechanisms in these two parts of the brain and could provide an important clue to help us to understand why certain brain regions are more susceptible to different neurodegenerative disease pathways.

No significant difference in the gene expression levels of *CDK5* within the frontal and temporal cortices of patients with PiD or FTDP-17 compared to controls was found. Decreased *CDK5* expression has not been reported in FTD before, however, it has been reported in brain regions susceptible to neurodegeneration in AD patients (Liang *et al.,* 2008, Liang *et al.,* 2010).

Levels of PAK3 protein are unchanged within the frontal cortices of patients with PiD. However, they are decreased within the frontal cortices of patients with FTDP-17. Decreased levels of PAK3 are associated with neurodegeneration and the loss of synapses (Chapter

1.3.3). Although levels of PAK3 protein have not been investigated in PiD or FTDP-17 patient brains, in AD levels of PAK3 have been reported to be decreased (Nguyen *et al.,* 2008; Zhao *et al.,* 2006). These results indicate that decreased PAK3 levels are not common to all tauopathies, at least in the frontal or temporal cortices, and that there are regional protein level differences in the brains of patients with FTDP-17.

Expression levels of *PAK3* were also found to be decreased in the frontal cortices of FTDP-17 patients compared to controls, however, were not significantly changed in the temporal cortices of these patients or within either cortex in PiD patients. Although levels of *PAK3* gene expression have not been investigated within the frontal or temporal cortices of patients with PiD, decreased gene expression has been reported in hiPSC-dopaminergic neurons derived from patients with V337M *MAPT* and N279K *MAPT* (Ehrlich *et al.,* 2015). Contrarily, within the midbrains of FTDP-17 patients carrying either N279K *MAPT* or P301L *MAPT, PAK3* levels were found to be unchanged in comparison to controls. Taken together, these results may indicate region specific alterations in *PAK3* gene expression in FTDP-17, which is in line with region specific changes in other tau kinases in AD (Liang *et al.,* 2008; Liang *et al.,* 2010). For example, *CDK5* expression is known to vary between different brain regions in normal physiological function (Wu *et al.,* 2000), AD patients (Liang *et al.,* 2008; Liang *et al.,* 2010) and in opiate users with AD-like brain changes (Anthony *et al.,* 2010).

6.4.5 Levels of synapsin I within PiD temporal cortex and FTDP-17 frontal cortex

Levels of synapsin I in the temporal cortices of patients with PiD were significantly decreased compared to controls, which implicates the loss of pre-synaptic proteins in PiD. This finding was expected, as the loss of synaptic proteins and synaptic dysfunction is a well recorded co-occurrence with tauopathy. Decreased levels of synapsin have been found in PiD patients' temporal cortices (Clare *et al*, 2010), frontal cortices (Ferrer, 1999) and hippocampi (Lippa, 2004). Furthermore, decreased pre-synaptic density was reported in the frontal cortices of patients with FTD (Brun *et al.,* 1995; Ferrer, 1999), although this group later reported no such change in the temporal cortices of these patients (Liu and Brun, 1996).

Unexpectedly, the level of synapsin I in the frontal cortices of patients with FTDP-17 was not significantly different compared to controls, suggesting no loss in pre-synaptic proteins. Synapses have been demonstrated to be lost in the frontal cortices of FTDP-17 patients (Brun

et al., 1995; Clare *et al.,* 2010; Liu and Brun, 1996; Mackenzie *et al.,* 2009). Counts and colleagues have provided evidence of varying levels of pre- and post-synaptic proteins across different brain regions of patients with AD and mild cognitive impairment MCI, compared to controls. The group demonstrated that while synaptophysin levels were reduced by 35 % in the temporal cortex but not the frontal cortex, drebrin levels were reduced in the temporal cortex but increased in the frontal cortex in patients with MCI (Counts *et al.,* 2006). This study, carried out by Counts and colleagues, suggests a disparity in the frontal and temporal cortices in terms of the loss of synaptic proteins and may explain why temporal cortical functions, such as memory and language, are lost early in AD, while frontal cortical functions such as executive function, are preserved in the early stages of disease. As the temporal cortices are primarily subject to neurodegeneration in patients with FTDP-17 caused by R406W and IVS 10+16, synaptic loss in the frontal cortices may be relatively spared. It is noted that these results contain an outlier in that control 5 (lane 5; Figure 6.18) (Table 1) has very low band density compared to the other two controls. Further research with a greater cohort of patients is required to confirm this result, which does not align with previous research. Unfortunately, due to a lack of tissue it was not possible to carry out western blots for frontal cortex PiD patients and controls, or for temporal cortex FTDP-17 patients.

6.4.6 Gene expression of *MAPT*, *CDK5* and *PAK3* within the nbM of patients with AD compared to controls

No change in the gene expression of *MAPT* was detected in AD patient nbM compared to controls. Previous reports on *MAPT* expression in AD are controversial as some studies report lower levels of *MAPT* expression (Fukasawa *et al.,* 2017), while others report no change in *MAPT* expression levels in AD brains (Farnsworth *et al.,* 2016; Fukasawa *et al.,* 2017). *MAPT* mRNA has previously been found to be decreased within the entorhinal cortex, hippocampus, middle temporal gyrus and posterior cingulate cortex of AD patients (Liang *et al.,* 2008).

Although gene expression of *CDK5* in the AD nbM was 40 % of that of controls, this result was not statistically significant. *CDK5* expression has been demonstrated to be decreased within the brains of AD patients (Liang *et al.,* 2008, Liang *et al.,* 2010; Fukasawa *et al.,* 2017), although this is debated (Tandon *et al.,* 2003; Borghi *et al.,* 2002). It should be noted however, that cohort sizes in the studies performed by Liang and colleagues were much greater than those performed by Tandon and colleagues (n=3 for both AD patients and

controls) and within the study published by Borghi and colleagues. The lack of statistically significant change in *PAK3* expression levels between AD patients and controls was also surprising, as PAK3 levels within the hippocampus have been demonstrated to be decreased with AD brains, animal models and cell-based models (Zhao *et al.,* 2006; Nguyen *et al.,* 2008). These results may be explained by variation between patients within the small cohort of patients examined in this study. Indeed, *CDK5* expression has previously been demonstrated to vary considerably between patients with AD (Tandon *et al.,* 2003). It may be necessary for increased numbers of patients to be included in studies investigating the expression of kinases which are known to be variable between patients to achieve a statistically significant result.

6.5 Chapter Summary

The results demonstrate that PiD and FTDP-17 share similarities in tau-related molecular pathology. Levels of total soluble tau protein were found to be unchanged in the frontal and temporal cortices of PiD patients, as well as within the frontal cortices of patients with FTDP-17, compared to controls. Additionally, *MAPT* gene expression levels were increased in the frontal cortex in both PiD and FTDP-17 patients compared to controls. Compared to controls, phosphorylation of tau at Ser396/404 was significantly increased, while phosphorylation at Ser202 was not significantly different, in both diseases. In both PiD frontal and temporal cortices, as well as FTDP-17 frontal cortices, total GSK3β protein levels and *GSK3β* expression were not significantly different to controls.

On the contrary, there are differences in tau-related molecular pathology between the two disease groups. In the frontal cortices, *PAK3* expression and protein levels were found to be significantly decreased in FTDP-17 patients but not in PiD patients. Significantly decreased levels of synapsin I were found in patients with PiD but not within patients with FTDP-17. These differences in kinase expression, kinase level and synapsin I may provide insight into the pathogenesis of both sporadic and familial FTD.

Brain region specific differences in protein levels and gene expression were also found in each disease and these differences were found to be unique to each form of FTD. PiD patients, *MAPT* expression levels and GSK3β activity levels were increased only within the frontal cortices, while *PAK3* expression levels were found to be decreased only in the frontal

cortices of FTDP-17 patients. These specific differences in *MAPT* expression, as well as *PAK3* expression and GSK3β activity levels may facilitate understanding into the area of pathogenesis initiation in the brains of these patients.

The limitations of using human brain tissue in research have been outlined in Chapter 1 (Chapter 1.4.1), however, it is worth reiterating that FTD is a particularly heterogenous disease and therefore a large cohort of patients is preferable for use alongside biomolecular investigation. While each sample from FTD patients came from either the frontal or temporal cortices, it is also important to note that some variability in this work may have been introduced through variation in the exact sampling area. To overcome this, future studies should be carried out on tissue from multiple sampling areas within each cortex. The western immunoblotting results in this chapter inform on the Sarkosyl soluble tau-related pathology in PiD and FTDP-17. Sarkosyl insoluble fractions typically include NFTs and other entangled proteins, including kinases such as Cdk5 and GSK3β. Future work carried out on Sarkosyl insoluble fractions, coupled with the work in this chapter, would allow a more comprehensive understanding of tau pathology in these tissues.

Chapter 7

Final discussion and future work

Despite decades of research and the thorough characterisation of tau pathology within the brains of patients with tauopathies, our knowledge of the molecular pathways involved in the etiopathology of these diseases remains inadequate. The complete elucidation of these pathways may be critical for the development of therapies capable of overcoming the progression of these diseases. One obstruction to progress is the lack of readily-available models that faithfully recapitulate the biomolecular pathways involved in the development of tauopathy in humans. Traditional animal models of tauopathy have failed to faithfully recapitulate human disease, resulting in the failure of many promising drugs to clinically translate (Sasaguri *et al*., 2017). Biomolecular studies of the human brain can be carried out using post-mortem tissue, however this represents end-stage disease rather than the state of the brain during pathogenesis.

Models of tauopathy have been developed through the differentiation of patient-derived human induced pluripotent stem cells (hiPSC) to produce disease-relevant cell types. While these models promise to facilitate investigation of the biomolecular pathways involved in early-stage disease, during which time we may be able to intercept therapeutically, the field is still in its infancy and it is important to research the applicability of these models.

The purpose of this PhD project was to investigate the ability of hiPSC models of tauopathy to inform on tau-related molecular pathology. hiPSC models of frontotemporal dementia with Parkinsonism linked to chromosome 17 (FTDP-17) and sporadic Alzheimer's disease (sAD) were developed through the derivation of vulnerable neuronal subtypes from hiPSC. The levels of tau protein and *MAPT* expression were determined alongside levels of tau phosphorylation at sites known to be aberrantly phosphorylated in tauopathy. The protein levels, activity and gene expression of three tau kinases previously implicated in tauopathy, GSK3β, Cdk5 and PAK3 (Chapter 1.3), were also investigated to understand the changes that occur in these during pathogenesis. Levels of synapsin I were also determined to understand whether the loss of synaptic proteins recognised in tauopathy is recapitulated in these

models. These changes in pathology were compared to those investigated within brain tissue in this study, and within the literature.

It should be noted that upon the inception of this project, it was not known that only foetal tau is expressed within hiPSC-neurons until approximately one year of culture has passed (Sposito *et al*., 2015), which will likely affect tau pathogenesis as these diseases occur in adults and involve all six tau isoforms.

7.1 The development of a model of frontotemporal dementia with Parkinsonism linked to chromosome 17 using induced pluripotent stem cell technology

The causal importance of tau protein in the pathogenesis of neurodegenerative disease was highlighted by the discovery that mutations of *MAPT* result in FTDP-17. As the underlying cause of sporadic tauopathy remains unclear, the development of models of tauopathy based on the expression of *MAPT* mutations offers the opportunity to investigate the molecular pathways involved in tau pathogenesis. To model FTDP-17, two hiPSC clones (V337M-C and V337M-E), derived from a patient carrying the missense mutation valine to methionine at 337 (V337M) *MAPT,* were differentiated to produce cortical glutamatergic neurons (CGNs) and cultured for 50 days.

It is not known whether tau pathogenesis in sporadic frontotemporal dementia (FTD) occurs through the same molecular pathways as at that within FTDP-17. Therefore, the tau-related molecular pathology discovered in this model was compared to that within the frontal and temporal cortices of patients with both FTDP-17 and Pick's disease (PiD). It is hoped that insights gained through the study FTDP-17 pathogenesis will also be applicable to sporadic forms of FTD, which are more common.

7.1.1 The ability of hiPSC-CGNs generated from a patient with V337M *MAPT* to model tau pathology in FTDP-17

7.1.1.1 Comparison of levels of tau protein and *MAPT* expression in hiPSC and brain tissue

Chromosomal microdeletions, microduplications and microtriplications involving *MAPT* have been demonstrated to cause syndromes involving mental retardation, thereby demonstrating the importance of changes in *MAPT* expression levels in neurological disease (Caillet-Boudin *et al.,* 2015). Despite this knowledge, few studies have examined the gene expression of *MAPT* in tauopathy.

In this study, hiPSC-CGNs derived from a patient carrying V337M *MAPT* were not found to have significantly different *MAPT* gene expression levels compared to controls, in line with the similar levels of *MAPT* gene expression found within the frontal and temporal cortices of FTDP-17 patients and temporal cortices of patients with PiD in this study. These results are in agreement with previous reports reporting similar levels of *MAPT* expression (van Eersel *et al.,* 2009; Adamec *et al.,* 2001). Therefore, levels of tau protein within V337M *MAPT* hiPSC-CGNs represent levels within the brain. *MAPT* expression was increased within the frontal cortices of patients with PiD, suggesting that alterations in *MAPT* expression, at least in the temporal cortex, are also distinguished between different frontotemporal dementias.

The expression of *MAPT* is regulated epigenetically by methylation. Generally, hypermethylation of *MAPT*, leading to decreased levels of tau protein, is associated with neuroprotective mechanisms; in reverse, hypomethylation of *MAPT* is associated with increased levels of tau protein and neurodegeneration (Caillet-Boudin *et al.,* 2015). Previous studies have shown that *MAPT* DNA methylation is altered within the brains of patients with tauopathy in a region-specific manner. For example, within the brains of patients with Parkinson's disease, in which tau pathology is recognised, hypermethylation of *MAPT* is associated with decreased tau protein and relative sparing (Coupland *et al.,* 2014). Additionally, the majority of *MAPT* methylation changes in the AD brain were found to occur within the temporal lobes, an area particularly vulnerable in this disease, and when modelled *in vitro* these changes brought about increased expression of tau (Iwata *et al*., 2014). Liang and colleagues have also reported region-specific reductions in *MAPT* expression within vulnerable areas of the brain, including the temporal cortex, of AD patients and this has also been hypothesised to be neuroprotective (Liang *et al.,* 2008). These studies suggest that in tauopathy, *MAPT* gene expression may vary in specific brain regions compared to healthy

brains and that this variation contributes to pathology. Further research into *MAPT* methylation changes due to disease would be useful to understand if this form of epigenetic regulation is affected in FTDP-17 and PiD. Indeed, highly reproducible DNA methylation changes are associated with human ageing (Koch et al., 2011) and may provide the link between age and tauopathy. Mice are often used in epigenetic studies, however, hiPSC-neuron models may be more ideal for this investigation due to the differences between mouse and human epigenetic regulation (Wagner, 2017).

In a previous study levels of *MAPT* expression were shown to correlate with tau protein expression (Trabunzi *et al*., 2012). Levels of soluble tau in the frontal cortices of patients with PiD may not represent *MAPT* expression because these protein levels do not take into account potential levels of excess, Sarkosyl-insoluble, aggregated tau. Further investigation into the insoluble levels of total tau protein, coupled with the reported levels of insoluble tau, may reveal a correlation in changes in tau protein levels with changes in *MAPT* expression in the frontal cortices of these patients.

7.1.1.2 Tau phosphorylation in hiPSC-neurons and brain tissue

The hallmark of tauopathies is the accumulation of hyperphosphorylated tau within the brain. Abnormal phosphorylation of tau initiates a pathological sequence of events, which ultimately leads to neurodegeneration. These include the loss of microtubule stability, dysfunction in cellular transport, the aggregation of tau, the loss of synapses and the dysregulation of critically important cellular pathways. Phosphorylation of tau in tauopathy is thought to occur sequentially. The sequential phosphorylation has been investigated within AD, but not FTD. In AD, phosphorylation at pThr231 is thought to be a very early event, which is followed by phosphorylation at pSer202 and subsequently pSer396/Ser404 (Luna-Munoz *et al*., 2007). Phosphorylation of tau at Ser396/404 is a well-known indicator of tau pathology and is associated with later stages of tau phosphorylation (Luna-Munoz *et al*., 2007). Tau was found to be abnormally phosphorylated in hiPSC-neurons carrying *MAPT* mutations compared to controls.

In FTDP-17 and PiD frontal cortices, levels of pSer396/404 were predictably increased. While increased phosphorylation at pSer396/404 was found in hiPSC-CGN derived from one clone, V337M-E, levels were not found to be significantly altered in the other ,V337M-C, indicating clonal variability.

Phosphorylation at Ser202 was found to be increased in V337M *MAPT* hiPSC, in line with previous studies demonstrating increased phosphorylation of tau within the midbrains of patients with this mutation (Ehrlich *et al*., 2015), PiD patient brains (Zhukareva *et al.,* 2002; Espinoza *et al.,* 2008; Koga *et al.,* 2017; van Eersel *et al.,* 2009; Nölle *et al.,* 2013) and within the brains of patients with FTDP-17 caused by G272V *MAPT* (Nölle *et al.,* 2013). Surprisingly, in this study, no significant change in pSer202 tau was determined in the frontal cortices of patients with FTDP-17, as well as the frontal and temporal cortices of PiD patients, contrary to previous reports. In each case the mean of the levels was found to be greater than that of controls, however, and there was a trend towards increased phosphorylation at this site within the frontal cortex of PiD patients. As discussed in Chapter 6 (Chapter 6.4.2), this may be due to heterogeneity and an increased cohort size may provide clarity on this result. Another reason for the lack of significantly increased phosphorylation at this site may be the fact the tau investigated was Sarkosyl-soluble tau, and tau phosphorylated at this site may have been sequestered into Sarkosyl-insoluble aggregations of tau, as it has been shown to decorate Pick Bodies previously (Zhukareva *et al.,* 2002; Espinoza *et al.,* 2008; Koga *et al.,* 2017; van Eersel *et al.,* 2009; Nölle *et al.,* 2013).

In V337M *MAPT* hiPSC-CGNs, tau phosphorylation at Thr231 was considerably decreased compared to controls while staining was too weak to detect levels on western immunoblots of lysates derived from brain tissue of controls, FTDP-17 patients or PiD patients. This was surprising, as increased levels of pThr231 tau within the brains of patients with AD are widely reported (Acker *et al.,* 2013; Beurger *et al*., 2002) and tau aggregations in FTLD patients positively immunostain with antibodies against pThr231 tau (Moszczynski *et al*., 2017). Interestingly, levels of pThr231 tau in the brains of patients with FTDP-17 (Shiarli *et al*., 2014) and in the CSF of patients with FTD (Buerger *et al*., 2002) are much closer to that of controls than AD and levels in CSF can be used to discriminate between the two diseases (Buerger *et al*., 2002). While further research into the levels of pThr231 tau within the brains of patients with FTDP-17 and PiD would be useful to understand if levels are decreased compared to controls, the results in V337M *MAPT* hiPSC-CGN suggest that in early disease tau phosphorylation at this site is decreased. Interestingly, phosphorylation of tau at Thr231 has been demonstrated to be a consequence of increased GSK3β activity leading to the detachment of tau from the microtubules (Moszczynski *et al*., 2014; Cho and Johnson, 2004).

7.1.3 Changes in kinase expression, levels and activity in hiPSC-neurons and brain tissue

The abnormal phosphorylation of tau occurs through dysregulation of tau kinases and phosphatases in tauopathy (Bodea *et al*., 2015; Dolan *et al*., 2010; Martin *et al*., 2013). The molecular pathways responsible for these alterations in these kinases and phosphatases are not well understood. Despite this, the involvement of GSK3β and Cdk5 in tauopathy is well reported (Dolan *et al*., 2010; Martin *et al*., 2013) and therapeutics targeting the activity of both kinases have been developed to limit tau phosphorylation; whilst promising in murine models of disease, the intended effects of these did not translate in humans (Vell *et al*., 2013; Tolosa *et al*., 2014; Lovestone *et al*., 2015). Comparatively little research has been carried out on the involvement of PAK3 in tauopathy, however, recently this kinase has been shown to be downregulated in V337M *MAPT* hiPSC-dopaminergic neurons (Ehrlich *et al*., 2015), indicating that it may be involved in pathogenesis.

The gene expression, protein levels and activity of Cdk5 and GSK3β were investigated, alongside the gene expression and protein levels of PAK3 to understand if these are altered in V337M *MAPT* hiPSC-CGNs and patient brain tissue. Through elucidating the mechanism, and time-frame (i.e. early-stage disease verses late-stage disease), during which these kinases become dysregulated in tauopathy we may be able to further refine therapeutics to render them effective.

CDK5 expression was not found to be significantly altered in V337M *MAPT* hiPSC-CGN or within both the frontal and temporal cortices of those with FTDP-17 and PiD, demonstrating that hiPSC carrying V337M *MAPT* recapitulate this lack of expression change. The activity of Cdk5, determined by an increase in p25 or a decrease in p35, was found to be increased in both V337M-hiPSC CGNs and within the frontal cortex of patients with PiD, demonstrating that Cdk5 activity in PiD is recapitulated in this model. Unfortunately, due to a lack of tissue p25 and p35 levels within the frontal cortex of FTDP-17 patients could not be examined. These results implicate alterations in Cdk5 kinase activity both in the pathogenesis and later stages of FTD-tau.

V337M *MAPT* hiPSC-CGN recapitulate altered protein levels of PAK3 within FTDP-17 brain tissue. PAK3 protein levels were significantly decreased in V337M *MAPT* hiPSC-CGNs derived from one hiPSC clone (V337M-C) and there was a trend towards decreased levels in CGNs derived from the other (V337M-E) ($p= 0.0601$). Reduced PAK3 levels were also found within

R406W and IVS 10+16 *MAPT* patient frontal and temporal cortices, demonstrating that a reduction in PAK3 protein levels is not specific only to FTDP-17 caused by the V337M *MAPT* mutation. Recently, it has been demonstrated that downregulation of PAK1 activity, which shares functional overlap with PAK3, during the treatment of dopaminergic neurons to induce oxidative stress, correlates with neurodegeneration (Kim *et al*., 2016). In light of this study, these results suggest that decreased PAK3 levels, within hiPSC-CGNs and cortex tissue, may be representative of neurodegenerative pathways. The recapitulation of these protein and gene expression changes demonstrate the suitability of this model for further investigation into this pathway and the activity levels of PAK3 in FTDP-17.On the other hand, in the frontal and temporal lobes of patients with PiD, levels of PAK3 protein were not found to be statistically different to those within controls, suggesting that changes in the protein levels of PAK3 are not involved in pathogenesis in this disease.

The gene expression of *PAK3* was not found to be statistically different in V337M *MAPT* hiPSC-CGNs, contrasting previously reported findings by Ehrlich and colleagues on expression levels within hiPSC-dopaminergic neurons (Ehrlich *et al*., 2015). Similarly, within the frontal and temporal cortices of PiD patients, as well as the temporal cortices of patients with FTDP-17, *PAK3* expression was not significantly different compared to controls. In line with these results, the expression of *PAK3* in the midbrains of V337M *MAPT* FTDP-17 patients has been measured previously and the authors concluded no change in gene expression within the midbrains of these patients (Ehrlich *et al*., 2015).

PAK3 expression was, however, found to be decreased within the frontal cortex of patients with FTDP-17, which may suggest that *PAK3* expression levels are altered in a regionally specific manner within the brains of these patients. One possible pathway through which *MAPT* mutations could cause a reduction in *PAK3* expression is through tau's role in the potentiation of activating protein 1 (AP-1) activity, which occurs in response to nerve growth factor (Leugers and Lee, 2010); AP-1 regulates the activity of PAK3 such that overexpression of AP-1 leads to increased levels of PAK3 expression (Parker *et al.,* 2013). Mutations in *MAPT* may hinder the ability of tau to influence the activity of AP-1, thereby resulting in decreased levels of PAK3.

Within V337M *MAPT* hiPSC-CGN, gene expression of *GSK3β* was not found to be significantly different in comparison to controls, recapitulating the gene expression levels found within the frontal and temporal cortices of patients with FTDP-17 or patients with PiD, in which

GSK3β gene expression was not found to be significantly different compared to controls. Total levels of GSK3β within V337M-CGN were found to be significantly increased within one clone, V337M-E, although unchanged within the other, V337M-C, indicating clonal variability in this model. Additionally, no significant differences compared to controls were found in the total levels of GSK3β within the frontal cortices of patients with FTDP-17 or PiD. Together, these results suggest that changes in the protein levels of GSK3β are not likely to be involved in disease pathogenesis or progression.

The activity of GSK3β was found to be decreased in V337M-E-CGN compared to controls, whereas it was found to be increased in the frontal cortices of PiD patients and unaltered in the temporal cortices of these patients. Additional research is required to understand whether GSK3β activity plays a role in disease pathogenesis or progression in FTD, however, these results indicate that GSK3β activity within PiD patient brain tissue is not recapitulated in this hiPSC model of FTDP-17.

The phosphorylated form of Akt, another tau kinases, was also investigated within the cells of this hiPSC-neuron and levels were found to similar compared to controls, suggesting that increased levels of the active, phosphorylated form of this tau kinase are not involved in FTDP-17.

7.1.4 Comparison of levels of synapsin I in hiPSC and brain tissue

The dysfunction and loss of synapses is thought to be an early event in tauopathy and to contribute to the dichotomous loss of neurons throughout the brain as functional connections between neurons are lost (Selkoe *et al*., 2002; Bodea *et al*., 2016). Hyperphosphorylated tau causes the loss of synapses through several pathways (Zhao *et al*., 2017; Spire-Jones *et al*., 2014). The levels of synapsin I, a pre-synaptic protein demonstrated previously to be lost in neurodegenerative disease, were determined within V337M *MAPT* hiPSC-CGNs to investigate the ability of these to recapitulate this aspect of disease. Levels of synapsin I were found to be decreased in hiPSC-CGNs, indicative of tauopathy and demonstrating that the loss of synaptic proteins is affected very early in disease pathogenesis, since these neurons are thought to be equivalent to foetal neurons in age. Although this is also strongly replicated in the PiD post-mortem temporal cortex, the reduction seen in the tissue from the FTDP-17 patients was not significant due to an outlier

in one of the controls. Replicate values from the controls were unsatisfactory but there was not enough tissue to replicate this experiment.

7.1.5 Summary of results

V337M *MAPT* hiPSC-CGNs recapitulated important tau-related pathology found in FTD patients, including the abnormal phosphorylation of tau and the loss of the pre-synaptic protein, synapsin I. This indicates that this model would be a useful tool for investigating the biomolecular pathways involved in aberrant tau phosphorylation and the early loss of synapses in FTD.

This study has also demonstrated the value of using hiPSC-CGN derived from patients with *MAPT* mutations to investigate biomolecular differences in disease, which may underlie the pathological phosphorylation of tau. The protein levels of PAK3, a tau kinase under-investigated in tauopathy, were found to be decreased within V337M *MAPT* hiPSC-CGNs as well as within the frontal and temporal cortices of patients with FTDP-17. Since *PAK3* expression was not found to be downregulated in V337M *MAPT* hiPSC-CGNs or the temporal cortices of patients with FTDP-17 this suggests that PAK3 levels are reduced through a pathological mechanism that does not target *PAK3* gene expression. Similarly, the results gained from V337M *MAPT* hiPSC-CGNs and the frontal cortices of patients with PiD in this study suggest the activity of the Cdk5 is increased, in FTD-tau.

Although protein levels of GSK3β and *GSK3β* gene expression were not significantly different compared to controls within the frontal and temporal cortices of FTDP-17 and PiD patients, or within V337M *MAPT* hiPSC-CGN, the activity of this kinase within V337M *MAPT* hiPSC-CGNs did not mirror that observed within tissue from either PiD or FTDP-17 patients. The inability of the model to replicate this aspect of tauopathy could be attributed to a number of limitations inherent in modelling with hiPSC-neurons. GSK3β is involved in neural development and these cultures of hiPSC-neurons, at day 50, are now thought to be equivalent in age to those within the developing foetus, exemplified by the production of only foetal tau isoforms in hiPSC-neurons before day 365 of culture (Sposito *et al*., 2015). The pathways altered in adults due to pathological tau leading to increased GSK3β activity may respond differently in these 'young' neurons. The limitation of age in hiPSC-neuron modelling is discussed later (Chapter 7.3.1). Furthermore, GSK3β is involved in a concert of cellular signalling pathways within the brain, some of which may be influenced by the

presence of other cell types within the brain. Increased GSK3β activity may not be recapitulated in this model, therefore, due to a lack of faithful recapitulation of the disease niche. This limitation is discussed later (Chapter 7.3.3). Levels of active GSK3β varied between the two clones indicating clonal variation, which is a limitation of hiPSC-models that is well reported (Hallman *et al*., 2015; Liang and Zhang, 2013) and discussed later (Chapter 7.3.4).

GSK3β activity is also regulated by phosphorylation of GSK3β at Ser9, which inhibits its activity (Hanger and Noble, 2011). It is possible that a more accurate depiction of GSK3β activity may be gained through analysis of levels of GSK3β phosphorylated at Ser9.

The lack of difference between *MAPT* expression in V337M *MAPT* hiPSC-CGNs mirrors *MAPT* expression within the FTDP-17 frontal and temporal cortices, as well as within the PiD temporal cortices, but not within the PiD frontal cortices where greater levels of *MAPT* expression were measured compared to controls. Further study is also required to understand the mechanisms behind region-specific and disease-specific *MAPT* expression changes in PiD frontal and temporal corticies.

7.2 The development of a model of Alzheimer's disease using pluripotent stem cell technology

Most AD models, including those developed using hiPSC technology, have been developed through the expression of mutations associated with familial AD (fAD), which is much more rare compared to sAD. sAD remains particularly difficult to model due to the unknown aetiology of the disease. Studies in which sAD has been modelled using patient derived hiPSC-neurons, have reported large phenotypic variation between lines from different patients; in studies by Israel and colleagues (Israel *et al*., 2012) as well as Kondo and colleagues (Kondo *et al*., 2013) only one out of two sAD lines studied demonstrated phenotypes comparable to those observed in hiPSC-neurons derived from patients with fAD. As sAD does not have a genetic cause, the use of gene editing techniques to create isogenic lines are not helpful here.

The aberrant molecular pathways involved in sAD are numerous, exceedingly complex and poorly understood; however, previous research has provided substantial evidence suggesting Aβ pathology initiates and exacerbates tau pathology through various pathways.

Therefore, during this project, a model of sAD was developed to investigate Aβ-induced tau pathogenesis and the same tau-related molecular pathology measured within V337M *MAPT* hiPSC-derived neurons was investigated in this model. The presence of neuronal varicosities was also investigated. These results were compared to those within the literature, while changes in gene expression levels of *MAPT, CDK5* and *PAK3* were also compared to those within the basal forebrain nucleus of Meynert (nbM) of AD patients compared to healthy patients.

To model sAD, the control hESC line Shef 6 and the control hiPSC line Nas 2 were differentiated to produce both bfCNs and CGNs, which are particularly vulnerable in this disease. Aβ 1-42 oligomers ($A\beta_{42}O$) were applied to the hPSC-neurons for 48 hours, at concentrations of 0.1, 0.5 and 1 μM, to investigate the molecular tau-related pathology induced by this treatment.

The following paragraphs review the molecular tau-related pathology found within these models and compare this to that observed within the nbM tissue of AD patients and to previously reported pathology.

7.2.1 The ability of hPSC-neurons treated with $A\beta_{42}O$ to model tau pathology in AD

7.2.1.1 *MAPT* expression, levels of tau and the phosphorylation of tau

The presence of increased levels of tau and abnormal hyperphosphorylation of tau are considered the hallmarks of AD pathology alongside Aβ pathology (Luna-Munoz *et al*., 2007) but these are not recapitulated within this sAD model. Levels of total tau were not increased within Nas 2-bfCNs, Shef 6-bfCNs or Shef 6-CGNs after the application of any concentration (0.1, 0.5 or 1 μM) of $A\beta_{42}O$ over 48 hours. While this was not surprising since no other sAD hiPSC-model has replicated the increased levels of tau found in the AD brain, recapitulation of increased tau levels has been achieved in two fAD hiPSC-models (Moore *et al*., 2015; Choi *et al*., 2014).

Through determining the properties of models in which increased total tau was demonstrated, we may be able to understand how this sAD model can be improved upon in the future. One sAD model, based on the application of Aβ to hiPSC-neurons over 8 days, reported similar levels of total tau after treatment (Nieweg *et al.,* 2015), which suggests that

the lack of recapitulation of increased total tau would not be overcome by lengthening the period of Aβ treatment from 48 hours up to 8 days. It remains to be determined whether treatment with $A\beta_{42}O$ throughout the differentiation and maturation of hiPSC-neuron cultures could bring about an increase in total tau. Additionally, hiPSC-CGNs within the model reported by Nieweg and colleagues were matured for approximately 14 weeks after the start of the differentiation protocol as opposed to 50 days for hiPSC-CGNs in this study, suggesting that further 'ageing' of the cells through prolonged culture would not coax the appearance of increased levels of tau either.

Moore and colleagues reported increased levels of total tau in V717L *APP* or *APP* duplication hiPSC-forebrain neurons cultured for 90 days. These cultures were described as three dimensional (3D) as these had developed into thick monolayer cultures over a culture period of 90 days (Moore *et al*., 2015). Choi and colleagues also reported increased total tau within 3xfAD (K670N/M671L,V717L *APP/*ΔE9 *PSEN1*) hiPSC-neurons cultured for approximately 70 days within a 3D culture system (Choi *et al*., 2014). As other hiPSC-models based on fAD mutations have also failed to demonstrate increased levels of tau protein, these models suggest that culture of hiPSC-neurons within 3D culture systems may allow for this aspect of AD to be replicated. One explanation for this, given by Moore and colleagues, could be that 3D culture systems allow for the accumulation of tau within neurons.

No statistically significant changes in tau phosphorylation levels at sites Ser202 or Ser396/404 were brought about through the treatment of hPSC-bfCNs with 0.1, 0.5 or 1 μM $A\beta_{42}O$ or of hPSC-CGNs treated with 0.5 μM $A\beta_{42}O$, over a period of 48 hours. Nieweg and colleagues reported increased levels of pSer202/Thr205 tau, as well as pThr231 tau, within hiPSC-neurons cultured for 14 weeks and treated with Aβ for 8 days (Nieweg *et al*., 2015), suggesting that increased 'ageing' of neurons through longer culture periods or the application of Aβ over a longer period may be necessary to achieve changes in ptau within sAD hiPSC-neuron models based on the application of Aβ to otherwise healthy neurons. Indeed, within studies using hiPSC-neurons derived from patients with fAD long-term culture has been demonstrated to be necessary before observed ptau levels significantly exceed those of controls. For example, Raja and colleagues detected increased ptau at 90 days but not at 60 days (Raja *et al.,* 2016).

No significant change in the expression of *MAPT* was found within hPSC-bfCNs and hPSC-CGNs treated with $A\beta_{42}O$, which reflects levels of *MAPT* expression within AD patient nucleus

basalis of Meynert (nbM) tissue found in this study. These results align with recently reported levels within AD brain tissue (Fukasawa *et al.,* 2017; Farnsworth *et al.,* 2016) and fAD hiPSC-glutamatergic neurons (Moore *et al.,* 2015).

7.2.2 Activity levels and expression of kinases

The levels, activity and gene expression of tau kinases GSK3β, Cdk5 and PAK3 were investigated within these hPSC-neurons after treatment with $A\beta_{42}O$. The purpose of this work was to investigate the AD-related pathways through which Aβ influences the tau kinases GSK3β, Cdk5 and PAK3.

Within Shef 6-CGN treated with 1 µM $A\beta_{42}O$ and Nas 2-bfCN treated with 0.5 or 1 µM $A\beta_{42}O$, no significant difference in the gene expression of *GSK3β* was found compared to controls, in line with levels found in AD patient nbM tissue. These results disagree with reported downregulation of *GSK3β* within hiPSC-neurons derived from a patient with sAD (Hossini *et al*., 2015). The activity of GSK3β has been demonstrated to be increased in V717L *APP* hiPSC-CGNs and a within mixed population of hiPSC-derived neurons carrying a duplication of APP (Muratore *et al*., 2014; Israel *et al*., 2012). In contrast, decreased GSK3β activity was indicated in Shef 6-CGN treated with 0.5 µM $A\beta_{42}O$, while no difference in activity was noted for Shef 6-CGN cultures treated with 1 µM $A\beta_{42}O$ in comparison to controls.

Similarly, in Nas 2-bfCN treated with 0.5 µM $A\beta_{42}O$ and Shef 6-bfCN treated with 1 µM $A\beta_{42}O$ *CDK5* gene expression was unchanged by treatment compared to controls. These results recapitulate *CDK5* expression levels within AD nbM tissue, which were found to be not significantly different to controls, despite a decrease of 40% in mean value of gene expression compared to controls. Within the literature, *CDK5* expression has been reported to be downregulated in studies using large cohorts of patients (Fukasawa et al., 2017; Liang et al., 2008), and within hiPSC-neurons derived from a sAD patient (Hallmann et al., 2015). However, no change in *CDK5* expression has also been reported upon comparison of AD brains and health patient brains (Tandon et al., 2002). Further investigation into the expression of *CDK5* is required to clear this point of contention within the literature. Within Shef-6 CGN treated with 1 µM $A\beta_{42}O$, levels of p35 were decreased, suggesting increased Cdk5 activity, however, this was not found within Nas2-bfCN treated with 0.5 µM $A\beta_{42}O$.

These results suggest that Cdk5 and GSK3β activity is affected in different ways within these two cell types; bfCNs and CGNs. As these represent the basal forebrain and cerebral cortex,

respectively, investigation using these may provide insight into the progression of AD. Additional research using these two hPSC-derived neuronal subtypes in tandem within investigations using hiPSC-neuron models would allow for further characterisation of their differences in response to $A\beta_{42}O$. Additionally, concurrent differentiation of hiPSC-bfCNs and hiPSC-CGNs from fAD patients would also be useful to confirm changes recognised through treatment with $A\beta_{42}O$ as fAD and sAD are generally associated with the same pattern of progression of aggregated Aβ and tau pathology in the brain.

The levels of PAK3 were unaltered by treatment of Shef 6-CGN or Nas 2-bfCN with 1 μM and 0.5 μM $A\beta_{42}O$, respectively. Additionally, gene expression of *PAK3* was also unaltered by these treatments. This result reflects gene expression within AD nbM tissue. These results disagree with previous research demonstrating that PAK3 levels are decreased within the AD brain, however, these were examined within the hippocampus (Nguyen et al., 2008; Zhao et al., 2006). It would be useful to carry out this investigation again with a larger cohort of patient brain tissue to rule out heterogeneity in the non-significant result.

7.2.3 Comparison of levels of synapsin I in hPSC-neurons treated with $A\beta_{42}O$

Tau and Aβ pathology have been linked to the loss of synapses in AD mouse models and within AD patient brains, a parameter that correlates with cognitive decline in this disease (Palop and Mucke, 2010; Palop *et al.,* 2006). Treatment of Shef 6-CGN with 1 μM $A\beta_{42}O$ replicated the loss of synaptic proteins reported in AD, indicating that this particular treatment of hPSC-derived CGNs would be useful for investigating the mechanisms underlying synaptic loss in this disease. Treatment of Nas 2-bfCN with 0.5 μM $A\beta_{42}O$, however, failed to replicate this important feature of neuropathology. This disparity could be due to differences in the reaction of the two cell types studied to the application of Aβ, discussed in Chapter 5 (Chapter 5). $A\beta_{42}O$ bring about missorting of tau into the dendrites, which leads to the loss synapses (Zempel *et al.*, 2010).

7.2.4 Varicosities

In Nas 2-bfCNs, treatment with 1 μM $A\beta_{42}O$ resulted in the development of varicosities within the lengths of select neurons containing mitochondria and an abnormal conformation of tau associated with tau pathology in AD. Axonal varicosities are well documented in AD (Geula *et al.,* 2008; Grutzendler *et al.,* 2007; Notter and Knuesel, 2013; Terwel *et al.,* 2002) and are

thought to represent microtubule transport dysfunction, leading to accumulation of cell organelles and pathological conformations of tau (Mertens *et al.,* 2013; Krstic and Knuesel, 2012; Khan and Bloom, 2016). These varicosities are found in AD and have been previously replicated in AD hiPSC-neurons (Choi et al., 2014).

7.2.5 Summary of results

This model failed to replicate reported hyperphosphorylation of tau in AD at phosphorylation sites pSer202 and pSer396/404. Since phosphorylation of tau is an important and invariable aspect of AD pathology this model may not be suitable for the investigation of pathology downstream of overt phosphorylation in tau. No changes in total tau levels, usually found to be increased within AD brains, was observed deeming this model unsuitable for studying the causal mechanisms of tau accumulation in AD.

The inability of this model to recapitulate important, previously reported AD pathology may be explained by more general limitations in modelling tauopathy using hiPSC-neuron models, described below (Chapter 7.3). However, it is possible that these limitations also arise from the limitations of 48-hour treatment with $A\beta_{42}O$ to model AD. This acute treatment may not be sufficient to induce changes that in human disease, culminate over decades to result in the pathogenic hallmarks of AD.

Nevertheless, treatment of Nas 2-bfCNs with 1μM $A\beta_{42}O$ did cause the appearance of varicosities in neurons, recapitulating these found within the AD brain and suggesting that microtubule transport was affected by the treatment. This model may, therefore, provide insights into microtubule transport deficits in AD within these human neurons. Furthermore, treatment of Shef 6-CGNs with 1μM $A\beta_{42}O$ replicated the loss of pre-synaptic proteins, through decreased levels of synapsin I, recognised as an early event in AD pathology.

Aβ-induced alterations in the activity of kinases were also recognised; levels of GSK3β activity were increased in Nas 2-bfCNs treated with 0.5 μM $A\beta_{42}O$. Additionally, decreased p35 levels, indicative of decreased Cdk5 activity, were found within Shef 6-CGN treated with 1 μM $A\beta_{42}O$. These results indicate that while overt changes in tau were not discovered, this model may be suitable for studying early changes in the molecular pathways that contribute to aberrant tau phosphorylation.

Finally, comparison of the different responses, in activity of tau kinases Cdk5 and GSK3β, to $A\beta_{42}O$ within these two cell types demonstrates that culture of specific neuronal subtypes derived from hiPSC may be used to understand the different behaviours of these cell types in AD. These differences in kinase activity may explain the regional progression of AD with further research.

7.3 Limitations and future development of models

7.3.1 Limitations of hiPSC-neuron models to recapitulate the aged phenotype of neurons in the brains of patients with tauopathy

Identifying phenotypes in hiPSC-neurons modelling tauopathies, where aging is the main risk factor, is challenging due to the current limitations of these models. Upon the inception of hiPSC-neuron models it was suggested that the epigenetic profile of the donor patient cells, also known as 'age memory', may be retained by these cells allowing for the production of 'aged' neurons. Since then, it has become apparent that the 'age memory' is lost during hiPSC-reprogramming (Miller *et al.,* 2013), therefore, the neurons derived from patient hiPSC-neurons are equivalent in age to those found during foetal development. In terms of modelling tauopathy this property of hiPSC-neurons is particularly problematic; firstly, it is believed younger neurons may be more resilient to neurodegeneration caused by tauopathy and so the changes brought on over decades within human aged-neurons may not be recapitulated in these; and secondly these neurons produce only the foetal isoform of tau (3R0N) until day 365 (Sposito *et al.,* 2015), whereas in AD and FTD all six isoforms of tau are involved in pathogenesis (Ghetti et al., 2015) preventing faithful recapitulation of disease. Additionally, foetal tau is heavily phosphorylated at many of the same sites found to be hyperphosphorylated in tauopathy, which may restrict identification of changes in phosphorylation of tau due to disease processes in these models.

Currently, we do not have an ideal solution enabling this challenge to be overcome as the neurobiology of aging is poorly understood and therefore cannot be accurately replicated *in vitro.* Protocols involving direct conversion of fibroblasts to neurons are reported to allow the production of neurons that retain the age-specific transcriptional profile of donor cells, which may support the development hiPSC-neuron models which are more susceptible to tau pathology (Mertens *et al.,* 2015). Miller and colleagues have expressed progerin, to

induce premature aging in hiPSC-neurons (Miller *et al.,* 2013); when paired with genetic alterations resulting in tauopathy, this may allow for overt tau pathology to be replicated in these models, however, it is unknown whether tau pathology will occur through alternate molecular pathways to those which occur within the human brains of patients with these diseases. Further optimisation of culture methods, for example through three dimensional (3D) culture, co-culture with other neural cell types and the use of optimised media compositions (Bardy *et al.,* 2015), have been demonstrated to support earlier maturation of neurons, which may also improve the ability of these models to recapitulate tau pathology.

7.3.2 Limitations of hiPSC-neuron models to recapitulate the latency of tau pathogenesis

In these age-related tauopathies, pathology develops and progresses over decades. Furthermore, there is evidence suggesting that, during the progression of disease, pathways responsible for tau pathogenesis become modulated; for example, levels of PAK3 are reduced in early AD, and increased in late-stage AD (Chapter 1.3.3). This may explain why tau hyperphosphorylation has not been observed in many hiPSC-models of tauopathy and why Raja and colleagues reported a lack of tau hyperphosphorylation in their hiPSC-model of AD at 60 days of culture, while at 90 days hyperphosphorylation of tau at Thr181 and Ser396 was detected (Raja *et al.,* 2016).

Although the ability to culture hiPSC-neurons for extended periods has been recently drastically improved, with hiPSC-neurons reportedly cultured for 365 days (Sposito *et al.,* 2015), this time period of culture falls short of the 30 or so years required for the development of tau pathology within the human brain. Furthermore, extended maintenance of these cultures is costly and technically challenging. One solution to overcome this challenge may involve subjecting the cultures to environmental stressors to coax the early appearance of overt pathology, however, this may lead to the development of models that recapitulate the overt pathology of disease through different molecular pathways to those that occur in the adult brain, further obscuring the development of therapeutics aimed at interrupting these pathways. This limitation of hiPSC-neuron modelling may constrain the use of the models for investigation of early-stage tau pathogenesis.

7.3.3 Limitations in recapitulating the disease niche

A conspicuous limitation in the use of hiPSC-neurons to model tauopathy is the difficulty in replicating the complex disease niche of the human brain. Some aspects of disease pathology have been demonstrated to be replicated *in vitro*, within this study and in previous studies detailed in Chapter 4.1 and Chapter 5.1, using hiPSC-neurons; however, the complex cytoarchitecture of the brain and the effects of interactions with other cell types in the brain are not modelled by monolayer cultures of pure hiPSC-neurons. While these limitations of *in vitro* modelling are challenging to overcome, recent advancements presage the possibility of more physiologically accurate cultures in the future.

Glial cells have important roles in tauopathy. In AD, astrocytes associate with Aβ plaques (Rinaldi and Caldwell, 2013), are capable of internalising and degrading Aβ (Wyss-Coray *et al.,* 2003; Koistinaho *et al.,* 2004) and exhibit cellular stress, which is thought to contribute to neurodegeneration through decreased antioxidant support of neurons (Abramov *et al.,* 2003). Microglial cells are important components of the inflammatory response recognised in AD pathology and microglial inflammatory activity has been demonstrated to be increased in AD, while protein clearance mechanisms are reduced (Sarlus and Heneka, 2017). Microglia also play important roles in the molecular pathways that transduce Aβ-induced tau hyperphosphorylation, illustrated by Figure 1.2.3 (Figure 8.1, Chapter 1.2.3), through increased inflammatory response. Future models of tauopathy would, therefore, benefit from the development of co-cultures of neurons with glial cells, aimed at replicating the disease niche more faithfully.

Culturing hiPSC-neurons with primary murine and human astrocytes supports long-term culture, shortens the maturation period of neurons and supports maturation of functional synaptic connections (Kuijlaars *et al.,* 2016; Odawara *et al.,* 2014). Astrocytes have now been derived from healthy, AD (Kondo *et al.,* 2013) and FTDP-17 (Hallmann *et al.,* 2017) patient hiPSC, which have also been demonstrated to improve the ability of neurons to produce mature action potentials and reduce variability associated with introducing astrocytes from different species or patients (Gunhanlar *et al.,* 2017). Recently, protocols for the derivation of microglia from hiPSC have been published (Haenseler *et al.,* 2017; Douvaras *et al.,* 2017; Muffat *et al.,* 2016); one of these studies exhibited greater physiological accuracy in these models, demonstrating a decreased pathogen-response pathway (Haenseler *et al.,* 2017).

Future research using these models may help us to understand more clearly the molecular influence of these glial cells in tau pathogenesis in neurons.

3D models of tauopathy have also been developed, which employ 3D scaffolds culture and the generation of cerebral organoids, described as miniature brain models, with discrete areas representing brain regions, in attempt to model the complexity of neural connectivity in the brain. Four publications detailing 3D AD hiPSC-neuron models have been published (Lee *et al.,* 2016; Zhang *et al.,* 2014; Choi *et al.,* 2014; Raja *et al.,* 2016), which demonstrated AD phenotypes that could not be observed in 2D models. Zhang and colleagues observed abnormal translocation of PAK within hiPSC-neurons in their 3D system, but not in a 2D system (Zhang *et al.,* 2014), while Choi and colleagues, along with Raja and colleagues, have developed the only hiPSC-models of AD in which aggregates of tau and Aβ within neurons were observed (Raja *et al.,* 2016; Choi *et al.,* 2014).

7.3.4 Overcoming clonal variability between hiPSC-neuron cultures

Clonal variability, which affects the disease phenotype modelled by hiPSC-neurons created from the same person's hiPSC, is well reported throughout the literature on modelling neurodegenerative disease using hiPSC-neurons (Hallmann *et al*., 2015; Martelli *et al.,* 2012; Ehrlich *et al.,* 2015; Yokobayashi *et al*., 2017; Sheridan *et al.,* 2011). A number of reasons have been suggested for this including sources of variation that occur during reprogramming and differentiation of these cells (Liang and Zhang, 2013; Vitale *et al*., 2012).

It is possible to use gene editing techniques, such as zinc finger nuclease editing technology (Hockemeyer *et al*., 2009) and CRISPR/Cas9 (Seah *et al*., 2015) to create isogenic lines to overcome this, provided the disease being modelled has a genetic basis. Future approaches to modelling may involve either genome editing or screening for clonal variability between lines in order to select lines that most successfully recapitulate disease.

7.4 Thesis summary

During this project a model of FTDP-17 was produced that is capable of recapitulating important aspects of tau-related molecular pathology found within the brains of patients with this disease, indicating that this model is useful for the investigation of tau pathogenesis within FTDP-17, and to a lesser extent PiD.

Within the hiPSC-neurons treated with $A\beta_{42}O$ to sAD, tau hyperphosphorylation or increased levels of tau found in AD were not recapitulated. These did recapitulate the appearance of varicosities within neurons and the loss of synaptic proteins due to the presence of Aβ. Interestingly, bfCNs and CGNs derived from pluripotent stem cells, that were treated with the same concentration of $A\beta_{42}O$, revealed different responses in the activity of tau kinases GSK3β and Cdk5. These differences, which occurred in the absence of tau hyperphosphorylation, suggest that early in disease the dysregulation of tau kinases may vary between specific cell types. Further clarification of these differences may inform on the regional progression of pathology within AD.

References

Abounit, S. *et al.* (2016) 'Tunneling nanotubes: A possible highway in the spreading of tau and other prion-like proteins in neurodegenerative diseases', *Prion*, pp. 344–351. doi: 10.1080/19336896.2016.1223003.

Abramov, A. Y. *et al.* (2003) 'Changes in intracellular calcium and glutathione in astrocytes as the primary mechanism of amyloid neurotoxicity.', *The Journal of neuroscience : the official journal of the Society for Neuroscience*, 23(12), pp. 5088–95.

Acker, C. M. *et al.* (2013) 'Sensitive quantitative assays for tau and phospho-tau in transgenic mouse models', *Neurobiology of Aging*, 34(1), pp. 338–350. doi: 10.1016/j.neurobiolaging.2012.05.010.

Adamec, E. *et al.* (2001) 'Tau protein expression in frontotemporal dementias', *Neuroscience Letters*, 315(1–2), pp. 21–24. doi: 10.1016/S0304-3940(01)02314-X.

Adamec, E. *et al.* (2001) 'Tau protein expression in frontotemporal dementias.', *Neuroscience letters*, 315(1–2), pp. 21–4.

Adem, A. *et al.* (1987) 'Muscarinic receptors in human SH-SY5Y neuroblastoma cell line: regulation by phorbol ester and retinoic acid-induced differentiation.', *Brain research*, 430(2), pp. 235–42.

Akhmanova, A. and Steinmetz, M. O. (2015) 'Control of microtubule organization and dynamics: two ends in the limelight', *Nature Reviews Molecular Cell Biology*. Nature Research, 16(12), pp. 711–726. doi: 10.1038/nrm4084.

Al-Bassam, J. *et al.* (2002) 'MAP2 and tau bind longitudinally along the outer ridges of microtubule protofilaments', *Journal of Cell Biology*, 157(7), pp. 1187–1196. doi: 10.1083/jcb.200201048.

Allen, K. M. *et al.* (1998) 'PAK3 mutation in nonsyndromic X-linked mental retardation.', *Nature genetics*. doi: 10.1038/1675.

Allen, M. *et al.* (2016) 'Human whole genome genotype and transcriptome data for Alzheimer's and other neurodegenerative diseases', *Scientific Data*, 3, p. 160089. doi: 10.1038/sdata.2016.89.

Almeida, C. G. *et al.* (2005) 'Beta-amyloid accumulation in APP mutant neurons reduces PSD-95 and GluR1 in synapses', *Neurobiology of Disease*, 20(2), pp. 187–198. doi: 10.1016/j.nbd.2005.02.008.

Alonso, A. D. C. *et al.* (2004) 'Promotion of hyperphosphorylation by frontotemporal dementia tau mutations', *Journal of Biological Chemistry*. doi: 10.1074/jbc.M405131200.

Alvarez, A., Munoz, J. P. and Maccioni, R. B. (2001) 'A Cdk5-p35 stable complex is involved in the beta-amyloid-induced deregulation of Cdk5 activity in hippocampal neurons', *Exp Cell Res*, 264(2), pp. 266–274. doi: 10.1006/excr.2001.5152.

Alvarez, G. *et al.* (1999) 'Lithium protects cultured neurons against ??-amyloid-induced neurodegeneration', *FEBS Letters*. doi: 10.1016/S0014-5793(99)00685-7.

Alvarez, G. *et al.* (1999) 'Lithium protects cultured neurons against beta-amyloid-induced neurodegeneration.', *FEBS letters*, 453(3), pp. 260–4.

Alzheimer's Association (2016) '2016 Alzheimer's Disease Facts and Figure', *Alzheimer's & Dementia*.

Alzheimer, A. (1907) 'Uber eine eigenartige Erkrankung der Hirnrinde.', *Allg Zeits Psychiatry Psychisch Y Gerichtlich Med*, 64, pp. 146–8. doi: 10.1002/ca.980080612.

An, W. F. *et al.* (2010) *Discovery of Potent and Highly Selective Inhibitors of GSK3b*, *Probe Reports from*

the NIH Molecular Libraries Program.

Li, T. and Paudel, H. K.(2006) 'Glycogen Synthase Kinase 3β Phosphorylates Alzheimer's Disease-Specific Ser396 of Microtubule-Associated Protein Tau by a Sequential Mechanism'. American Chemical Society . doi: 10.1021/BI051634R.

Andreadis, A. *et al*. (1995) 'Relative exon affinities and suboptimal splice site signals lead to non-equivalence of two cassette exons', *Nucleic Acids Research*, 23(17), pp. 3585–3593. doi: 10.1093/nar/23.17.3585.

Andreadis, a, Brown, W. M. and Kosik, K. S. (1992) 'Structure and novel exons of the human tau gene.', *Biochemistry*, 31(43), pp. 10626–10633. doi: 10.1021/bi00158a027.

Angelo, M., Plattner, F. and Giese, K. P. (2006) 'Cyclin-dependent kinase 5 in synaptic plasticity, learning and memory', *Journal of Neurochemistry*, pp. 353–370.

Anstey, K. J., Mack, H. a and Cherbuin, N. (2009) 'Alcohol consumption as a risk factor for dementia and cognitive decline: meta-analysis of prospective studies.', *The American journal of geriatric psychiatry : official journal of the American Association for Geriatric Psychiatry*, 17(7), pp. 542–555.

Aplin, A. E. *et al.* (1996) 'In vitro phosphorylation of the cytoplasmic domain of the amyloid precursor protein by glycogen synthase kinase-3beta.', *Journal of neurochemistry*, 67(2), pp. 699–707.

Aplin, A. E. *et al.* (1997) 'Effect of increased glycogen synthase kinase-3 activity upon the maturation of the amyloid precursor protein in transfected cells.', *Neuroreport*, 8(3), pp. 639–43.

Arawaka, S. *et al.* (1999) 'The tau mutation (val337met) disrupts cytoskeletal networks of microtubules.', *Neuroreport*, 10(5), pp. 993–7.

Arendt, T. *et al.* (1983) 'Loss of neurons in the nucleus basalis of Meynert in Alzheimer's disease, paralysis agitans and Korsakoff's Disease.', *Acta neuropathologica*, 61(2), pp. 101–8.

Arendt, T. *et al.* (2003) 'Reversible paired helical filament-like phosphorylation of tau is an adaptive process associated with neuronal plasticity in hibernating animals.', *The Journal of neuroscience : the official journal of the Society for Neuroscience*, 23(18), pp. 6972–81.

Arendt, T. and Bullmann, T. (2013) 'Neuronal plasticity in hibernation and the proposed role of the microtubule-associated protein tau as a "master switch" regulating synaptic gain in neuronal networks', *American Journal of Physiology-Regulatory, Integrative and Comparative Physiology*, 305(5), pp. R478–R489. doi: 10.1152/ajpregu.00117.2013.

Arias-Romero, L. E. and Chernoff, J. (2008) 'A tale of two Paks', *Biology of the Cell*, 100(2), pp. 97–108. doi: 10.1042/BC20070109.

Arsenault, D. *et al.* (2013a) 'PAK Inactivation Impairs Social Recognition in 3xTg-AD Mice without Increasing Brain Deposition of Tau and A', *Journal of Neuroscience*, 33(26), pp. 10729–10740. doi: 10.1523/JNEUROSCI.1501-13.2013.

Arsenault, D. *et al.* (2013b) 'PAK Inactivation Impairs Social Recognition in 3xTg-AD Mice without Increasing Brain Deposition of Tau and A', *Journal of Neuroscience*, 33(26), pp. 10729–10740. doi: 10.1523/JNEUROSCI.1501-13.2013.

Asada, A. *et al.* (2008) 'Myristoylation of p39 and p35 is a determinant of cytoplasmic or nuclear localization of active cycline-dependent kinase 5 complexes', *Journal of Neurochemistry*, 106(3), pp. 1325–1336.

Asrar, S. *et al.* (2009) 'Regulation of hippocampal long-term potentiation by p21-activated protein kinase 1 (PAK1)', *Neuropharmacology*, 56(1), pp. 73–80. doi: 10.1016/j.neuropharm.2008.06.055.

Augustinack, J., Schneider, A. and , Mandelkow, E., Hyman, B. (2002) 'Specific tau phosphorylation

sites correlate with severity of neuronal cytopathology in Alzheimer's disease', *Acta Neuropathol*, 103, pp. 26–35.

Augustinack, J. C. *et al.* (2002) 'Colocalization and fluorescence resonance energy transfer between cdk5 and AT8 suggests a close association in pre-neurofibrillary tangles and neurofibrillary tangles.', *Journal of neuropathology and experimental neurology*, 61(6), pp. 557–564.

Auld, D. S. *et al.* (2002) 'Alzheimer's disease and the basal forebrain cholinergic system : relations to B-amyloid peptides , cognition , and treatment strategies', *Progress in Neurobiology*.

AVILA, J. *et al.* (2004) 'Role of Tau Protein in Both Physiological and Pathological Conditions', *Physiological Reviews*, 84(2), pp. 361–384. doi: 10.1152/physrev.00024.2003.

Azorsa, D. O. *et al.* (2010) 'High-content siRNA screening of the kinome identifies kinases involved in Alzheimer's disease-related tau hyperphosphorylation'. doi: 10.1186/1471-2164-11-25.

Baba, Y. *et al.* (2005) 'The effect of tau genotype on clinical features in FTDP-17.', *Parkinsonism & related disorders*. Elsevier BV, 11(4), pp. 205–8. doi: 10.1016/j.parkreldis.2005.01.003.

Bagrodia, S. and Cerione, R. A. (1999) 'PAK to the future', *Trends in Cell Biology*, pp. 350–355. doi: 10.1016/S0962-8924(99)01618-9.

Ballesteros-Yáñez, I. *et al.* (2006) 'Density and morphology of dendritic spines in mouse neocortex', *Neuroscience*, 138(2), pp. 403–409. doi: 10.1016/j.neuroscience.2005.11.038.

Bardy, C. *et al.* (2015) 'Neuronal medium that supports basic synaptic functions and activity of human neurons in vitro', *Proceedings of the National Academy of Sciences*, 112(20), pp. E2725–E2734. doi: 10.1073/pnas.1504393112.

Barini, E. *et al.* (2016) 'Metformin promotes tau aggregation and exacerbates abnormal behavior in a mouse model of tauopathy', *Molecular Neurodegeneration*. doi: 10.1186/s13024-016-0082-7.

de Barreda, E. G. *et al.* (2010) 'Tau-knockout mice show reduced GSK3-induced hippocampal degeneration and learning deficits', *Neurobiology of Disease*, 37(3), pp. 622–629. doi: 10.1016/j.nbd.2009.11.017.

Bartus, R. T. *et al.* (1982) 'The cholinergic hypothesis of geriatric memory dysfunction.', *Science (New York, N.Y.)*, 217(4558), pp. 408–14.

Basiri, K., Ansari, B. and Meamar, R. (2015) 'Frontotemporal dementia parkinsonism: Clinical findings in a large Iranian family', *Advanced Biomedical Research*, 4(1), p. 37. doi: 10.4103/2277-9175.151242.

Bates, L. E. and Silva, J. C. (2017) 'Reprogramming human cells to naïve pluripotency: how close are we?', *Current Opinion in Genetics & Development*, 46, pp. 58–65. doi: 10.1016/j.gde.2017.06.009.

Baumann, K. *et al.* (1993) 'Abnormal Alzheimer-like phosphorylation of tau-protein by cyclin-dependent kinases cdk2 and cdk5', *FEBS Letters*, 336(3), pp. 417–424.

Beevers, J. E., Caffrey, T. M. and Wade-Martins, R. (no date) 'Induced pluripotent stem cell (iPSC)-derived dopaminergic models of Parkinson's disease Parkinson's disease'. doi: 10.1042/BST20130194.

Behnam, M. *et al.* (2015) 'Homozygous MAPT R406W mutation causing FTDP phenotype: A unique instance of a unique mutation', *Gene*. doi: 10.1016/j.gene.2015.06.033.

Bellocchio, E. E. *et al.* (2000) 'Uptake of glutamate into synaptic vesicles by an inorganic phosphate transporter.', *Science (New York, N.Y.)*, 289(5481), pp. 957–60.

Benavides-Piccione, R. *et al.* (2006) 'Dendritic Size of Pyramidal Neurons Differs among Mouse Cortical Regions', *Cerebral Cortex*, 16(7), pp. 990–1001. doi: 10.1093/cercor/bhj041.

Bennett, D. A. *et al.* (2004) 'Neurofibrillary Tangles Mediate the Association of Amyloid Load with

Clinical Alzheimer Disease and Level of Cognitive Function', *Archives of Neurology*, 61(3), pp. 378–384. doi: 10.1001/archneur.61.3.378.

Beydoun, M. A., Beydoun, H. A. and Wang, Y. (2008) 'Obesity and central obesity as risk factors for incident dementia and its subtypes: a systematic review and meta-analysis', *Obesity Reviews*, 9(3), pp. 204–218. doi: 10.1111/j.1467-789X.2008.00473.x.

Bilic, J. and Belmonte, J. C. I. (2012) 'Concise Review: Induced Pluripotent Stem Cells Versus Embryonic Stem Cells: Close Enough or Yet Too Far Apart?', *STEM CELLS*, 30(1), pp. 33–41. doi: 10.1002/stem.700.

Billings, L. M. *et al.* (2005) 'Intraneuronal Abeta causes the onset of early Alzheimer's disease-related cognitive deficits in transgenic mice.', *Neuron*, 45(5), pp. 675–88. doi: 10.1016/j.neuron.2005.01.040.

Billingsley, M. L. and Kincaid, R. L. (1997) 'Regulated phosphorylation and dephosphorylation of tau protein: effects on microtubule interaction, intracellular trafficking and neurodegeneration.', *The Biochemical journal*, pp. 577–91.

Bird, T. D. (1993) *Early-Onset Familial Alzheimer Disease*, *GeneReviews(®)*. University of Washington, Seattle. Available at: http://www.ncbi.nlm.nih.gov/pubmed/20301414

Bird, T. D. *et al.* (1997) 'Chromosome 17 and hereditary dementia: linkage studies in three non-Alzheimer families and kindreds with late-onset FAD', *Neurology*.

Bissonnette, C. J. *et al.* (2011) 'The controlled generation of functional basal forebrain cholinergic neurons from human embryonic stem cells.', *Stem Cells*. doi: 10.1002/stem.626.

Blalock, E. M. *et al.* (2004) 'Incipient Alzheimer's disease: microarray correlation analyses reveal major transcriptional and tumor suppressor responses.', *Proceedings of the National Academy of Sciences of the United States of America*. National Academy of Sciences, 101(7), pp. 2173–8. doi: 10.1073/pnas.0308512100.

Boda, B. *et al.* (2004) 'The mental retardation protein PAK3 contributes to synapse formation and plasticity in hippocampus.', *The Journal of neuroscience : the official journal of the Society for Neuroscience*. doi: 10.1523/JNEUROSCI.2931-04.2004.

Bode, D. C., Baker, M. D. and Viles, J. H. (2017) 'Differential ion channel formation by Aβ 40 and Aβ 42 Ion Channel Formation by Amyloid-β 42 Oligomers but not Amyloid-β 40 in Cellular Membranes Differential ion channel formation by Aβ 40 and Aβ 42', *at University of Bristol Library Services on*. doi: 10.1074/jbc.M116.762526.

Boisvert, E. M. *et al.* (2013) 'The specification of telencephalic glutamatergic neurons from human pluripotent stem cells.', *Journal of visualized experiments : JoVE*. doi: 10.3791/50321.

Bolmont, T. *et al.* (2007a) 'Induction of tau pathology by intracerebral infusion of amyloid-beta -containing brain extract and by amyloid-beta deposition in APP x Tau transgenic mice.', *The American journal of pathology*. doi: 10.2353/ajpath.2007.070403.

Bolmont, T. *et al.* (2007b) 'Induction of tau pathology by intracerebral infusion of amyloid-beta -containing brain extract and by amyloid-beta deposition in APP x Tau transgenic mice.', *The American journal of pathology*. American Society for Investigative Pathology, 171(6), pp. 2012–20. doi: 10.2353/ajpath.2007.070403.

Borghi, R. *et al.* (2002) 'Increase of cdk5 is related to neurofibrillary pathology in progressive supranuclear palsy.', *Neurology*, 58(4), pp. 589–92.

Bories, C. *et al.* (2017) 'Transgenic autoinhibition of p21-activated kinase exacerbates synaptic impairments and fronto-dependent behavioral deficits in an animal model of Alzheimer's disease.', *Aging*. Impact Journals, LLC, 9(5), pp. 1386–1403. doi: 10.18632/aging.101239.

Boutajangout, A., Sigurdsson, E. M. and Krishnamurthy, P. K. (2011) 'Tau as a therapeutic target for

Alzheimer's disease.', *Current Alzheimer research*. NIH Public Access, 8(6), pp. 666–77.

Braak, H. *et al.* (2006) 'Staging of Alzheimer disease-associated neurofibrillary pathology using paraffin sections and immunocytochemistry', *Acta Neuropathologica*, 112(4), pp. 389–404. doi: 10.1007/s00401-006-0127-z.

Braak, H. *et al.* (2011) 'Stages of the Pathologic Process in Alzheimer Disease: Age Categories From 1 to 100 Years', *Journal of Neuropathology & Experimental Neurology*. doi: 10.1097/NEN.0b013e318232a379.

Braak, H. and Braak, E. (1991) 'Acta H â€™ pathologica Neuropathological stageing of Alzheimer-related changes', *Acta Neuropathol*. doi: 10.1007/BF00308809.

Braak, H. and Braak, E. (1995) 'Staging of alzheimer's disease-related neurofibrillary changes', *Neurobiology of Aging*, 16(3), pp. 271–278.

Braak, H. and Braak, E. (1996) 'Evolution of the neuropathology of Alzheimer's disease', *Acta Neurologica Scandinavica*, 94(SUPPL.165), pp. 3–12. doi: 10.1111/j.1600-0404.1996.tb05866.x.

Bramblett, G. T. *et al.* (1993) 'Abnormal tau phosphorylation at Ser396 in alzheimer's disease recapitulates development and contributes to reduced microtubule binding', *Neuron*. doi: 10.1016/0896-6273(93)90057-X.

Brandt, R., Hundelt, M. and Shahani, N. (2005) 'Tau alteration and neuronal degeneration in tauopathies: mechanisms and models', *Biochimica et Biophysica Acta (BBA) - Molecular Basis of Disease*, 1739(2–3), pp. 331–354. doi: 10.1016/j.bbadis.2004.06.018.

Brown, M. *et al.* (2004) 'Alpha2-chimaerin, cyclin-dependent Kinase 5/p35, and its target collapsin response mediator protein-2 are essential components in semaphorin 3A-induced growth-cone collapse.', *The Journal of neuroscience : the official journal of the Society for Neuroscience*, 24(41), pp. 8994–9004. Available at: http://www.jneurosci.org/cgi/doi/10.1523/JNEUROSCI.3184-04.2004%5Cnhttp://www.ncbi.nlm.nih.gov/pubmed/15483118.

Brownlees, J. *et al.* (1997) 'Tau phosphorylation in transgenic mice expressing glycogen synthase kinase-3beta transgenes.', *Neuroreport*, 8(15), pp. 3251–5.

Brun, A. *et al.* (1995) 'Synapse loss and gliosis in the molecular layer of the cerebral cortex in Alzheimer's disease and in frontal lobe degeneration.', *Neurodegeneration : a journal for neurodegenerative disorders, neuroprotection, and neuroregeneration*, 4(2), pp. 171–7.

Buckner, R. L. *et al.* (2008) '*The Brain's Default Network*', *Annals of the New York Academy of Sciences*, 1124(1), pp. 1–38. doi: 10.1196/annals.1440.011.

Buée, L. *et al.* (2000) 'Tau protein isoforms, phosphorylation and role in neurodegenerative disorders', *Brain Research Reviews*, 33(1), pp. 95–130.

Buée, L. and Delacourte, A. (1999) 'Comparative Biochemistry of Tau in Progressive Supranuclear Palsy, Corticobasal Degeneration, FTDP-17 and Pick's Disease', *Brain pathology*, 9, pp. 681–693.

Bugiani, O. *et al.* (1999) 'Frontotemporal dementia and corticobasal degeneration in a family with a P301S mutation in tau.', *Journal of neuropathology and experimental neurology*. doi: 10.1097/00005072-199906000-00011.

Burk, K. *et al.* (2017) 'EndophilinAs regulate endosomal sorting of BDNF-TrkB to mediate survival signaling in hippocampal neurons', *Scientific Reports*, 7(1), p. 2149.

Busciglio, J. *et al.* (1995) 'beta-amyloid fibrils induce tau phosphorylation and loss of microtubule binding.', *Neuron*, 14(4), pp. 879–88.

Cabana, M. D. *et al.* (1999) 'Why don't physicians follow clinical practice guidelines? A framework for

improvement.', *JAMA*, 282(15), pp. 1458–65.

Cabezas-Opazo, F. A. *et al.* (2015) 'Mitochondrial Dysfunction Contributes to the Pathogenesis of Alzheimer's Disease', *Oxidative Medicine and Cellular Longevity*. doi: 10.1155/2015/509654.

Caceres, A. and Kosik, K. S. (1990) 'Inhibition of neurite polarity by tau antisense oligonucleotides in primary cerebellar neurons.', *Nature*. doi: 10.1038/343461a0.

Caffrey, T. M. *et al.* (2006) 'Haplotype-specific expression of exon 10 at the human MAPT locus', *Human Molecular Genetics*, 15(24), pp. 3529–3537. doi: 10.1093/hmg/ddl429.

Cai, F. *et al.* (2008) 'Redox modulation of long-term potentiation in the hippocampus via regulation of the glycogen synthase kinase-3β pathway', *Free Radical Biology and Medicine*, 45(7), pp. 964–970. doi: 10.1016/j.freeradbiomed.2008.06.014.

Caillet-Boudin, M.-L. *et al.* (2015) 'Regulation of human MAPT gene expression', *Mol Neurodegener.*, 10: 28. doi: 10.1186/s13024-015-0025-8.

Camins, A. *et al.* (2006) 'The role of CDK5/P25 formation/inhibition in neurodegeneration.', *Drug news & perspectives*, 19(8), pp. 453–60.

Campos-Pea, V. and Antonio, M. (2014) 'Alzheimer Disease: The Role of Aβ in the Glutamatergic System', in *Neurochemistry*. InTech. doi: 10.5772/57367.

Candela, S. *et al.* (2013) 'Heterogeneous pathologies associated with dementia in Parkinsonism share a prion-like spreading mechanism.', *Archives italiennes de biologie*, 151(4), pp. 169–78.

Candy, J. *et al.* (1983) 'Pathological changes in the nucleus of meynert in Alzheimer's and Parkinson's diseases', *Journal of the Neurological Sciences*. Elsevier, 59(2), pp. 277–289.

Caraci, F. *et al.* (2010) 'Depression and Alzheimer's disease: Neurobiological links and common pharmacological targets', *European Journal of Pharmacology*, pp. 64–71. doi: 10.1016/j.ejphar.2009.10.022.

Carney, R. M. *et al.* (2014) 'Parkinsonism and distinct dementia patterns in a family with the MAPT R406W mutation', *Alzheimer's & Dementia*, 10(3), pp. 360–365. doi: 10.1016/j.jalz.2013.02.011.

Castaño, Z., Gordon-Weeks, P. R. and Kypta, R. M. (2010) 'The neuron-specific isoform of glycogen synthase kinase-3β is required for axon growth', *Journal of Neurochemistry*, 113(1), pp. 117–130. doi: 10.1111/j.1471-4159.2010.06581.x.

Chabrier, M. A. *et al.* (2014) 'Synergistic effects of amyloid-beta and wild-type human tau on dendritic spine loss in a floxed double transgenic model of Alzheimer's disease', *Neurobiology of Disease*. doi: 10.1016/j.nbd.2014.01.007.

Chai, X. *et al*. (2012) 'Constitutive secretion of tau protein by an unconventional mechanism', *Neurobiology of Disease*, 48(3), pp. 356–366. doi: 10.1016/j.nbd.2012.05.021.

Chalecka-Franaszek, E. and Chuang, D. M. (1999) 'Lithium activates the serine/threonine kinase Akt-1 and suppresses glutamate-induced inhibition of Akt-1 activity in neurons.', *Proceedings of the National Academy of Sciences of the United States of America*, 96(15), pp. 8745–50.

Chambers, S. M. *et al.* (2009) 'Highly efficient neural conversion of human ES and iPS cells by dual inhibition of SMAD signaling', *Nature Biotechnology*. doi: 10.1038/nbt.1529.

Chang, C.-Y. *et al.* (2015) 'N-butylidenephthalide Attenuates Alzheimer's Disease-Like Cytopathy in Down Syndrome Induced Pluripotent Stem Cell-Derived Neurons', *Scientific Reports*, 5(1), p. 8744. doi: 10.1038/srep08744.

Chang, K.-H. *et al.* (2010) 'Cdk5 is a major regulator of p38 cascade: relevance to neurotoxicity in Alzheimer's disease', *Journal of Neurochemistry*, 113(5), pp. 1221–9. doi: 10.1111/j.1471-

4159.2010.06687.x.

Chauhan, N. B. *et al.* (2005) 'Propentofylline attenuates tau hyperphosphorylation in Alzheimer's Swedish mutant model Tg2576', *Neuropharmacology*, 48(1), pp. 93–104.

Chen, G. *et al.* (2011) 'Chemically defined conditions for human iPSC derivation and culture', *Nature Methods*, 8(5), pp. 424–429. doi: 10.1038/nmeth.1593.

Chen, J. *et al.* (2017) 'Genome-wide association study identifies MAPT locus influencing human plasma tau levels.', *Neurology*. Lippincott Williams & Wilkins, 88(7), pp. 669–676.

Chen, J. *et al.* (2006) 'Activity-dependent Synaptic Wnt Release Regulates Hippocampal Long Term Potentiation', *Journal of Biological Chemistry*, 281(17), pp. 11910–11916.

Cheng, J. S. *et al.* (2014) 'Tau Reduction Diminishes Spatial Learning and Memory Deficits after Mild Repetitive Traumatic Brain Injury in Mice', *PLoS ONE*. Edited by M. Ohno. Public Library of Science, 9(12), p. e115765..

Cheung, Z. H. *et al.* (2008) 'Cyclin-Dependent Kinase 5 Supports Neuronal Survival through Phosphorylation of Bcl-2', *The Journal of Neuroscience*, 28(19), pp. 4872–4877.

Chi, S. *et al.* (2014) 'Depression in Alzheimer's disease: epidemiology, mechanisms, and management.', *Journal of Alzheimer's disease : JAD*, 42(3), pp. 739–55. doi: 10.3233/JAD-140324.

Chinwalla, A. T. *et al.* (2002) 'Initial sequencing and comparative analysis of the mouse genome', *Nature*, 420(6915), pp. 520–562. doi: 10.1038/nature01262.

Cho, J.-H. and Johnson, G. V. W. (2004) 'Glycogen synthase kinase 3beta phosphorylates tau at both primed and unprimed sites. Differential impact on microtubule binding.', *The Journal of biological chemistry*. American Society for Biochemistry and Molecular Biology, 278(1), pp. 187–93.

Cho, J.-H. and Johnson, G. V. W. (2003) 'Primed phosphorylation of tau at Thr231 by glycogen synthase kinase 3β (GSK3β) plays a critical role in regulating tau's ability to bind and stabilize microtubules', *Journal of Neurochemistry*. Blackwell Science Ltd, 88(2), pp. 349–358.

Choi, S. H. *et al.* (2014) 'A three-dimensional human neural cell culture model of Alzheimer's disease', *Nature*, 515(7526), pp. 274–278.

Chun, W. and Johnson, G. V. W. (2007) 'Activation of glycogen synthase kinase 3beta promotes the intermolecular association of tau. The use of fluorescence resonance energy transfer microscopy.', *The Journal of biological chemistry*. American Society for Biochemistry and Molecular Biology, 282(32), pp. 23410–7.

Ciani, L. *et al.* (2004) 'A divergent canonical WNT-signaling pathway regulates microtubule dynamics', *The Journal of Cell Biology*, 164(2), pp. 243–253. doi: 10.1083/jcb.200309096.

Clare, R. *et al.* (2010) 'Synapse loss in dementias', *Journal of Neuroscience Research*. Wiley Subscription Services, Inc., A Wiley Company, 88(10), pp. 2083–2090. doi: 10.1002/jnr.22392.

Clavaguera, F. *et al.* (2009) 'Transmission and spreading of tauopathy in transgenic mouse brain', *Nature Cell Biology*. doi: 10.1038/ncb1901.

Clavaguera, F. *et al.* (2013) 'Brain homogenates from human tauopathies induce tau inclusions in mouse brain', *Proceedings of the National Academy of Sciences*. doi: 10.1073/pnas.1301175110.

Clavaguera, F. *et al.* (2015) 'Invited review: Prion-like transmission and spreading of tau pathology', *Neuropathology and Applied Neurobiology*. doi: 10.1111/nan.12197.

Clayton, E. L. *et al.* (2010) 'Dynamin I phosphorylation by GSK3 controls activity-dependent bulk endocytosis of synaptic vesicles', *Nature Neuroscience*, 13(7), pp. 845–851. doi: 10.1038/nn.2571.

Clayton, E. L. *et al.* (2015) 'Frontotemporal dementia caused by CHMP2B mutation is characterised by neuronal lysosomal storage pathology', *Acta Neuropathologica*. Springer Berlin Heidelberg, 130(4), pp. 511–523.

Conde, C. and Cáceres, A. (2009) 'Microtubule assembly, organization and dynamics in axons and dendrites', *Nature Reviews Neuroscience*, 10(5), pp. 319–332. doi: 10.1038/nrn2631.

Connell, J. W. *et al.* (2001) 'Effects of FTDP-17 mutations on the in vitro phosphorylation of tau by glycogen synthase kinase 3β identified by mass spectrometry demonstrate certain mutations exert long-range conformational changes', *FEBS Letters*, 493(1), pp. 40–44.

Connell, J. W. *et al.* (2005) 'Quantitative analysis of tau isoform transcripts in sporadic tauopathies', *Molecular Brain Research*, 137(1–2), pp. 104–109. doi: 10.1016/j.molbrainres.2005.02.014.

Contreras-Vallejos, E. *et al.* (2014) 'Searching for novel Cdk5 substrates in brain by comparative phosphoproteomics of wild type and Cdk5-/- mice', *PLoS ONE*. Public Library of Science, 9(3).

Cook, C. *et al.* (2014) 'Acetylation of the KXGS motifs in tau is a critical determinant in modulation of tau aggregation and clearance', *Human Molecular Genetics*. doi: 10.1093/hmg/ddt402.

Counts, S. E. *et al.* (2006) 'Differential Expression of Synaptic Proteins in the Frontal and Temporal Cortex of Elderly Subjects With Mild Cognitive Impairment', *Journal of Neuropathology & Experimental Neurology*, 65(6), pp. 592–601.

Counts, S. E. *et al.* (2012) 'Hippocampal drebrin loss in mild cognitive impairment.', *Neuro-degenerative diseases*. Karger Publishers, 10(1–4), pp. 216–9.

Coupland, K. G. *et al.* (2014) 'DNA methylation of the *MAPT* gene in Parkinson's disease cohorts and modulation by vitamin E *In Vitro*', *Movement Disorders*, 29(13), pp. 1606–1614.

Coyle, J. T., Price, D. L. and DeLong, M. R. (1983) 'Alzheimer's disease: a disorder of cortical cholinergic innervation.', *Science (New York, N.Y.)*. American Association for the Advancement of Science, 219(4589), pp. 1184–90. doi: 10.1126/SCIENCE.6338589.

Crawford, T. Q. and Roelink, H. (2007) 'The Notch response inhibitor DAPT enhances neuronal differentiation in embryonic stem cell-derived embryoid bodies independently of sonic hedgehog signaling', *Developmental Dynamics*, 236(3), pp. 886–892. doi: 10.1002/dvdy.21083.

Crescenzi, R. *et al.* (2014) 'In vivo measurement of glutamate loss is associated with synapse loss in a mouse model of tauopathy.', *NeuroImage*. NIH Public Access, 101, pp. 185–92. doi: 10.1016/j.neuroimage.2014.06.067.

Crompton, L. A. *et al.* (2013) 'Stepwise, non-adherent differentiation of human pluripotent stem cells to generate basal forebrain cholinergic neurons via hedgehog signaling', *Stem Cell Research*. doi: 10.1016/j.scr.2013.08.002.

Cross, D. A. *et al.* (1994) 'The inhibition of glycogen synthase kinase-3 by insulin or insulin-like growth factor 1 in the rat skeletal muscle cell line L6 is blocked by wortmannin, but not by rapamycin: evidence that wortmannin blocks activation of the mitogen-activated protein kinase pathway in L6 cells between Ras and Raf.', *The Biochemical journal*, 303 (Pt 1), pp. 21–6.

Cross, D. A. E. *et al.* (1995) 'Inhibition of glycogen synthase kinase-3 by insulin mediated by protein kinase B', *Nature*, 378(6559), pp. 785–789. doi: 10.1038/378785a0.

Crouch, P. J. *et al.* (2009) 'Increasing Cu bioavailability inhibits Abeta oligomers and tau phosphorylation.', *Proceedings of the National Academy of Sciences of the United States of America*. National Academy of Sciences, 106(2), pp. 381–6. doi: 10.1073/pnas.0809057106.

Cruts, M., Theuns, J. and Van Broeckhoven, C. (2012) 'Locus-specific mutation databases for neurodegenerative brain diseases', *Human Mutation*, 33(9), pp. 1340–1344. doi:

10.1002/humu.22117.

Cruz, J. C. *et al.* (2003) 'Aberrant Cdk5 activation by p25 triggers pathological events leading to neurodegeneration and neurofibrillary tangles', *Neuron*, 40(3), pp. 471–483.

Cruz, J. C. *et al.* (2006) 'P25/Cyclin-Dependent Kinase 5 Induces Production and Intraneuronal Accumulation of Amyloid Beta in Vivo.', *The Journal of neuroscience : the official journal of the Society for Neuroscience*, 26(41), pp. 10536–10541.

Cuchillo-Ibanez, I. *et al.* (2008) 'Phosphorylation of tau regulates its axonal transport by controlling its binding to kinesin.', *The FASEB journal : official publication of the Federation of American Societies for Experimental Biology*. doi: 10.1096/fj.08-109181.

Czapski, G. A. *et al.* (2011) 'Alterations of Cyclin dependent kinase 5 expression and phosphorylation in Amyloid precursor protein (APP)-transfected PC12 cells', *FEBS Letters*, 585(8), pp. 1243–1248.

DaRocha-Souto, B. *et al.* (2012) 'Activation of glycogen synthase kinase-3 beta mediates β-amyloid induced neuritic damage in Alzheimer's disease', *Neurobiology of Disease*, 45(1), pp. 425–437.

Davis, E. K., Zou, Y. and Ghosh, A. (2008) 'Wnts acting through canonical and noncanonical signaling pathways exert opposite effects on hippocampal synapse formation', *Neural Development*, 3(1), p. 32.

Dawson, H. N. *et al.* (2001) 'Inhibition of neuronal maturation in primary hippocampal neurons from tau deficient mice.', *Journal of cell science*, 114(Pt 6), pp. 1179–87.

Dayanandan, R., Van Slegtenhorst, M., Mack, T. G. A., *et al.* (1999) 'Mutations in tau reduce its microtubule binding properties in intact cells and affect its phosphorylation', *FEBS Letters*. doi: 10.1016/S0014-5793(99)00222-7.

Dayanandan, R., Van Slegtenhorst, M., Mack, T. G. A., *et al.* (1999) 'Mutations in tau reduce its microtubule binding properties in intact cells and affect its phosphorylation', *FEBS Letters*, 446(2–3), pp. 228–232.

de Calignon, A. *et al.* (2012) 'Propagation of Tau Pathology in a Model of Early Alzheimer's Disease', *Neuron*, 73(4), pp. 685–697.

Decker, H. *et al.* (2010) 'Amyloid- Peptide Oligomers Disrupt Axonal Transport through an NMDA Receptor-Dependent Mechanism That Is Mediated by Glycogen Synthase Kinase 3 in Primary Cultured Hippocampal Neurons', *Journal of Neuroscience*, 30(27), pp. 9166–9171.

Delacourte, A. *et al.* (1996) 'Specific pathological Tau protein variants characterize Pick's disease.', *Journal of neuropathology and experimental neurology*, 55(2), pp. 159–68.

Delacourte, A. *et al.* (1998) 'Vulnerable neuronal subsets in Alzheimer's and Pick's disease are distinguished by their isoform distribution and phosphorylation', *Annals of Neurology*. Wiley Subscription Services, Inc., A Wiley Company, 43(2), pp. 193–204.

Delcommenne, M. *et al.* (1998) 'Phosphoinositide-3-OH kinase-dependent regulation of glycogen synthase kinase 3 and protein kinase B/AKT by the integrin-linked kinase.', *Proceedings of the National Academy of Sciences of the United States of America*, 95(19), pp. 11211–6.

Deng, Y. *et al.* (2014) 'β-Amyloid impairs the regulation of N-methyl-D-aspartate receptors by glycogen synthase kinase 3', *Neurobiology of Aging*, 35(3), pp. 449–459. doi: 10.1016/j.neurobiolaging.2013.08.031.

Denk, F. and Wade-Martins, R. (2009) 'Knock-out and transgenic mouse models of tauopathies', *Neurobiology of Aging*, pp. 1–13. doi: 10.1016/j.neurobiolaging.2007.05.010.

Dennis, E. L. and Thompson, P. M. (2014) 'Functional brain connectivity using fMRI in aging and Alzheimer's disease.', *Neuropsychology review*. NIH Public Access, 24(1), pp. 49–62. doi:

10.1007/s11065-014-9249-6.

Desikan, R. S. *et al.* (2012) 'Amyloid-β–Associated Clinical Decline Occurs Only in the Presence of Elevated P-tau', *Archives of Neurology*, 69(6), pp. 709–13. doi: 10.1001/archneurol.2011.3354.

Deture, M. *et al.* (2000) 'Missense tau mutations identified in FTDP-17 have a small effect on tau-microtubule interactions', *Brain Research*. doi: 10.1016/S0006-8993(99)02124-1.

DeTure, M. *et al.* (2002) 'Tau assembly in inducible transfectants expressing wild-type or FTDP-17 tau.', *The American journal of pathology*. doi: 10.1016/S0002-9440(10)64448-3.

Devine, M. J. *et al.* (2011) 'Parkinson's disease induced pluripotent stem cells with triplication of the α-synuclein locus', *Nature Communications*. doi: 10.1038/ncomms1453.

Dhariwala, F. A. and Rajadhyaksha, M. S. (2008) 'An unusual member of the Cdk family: Cdk5', *Cellular and Molecular Neurobiology*, pp. 351–369. doi: 10.1007/s10571-007-9242-1.

Dhavan, R. and Tsai, L. H. (2001) 'A decade of CDK5.', *Nature reviews. Molecular cell biology*, 2(10), pp. 749–759.

Dickey, C. A. *et al.* (2006) 'The high-affinity HSP90-CHIP complex recognizes and selectively degrades phosphorylated tau client proteins', *Journal of Clinical Investigation*, 117(3), pp. 648–658. doi: 10.1172/JCI29715.

Dickson, D. W. *et al.* (2011) 'Neuropathology of Frontotemporal Lobar Degeneration-Tau (FTLD-Tau)', *Journal of Molecular Neuroscience*, 45(3), pp. 384–389. doi: 10.1007/s12031-011-9589-0.

Dill, J. *et al.* (2008) 'Inactivation of Glycogen Synthase Kinase 3 Promotes Axonal Growth and Recovery in the CNS', *Journal of Neuroscience*, 28(36).

Ding, Y. *et al.* (2015) 'Inhibition of Nischarin Expression Promotes Neurite Outgrowth through Regulation of PAK Activity', *PLOS ONE*. Edited by E. Manser. Public Library of Science, 10(12), p. e0144948. doi: 10.1371/journal.pone.0144948.

Dixit, R. *et al.* (2008) 'Differential regulation of dynein and kinesin motor proteins by tau.', *Science (New York, N.Y.)*. doi: 10.1126/science.1152993.

Doble, B. W. and Woodgett, J. R. (2003) 'GSK-3: tricks of the trade for a multi-tasking kinase.', *Journal of cell science*, 116(Pt 7), pp. 1175–86.

Domoto-Reilly, K. *et al.* (2017) 'Unusually long duration and delayed penetrance in a family with FTD and mutation in *MAPT* (V337M)', *American Journal of Medical Genetics Part B: Neuropsychiatric Genetics*, 174(1), pp. 70–74. doi: 10.1002/ajmg.b.32443.

Doran, M., du Plessis, D. G., *et al.* (2007) 'Familial Early-Onset Dementia With Tau Intron 10 + 16 Mutation With Clinical Features Similar to Those of Alzheimer Disease', *Archives of Neurology*, 64(10), p. 1535. doi: 10.1001/archneur.64.10.1535.

Doran, M., du Plessis, D. G., *et al.* (2007) 'Familial early-onset dementia with tau intron 10 + 16 mutation with clinical features similar to those of Alzheimer disease.', *Archives of neurology*. doi: 10.1001/archneur.64.10.1535.

Douvaras, P. *et al.* (2017) 'Directed Differentiation of Human Pluripotent Stem Cells to Microglia.', *Stem cell reports*. Elsevier, 8(6), pp. 1516–1524. doi: 10.1016/j.stemcr.2017.04.023.

Drewes, G. *et al.* (1995) 'Microtubule-associated protein/microtubule affinity-regulating kinase (p110mark): A novel protein kinase that regulates tau-microtubule interactions and dynamic instability by phosphorylation at the Alzheimer-specific site serine 262', *Journal of Biological Chemistry*, 270(13), pp. 7679–7688.

Drubin, D. G. and Kirschner, M. W. (1986) 'Tau protein function in living cells', *J Cell Biol*.

Duan, L. *et al.* (2014) 'Stem cell derived basal forebrain cholinergic neurons from Alzheimer's disease patients are more susceptible to cell death', *Molecular Neurodegeneration*. doi: 10.1186/1750-1326-9-3.

Duan, N. *et al*. (2013) 'Single-patient (n-of-1) trials: a pragmatic clinical decision methodology for patient-centered comparative effectiveness research', *Journal of Clinical Epidemiology*, 66(8), pp. S21–S28. doi: 10.1016/j.jclinepi.2013.04.006.

Ebneth, A. *et al.* (1998) 'Overexpression of tau protein inhibits kinesin-dependent trafficking of vesicles, mitochondria, and endoplasmic reticulum: implications for Alzheimer's disease.', *The Journal of cell biology*. The Rockefeller University Press, 143(3), pp. 777–94.

Ebrahimi, B. (2015) 'Reprogramming barriers and enhancers: strategies to enhance the efficiency and kinetics of induced pluripotency.', *Cell regeneration (London, England)*. doi: 10.1186/s13619-015-0024-9.

Eckermann, K. *et al.* (2007) 'The β-Propensity of Tau Determines Aggregation and Synaptic Loss in Inducible Mouse Models of Tauopathy', *Journal of Biological Chemistry*, 282(43), pp. 31755–31765.

van Eersel, J. *et al.* (2009) 'Phosphorylation of soluble tau differs in Pick's disease and Alzheimer's disease brains', *Journal of Neural Transmission*, 116(10), pp. 1243–1251.

Ehrlich, M. *et al.* (2015) 'Distinct Neurodegenerative Changes in an Induced Pluripotent Stem Cell Model of Frontotemporal Dementia Linked to Mutant TAU Protein', *Stem Cell Reports*. doi: 10.1016/j.stemcr.2015.06.001.

Eickholt, B. J. *et al.* (2002) 'An inactive pool of GSK-3 at the leading edge of growth cones is implicated in Semaphorin 3A signaling', *The Journal of Cell Biology*, 157(2), pp. 211–217.

Eiraku, M. *et al.* (2008) 'Self-Organized Formation of Polarized Cortical Tissues from ESCs and Its Active Manipulation by Extrinsic Signals', *Cell Stem Cell*. doi: 10.1016/j.stem.2008.09.002.

Eldar-Finkelman, H. and Martinez, A. (2011) 'GSK-3 Inhibitors: Preclinical and Clinical Focus on CNS.', *Frontiers in molecular neuroscience*. Frontiers Media SA, 4, p. 32. doi: 10.3389/fnmol.2011.00032.

Elston, G. N. *et al.* (2011) 'Pyramidal cells in prefrontal cortex of primates: marked differences in neuronal structure among species.', *Frontiers in neuroanatomy*. Frontiers Media SA, 5, p. 2. doi: 10.3389/fnana.2011.00002.

Embi, N. *et al.* (1980) 'Glycogen synthase kinase-3 from rabbit skeletal muscle. Separation from cyclic-AMP-dependent protein kinase and phosphorylase kinase.', *European journal of biochemistry*, 107(2), pp. 519–27.

Encinas, M. *et al.* (2000) 'Sequential treatment of SH-SY5Y cells with retinoic acid and brain-derived neurotrophic factor gives rise to fully differentiated, neurotrophic factor-dependent, human neuron-like cells', *Journal of Neurochemistry*, 75(3), pp. 991–1003. doi: 10.1046/j.1471-4159.2000.0750991.x.

Engel, T. *et al.* (2006) 'Chronic lithium administration to FTDP-17 tau and GSK-3β overexpressing mice prevents tau hyperphosphorylation and neurofibrillary tangle formation, but pre-formed neurofibrillary tangles do not revert', *Journal of Neurochemistry*. doi: 10.1111/j.1471-4159.2006.04139.x.

Engel, T. *et al.* (2008) 'Hippocampal neuronal subpopulations are differentially affected in double transgenic mice overexpressing frontotemporal dementia and parkinsonism linked to chromosome 17 tau and glycogen synthase kinase-3β', *Neuroscience*, 157(4), pp. 772–780.

Englund, C. *et al.* (2005) 'Pax6, Tbr2, and Tbr1 Are Expressed Sequentially by Radial Glia, Intermediate Progenitor Cells, and Postmitotic Neurons in Developing Neocortex', *Journal of Neuroscience*, 25(1), pp. 247–251.

Espinoza, M. *et al.* (2008) 'Differential incorporation of tau isoforms in Alzheimer's disease.', *Journal of Alzheimer's disease : JAD*, 14(1), pp. 1–16.

Esteras, N. *et al.* (2017) 'Mitochondrial hyperpolarization in iPSC-derived neurons from patients of FTDP-17 with 10+16 MAPT mutation leads to oxidative stress and neurodegeneration', *Redox Biology*. doi: 10.1016/j.redox.2017.03.008.

Evergren, E. *et al.* (2007) 'The synapsin cycle: A view from the synaptic endocytic zone', *Journal of Neuroscience Research*, 85(12), pp. 2648–2656. doi: 10.1002/jnr.21176.

Fang, W. Q. *et al.* (2011) 'Cdk5-Mediated Phosphorylation of Axin Directs Axon Formation during Cerebral Cortex Development', *Journal of Neuroscience*, 31(38), pp. 13613–13624.

Farg, M. A. *et al.* (2014) 'C9ORF72, implicated in amytrophic lateral sclerosis and frontotemporal dementia, regulates endosomal trafficking', *Human Molecular Genetics*, 23(13), pp. 3579–3595.

Farnsworth, B. *et al.* (2016) 'Gene Expression of Quaking in Sporadic Alzheimer's Disease Patients is Both Upregulated and Related to Expression Levels of Genes Involved in Amyloid Plaque and Neurofibrillary Tangle Formation', *Journal of Alzheimer's Disease*, 53(1), pp. 209–219.

De Felice, F. G. *et al.* (2008) 'Alzheimer's disease-type neuronal tau hyperphosphorylation induced by Aβ oligomers', *Neurobiology of Aging*. doi: 10.1016/j.neurobiolaging.2007.02.029.

Ferreira, S. T. and Klein, W. L. (2011) 'The Aβ oligomer hypothesis for synapse failure and memory loss in Alzheimer's disease.', *Neurobiology of learning and memory*. NIH Public Access, 96(4), pp. 529–43. doi: 10.1016/j.nlm.2011.08.003.

Ferrer, I. (1999) 'Neurons and their dendrites in frontotemporal dementia.', *Dementia and geriatric cognitive disorders*. Karger Publishers, 10 Suppl 1(Suppl. 1), pp. 55–60. doi: 51214.

Finger, E. C. (2016) 'Frontotemporal Dementias.', *Continuum (Minneapolis, Minn.)*. American Academy of Neurology, 22(2 Dementia), pp. 464–89.

Fong, H. *et al.* (2013) 'Genetic correction of tauopathy phenotypes in neurons derived from human induced pluripotent stem cells.', *Stem cell reports*. Elsevier, 1(3), pp. 226–34.

De Forges, H., Bouissou, A. and Perez, F. (2012) 'Interplay between microtubule dynamics and intracellular organization', *International Journal of Biochemistry and Cell Biology*. doi: 10.1016/j.biocel.2011.11.009.

Forman, M. (2004) 'Genotype-phenotype correlations in FTDP-17: does form follow function?', *Experimental Neurology*, 187(2), pp. 229–234. doi: 10.1016/j.expneurol.2004.01.031.

Foster, N. L. *et al.* (1997) 'Frontotemporal dementia and parkinsonism linked to chromosome 17', *Annals of Neurology*. doi: 10.1186/1750-1172-1-30.

Francis, P. T. *et al.* (1993) 'Cortical Pyramidal Neurone Loss May Cause Glutamatergic Hypoactivity and Cognitive Impairment in Alzheimer's Disease: Investigative and Therapeutic Perspectives', *Journal of Neurochemistry*. Blackwell Publishing Ltd, 60(5), pp. 1589–1604.

Francis, P. T. (2003) 'Glutamatergic systems in Alzheimer's disease', *International Journal of Geriatric Psychiatry*, 18(S1), pp. S15–S21. doi: 10.1002/gps.934.

Franco, R. and Cedazo-Minguez, A. (2014) 'Successful therapies for Alzheimer's disease: Why so many in animal models and none in humans?', *Frontiers in Pharmacology*. doi: 10.3389/fphar.2014.00146.

Frandemiche, M. L. *et al.* (2013) 'Activity-Dependent Tau Protein Translocation to Excitatory Synapse Is Disrupted by Exposure to Amyloid-Beta Oligomers'. doi: 10.1523/JNEUROSCI.4261-13.2014.

Frappier, T. *et al.* (1999) 'Abnormal microtubule packing in processes of SF9 cells expressing the FTDP-17 V337M tau mutation', *FEBS Letters*. doi: 10.1016/S0014-5793(99)00902-3.

Frappier, T. F. *et al.* (1994) 'Regulation of Microtubule Microtubule Spacing and Bundling', *Journal of Neurochemistry*, 63(6), pp. 2288–2294. doi: 10.1046/j.1471-4159.1994.63062288.x.

Frautschy, S. A. *et al.* (1991) 'Effects of injected Alzheimer beta-amyloid cores in rat brain', *Proc Natl Acad Sci U S A*. doi: 10.1073/pnas.88.19.8362.

Frisardi, V. *et al.* (2011) 'Late-life depression and Alzheimer's disease: The glutamatergic system inside of this mirror relationship', 6(3), pp. 4–4. doi: 10.1016/j.brainresrev.2011.04.003.

Frost, B. *et al.* (2009) 'Propagation of Tau Misfolding from the Outside to the Inside of a Cell', *Journal of Biological Chemistry*, 284(19), pp. 12845–12852. doi: 10.1074/jbc.M808759200.

Fuchsova, B. *et al.* (2016) 'Expression of p21-activated kinases 1 and 3 is altered in the brain of subjects with depression', *Neuroscience*, 333, pp. 331–344. doi: 10.1016/j.neuroscience.2016.07.037.

Fukasawa, J. T. *et al.* (2017) 'CDK5 and MAPT Gene Expression in Alzheimer's Disease Brain Samples', *Current Alzheimer Research*, 14. doi: 10.2174/1567205014666170713160407.

Fukuda, S. *et al.* (2003) 'Two distinct subpopulations of nestin-positive cells in adult mouse dentate gyrus.', *The Journal of neuroscience : the official journal of the Society for Neuroscience*. doi: 23/28/9357 [pii].

Furukawa, K. *et al.* (1996) 'Increased activity-regulating and neuroprotective efficacy of alpha-secretase-derived secreted amyloid precursor protein conferred by a C-terminal heparin-binding domain.', *Journal of neurochemistry*, 67(5), pp. 1882–96.

Fusaki, N. *et al.* (2009) 'Efficient induction of transgene-free human pluripotent stem cells using a vector based on Sendai virus, an RNA virus that does not integrate into the host genome', *Proceedings of the Japan Academy, Series B*, 85(8), pp. 348–362.

Fuster-Matanzo, A. *et al.* (2011) 'Different Susceptibility to Neurodegeneration of Dorsal and Ventral Hippocampal Dentate Gyrus: A Study with Transgenic Mice Overexpressing GSK3β', *PLoS ONE*. Edited by C.-X. Gong. Public Library of Science, 6(11), p. e27262. doi: 10.1371/journal.pone.0027262.

Gao, C. and Chen, Y.-G. (2010) 'Dishevelled: The hub of Wnt signaling', *Cellular Signalling*, 22(5), pp. 717–727. doi: 10.1016/j.cellsig.2009.11.021.

Garver, T. D. *et al.* (1996) 'Microtubule assembly competence analysis of freshly-biopsied human tau, dephosphorylated tau, and Alzheimer tau.', *Journal of neuroscience research*, 44(1), pp. 12–20.

Geerts, H. (2009) 'Of Mice and Men', *CNS Drugs*, 23(11), pp. 915–926. doi: 10.2165/11310890-000000000-00000.

Gendron, T. F. and Petrucelli, L. (2009) 'The role of tau in neurodegeneration', *Molecular Neurodegeneration*, 4(1), p. 13. doi: 10.1186/1750-1326-4-13.

Geraldo, S. and Gordon-Weeks, P. R. (2009) 'Cytoskeletal dynamics in growth-cone steering', *Journal of Cell Science*, 122(20), pp. 3595–3604. doi: 10.1242/jcs.042309.

Geula, C. *et al.* (2008) 'Cholinergic Neuronal and Axonal Abnormalities Are Present Early in Aging and in Alzheimer Disease', *Journal of Neuropathology & Experimental Neurology*, 67(4), pp. 309–318.

Ghetti, B. *et al.* (2015) 'Invited review: Frontotemporal dementia caused by microtubule-associated protein tau gene (MAPT) mutations: A chameleon for neuropathology and neuroimaging', *Neuropathology and Applied Neurobiology*, pp. 24–46.

Giese, K. P. (2009) 'GSK-3: A key player in neurodegeneration and memory', *IUBMB Life*, pp. 516–521.

Giese, K. P. (2014) 'Generation of the Cdk5 activator p25 is a memory mechanism that is affected in early Alzheimer's disease.', *Frontiers in molecular neuroscience*, 7(May), p. 36.

Gilbert, S. F. (2000) *Developmental biology*. Sinauer Associates. Available at: https://www.ncbi.nlm.nih.gov/books/NBK9983/

Gilson, V. *et al.* (2015) 'Effects of Low Amyloid-β (Aβ) Concentration on Aβ1-42 Oligomers Binding and GluN2B Membrane Expression.', *Journal of Alzheimer's disease : JAD*. IOS Press, 47(2), pp. 453–66. doi: 10.3233/JAD-142529.

Goard, M. and Dan, Y. (2009) 'Basal forebrain activation enhances cortical coding of natural scenes', *Nature Neuroscience*, 12(11), pp. 1444–1449. doi: 10.1038/nn.2402.

Goate, A. *et al.* (1991) 'Segregation of a missense mutation in the amyloid precursor protein gene with familial Alzheimer's disease', *Nature*, 349(6311), pp. 704–706. doi: 10.1038/349704a0.

Goedert, M. *et al.* (1989) 'Multiple isoforms of human microtubule-associated protein tau: sequences and localization in neurofibrillary tangles of Alzheimer's disease', *Neuron*, 3(4), pp. 519–526.

Goedert, M. (1993) 'Tau protein and the neurofibrillary pathology of Alzheimer's disease.', *Trends in neurosciences*, 16(11), pp. 460–5.

Goedert, M. *et al.* (1993) 'The abnormal phosphorylation of tau protein at Ser-202 in Alzheimer disease recapitulates phosphorylation during development.', *Proceedings of the National Academy of Sciences of the United States of America*, 90(11), pp. 5066–70.

Goedert, M. *et al.* (2012) 'Frontotemporal dementia: implications for understanding Alzheimer disease', *Cold Spring Harb Perspect Med*. doi: 10.1101/cshperspect.a006254.

Goedert, M. and Jakes, R. (1990) 'Expression of separate isoforms of human tau protein: correlation with the tau pattern in brain and effects on tubulin polymerization.', *The EMBO journal*, 9(13), pp. 4225–4230.

Goedert, M. *et al.* (1995) 'Monoclonal antibody AT8 recognises tau protein phosphorylated at both serine 202 and threonine 205.', *Neuroscience letters*, 189(3), pp. 167–9.

Goedert, M. and Spillantini, M. G. (2000) 'Tau mutations in frontotemporal dementia FTDP-17 and their relevance for Alzheimer's disease', *Biochimica et Biophysica Acta - Molecular Basis of Disease*. doi: 10.1016/S0925-4439(00)00037-5.

Gong, C.-X. and Iqbal, K. (2008) 'Hyperphosphorylation of microtubule-associated protein tau: a promising therapeutic target for Alzheimer disease.', *Current medicinal chemistry*. NIH Public Access, 15(23), pp. 2321–8.

Gong, C. X. *et al.* (1993) 'Phosphoprotein phosphatase activities in Alzheimer disease brain.', *Journal of neurochemistry*, 61(3), pp. 921–7.

Goni-Oliver, P. *et al.* (2007) 'N-terminal Cleavage of GSK-3 by Calpain: A new form of GSK-3 regulation', *Journal of Biological Chemistry*, 282(31), pp. 22406–22413.

Goold, R. G. and Gordon-Weeks, P. R. (2004) 'Glycogen synthase kinase 3β and the regulation of axon growth: Figure 1', *Biochemical Society Transactions*, 32(5), pp. 809–811.

Gordon, J. *et al.* (2013) 'General overview of neuronal cell culture.', *Methods in molecular biology (Clifton, N.J.)*. NIH Public Access, 1078, pp. 1–8. doi: 10.1007/978-1-62703-640-5_1.

Gotz, J. *et al.* (2001) 'Formation of Neurofibrillary Tangles in P301L Tau Transgenic Mice Induced by Abeta 42 Fibrils', *Science*, 293(5534), pp. 1491–1495. doi: 10.1126/science.1062097.

Götz, J. and Ittner, L. M. (2008) 'Animal models of Alzheimer's disease and frontotemporal dementia', *Nature Reviews Neuroscience*. Nature Publishing Group, 9(7), pp. 532–544. doi: 10.1038/nrn2420.

Gousset, K. *et al.* (2009) 'Prions hijack tunnelling nanotubes for intercellular spread', *Nature Cell Biology*, 11(3), pp. 328–336. doi: 10.1038/ncb1841.

Greco, S. J. *et al.* (2009) 'Leptin inhibits glycogen synthase kinase-3β to prevent tau phosphorylation in neuronal cells', *Neuroscience Letters*, 455(3), pp. 191–194. doi: 10.1016/j.neulet.2009.03.066.

Greenamyre, J. T. (1986) 'The Role of Glutamate in Neurotransmission and in Neurologic Disease', *Archives of Neurology*. American Medical Association, 43(10), pp. 1058–1063.

Greenamyre, J. T. *et al.* (1988) 'Glutamate transmission and toxicity in Alzheimer's disease.', *Progress in neuro-psychopharmacology & biological psychiatry*, 12(4), pp. 421–30.

Greenfield, S. *et al.* (2007) 'Heterogeneity of Treatment Effects: Implications for Guidelines, Payment, and Quality Assessment', *The American Journal of Medicine*, 120(4), pp. S3–S9.

Grutzendler, J. *et al.* (2007) 'Various Dendritic Abnormalities Are Associated with Fibrillar Amyloid Deposits in Alzheimer's Disease', *Annals of the New York Academy of Sciences*, 1097(1), pp. 30–39.

Grynspan, F. *et al.* (1997) 'Active site-directed antibodies identify calpain II as an early- appearing and pervasive component of neurofibrillary pathology in Alzheimer's disease', *Brain Research*, 763(2), pp. 145–158.

Guidato, S. *et al.* (1998) 'Cyclin D2 interacts with cdk-5 and modulates cellular cdk-5/p35 activity.', *Journal of neurochemistry*, 70(1), pp. 335–340.

Gunhanlar, N. *et al.* (2017) 'A simplified protocol for differentiation of electrophysiologically mature neuronal networks from human induced pluripotent stem cells', *Molecular Psychiatry*. Nature Publishing Group. doi: 10.1038/mp.2017.56.

Guo, J.-P. *et al.* (2006) 'Abeta and tau form soluble complexes that may promote self aggregation of both into the insoluble forms observed in Alzheimer's disease', *Proceedings of the National Academy of Sciences*. doi: 10.1073/pnas.0509386103.

Guo, J. L. and Lee, V. M.-Y. (2011) 'Seeding of normal Tau by pathological Tau conformers drives pathogenesis of Alzheimer-like tangles.', *The Journal of biological chemistry*. American Society for Biochemistry and Molecular Biology, 286(17), pp. 15317–31. doi: 10.1074/jbc.M110.209296.

Haddadi, M. *et al.* (2016) 'Biochemical and Behavioral Evaluation of Human MAPT Mutations in Transgenic Drosophila melanogaster', *Biochemical Genetics*. Springer US, 54(1), pp. 61–72.

Haenseler, W. *et al.* (2017) 'A Highly Efficient Human Pluripotent Stem Cell Microglia Model Displays a Neuronal-Co-culture-Specific Expression Profile and Inflammatory Response.', *Stem cell reports*. Elsevier, 8(6), pp. 1727–1742.

Halevy, T. and Urbach, A. (2014) 'Comparing ESC and iPSC-Based Models for Human Genetic Disorders.', *Journal of clinical medicine*. Multidisciplinary Digital Publishing Institute (MDPI), 3(4), pp. 1146–62.

Hall, A. C., Lucas, F. R. and Salinas, P. C. (2000) 'Axonal Remodeling and Synaptic Differentiation in the Cerebellum Is Regulated by WNT-7a Signaling', *Cell*, 100(5), pp. 525–535. doi: 10.1016/S0092-8674(00)80689-3.

Halliday, G. *et al.* (2012) 'Mechanisms of disease in frontotemporal lobar degeneration: gain of function versus loss of function effects.', *Acta neuropathologica*. NIH Public Access, 124(3), pp. 373–82.

Hallmann, A.-L. *et al.* (2017) 'Astrocyte pathology in a human neural stem cell model of frontotemporal dementia caused by mutant TAU protein.', *Scientific reports*. Nature Publishing Group, 7, p. 42991.

Hamdane, M. *et al.* (2005) 'p25/Cdk5-mediated retinoblastoma phosphorylation is an early event in neuronal cell death.', *Journal of cell science*, 118(Pt 6), pp. 1291–8.

Hamos, J. E. *et al*. (1989) 'Synaptic loss in Alzheimer's disease and other dementias.', *Neurology*, 39(3),

pp. 355–61.

Han, D. *et al.* (2009) 'Familial FTDP-17 Missense Mutations Inhibit Microtubule Assembly-promoting Activity of Tau by Increasing Phosphorylation at Ser 202 in Vitro'. doi: 10.1074/jbc.M901095200.

Han, P. (2005) 'Suppression of Cyclin-Dependent Kinase 5 Activation by Amyloid Precursor Protein: A Novel Excitoprotective Mechanism Involving Modulation of Tau Phosphorylation', *Journal of Neuroscience*, 25(50), pp. 11542–11552.

Hanger, D. P. *et al.* (1992) 'Glycogen synthase kinase-3 induces Alzheimer's disease-like phosphorylation of tau: Generation of paired helical filament epitopes and neuronal localisation of the kinase', *Neuroscience Letters*, 147(1), pp. 58–62.

Hanger, D. P. *et al.* (2007) 'Novel phosphorylation sites in tau from Alzheimer brain support a role for casein kinase 1 in disease pathogenesis.', *The Journal of biological chemistry*. American Society for Biochemistry and Molecular Biology, 282(32), pp. 23645–54.

Hanger, D. P. *et al.* (2014) 'Intracellular and extracellular roles for tau in neurodegenerative disease', *Journal of Alzheimer's Disease*. doi: 10.3233/JAD-132054.

Hanger, D. P. *et al.* (2009) 'Tau phosphorylation: the therapeutic challenge for neurodegenerative disease', *Trends in Molecular Medicine*. doi: 10.1016/j.molmed.2009.01.003.

Hanger, D. P. and Noble, W. (2011) 'Functional Implications of Glycogen Synthase Kinase-3-Mediated Tau Phosphorylation', *SAGE-Hindawi Access to Research International Journal of Alzheimer's Disease*, 11. doi: 10.4061/2011/352805.

Harada, T. and Kuroda, R. (2011) 'CD measurements of ??-amyloid (1-40) and (1-42) in the condensed phase', *Biopolymers*. doi: 10.1002/bip.21543.

Hardy, J. (2014) 'The genetics of frontotemporal dementia [video file]'. The Biomedical and Life Sciences Collection, Henry Stewart Talks. Available at: https://hstalks.com/bs/2835.

Hardy, J. A. and Higgins, G. A. (1992) 'Alzheimer's disease: the amyloid cascade hypothesis.', *Science (New York, N.Y.)*, 256(5054), pp. 184–5.

Hardy, J. and Selkoe, D. J. (2002) 'The amyloid hypothesis of Alzheimer's disease: progress and problems on the road to therapeutics.', *Science (New York, N.Y.)*. doi: 10.1126/science.1072994.

Harold, D. *et al.* (2009) 'Genome-wide association study identifies variants at CLU and PICALM associated with Alzheimer's disease', *Nature Genetics*, 41(10), pp. 1088–1093. doi: 10.1038/ng.440.

Harris, J. A. *et al.* (2012) 'Human P301L-Mutant Tau Expression in Mouse Entorhinal-Hippocampal Network Causes Tau Aggregation and Presynaptic Pathology but No Cognitive Deficits', *PLoS ONE*. Edited by T. Ikezu, 7(9), p. e45881.

Hasegawa, M. *et al.* (1998) 'Tau proteins with FTDP-17 mutations have a reduced ability to promote microtubule assembly', *FEBS Letters*. doi: 10.1016/S0014-5793(98)01217-4.

Hashiguchi, M. *et al.* (2002) 'Truncation of CDK5 activator p35 induces intensive phosphorylation of Ser202/Thr205 of human tau', *Journal of Biological Chemistry*, 277(46), pp. 44525–44530.

Hashiguchi, M. and Hashiguchi, T. (2013) 'Kinase–Kinase Interaction and Modulation of Tau Phosphorylation', in *International review of cell and molecular biology*, pp. 121–160.

Hawasli, A. H. *et al.* (2007) 'Cyclin-dependent kinase 5 governs learning and synaptic plasticity via control of NMDAR degradation.', *Nature neuroscience*, 10(7), pp. 880–6.

Hayashi, K. *et al.* (2006) 'Phosphorylation of the tubulin-binding protein, stathmin, by Cdk5 and MAP kinases in the brain', *Journal of Neurochemistry*, 99(1), pp. 237–250.

Hayashi, M. L. *et al.* (2004) 'Altered Cortical Synaptic Morphology and Impaired Memory Consolidation in Forebrain- Specific Dominant-Negative PAK Transgenic Mice', *Neuron*, 42(5), pp. 773–787. doi: 10.1016/j.neuron.2004.05.003.

Hayashi, M. L. *et al.* (2007) 'Inhibition of p21-activated kinase rescues symptoms of fragile X syndrome in mice', *Proceedings of the National Academy of Sciences*, 104(27), pp. 11489–11494. doi: 10.1073/pnas.0705003104.

Heins, N. *et al.* (2002) 'Glial cells generate neurons: the role of the transcription factor Pax6', *Nature Neuroscience*, 5(4), pp. 308–315. doi: 10.1038/nn828.

Hellstrand, E. *et al.* (2010) 'Amyloid β-protein aggregation produces highly reproducible kinetic data and occurs by a two-phase process', *ACS Chemical Neuroscience*. doi: 10.1021/cn900015v.

Hemmings, B. A. *et al.* (1981) 'Purification of Glycogen Synthase Kinase 3 from Rabbit Skeletal Muscle.. Copurification with the Activating Factor (FA)of the (Mg-ATP) Dependent Protein Phosphatase.', *European Journal of Biochemistry*. Blackwell Publishing Ltd, 119(3), pp. 443–451.

Héraud, C. *et al.* (2014) 'Increased misfolding and truncation of tau in APP/PS1/tau transgenic mice compared to mutant tau mice', *Neurobiology of Disease*, 62, pp. 100–112. doi: 10.1016/j.nbd.2013.09.010.

Hernández, F. *et al.* (2009a) 'The role of GSK3 in Alzheimer disease', *Brain Research Bulletin*, pp. 248–250.

Hernandez, P. *et al.* (2009b) 'Tau phosphorylation by cdk5 and Fyn in response to amyloid peptide Aβ 25-35: Involvement of lipid rafts', *Journal of Alzheimer's Disease*, 16(1), pp. 149–156.

Hertel, C. *et al.* (1997) 'Inhibition of the electrostatic interaction between beta-amyloid peptide and membranes prevents beta-amyloid-induced toxicity.', *Proceedings of the National Academy of Sciences of the United States of America*.

Hevner, R. F. *et al.* (2001) 'Tbr1 regulates differentiation of the preplate and layer 6.', *Neuron*, 29(2), pp. 353–66.

Hevner, R. F. *et al.* (2006) 'Transcription factors in glutamatergic neurogenesis: Conserved programs in neocortex, cerebellum, and adult hippocampus', *Neuroscience Research*, 55(3), pp. 223–233. doi: 10.1016/j.neures.2006.03.004.

Hewitt, K. J. and Garlick, J. A. (2013) 'Cellular reprogramming to reset epigenetic signatures', *Molecular Aspects of Medicine*. doi: 10.1016/j.mam.2012.08.002.

Hirschbichler, S. T. *et al.* (2015) 'Classic PD-like rest tremor associated with the tau p.R406W mutation.', *Parkinsonism & related disorders*. Elsevier, 21(8), pp. 1002–4. doi: 10.1016/j.parkreldis.2015.05.012.

Hisanaga, S. and Endo, R. (2010) 'Regulation and role of cyclin-dependent kinase activity in neuronal survival and death.', *Journal of neurochemistry*, 115(6), pp. 1309–21.

Hlavanda, E. *et al.* (2007) 'Phosphorylation blocks the activity of tubulin polymerization-promoting protein (TPPP): Identification of sites targeted by different kinases', *Journal of Biological Chemistry*, 282(40), pp. 29531–29539.

Hodges, J. R. (2001) 'Frontotemporal dementia (Pick's disease): Clinical features and assessment', *Neurology*. Lippincott Williams & Wilkins, 56(Supplement 4), pp. S6–S10.

Hoffmann, N. A. *et al.* (2013) 'Impaired plasticity of cortical dendritic spines in P301S tau transgenic mice.', *Acta neuropathologica communications*. BioMed Central, 1, p. 82. doi: 10.1186/2051-5960-1-82.

Höglund, K. *et al.* (2008) 'Prediction of Alzheimer's disease using a cerebrospinal fluid pattern of C-terminally truncated β-amyloid peptides', *Neurodegenerative Diseases*. doi: 10.1159/000119457.

Holderness Parker, N. *et al.* (2013) 'p21-Activated Kinase 3 (PAK3) Is an AP-1 Regulated Gene Contributing to Actin Organisation and Migration of Transformed Fibroblasts', *PLoS ONE*. doi: 10.1371/journal.pone.0066892.

Holmes, B. B. *et al.* (2013) 'Heparan sulfate proteoglycans mediate internalization and propagation of specific proteopathic seeds', *Proceedings of the National Academy of Sciences*, 110(33), pp. E3138–E3147. doi: 10.1073/pnas.1301440110.

Hong, M. *et al.* (1998) 'Mutation-specific functional impairments in distinct tau isoforms of hereditary FTDP-17.', *Science (New York, N.Y.)*, 282(5395), pp. 1914–7.

Hong, S. *et al.* (2016) 'Complement and microglia mediate early synapse loss in Alzheimer mouse models.', *Science (New York, N.Y.)*. American Association for the Advancement of Science, 352(6286), pp. 712–716..

Hooper, C. *et al.* (2007) 'Glycogen synthase kinase-3 inhibition is integral to long-term potentiation', *European Journal of Neuroscience*, 25(1), pp. 81–86. doi: 10.1111/j.1460-9568.2006.05245.x.

Hoshi, M. *et al.* (2003) 'Spherical aggregates of beta-amyloid (amylospheroid) show high neurotoxicity and activate tau protein kinase I/glycogen synthase kinase-3beta.', *Proceedings of the National Academy of Sciences of the United States of America*. National Academy of Sciences, 100(11), pp. 6370–5.

Hossini, A. M. *et al.* (2015) 'Induced pluripotent stem cell-derived neuronal cells from a sporadic Alzheimer's disease donor as a model for investigating AD-associated gene regulatory networks', *BMC Genomics*. doi: 10.1186/s12864-015-1262-5\rs12864-015-1262-5 [pii].

Hsiao, Y.-H. *et al.* (2008) 'N-acetylcysteine prevents beta-amyloid toxicity by a stimulatory effect on p35/cyclin-dependent kinase 5 activity in cultured cortical neurons.', *Journal of neuroscience research*. doi: 10.1002/jnr.21710.

Huang, E. P. (1998) 'Synaptic plasticity: going through phases with LTP.', *Current biology : CB*, 8(10), pp. R350-2.

Huang, W. *et al.* (2011) 'p21-Activated Kinases 1 and 3 Control Brain Size through Coordinating Neuronal Complexity and Synaptic Properties', *Molecular and Cellular Biology*, 31(3), pp. 388–403. doi: 10.1128/MCB.00969-10.

Humbert, S. *et al.* (2000) 'P39 Activates Cdk5 in Neurons, and Is Associated With the Actin Cytoskeleton.', *Journal of cell science*, 113 (Pt 6, pp. 975–983.

Hurtado, D. E. *et al.* (2012) 'Selectively Silencing GSK-3 Isoforms Reduces Plaques and Tangles in Mouse Models of Alzheimer's Disease', *Journal of Neuroscience*. doi: 10.1523/JNEUROSCI.0889-12.2012.

Hutton, M. *et al.* (1998) 'Association of missense and 5'-splice-site mutations in tau with the inherited dementia FTDP-17.', *Nature*, 393(6686), pp. 702–5.

Hye, A. *et al.* (2004) 'Glycogen synthase kinase-3 is increased in white cells early in Alzheimer's disease', *Neuroscience Letters*, 373(1), pp. 1–4. doi: http://dx.doi.org/10.1016/j.neulet.2004.10.031.

Iba, M. *et al.* (2013) 'Synthetic Tau Fibrils Mediate Transmission of Neurofibrillary Tangles in a Transgenic Mouse Model of Alzheimer's-Like Tauopathy', *Journal of Neuroscience*. doi: 10.1523/JNeurosci.2642-12.2013.

Iijima, K. *et al.* (2000) 'Neuron-specific phosphorylation of Alzheimer's beta-amyloid precursor protein by cyclin-dependent kinase 5.', *Journal of neurochemistry*, 75(3), pp. 1085–91.

Ikeda, M. *et al.* (2005) 'Accumulation of filamentous tau in the cerebral cortex of human tau R406W transgenic mice.', *The American journal of pathology*. American Society for Investigative Pathology, 166(2), pp. 521–31.

Ikeuchi, T. *et al.* (2008) 'Mutational analysis in early-onset familial dementia in the Japanese population. The role of PSEN1 and MAPT R406W mutations.', *Dementia and geriatric cognitive disorders*. Karger Publishers, 26(1), pp. 43–9. doi: 10.1159/000141483.

Illenberger, S. *et al.* (1998) 'The Endogenous and Cell Cycle-dependent Phosphorylation of tau Protein in Living Cells : Implications for Alzheimer ' s Disease', *Molecular Biology of the Cell*, 9(June), pp. 1495–1512.

Imahori, K. and Uchida, T. (1997) 'Physiology and pathology of tau protein kinases in relation to Alzheimer's disease.', *Journal of biochemistry*, 121(2), pp. 179–88.

Imamura, K. *et al.* (2016) 'Calcium dysregulation contributes to neurodegeneration in FTLD patient iPSC-derived neurons', *Scientific Reports*. doi: 10.1038/srep34904.

Inestrosa, N. C. and Varela-Nallar, L. (2014) 'Wnt signaling in the nervous system and in Alzheimer's disease', *Journal of Molecular Cell Biology*, 6(1), pp. 64–74. doi: 10.1093/jmcb/mjt051.

Iovino, M. *et al.* (2015) 'Early maturation and distinct tau pathology in induced pluripotent stem cell-derived neurons from patients with MAPT mutations', *Brain*. doi: 10.1093/brain/awv222.

Iqbal, K. *et al.* (1998) 'Mechanisms of neurofibrillary degeneration and the formation of neurofibrillary tangles', in. Springer, Vienna, pp. 169–180. doi: 10.1007/978-3-7091-6467-9_15.

Iqbal, K. *et al.* (2010) 'Tau in Alzheimer disease and related tauopathies.', *Current Alzheimer research*. NIH Public Access, 7(8), pp. 656–64.

Irwin, D. J. *et al.* (2013) 'Acetylated tau neuropathology in sporadic and hereditary tauopathies.', *The American journal of pathology*. American Society for Investigative Pathology, 183(2), pp. 344–51. doi: 10.1016/j.ajpath.2013.04.025.

Ishida, C. *et al.* (2015) 'Frontotemporal dementia with parkinsonism linked to chromosome 17 with the *MAPT* R406W mutation presenting with a broad distribution of abundant senile plaques', *Neuropathology*, 35(1), pp. 75–82. doi: 10.1111/neup.12154.

Ishizawa, K. *et al.* (2000) 'A double-labeling immunohistochemical study of tau exon 10 in Alzheimer's disease, progressive supranuclear palsy and Pick's disease', *Acta Neuropathologica*. Springer-Verlag, 100(3), pp. 235–244. doi: 10.1007/s004019900177.

Israel, M. A. *et al.* (2012) 'Probing sporadic and familial Alzheimer's disease using induced pluripotent stem cells', *Nature*. doi: 10.1038/nature10821.

Ittner, L. M. *et al.* (2010) 'Dendritic function of tau mediates amyloid-beta toxicity in Alzheimer's disease mouse models.', *Cell*, 142(3), pp. 387–97. doi: 10.1016/j.cell.2010.06.036.

Iwata, A. *et al.* (2014) 'Altered CpG methylation in sporadic Alzheimer's disease is associated with APP and MAPT dysregulation', *Human Molecular Genetics*. Oxford University Press, 23(3), pp. 648–656.

Jack, C. R. *et al.* (1998) 'Rate of medial temporal lobe atrophy in typical aging and Alzheimer's disease.', *Neurology*. Lippincott Williams & Wilkins, 51(4), pp. 993–9.

Janocko, N. J. *et al.* (2012) 'Neuropathologically defined subtypes of Alzheimer's disease differ significantly from neurofibrillary tangle-predominant dementia', *Acta Neuropathologica*, 124(5), pp. 681–692. doi: 10.1007/s00401-012-1044-y.

Janssen, J. C. *et al.* (2002) 'Clinical features of frontotemporal dementia due to the intronic tau 10(+16) mutation.', *Neurology*, 58(8), pp. 1161–8.

Janssen, J. C. *et al.* (2003) 'Early onset familial Alzheimer's disease: Mutation frequency in 31 families.', *Neurology*, 60(2), pp. 235–9.

Jarosz-Griffiths, H. H. *et al.* (2016) 'Amyloid-β Receptors: The Good, the Bad, and the Prion Protein', *Journal of Biological Chemistry*, 291(7), pp. 3174–3183. doi: 10.1074/jbc.R115.702704.

Jenkins, S. M. and Johnson, G. V (1999) 'Modulation of tau phosphorylation within its microtubule-binding domain by cellular thiols.', *Journal of neurochemistry*, 73(5), pp. 1843–50.

Jiang, H. *et al.* (2005) 'Both the Establishment and the Maintenance of Neuronal Polarity Require Active Mechanisms', *Cell*, 120(1), pp. 123–135. doi: 10.1016/j.cell.2004.12.033.

Jicha, G. A. *et al.* (1997) 'Alz-50 and MC-1, a new monoclonal antibody raised to paired helical filaments, recognize conformational epitopes on recombinant tau', *Journal of Neuroscience Research*.

Jicha, G. A. *et al.* (1999) 'Altered conformation of recombinant frontotemporal dementia-17 mutant tau proteins', *Neuroscience Letters*. doi: 10.1016/S0304-3940(98)00980-X.

Jin, M. *et al.* (2011) 'Soluble amyloid beta-protein dimers isolated from Alzheimer cortex directly induce Tau hyperphosphorylation and neuritic degeneration.', *Proceedings of the National Academy of Sciences of the United States of America*. National Academy of Sciences, 108(14), pp. 5819–24.

Jin, N. *et al.* (2015a) 'Truncation and Activation of Dual Specificity Tyrosine Phosphorylation-regulated Kinase 1A by Calpain I: A molecular mechanism linked to tau pathology in alzheimer disease.', *The Journal of biological chemistry*. American Society for Biochemistry and Molecular Biology, 290(24), pp. 15219–37.

Jin, N. *et al.* (2015b) 'Truncation and activation of GSK-3β by calpain I: a molecular mechanism links to tau hyperphosphorylation in Alzheimer's disease.', *Scientific reports*. Nature Publishing Group, 5, p. 8187. doi: 10.1038/srep08187.

Johansson, S. *et al.* (2006) 'Increased tau phosphorylation at the Ser396 epitope after amyloid beta-exposure in organotypic cultures', *NeuroReport*, 17(9), pp. 907–911.

Jonckheere, A. *et al.* (2012) 'Mitochondrial ATP synthase: architecture, function and pathology', *Journal of Inherited Metabolic Disease*. doi: 10.1007/s10545-011-9382-9.

Josephs, K. A. *et al.* (2005) 'Survival in two variants of tau-negative frontotemporal lobar degeneration: FTLD-U vs FTLD-MND', *Neurology*. doi: 10.1212/01.wnl.0000173178.67986.7f.

Jung, D.-W. *et al.* (2014) 'Reprogram or Reboot: Small Molecule Approaches for the Production of Induced Pluripotent Stem Cells and Direct Cell Reprogramming', *ACS Chemical Biology*. American Chemical Society, 9(1), pp. 80–95. doi: 10.1021/cb400754f.

Kadavath, H. *et al.* (2015) 'Tau stabilizes microtubules by binding at the interface between tubulin heterodimers.', *Proceedings of the National Academy of Sciences of the United States of America*. doi: 10.1073/pnas.1504081112.

Kaivorinne, A.-L. *et al.* (2008) 'Role of MAPT mutations and haplotype in frontotemporal lobar degeneration in Northern Finland', *BMC Neurology*, 8(1), p. 48. doi: 10.1186/1471-2377-8-48.

Kaneko, Y. *et al.* (2000) 'Musashi1: an evolutionally conserved marker for CNS progenitor cells including neural stem cells.', *Developmental neuroscience*. doi: 10.1159/000017435.

Kanemaru, K. *et al.* (1992) 'Fetal-type phosphorylation of the tau in paired helical filaments.', *Journal of neurochemistry*, 58(5), pp. 1667–75.

Kanungo, J. *et al.* (2009) 'Targeting Cdk5 activity in neuronal degeneration and regeneration', *Cellular and Molecular Neurobiology*, pp. 1073–1080.

Kar, S. *et al.* (2003) 'Repeat motifs of tau bind to the insides of microtubules in the absence of taxol',

EMBO Journal, 22(1), pp. 70–77. doi: 10.1093/emboj/cdg001.

Kaufman, S. K. *et al.* (2017) 'Characterization of tau prion seeding activity and strains from formaldehyde-fixed tissue', *Acta Neuropathologica Communications*. BioMed Central, 5(1), p. 41. doi: 10.1186/s40478-017-0442-8.

Kawauchi, T. *et al.* (2005) 'MAP1B phosphorylation is differentially regulated by Cdk5/p35, Cdk5/p25, and JNK', *Biochemical and Biophysical Research Communications*, 331(1), pp. 50–55.

Kawauchi, T. (2014) 'Cdk5 regulates multiple cellular events in neural development, function and disease', *Development Growth and Differentiation*. Blackwell Publishing, 56(5), pp. 335–348.

Kelly, M. L. and Chernoff, J. (2011) 'COMMENTARY Getting Smart about p21-Activated Kinases', *Molecular and cellular biologY*, 31(3), pp. 386–387. doi: 10.1128/MCB.01267-10.

Kerbler, G. M. *et al.* (2015) 'Basal forebrain atrophy contributes to allocentric navigation impairment in Alzheimer's disease patients', *Frontiers in Aging Neuroscience*, 7(SEP). doi: 10.3389/fnagi.2015.00185.

Kertesz, A. (2003) 'Pick Complex: An Integrative Approach to Frontotemporal Dementia', *The Neurologist*, 9(6), pp. 311–317. doi: 10.1097/01.nrl.0000094943.84390.cf.

Kfoury, N. *et al.* (2012) 'Trans-cellular propagation of Tau aggregation by fibrillar species.', *The Journal of biological chemistry*. American Society for Biochemistry and Molecular Biology, 287(23), pp. 19440–51.

Khan, S. S. and Bloom, G. S. (2016) 'Tau: The Center of a Signaling Nexus in Alzheimer's Disease', *Frontiers in Neuroscience*. doi: 10.3389/fnins.2016.00031.

Killick, R. *et al.* (2014) 'Clusterin regulates β-amyloid toxicity via Dickkopf-1-driven induction of the wnt–PCP–JNK pathway', *Molecular Psychiatry*. Nature Publishing Group, 19(1), pp. 88–98. doi: 10.1038/mp.2012.163.

Kim, J. K. *et al.* (2010) 'Epigenetic memory in induced pluripotent stem cells', *Nature*.

Kimura, R. *et al.* (2007) 'The DYRK1A gene, encoded in chromosome 21 Down syndrome critical region, bridges between β-amyloid production and tau phosphorylation in Alzheimer disease', *Human Molecular Genetics*, 16(1), pp. 15–23. doi: 10.1093/hmg/ddl437.

Kimura, T. *et al.* (2013) 'Isomerase Pin1 stimulates dephosphorylation of Tau protein at cyclin-dependent kinase (Cdk5)-dependent Alzheimer phosphorylation sites', *Journal of Biological Chemistry*, 288(11), pp. 7968–7977.

Kimura, T. *et al.* (2014) 'Physiological and pathological phosphorylation of tau by Cdk5'. doi: 10.3389/fnmol.2014.00065.

Kimura, T. *et al.* (2016) 'Quantitative and combinatory determination of in situ phosphorylation of tau and its FTDP-17 mutants.', *Scientific reports*. doi: 10.1038/srep33479.

Kimura, T. *et al.* (1996) 'Sequential changes of tau-site-specific phosphorylation during development of paired helical filaments.', *Dementia (Basel, Switzerland)*, 7(4), pp. 177–81.

Kirschenbaum, F. *et al.* (2001a) 'Glycogen Synthase Kinase-3β Regulates Presenilin 1 C-terminal Fragment Levels', *Journal of Biological Chemistry*, 276(33), pp. 30701–30707. doi: 10.1074/jbc.M102849200.

Kirschenbaum, F. *et al.* (2001b) 'Substitution of a Glycogen Synthase Kinase-3β Phosphorylation Site in Presenilin 1 Separates Presenilin Function from β-Catenin Signaling', *Journal of Biological Chemistry*, 276(10), pp. 7366–7375. doi: 10.1074/jbc.M004697200.

Kirschner, M. and Mitchison, T. (1986) 'Beyond self-assembly: from microtubules to morphogenesis.',

Cell, 45(3), pp. 329–42.

Klein, W. L. (2013) 'Synaptotoxic amyloid-β oligomers: a molecular basis for the cause, diagnosis, and treatment of Alzheimer's disease?', *Journal of Alzheimer's disease : JAD*, 33 Suppl 1, pp. S49-65. doi: 10.3233/JAD-2012-129039.

Koch, G. *et al.* (2012) 'Impaired LTP- but not LTD-like cortical plasticity in Alzheimer's disease patients.', *Journal of Alzheimer's disease : JAD*, 31(3), pp. 593–9. doi: 10.3233/JAD-2012-120532.

Koga, S. *et al.* (2017) 'Fluorescence and autoradiographic evaluation of tau PET ligand PBB3 to α-synuclein pathology', *Movement Disorders*, 32(6), pp. 884–892. doi: 10.1002/mds.27013.

Koh, S.-H. *et al.* (2008) 'Amyloid-beta-induced neurotoxicity is reduced by inhibition of glycogen synthase kinase-3', *Brain Research*, 1188, pp. 254–262. doi: 10.1016/j.brainres.2007.10.064.

Koistinaho, M. *et al.* (2004) 'Apolipoprotein E promotes astrocyte colocalization and degradation of deposited amyloid-β peptides', *Nature Medicine*, 10(7), pp. 719–726. doi: 10.1038/nm1058.

Kolarova, M. *et al.* (2012) 'Structure and Pathology of Tau Protein in Alzheimer Disease', *International Journal of Alzheimer's Disease*. Hindawi, 2012, pp. 1–13. doi: 10.1155/2012/731526.

Kondo, T. *et al.* (2013) 'Modeling Alzheimer's disease with iPSCs reveals stress phenotypes associated with intracellular Aβ and differential drug responsiveness', *Cell Stem Cell*, 12(4). doi: 10.1016/j.stem.2013.01.009.

Kopeikina, K. J. *et al.* (2011) 'Tau accumulation causes mitochondrial distribution deficits in neurons in a mouse model of tauopathy and in human Alzheimer's disease brain.', *The American journal of pathology*. American Society for Investigative Pathology, 179(4), pp. 2071–82.

Kosik, K. S. *et al.* (1989) 'Developmentally regulated expression of specific tau sequences.', *Neuron*, 2(4), pp. 1389–97.

Kovalevich, J. and Langford, D. (2013) 'Considerations for the Use of SH-SY5Y Neuroblastoma Cells in Neurobiology', in *Neuronal Cell Culture*. doi: 10.1007/978-1-62703-640-5_2.

Kozikowski, A. P. *et al.* (2006) 'Highly Potent and Specific GSK-3β Inhibitors That Block Tau Phosphorylation and Decrease α-Synuclein Protein Expression in a Cellular Model of Parkinson's Disease', *ChemMedChem*. WILEY-VCH Verlag, 1(2), pp. 256–266. doi: 10.1002/cmdc.200500039.

Kraemer, B. C. *et al.* (2003) 'Neurodegeneration and defective neurotransmission in a Caenorhabditis elegans model of tauopathy', *Proceedings of the National Academy of Sciences*, 100(17), pp. 9980–9985. doi: 10.1073/pnas.1533448100.

Kraemer, B. C. *et al.* (2006) 'Molecular pathways that influence human tau-induced pathology in Caenorhabditis elegans', *Human Molecular Genetics*, 15(9), pp. 1483–1496. doi: 10.1093/hmg/ddl067.

Kreis, P. and Barnier, J. V. (2009) 'PAK signalling in neuronal physiology', *Cellular Signalling*. doi: 10.1016/j.cellsig.2008.11.001.

Krishtal, J. *et al.* (2015) 'Toxicity of amyloid beta 1-40 and 1-42 on SH-SY5Y cell line', *SpringerPlus*. Springer, 4(Suppl 1), p. P19. doi: 10.1186/2193-1801-4-S1-P19.

Krstic, D. and Knuesel, I. (2012) 'Deciphering the mechanism underlying late-onset Alzheimer disease', *Nature Reviews Neurology*. doi: 10.1038/nrneurol.2012.236.

Krylova, O. *et al.* (2000) 'Dishevelled-1 regulates microtubule stability: a new function mediated by glycogen synthase kinase-3beta.', *The Journal of cell biology*. The Rockefeller University Press, 151(1), pp. 83–94.

Ksiezak-Reding, H. *et al.* (2003a) 'Akt/PKB kinase phosphorylates separately Thr212 and Ser214 of tau protein in vitro', *Biochimica et Biophysica Acta - Molecular Basis of Disease*, 1639(3), pp. 159–168.

Ksiezak-Reding, H. *et al.* (2003b) 'Akt/PKB kinase phosphorylates separately Thr212 and Ser214 of tau protein in vitro', *Biochimica et Biophysica Acta - Molecular Basis of Disease*. doi: 10.1016/j.bbadis.2003.09.001.

Kuhn, J. *et al.* (2015) 'Deep brain stimulation of the nucleus basalis of Meynert in Alzheimer's dementia.', *Molecular psychiatry*. doi: 10.1038/mp.2014.32.

Kuijlaars, J. *et al.* (2016) 'Sustained synchronized neuronal network activity in a human astrocyte co-culture system', *Scientific Reports*. Nature Publishing Group, 6(1), p. 36529. doi: 10.1038/srep36529.

Kuo, Y.-M. *et al.* (1996) 'Water-soluble A(N-40, N-42) Oligomers in Normal and Alzheimer Disease Brains', *Journal of Biological Chemistry*. doi: 10.1074/jbc.271.8.4077.

Kusakawa, G. I. *et al.* (2000) 'Calpain-dependent proteolytic cleavage of the p35 cyclin-dependent kinase 5 activator to p25', *Journal of Biological Chemistry*, 275(22), pp. 17166–17172.

Kyoung Pyo, H. *et al.* (2004) 'Phosphorylation of tau at THR212 and SER214 in human neuronal and glial cultures: The role of AKT', *Neuroscience*. doi: 10.1016/j.neuroscience.2004.05.036.

De La Mota-Peynado, A. *et al.* (2011) 'Identification of the atypical MAPK Erk3 as a novel substrate for p21-activated Kinase (Pak) activity', *Journal of Biological Chemistry*. doi: 10.1074/jbc.M110.181743.

Lambert, J.-C. *et al.* (2009) 'Genome-wide association study identifies variants at CLU and CR1 associated with Alzheimer's disease', *Nature Genetics*, 41(10), pp. 1094–1099. doi: 10.1038/ng.439.

Lambourne, S. L. *et al.* (2005) 'Increased tau Phosphorylation on Mitogen-Activated Protein Kinase Consensus Sites and Cognitive Decline in Transgenic Models for Alzheimer's Disease and FTDP-17: Evidence for Distinct Molecular Processes Underlying tau Abnormalities', *Molecular and Cellular Biology*, 25(1), pp. 278–293. doi: 10.1128/MCB.25.1.278-293.2005.

Lancaster, M. A. *et al.* (2012) 'Cerebral organoids model human brain development and microcephaly.', *Nature*. doi: 10.1038/nature12517.

Landes, A. M. *et al.* (2001) 'Apathy in Alzheimer's disease', *Journal of the American Geriatrics Society*, 49(12), pp. 1700–1707. doi: 10.1046/j.1532-5415.2001.49282.x.

LaPointe, N. E. *et al.* (2009) 'The amino terminus of tau inhibits kinesin-dependent axonal transport: Implications for filament toxicity', *Journal of Neuroscience Research*, 87(2), pp. 440–451. doi: 10.1002/jnr.21850.

Larner, A. and Doran, M. (2008) 'Clinical Heterogeneity Associated with Tau Gene Mutations', *European Neurological Review*, 3(2), p. 31. doi: 10.17925/ENR.2008.03.02.31.

Larner, A. J. (2008) 'Mutation Negative Early-onset Familial Alzheimer Disease???: Consider Screening for Tau Gene Mutations', *Alzheimer Disease & Associated Disorders*, 22(2), pp. 194–195.

Larner, A. J. (2009) 'Intrafamilial clinical phenotypic heterogeneity with MAPT gene splice site IVS10+16C>T mutation', *Journal of the Neurological Sciences*, 287(1–2), pp. 253–256.

Larner, A. J. and Doran, M. (2006) 'Clinical phenotypic heterogeneity of Alzheimer's disease associated with mutations of the presenilin–1 gene', *Journal of Neurology*, 253(2), pp. 139–158. doi: 10.1007/s00415-005-0019-5.

Lasagna-Reeves, C. A. *et al.* (2012) 'Alzheimer brain-derived tau oligomers propagate pathology from endogenous tau.', *Scientific reports*. Nature Publishing Group, 2, p. 700. doi: 10.1038/srep00700.

Lau, K.-F. *et al.* (2002) 'Cyclin-dependent kinase-5/p35 phosphorylates Presenilin 1 to regulate carboxy-terminal fragment stability.', *Molecular and cellular neurosciences*, 20(1), pp. 13–20.

Laurijssens, B. *et al.* (2013) 'Animal models of Alzheimer's disease and drug development'. doi: 10.1016/j.ddtec.2012.04.001.

Leclerc, S. *et al.* (2001) 'Indirubins inhibit glycogen synthase kinase-3 beta and CDK5/p25, two protein kinases involved in abnormal tau phosphorylation in Alzheimer's disease. A property common to most cyclin-dependent kinase inhibitors?', *The Journal of biological chemistry*. American Society for Biochemistry and Molecular Biology, 276(1), pp. 251–60. doi: 10.1074/jbc.M002466200.

Lee, H.-K. *et al.* (2016) 'Three Dimensional Human Neuro-Spheroid Model of Alzheimer's Disease Based on Differentiated Induced Pluripotent Stem Cells', *PLOS ONE*. Edited by R. Yan. Public Library of Science, 11(9), p. e0163072. doi: 10.1371/journal.pone.0163072.

Lee, H. G. *et al.* (2002) 'Differential regulation of glutamate receptors in Alzheimer's disease', *Neurosignals*. doi: 10.1159/000067427 [doi]\rnsg11282 [pii].

Lee, K. Y. *et al.* (1999) 'Elevated neuronal Cdc2-like kinase activity in the Alzheimer disease brain.', *Neuroscience research*, 34(1), pp. 21–9.

Lee, M. *et al.* (2000) 'Neurotoxicity induces cleavage of p35 to p25 by calpain', *Nature*. Nature Publishing Group, 405(6784), pp. 360–364. doi: 10.1038/35012636.

Lee, N. *et al.* (1997) 'Activation of hPAK65 by caspase cleavage induces some of the morphological and biochemical changes of apoptosis', *Cell Biology*, 94, pp. 13642–13647.

Lee, V. M.-Y. *et al.* (2001) 'Neurodegenerative Tauopathies', *Annual review of neuroscience*, 24, pp. 1121–159. doi: 10.1146/annurev.neuro.24.1.1121.

Lee, V. M. Y. *et al.* (2011) 'Developing therapeutic approaches to tau, selected kinases, and related neuronal protein targets.', *Cold Spring Harbor perspectives in medicine*. doi: 10.1101/cshperspect.a006437.

Lee, Y. *et al.* (2010) 'Systematic review of health behavioral risks and cognitive health in older adults', *International Psychogeriatrics*, 22(2), p. 174. doi: 10.1017/S1041610209991189.

Lei, P. *et al.* (2011) 'GSK-3 in Neurodegenerative Diseases', *International Journal of Alzheimer's Disease*. Hindawi Publishing Corporation, 2011, pp. 1–9.

Leroy, K. *et al.* (2002) 'The active form of glycogen synthase kinase-3beta is associated with granulovacuolar degeneration in neurons in Alzheimer's disease.', *Acta neuropathologica*, 103(2), pp. 91–9. doi: 10.1007/s004010100435.

Leroy, K. *et al.* (2012) 'Lack of tau proteins rescues neuronal cell death and decreases amyloidogenic processing of APP in APP/PS1 mice', *American Journal of Pathology*. doi: 10.1016/j.ajpath.2012.08.012.

Leroy, K. *et al.* (2007) 'Increased level of active GSK-3? in Alzheimer's disease and accumulation in argyrophilic grains and in neurones at different stages of neurofibrillary degeneration', *Neuropathology and Applied Neurobiology*, 33(1), pp. 43–55.

Leugers, C. J. and Lee, G. (2010) 'Tau potentiates nerve growth factor-induced mitogen-activated protein kinase signaling and neurite initiation without a requirement for microtubule binding', *Journal of Biological Chemistry*. doi: 10.1074/jbc.M110.105387.

Levy-Lahad, E. *et al.* (1995) 'Candidate gene for the chromosome 1 familial Alzheimer's disease locus.', *Science (New York, N.Y.)*, 269(5226), pp. 973–7.

Lew, J. *et al.* (1994) 'A brain-specific activator of cyclin-dependent kinase 5', *Nature*, 371(6496), pp. 423–426.

Lewis, J. *et al.* (2001) 'Enhanced neurofibrillary degeneration in transgenic mice expressing mutant tau and APP.', *Science*. doi: 10.1126/science.1058189.

Li, B.-S. *et al.* (2002) 'Cyclin-dependent kinase 5 prevents neuronal apoptosis by negative regulation of

c-Jun N-terminal kinase 3.', *The EMBO journal*, 21(3), pp. 324–333. doi: 10.1093/emboj/21.3.324.

Li, G. *et al.* (2003) 'Stabilization of the cyclin-dependent kinase 5 activator, p35, by paclitaxel decreases β-amyloid toxicity in cortical neurons', *Journal of Neurochemistry*, 84(2), pp. 347–362.

Li, T. *et al.* (2006) 'Cyclin-dependent protein kinase 5 primes microtubule-associated protein tau site-specifically for glycogen synthase kinase 3beta.', *Biochemistry*, 45(10), pp. 3134–45. doi: 10.1021/bi051635j.

Li, W. *et al.* (2016) 'p39 Is Responsible for Increasing Cdk5 Activity during Postnatal Neuron Differentiation and Governs Neuronal Network Formation and Epileptic Responses', *Journal of Neuroscience*, 36(44), pp. 11283–11294. doi: 10.1523/JNEUROSCI.1155-16.2016.

Liang, G. and Zhang, Y. (2013) 'Genetic and epigenetic variations in iPSCs: potential causes and implications for application.', *Cell stem cell*. NIH Public Access, 13(2), pp. 149–59. doi: 10.1016/j.stem.2013.07.001.

Liang, W. S. *et al.* (2008) 'Altered neuronal gene expression in brain regions differentially affected by Alzheimer's disease: a reference data set.', *Physiological genomics*. NIH Public Access, 33(2), pp. 240–56. doi: 10.1152/physiolgenomics.00242.2007.

Liang, W. S. *et al.* (2010) 'Neuronal gene expression in non-demented individuals with intermediate Alzheimer's Disease neuropathology.', *Neurobiology of aging*. NIH Public Access, 31(4), pp. 549–66. doi: 10.1016/j.neurobiolaging.2008.05.013.

Lightcap, C. M. *et al.* (2009) 'Interaction with LC8 is required for Pak1 nuclear import and is indispensable for zebrafish development.', *PloS one*. Public Library of Science, 4(6), p. e6025. doi: 10.1371/journal.pone.0006025.

Lim, J. P. and Gleeson, P. A. (2011) 'Macropinocytosis: an endocytic pathway for internalising large gulps', *Immunology and Cell Biology*, 89(8), pp. 836–843. doi: 10.1038/icb.2011.20.

Lindquist, S. G. *et al.* (2008) 'Alzheimer disease-like clinical phenotype in a family with FTDP-17 caused by a MAPT R406W mutation', *European Journal of Neurology*. Blackwell Publishing Ltd, 15(4), pp. 377–385.

Lindwall, G. and Cole, R. D. (1984) 'Phosphorylation affects the ability of tau protein to promote microtubule assembly.', *The Journal of biological chemistry*, 259(8), pp. 5301–5.

Lippa, C. F. (2004) 'Synaptophysin immunoreactivity in Pick's disease: Comparison with Alzheimer's disease and dementia with Lewy bodies', *American Journal of Alzheimer's Disease & Other Dementiasr*. Sage PublicationsSage CA: Thousand Oaks, CA, 19(6), pp. 341–344.

Lisman, J. (2003) 'Long-term potentiation: outstanding questions and attempted synthesis', *Philosophical Transactions of the Royal Society B: Biological Sciences*, 358(1432), pp. 829–842. doi: 10.1098/rstb.2002.1242.

Liu, A. K. L. *et al.* (2015) 'Nucleus basalis of Meynert revisited: anatomy, history and differential involvement in Alzheimer's and Parkinson's disease', *Acta Neuropathologica*. Springer Berlin Heidelberg, 129(4), pp. 527–540. doi: 10.1007/s00401-015-1392-5.

Liu, C.-C. *et al.* (2013) 'Apolipoprotein E and Alzheimer disease: risk, mechanisms and therapy', *Nature Reviews Neurology*. Nature Publishing Group, 9(2), pp. 106–118. doi: 10.1038/nrneurol.2012.263.

Liu, L. *et al.* (2012) 'Trans-synaptic spread of tau pathology in vivo', *PLoS ONE*. doi: 10.1371/journal.pone.0031302.

Liu, S.-L. *et al.* (2016) 'The Role of Cdk5 in Alzheimer's Disease', *Molecular Neurobiology*, 53(7), pp. 4328–4342.

Liu, X. and Brun, A. (1996) 'regional and laminar synaptic pathology in frontal lobe degeneration of non-alzheimer type', *International Journal of Geriatric Psychiatry*. John Wiley & Sons, Ltd., 11(1), pp. 47–55.

Lleó, A. *et al.* (2002) 'Frequency of mutations in the presenilin and amyloid precursor protein genes in early-onset Alzheimer disease in Spain.', *Archives of neurology*, 59(11), pp. 1759–63.

Llorens-Martín, M. *et al.* (2014) 'GSK-3β, a pivotal kinase in Alzheimer disease'. doi: 10.3389/fnmol.2014.00046.

Loh, Y.-H. *et al.* (2009) 'Generation of induced pluripotent stem cells from human blood.', *Blood*. American Society of Hematology, 113(22), pp. 5476–9. doi: 10.1182/blood-2009-02-204800.

Lopes, F. M. *et al.* (2010) 'Comparison between proliferative and neuron-like SH-SY5Y cells as an in vitro model for Parkinson disease studies', *Brain Research*, 1337, pp. 85–94. doi: 10.1016/j.brainres.2010.03.102.

Lopes, J. P. *et al.* (2007) 'Role of cyclin-dependent kinase 5 in the neurodegenerative process triggered by amyloid-beta and prion peptides: Implications for Alzheimer's disease and prion-related encephalopathies', *Cellular and Molecular Neurobiology*, 27(7), pp. 943–957. doi: 10.1007/s10571-007-9224-3.

Lopes, J. P. *et al.* (2010) 'Neurodegeneration in an A beta-induced model of Alzheimer's disease: the role of Cdk5', *Aging Cell*. doi: 10.1111/j.1474-9726.2009.00536.x.

Love, S. *et al.* (1988) 'Alz-50, ubiquitin and tau immunoreactivity of neurofibrillary tangles, Pick bodies and Lewy bodies.', *Journal of neuropathology and experimental neurology*, 47(4), pp. 393–405.

Lovestone, S. *et al.* (1994) 'Alzheimer's disease-like phosphorylation of the microtubule-associated protein tau by glycogen synthase kinase-3 in transfected mammalian cells', *Current Biology*, 4(12), pp. 1077–1086.

Lovestone, S. *et al.* (1996) 'Phosphorylation of tau by glycogen synthase kinase-3β in intact mammalian cells: The effects on the organization and stability of microtubules', *Neuroscience*, 73(4), pp. 1145–1157.

Lovestone, S. *et al.* (2014) 'A Phase II Trial of Tideglusib in Alzheimer's Disease.', *Journal of Alzheimer's disease : JAD*, 45(1), pp. 75–88. doi: 10.3233/JAD-141959.

Lu, F.-P. *et al.* (2009) 'Diabetes and the Risk of Multi-System Aging Phenotypes: A Systematic Review and Meta-Analysis', *PLoS ONE*. Edited by C. Zhang, 4(1), p. e4144. doi: 10.1371/journal.pone.0004144.

Lu, M. and Kosik, K. S. (2001) 'Competition for microtubule-binding with dual expression of tau missense and splice isoforms.', *Molecular biology of the cell*, 12(1), pp. 171–84.

Lucas, F. R. *et al.* (1998) 'Inhibition of GSK-3beta leading to the loss of phosphorylated MAP-1B is an early event in axonal remodelling induced by WNT-7a or lithium.', *Journal of cell science*, 111 (Pt 10), pp. 1351–61.

Lucas, F. R. and Salinas, P. C. (1997) 'WNT-7a Induces Axonal Remodeling and Increases Synapsin I Levels in Cerebellar Neurons', *Developmental Biology*, 192(1), pp. 31–44. doi: 10.1006/dbio.1997.8734.

Lucas, J. J. (2001) 'Decreased nuclear beta-catenin, tau hyperphosphorylation and neurodegeneration in GSK-3beta conditional transgenic mice', *The EMBO Journal*, 20(1), pp. 27–39. doi: 10.1093/emboj/20.1.27.

Luna-Munoz, J. *et al.* (2014) 'Accumulation of Abnormally Processed Tau Protein in Neuronal Cells as a Biomarker for Dementia', in *Neurochemistry*. InTech. doi: 10.5772/58305.

Luna-Muñoz, J. *et al.* (2007) 'Earliest stages of tau conformational changes are related to the appearance of a sequence of specific phospho-dependent tau epitopes in Alzheimer's disease.', *Journal of Alzheimer's disease : JAD*, 12(4), pp. 365–75.

Lund, E. T. *et al.* (2001) 'Characterization of the in vitro phosphorylation of human tau by tau protein kinase II (cdk5/p20) using mass spectrometry.', *Journal of neurochemistry*, 76, pp. 1221–1232.

Ly, P. T. T. *et al.* (2013) 'Inhibition of GSK3β-mediated BACE1 expression reduces Alzheimer-associated phenotypes.', *The Journal of clinical investigation*. American Society for Clinical Investigation, 123(1), pp. 224–35. doi: 10.1172/JCI64516.

Ma, Q.-L. *et al.* (2008) 'p21-activated Kinase-aberrant Activation and Translocation in Alzheimer Disease Pathogenesis', *Journal of Biological Chemistry*, 283(20), pp. 14132–14143.

Ma, Q.-L. *et al.* (2009) 'Beta-amyloid oligomers induce phosphorylation of tau and inactivation of insulin receptor substrate via c-Jun N-terminal kinase signaling: suppression by omega-3 fatty acids and curcumin.', *The Journal of neuroscience : the official journal of the Society for Neuroscience*. Society for Neuroscience, 29(28), pp. 9078–89. doi: 10.1523/JNEUROSCI.1071-09.2009.

Ma, Q. L. *et al.* (2006) 'Antibodies against β-amyloid reduce Aβ oligomers, glycogen synthase kinase-3β activation and phosphorylation in vivo and in vitro', *Journal of Neuroscience Research*. doi: 10.1002/jnr.20734.

Ma, T. *et al.* (2009) 'Statin's Excitoprotection Is Mediated by sAPP and the Subsequent Attenuation of Calpain-Induced Truncation Events, Likely via Rho-ROCK Signaling', *Journal of Neuroscience*, 29(36), pp. 11226–11236. doi: 10.1523/JNEUROSCI.6150-08.2009.

Maas, T. *et al.* (2000) 'Interaction of tau with the neural membrane cortex is regulated by phosphorylation at sites that are modified in paired helical filaments', *Journal of Biological Chemistry*, 275(21), pp. 15733–15740. doi: 10.1074/jbc.M000389200.

Mair, W. *et al.* (2016) 'FLEXITau: Quantifying Post-translational Modifications of Tau Protein in Vitro and in Human Disease', *Analytical Chemistry*. doi: 10.1021/acs.analchem.5b04509.

Majounie, E. *et al.* (2013) 'Variation in tau isoform expression in different brain regions and disease states', *Neurobiology of Aging*, 34(7). doi: 10.1016/j.neurobiolaging.2013.01.017.

Malatesta, P. *et al.* (2000) 'Isolation of radial glial cells by fluorescent-activated cell sorting reveals a neuronal lineage.', *Development (Cambridge, England)*, 127(24), pp. 5253–63.

Malenka, R. C. and Bear, M. F. (2004) 'LTP and LTD', *Neuron*, 44(1), pp. 5–21. doi: 10.1016/j.neuron.2004.09.012.

Malinow, R. (2011) 'New developments on the role of NMDA receptors in Alzheimer's disease', *Curr Opin Neurobiol*. doi: S0959-4388(11)00145-0 [pii]\r10.1016/j.conb.2011.09.001.

Malinow, R. and Malenka, R. C. (2002) 'AMPA receptor trafficking and synaptic plasticity', *Annu Rev Neurosci*. doi: 10.1146/annurev.neuro.25.112701.142758.

Mallon, B. S. *et al.* (2014) 'Comparison of the molecular profiles of human embryonic and induced pluripotent stem cells of isogenic origin.', *Stem cell research*. NIH Public Access, 12(2), pp. 376–86. doi: 10.1016/j.scr.2013.11.010.

Malm, T. M. *et al.* (2007) 'Pyrrolidine Dithiocarbamate Activates Akt and Improves Spatial Learning in APP/PS1 Mice without Affecting β-Amyloid Burden', *Journal of Neuroscience*, 27(14).

Mandelkow, E.-M. *et al.* (1992) 'Glycogen synthase kinase-3 and the Alzheimer-like state of microtubule-associated protein tau', *FEBS Letters*, 314(3), pp. 315–321. doi: 10.1016/0014-5793(92)81496-9.

Mandelkow, E. M. *et al.* (1996) 'Structure, microtubule interactions, and phosphorylation of tau protein.', *Annals of the New York Academy of Sciences*, 777, pp. 96–106. doi: 10.1111/j.1749-6632.1996.tb34407.x.

Mann, D. M. A. *et al.* (2001) 'Amyloid β protein deposition in patients with frontotemporal lobar degeneration: relationship to age and apolipoprotein E genotype', *Neuroscience Letters*. Elsevier, 304(3), pp. 161–164. doi: 10.1016/S0304-3940(01)01785-2.

Manuel, M. N. *et al.* (2015) 'Regulation of cerebral cortical neurogenesis by the Pax6 transcription factor.', *Frontiers in cellular neuroscience*. Frontiers Media SA, 9, p. 70. doi: 10.3389/fncel.2015.00070.

Martelli, A. *et al.* (2012) 'Understanding the genetic and molecular pathogenesis of Friedreich's ataxia through animal and cellular models.', *Disease models & mechanisms*. The Company of Biologists Ltd, 5(2), pp. 165–76. doi: 10.1242/dmm.008706.

Martin, L. *et al.* (2009) 'Inhibition of glycogen synthase kinase-3β downregulates total tau proteins in cultured neurons and its reversal by the blockade of protein phosphatase-2A', *Brain Research*, 1252, pp. 66–75.

Martin, L. *et al.* (2013) 'Tau protein kinases: Involvement in Alzheimer's disease', *Ageing Research Reviews*, 12(1), pp. 289–309. doi: 10.1016/j.arr.2012.06.003.

Martin, L. *et al.* (2011) 'Post-translational modifications of tau protein: Implications for Alzheimer's disease', *Neurochemistry International*, 58(4), pp. 458–471.

Martins, I. C. *et al.* (2008) 'Lipids revert inert Aβ amyloid fibrils to neurotoxic protofibrils that affect learning in mice', *The EMBO Journal*, 27(1), pp. 224–233. doi: 10.1038/sj.emboj.7601953.

Matsumura, N., Yamazaki, T. and Ihara, Y. (1999) 'Stable expression in Chinese hamster ovary cells of mutated tau genes causing frontotemporal dementia and parkinsonism linked to chromosome 17 (FTDP-17).', *The American journal of pathology*. American Society for Investigative Pathology, 154(6), pp. 1649–56.

Matsuo, E. S. *et al.* (1994) 'Biopsy-derived adult human brain tau is phosphorylated at many of the same sites as Alzheimer's disease paired helical filament tau.', *Neuron*, 13(4), pp. 989–1002.

Mattson, M. P. *et al.* (1993) 'Evidence for excitoprotective and intraneuronal calcium-regulating roles for secreted forms of the beta-amyloid precursor protein.', *Neuron*, 10(2), pp. 243–54.

Mazanetz, M. P. and Fischer, P. M. (2007) 'Untangling tau hyperphosphorylation in drug design for neurodegenerative diseases', *Nature Reviews Drug Discovery*, 6(6), pp. 464–479. doi: 10.1038/nrd2111.

McGaughy, J. (2005) 'Cholinergic Deafferentation of the Entorhinal Cortex in Rats Impairs Encoding of Novel But Not Familiar Stimuli in a Delayed Nonmatch-to-Sample Task', *Journal of Neuroscience*, 25(44), pp. 10273–10281.

McMillan, P. *et al.* (2008) 'Tau isoform regulation is region- and cell-specific in mouse brain.', *The Journal of comparative neurology*. NIH Public Access, 511(6), pp. 788–803. doi: 10.1002/cne.21867.

McPhie, D. L. *et al.* (2003) 'DNA synthesis and neuronal apoptosis caused by familial Alzheimer disease mutants of the amyloid precursor protein are mediated by the p21 activated kinase PAK3.', *The Journal of neuroscience : the official journal of the Society for Neuroscience*, 23(17), pp. 6914–27.

Medina, M. *et al.* (2016) 'New Features about Tau Function and Dysfunction.', *Biomolecules*. Multidisciplinary Digital Publishing Institute (MDPI), 6(2). doi: 10.3390/biom6020021.

Meng, J. *et al.* (2005) 'Abnormal Long-Lasting Synaptic Plasticity and Cognition in Mice Lacking the Mental Retardation Gene Pak3', *Journal of Neuroscience*, 25(28).

Mertens, J. *et al.* (2013) 'Embryonic Stem CelleBased Modeling of Tau Pathology in Human Neurons', *The American Journal of Pathology*, 182, pp. 1769–1779. doi: 10.1016/j.ajpath.2013.01.043.

Mertens, J. *et al.* (2015) 'Directly Reprogrammed Human Neurons Retain Aging-Associated Transcriptomic Signatures and Reveal Age-Related Nucleocytoplasmic Defects', *Cell Stem Cell*. Broad Institute of MIT and Harvard, 17(6), pp. 705–718. doi: 10.1016/j.stem.2015.09.001.

Meyer-Luehmann, M. *et al.* (2008) 'Rapid appearance and local toxicity of amyloid-β plaques in a mouse model of Alzheimer's disease', *Nature*, 451(7179), pp. 720–724. doi: 10.1038/nature06616.

Micheva, K. D. *et al.* (2010) 'Single-synapse analysis of a diverse synapse population: proteomic imaging methods and markers.', *Neuron*. NIH Public Access, 68(4), pp. 639–53. doi: 10.1016/j.neuron.2010.09.024.

Miller, J. D. *et al.* (2013) 'Human iPSC-based modeling of late-onset disease via progerin-induced aging', *Cell Stem Cell*. doi: 10.1016/j.stem.2013.11.006.

Minden, A. (2012) 'PAK4–6 in cancer and neuronal development', *Cellular Logistics*, 2(2), pp. 95–104. doi: 10.4161/cl.21171.

Mitalipov, S. and Wolf, D. (2009) 'Totipotency, Pluripotency and Nuclear Reprogramming', in *Engineering of Stem Cells*. Berlin, Heidelberg: Springer Berlin Heidelberg, pp. 185–199. doi: 10.1007/10_2008_45.

Miyajima, M. *et al.* (1995) 'Cyclin E is expressed in neurons and forms complexes with cdk5.', *Neuroreport*, pp. 1130–2.

Miyata, T. *et al.* (2001) 'Asymmetric inheritance of radial glial fibers by cortical neurons.', *Neuron*, 31(5), pp. 727–41.

Moore, S. *et al.* (2015) 'APP Metabolism Regulates Tau Proteostasis in Human Cerebral Cortex Neurons', *Cell Reports*. doi: 10.1016/j.celrep.2015.03.068.

Moreira, P. I. *et al.* (2010) 'Mitochondrial dysfunction is a trigger of Alzheimer's disease pathophysiology', *Mitochondrial Dysfunction*.

Moreno, F. J. *et al.* (1995) 'Glycogen synthase kinase 3 phosphorylates recombinant human tau protein at serine-262 in the presence of heparin (or tubulin)', *FEBS Letters*, 372(1), pp. 65–68. doi: 10.1016/0014-5793(95)00934-2.

Morfini, G. *et al.* (2004) 'A novel CDK5-dependent pathway for regulating GSK3 activity and kinesin-driven motility in neurons.', *The EMBO journal*, 23(11), pp. 2235–45.

Morris, H. R. *et al.* (2003) 'Tau exon 10 +16 mutation FTDP-17 presenting clinically as sporadic young onset PSP.', *Neurology*, 61(1), pp. 102–4.

Morris, J. K. *et al.* (2017) 'Aerobic exercise for Alzheimer's disease: A randomized controlled pilot trial', *PLoS ONE*, 12(2). doi: 10.1371/journal.pone.0170547.

Morrissette, D. A. *et al.* (2009) 'Relevance of transgenic mouse models to human Alzheimer disease.', *The Journal of biological chemistry*. American Society for Biochemistry and Molecular Biology, 284(10), pp. 6033–7. doi: 10.1074/jbc.R800030200.

Moszczynski, A. J. *et al.* (2017) 'Threonine175, a novel pathological phosphorylation site on tau protein linked to multiple tauopathies', *Acta Neuropathologica Communications*. BioMed Central, 5(1), p. 6. doi: 10.1186/s40478-016-0406-4.

Muffat, J. *et al.* (2016) 'Efficient derivation of microglia-like cells from human pluripotent stem cells', *Nature Medicine*, 22(11), pp. 1358–1367. doi: 10.1038/nm.4189.

Murata, Y. and Constantine-Paton, M. (2013) 'Postsynaptic Density Scaffold SAP102 Regulates Cortical

Synapse Development through EphB and PAK Signaling Pathway', *Journal of Neuroscience*, 33(11), pp. 5040–5052.

Muratore, C. R. *et al.* (2014) 'The familial Alzheimer's disease APPV717I mutation alters APP processing and Tau expression in iPSC-derived neurons.', *Human molecular genetics*. Oxford University Press, 23(13), pp. 3523–36. doi: 10.1093/hmg/ddu064.

Murray, M. E. *et al.* (2014) 'Clinicopathologic assessment and imaging of tauopathies in neurodegenerative dementias', *Alzheimer's Research & Therapy*, 6(1), p. 1. doi: 10.1186/alzrt231.

Myers, A. J. *et al.* (2007) 'The MAPT H1c risk haplotype is associated with increased expression of tau and especially of 4 repeat containing transcripts', *Neurobiology of Disease*, 25(3), pp. 561–570. doi: 10.1016/j.nbd.2006.10.018.

Naisbitt, S. *et al.* (2000) 'Interaction of the Postsynaptic Density-95/Guanylate Kinase Domain-Associated Protein Complex with a Light Chain of Myosin-V and Dynein', *Journal of Neuroscience*, 20(12).

Nakashima, H. *et al.* (2005) 'Chronic lithium treatment decreases tau lesions by promoting ubiquitination in a mouse model of tauopathies', *Acta Neuropathologica*. Springer-Verlag, 110(6), pp. 547–556. doi: 10.1007/s00401-005-1087-4.

Nakayama, A. Y. *et al.* (2000) 'Small GTPases Rac and Rho in the maintenance of dendritic spines and branches in hippocampal pyramidal neurons.', *The Journal of neuroscience : the official journal of the Society for Neuroscience*. Society for Neuroscience, 20(14), pp. 5329–38.

Nakayama, T. *et al.* (1999) 'Role of Cdk5 and tau phosphorylation in heterotrimeric G protein-mediated retinal growth cone collapse', *Journal of Neurobiology*, 41(3), pp. 326–339.

Narasimhan, S. *et al.* (2017) 'Pathological Tau Strains from Human Brains Recapitulate the Diversity of Tauopathies in Nontransgenic Mouse Brain.', *The Journal of neuroscience : the official journal of the Society for Neuroscience*. Society for Neuroscience, 37(47), pp. 11406–11423.

Ng, A. S. L. *et al.* (2015) 'Young-onset frontotemporal dementia in a homozygous tau R406W mutation carrier', *Annals of Clinical and Translational Neurology*, 2(12), pp. 1124–1128. doi: 10.1002/acn3.265.

Nguyen, T.-V. V. *et al.* (2008) 'Signal transduction in Alzheimer disease: p21-activated kinase signaling requires C-terminal cleavage of APP at Asp664', *Journal of Neurochemistry*. Blackwell Publishing Ltd, 104(4), pp. 1065–1080. doi: 10.1111/j.1471-4159.2007.05031.x.

Nieweg, K. *et al.* (2015) 'Alzheimer's disease-related amyloid-β induces synaptotoxicity in human iPS cell-derived neurons', 6. doi: 10.1038/cddis.2015.72.

Nistor, P. A. *et al.* (2015) 'Long-term culture of pluripotent stem-cell-derived human neurons on diamond – A substrate for neurodegeneration research and therapy', *Biomaterials*, 61, pp. 139–149.

Noble, W. *et al.* (2003) 'Cdk5 is a key factor in tau aggregation and tangle formation in vivo', *Neuron*. doi: 10.1016/S0896-6273(03)00259-9.

Noble, W. *et al.* (2005) 'Inhibition of glycogen synthase kinase-3 by lithium correlates with reduced tauopathy and degeneration in vivo.', *Proceedings of the National Academy of Sciences of the United States of America*. National Academy of Sciences, 102(19), pp. 6990–5.

Noctor, S. C. *et al.* (2001) 'Neurons derived from radial glial cells establish radial units in neocortex', *Nature*, 409(6821), pp. 714–720. doi: 10.1038/35055553.

Nölle, A. *et al.* (2013) 'Ubiquilin 2 is not associated with tau pathology.', *PloS one*. Public Library of Science, 8(9), p. e76598. doi: 10.1371/journal.pone.0076598.

Notter, T. and Knuesel, I. (2013) 'Reelin immunoreactivity in neuritic varicosities in the human

hippocampal formation of non-demented subjects and Alzheimer's disease patients.', *Acta neuropathologica communications*. BioMed Central, 1, p. 27. doi: 10.1186/2051-5960-1-27.

Oberheim, N. A. *et al.* (2006) 'Astrocytic complexity distinguishes the human brain', *Trends in Neurosciences*, 29(10), pp. 547–553. doi: 10.1016/j.tins.2006.08.004.

Oberheim, N. A. *et al.* (2009) 'Uniquely hominid features of adult human astrocytes.', *The Journal of neuroscience : the official journal of the Society for Neuroscience*. NIH Public Access, 29(10), pp. 3276–87. doi: 10.1523/JNEUROSCI.4707-08.2009.

Obermeier, A. *et al.* (1998) 'PAK promotes morphological changes by acting upstream of Rac', *The EMBO Journal*, 17(15), pp. 4328–4339.

Oda, Y. (1999) 'Choline acetyltransferase: the structure, distribution and pathologic changes in the central nervous system.', *Pathology international*. doi: 10.1046/j.1440-1827.1999.00977.x.

Odawara, A. *et al.* (2014) 'Long-term electrophysiological activity and pharmacological response of a human induced pluripotent stem cell-derived neuron and astrocyte co-culture', *Biochemical and Biophysical Research Communications*, 443(4), pp. 1176–1181. doi: 10.1016/j.bbrc.2013.12.142.

Oddo, S. (2003) 'Amyloid deposition precedes tangle formation in a triple transgenic model of Alzheimer's disease', *Neurobiology of Aging*, 24(8), pp. 1063–1070. doi: 10.1016/j.neurobiolaging.2003.08.012.

Oddo, S. *et al.* (2003) 'Triple-transgenic model of Alzheimer's Disease with plaques and tangles: Intracellular Aβ and synaptic dysfunction', *Neuron*, 39(3), pp. 409–421.

Oddo, S. *et al.* (2004) 'Aβ immunotherapy leads to clearance of early, but not late, hyperphosphorylated tau aggregates via the proteasome', *Neuron*. doi: 10.1016/j.neuron.2004.07.003.

Oddo, S. *et al.* (2006) 'Reduction of soluble A?? and tau, but not soluble A?? alone, ameliorates cognitive decline in transgenic mice with plaques and tangles', *Journal of Biological Chemistry*, 281(51), pp. 39413–39423.

Okabe, M. *et al.* (2009) 'Definitive proof for direct reprogramming of hematopoietic cells to pluripotency.', *Blood*. American Society of Hematology, 114(9), pp. 1764–7. doi: 10.1182/blood-2009-02-203695.

Okita, K. *et al.* (2008) 'Generation of mouse induced pluripotent stem cells without viral vectors.', *Science (New York, N.Y.)*, 322(5903), pp. 949–53. doi: 10.1126/science.1164270.

de Oliveira, R. M. *et al.* (2017) 'The mechanism of sirtuin 2–mediated exacerbation of alpha-synuclein toxicity in models of Parkinson disease', *PLOS Biology*. Edited by G. Bates. Public Library of Science, 15(3), p. e2000374. doi: 10.1371/journal.pbio.2000374.

Olton, D. S. (1990) 'Dementia: animal models of the cognitive impairments following damage to the basal forebrain cholinergic system.', *Brain research bulletin*.

Ostojic, J. *et al.* (2004) 'The Tau R406W Mutation Causes Progressive Presenile Dementia with Bitemporal Atrophy', *Dementia and Geriatric Cognitive Disorders*, 17(4), pp. 298–301.

Otth, C. *et al.* (2002) 'AbetaPP induces cdk5-dependent tau hyperphosphorylation in transgenic mice Tg2576.', *Journal of Alzheimer's disease : JAD*, 4(5), pp. 417–430.

Otvos, L. *et al.* (1994) 'Monoclonal antibody PHF???1 recognizes tau protein phosphorylated at serine residues 396 and 404', *Journal of Neuroscience Research*. doi: 10.1002/jnr.490390607.

Paglini, G. *et al.* (1998) 'Evidence for the participation of the neuron-specific CDK5 activator P35 during laminin-enhanced axonal growth.', *The Journal of neuroscience : the official journal of the Society for*

Neuroscience, 18(23), pp. 9858–9869.

Paglini, G. and Cáceres, A. (2001) 'The role of the Cdk5-p35 kinase in neuronal development', *European Journal of Biochemistry*. Blackwell Science Ltd, 268(6), pp. 1528–1533. doi: 10.1046/j.1432-1327.2001.02023.x.

Påhlman, S. *et al.* (1981) 'Phenotypic changes of human neuroblastoma cells in culture induced by 12-O-tetradecanoyl-phorbol-13-acetate.', *International journal of cancer*, 28(5), pp. 583–9.

Påhlman, S. *et al.* (1984) 'Retinoic acid-induced differentiation of cultured human neuroblastoma cells: a comparison with phorbolester-induced differentiation.', *Cell differentiation*, 14(2), pp. 135–44.

Paholikova, K. *et al.* (2015) 'N-terminal truncation of microtubule associated protein tau dysregulates its cellular localization', *Journal of Alzheimer's Disease*. doi: 10.3233/JAD-140996.

Palmer, A. M. and Gershon, S. (1990) 'Is the neuronal basis of Alzheimer's disease cholinergic or glutamatergic?', *FASEB journal: official publication of the Federation of American Societies for Experimental Biology*, 4(10), pp. 2745–52.

Palop, J. J. *et al.* (2006) 'A network dysfunction perspective on neurodegenerative diseases', *Nature*, 443(7113), pp. 768–773. doi: 10.1038/nature05289.

Palop, J. J. and Mucke, L. (2010) 'Amyloid-β–induced neuronal dysfunction in Alzheimer's disease: from synapses toward neural networks', *Nature Neuroscience*, 13(7), pp. 812–818. doi: 10.1038/nn.2583.

Pandey, M. K. and DeGrado, T. R. (2016) 'Glycogen Synthase Kinase-3 (GSK-3)-Targeted Therapy and Imaging.', *Theranostics*. Ivyspring International Publisher, 6(4), pp. 571–93. doi: 10.7150/thno.14334.

Parameshwaran, K. *et al.* (2007) 'Amyloid β-peptide Aβ1–42 but not Aβ1–40 attenuates synaptic AMPA receptor function', *Synapse*. Wiley Subscription Services, Inc., A Wiley Company, 61(6), pp. 367–374. doi: 10.1002/syn.20386.

Pascoal, T. A. *et al.* (2017) 'Amyloid-β and hyperphosphorylated tau synergy drives metabolic decline in preclinical Alzheimer's disease', *Molecular Psychiatry*. Nature Publishing Group, 22(2), pp. 306–311. doi: 10.1038/mp.2016.37.

Passant, U. *et al.* (2004) 'Familial Presenile Dementia with Bitemporal Atrophy', *Dementia and Geriatric Cognitive Disorders*, 17(4), pp. 287–292. doi: 10.1159/000077156.

Pastor, P. *et al.* (2002) 'Further extension of the H1 haplotype associated with progressive supranuclear palsy', *Movement Disorders*. Wiley Subscription Services, Inc., A Wiley Company, 17(3), pp. 550–556. doi: 10.1002/mds.10076.

Pastor, P. *et al.* (2015) 'MAPT H1 Haplotype is Associated with Late-Onset Alzheimer's Disease Risk in APOE ε4 Noncarriers: Results from the Dementia Genetics Spanish Consortium', *Journal of Alzheimer's Disease*. IOS Press, 49(2), pp. 343–352. doi: 10.3233/JAD-150555.

Patrick, G. N. *et al.* (1998) 'p35, the neuronal-specific activator of cyclin-dependent kinase 5 (Cdk5) is degraded by the ubiquitin-proteasome pathway', *Journal of Biological Chemistry*, 273(37), pp. 24057–24064.

Patrick, G. N. *et al.* (1999) 'Conversion of p35 to p25 deregulates Cdk5 activity and promotes neurodegeneration', *Nature*, 402(6762), pp. 615–622.

Patzke, H. and Tsai, L. H. (2002) 'Calpain-mediated cleavage of the cyclin-dependent kinase-5 activator p39 to p29', *Journal of Biological Chemistry*, 277(10), pp. 8054–8060.

Pei, J. J. *et al.* (1997) 'Distribution, levels, and activity of glycogen synthase kinase-3 in the Alzheimer disease brain.', *Journal of neuropathology and experimental neurology*, 56(1), pp. 70–8.

Pei, J. J. *et al.* (1998) 'Accumulation of cyclin-dependent kinase 5 (cdk5) in neurons with early stages

of Alzheimer's disease neurofibrillary degeneration', *Brain Research*, 797(2), pp. 267–277.

Pei, J. J. *et al.* (2001) 'Localization of active forms of C-jun kinase (JNK) and p38 kinase in Alzheimer's disease brains at different stages of neurofibrillary degeneration', *Journal of Alzheimer's disease : JAD*, 3(1), pp. 41–48.

Peineau, S. *et al.* (2007) 'LTP Inhibits LTD in the Hippocampus via Regulation of GSK3??', *Neuron*. doi: 10.1016/j.neuron.2007.01.029.

Peippo, M. *et al.* (2007) 'PAK3 related mental disability: Further characterization of the phenotype', *American Journal of Medical Genetics, Part A*. doi: 10.1002/ajmg.a.31956.

Perdahl, E. *et al.* (1984) 'Synapsin I (protein I) in different brain regions in senile dementia of Alzheimer type and in multiinfarct dementia', *Journal of Neural Transmission*. Springer-Verlag, 60(2), pp. 133–141. doi: 10.1007/BF01245030.

Pérez, M. *et al.* (2003) 'Chronic lithium treatment decreases mutant tau protein aggregation in a transgenic mouse model', *Journal of Alzheimer's Disease*. IOS Press, 5(4), pp. 301–308. doi: 10.3233/JAD-2003-5405.

Peter-Derex, L. *et al.* (2015) 'Sleep and Alzheimer's disease', *Sleep Medicine Reviews*, pp. 29–38. doi: 10.1016/j.smrv.2014.03.007.

Petry, F. R. *et al.* (2014) 'Specificity of anti-tau antibodies when analyzing mice models of Alzheimer's disease: problems and solutions.', *PloS one*. Public Library of Science, 9(5), p. e94251. doi: 10.1371/journal.pone.0094251.

Phiel, C. J. *et al.* (2003) 'GSK-3alpha regulates production of Alzheimer's disease amyloid-beta peptides.', *Nature*, 423(lane 2), pp. 435–439. doi: 10.1038/nature01640.

Pickering-Brown, S. M. *et al.* (2002) 'Inherited frontotemporal dementia in nine British families associated with intronic mutations in the tau gene.', *Brain : a journal of neurology*, 125(Pt 4), pp. 732–51.

Piguet, O. *et al.* (2011) 'Behavioural-variant frontotemporal dementia: diagnosis, clinical staging, and management', *The Lancet Neurology*, 10(2), pp. 162–172. doi: 10.1016/S1474-4422(10)70299-4.

Pijuan-Galitó, S. *et al.* (2016) 'Human serum-derived protein removes the need for coating in defined human pluripotent stem cell culture', *Nature Communications*. Nature Publishing Group, 7, p. 12170. doi: 10.1038/ncomms12170.

Pinto, L. *et al.* (2013) 'Fast modulation of visual perception by basal forebrain cholinergic neurons', *Nature Neuroscience*, 16(12), pp. 1857–1863.

Pittman, A. M., Fung, H.-C. and de Silva, R. (2006) 'Untangling the tau gene association with neurodegenerative disorders', *Human Molecular Genetics*, 15, pp. R188–R195.

Plattner, F., Angelo, M. and Giese, K. P. (2006) 'The roles of cyclin-dependent kinase 5 and glycogen synthase kinase 3 in tau hyperphosphorylation.', *The Journal of biological chemistry*, 281(35), pp. 25457–65.

Pooler, A. M. *et al.* (2013) 'Physiological release of endogenous tau is stimulated by neuronal activity', *EMBO reports*, 14(4), pp. 389–394. doi: 10.1038/embor.2013.15.

Pooler, A. M. *et al.* (2015) 'Amyloid accelerates tau propagation and toxicity in a model of early Alzheimer's disease.', *Acta neuropathologica communications*. doi: 10.1186/s40478-015-0199-x.

Poorkaj, P. *et al.* (1998) 'Tau is a candidate gene for chromosome 17 frontotemporal dementia.', *Annals of neurology*. doi: 10.1002/ana.410430617.

Porquet, D. *et al.* (2015) 'Amyloid and tau pathology of familial Alzheimer's disease APP/PS1 mouse

model in a senescence phenotype background (SAMP8)', *PLOS Biology*, 37(1), p. 9747.

Powell, P. P. *et al.* (1991) 'Temporal, differential and regional expression of mRNA for basic fibroblast growth factor in the developing and adult rat brain.', *Brain research. Molecular brain research*, 11(1), pp. 71–7.

Prado, V. F. *et al.* (2016) 'Cholinergic circuits in cognitive flexibility', *Neuroscience*. doi: 10.1016/j.neuroscience.2016.09.013.

Pratt, K. G. *et al.* (2008) 'Dynamics underlying synaptic gain between pairs of cortical pyramidal neurons', *Developmental Neurobiology*, 68(2), pp. 143–151. doi: 10.1002/dneu.20577.

Price, D. L. *et al.* (1998) 'ALZHEIMER'S DISEASE: Genetic Studies and Transgenic Models', *Annual Review of Genetics*, 32(1), pp. 461–493. doi: 10.1146/annurev.genet.32.1.461.

Procter, A. W., Qurne, M. and Francis, P. T. (1999) 'Neurochemical features of frontotemporal dementia.', *Dementia and geriatric cognitive disorders*, 10 Suppl 1, pp. 80–4. doi: 51219.

Prusiner, S. B. (1982) 'Novel proteinaceous infectious particles cause scrapie.', *Science (New York, N.Y.)*, 216(4542), pp. 136–44.

Prüßing, K., Voigt, A. and Schulz, J. B. (2013) 'Drosophila melanogaster as a model organism for Alzheimer's disease', *Molecular Neurodegeneration*, 8.

Puri, M. C. and Nagy, A. (2012) 'Concise Review: Embryonic Stem Cells Versus Induced Pluripotent Stem Cells: The Game Is On', *STEM CELLS*, 30(1), pp. 10–14. doi: 10.1002/stem.788.

Purro, S. A. *et al.* (2008) 'Wnt Regulates Axon Behavior through Changes in Microtubule Growth Directionality: A New Role for Adenomatous Polyposis Coli', *Journal of Neuroscience*, 28(34), pp. 8644–8654.

Qi, Y. *et al.* (2017) 'Combined small-molecule inhibition accelerates the derivation of functional cortical neurons from human pluripotent stem cells', *Nature Biotechnology*. doi: 10.1038/nbt.3777.

Qing, H. *et al.* (2008) 'Valproic acid inhibits Aβ production, neuritic plaque formation, and behavioral deficits in Alzheimer's disease mouse models', *The Journal of Experimental Medicine*, 205(12), pp. 2781–2789.

Qiu, C. *et al.* (2005) 'The age-dependent relation of blood pressure to cognitive function and dementia', *Lancet Neurology*, pp. 487–499. doi: 10.1016/S1474-4422(05)70141-1.

Quigley, C. *et al.* (2010) 'Feature-selective attention: Evidence for a decline in old age', *Neuroscience Letters*, 474(1), pp. 5–8. doi: 10.1016/j.neulet.2010.02.053.

Rademakers, R. *et al.* (2003) 'Tau (MAPT) mutation Arg406Trp presenting clinically with Alzheimer disease does not share a common founder in Western Europe', *Human Mutation*, 22(5), pp. 409–411.

Raj, A. *et al.* (2012) 'A Network Diffusion Model of Disease Progression in Dementia', *Neuron*, 73(6), pp. 1204–1215. doi: 10.1016/j.neuron.2011.12.040.

Raja, W. K. *et al.* (2016) 'Self-Organizing 3D Human Neural Tissue Derived from Induced Pluripotent Stem Cells Recapitulate Alzheimer's Disease Phenotypes', *PLOS ONE*. Edited by J. Padmanabhan. Public Library of Science, 11(9), p. e0161969. doi: 10.1371/journal.pone.0161969.

Rametti, A. *et al.* (2008) 'Lithium down-regulates tau in cultured cortical neurons: A possible mechanism of neuroprotection', *Neuroscience Letters*, 434(1), pp. 93–98.

Ramot, D. *et al.* (2008) 'Bidirectional temperature-sensing by a single thermosensory neuron in C. elegans', *Nature Neuroscience*, 11(8), pp. 908–915.

Ramsden, M. *et al.* (2005) 'Age-Dependent Neurofibrillary Tangle Formation, Neuron Loss, and Memory Impairment in a Mouse Model of Human Tauopathy (P301L)'. doi: 10.1523/JNEUROSCI.3279-05.2005.

Ramser, E. M. *et al.* (2013) 'Amyloid-β oligomers induce tau-independent disruption of BDNF axonal transport via calcineurin activation in cultured hippocampal neurons.', *Molecular biology of the cell*. American Society for Cell Biology, 24(16), pp. 2494–505. doi: 10.1091/mbc.E12-12-0858.

Rankin, C. *et al.* (2007) 'Tau phosphorylation by GSK-3beta promotes tangle-like filament morphology.', *Molecular neurodegeneration*, 2(12), p. 12.

Rao, M. S. and Malik, N. (2012) 'Assessing iPSC reprogramming methods for their suitability in translational medicine.', *Journal of cellular biochemistry*. NIH Public Access, 113(10), pp. 3061–8. doi: 10.1002/jcb.24183.

Rapoport, M. *et al.* (2002) 'Tau is essential to beta -amyloid-induced neurotoxicity.', *Proceedings of the National Academy of Sciences of the United States of America*. National Academy of Sciences, 99(9), pp. 6364–9.

Reddy, P. H. (2013) 'Amyloid beta-induced glycogen synthase kinase 3β phosphorylated VDAC1 in Alzheimer's disease: Implications for synaptic dysfunction and neuronal damage', *Biochimica et Biophysica Acta (BBA) - Molecular Basis of Disease*, 1832(12), pp. 1913–1921.

Reed, L. A. *et al.* (2000) 'Phenotypic correlations in FTDP-17.', *Neurobiology of aging*, 22(1), pp. 89–107.

Regan, P. *et al.* (2015) 'Tau Phosphorylation at Serine 396 Residue Is Required for Hippocampal LTD', *Journal of Neuroscience*, 35(12), pp. 4804–4812.

Revett, T. J. *et al.* (2013) 'Glutamate system, amyloid β peptides and tau protein: Functional interrelationships and relevance to Alzheimer disease pathology', *Journal of Psychiatry and Neuroscience*. doi: 10.1503/jpn.110190.

Reynolds, C. H. *et al.* (2000) 'Phosphorylation sites on tau identified by nanoelectrospray mass spectrometry: differences in vitro between the mitogen-activated protein kinases ERK2, c-Jun N-terminal kinase and P38, and glycogen synthase kinase-3beta.', *Journal of neurochemistry*, 74(4), pp. 1587–95.

Riederer, B. M. *et al.* (2001) 'Differential phosphorylation of tau proteins during kitten brain development and Alzheimer's disease.', *Journal of neurocytology*, 30(2), pp. 145–58.

Rinaldi, F. and Caldwell, M. A. (2013) 'Modeling astrocytic contribution toward neurodegeneration with pluripotent stem cells', *NeuroReport*, 24(18), pp. 1053–1057.

Rizzu, P. *et al.* (1999) 'High Prevalence of Mutations in the Microtubule-Associated Protein Tau in a Population Study of Frontotemporal Dementia in the Netherlands', *The American Journal of Human Genetics*, 64(2), pp. 414–421. doi: 10.1086/302256.

Roberson, E. D. *et al.* (2007) 'Reducing Endogenous Tau Ameliorates Amyloid ß-Induced Deficits in an Alzheimer's Disease Mouse Model', *Science*, 316(5825).

Rocher, A. B. *et al.* (2010) 'Structural and functional changes in tau mutant mice neurons are not linked to the presence of NFTs', *Experimental Neurology*, 223(2), pp. 385–393. doi: 10.1016/j.expneurol.2009.07.029.

Rockenstein, E. *et al.* (2007) 'Neuroprotective Effects of Regulators of the Glycogen Synthase Kinase-3 Signaling Pathway in a Transgenic Model of Alzheimer's Disease Are Associated with Reduced Amyloid Precursor Protein Phosphorylation', *Journal of Neuroscience*, 27(8), pp. 1981–1991.

Rogaeva, E. *et al.* (2007) 'The neuronal sortilin-related receptor SORL1 is genetically associated with Alzheimer disease', *Nature Genetics*. Nature Publishing Group, 39(2), pp. 168–177. doi: 10.1038/ng1943.

Rogaeva, E. A. *et al.* (2001) 'Screening for PS1 mutations in a referral-based series of AD cases: 21 novel mutations.', *Neurology*, 57(4), pp. 621–5.

Roher, A. E. *et al.* (1993) 'Structural alterations in the peptide backbone of beta-amyloid core protein may account for its deposition and stability in Alzheimer's disease.', *The Journal of biological chemistry*, 268(5), pp. 3072–83.

Rohn, T. T. and T., T. (2013) 'The triggering receptor expressed on myeloid cells 2: "TREM-ming" the inflammatory component associated with Alzheimer's disease.', *Oxidative medicine and cellular longevity*. Hindawi, 2013, p. 860959.

Roll-Mecak, A. and McNally, F. J. (2010) 'Microtubule-severing enzymes', *Current Opinion in Cell Biology*. doi: 10.1016/j.ceb.2009.11.001.

Rösner, H. *et al.* (1995) 'Developmental expression of tau proteins in the chicken and rat brain: rapid down-regulation of a paired helical filament epitope in the rat cerebral cortex coincides with the transition from immature to adult tau isoforms.', *International journal of developmental neuroscience : the official journal of the International Society for Developmental Neuroscience*, 13(6), pp. 607–17.

Rosso, S. M. *et al.* (2003) 'Total tau and phosphorylated tau 181 levels in the cerebrospinal fluid of patients with frontotemporal dementia due to P301L and G272V tau mutations.', *Archives of neurology*. doi: 10.1001/archneur.60.9.1209.

Rossor, M. N. *et al.* (2010) 'The diagnosis of young-onset dementia', *The Lancet Neurology*, 9(8), pp. 793–806. doi: 10.1016/S1474-4422(10)70159-9.

Rouhani, F. *et al.* (2014) 'Genetic Background Drives Transcriptional Variation in Human Induced Pluripotent Stem Cells', *PLoS Genetics*. Edited by G. Gibson. Public Library of Science, 10(6), p. e1004432.

Rui, Y. *et al.* (2006) 'Acute impairment of mitochondrial trafficking by beta-amyloid peptides in hippocampal neurons.', *The Journal of neuroscience : the official journal of the Society for Neuroscience*. Society for Neuroscience, 26(41), pp. 10480–7.

Rui, Y. *et al.* (2013) 'Activity-dependent regulation of dendritic growth and maintenance by glycogen synthase kinase 3β.', *Nature communications*. NIH Public Access, 4, p. 2628.

Russ, C. *et al.* (2001) 'The extended haplotype of the microtubule associated protein tau gene is not associated with Pick's disease.', *Neuroscience letters*, 299(1–2), pp. 156–8.

Ryder, J. *et al.* (2003) 'Divergent roles of GSK3 and CDK5 in APP processing', *Biochemical and Biophysical Research Communications*, 312(4), pp. 922–929.

Ryu, J. K. *et al.* (2004) 'Minocycline inhibits neuronal death and glial activation induced by ?-amyloid peptide in rat hippocampus', *Glia*, 48(1), pp. 85–90. doi: 10.1002/glia.20051.

Saeki, K. *et al.* (2011) 'Glycogen synthase kinase-3β2 has lower phosphorylation activity to tau than glycogen synthase kinase-3β1.', *Biological & pharmaceutical bulletin*, 34(1), pp. 146–9.

Sakakibara, S. *et al.* (1996) 'Mouse-Musashi-1, a neural RNA-binding protein highly enriched in the mammalian CNS stem cell', *Developmental biology*. doi: 10.1006/dbio.1996.0130.

Sakaue, F. *et al.* (2005) 'Phosphorylation of FTDP-17 mutant tau by cyclin-dependent kinase 5 complexed with p35, p25, or p39', *Journal of Biological Chemistry*, 280(36), pp. 31522–31529.

Salinas, P. C. (2005) 'Retrograde signalling at the synapse: a role for Wnt proteins', *Biochemical Society Transactions*, 33(6), p. 1295. doi: 10.1042/BST20051295.

Saman, S. *et al.* (2012) 'Exosome-associated Tau Is Secreted in Tauopathy Models and Is Selectively Phosphorylated in Cerebrospinal Fluid in Early Alzheimer Disease', *Journal of Biological Chemistry*, 287(6), pp. 3842–3849.

Sanders, D. W. *et al.* (2014) 'Distinct Tau Prion Strains Propagate in Cells and Mice and Define Different Tauopathies', *Neuron*. Cell Press, 82(6), pp. 1271–1288. doi: 10.1016/J.NEURON.2014.04.047.

Sang, H. *et al.* (2001) 'Phosphorylation of tau by glycogen synthase kinase 3β in intact mammalian cells influences the stability of microtubules', *Neuroscience Letters*, 312(3), pp. 141–144.

Santa-Maria, I. *et al.* (2012) 'Paired Helical Filaments from Alzheimer Disease Brain Induce Intracellular Accumulation of Tau Protein in Aggresomes', *Journal of Biological Chemistry*, 287(24), pp. 20522–20533.

Santacruz, K. *et al.* (2005) 'Tau suppression in a neurodegenerative mouse model improves memory function.', *Science (New York, N.Y.)*. NIH Public Access, 309(5733), pp. 476–81.

Santarella, R. A. *et al.* (2004) 'Surface-decoration of microtubules by human tau', *Journal of Molecular Biology*, 339(3), pp. 539–553.

Sarlus, H. and Heneka, M. T. (2017) 'Microglia in Alzheimer's disease', *Journal of Clinical Investigation*, 127(9), pp. 3240–3249.

De Sarno, P. *et al.* (2002) 'Regulation of Akt and glycogen synthase kinase-3 beta phosphorylation by sodium valproate and lithium.', *Neuropharmacology*, 43(7), pp. 1158–64.

Savva, G. M., Stephan, B. C. M. and Alzheimer's Society Vascular Dementia Systematic Review Group, the A. S. V. D. S. R. (2010) 'Epidemiological studies of the effect of stroke on incident dementia: a systematic review.', *Stroke*. American Heart Association, Inc., 41(1), pp. e41-6. doi: 10.1161/Strokeaha.109.559880.

Sayas, C. L. *et al.* (2015) 'Tau regulates the localization and function of End-binding proteins 1 and 3 in developing neuronal cells', *Journal of Neurochemistry*, 133(5), pp. 653–667.

Schaffer, B. A. J. *et al.* (2008) 'Association of GSK3B With Alzheimer Disease and Frontotemporal Dementia', *Archives of Neurology*, 65(10), pp. 1368–74.

Scheff, S. W. *et al.* (2006) 'Hippocampal synaptic loss in early Alzheimer's disease and mild cognitive impairment', *Neurobiology of Aging*, 27(10), pp. 1372–1384.

Scheuner, D. *et al.* (1996) 'Secreted amyloid beta-protein similar to that in the senile plaques of Alzheimer's disease is increased in vivo by the presenilin 1 and 2 and APP mutations linked to familial Alzheimer's disease.', *Nature medicine*, 2(8), pp. 864–70.

Schlaeger, T. M. *et al.* (2015) 'A comparison of non-integrating reprogramming methods.', *Nature biotechnology*. NIH Public Access, 33(1), pp. 58–63. doi: 10.1038/nbt.3070.

Schmitz, T. W. *et al.* (2014) 'Distinguishing attentional gain and tuning in young and older adults', *Neurobiology of Aging*, 35(11), pp. 2514–2525. doi: 10.1016/j.neurobiolaging.2014.04.028.

Schmitz, T. W. *et al.* (2016) 'Basal forebrain degeneration precedes and predicts the cortical spread of Alzheimer's pathology', *Nature Communications*. Nature Publishing Group, 7, p. 13249. doi: 10.1038/ncomms13249.

Schmitz, T. W. *et al.* (2010) 'Failing to Ignore: Paradoxical Neural Effects of Perceptual Load on Early Attentional Selection in Normal Aging', *Journal of Neuroscience*, 30(44), pp. 14750–14758.

Seeley, W. W. *et al.* (2006) 'Early frontotemporal dementia targets neurons unique to apes and humans', *Annals of Neurology*. Wiley Subscription Services, Inc., A Wiley Company, 60(6), pp. 660–667.

Seeley, W. W. *et al.* (2009) 'Neurodegenerative Diseases Target Large-Scale Human Brain Networks', *Neuron*.

Selkoe, D. J. (2011) 'Alzheimer's Disease', *Cold Spring Harbor Perspectives in Biology*, 3(7), pp. a004457–a004457. doi: 10.1101/cshperspect.a004457.

Selkoe, D. J. and Hardy, J. (2016) 'The amyloid hypothesis of Alzheimer's disease at 25 years.', *EMBO molecular medicine*. Wiley-Blackwell, 8(6), pp. 595–608. doi: 10.15252/emmm.201606210.

Sengupta, A. *et al.* (1998) 'Phosphorylation of Tau at Both Thr 231 and Ser 262 Is Required for Maximal Inhibition of Its Binding to Microtubules', *Archives of Biochemistry and Biophysics*, 357(2), pp. 299–309.

Sengupta, A. *et al.* (2006) 'Regulation of phosphorylation of tau by cyclin-dependent kinase 5 and glycogen synthase kinase-3 at substrate level', *FEBS Letters*, 580(25), pp. 5925–5933.

Seok, J. *et al.* (2013) 'Genomic responses in mouse models poorly mimic human inflammatory diseases.', *Proceedings of the National Academy of Sciences of the United States of America*. National Academy of Sciences, 110(9), pp. 3507–12.

Sepulveda, F. J. *et al.* (2010a) 'Synaptotoxicity of Alzheimer Beta Amyloid Can Be Explained by Its Membrane Perforating Property', *PLoS ONE*. Edited by H. E. Gendelman. Public Library of Science, 5(7), p. e11820.

Sepulveda, F. J. *et al.* (2010b) 'Synaptotoxicity of Alzheimer Beta Amyloid Can Be Explained by Its Membrane Perforating Property', *PLoS ONE*. Edited by H. E. Gendelman. (Sinauer Associates, Inc.), 5(7), p. e11820. doi: 10.1371/journal.pone.0011820.

Serenó, L. *et al.* (2009) 'A novel GSK-3β inhibitor reduces Alzheimer's pathology and rescues neuronal loss in vivo', *Neurobiology of Disease*, 35(3), pp. 359–367.

Seshadri, S. *et al.* (2010) 'Genome-wide Analysis of Genetic Loci Associated With Alzheimer Disease', *JAMA*, 303(18), p. 1832. doi: 10.1001/jama.2010.574.

Seubert, P. *et al.* (1992) 'Isolation and quantification of soluble Alzheimer's β-peptide from biological fluids', *Nature*, 359(6393), pp. 325–327. doi: 10.1038/359325a0.

Shah, K. and Lahiri, D. K. (2016) 'A Tale of the Good and Bad: Remodeling of the Microtubule Network in the Brain by Cdk5', *Molecular Neurobiology*, 5 March, pp. 1–14.

Shahpasand, K. *et al.* (2012) 'Regulation of mitochondrial transport and inter-microtubule spacing by tau phosphorylation at the sites hyperphosphorylated in Alzheimer's disease.', *The Journal of neuroscience : the official journal of the Society for Neuroscience*. Society for Neuroscience, 32(7), pp. 2430–41.

Sheridan, S. D. *et al.* (2011) 'Epigenetic Characterization of the FMR1 Gene and Aberrant Neurodevelopment in Human Induced Pluripotent Stem Cell Models of Fragile X Syndrome', *PLoS ONE*. Edited by M. R. Cookson, 6(10), p. e26203. doi: 10.1371/journal.pone.0026203.

Sherrington, R. *et al.* (1995) 'Cloning of a gene bearing missense mutations in early-onset familial Alzheimer's disease', *Nature*, 375(6534), pp. 754–760.

Shi, H.-R. *et al.* (2008) '17β-estradiol attenuates glycogen synthase kinase-3β activation and tau hyperphosphorylation in Akt-independent manner', *Journal of Neural Transmission*. Springer Vienna, 115(6), pp. 879–888.

Shi, S.-H. *et al.* (2004) 'APC and GSK-3β Are Involved in mPar3 Targeting to the Nascent Axon and Establishment of Neuronal Polarity', *Current Biology*, 14(22), pp. 2025–2032. doi: 10.1016/j.cub.2004.11.009.

Shi, Y. *et al.* (2012a) 'A Human Stem Cell Model of Early Alzheimer's Disease Pathology in Down Syndrome', *Science Translational Medicine*, 4(124), p. 124ra29-124ra29. doi: 10.1126/scitranslmed.3003771.

Shi, Y. *et al.* (2012b) 'Human cerebral cortex development from pluripotent stem cells to functional excitatory synapses.', *Nature neuroscience*, 15(3), pp. 477–86, S1. doi: 10.1038/nn.3041.

Shiarli, A.-M. *et al.* (2006) 'Comparison of extent of tau pathology in patients with frontotemporal dementia with Parkinsonism linked to chromosome 17 (FTDP-17), frontotemporal lobar degeneration with Pick bodies and early onset Alzheimer's disease', *Neuropathology and Applied Neurobiology*, 32(4), pp. 374–387.

Shim, S. B. *et al.* (2007) 'Tau overexpression in transgenic mice induces glycogen synthase kinase 3β and β-catenin phosphorylation', *Neuroscience*, 146(2), pp. 730–740. doi: 10.1016/j.neuroscience.2007.01.041.

Shipton, O. A. *et al.* (2011) 'Tau protein is required for amyloid {beta}-induced impairment of hippocampal long-term potentiation.', *The Journal of neuroscience : the official journal of the Society for Neuroscience*. doi: 10.1523/Jneurosci.2610-10.2011.

Shukla, V. *et al.* (2012) 'Deregulated Cdk5 activity is involved in inducing Alzheimer's disease.', *Archives of medical research*. NIH Public Access, 43(8), pp. 655–62.

Sigurdsson, E. M. *et al.* (1997) 'Laterality in the histological effects of injections of amyloid-beta 25-35 into the amygdala of young Fischer rats', *J Neuropathol Exp Neurol*. doi: 10.1017/CBO9781107415324.004.

Silva, M. C. *et al.* (2016) 'Human iPSC-Derived Neuronal Model of Tau-A152T Frontotemporal Dementia Reveals Tau-Mediated Mechanisms of Neuronal Vulnerability.', *Stem cell reports*. Elsevier, 7(3), pp. 325–40.

Šimić, G. *et al.* (2016) 'Tau protein hyperphosphorylation and aggregation in alzheimer's disease and other tauopathies, and possible neuroprotective strategies', *Biomolecules*. doi: 10.3390/biom6010006.

Sims, N. R. *et al.* (1983) 'Presynaptic Cholinergic Dysfunction in Patients with Dementia', *Journal of Neurochemistry*, 40(2), pp. 503–509. doi: 10.1111/j.1471-4159.1983.tb11311.x.

Siuda, J. *et al*. (2014) 'Parkinsonian syndrome in familial frontotemporal dementia.', *Parkinsonism & related disorders*. NIH Public Access, 20(9), pp. 957–64. doi: 10.1016/j.parkreldis.2014.06.004.

Sjögren, M. *et al.* (2001) 'Both total and phosphorylated tau are increased in Alzheimer's disease.', *Journal of neurology, neurosurgery, and psychiatry*, 70(5), pp. 624–30.

Smith, R. *et al.* (2016) '18F-AV-1451 tau PET imaging correlates strongly with tau neuropathology in *MAPT* mutation carriers', *Brain*. doi: 10.1093/brain/aww163.

Snyder, S. W. *et al.* (1994) 'Amyloid-beta aggregation: selective inhibition of aggregation in mixtures of amyloid with different chain lengths', *Biophysical Journal*, 67(3), pp. 1216–1228. doi: 10.1016/S0006-3495(94)80591-0.

Sofola, O. *et al.* (2010) 'Inhibition of GSK-3 Ameliorates Aβ Pathology in an Adult-Onset Drosophila Model of Alzheimer's Disease', *PLoS Genetics*. Edited by B. Lu. Public Library of Science, 6(9), p. e1001087. doi: 10.1371/journal.pgen.1001087.

Song, L. *et al.* (2015) 'Analysis of tau post-translational modifications in rTg4510 mice, a model of tau pathology', *Molecular Neurodegeneration*, 10(1), p. 14. doi: 10.1186/s13024-015-0011-1.

Sontag, E. *et al.* (1996) 'Regulation of the phosphorylation state and microtubule-binding activity of Tau by protein phosphatase 2A.', *Neuron*, 17(6), pp. 1201–7.

Sparks, D. L. *et al.* (1994) 'Neurochemical and histopathologic alterations characteristic of Pick's disease in a non-demented individual.', *Journal of neuropathology and experimental neurology*, 53(1), pp. 37–42.

Sperbera, B. R. *et al.* (1995) 'Glycogen synthase kinase-3β phosphorylates tau protein at multiple sites in intact cells', *Neuroscience Letters*, 197(2), pp. 149–153. doi: 10.1016/0304-3940(95)11902-9.

Spillantini, M. G. *et al.* (1997) 'Familial multiple system tauopathy with presenile dementia: A disease with abundant neuronal and glial tau filaments', *Proceedings of the National Academy of Sciences*, 94(8), pp. 4113–4118. doi: 10.1073/pnas.94.8.4113.

Spina, S. *et al.* (2017) 'Frontotemporal dementia with the V337M MAPT mutation', *Neurology*. doi: 10.1212/WNL.0000000000003636.

Spires-Jones, T. L. and Hyman, B. T. (2014) 'The intersection of amyloid beta and tau at synapses in Alzheimer's disease.', *Neuron*. NIH Public Access, 82(4), pp. 756–71.

Spires, T. L. *et al.* (2006) 'Region-specific dissociation of neuronal loss and neurofibrillary pathology in a mouse model of tauopathy.', *The American journal of pathology*, 168(5), pp. 1598–607.

Spittaels, K. *et al.* (2000) 'Glycogen synthase kinase-3beta phosphorylates protein tau and rescues the axonopathy in the central nervous system of human four-repeat tau transgenic mice.', *The Journal of biological chemistry*. American Society for Biochemistry and Molecular Biology, 275(52), pp. 41340–9.

Sposito, T. *et al.* (2015) 'Developmental regulation of tau splicing is disrupted in stem cell-derived neurons from frontotemporal dementia patients with the 10 + 16 splice-site mutation in *MAPT*', *Human Molecular Genetics*. doi: 10.1093/hmg/ddv246.

Sproul, A. A. *et al.* (2014) 'Characterization and molecular profiling of PSEN1 familial Alzheimer's disease iPSC-derived neural progenitors', *PloS one*. doi: 10.1371/journal.pone.0084547.

Squire, L. R. and Zola-Morgan, S. (1991) 'The medial temporal lobe memory system.', *Science*, 253(5026), pp. 1380–1386. doi: 10.1126/science.1896849.

Stamer, K. *et al.* (2002) 'Tau blocks traffic of organelles, neurofilaments, and APP vesicles in neurons and enhances oxidative stress', *The Journal of Cell Biology*, 156(6), pp. 1051–1063.

Stancu, I.-C. *et al.* (2014) 'Models of β-amyloid induced Tau-pathology: the long and folded road to understand the mechanism', 9, pp. 1–14. doi: 10.1186/1750-1326-9-51.

Stanford, P. *et al.* (2004) 'Frequency of tau mutations in familial and sporadic frontotemporal dementia and other tauopathies', *Journal of Neurology*, 251(9), pp. 1098–104.

Stanford, P. M. *et al.* (2003) 'Mutations in the tau gene that cause an increase in three repeat tau and frontotemporal dementia', *Brain*. Oxford University Press, 126(4), pp. 814–826.

Stanton, P. K. (1996) 'LTD, LTP, and the sliding threshold for long-term synaptic plasticity', *Hippocampus*, 6(1), pp. 35–42.

Stefanova, N. A. *et al.* (2016) 'An antioxidant specifically targeting mitochondria delays progression of Alzheimer's disease-like pathology.', *Aging*. Impact Journals, LLC, 8(11), pp. 2713–2733.

Stokin, G. B. (2005) 'Axonopathy and Transport Deficits Early in the Pathogenesis of Alzheimer's Disease', *Science*, 307(5713), pp. 1282–1288.

Stoothoff, W. *et al.* (2009) 'Differential effect of three-repeat and four-repeat tau on mitochondrial axonal transport', *Journal of Neurochemistry*. doi: 10.1111/j.1471-4159.2009.06316.x.

Su, B. *et al.* (2008) 'Physiological regulation of tau phosphorylation during hibernation.', *Journal of neurochemistry*. NIH Public Access, 105(6), pp. 2098–108.

Su, B. *et al.* (2010) 'Abnormal mitochondrial dynamics and neurodegenerative diseases', *Biochimica et Biophysica Acta (BBA) - Molecular Basis of Disease*, 1802(1), pp. 135–142.

Sullivan, S. E. and Young-Pearse, T. (2015) 'Induced pluripotent stem cells as a discovery tool for Alzheimer's disease.', *Brain research*. doi: 10.1016/j.brainres.2015.10.005.

Sumi, S. M. *et al.* (1992) 'Familial presenile dementia with psychosis associated with cortical neurofibrillary tangles and degeneration of the amygdala.', *Neurology*. Lippincott Williams & Wilkins, 42(1), pp. 120–7. doi: 10.1212/WNL.42.1.120.

Sun, K. H. *et al.* (2008) 'Deregulated Cdk5 promotes oxidative stress and mitochondrial dysfunction', *Journal of Neurochemistry*, 107(1), pp. 265–278.

Swatton, J. E. *et al.* (2004) 'Increased MAP kinase activity in Alzheimer's and Down syndrome but not in schizophrenia human brain', *European Journal of Neuroscience*, 19(10), pp. 2711–2719.

Van Swieten, J. C. *et al.* (1999) 'Phenotypic variation in hereditary frontotemporal dementia with tau mutations', *Annals of Neurology*. doi: 10.1002/1531-8249(199910)46:4<617::AID-ANA10>3.0.CO;2-I.

Szczepanowska, J. (2009) 'Involvement of Rac/Cdc42/PAK pathway in cytoskeletal rearrangements.', *Acta biochimica Polonica*, 56(2), pp. 225–34.

del Ser, T. *et al.* (2013) 'A phase II randomized, double-blind, parallel group, 26-week study of GSK-3 inhibitor tideglusib in Alzheimer's disease (argo trial)', *Alzheimer's and Dementia*. Elsevier Inc. (Alzheimer's Association International Conference 2013. Boston, MA United States. Conference Start: 20130713. Conference End: 20130718.), pp. P689–P690.

Takahashi, K. and Yamanaka, S. (2006) 'Induction of Pluripotent Stem Cells from Mouse Embryonic and Adult Fibroblast Cultures by Defined Factors', *Cell*, 126(4), pp. 663–676.

Takahashi, M. *et al.* (1999) 'Lithium inhibits neurite growth and tau protein kinase I/glycogen synthase kinase-3beta-dependent phosphorylation of juvenile tau in cultured hippocampal neurons.', *Journal of neurochemistry*, 73(5), pp. 2073–83.

Takashima, A. *et al.* (1993) 'Tau protein kinase I is essential for amyloid beta-protein-induced neurotoxicity.', *Proceedings of the National Academy of Sciences of the United States of America*. National Academy of Sciences, 90(16), pp. 7789–93.

Takashima, A. *et al.* (1996) 'Exposure of rat hippocampal neurons to amyloid beta peptide (25-35) induces the inactivation of phosphatidyl inositol-3 kinase and the activation of tau protein kinase I/glycogen synthase kinase-3 beta.', *Neuroscience letters*, 203(1), pp. 33–6.

Takashima, A. *et al.* (1998) 'Activation of tau protein kinase I/glycogen synthase kinase-3β by amyloid β peptide (25–35) enhances phosphorylation of tau in hippocampal neurons', *Neuroscience Research*, 31(4), pp. 317–323.

Takauchi, S. *et al.* (1984) 'An ultrastructural study of Pick bodies.', *Acta neuropathologica*, 64(4), pp. 344–8.

Tan, M.-S., Yu, J.-T. and Tan, L. (2013) 'Bridging integrator 1 (BIN1): form, function, and Alzheimer's disease', *Trends in Molecular Medicine*, 19(10), pp. 594–603. doi: 10.1016/j.molmed.2013.06.004.

Tanaka, T. *et al.* (2004) 'Cdk5 Phosphorylation of Doublecortin Ser297 Regulates Its Effect on Neuronal Migration', *Neuron*, 41(2), pp. 215–227.

Tandon, A. *et al.* (2003) 'Brain levels of CDK5 activator p25 are not increased in Alzheimer's or other neurodegenerative diseases with neurofibrillary tangles', *Journal of Neurochemistry*, 86(3), pp. 572–581.

Tanemura, K. *et al.* (2002) 'Neurodegeneration with tau accumulation in a transgenic mouse expressing V337M human tau.', *The Journal of neuroscience : the official journal of the Society for Neuroscience*. doi: 22/1/133 [pii].

Tang, D. *et al.* (1997) 'Cyclin-dependent kinase 5 (Cdk5) activation domain of neuronal Cdk5 activator. Evidence of the existence of cyclin fold in neuronal Cdk5a activator', *Journal of Biological Chemistry*, 272(19), pp. 12318–12327.

Taniguchi, S. *et al.* (2001) 'Calpain-mediated degradation of p35 to p25 in postmortem human and rat brains', *FEBS Letters*, 489(1), pp. 46–50.

Taniguchi, S. *et al.* (2001) 'Calpain-mediated degradation of p35 to p25 in postmortem human and rat brains.', *FEBS letters*, 489(1), pp. 46–50.

Tanokashira, D. *et al.* (2017) 'The neurotoxicity of amyloid β-protein oligomers is reversible in a primary neuron model', *Molecular Brain*. doi: 10.1186/s13041-016-0284-5.

Tardivel, M. *et al.* (2016) 'Tunneling nanotube (TNT)-mediated neuron-to neuron transfer of pathological Tau protein assemblies', *Acta Neuropathologica Communications*, 4(1), p. 117. doi: 10.1186/s40478-016-0386-4.

Tashiro, K. *et al.* (1997) 'Somatodendritic localization of phosphorylated tau in neonatal and adult rat cerebral cortex.', *Neuroreport*, 8(12), pp. 2797–2801. doi: 10.1097/00001756-199708180-00029.

Tatebayashi, Y. *et al.* (2004) 'Role of tau phosphorylation by glycogen synthase kinase-3β in the regulation of organelle transport', *Journal of Cell Science*, 117(9).

Tedde, A. *et al.* (2003) 'Identification of New Presenilin Gene Mutations in Early-Onset Familial Alzheimer Disease', *Archives of Neurology*, 60(11), p. 1541. doi: 10.1001/archneur.60.11.1541.

Tell, V. and Hilgeroth, A. (2013) 'Recent developments of protein kinase inhibitors as potential AD therapeutics.', *Frontiers in cellular neuroscience*. Frontiers Media SA, 7, p. 189. doi: 10.3389/fncel.2013.00189.

Terracciano, C. *et al.* (2010) 'In APP-overexpressing cultured human muscle fibers proteasome inhibition enhances phosphorylation of AÎ²PP751 and GSK3Î² activation: effects mitigated by lithium and apparently relevant to sporadic inclusion-body myositis', *Journal of Neurochemistry*, 112(2), pp. 389–396. doi: 10.1111/j.1471-4159.2009.06461.x.

Terwel, D. *et al.* (2008) 'Amyloid Activates GSK-3β to Aggravate Neuronal Tauopathy in Bigenic Mice', *The American Journal of Pathology*, 172(3), pp. 786–798.

Terwel, D. *et al*. (2002) 'Axonal Transport, Tau Protein, and Neurodegeneration in Alzheimer's Disease', *NeuroMolecular Medicine*. Humana Press, 2(2), pp. 151–166. doi: 10.1385/NMM:2:2:151.

Teschendorf, D. and Link, C. D. (2009) 'What have worm models told us about the mechanisms of neuronal dysfunction in human neurodegenerative diseases?', *Molecular Neurodegeneration*, 4(1), p. 38. doi: 10.1186/1750-1326-4-38.

Thévenot, E. *et al.* (2011) 'p21-activated kinase 3 (PAK3) protein regulates synaptic transmission through its interaction with the Nck2/Grb4 protein adaptor', *Journal of Biological Chemistry*. doi: 10.1074/jbc.M111.262246.

Tiiman, A. *et al.* (2015) 'In vitro fibrillization of Alzheimer's amyloid-?? peptide (1-42)', *AIP Advances*. doi: 10.1063/1.4921071.

Tolosa, E. *et al.* (2014) 'A phase 2 trial of the GSK-3 inhibitor tideglusib in progressive supranuclear palsy', *Movement Disorders*. doi: 10.1002/mds.25824.

Tong, L. *et al.* (2015) 'The Role of SUMO-Conjugating Enzyme Ubc9 in the Neuroprotection of Isoflurane Preconditioning Against Ischemic Neuronal Injury', *Molecular Neurobiology*, 51(3), pp. 1221–1231. doi: 10.1007/s12035-014-8797-3.

Torrent, L. and Ferrer, I. (2012) 'PP2A and Alzheimer disease.', *Current Alzheimer research*, 9(2), pp. 248–56.

Tosetti, P. *et al*. (1998) 'Functional changes in potassium conductances of the human neuroblastoma cell line SH-SY5Y during in vitro differentiation.', *Journal of neurophysiology*, 79(2), pp. 648–58.

Town, T. *et al.* (2002) 'p35/Cdk5 pathway mediates soluble amyloid-?? peptide-induced tau phosphorylation in vitro', *Journal of Neuroscience Research*, pp. 362–372.

Trabzuni, D. *et al.* (2012) 'MAPT expression and splicing is differentially regulated by brain region: relation to genotype and implication for tauopathies.', *Human molecular genetics*. Oxford University Press, 21(18), pp. 4094–103.

Trinczek, B. *et al.* (1999) 'Tau regulates the attachment/detachment but not the speed of motors in microtubule-dependent transport of single vesicles and organelles.', *Journal of cell science*, 112 (Pt 14), pp. 2355–67.

Trivedi, N. *et al.* (2005) 'Glycogen synthase kinase-3 phosphorylation of MAP1B at Ser1260 and Thr1265 is spatially restricted to growing axons', *Journal of Cell Science*, 118(5), pp. 993–1005.

Trojanowski, J. Q. *et al.* (1989) 'Distribution of tau proteins in the normal human central and peripheral nervous system', *J Histochem Cytochem*, 37(2), pp. 209–215.

Tsai, L. H. *et al.* (1994) 'P35 Is a Neural-Specific Regulatory Subunit of Cyclin-Dependent Kinase 5.', *Nature*, 371(6496), pp. 419–423.

Tseng, H. C. *et al.* (2002) 'A survey of Cdk5 activator p35 and p25 levels in Alzheimer's disease brains', *FEBS Letters*, 523(1–3), pp. 58–62.

Twomey, C. and McCarthy, J. V. (2006) 'Presenilin-1 is an unprimed glycogen synthase kinase-3β substrate', *FEBS Letters*, 580(17), pp. 4015–4020. doi: 10.1016/j.febslet.2006.06.035.

Uchida, T. *et al.* (1994) 'Precursor of cdk5 activator, the 23 kDa subunit of tau protein kinase II: Its sequence and developmental change in brain', *FEBS Letters*, 355(1), pp. 35–40.

Um, J. W. *et al.* (2013) 'Metabotropic glutamate receptor 5 is a coreceptor for Alzheimer abeta oligomer bound to cellular prion protein', *Neuron*. doi: 10.1016/j.neuron.2013.06.036.

Umeda, T. *et al.* (2013) 'Neurodegenerative Disorder FTDP-17–Related Tau Intron 10 +16C→T Mutation Increases Tau Exon 10 Splicing and Causes Tauopathy in Transgenic Mice', *The American Journal of Pathology*, 183(1), pp. 211–225.

Ungureanu, A.-A. *et al.* (2016) 'Amyloid beta oligomers induce neuronal elasticity changes in age-dependent manner: a force spectroscopy study on living hippocampal neurons', *Scientific Reports*. Nature Publishing Group, 6(1), p. 25841.

Usenovic, M. *et al.* (2015) 'Internalized Tau Oligomers Cause Neurodegeneration by Inducing Accumulation of Pathogenic Tau in Human Neurons Derived from Induced Pluripotent Stem Cells.', *The Journal of Neuroscience*, 35(42). doi: 10.1523/JNEUROSCI.1523-15.2015.

Utreras, E. *et al*. (2009) 'Cyclin-dependent kinase 5 activator p35 over-expression and amyloid beta synergism increase apoptosis in cultured neuronal cells', *Neuroscience*, 161(4), pp. 978–987.

Utton, M. A. *et al.* (2001) 'Functional Differences of Tau Isoforms Containing 3 or 4 C-terminal Repeat Regions and the Influence of Oxidative Stress', *Journal of Biological Chemistry*, 276(36), pp. 34288–34297.

Utton, M. A. *et al.* (1997) 'Phosphorylation of tau by glycogen synthase kinase 3β affects the ability of tau to promote microtubule self-assembly', *Biochemical Journal*, 323(3).

Vandersteen, A. *et al.* (2012) 'Molecular plasticity regulates oligomerization and cytotoxicity of the multipeptide-length amyloid-β peptide pool.', *The Journal of biological chemistry*. American Society for Biochemistry and Molecular Biology, 287(44), pp. 36732–43. doi: 10.1074/jbc.M112.394635.

Vannucci, L. *et al.* (2013) 'Viral vectors: a look back and ahead on gene transfer technology.', *The new microbiologica*, 36(1), pp. 1–22. Available at: http://www.ncbi.nlm.nih.gov/pubmed/23435812.

Vazin, T. *et al.* (2014) 'Efficient derivation of cortical glutamatergic neurons from human pluripotent stem cells: A model system to study neurotoxicity in Alzheimer's disease', *Neurobiology of Disease*.

Verheyen, A. *et al.* (2015) 'Using human iPSC-derived neurons to model TAU aggregation', *PLoS ONE*. doi: 10.1371/journal.pone.0146127.

Verma, M., Vats, A. and Taneja, V. (2015) 'Toxic species in amyloid disorders: Oligomers or mature fibrils.', *Annals of Indian Academy of Neurology*. Medknow Publications, 18(2), pp. 138–45.

Vetrivel, K. S. *et al.* (2006) 'Pathological and physiological functions of presenilins.', *Molecular Neurodegeneration*, 1(1), p. 4. doi: 10.1186/1750-1326-1-4.

Vingtdeux, V. *et al.* (2011) 'AMPK is abnormally activated in tangle-and pre-tangle-bearing neurons in Alzheimer's disease and other tauopathies', *Acta Neuropathologica*. doi: 10.1007/s00401-010-0759-x.

Vitale, A. M. *et al.* (2012) 'Variability in the Generation of Induced Pluripotent Stem Cells: Importance for Disease Modeling', *STEM CELLS Translational Medicine*. AlphaMed Press, 1(9), pp. 641–650.

Vossel, K. A. *et al.* (2010) 'Tau reduction prevents Abeta-induced defects in axonal transport.', *Science*, 330(6001), p. 198.

Wada, Y. *et al.* (1998) 'Microtubule-stimulated phosphorylation of tau at Ser202 and Thr205 by cdk5 decreases its microtubule nucleation activity.', *Journal of biochemistry*, 124(4), pp. 738–46.

Wang, H. Y. *et al.* (2000) 'beta-Amyloid(1-42) binds to alpha7 nicotinic acetylcholine receptor with high affinity. Implications for Alzheimer's disease pathology.', *J.Biol.Chem.*

Wang, Q. M. *et al.* (1994) 'Glycogen synthase kinase-3?? is a dual specificity kinase differentially regulated by tyrosine and serine/threonine phosphorylation', *Journal of Biological Chemistry*, 269(20), pp. 14566–14574.

Wang, W. *et al.* (2008) 'Chromosomal transposition of PiggyBac in mouse embryonic stem cells', *Proceedings of the National Academy of Sciences*, 105(27), pp. 9290–9295. doi: 10.1073/pnas.0801017105.

Wang, Y. *et al.* (2017) 'The release and trans-synaptic transmission of Tau via exosomes', *Molecular Neurodegeneration*. doi: 10.1186/s13024-016-0143-y.

Wang, Y. and Mandelkow, E. (2015) 'Tau in physiology and pathology.', *Nature reviews. Neuroscience*, 17(1). doi: 10.1038/nrn.2015.1.

Warmus, B. A. *et al.* (2014) 'Tau-mediated NMDA receptor impairment underlies dysfunction of a selectively vulnerable network in a mouse model of frontotemporal dementia.', *The Journal of neuroscience : the official journal of the Society for Neuroscience*. Society for Neuroscience, 34(49), pp. 16482–95.

Warren, L. *et al.* (2010) 'Highly efficient reprogramming to pluripotency and directed differentiation of human cells with synthetic modified mRNA', *Cell Stem Cell*, 7(5), pp. 618–630. doi: 10.1016/j.stem.2010.08.012.

Weaver, C. L. *et al.* (no date) 'Conformational change as one of the earliest alterations of tau in Alzheimer's disease.', *Neurobiology of aging*, 21(5), pp. 719–27.

Weintraub, S., Wicklund, A. H. and Salmon, D. P. (2012) 'The neuropsychological profile of Alzheimer disease', *Cold Spring Harbor Perspectives in Medicine*. doi: 10.1101/cshperspect.a006171.

Wen, Y. *et al.* (2008) 'Interplay between cyclin-dependent kinase 5 and glycogen synthase kinase 3beta mediated by neuregulin signaling leads to differential effects on tau phosphorylation and amyloid precursor protein processing', *J Neurosci*, 28(10), pp. 2624–2632. doi: 10.1523/JNEUROSCI.5245-07.2008.

Westphal, R. S. *et al.* (1999) 'Identification of kinase-phosphatase signaling modules composed of p70 S6 kinase-protein phosphatase 2A (PP2A) and p21-activated kinase-PP2A.', *The Journal of biological chemistry*. American Society for Biochemistry and Molecular Biology, 274(2), pp. 687–92. doi: 10.1074/JBC.274.2.687.

Whitehouse, P. *et al.* (1982) 'Alzheimer's disease and senile dementia: loss of neurons in the basal forebrain', *Science*. American Association for the Advancement of Science, 215(4537), pp. 1237–1239. doi: 10.1126/science.7058341.

Whitwell, J. L. *et al.* (2009a) 'Atrophy patterns in IVS10+16, IVS10+3, N279K, S305N, P301L, and V337M MAPT mutations', *Neurology*, 73(13), pp. 1058–1065. doi: 10.1212/WNL.0b013e3181b9c8b9.

Whitwell, J. L. *et al.* (2009b) 'Atrophy patterns in IVS10+16, IVS10+3, N279K, S305N, P301L, and V337M MAPT mutations', *Neurology*. doi: 10.1212/WNL.0b013e3181b9c8b9.

Wicklund, L. *et al.* (2010) 'Beta-amyloid 1-42 oligomers impair function of human embryonic stem cell-derived forebrain cholinergic neurons', *PLoS One*. doi: 10.1371/journal.pone.0015600.

Wicklund, L. *et al.* (2010) 'B-Amyloid 1-42 Oligomers Impair Function of Human Embryonic Stem Cell-Derived Forebrain Cholinergic Neurons.', *PloS one*. doi: 10.1371/journal.pone.0015600.

Winder-Rhodes, S. E. *et al.* (2015) 'Association between MAPT haplotype and memory function in patients with Parkinson's disease and healthy aging individuals.', *Neurobiology of aging*. Elsevier, 36(3), pp. 1519–28. doi: 10.1016/j.neurobiolaging.2014.12.006.

Windisch, M. (2014) 'We Can Treat Alzheimer's Disease Successfully in Mice but Not in Men: Failure in Translation? A Perspective', *Neurodegenerative Diseases*, 13(2–3), pp. 147–150. doi: 10.1159/000357568.

Wirths, O. and Bayer, T. A. (2008) 'Motor impairment in Alzheimer's disease and transgenic Alzheimer's disease mouse models', in *Genes, Brain and Behavior*, pp. 1–5. doi: 10.1111/j.1601-183X.2007.00373.x.

Wittmann, C. W. (2001) 'Tauopathy in Drosophila: Neurodegeneration Without Neurofibrillary Tangles', *Science*, 293(5530), pp. 711–714. doi: 10.1126/science.1062382.

Wolfe, M. S. (2008) 'Tau Mutations in Neurodegenerative Diseases * Normal Tau Function and Isoforms'. doi: 10.1074/jbc.R800013200.

Woltjen, K. *et al.* (2009) 'PiggyBac transposition reprograms fibroblasts to induced pluripotent stem cells', *Nature*, 458(7239), pp. 766–770. doi: 10.1038/nature07863.

Woodbury, M. E. and Ikezu, T. (2014) 'Fibroblast growth factor-2 signaling in neurogenesis and neurodegeneration.', *Journal of neuroimmune pharmacology : the official journal of the Society on NeuroImmune Pharmacology*. NIH Public Access, 9(2), pp. 92–101. doi: 10.1007/s11481-013-9501-5.

Woodgett, J. R. (1990) 'Molecular cloning and expression of glycogen synthase kinase-3/factor A.', *The EMBO journal*. European Molecular Biology Organization, 9(8), pp. 2431–8.

Woolf, N. J. (1991) 'Cholinergic systems in mammalian brain and spinal cord', *Progress in Neurobiology*, pp. 475–524. doi: 10.1016/0301-0082(91)90006-M.

Wren, M. C. *et al.* (2015) 'Frontotemporal dementia-associated N279K tau mutant disrupts subcellular vesicle trafficking and induces cellular stress in iPSC-derived neural stem cells', *Molecular Neurodegeneration*. doi: 10.1186/s13024-015-0042-7.

Wren, M. C. *et al.* (2015) 'Frontotemporal dementia-associated N279K tau mutant disrupts subcellular vesicle trafficking and induces cellular stress in iPSC-derived neural stem cells.', *Molecular Neurodegeneration*. doi: 10.1186/s13024-015-0042-7.

Wszolek, Z. K. *et al.* (2003) 'Hereditary tauopathies and parkinsonism.', *Advances in neurology*, 91, pp. 153–63.

Wu, D.-C. *et al.* (2000) 'The Expression of Cdk5, p35, p39, and Cdk5 Kinase Activity in Developing, Adult, and Aged Rat Brains', *Neurochemical Research*. Kluwer Academic Publishers-Plenum Publishers, 25(7), pp. 923–929. doi: 10.1023/A:1007544106645.

Wu, D. and Pan, W. (2010) 'GSK3: a multifaceted kinase in Wnt signaling', *Trends in Biochemical Sciences*, 35(3), pp. 161–168. doi: 10.1016/j.tibs.2009.10.002.

Wu, H. *et al.* (2014) 'Complete morphologies of basal forebrain cholinergic neurons in the mouse', *eLife*. doi: 10.7554/eLife.02444.

Wu, J. W. *et al.* (2013) 'Small Misfolded Tau Species Are Internalized via Bulk Endocytosis and Anterogradely and Retrogradely Transported in Neurons', *Journal of Biological Chemistry*, 288(3), pp. 1856–1870. doi: 10.1074/jbc.M112.394528.

Wu, J. W. *et al.* (2016) 'Neuronal activity enhances tau propagation and tau pathology in vivo', *Nature Neuroscience*, 19(8), pp. 1085–1092. doi: 10.1038/nn.4328.

Wu, X. *et al.* (2011) 'Skin Stem Cells Orchestrate Directional Migration by Regulating Microtubule-ACF7 Connections through GSK3β', *Cell*, 144(3), pp. 341–352. doi: 10.1016/j.cell.2010.12.033.

Wyss-Coray, T. *et al.* (2003) 'Adult mouse astrocytes degrade amyloid-β in vitro and in situ', *Nature Medicine*, 9(4), pp. 453–457. doi: 10.1038/nm838.

Xu, X. *et al.* (2013) 'Prevention of beta-amyloid induced toxicity in human iPS cell-derived neurons by inhibition of Cyclin-dependent kinases and associated cell cycle events', *Stem Cell Res*. doi: 10.1016/j.scr.2012.11.005.

Yagi, T. *et al.* (2011) 'Modeling familial Alzheimer's disease with induced pluripotent stem cells', *Human Molecular Genetics*. doi: 10.1093/hmg/ddr394.

Yamada, K. *et al.* (2014) 'Neuronal activity regulates extracellular tau in vivo.', *The Journal of experimental medicine*. Rockefeller University Press, 211(3), pp. 387–93. doi: 10.1084/jem.20131685.

Yan, S. D. *et al.* (1994) 'Glycated tau protein in Alzheimer disease: a mechanism for induction of oxidant stress.', *Proceedings of the National Academy of Sciences of the United States of America*, 91(16), pp. 7787–91. doi: 10.1073/pnas.91.16.7787.

Yao, H.-B. *et al.* (2002) 'Expression of glycogen synthase kinase-3 isoforms in mouse tissues and their transcription in the brain.', *Journal of chemical neuroanatomy*, 23(4), pp. 291–7.

Yokobayashi, S. *et al.* (2017) 'Clonal variation of human induced pluripotent stem cells for induction into the germ cell fate†', *Biology of Reproduction*. Oxford University Press, 96(6), pp. 1154–1166. doi: 10.1093/biolre/iox038.

Yoshimura, T. *et al.* (2005) 'GSK-3β Regulates Phosphorylation of CRMP-2 and Neuronal Polarity', *Cell*, 120(1), pp. 137–149. doi: 10.1016/j.cell.2004.11.012.

Yoshiyama, Y. (2008) '[Neurodegeneration and inflammation: analysis of a FTDP-17 model mouse].', *Rinsho shinkeigaku = Clinical neurology*, 48(11), pp. 910–2.

Yoshiyama, Y. *et al.* (2001) 'Frontotemporal dementia and tauopathy', *Current Neurology and Neuroscience Reports*. Current Medicine Group, 1(5), pp. 413–421. doi: 10.1007/s11910-001-0100-0.

Young, J. E. E. *et al.* (2015) 'Elucidating molecular phenotypes caused by the SORL1 Alzheimer's disease genetic risk factor using human induced pluripotent stem cells', *Cell Stem Cell*. doi: 10.1016/j.stem.2015.02.004.

Yu, J. *et al.* (2007) 'Induced Pluripotent Stem Cell Lines Derived from Human Somatic Cells', *Science*, 318(5858), pp. 1917–1920. doi: 10.1126/science.1151526.

Yu, J. *et al.* (2011) 'Efficient Feeder-Free Episomal Reprogramming with Small Molecules', *PLoS ONE*. Edited by M. Pera. Public Library of Science, 6(3), p. e17557. doi: 10.1371/journal.pone.0017557.

Yusa, K. *et al.* (2009) 'Generation of transgene-free induced pluripotent mouse stem cells by the piggyBac transposon', *Nature Methods*, 6(5), pp. 363–369. doi: 10.1038/nmeth.1323.

Zaborszky, L., van den Pol, A. N. and Gyengesi, E. (2012) 'The Basal Forebrain Cholinergic Projection System in Mice', in *The Mouse Nervous System*, pp. 684–718. doi: 10.1016/B978-0-12-369497-3.10028-7.

Zang, M. *et al.* (2001) 'Microtubule integrity regulates Pak leading to Ras-independent activation of Raf-1. insights into mechanisms of Raf-1 activation.', *The Journal of biological chemistry*. American Society for Biochemistry and Molecular Biology, 276(27), pp. 25157–65.

van der Zee, J. and Van Broeckhoven, C. (2014) 'Dementia in 2013: Frontotemporal lobar degeneration—building on breakthroughs', *Nature Reviews Neurology*, 10(2), pp. 70–72. doi: 10.1038/nrneurol.2013.270.

Zempel, H. *et al.* (2010) 'A Oligomers Cause Localized Ca2+ Elevation, Missorting of Endogenous Tau into Dendrites, Tau Phosphorylation, and Destruction of Microtubules and Spines', *Journal of Neuroscience*. BioMed Central, 30(36), pp. 11938–11950.

Zeng, H. *et al.* (2010) 'Specification of region-specific neurons including forebrain glutamatergic neurons from human induced pluripotent stem cells', *PLoS ONE*. doi: 10.1371/journal.pone.0011853.

Zetterberg, H. *et al.* (2013) 'Plasma tau levels in Alzheimer's disease.', *Alzheimer's research & therapy*. BioMed Central, 5(2), p. 9. doi: 10.1186/alzrt163.

Zhang, D. *et al.* (2014) 'A 3D Alzheimer's disease culture model and the induction of P21-activated kinase mediated sensing in iPSC derived neurons', *Biomaterials*, 35(5), pp. 1420–1428.

Zhang, H. *et al.* (2005) 'A GIT1/PIX/Rac/PAK signaling module regulates spine morphogenesis and synapse formation through MLC.', *The Journal of neuroscience : the official journal of the Society for Neuroscience*. Society for Neuroscience, 25(13), pp. 3379–88. doi: 10.1523/JNEUROSCI.3553-04.2005.

Zhang, H. *et al.* (2012) 'Proteolytic processing of Alzheimer's β-amyloid precursor protein.', *Journal of neurochemistry*. NIH Public Access, 120 Suppl 1(Suppl 1), pp. 9–21. doi: 10.1111/j.1471-4159.2011.07519.x.

Zhang, Y. (2013) 'Caspases in Alzheimer's Disease', in *Neurodegenerative Diseases*. InTech. doi: 10.5772/54627.

Zhang, Z. *et al.* (2011) 'Inhibition of glycogen synthase kinase-3β by Angelica sinensis extract decreases β-amyloid-induced neurotoxicity and tau phosphorylation in cultured cortical neurons', *Journal of*

Neuroscience Research. Wiley Subscription Services, Inc., A Wiley Company, 89(3), pp. 437–447. doi: 10.1002/jnr.22563.

Zhao, L. *et al.* (2006) 'Role of p21-activated kinase pathway defects in the cognitive deficits of Alzheimer disease', *Nature Neuroscience*, 9(2), pp. 234–242. doi: 10.1038/nn1630.

Zheng-Fischhöfer, Q. *et al.* (1998) 'Sequential phosphorylation of Tau by glycogen synthase kinase-3β and protein kinase A at Thr212 and Ser214 generates the Alzheimer-specific epitope of antibody AT100 and requires a paired-helical-filament-like conformation', *Eur. J. Biochem*, 252, pp. 542–552.

Zheng, W.-H. *et al.* (2002) 'Amyloid beta peptide induces tau phosphorylation and loss of cholinergic neurons in rat primary septal cultures.', *Neuroscience*, 115(1), pp. 201–11.

Zheng, Y. *et al.* (2002) 'A peptide derived from cyclin-dependent kinase activator (p35) specifically inhibits Cdk5 activity and phosphorylation of tau protein in transfected cells', *European Journal of Biochemistry*. Blackwell Science Ltd, 269(18), pp. 4427–4434. doi: 10.1046/j.1432-1033.2002.03133.x.

Zheng, Y.-L. *et al.* (2005) 'A Cdk5 inhibitory peptide reduces tau hyperphosphorylation and apoptosis in neurons', *The EMBO Journal*, 24(1), pp. 209–220. doi: 10.1038/sj.emboj.7600441.

Zheng, Y. L. *et al.* (2010) 'A 24-residue peptide (p5), derived from p35, the Cdk5 neuronal activator, specifically inhibits Cdk5-p25 hyperactivity and tau hyperphosphorylation', *Journal of Biological Chemistry*, 285(44), pp. 34202–34212. doi: 10.1074/jbc.M110.134643.

Zhou, J. *et al.* (2012) 'Predicting Regional Neurodegeneration from the Healthy Brain Functional Connectome', *Neuron*, 73(6), pp. 1216–1227. doi: 10.1016/j.neuron.2012.03.004.

Zhou, Y. *et al.* (2014) 'Intracellular clusterin interacts with brain isoforms of the bridging integrator 1 and with the microtubule-associated protein Tau in Alzheimer's Disease', *PLoS ONE*. doi: 10.1371/journal.pone.0103187.

Zhu, L.-Q. *et al.* (2007) 'Activation of Glycogen Synthase Kinase-3 Inhibits Long-Term Potentiation with Synapse-Associated Impairments', *Journal of Neuroscience*, 27(45), pp. 12211–12220.

Zhu, X. *et al.* (2001) 'Activation of MKK6, an upstream activator of p38, in Alzheimer's disease', *Journal of Neurochemistry*, 79(2), pp. 311–318.

Zhu, X.-C. *et al.* (2015) 'Rate of early onset Alzheimer's disease: a systematic review and meta-analysis.', *Annals of translational medicine*. AME Publications, 3(3), p. 38. doi: 10.3978/j.issn.2305-5839.2015.01.19.

Zhukareva, V. *et al.* (2002) 'Sporadic Pick's disease: A tauopathy characterized by a spectrum of pathological tau isoforms in gray and white matter', *Annals of Neurology*. Wiley Subscription Services, Inc., A Wiley Company, 51(6), pp. 730–739.

Zilka, N. *et al.* (2006) 'Truncated tau from sporadic Alzheimer's disease suffices to drive neurofibrillary degeneration in vivo', *FEBS Letters*. doi: 10.1016/j.febslet.2006.05.029.

Zimmerman, L. *et al.* (1994) 'Independent regulatory elements in the nestin gene direct transgene expression to neural stem cells or muscle precursors [published erratum appears in Neuron 1994 Jun;12(6):following 1388]', *Neuron*. doi: 10.1016/0896-6273(94)90148-1.